Institut für Geowissenschaften
Matematisch-Naturwissenschaftliche Fakultät
Univesität Potsdam

MELT INCLUSIONS IN MAFIC ROCKS AS WITNESSES OF METASOMATISM IN THE BOHEMIAN MASSIF

Dissertation
von

Alessia Borghini

Kumulative Dissertation
zur Erlangung des akademischen Grades
“Doctor rerum naturalium”

Dr. rer. nat.

in der Wissenschaftsdisziplin
PETROLOGIE

eingereicht an der
Mathematisch-Naturwissenschaften Fakultät
Institut für Geowissenschaften
der Universität Potsdam

Potsdam, den 6. Juli 2020

Supervisor:
Prof. Dr. Patrick J. O'Brien, Universität Potsdam

Reviewers:
Prof. Dr. Patrick J. O'Brien, Universität Potsdam
Prof. Dr. Bernardo Cesare, Universita' degli Studi di Padova
Assoc. Prof. Dr. Vojtěch Janoušek, Czech Geological Survey

Published online in the
Institutional Repository of the University of Potsdam:
https://doi.org/10.25932/publishup-47363
https://nbn-resolving.org/urn:nbn:de:kobv:517-opus4-473639

A Laura e Cesare

Declaration of Authorship

I confirm that I independently authored this thesis entitled" Melt inclusions in mafic rocks as witnesses of metasomatism in the Bohemian Massif" without the use of any other sources than the ones indicated. This work has been funded by the German Federal Ministry for Education and Research and the Deutsche Forschungsgemeinschaft (DFG; projects FE 1527/2-1 and FE 1527/2-2 to Silvio Ferrero) and it has not been submitted to any other institution of higher education.

Abstract

Orogenic peridotites represent portions of upper subcontinental mantle now incorporated in mountain belts. They often contain layers, lenses and irregular bodies of pyroxenite and eclogite. The origin of this heterogeneity and the nature of these layers is still debated but it is likely to involve processes such as transient melts coming from the crust or the mantle and segregating in magma conduits, crust-mantle interaction, upwelling of the asthenosphere and metasomatism. All these processes occur in the lithospheric mantle and are often related with the subduction of crustal rocks to mantle depths. In fact, during subduction, fluids and melts are released from the slab and can interact with the overlying mantle, making the study of deep melts in this environment crucial to understand mantle heterogeneity and crust-mantle interaction. The aim of this thesis is precisely to better constrain how such processes take place studying directly the melt trapped as primary inclusions in pyroxenites and eclogites. The Bohemian Massif, crystalline core of the Variscan belt, is targeted for these purposes because it contains orogenic peridotites with layers of pyroxenite and eclogite and other mafic rocks enclosed in felsic high pressure and ultra-high pressure crustal rocks. Within this Massif mafic rocks from two areas have been selected: the garnet clinopyroxenite in orogenic peridotite of the Granulitgebirge and the ultra-high pressure eclogite in the diamond-bearing gneisses of the Erzgebirge. In both areas primary melt inclusions were recognized in the garnet, ranging in size between 2-25 μm and with different degrees of crystallization, from glassy to polycrystalline. They have been investigated with Micro Raman spectroscopy and EDS mapping and the mineral assemblage is kumdykolite, phlogopite, quartz, kokchetavite, phase with a main Raman peak at 430 cm^{-1}, phase with a main Raman peak at 412 cm^{-1}, white mica and calcite with some variability in relative abundance depending on the case study. In the Granulitgebirge osumilite and pyroxene are also present, whereas calcite is one of the main phases in the Erzgebirge. The presence of glass and the mineral assemblage in the nanogranitoids suggest that they were former droplets of melt trapped in the garnet while it was growing. Glassy inclusions and re-homogenized nanogranitoids show a silicate melt that is granitic, hydrous, high in alkalis and weakly peraluminous. The melt is also enriched in both case studies in Cs, Pb, Rb, U, Th, Li and B suggesting the involvement of crustal component, i.e. white mica (main carrier of Cs, Pb, Rb, Li and B), and a fluid (Cs, Th and U) in the melt producing reaction. The whole rock in both cases mainly consists of garnet and clinopyroxene with, in Erzgebirge samples, the additional presence of quartz both in the matrix and as a polycrystalline inclusion in the garnet. The latter is interpreted as a quartz pseudomorph after coesite and occurs in the same microstructural position as the melt inclusions. Both rock types show a crustal and

subduction zone signature with garnet and clinopyroxene in equilibrium. Melt was likely present during the metamorphic peak of the rock, as it occurs in garnet.

Our data suggest that the processes most likely responsible for the formation of the investigated rocks in both areas is a metasomatic reaction between a melt produced in the crust and mafic layers formerly located in the mantle wedge for the Granulitgebirge and in the subducted continental crust itself in the Erzgebirge. Thus metasomatism in the first case took place in the mantle overlying the slab, whereas in the second case metasomatism took place in the continental crust that already contained, before subduction, mafic layers. Moreover, the presence of former coesite in the same microstructural position of the melt inclusions in the Erzgebirge garnets suggest that metasomatism took place at ultra-high pressure conditions.

Summarizing, in this thesis we provide new insights into the geodynamic evolution of the Bohemian Massif based on the study of melt inclusions in garnet in two different mafic rock types, combining the direct microstructural and geochemical investigation of the inclusions with the whole-rock and mineral geochemistry. We report for the first time data, directly extracted from natural rocks, on the metasomatic melt responsible for the metasomatism of several areas of the Bohemian Massif. Besides the two locations here investigated, belonging to the Saxothuringian Zone, a signature similar to the investigated melt is clearly visible in pyroxenite and peridotite of the T-7 borehole (again Saxothuringian Zone) and the durbachite suite located in the Moldanubian Zone.

Allgemeine Zusammenfassung

Die Präsenz orogener Peridotite - metamorphosierte Bestanteile des Mantels -, die in Gebirgen auftreten, belegt, dass der Erdmantel an Kontinent-Kontinent-Kollisionen beteiligt sein kann. Solche orogenen Peridotite sind häufig heterogen, da sie Pyroxenit- und Eklogitlagen und Linsen enthalten, d.h. Hochdruckgesteine, die aus Granat und Klinopyroxen bestehen. Die meisten Prozesse, die für diese Heterogenität verantwortlich sind, involvieren Schmelzen, die durch den Mantel migrieren und dabei zu dessen Metasomatose oder zu der Anreicherung von Granat und Klinopyroxen in Adern und Kanälen führen. Ein weiterer Prozess kann auch das Recyceln subduzierter ozeanischer Kruste im Erdmantel sein. Im Allgemeinen finden all diese Prozesse während der Subduktion der Kruste in Manteltiefe statt. Unter diesen Bedingungen stehen die Krustengesteine im direkten Kontakt mit den Mantelgesteinen und die dabei freigesetzten Fluide oder Schmelzen können mit den Peridotiten wechselwirken. Letztere können anschließend von den Krustengesteinen aufgenommen und zur Erdoberfläche exhumiert werden, wo sie untersucht werden können. Diese Arbeit fokussiert sich vor allem auf die Untersuchung der Pyroxenit- und Eklogitbildung sowie auf die Wechselwirkung zwischen Schmelze und Gestein während der Subduktion der Kontinentalkruste in Manteltiefe. Dafür ist das Böhmische Massiv die ideale geologische Umgebung, da es erhebliche Mengen an Pyroxeniten und Eklogiten enthält, die sich in einigen Fällen in orogenen Peridotiten befinden, und die alle in einer ehemals tief subduziertern kontinentalern Kruste eingegliedert wurden. Um die Zielstellung zu erreichen, wurde die Schmelze mit einem neuartigen Ansatz untersucht, wobei diese hier direkt in primären Schmelzeinschlüssen, die im Granat eingeschlossenen sind, untersucht wird. Es wurden zwei Gebiete mit Pyroxeniten und Eklogiten, die Schmelzeinschlüsse enthalten, ausgewählt, ein Pyroxenit aus dem Granulitgebirge und ein Ultrahochdruck-Eklogit aus dem Erzgebirge (Sachsen, Deutschland). Die Einschlüsse bestehen aus einer granitischen, wasserhaltigen Schmelze krustaler Herkunft. Das Auftreten der im Granat unregelmäßig verteilten Einschlüsse bestätigt das Vorhandensein von Schmelze während der Peakmetamorphose. Da die Schmelzen in beiden Fällen ähnlich sind, schlussfolgern wir daraus, dass beide Gesteinsarten durch metasomatische Prozesse infolge der Wechselwirkung von silikatreicher Schmelze und mafischen Lagen gebildete wurden. Im Granulitgebirge ging die Schmelze eine Wechselwirkung mit mafischen Lagen im Mantel ein und erst später wurde der Wirtsperidotit einschließlich der neugebildeten Pyroxenit- und Eklogitlagen in die subduzierte Kruste eingebaut. Im Fall der Pyroxenite und Eklogite des Erzgebirges fand die Metasomatose stattdessen in der kontinentalen Kruste statt. Hier ging die Schmelze eine Wechselwirkung mit mafischen Lagen ein, die sich bereits vor der Subduktion in der Kruste befunden hatten. Im letzteren Fall belegt der Hinweis auf ehemaligen Coesit , d. h. auf ein Mineral, das Tiefen >95 km anzeigt, welches anwesend war während der Metasomatose, dass die Prozesse in größeren Tiefen stattfanden als im Granulitgebirge.

Acknowledgments

This thesis is the result of a path in which I learned a lot and not only not only how to be a scientist but also from personal perspective. It could have not been possible without the help and support of many people.

First, I would like to thank my supervisor Patrick O'Brien for helping me to address the scientific questions, teaching me how to be critic about my data and stimulating me with many scientific discussions. I would like to express my deep gratitude to my advisor Silvio Ferrero for constantly supporting me and guiding me in all the different and exciting aspects of the melt inclusions study, but also for listening and giving advices in scientific and personal matters. I would like to thank both because they allowed me to present my work all over the world and they made me grow as a scientist.

I would like to thank Manfred Strecker for his support and advices, Christina Günter for her help inside and outside the lab, Martin Ziemann for the assistance, Martin Timmerman for scientific discussion and together with Martin Ziemann for the translation of my abstract in German. My gratitude goes also to Valby van Schijndel for her time and Uwe Alterberger. My work on nanogranitoids would not be completed without the help of Bernd Wunder, Oscar Laurent, Lutz Hecht, Felix Kaufmann, Peter Czaja, Giulio Borghini and Sula Milani: thanks to all of you. My gratitude goes also to Christine Fischer in particular and Marcel and Martin for the sample preparation.

Of course there is not just science, I would like to thank all the administrative staff of the University of Potsdam and in particular Tanja Klaka-Tauscher, Cornelia Becker, Ines Münch, Corinna Kallich, Martina Heidemann, Juliane Gross and Claudia Rössling.

My experience here has been great thanks to my colleagues, officemates and friends especially, Sebastian Zapata, Lélia Libon, Iris van der Veen, Stephanie Olen, Fabiana Castino, Iris Wannhoff, Veronica Torres Acosta, Melanie Lorenz, Nicole Köllner, Roberta Spallanzani, Melanie Olschimke, Nicolas Christ, Magda Patyniak, Sara Savi, Federico Ibarra, Ahmad Arnous, Niels Meijer and Irum Khan.

My life here wouldn't have been the same without Fede and Maya that I thank for their constant presence and support. Thank you also to Leila, Linda, Emelie and Patrick.

A special thanks goes to my friends around Europe especially to Marty, Pinny, Fede, Giulia, Marghe, Carlot, Frollo, Marly, Fede and Stefano.

Last but the least, I would like to thank my mom Laura, my dad Cesare and my brother Nicoló for all the unconditional support in all my choices, if I manage to reach this goal is thanks to you. I finally would like to thank my aunt Anna, my grandma Sara and all my family.

CONTENTS

LIST OF FIGURES

LIST OF TABLES

LIST OF ABBREVIATIONS

Most of the abbreviation used on this thesis come from Whitney and Evans (2010) here a list of the abbreviation that are not included in that list:

Wm = white mica

Qtz = quartz

Kml = kumdykolite

Kok = Kokchetavite

1. INTRODUCTION

The investigation of the composition and evolution of Earth's mantle is fundamental to unravel the origin and chemical differentiation of our planet (Anderson, 1989). The mantle can be directly investigated by targeting orogenic peridotites, portions of which are now incorporated in orogenic belts. Garnet-bearing Alpine-type or orogenic peridotites tectonically emplaced in high pressure (HP) and ultra-high pressure (UHP) continental crustal sequences (e.g. metagranites and metapelites; Medaris and Carswell, 1990; Brueckner, 1998; Medaris, 1999; Brueckner and Medaris, 2000; Kotková et al., 2011; Bodinier and Godard, 2014) are a common feature of most studied orogenic belts formed by continent-continent collision in Europe: the Caledonides, Variscides and Alps (Fig. 1.1).

Figure 1.1. Map of Europe with highlighted the three main orogens (after Neubauer, 2009): Caledonian, Variscan and Alpine and the main location of orogenic peridotite reported in italic.

The orogenic peridotites represent an important source of information on (i) the physical and chemical characteristic of the upper mantle, (ii) the metamorphic conditions of the thickened continental crust, (iii) the nature of crust-mantle interaction in continental subduction settings, (iv) transport, reaction and storage of fluids/melts in supra-subduction mantle wedges, and (v) subduction and exhumation mechanisms (Medaris, 1999; Bodinier and Godard, 2014 and references therein).

Orogenic peridotites have been classified according to their tectonothermal setting (Fig. 1.2) by Brueckner and Medaris (2000) as *crustal* and *mantle* peridotites.

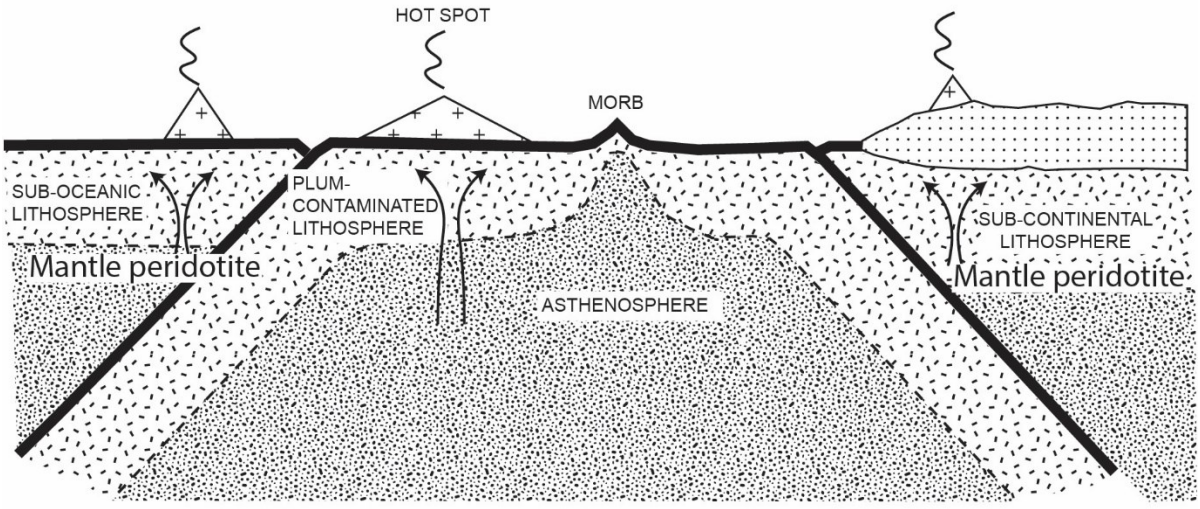

Figure 1.2. Initial mantle environment of HP-UHP mantle peridotites (modified after Brueckner and Medaris, 2000).

Crustal peridotites occur in the crust at shallow level prior to subduction and share a metamorphic history with the crust. *Mantle* peridotites intrude the crust from the mantle wedge and are exhumed to the surface along continent-continent sutures or the active continental margin (Brueckner and Medaris, 2000; Bodinier and Godard, 2014). They are divided into *subduction zone* and *relict* peridotites and this thesis focused in particular on the *subduction zone* type. Among subduction zone peridotites, Brueckner and Medaris (2000) recognized prograde, HP-high temperature (HT) and ultra-high temperature (UHT) peridotites based on the mantle source and P-T conditions at the moment of emplacement. The prograde peridotites intrude the crust at shallow levels (20 - 50 km) during subduction and they acquire their garnet-bearing assemblage through subsequent prograde metamorphism whereas the HP-HT ones are incorporated into the crust already in the garnet stability field (> 50 km), e.g., Nové Dvory type in the Gföhl Nappe, Bohemian Massif

(Medaris et al., 1995). The UHT peridotites intrude the crust at UHT conditions in the spinel stability field as a result of asthenospheric upwelling and they recrystallize in a second event as garnet-bearing ones (Kotková et al., 2011), e.g., Mohelno type in the Gföhl Nappe, Bohemian Massif (Medaris et al., 1995) and Ronda and Beni Bousera, Betic-Rif Belt (Pearson et al., 1991). Prograde and HP-HT peridotite can be transferred from the mantle wedge (hanging wall) to the slab (crustal footwall) because of a gravitational instability due to a denser body lying on a lighter one (Brueckner, 1998). If the interface between slab and mantle becomes hot or wet, peridotite can deform via ductile flow and sink in the underlying crust as mantle blobs (Brueckner, 1998). From the moment of the incorporation, peridotites share their evolution with the crust and are exhumed with it (Brueckner, 1998; Medaris, 1999; Brueckner and Medaris, 2000).

A common feature of the alpine type peridotites occurring in orogenic belts, independent from their chemistry, is that they are heterogeneous. In fact, they contain lenses, irregular bodies and dykes of pyroxenites and eclogites (Allègre and Turcotte, 1986; Medaris and Carswell, 1990; Medaris et al., 1995, 2006; Garrido and Bodinier, 1999; Brueckner and Medaris, 2000; Bodinier and Godard, 2014; Borghini et al., 2018). Both rock types have garnet and pyroxene as main rock-forming phases, and are generally classified as pyroxenites or eclogites based on their chemical features of both whole-rock and mineral phases (see chapter 4 for a detailed discussion). The petrological and chemical features of both pyroxenites and eclogites, their formation in relationship to deep melts and melt-rock interaction in subduction zones are the main topics of the presented doctoral thesis.

1.1 PYROXENITE AND ECLOGITE AS WITNESSES OF MANTLE HETEROGENEITY

In 1964, Gast et al. have shown that the distribution of the radiogenic isotopes of Sr and Pb was not homogeneous in the Earth's upper mantle. Since then, the chemical heterogeneity of the mantle has been extensively documented (Allegre et al., 1980 and reference therein). It is mainly controlled by plate tectonics (Isabel Varas-Reus et al., 2018) that, with generation and subduction of oceanic crust and continental lithosphere, allow crust-mantle interaction and mantle re-fertilization (Marchesi et al., 2013). As stated above, this heterogeneity can be directly observed not only in the orogenic peridotites, which frequently enclose pyroxenite and eclogite veins and lenses (see references above), but also in basalts containing different ultramafic and mafic xenoliths and nodules (Frey, 1980; Irving, 1980; Schmidt et al., 2003), as well as in

kimberlite pipes (Boyd and Meyer, 1979; Nixon et al., 1981). The investigation of orogenic peridotite provides insights into the evolution of the whole lithosphere. Pyroxenite and eclogite, in particular, are believed to play an important role in the petrogenesis of mid-ocean ridge basalts (MORB; see (Hirschmann and Stolper, 1996; Pertermann and Hirschmann, 2003; Sobolev et al., 2007; Lambart et al., 2013, 2016) and ocean island basalts (OIB; see Mallik and Dasgupta, 2012; Lambart et al., 2013) because of their lower solidus temperature and higher melt productivity at HP than the host peridotite (Hirschmann and Stolper, 1996; Yaxley and Green, 1998; Kogiso et al., 2004; Lambart et al., 2012). Moreover, they have a wide compositional variability and thus the possibility to produce, by partial melting, melts from silica-oversaturated to undersaturated types (Kogiso et al., 2004; Montanini and Tribuzio, 2015). Thus, the investigation of the origin and nature of pyroxenite and eclogite lenses and layers is fundamental for a better understanding of the mantle heterogeneity, the evolution of the lithosphere and the origin of mantle-related magmatism. The origin of these bodies is still debated, but has been explained with a variety of processes including fluid/melt migration in the mantle, crust-mantle interaction and asthenospheric upwelling (Downes, 2007; Bodinier and Godard, 2014). The main genetic processes so far proposed are: (i) HP crystals segregation from mafic melt mainly in a magma conduit (Irving, 1980; Medaris et al., 1995, 2006; Becker, 1996; Downes, 2007; Bodinier and Godard, 2014; Svojtka et al., 2016); (ii) recycling of oceanic crust in the convective mantle (Allègre and Turcotte, 1986; Kornprobst et al., 1990; Blichert-Toft et al., 1999; Bodinier and Godard, 2014; Montanini and Tribuzio, 2015; Isabel Varas-Reus et al., 2018); (iii) HP-lower temperature recrystallization from pyroxene megacrysts (Carswell and Jamtveit, 1990; Becker, 1997; Massone and Bautsch, 2002; Faryad et al., 2009; Schmädicke et al., 2010); (iv) fluid/melt-rock interaction with melts of mantle or crustal origin (Garrido and Bodinier, 1999; Malaspina et al., 2006, 2009; Downes, 2007; Vrijmoed et al., 2013) and (v) HP recrystallization of gabbroic cumulates from oceanic crust (Obata et al., 2006; Svojtka et al., 2016). The last genetic process has been proposed exclusively for Nové Dvory kyanite eclogite and pyroxenites of the Bečváry locality both from the Gföhl Unit, Moldanubian Zone, Bohemian Massif (Czech Republic) and for the corundum-bearing garnet clinopyroxenite at Beni Bousera, Betic-Rif Belt (north Morocco; Kornprobst et al., 1990). As the last process has been proposed only for few restricted areas, it will not be discussed further in the present introduction.

1.1.1 HP CUMULATE

The majority of authors propose HP segregation of garnet and clinopyroxene ± trapped fluid from a transient basaltic melt in magma conduits to produce garnet pyroxenites (Irving, 1980;

Medaris et al., 1995, 2006, 2013; Becker, 1996; Downes, 2007; Bodinier and Godard, 2014; Svojtka et al., 2016). The origin of this melt is either from the mantle asthenosphere (Frey, 1980; Irving, 1980; Becker, 1996; Schmädicke et al., 2010) that, after ascent and cooling, crystallizes in the deep lithosphere (Becker, 1996) or from subducted oceanic crust including subducted sediments (Medaris et al., 1995, 2006; Schmädicke et al., 2010). Irving (1980) suggested that the process of segregation inside the conduit is gravity independent because it is not necessarily vertical, and takes place via a flow crystallization mechanism in which the liquidus crystals are plating the host peridotites walls (Fig. 1.3). If the magma flow rate is slow then the crystals would be continuously plated on the conduit walls as the magma moved through (Irving, 1980).

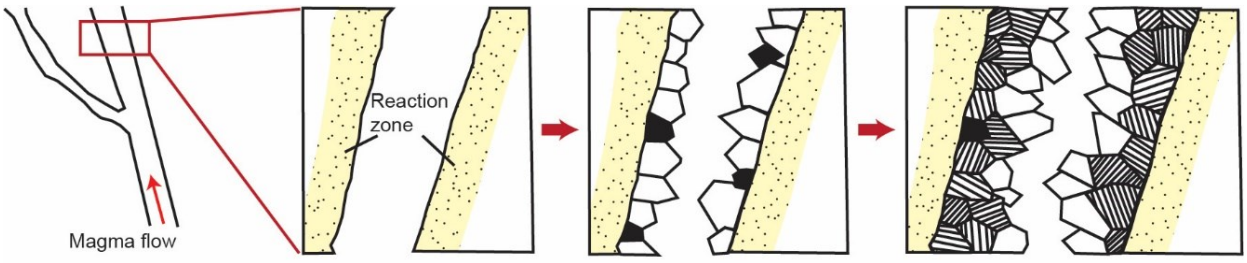

Figure 1.3. Model for the formation of pyroxenite via crystal segregation in a magma conduit (modified after Irving, 1980). Basaltic magma flows and plates the conduit walls where crystals precipitate. The type of crystals depends on P, temperature difference between magma and wall rock, channel width, magma flow rate and others factors (Irving, 1980)

Generally, this type of pyroxenite shows a modal layering of garnet and clinopyroxene with a modal variation visible at both outcrop and thin section scale (see Svojtka et al., 2016 Supplementary Data Fig. A2). The chemical variation in the pyroxenite indicates a fractional crystallization and reaction with the wall-rock peridotite whereas in the eclogite it can be due just to the fractional crystallization (Medaris et al., 1995). Other evidences are: igneous texture, crosscutting relationship and HREE enrichment indicative of garnet segregation (Bodinier and Godard, 2014); absence of any prograde metamorphic feature such a zoning in the garnet and large degree of scatter in oxide variation diagrams (Medaris et al., 1995, 2006; Svojtka et al., 2016); sometimes diffusive contacts with the host peridotite, high Ni contents and bulk-rock Mg# between 81.3-90.4: all features consistent with a reaction between the transient melt and the host peridotite (Svojtka et al., 2016). This origin has been proposed for most of the pyroxenites enclosed in peridotite of the Moldanubian Zone, Bohemian Massif (Czech Republic: Medaris et al., 1995, 2005, 2006; Svojtka et al., 2016; lower Austria: Becker, 1996), some pyroxenite in mantle xenoliths (Frey and Prinz, 1978; Irving, 1980), some pyroxenite layers in the Ronda

peridotite, Betic-Rif Belt (south Spain; Suen and Frey, 1987) and pyroxenite from Beni Bousera (Pearson et al., 1993).

1.1.2 SUBDUCTED CRUST RECYCLED IN THE MANTLE

Allegre et al. (1980) and Allègre and Turcotte (1986) proposed a genetic model stating that the pyroxenite and eclogite of the upper mantle represent pieces of subducted ancient oceanic crust recycled in the convective mantle. This model is called the “marble-cake model” (Fig. 1.4) because of the mantle appearance with these stripes of oceanic crust stretched and extensively deformed, but not completely destroyed and homogenized (Allègre and Turcotte, 1986). This model is based mainly on the extreme difference in isotopic composition in the mafic rocks and their isotopic differences with the peridotites (Bodinier and Godard, 2014 and references therein). Both the presence of positive Eu anomalies in some garnet pyroxenite (e.g. Ronda and Beni Bousera; Kornprost et al., 1990) and the isotopic variability of oceanic basalts support the hypothesis of recycled oceanic (Allègre and Turcotte, 1986) and continental crust in the mantle (Stracke, 2012). In addition, some garnet pyroxenites show trace element signatures, e.g., positive Sr and Eu anomalies, similar to those of the lower oceanic crust (Kornprobst et al., 1990; Garrido and Bodinier, 1999; Morishita et al., 2003; Montanini et al., 2012; Marchesi et al., 2013; Montanini and Tribuzio, 2015) and an isotopic compositional variation akin to the recycled oceanic crust component observed in oceanic basalts (Pearson et al., 1991; Blichert-Toft et al., 1999; Pearson and Nowell, 2004). The marble-cake model has been suggested for the genesis of garnet pyroxenite of the External Ligurian ophiolites (Northern Apennine, Italy; Montanini and Tribuzio, 2015), garnet pyroxenite of Beni Bousera (Kornprobst et al., 1990; Blichert-Toft et al., 1999) and garnet pyroxenite of Ronda (Morishita et al., 2003).

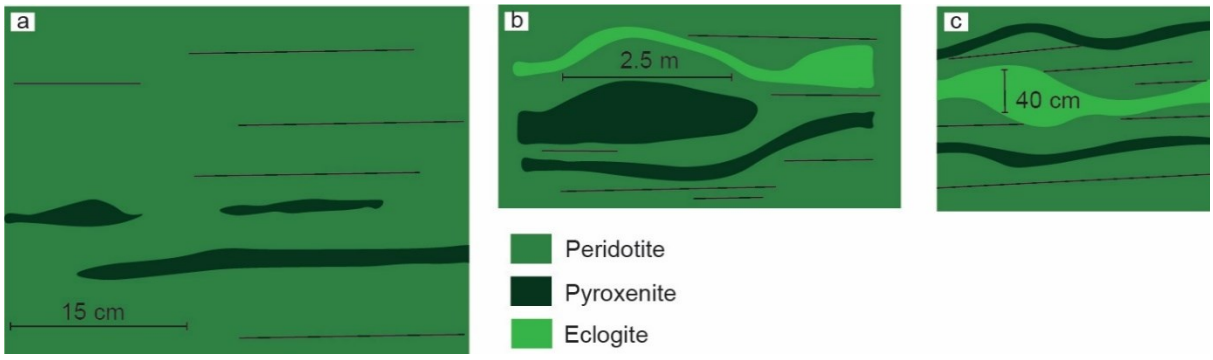

Figure 1.4. Marble-cake model: a) sketch of Beni Bousera garnet and spinel pyroxenite boudinaged layers in peridotite (drawing after Fig. 6a of Frets et al., 2014); b) and c) sketch of eclogite and pyroxenite strips in peridotite (modified after Allègre and Turcotte, 1986).

A more modern version of the marble-cake model suggests that UHP garnet pyroxenites would be restite formed after variable degrees of HP partial melting of ancient subducted oceanic crust with or without continental crust (Isabel Varas-Reus et al., 2018). Oceanic and continental crust would have been recycled into the convective mantle and thereby stirred into the lithosphere. This model has been applied in particular to the genesis of the UHP garnet pyroxenites of Ronda and Beni Bousera. The possibility of recycling continental crust in the convective mantle has also been reported for the UHP metasediments close to the serpentinite of the Dunkelsteiner Wald, Lower Austria, Bohemian Massif (west of Vienna; Becker and Altherr, 1992).

1.1.3 HP RECRYSTALLIZATION OF PYROXENE MEGACRYSTS

Garnet pyroxenite can represent the result of a stress-induced recrystallization of HT (1300–1400°C), highly aluminous pyroxene megacrysts typically at HP and lower temperature with a growth of exsolution-like lamellar garnet and low-Al pyroxene. The rock becomes a fine-grained, granoblastic garnet pyroxenite with generally two pyroxenes (orthopyroxene-rich or clinopyroxene-rich, depending on whether they derived from orthopyroxene or clinopyroxene megacrysts, respectively) as a result of continued deformation. The new phases are growing at solid state conditions, without the contribution of the melt (Carswell & Jamtveit, 1990; Faryad et al., 2009; Massonne and Bautsch, 2002; Medaris et al., 2005; Schmädicke et al., 2010). Megacrysts originate in the asthenospheric mantle by interaction between mantle and mantle-derived melts, which produced mono-mineralic equigranular layers of clinopyroxene and/or orthopyroxene and/or garnet. Examples of this process are garnet pyroxenites of Reinsdorf, Granulitgebirge, Bohemian Massif (Germany; Massonne and Bautsch, 2002; Schmädicke et al., 2010), some garnet pyroxenite of the Gföhl unit, Moldanubian Zone, Bohemian Massif (Czech Republic; Faryad et al., 2009) or garnet clinopyroxenite of Lower Austria, Moldanubian Zone (Becker, 1996).

1.1.4 FLUID/MELT-ROCK INTERACTION: METASOMATISM

Another process proposed for the genesis of the garnet pyroxenite is the metasomatic interaction between a fluid/melt and the peridotites (Malaspina et al., 2006, 2009; Vrijmoed et al., 2013). The metasomatism would take place in the mantle wedge where fluids and melts released by the subducted slab can infiltrate the mantle and react with the peridotites (Malaspina et al., 2006, 2009; Vrijmoed et al., 2013). The interaction between peridotites and silicic fluids/melts produces generally new phases, such as orthopyroxene, amphibole and phlogopite (i.e. modal

metasomatism; Carroll and Wyllie, 1990; Schiano et al., 1995; Becker, 1996; Zanetti et al., 1999; Becker et al., 2001; Prouteau et al., 2001; Rampone and Morten, 2001; Scaillet and Prouteau, 2001; Scambelluri et al., 2006; Zhang et al., 2007, 2011; Cannao` and Malaspina, 2018) and more rarely also apatite, dolomite and allanite (Obata and Morten, 1987; Tumiati et al., 2003), often mixed with peridotite relicts. In addition to the presence of new phases, peridotites are enriched in LILE, LREE, Sr (Schiano et al., 1995; Becker, 1996; Zanetti et al., 1999; Becker et al., 2001; Prouteau et al., 2001; Rampone and Morten, 2001; Scambelluri et al., 2006; Zhang et al., 2007; Zhang et al., 2011) and Li, U and Pb - typical elements related to subduction zone fluids (Scambelluri et al., 2006).

In some cases, the metasomatic interaction produces a blocks-and-veins texture in which the blocks are made of unmetasomatized or slightly metasomatized peridotite separated by different generation of veins with different compositions (Vrijmoed et al., 2013). These veins represent a sequence of metasomatic reaction zones developed along a fracture system. Here the metasomatism took place via influx of metasomatic agents through a network of thin fissures until the end mass transport (Vrijmoed et al., 2013). Moreover, metasomatism can also be cryptic and inferred just by the enrichment of incompatible elements in both the bulk rock and the mineral phases (Medaris et al., 2015) or by the presence of melt inclusions with a particular composition (Malaspina et al., 2006, 2009; Borghini et al., 2018).

The production of pyroxenite can be the result of mixing of variable proportions of a silica-rich melt and peridotite (Sobolev et al. 2007). This production of pyroxenite is thought to be the process responsible for the refertilization of the mantle (Kelemen et al., 1997; Yaxley and Green, 1998). Examples of these processes are considered to be the UHP Svartberget garnet peridotite, Western Gneiss Region (Norway; Vrijmoed et al., 2013), Bardane peridotite (Norway; Van Roermund et al., 2002), the Finero phlogopite peridotite Massif, Western Alps (Italy; (Zanetti et al., 1999; Raffone et al., 2006), the Ulten Zone garnet peridotite in the Eastern Alps (Italy; Rampone and Morten, 2001; Scambelluri et al., 2006), the UHP Sulu garnet peridotite (Eastern China; Malaspina et al., 2009) and UHP garnet orthopyroxenite from the Dabie Shan (Eastern China; Malaspina et al., 2006, 2009), Lherz peridotite Massif (France; (Bodinier et al., 1990, 2004; Woodland et al., 1996), garnet peridotite and pyroxenite of the T-7 borehole in the Saxothuringian Zone, Bohemian Massif (Germany; Medaris et al., 2015). For a detailed discussion on the role of the fluid in subduction zone see the next section of the introduction (§ 1.2).

1.2 ORIGIN OF DEEP MELTS IN SUBDUCTION SETTINGS

Most of the processes proposed for the genesis of pyroxenite and eclogite discussed above, consider fluid and melts to play an important role. It is then crucial to understand where the fluid can be produced and how it interacts with the peridotite. Fluids and melts can be originated by partial melting of peridotite in the mantle (see 1.3.1) or by the slab dehydration during the subduction of the crust at mantle depth (see 1.3.2). Peridotites can partially melt as a result of asthenospheric upwelling (e.g. beneath the mid-oceanic ridges, oceanic islands, continental rifts and possibly also subduction zones; Hirschmann et al., 1998) or due to release of H_2O from the subducted slab into the mantle wedge thus lowering the solidus temperature (Elliott et al., 1997). In general, the melt composition obtained from the partial melting of the upper mantle is controlled by olivine and pyroxene in peridotite and mainly by pyroxene in olivine-free hybrid pyroxenites, i.e., pyroxenites generated by the interaction of high silica-eclogite derived melt and the peridotite (Sobolev et al., 2007).

1.2.1 PARTIAL MELTING OF PERIDOTITE

Several experiments have provided constraints for the solidus of peridotite at different conditions: (i) dry, i.e., without free H_2O and without hydrous phases (Takahashi and Kushiro, 1983; Falloon et al., 1988, 1997; Hirose and Kushiro, 1993; Herzberg and Zhang, 1996; Hirschmann et al., 1998; Hirschmann, 2000); (ii) with H_2O present (Kawamoto and Holloway, 1997); or (iii) with a hydrous phase such as phlogopite or amphibole present (Fumagalli et al., 2009; Kessel et al., 2015; Condamine et al., 2016; Förster et al., 2017). In all the different cases, the melt contains less SiO_2 and Al_2O_3 and more MgO and FeO as a function of pressure increase (Herzberg and Zhang, 1996; Kawamoto and Holloway, 1997). Experiments done on two types of spinel lherzolites at dry conditions, pressures between 1 and 3 GPa and in a temperature range between 1250° and 1525°C, have obtained melts with alkali-olivine basalts and olivine tholeiite compositions (Hirose and Kushiro, 1993). The concentration of major elements varies based on the composition of the source lherzolite, the increasing of pressure and melting degree. SiO_2 is little related with the composition of the source and the degree of melting, whereas it is strongly inversely correlated with pressure. MgO is controlled mainly by temperature and increases when temperature increases. FeO, Al_2O_3, CaO and the incompatible elements are instead affected by the composition of the source and the degree of partial melting (Hirose and Kushiro, 1993). Two aspects have to be taken into account in the case of a H_2O-saturated melting of peridotite: presence of H_2O-rich fluid, and the presence and stability field of hydrous minerals (see also

1.2.2). These two aspects restrict the range at which melting can take place at depth (between 90 and 330 km; Kawamoto and Holloway, 1997). Melting in the presence of H_2O not only lowers the melting temperature, but it also affects the melt composition: at 1 GPa the melts are andesitic or dacitic in the presence of H_2O and basaltic for dry peridotite (Kushiro, 1972; Green, 1973). Moreover, the melt produced is generally SiO_2-poor when the melting reaction is due to the break-down of phlogopite in the absence of fluids. This latter possibility is similar to the condition of anhydrous partial melting of peridotite described above and the melt evolves from silica-undersaturated foidite to trachybasalt with increase degree of melting (Condamine et al., 2016).

1.2.2 MELTING OF DEEPLY SUBDUCTED CRUSTAL ROCKS

The interaction of peridotite with aqueous fluids or hydrous melts is a common process in the upper mantle. This is clearly the case with the petrogenesis of arc lavas which mixes components from the mantle wedge, as well as fluids and melts from subducted basaltic and sedimentary rocks and from shallow crustal interaction and contamination (Becker et al., 2000; Moyen and Martin, 2012; Scambelluri et al., 2019; Fig. 1.5).

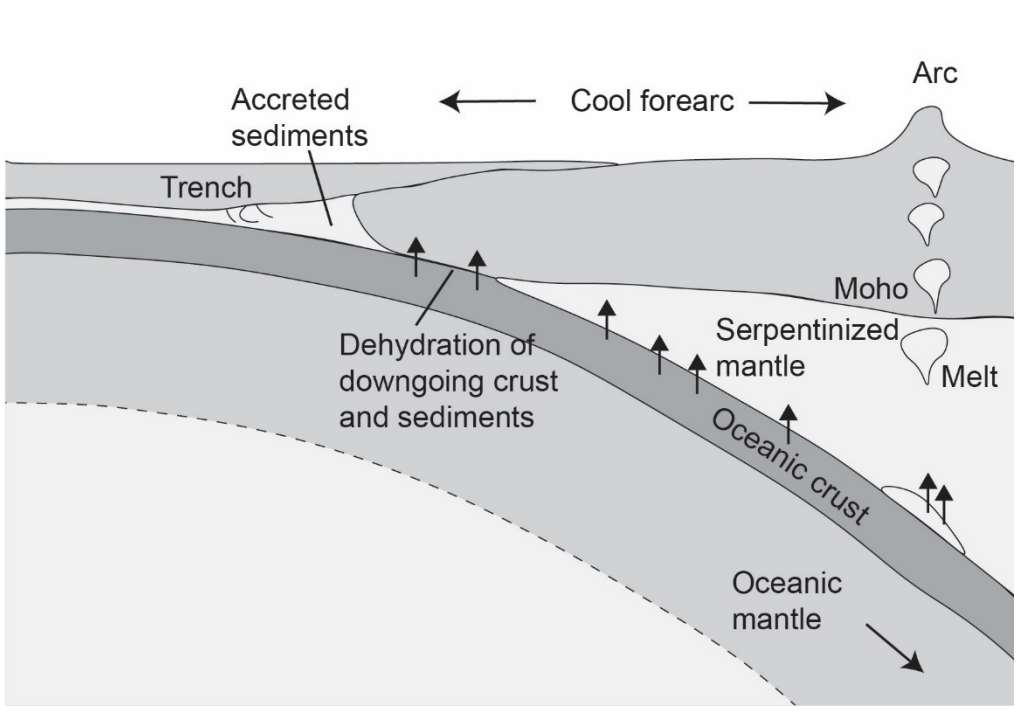

Figure 1.5. Scheme of crust dehydration and fluid release during subduction zone (modified after (Hyndman and Peacock, 2003).

The arc lavas are generally enriched in LILE and LREE compared with MORB and they represent evidence of deep recycling of elements in the subduction zone (Cannao` and Malaspina, 2018).

During subduction, oceanic and continental crusts are the carrier of elements, mainly LILE, LREE, Th, U and H_2O, that are stored mainly in hydrous phases such as phengite and phlogopite (Hermann and Green, 2001), lawsonite, serpentine, zoisite and amphibole (Cannaó and Malaspina, 2018). These phases break down and release fluids/melts that have a crucial role in the H_2O, halogen and LILE cycles and are among the most suitable agents for slab-to-mantle element transfer and mantle metasomatism and melting (Scambelluri et al., 2006; Fumagalli et al., 2009; Condamine et al., 2016). The melting of the oceanic crust is the subject of several experiments (Rapp et al., 1991; Peacock et al., 1994; Rapp and Watson, 1995; Yogodzinski et al., 2001; Klemme et al., 2002; Martin et al., 2005; Yaxley et al., 2007; Bouilhol et al., 2015) because of the possible link between eclogite/amphibolite melting and genesis of TTGs characteristic of Archean terranes (Martin et al., 2005; Moyen and Martin, 2012; Johnson et al., 2017). Experiments show that the partial melting of an eclogite produces tonalitic, trondhjemitic and dacitic melt such as the adakite arc lavas considered the modern equivalent of TTGs (Martin et al., 2005; Moyen and Martin, 2012). The felsic melt before ascent interacts with the peridotite and becomes richer in MgO, Ni and Cr. Adakite melt trace elements have a peculiar signature with low Y and HREE, high Sr and $(La/Yb)_N$>10 considered a feature of the melting of the oceanic crust at mantle depth (Martin et al., 2005).

1.3 NOVEL INVESTIGATION APPROACH: FLUID AND MELT INCLUSIONS STUDIES

The occurrence in minerals from garnet peridotite and pyroxenite of inclusions containing fluids, melts and multiphase solid inclusions was already reported for several ultramafic terranes (Schiano et al., 1995; Malaspina et al., 2006, 2009; Faryad et al., 2013; Borghini et al., 2018; Čopjaková and Kotková, 2018; Naemura et al., 2018; Sobolev, 2019). The investigation of preserved primary fluid and melt inclusions is the most direct approach to acquire crucial information about the genesis of both fluids and/or melts and their hosts (Ferrero and Angel, 2018). These inclusions, in fact, are isolated from the surrounding environment and the physio-chemical evolution of the rock along the path from subduction at mantle depth to exhumation (Ferrero and Angel, 2018). They record the fluid and/or melt composition at the moment of entrapment during the crystal growth. They provide important information about the chemistry of

the melt and the phase/phases and the rock involved in the melt production (see Chapter 2-3-4-5 of this thesis).

In the last two decades, the study of melt inclusions has been expanded to the metamorphic field, focusing on inclusions in migmatites and granulites, and the study of crustal anatexis (Cesare et al., 2009, 2015; Ferrero et al., 2015, 2016b, 2016a, 2018b; Bartoli et al., 2015, 2016a; Acosta-Vigil et al., 2016, 2017a; Bartoli, 2017, 2019; Tacchetto et al., 2018; Carvalho et al., 2018; Ferrero and Angel, 2018). Such investigations target primary melt inclusions that can display different degrees of crystallization from glassy to nanogranitoids, i.e., fully crystallized cryptocrystalline aggregates with a granitoid composition (Cesare et al., 2015). These inclusions can be defined as former droplets of melt because of their mineral assemblage and the presence of glass, trapped in the garnet while it was growing (Ferrero et al., 2012). So far, the genesis of these melt inclusions has been ascribed to partial melting of migmatites/granulites. The rock is melting and producing at the same time melt and peritectic phases (Cesare et al., 2015).

In the last few years, the melt inclusions investigation has been expanded to mafic and ultramafic rocks (Borghini et al., 2018; Ferrero et al., 2018a; Naemura et al., 2018). The new findings of Borghini et al. (2018, submitted; Chapter 3-4 of this thesis) show that primary melt inclusions in garnet may preserve deep melts infiltrating the host rock rather than melt internally produced via partial melting of the rock in which they occur. Such a discovery paves the way for a new approach to the investigation of metasomatic processes based on the characterization of melt inclusions in metamorphic rocks.

1.4 RESEARCH QUESTIONS

This thesis focusses on unravelling the melt-related processes in silica-poor rocks enclosed in a crustal sequence involved in subduction and continent-continent collision. In particular, the main goal is to determine the genetic processes involved in the formation of pyroxenite and eclogite using a novel approach: the direct investigation of the melt preserved as primary melt inclusions (Cesare et al., 2015) in both rock types. The investigation has been performed on the pyroxenites of the Granulitgebirge and the UHP eclogite of Saidenbach Reservoir, Erzgebirge, both located in Saxony, Germany.

The main research questions are the following:

1) **Are the targeted inclusions real former droplets of deep melt? What information we can obtain from them?** (Chapter 2)

2) **Which is the composition of the melt in the pyroxenite of the Granulitgebirge? How does the melt relate to the host rock?** (Chapter 3)

3) **Which are the possible genetic processes responsible for the formation of the melt-bearing pyroxenites of the Granulitgebirge? Are there similar rocks or melt signature elsewhere in the Bohemian Massif?** (Chapter 4)

4) **Which is the composition of the melt in the UHP eclogite of the Erzgebirge? Which is its possible source, and which possible genetic processes are responsible for the presence of such melt?** (Chapter 5)

5) **Are the two investigated melts in the pyroxenite and the eclogite genetically related? How can their presence be explained in the framework of the geodynamic evolution of the Bohemian Massif?** (Chapter 6)

1.5 THESIS STRUCTURE

This thesis is a cumulative work that contains two published peer-reviewed manuscripts - a book chapter (Chapter 2) and a paper (Chapter 3) -, one manuscript under review (Chapter 4), an additional manuscript to be submitted for publication to an internationally renowned, peer-reviewed scientific journal (Chapter 5) and a final discussion chapter (Chapter 6). Chapters from 2 to 5 answer to the research questions listed above (see 1.3) and Chapter 6 discusses the results and conclusions of the previous chapters. Below, I will illustrate the different chapters highlighting in which part of the thesis each research question has been addressed.

Chapter 2 comprises the book chapter "*A treasure chest full of nanogranitoids: an archive to investigate crustal melting in the Bohemian Massif*" (published in *Metamorphic Geology: Microscale to Mountain Belts,* 2018, Special Publication 478, eds Ferrero S., Lanari P., Goncalves P. & Grosch E.G., *Gological Society of London*) and addresses the research question 1. This manuscript reports a compilation of all the localities in the Bohemian Massif that contain nanogranitoids identified to the present date. It provides guidelines for the recognition of the nanogranitoids and an overview of the qualitative and quantitative constrains that they provide on melting processes, the nature of the melt and the fluid involved in these processes. Moreover, it

discusses the melt signature derived by the study of the trace elements and on the P-T constrains on mutual stability of melt and host provided by the re-homogenization experiments.

Chapter 3 comprises the paper *"Granitoids melt inclusions in orogenic peridotite and origin of garnet clinopyroxenite"* (published in *Geology*, 2018, v. 46, pp. 1007-1010, DOI: 10.1130/G45316.1) that addresses the second research question. This paper reports the first finding of primary granitic melt inclusions, both polycrystalline and glassy, in rocks of mantle affinity such as garnet clinopyroxenite enclosed in the orogenic garnet peridotite of the Granulitgebirge (Bohemian Massif). The results here presented show that the melt was involved in the formation of the garnet clinopyroxenites. Two possible genetic processes, partial melting and metasomatism, have been proposed and discussed in the paper, using geochemical and microstructural data collected up to early 2018.

Chapter 4 comprises the paper *"Cryptic metasomatic agent measured in situ in Variscan mantle rocks: melt inclusions in garnet of eclogite/pyroxenites, Granulitgebirge, Germany"* (submitted to *Journal of Metamorphic Geology*). This manuscript, which addresses the third research questions, integrates geochemical data from the melt and mineral phases and bulk rock on the pyroxenites. In the paper it is proposed that the garnet clinopyroxenites formed as result of metasomatism, and thus the trapped melt most likely represent the preserved metasomatic agent responsible for the formation of the whole rock. This paper also addresses the mutual relationship between the investigated rocks and the other pyroxenites reported in the Bohemian Massif, extensively studied in the past decades by several authors. Moreover, the possibility is also discussed here that a melt with similar geochemical signature is involved in the metasomatism of another peridotite body in the Bohemian Massif and in the genesis of unusual ultrapotassic magmatic rocks, i.e. durbachite.

Chapter 5 comprises the manuscript *"Melt inclusions in UHP eclogite of the Saidenbach reservoir: the first preserved melt found in ultrahigh pressure rocks"* (it will be submitted in a peer-reviewed journal). This paper addresses the fourth research questions and focus on the nature of the melt inclusions in the Saidenbach eclogite. The geochemical relationships between melt, mineral phases and bulk rock is discussed in detail and compared with the rare similar case studies already reported in literature.

Chapter 6 combines the principal results of the individual studies and discusses the relationship between the pyroxenite and the eclogite in terms of melt composition and geodynamic evolution of the Bohemian Massif during the Variscan orogeny. This chapter addresses the last

research question and highlights the possible future directions of the investigation of nanogranitoids in mafic rock.

1.6 PUBLICATIONS AND AUTHOR CONTRIBUTIONS

Most of the work described in this thesis has been carried out by the author. Chapters 2 is a chapter in the book “Metamorphic Geology: Microscale to Mountain Belts”, edited by the Geological Society of London, whereas chapter 3 is published in an international peer-reviewed journals and Chapter 4 has been submitted and is currently under review.

Chapter 2 Ferrero, S., O’Brien, P.J., **Borghini, A.,** Wunder, B., Wälle, M., Günter, C., and Ziemann, M.A., 2018. A treasure chest full of nanogranitoids: an archive to investigate crustal melting in the Bohemian Massif. In: Ferrero, S., Lanari, P., Goncalves, P. & Grosch, E.G., (Eds): Metamorphic Geology: Microscale to Mountain Belts. *Geological society, London, Special Publication*, 478.

Silvio Ferrero designed and wrote the paper. Alessia Borghini participated to sample collection along with Patrick O’Brien. Silvio Ferrero performed re-homogenization experiments with Bernd Wunder, the laser ablation analyses with Marcus Wälle, EMPA analyses on mineral phases and glassy inclusions with Christina Günter. Alessia Borghini collected part of the MicroRaman spectroscopy data on polycrystalline and glassy inclusions from several of the case studies reported in the manuscript, with the technical support of Martin A. Ziemann. All the authors contributed to interpretation and discussion of the results.

Chapter 3 **Borghini, A.,** Ferrero, S., Wunder, B., Laurent, O., O’Brien, P.J., and Ziemann, M.A., 2018. Granitoids melt inclusions in orogenic peridotite and origin of garnet clinopyroxenite. *Geology*, 46 (11), 1007-1010.

Alessia Borghini conducted field work, designed the manuscript and the artwork, after discussion and in collaboration with Silvio Ferrero and Patrick O’Brien. Alessia Borghini performed: the samples investigated via Raman spectroscopy with the technical support of Martin A. Ziemann, the re-homogenization experiments with Bernd Wunder and the laser ablation analyses on the melt inclusions with Oscar Laurent. Silvio Ferrero, Patrick O’Brien and Oscar Laurent contribute to the data processing and discussion on data interpretations.

Chapter 4 **Borghini, A.,** Ferrero, S., O'Brien, P.J., Laurent, O., Günter, C., and Ziemann, M.A., submitted. Cryptic metasomatic agent measured in situ in Variscan mantle rocks: melt inclusions in garnet of eclogite/pyroxenite, Granulitgebirge, Germany.

Alessia Borghini conducted field work, designed the manuscript and the artwork. Alessia Borghini performed: the laser ablation analyses on melt inclusions and mineral phases with Oscar Laurent, the sample investigation using the Raman with the technical support of Martin A. Ziemann and EMPA with the support of Christina Günter. Alessia Borghini, Silvio Ferrero and Patrick O'Brien extensively discussed about the petrological and geochemical aspects and the possible implications for the geodynamic evolution of the orogeny.

2 A TREASURE CHEST FULL OF NANOGRANITOIDS: AN ARCHIVE TO INVESTIGATE CRUSTAL MELTING IN THE BOHEMIAN MASSIF

SILVIO FERRERO[1,2], PATRICK J. O'BRIEN[1], ALESSIA BORGHINI[1], BERND WUNDER[3], MARKUS WÄLLE[4], CHRISTINA GÜNTER[1] AND MARTIN A. ZIEMANN[1]

[1]Institute für Geowissenschaften, Universität Potsdam, [2]Musem für Naturkunde (MfN), Berlin, [3]Helmholtz-Zentrum, GFZ, Potsdam, [4]Memorial Univeristy, Canada.

Geological Society (2018), London, Special Publication, 478, doi: 10.1144/SP478.19.]

ABSTRACT

The central European Bohemian Massif has undergone over two centuries of scientific investigation which has made it a pivotal area for the development and testing of modern geological theories. The discovery of melt inclusions in high-grade rocks, either crystallized as *nanogranitoids* or glassy, prompted the re-evaluation of the area with an "inclusionist" eye. Melt inclusions have been identified in a wide range of rocks, including felsic/perpotassic granulites, migmatites, eclogites and garnet clinopyroxenites, all the result of melting events albeit over a wide range of pressure/temperature conditions (800°C–1000°C / 0.5–5 GPa). This contribution provides an overview of such inclusions and discusses the qualitative and quantitative constraints they provide for melting processes, and to the nature of melts and fluids involved in these processes. In particular, data on trace element signatures of melt inclusions trapped at mantle depths are presented and discussed. Moreover, experimental re-homogenization of nanogranitoids provided microstructural criteria allowing assessment of the conditions at which melt and host are mutually stable during melting. Overall this work aims to provide guidelines and suggestions for petrologists wishing to explore the fascinating field of melt inclusions in metamorphic terranes worldwide, based on the newest discoveries from the still enigmatic Bohemian Massif.

2.1 INTRODUCTION

Partial melting plays a pivotal role for the human race as it is the main agent responsible for the geochemical differentiation of the continental crust, a process responsible for re-mobilization of metals and other elements of strategic importance and their emplacement into "harvestable" ore deposits close to the surface (Lundstrom and Glazner, 2016). High grade, high pressure (HP) and ultrahigh pressure (UHP) terranes of crustal affinity are the only archive that grants us direct access to the deep rocks where partial melting took place, thus allowing us to directly investigate its mechanisms. An excellent example of how influential crustal melting processes are for human history is represented by the long standing interest in the geology of the Bohemian Massif. The most extensive manifestation of the Variscan orogeny in Europe, it has held a prominent role in the economic and scientific development of Europe across the centuries. This area was a major source of metallic ores since pre-historic times (Taylor, 1983; Bouzek et al., 1989), and in the last three centuries has played a major role in the industrialization of Central and Eastern Europe, with key areas even deriving their geographic name directly from the abundance of ore deposits, e.g. the German Erzgebirge or Czech Krušné hory: both meaning "Ore mountains" in English. The large economic interests involved in the exploitation of the mineral resources of the Bohemian Massif prompted since the early days of geological studies a vast scientific effort aimed at understanding its evolution. Agricola's 1556 publication "*De re metallica*" initiated the scientific study of ore minerals and the founding (in 1765) of the Mining Academy in Freiberg (Erzgebirge) resulted in a more systematic development of theories to understand the crust and its development. Most notable from the Freiberg school was Abraham Gottlob Werner's "Neptunist" view of rock formation, involving sedimentation in the early oceans even of basalt, countering a "Plutonist" standpoint championed by e.g. James Hutton which had recognized the importance of magmas in the evolution of rocks such as granite and basalt.

The type locality of granulite, i.e. a high grade anhydrous metamorphic rock, is in the northern part of the Bohemian Massif (Weiss, 1803), whereas in the same area the first diamond ever reported in Europe was discovered in 1870 (see e.g. Kotková et al., 2011). Despite two centuries of scientific investigation of the Bohemian Massif research is still thriving to the present day. As analytical techniques improve in spatial resolution and sensitivity, old studies are improved and reevaluated and new discoveries are being made continuously (see e.g. the modern diamonds identified by Nasdala and Massonne, 2000, or preserved coesite, Massonne, 2001). As new models and theories are created, they find direct application and a suitable testing ground for their refinement in the rocks of the Bohemian Massif.

One of the most direct examples of how new approaches to the investigation of natural processes found a perfect application in the Bohemian Massif is the investigation of anatectic melt inclusions (MI) in metamorphic rocks, i.e. *nanogranitoids* (Cesare et al., 2015). These unadulterated droplets of melt, between 5 and 50 μm in size, are a rather recent discovery in regionally metamorphosed migmatites, first reported by Cesare et al. (2009). Previously MI of anatectic origin were reported only in a rather unique case study, that of granulitic enclaves of the Neogene Volcanic Province (NVP) in Southern Spain (Cesare et al., 1997; Cesare and Gomez-Pugnaire, 2001; Acosta-Vigil et al., 2007, 2010, 2012; Ferrero et al., 2011). Important crustal rocks involved in continent-continent collision are silica- and alumina-rich metasediments with significant amounts of iron and magnesium. When the continental crust undergoes anatexis, the resultant melt can only accommodate a limited amount of alumina, iron and magnesium, with the last two elements slightly increasing at T>900°C (Johannes and Holtz, 1996). The excess Al, Fe and Mg not required in the melt itself then combine to form aluminous peritectic minerals, such as garnet at mid-to-lower crustal conditions, which grows synchronously with melt production (Sawyer et al., 2011). Importantly, both melt and garnet are in equilibrium during inclusion formation because they are simultaneously generated from the same, incongruous, melting reaction (Cesare et al. 2015). This is fundamentally different from magmatic MI, where the minerals host instead an already modified – fractionated – melt (Audetát and Lowenstern, 2014). Such granitoid “embryos” (Bartoli et al., 2014) in peritectic phases thus preserve a snapshot of the most pristine stage of the melt evolution: this is the closest point we can get to the moment in which the crust started to melt.

The characterization of these inclusions rapidly became a new powerful tool enabling metamorphic petrologists to understand, and for the first time quantify, partial melts directly in natural rocks (Bartoli et al., 2016a; Acosta-Vigil et al., 2017a). In the present contribution we discuss the importance of this novel finding for the already extensively investigated Bohemian Massif and the novel information about partial melting in collisional settings they provide. In the first part we will present the characteristic features of anatectic MI and of their host rocks, providing the most comprehensive and up-to-date overview of MI discoveries in the Bohemian Massif. The qualitative constraints which can be derived for the PT conditions of equilibration of the host rock via MI investigation will be then discussed. In the second part we will illustrate the kinds of novel quantitative information on deep melts generated by nanogranitoid investigation using, as an example, the first and most investigated case study of nanogranitoids in the Bohemian Massif, the preserved near UHP MI of the Orlica-Śnieżnik dome (OSD) in the Polish Sudetes (Ferrero et al., 2015, 2016b). Novel data on the trace element signature of this deep melt

are presented and discussed in the light of the existent knowledge on melting processes during crustal subduction. Finally, we will show how novel constraints on the mutual stability of melt and host garnet are generated as an intriguing by-product of the re-homogenization experiments we have performed: an integral part of nanogranitoid investigation. Our final aim is to provide microstructural guidelines and methodological suggestions for natural scientists who wish to delve into the fascinating field of investigation of MI in metamorphic rocks from other metamorphic terranes worldwide, using the knowledge gained by our study of the wide and varied range of Bohemian Massif rocks which are still capable of springing surprises.

2.2 IDENTIFICATION OF NANOGRANITOIDS IN THE BOHEMIAN MASSIF

The Bohemian Massif consists of extensive bodies of magmatic and metamorphic rocks of mainly continental origin (Matte et al., 1990; Franke, 2000) with a complex evolution, in most cases involving a high temperature history, albeit at a range of pressures, in some cases reaching the stability field of coesite and diamond (Nasdala and Massonne, 2000; Massonne, 2001; Kotková et al., 2011; Perraki and Faryad, 2014). Due to the low percentage of outcrops in the area, large scale correlation has always been difficult, so much so that still now, after centuries of study, the precise geodynamic processes which resulted in the formation of the Massif are still a topic of intense debate (e.g. Matte, 1998; O'Brien, 2000; Massonne and O'Brien, 2003; Schulmann et al., 2014). Unsurprisingly, a large part of the knowledge available on the Bohemian Massif derives from petrological studies at the microscale, where countless investigations have produced an extremely large body of data (e.g. Carswell and O'Brien, 1993; Massonne and O'Brien, 2003; Janoušek et al., 2004; Massonne, 2011 and references therein)**.** Despite their extensive investigation, the re-evaluation of high temperature rocks from this area with an "inclusionist" eye has shown that MI are rather common in the Bohemian Massif, and can be successfully investigated to provide novel information on partial melting in subduction-collision settings.

In general, melt droplets in regionally metamorphosed high grade rocks are mostly crystallized to aggregates of quartz + feldspar(s) + OH-bearing phase(s) as "nanogranitoids" (Cesare et al. 2015; see also Cesare et al. 2009; Ferrero et al. 2012; Bartoli et al. 2016a) which may also contain liquid H_2O in interstitial position as verifiable via Micro-Raman spectroscopy (Ferrero, unpublished data). Glass-bearing, partially crystallized inclusions (Ferrero et al. 2012, 2015) and, more rarely, monophase glass inclusions (Cesare et al. 2009) may occur in the same

cluster along with fully crystallized inclusions. The variable behavior of the different volumes of melt is most likely dependent on kinetic factors (Cesare et al. 2015; see also Ferrero and Angel 2018). The first tool one must employ to identify the occurrence of nanogranitoids in a rock is optical microscopy: their often isometric shape (Figs. 2.2c, g, n) and generally polycrystalline nature (Figs 2.2d, h, o) are for example prominent petrographic features (Cesare et al., 2015). Glassy inclusions appear isotropic under crossed polars, but further in situ analysis, e.g. via Raman spectroscopy (e.g. Cesare et al. 2009) is often required to confidently rule out whether they are just rounded crystals of quartz or plagioclase with very low interference colors. At present, primary glassy or crystallized MI in garnet have been identified in samples from thirteen localities of the Bohemian Massif as indicated in Fig. 2.1 and reported in Table 2.1. Whereas the former melt nature of glassy inclusions is self-evident, the polycrystalline inclusions identified in rocks of the Bohemian Massif must satisfy two criteria to be considered as former melt droplets, and thus included in table 2.1: 1) they must contain a phase assemblage consistent with the crystallization of a silicate melt, verified via EDS mapping, BSE imaging and/or Micro-Raman spectroscopy (Fig. 2.1), and 2) they must be demonstrably confined in the host mineral when observed in thin or doubly polished thick section. In some cases (Ferrero et al., 2015, 2016a) the reported nanogranitoids have already been experimentally re-homogenized via piston cylinder apparatus, thus confirming their former nature as trapped melts. Other works report polycrystalline inclusions whose phase assemblage is consistent with melt crystallization, and were therefore proposed by the authors to originally contain melt (Stöckhert et al., 2001, 2009; Faryad et al., 2013; Kotkova et al., 2014; Acosta-Vigil et al., 2017b).

Following the criteria reported above, former MI can be confidently identified in 16 localities spanning the whole massif - the pertinent references are reported in Table 2.1. So far nanogranitoids in the Bohemian Massif were recognized only in peritectic garnet, the host of most of the reported occurrences of nanogranitoids worldwide (Cesare et al. 2015). Most of the findings are from the Moldanubian zone with ten localities (Althütte, Stückstein, Winklarn quarry, Plešovice quarry, Ktiš, Kutná Hora Complex, Plaimberg, Steinaweg, Hartsteinwerk Loja quarry and one unnamed locality in the Bavarian Unit), the Granulitgebirge with three findings (Mohsdorf, Rubinberg/Klatschmühle and Waldheim), the Polish Sudetes with two occurrences (Stary Gierałtów and Zagórze Śląskie), one in the Erzgebirge area (Forchheim near the Saidenbach reservoir) and one from the T7 borehole south of the Erzgebirge area (Staré in the České Středohoří Mountains). The host rocks are extremely variable, encompassing felsic and/or perpotassic granulite, stromatic migmatite/paragneiss, eclogite and garnet clinopyroxenite. The conditions of melt entrapment, which corresponds to the garnet formation conditions, span the

whole field of high temperature metamorphism, from 750-800°C and 0.5 GPa in the metasediments of Althütte to >1000°C and 4-5 GPa in the Erzgebirge (Table 2.1).

Primary melt inclusions in garnet	Rock type	Composition of the coexistent fluid (when present)	References about MI±FI	Host mineral formation	Protolith	Related Reference	Peculiar features
West Sudetes							
(1) Stary Gierałtów (Orlica-Śnieżnik Dome)	HP Felsic granulites	-	Ferrero et al. (2015, 2016)	875°C, 2.7 Gpa	Granitoids	Ferrero et al. (2015)	Kumdykolite, Kokchetavite, Cristobalite, Glass
(2) Zagórze Śląskie (Góry Sowie Block)		-	Słupski et al. (2018)	?	Granitoids?	Kryza et al. (1996)	Kumdykolite, Kokchetavite, Cristobalite
Moldanubian zone							
(3) Althütte (Oberpfalz)	Stromatic Migmatites	CO_2+N_2 ±Siderite	Ferrero et al. (2016b)	825°C, 0.5-0.8 Gpa	Pelites with carbonatic lenses	Kalt et al. (1999)	Melt-melt-fluid immiscibility, carbonatititc melt, cristobalite
(4) Stückstein (Oberpfalz)	Stromatic Migmatites	CH_4+N_2±CO_2±Carbonate	Ferrero (this study); Wannhoff et al. (2018)	~800°C, 0.5-0.7 Gpa	Pelites	Kalt et al. (1999)	Melt-fluid immiscibility, Kumdykolite, Cristobalite
(5) Winklarn quarry		-	Ferrero (this study)	?	Pelites	?	MI only in low-Ca, external rim of garnet
(6) Plešovice quarry (Blanský les Massif)	Perpotassic Granulites	-	Ferrero (this study)	>950°C, 2.2-2.3 Gpa	Granitoids?	Vrána (1989),Janoušek et al. (2007), Vrána et al. (2013)	Widespread rutile exsolutions, large zircons
(7) Ktiš	HP Garnet-rich gneiss	CO_2+N_2 ±Carbonate	Ferrero (this study)	700-900°C, 1.5-2.3 Gpa	Pelites	Kobayashi et al. (2011)	Melt-fluid immiscibility
(8) Kutná Hora	HP Felsic granulites	-	-	700-750°C, 4.0 Gpa	?	Perraki & Faryad (2014)	Kumdykolite
(9) Steinaweg (Dunkelsteinerwald)	HP Felsic granulites	-	P. Schantl (Pers. Comm)	800-850°C, 1.2-2.5 Gpa	Granitoids	Schantl et al. (2018)	-
(10) Plaimberg (Dunkelsteinerwald)	UHP Cpx-rich Eclogites	-	Faryad et al. (2013)	1000-1200°C, 4-5 Gpa	?	Faryad et al., 2013	-
(11) Hartsteinwerk Loja quarry (Drosendord Unit)	LP, Grt-Kfs-Sil gneisses	-	D. Sorger (Pers. Comm)	750-800°C, 0.6-0.9 Gpa	Pelites	-	-
(12) Bavarian Unit	LP, Grt-Crd-Sil gneisses	-	D. Sorger (Pers. Comm)	830-910°C, 0.6 Gpa	Pelites	Sorger et al (2018)	-
Saxo-Thuringian Zone							
Granulitgebirge							
(13) Rubinberg, Klatschmühle, Waldheim	Garnet-clinopyroxenites	-	Borghini (submitted)	>1000°C, 1.5 - 2.0 Gpa	?	O'Brien & Rötzler (2003)	Kumdykolite, Kokchetavite, Osumilite, Glass
(14) Mohsdorf	HP felsic granulites	-	Ferrero (this study)	>1000°C, 1.6 Gpa	Granitoids	O'Brien & Rötzler (2003)	-
Erzgebirge							
(15) Saidenbach	Quartz-feldspathic rocks	-	Stöckhert et al. (2001, 2009); Acosta-Vigil et al. (2017b)	1000°C, 4-5 GPa	Pelites	Stöckhert et al. (2001, 2009)	Diamond, glass
(16) T7 borehole		-	Kotkova et al. (2014)	1000°C, 4-5 GPa	Pelites	Kotková et al. (2011)	Kumdykolite, Diamond

Table 2.1. Localities of the Bohemian Massif where primary melt inclusions in high-grade rocks were reported, their most peculiar features, protolith, likely P-T conditions of melting and pertinent reference (Vrána, 1989; Kryza et al., 1996; Kalt et al., 1999; Stöckhert et al., 2001, 2009; O'Brien and Rötzler, 2003; Janousek et al., 2007; Kobayashi et al., 2011; Kotková et al., 2011; Vrána et al., 2013; Faryad et al., 2013; Perraki and Faryad, 2014; Kotkova et al., 2014; Ferrero et al., 2015, 2016b; Acosta-Vigil et al., 2017b; Borghini et al., 2018; Schantl et al., 2018; Slupski et al., 2018; Sorger et al., 2018; Wannhoff et al., 2018).

A further intriguing aspect is the common presence of polymorphs of quartz and feldspars (cristobalite, kumdykolite or kokchetavite) in crystallized MI which can be swiftly identified using Raman spectroscopy (Ferrero et al., 2016b, 2018a; Ferrero and Angel, 2018). In the Bohemian Massif such phases were identified in six localities out of sixteen (column "peculiar features" in table 2.1). The nature and significance of the polymorphs are discussed in much greater detail elsewhere (Ferrero and Angel 2018) and for this reason they will not be mentioned any further in the present contribution.

2.3 QUALITATIVE CONSTRAINTS ON PARTIAL MELTING PROCESSES FROM NANOGRANITOID MICROSTRUCTURES

Nanogranitoids provide both qualitative and quantitative constraints for the high temperature history of partially melted rocks. As a qualitative constraint, primary MI constrains the presence of melt during growth of the inclusions' host, and this can be used as direct evidence that the host phase is a peritectic phase product of a partial melting reaction, a most useful feature especially when other typical evidence such as leucosomes are absent in the rocks under investigation. A good example is represented by the HP granulites visible at the quarry of Mohsdorf (Granulitgebirge, Fig. 2.2a-d), whose peak assemblage is characterized by garnet, kyanite and ternary feldspar (O´Brien and Rötzler, 2003). Here nanogranitoids occur in the inner part of garnets, while leucosome domains- direct indicators of melting- are indistinguishable from the quartzo-feldspatic matrix of the rock. The identification of melt in garnet thus suggests partial melting with garnet production at mantle depths, very close to or directly at the deepest conditions of re-equilibration of these HP felsic granulites, similarly to what was recently proposed for similar HP granulites of the Orlica-Śnieżnik Dome (Budzyń et al., 2015; Ferrero et al., 2015; Walczak et al., 2017). The link between the presence of MI in garnet and partial melting event is of course only valid if the garnet is exclusively of metamorphic origin, as magmatic garnet containing MI of parental magma could theoretically be already present in suitable protoliths before partial melting (e.g. Clarke et al., 2013; Xia and Zhou, 2017). Although such a possibility should always be taken into account for the correct identification of nanogranitoids sensu strictu (i.e. of anatectic origin), at present no magmatic MI (i.e., MI trapped during cooling) have ever been reported in garnet from migmatites.

Nanogranitoids may also occur exclusively in a particular zone of a compositionally-zoned host, as reported in garnets from Kali Gandaki (Himalaya) where the inclusions occur in an annulum in the inner part of the garnet (Carosi et al., 2015). In such a case only the inclusion-bearing portion of the mineral can be confidently associated with a partial melting event. Similarly in the Bohemian Massif, some coarse-grained garnet + biotite + sillimanite migmatites of the Winklarn quarry (Moldanubian Zone) contain nanogranitoids exclusively in the low-Ca rim overgrowth of the garnet (Fig. 2.2e-h), although the garnet core grew under higher pressure (kyanite field) conditions. Associated eclogitic (Scott et al., 2013) also underwent the same LP-HT stage.

Nanogranitoids in garnet allow furthermore the "bracketing" of the melting event into a precise point in time of the history of the host rock, as host age may be determined via in situ

analyses on garnet and/or of accessory minerals. For example, nanogranitoids have been recently identified in the renowned zircon-rich perpotassic granulites of the Plešovice quarry in the Blanský les Massif of the Bohemian Massif (see table 2.1. Fig 2.1, 2.2i-o). These rocks consist mainly of abundant garnet porphyroblasts partially overgrown by biotite, hosted in a feldspar-rich matrix with minor quartz. Such garnets contain a large amount of mineral inclusions, especially needles of apatite and rutile (Vrána, 1989), as well as unevenly distributed nanogranitoids, with more defined clusters located close to the rim – although no zonation in major or trace elements is visible in the host garnet. The most notable and apparent feature of these rocks is the presence of mm-sized euhedral zircons both as mineral inclusions in garnet and in the matrix. The zircons are used as reference material for geochronology and dated via different techniques at 337 Ma (Sláma et al., 2008), which many authors identify as the age of peak metamorphism and garnet production (Vrána 1989; Vrána et al. 2013). In this case, nanogranitoids directly testify to the presence of melt during garnet growth at 337 Ma, a scenario consistent with the interpretation of these rocks as the result of “non-congruent partial melting of crustal rocks and their crystallization under upper mantle conditions” proposed by Vrána (1989).

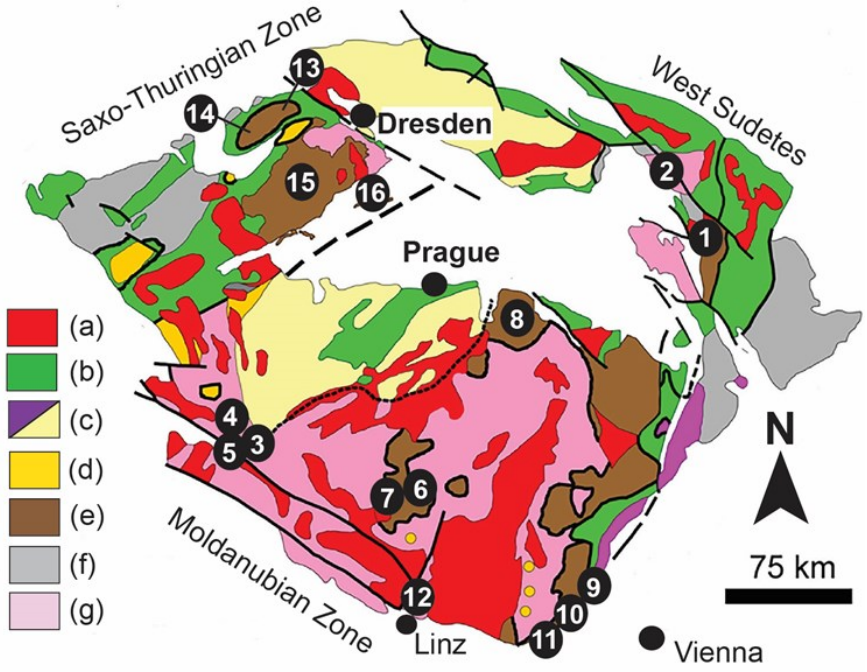

Figure 2.1. Map of the Bohemian Massif with localities of melt inclusions in metamorphic rocks. (**a**) Variscan granites; (**b**) Low T metamorphic rocks; (**c**) Pre-Variscan crystalline rocks; (**d**) Eclogites older than 370 Ma with associated spinel-peridotites; (**e**) Granulites, eclogites, garnet peridotites with age 340 Ma, in some cases containing diamond and/or coesite; (**f**) Carboniferous units; (**g**) Medium-to-high T metamorphism (highly simplified after Franke *et al.* 2000). The numbers refer to the localities reported in table 1 where nanogranitoids were identified.

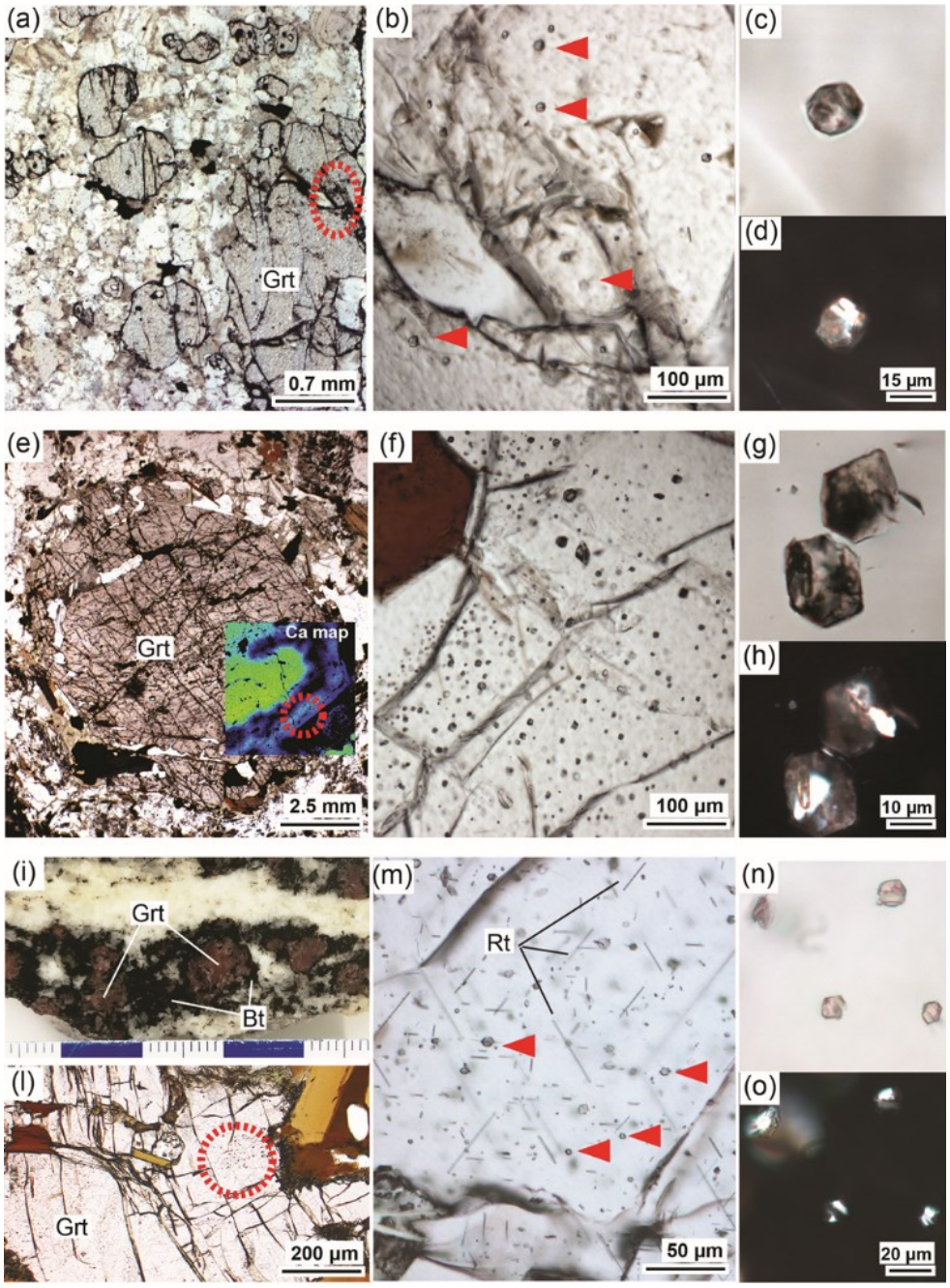

Figure 2.2. Optical features and microstructures of nanogranitoid-bearing rocks from the Bohemian Massif. (**a**) HP felsic granulites from Mohsdorf (SW portion of Granulitgebirge), where nanogranitoids are rare and scattered in HP garnets (**b**) and can be identified via optical microscopy in (**c** and **d**); (**e**) metapelites from Winklarn (close to the Czech/German border in the Moldanubian Zone), with clusters (**f**) of polycrystalline inclusions (**g,h**); (**i**) perpotassic granulites from Plešovice (Blanský les Massif, central Moldanubian Zone) with large garnets partially resorbed by biotite (**l**). Several rounded inclusions occur in clusters (**m**) along with rutile needles (possibly exsolutions) and show a clearly polycrystalline nature (**n** and **o**). (**d**), (**h**) and (**o**): transmitted light with crossed polars. Dashed red circles: location of the inclusions in the sample. Red arrows: nanogranitoids.

2.3.1 FLUIDS DURING ANATEXIS

Fluids are the main agents promoting metamorphic reaction, including partial melting, in rocks. The generation of melt starting from a subsolidus mineral assemblage requires indeed the presence of H_2O to stabilize silicate melts under an extensive range of physicochemical conditions, and only at temperatures far in excess of 1000°C – rarely reached in collisional settings – can melting take place under dry conditions (Johannes and Holtz, 1996). The necessary H_2O is either already in the system (or introduced into it, see Weinberg and Hasalová, 2015) or is it provided by the breakdown of OH-bearing phases during dehydration melting reactions (Le Breton and Thompson, 1988; Thompson, 1988; Vielzeuf and Montel, 1994; Sawyer et al., 2011). When the rocks involved in melting are metasediments, graphite is often present and constrains the composition of the fluid in the COH field, regardless of whether H_2O was externally derived (Cesare, 1995) or produced internally, i.e. as the result of mica breakdown (Cesare et al., 2005). Experimental work showed that under crustal conditions silicate melt produced in the presence of COH fluid may result in a condition of fluid-melt immiscibility, with coexistence of an H_2O -bearing melt and a CO_2-rich fluid (Holloway, 1976; Tamic et al., 2001). The microstructural expression of this phenomenon is coexisting primary melt and fluid inclusions belonging to the same cluster within peritectic phases: an occurrence reported so far in granulitic enclaves in dacitic lavas from southern Spain (Cesare et al., 2007; Ferrero et al., 2011) and garnet xenocrysts in granodioritic plutons from Tunisia (Ferrero et al., 2014), whose investigation largely confirmed previous experimental findings. Our work on inclusions of the Bohemian Massif has shown extensive evidence of immiscibility between a silicate melt and a COH(N) fluid in regionally metamorphosed migmatites of the Moldanubian Zone with sedimentary protolith (Figure 2.3). In the Bayerischer Wald (Fig. 2.1) samples from the adjacent (only 5 km apart) localities of Stückstein (Fig. 2.3a) and Althütte (Ferrero et al. 2016a) show extensive evidence of melting, i.e. exhibit abundant leucosome. Anatexis occurred in the sillimanite stability field, as testified by the abundance of this phase both as mineral inclusions in garnet and in the matrix where it defines the foliation along with biotite. Inclusion-bearing garnets are wrapped by the foliation and show partial resorption via coronitic reactions, with production of cordierite and/or plagioclase (Kalt et al. 1999). At Stückstein melt and fluid inclusions occur throughout the most resorbed garnets as clusters (Fig. 2.3b), and their respective nature of polycrystalline aggregates and fluids is easily verified via BSE imaging (Figs. 2.3c,d). Althütte samples, in contrast, show garnet containing primary inclusions of silicate melt, fluid and a Ca-rich carbonatitic melt, a so far unique finding which indicates triple immiscibility during crustal melting as well as carbonatite production under mid-to-shallow crustal conditions (Ferrero et al. 2016a). The garnet-rich gneisses of Ktiš in the Lhenice Shear Zone

show again evidence of melt-fluid immiscibility, based on the presence of primary nanogranitoids and fluid inclusions in the same cluster within garnet (Fig. 2.3e,f,g,h).

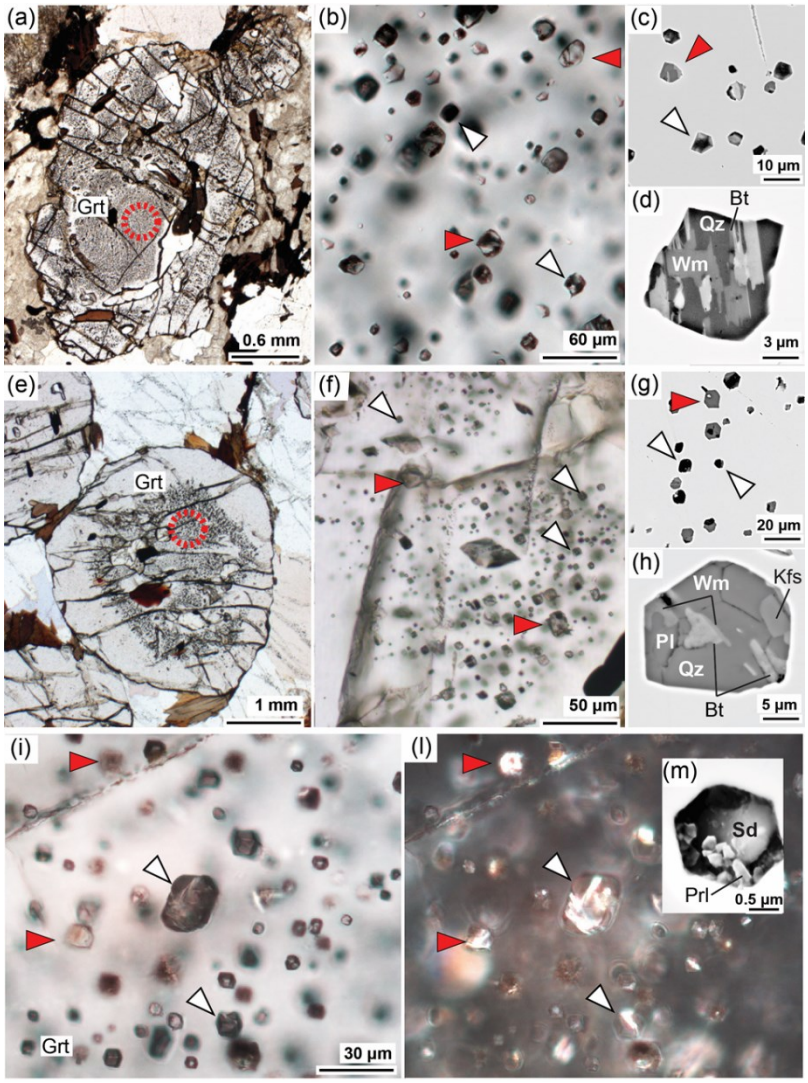

Figure 2.3. Microstructural evidence of fluid-melt immiscibility during anatexis. (**a**) low-to-medium pressure metasediments from Stückstein (close to the Czech/German border in the Moldanubian Zone) with extremely abundant fluid and (former) melt inclusions (**b**). BSE images (**c**) show the occurrence of polycrystalline inclusions, i.e. nanogranitoids (**d**), associated with holes formerly occupied by fluids; (**e**) HP metapelites from Ktiš (Lhenice Shear Zone, central Moldanubian Zone) with fluid and (former) melt inclusions (**f**), clearly visible in BSE images (**g** and **h**). (**i**) Fluid and melt inclusions in sillimanite-bearing metapelites from Althütte (close to the Czech/German border in the Moldanubian Zone, see Ferrero *et al.* 2016a for more details), where optical observation under crossed polars show how both inclusion types could show multiple birefringent phases, thus hampering the distinction between fluids and nanogranitoids by optical means only (**l**). (**m**) BSE image of open fluid inclusion where pyrophyllite and siderite can be recognized via EDS analyses. Dashed red circles and red arrows: see caption Fig. 2. White arrows: fluid inclusions.

Partial melting, however, took place under HP conditions, as indicated by kyanite present as mineral inclusions in garnet as reported by Kobayashi et al. (2011) who identified COHN fluid inclusions but no nanogranitoids. It is worth pointing out that nanogranitoids and fluid inclusions exhibit a similar appearance under the optical microscope, both being relatively dark due either to the abundance of tiny phases (nanogranitoids) or the rather common presence of CO_2 (Touret, 2001). In both cases the inclusions frequently contain multiple birefringent phases (Figs. 2.3i, l).

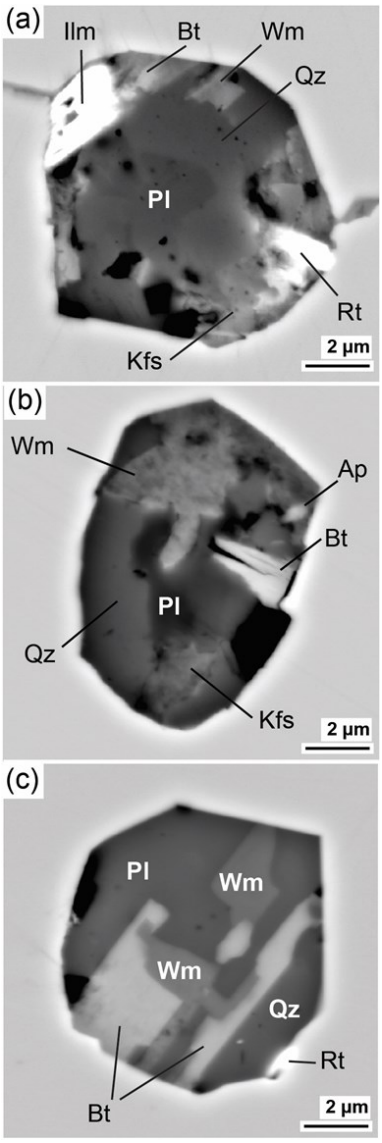

Figure 2.4. Back scattered electron (BSE) images of nanogranitoids from Mohsdorf (**a**), Winklarn (**b**) and Plešovice (**c**), for more details see caption Fig. 2. The inclusions generally show linear boundaries, occasionally defining a well-developed negative crystal shape mimicking the host garnet. Mineral abbreviations are from Whitney and Evans (2010).

In nanogranitoids these phases are mostly the products of melt crystallization (Fig. 2.4), whereas in fluid inclusions they may be (1) trapped phases (most commonly apatites, rutiles, zircons), daughter phases (e.g. calcite or magnesite, see e.g. Ferrero et al. 2018a) and/or step-daughter

phases (e.g. pyrophyllite, siderite, cristobalite) resulting from fluid-host interaction after entrapment (Ferrero et al. 2014, 2016a; see also Fig. 2.3m). If all these inclusions with multiple phases are at first identified as nanogranitoids, their abundance in the clusters may be largely overestimated and the presence of fluid erroneously considered negligible or, in the worst case, completely overlooked. Ultimately, the real nature of the inclusions can be ascertained only via Micro-Raman spectroscopy (Tsunogae et al., 2008; Lamadrid et al., 2014). In addition, microthermometric studies can be undertaken to observe possible phase transitions occurring in the inclusions (Andersen et al., 1990; Huizenga et al., 2014), thus confirming the presence of fluid – this may however be extremely difficult at times because of the combined effect of small size (especially in inclusions <5 μm) and dark color of the fluid inclusions.

2.4 QUANTITATIVE CONSTRAINTS ON MELTING PROCESSES

Melt inclusions provide quantitative information directly on the chemistry of the melt hosted in natural rocks. In situ analyses of major elements, trace elements and volatiles requires, however, that they are homogenous in composition, exposed on the surface of the sample, and of a size suitable for investigation via the analytical technique of choice. In the regionally metamorphosed rocks so far investigated preserved glass is rather rare whereas partially crystallized and fully crystallized inclusions are far more common (Ferrero et al. 2012, 2015b). Nanogranitoids need therefore to be re-homogenized experimentally via a piston cylinder apparatus at the pressure-temperature conditions of formation (Bartoli et al., 2013a, 2016a; Ferrero et al., 2015). After quenching to a homogeneous glass, major elements can be measured with a common electron microprobe (EMP). The smallest available diameter for the electron beam of the most commonly available EMP is ~1 μm, but in order to avoid the acquisition of signal from the surrounding host the smallest glass inclusion should be at least 4 μm across because of the effective volume of material excited by the electron beam (e.g. Ferrero et al. 2012). Such conditions are far from the optimal ones recommended to avoid alkali-loss during the analyses of alkali-rich glasses, i.e. a diameter of 20 μm (Morgan and London, 1996, 2005). The alkali-loss experienced by the glass during EMP analyses on anatectic MI is therefore estimated (and corrected) using secondary glass standards, following the procedure devised by Morgan & London (2005). More than a decade of anatectic MI investigation suggests that this approach is successful, despite some initial criticism (Clemens, 2009). The H_2O content of the melt has been

measured in situ within inclusions with size ≥5 μm via quantitative Raman spectroscopy (Bartoli et al. 2013, Ferrero et al. 2015) and via NanoSIMS (Bartoli et al., 2014; Acosta-Vigil et al., 2016).

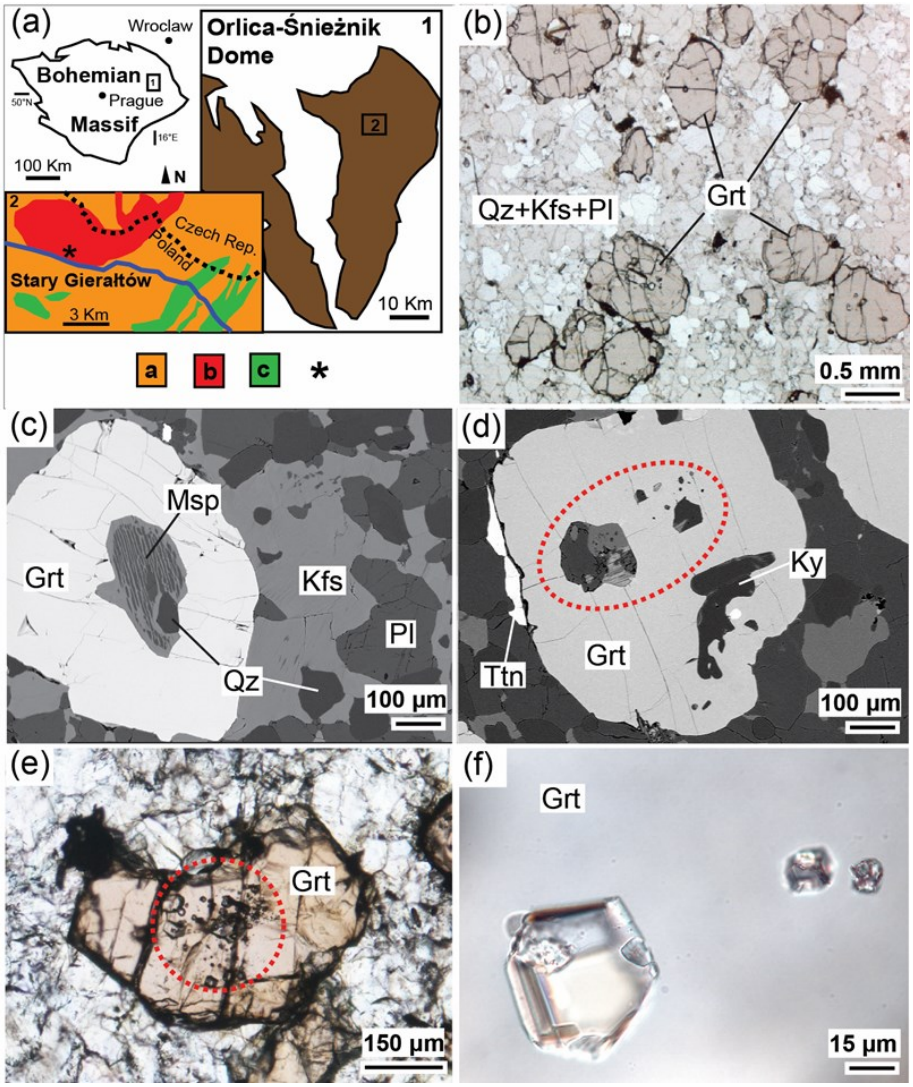

Figure 2.5. HP felsic granulites from Orlica-Śnieżnik, Polish Sudetes. (**a**) geological sketch of the Bohemian Massif (modified after Anczkiewicz *et al.* 2007) with the location of the Orlica-Śnieżnik (1) and the location of the granulite body (2) along the river at Stary Gierałtów. Star: sampling locality, a: Orlica-Śnieżnik gneisses, b: granulites, c: micaschists; (**b**) microstructural aspect of the investigated granulites, microphotograph in transmitted light; (**c**) mesoperthite in peak garnet, BSE image; (**d**) garnet containing crystallized melt inclusions and melt pockets (red dashed circle) and kyanite mineral inclusion, BSE image; (**e**) garnet with a cluster of small nanogranitoids (red dashed circle), microphotograph in transmitted light of a doubly-polished thick section; (**f**) close-up of the investigated inclusions in garnet, photomicrograph in transmitted light.

The trace element (TE) signature of the melt is one of the most fundamental pieces of information to understand chemical differentiation and can be investigated via laser ablation inductively coupled plasma mass spectrometry (LA-ICPMS). LA-ICPMS analyses can acquire a significant signal of the MI glass, without interference from the host, using a laser beam between 15 and 40 μm in diameter, thus limiting its applicability to relatively large inclusions, i.e. >>20 μm in diameter such as the ones in granulitic enclaves investigated by Acosta-Vigil et al. (2010). Most of the inclusions investigated so far in common regional high grade terranes are however between 5 and 25 microns across (Cesare et al. 2015). This limitation has been circumvented by ablating the whole inclusion and subtracting the host component (Halter et al., 2002; Stepanov et al., 2016; see also next paragraph). Such an approach allows quantitative geochemical information to be obtained on inclusions with a size of 10-20 μm. A precise knowledge of the major element contents of the glass, which can only be obtained via EMP, is nonetheless required to deconvolute the mixed inclusion + host signal. Previous studies (Acosta-Vigil et al. 2010, 2012; Bartoli et al. 2016a) have proven that major elements and incompatible trace elements (TE) of the MI are representative of the original melt composition, whereas TE compatible with the host mineral are generally affected by a boundary layer effect, commonly observed in magmatic MI (Baker, 2008). Investigation of partial melt TE provides fundamental insights on the behavior of accessory phases such as zircon, apatite and monazite, common repositories of most trace elements, during crustal subduction and anatexis (Yakymchuk, 2017). Furthermore the investigation of TE in the melt is a powerful tool to identify the mechanisms responsible for melt generation (i.e., equilibrium/disequilibrium melting, melting reactions; Acosta-Vigil et al. 2010; 2012; 2017a, Ferrero et al. 2016a). In high grade, partially melted rocks this task is often impossible by petrological investigation of the host rock alone. Mineralogical evidence, e.g. “relicts” of the minerals involved in the partial melting reaction, are often absent because they are either completely consumed or extensively re-equilibrated during the post-peak metamorphic history (Acosta-Vigil et al. 2010, 2016, 2017a). This aspect will be illustrated in the next section presenting the novel data on TE of near UHP melt enclosed in the Orlica-Śnieżnik Dome felsic granulites of the Polish Sudetes.

2.4.1 PRESERVED MELT OF THE NEAR-UHP MELT INCLUSIONS OF THE OSD FELSIC GRANULITES, BOHEMIAN MASSIF

The Orlica-Śnieżnik Dome (OSD) is located at the NE of the Bohemian Massif (Fig. 2.5a). It consists of amphibolite facies orthogneisses with HP/UHP rock inliers and subordinate staurolite-grade metasediments (Don et al., 1990). Intrusion of the granitoid protolith of the Orlica-

Śnieżnik granulites occurred at c. 520 – 490 Ma, (Oliver et al., 1993; Kröner et al., 2001; Štípská et al., 2004). The whole complex then underwent high grade metamorphism during the Variscan orogeny (c. 350 – 330 Ma, see e.g. (Turniak et al., 2000; Gordon et al., 2005; Lange et al., 2005; Bröcker et al., 2009). Several HP/UHP eclogite bodies and one large body of felsic granulite with mafic granulite lenses also occur. All the granulite samples from this area come from the most well-known and best-preserved in situ outcrop at Stary Gierałtów (Fig. 2.5a) on the Biała Lądecka River bank (50º18,509`, E 016º56,032`). Garnet (<2mm in size) forms modally 30-40% of the rock, and is scattered in a leucocratic matrix of quartz, plagioclase and perthitic feldspar (Fig. 2.5b). Garnet contains mesoperthite (Fig. 2.5c), kyanite (Fig. 2.5d), quartz and rare clinopyroxene as mineral inclusions alongside the nanogranitoids. Only one generation of garnet has been identified in these rocks, and it is rich in almandine and grossular component (Table 2.2), with a very weak zoning characterized by a slight decrease in almandine and grossular toward the rim balanced by pyrope increase (Walczak et al. 2017). Nanogranitoids in these rocks always occur in the garnet core. Generally partial melting is expected to have produced a limited amount of melt in the felsic granulites of the Bohemian Massif (Janoušek et al. 2004), and no clear evidence of melting, e.g. leucosome layers, can be identified easily at the outcrop scale due to the felsic nature of the rocks - layers of both crystallized melt and the recrystallized matrix would indeed appear leucocratic. At the microscale, however, several cuspate lobate microstructures can be identified under high magnification both in electron (Fig. 2.6a) and optical microscope (Fig. 2.6b). Such features are more commonly observed in rocks melted at lower P and are commonly interpreted as pseudomorphs after melt-filled pores (Holness and Sawyer, 2008; Holness et al., 2011; Vernon, 2011; Ferrero et al., 2012), thus further supporting the presence of melt during the metamorphic history of the rock. Whereas no UHP phase, i.e. coesite and/or diamond, was ever identified in the area, some authors reported aggregates of polycrystalline quartz which they interpreted as indicative of the former presence of coesite (e.g. Bakun-Czubarow, 1991; Bröcker and Klemd, 1996). Microstructures with similar appearance were identified during the investigation of the nanogranitoids, but Raman investigation revealed the presence of plagioclase, undetectable by optical means only because of its small size, along with quartz in these polycrystalline aggregates (Fig. 2.6c). Thus our interpretation is that this Qz + Pl aggregate is a part of nanogranitoid with size much larger than the thickness of the thin section under investigation (compare with Fig. 2.2b in Ferrero et al. 2015) or even a melt-bearing pocket possibly connected with the matrix, both because of its polyphasic nature and the presence of pseudomorphs after melt within the polycrystalline aggregate (gray arrow in Fig. 2.6c). This represents therefore a major caveat: the former presence of coesite can be erroneously inferred

if the presence of crystallized MI is not recognized, thus leading to significant overestimates of the equilibration pressure of the host rocks.

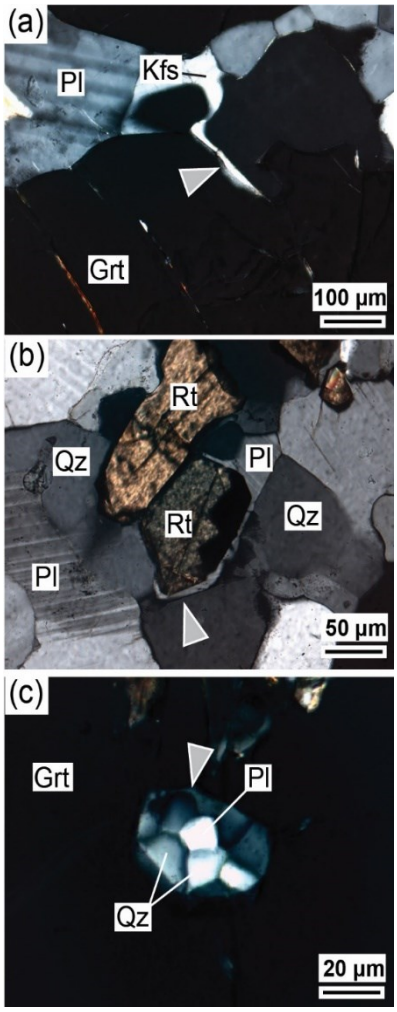

Figure 2.6. Microstructural evidence for presence of melt. Gray arrow: melt pseudomorphs. (**a**) K-feldspar forming a melt pseudomorph at the contact between matrix and garnet, photomicrographs in crossed polars. (**b**) Melt pseudomorph of plagioclase around rutile, microphotograph in transmitted light; (**c**) "pseudo" quartz pseudomorph after coesite, photomicrographs in crossed polars. The phases within the inclusion were checked via Raman spectroscopy.

	Grt	Exp. Grt	Msp in	Ep
Name (wt%)	312 (core)	exp.2	av2	254
Na_2O	0.04	0.13	4.48	0.01
MgO	2.67	6.32	0.00	0.01
Al_2O_3	21.47	21.14	19.94	23.86
SiO_2	38.11	37.92	65.18	37.58
K_2O	0.00	0.03	9.27	0.00
CaO	10.80	5.09	0.67	22.73
TiO_2	0.16	1.00	0.01	0.21
Cr_2O_3	0.00	0.01	n.a.	n.a.
MnO	0.48	0.08	0.01	0.10
FeO	26.22	26.96	0.25	13.87
Total	99.95	98.66	99.81	98.37
	12 (O)	12 (O)	8 (O)	12.5 (O)
Si	3.002	2.99	2.943	3.056
Ti	0.010	0.06	0.000	0.013
Al	1.993	1.97	1.061	2.287
Cr	0.000	0.00	0.000	0.000
Fe^{3+}	0.000	0.00	0.000	0.000
Fe^{2+}	1.727	1.78	0.010	0.943
Mn	0.032	0.01	0.000	0.007
Mg	0.314	0.74	0.000	0.001
Ca	0.911	**0.43**	0.032	1.980
Na	0.005	0.02	0.392	0.001
K	0.000	0.00	0.562	0.000
Alm	58	60	-	-
Pyp	11	25	-	-
Sps	1	0	-	-
Grs	31	15	-	-
Ab %	-	-	41	-
An %	-	-	4	-
Or %	-	-	55	-
Mg# / Ps	0.15	0.29	-	0.29

*Garnet analysis is the representative of the composition of the garnet near the nanogranitoids.

Table 2.2. Representative EMP analyses on mineral phases in Orlica-Śnieżnik Dome granulites and experimental garnet from experiment 2 (see Table 5). The garnet analyses 312 is the representative of the composition of the garnet near the nanogranitoids

Decompressional melting is by far the most commonly proposed mechanism to explain the presence of partial melts in deeply subducted HP/UHP metamorphic terranes of crustal affinity, see e.g. the Dabie-Sulu orogen (Liu et al., 2013; Gao et al., 2017 and references therein).

The discovery of nanogranitoids in peak garnet of the OSD granulites instead directly supports the interpretation that melting occurred at the HP metamorphic peak, thus still on the prograde path, as already proposed for other HP felsic granulites of the Bohemian Massif (O'Brien and Rötzler 2003). Partial melting of crustal rocks at mantle depth, e.g. in the case OSD granulites almost 90 km (corresponding to the metamorphic peak pressure of 2.7 GPa) and 900°C (Ferrero et al. 2015b) appears difficult to achieve because crustal material is likely to melt much earlier during subduction, i.e. at lower temperatures (700-800°C) and pressures still in the sillimanite stability field (e.g. Vielzeuf and Montel, 1994; Montel and Vielzeuf, 1997). An influential factor in our case is the extremely dry character of the protolith (0.44 wt% on LOI, see data repository in Ferrero et al. 2015) that most likely delayed the onset of melting, also helped by the very high *dP/dT* gradient (Ferrero et al. 2015).

	Re-homogenized nanogranitoids												OSD	GAL
Name (Wt%)	*31*	*41*	*42*	*5*	*MIe8**	*27*	*80**	*81**	*6**	*2*	***av.***	*std. dev*	*Bulk*	*av. MI (n=24)*
SiO_2	68.85	69.58	70.36	68.02	67.79	67.20	67.59	67.92	68.34	68.87	**68.45**	0.97	65.67	73.90
TiO_2	0.12	0.25	0.16	0.00	0.09	0.06	0.18	0.09	0.03	0.00	**0.10**	0.08	0.68	0.04
Al_2O_3	13.64	12.91	12.73	14.20	13.98	13.26	14.07	14.01	14.64	13.17	**13.66**	0.62	14.56	12.05
FeO	2.01	2.40	2.34	1.39	1.32	2.60	1.25	1.16	1.20	1.94	**1.76**	0.56	6.80	1.30
MnO	0.00	0.00	0.00	0.00	0.00	0.00	0.00	0.00	0.00	0.00	**0.00**	0.00	0.11	0.08
MgO	0.12	0.08	0.06	0.07	0.09	0.02	0.04	0.05	0.11	0.00	**0.06**	0.04	0.79	0.12
CaO	0.79	0.48	0.44	0.67	0.71	0.52	0.52	0.55	0.97	0.87	**0.65**	0.18	3.55	0.26
Na_2O	3.76	4.24	3.77	4.26	5.21	5.19	4.50	4.15	4.69	3.49	**4.32**	0.58	3.43	3.43
K_2O	4.15	4.23	4.28	4.37	4.74	4.79	4.94	4.93	3.56	4.16	**4.41**	0.43	2.53	5.90
P_2O_5	0.05	0.00	0.03	0.00	0.00	0.00	0.00	0.10	0.03	0.00	**0.02**	0.03	0.24	0.07
TOTAL	93.48	94.16	94.16	92.98	93.92	93.63	93.08	92.94	93.57	92.49	**93.44**	0.56	98.36	95.50
Q	28	26	29	24	17	17	20	23	24	29	**24**	4	23	31
C	2	0	1	1	0	0	0	1	1	1	**0**	1	0	0
Or	25	25	25	26	28	28	29	29	21	25	**27**	3	15	35
Ab	32	36	32	36	44	42	38	35	40	29	**36**	5	29	28
An	4	2	2	3	1	0	3	2	5	4	**4**	1	16	0
Hy	4	4	4	3	1	4	2	2	2	4	**4**	1	14	2
ASI	1.13	1.04	1.09	1.10	0.93	0.90	1.03	1.06	1.10	1.11	**1.03**	0.08	0.98	0.98
H_2O by diff	6.52	5.84	5.84	7.02	6.08	6.37	6.92	7.06	6.43	7.51	**5.97**	0.56	0,44**	4.50
Mg#	0.10	0.06	0.04	0.08	0.11	0.01	0.05	0.07	0.14	0.00	**0.06**	0.04	0.17	0.12
K_2O/Na_2O	1.10	1.00	1.13	1.03	0.91	0.92	1.10	1.19	0.76	1.19	**1.06**	0.14	0.74	1.92
K_2O/H_2O	0.64	0.72	0.73	0.62	0.78	0.75	0.71	0.70	0.55	0.55	**0.75**	0.08	1.54	1.31

Table 2.3. Representative EMP analyses of re-homogenized nanogranitoids from Orlica-Śnieżnik felsic granulites. Analyses marked with * are re-homogenized inclusions containing trapped quartz. OSD: Orlica-Śnieżnik leucogranulites bulk chemistry from Walczak (2011). GAL: average composition of 24 preserved glassy inclusions from garnet xenocrysts of peritectic origin in the plutons of La Galite Archipelago, Tunisia (data from Ferrero et al. 2014). **=LOI. ASI: Alumina Saturation Index (molar $Al_2O_3/CaO+Na_2O+K_2O$). Mg#= molar MgO/(MgO+FeO)

2.4.2 NANOGRANITOID-BASED CONSTRAINTS ON MELTING REACTIONS AND GEODYNAMIC HISTORY OF HOST ROCKS

The melt in the OSD granulites is H_2O-bearing, granitic in composition and metaluminous to slightly peraluminous (Table 2.3; Ferrero et al. 2015). The latter feature was already observed in the inclusions of La Galite Archipelago, Tunisia (Ferrero et al. 2014) and interpreted as the result of the melting of a magmatic protolith (a feature in common with the OSD granulites, see previous paragraph) rather than a metasedimentary protolith, which would have instead resulted in a more peraluminous melt (Bartoli et al. 2016a). The event recorded by the investigated nanogranitoids represents the first melt-producing event in the OSD granulites during Variscan orogeny. At the onset of melting the melt composition is influenced chiefly by the nature of the melting reaction (e.g. fluid-present vs fluid absent, e.g. Weinberg and Hasalova 2015) and of the crystalline phases consumed during melting (Acosta-Vigil et al. 2010), but also by more complex processes such as mineral –melt interface processes, element diffusion both in melt and minerals and mineral re-crystallization (Acosta-Vigil et al. 2017a), all processes operating concomitantly during melt production. Whereas kyanite and mesoperthite occur as mineral inclusions in the inclusion-bearing garnets, no relicts of the OH-bearing reactants involved in the melting reaction can be identified, thus hampering a more precise characterization of the melting process. For this reason TE in inclusions and garnet have been analyzed at the Department of Earth Sciences, ETH Zürich with LA-ICPMS. Nanogranitoids of workable size (generally >10 μm), located under the surface of the samples, were selected via optical microscopy in chips of doubly-polished garnets and their assemblage checked via Raman spectroscopy before LA-ICPMS analysis in order to avoid inclusions containing TE-rich trapped phases such as zircon, apatite or rutile, that are likely to provide TE contents unrepresentative of the original melt. The acquired signals were processed using the software SILLS (Guillong et al., 2008) subtracting the contribution of the host to the total signal (Halter et al. 2002). The concentrations determined by EMP of K_2O as inclusion-dominated and FeO as host-dominated tracers were used to deconvolute the signal. Using this approach, both major elements and TE which are strongly enriched in the host (e.g. Y and HREE in the case of garnet-hosted inclusions) are normally not quantifiable in the inclusions due to the dominating host signal. The average calculated concentrations of the detected elements are reported in Table 2.4, and the whole dataset acquired on these inclusions in the Supplementary material Table 2.S1. More details on the analytical procedure are available in Ferrero et al. (2016a).

Our geochemical data show a variability of at least one order of magnitude, very similar to those of the lower P Ojen migmatites (Southern Spain) analyzed with similar procedure by Bartoli et al. (2016a). Such variability may be the result of an incomplete subtraction of the host contribution to the signal, and/or the presence of very small TE-rich accessory phases trapped in

the inclusions and not detectable via optical or spectroscopical means (Stepanov et al. 2016). Despite this, after normalization the TE signature of the OSD inclusions visible in Fig. 2.7a provides novel geochemical constraints for deep melts. The envelope of the TE patterns of the nanogranitoids shows some significant differences with respect to the host rock. Cs, Rb and Li are much higher (up to one order of magnitude) than in the bulk rock, where Cs and Rb are below the detection limit and Li was not measured (Table 2.4).

	Nanogranitoids	HO50	HO33	OSD Garnet	
(ppm)	(n=27)	(n=18)	(n=5)	bulk	(n=5)
Li	105	114	276	-	5.0
B	-	185	449	-	3.5
P	352	1890	-	2500	96
Sc	22	2	-	21	73
Ti	671	541	576	6920	719
V	21	0.52	0.16	23	25
Co	12	-	-	5	28
Zn	455	60	53	80	379
Rb	507	211	237	56	0.4
Sr	39	165	112	119	0.1
Zr	125	32	28	308	30
Nb	0.9	12	16	10	0.03
Cs	6.7	31	31	< 0.1	0.04
Ba	770	308	235	1074	0.6
La	12.6	4.5	4.0	35.0	0.2
Ce	18.3	10.0	8.6	73.2	2.7
Pr	2.6	1.1	1.0	9.9	1.6
Nd	11.3	4.3	3.4	36.8	24.2
Sm	7.0	1.3	1.0	8.3	20.4
Eu	1.4	1.3	0.8	1.7	5.1
Gd	10.9	1.3	1.0	9.1	35.3
Hf	4.6	0.9	-	8.4	0.46
Ta	0.1	2.7	-	0.2	0.01
Pb	0.5	78	61	< 5	0.04
Th	0.2	1.3	1.1	0.4	0.01
U	0.6	4.5	4.2	0.4	0.02
Tb	-	0.21	-	1.46	3.6
Dy	-	1.00	0.72	8.80	27.5
Ho	-	0.16	-	1.87	6.0
Er	-	0.21	0.13	5.95	15.1
Tm	-	0.05	-	0.86	1.9
Yb	-	0.09	0.05	5.37	11.8
Lu	-	0.06	0.02	0.80	1.4

Table 2.4. LA-ICP-MS analyses on nanogranitoids below the surface (OSD granulites) and average composition of the host garnet surrounding the inclusions. Average values of analyses from MI in garnet from the samples HO50 and HO33 from Acosta-Vigil et al. (2010) are also reported. Bulk rock composition for the OSD granulites is from Walczak (2011)

The abundance of some large ion lithophile elements (LILE) such as Cs and Rb is consistent with the consumption of an OH-bearing phase, most likely a phyllosilicate, during the melt-producing reaction. Considering the other TE investigated in the nanogranitoids, in the melt Nb, Ta and Ti are significantly lower and Zr, Hf, LREE moderately lower than in the host rock. Ba, Th, U, Gd, V, Zn, Sc and Co show instead rather similar abundance. The most important repositories of TE in the OSD granulites are accessory minerals such as rutile, zircon, apatite and magmatic epidote,

often characterized by an allanitic core (Ferrero et al. 2015). Nb, Ta and, to a minor extent, V are mainly hosted in rutile (Luvizotto et al., 2009), Zr and Hf in zircon and REE in apatite and epidote (Bea, 1996; Acosta-Vigil et al., 2010).

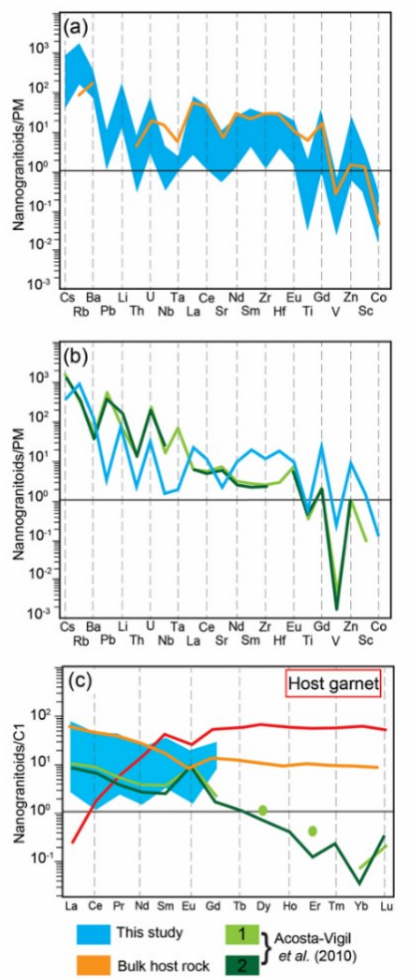

Figure 2.7. Trace elements in nanogranitoids of the OSD granulites, reported as the envelope of 27 analyses (see Supplementary Material A, Table S2.1). For the nanogranitoids only the TE above the detection limit have been reported in the diagram; for the complete dataset see Table S2.1. (**a**) Primitive mantle (PM) -normalized pattern of trace elements of the investigated inclusions and bulk rock of the host felsic granulites. (**b**) PM-normalized pattern of average values of trace elements of the investigated inclusions and the averages MI in garnet from granulitic enclaves of Acosta-Vigil et al. (2010); (**c**) Chondrite (C1)-normalized REE pattern. Both PM and C1 values are from Sun and McDonough (1989). Average of MI in grt from samples HO50 (1) and HO33 (2) respectively are from Acosta-Vigil et al. (2010). Bulk rock composition of OSD granulites is from Walczak (2011).

(a)

(ppm)	Zr	T	T_{min}	T_{max}
Max	295	**770**	753	788
Min	14	**521**	511	530
Average	129	**688**	674	703
Expected	700	**873**	852	894
Bulk rock	308	**775**	758	793

(b)

Figure 2.8. (**a**) Zircon saturation calculation for the OSD nanogranitoids (n=26), the measured Zr values for the whole dataset are reported in table S1. (**b**) Boxplot of zircon saturation temperatures. The equation for this calculation was derived by Boehnke et al. (2013) as T (°C)= 10108/[ln(497644/Zr_{melt})+(1.16±0.15)*(M-1)+(1.48±0.09)]-273.15, where Zr_{melt}=Zr content in the melt and M is the molar ratio 100*(Na+K+2Ca)/Al*Si. For the OSD nanogranitoids the value M was calculated from the average major elements composition of the inclusions as reported in Table 3 and corresponds to 1.669.

The melt is generally lower in these elements than the bulk rock, suggesting that all these phases were not involved significantly in melt production, a notion supported also by the common occurrence of rutile, zircon, apatite and epidote as mineral inclusions both in the nanogranitoids and in the inclusion-bearing garnet cores (Ferrero et al. 2015). The stability of apatite during melting is consistent with the lower amount of P observed in the melt with respect to the host rock (ca. one order of magnitude, 352 vs 2500 ppm, Table 2.4). To evaluate whether zircon was dissolved during melting, the zircon saturation temperature of the trapped melt was calculated using the equation of Boehnke et al. (2013) derived by zircon dissolution experiments up to 2.5 GPa. The calculated temperatures are in the range ~520±10°C and 770±20°C (Fig. 8a), significantly below the T of 875°C observed during nanogranitoid re-homogenization experiments and calculated via geothermometry. In our opinion this is a further evidence that zircon did not dissolved during the melting event, at least not enough for the melt to achieve saturation in Zr. Indeed, based on the same equation, the amount of Zr expected in a Zr-saturated melt at 875°C would be ~700 ppm (Fig. 2.8b), 2.5 times higher than the highest value measured in the nanogranitoids (295 ppm, Fig. 2.8a). This is furthermore confirmed by previous studies based on REE partitioning between zircon and garnet (Walczak et al. 2017) which show instead that the zircon growth during Variscan metamorphism post-dated partial melting, as it took place already on the retrograde path, during the formation of the garnet rim – notably free of nanogranitoids. Although in situ zircon studies on the OSD granulites are missing, it is likely that the zircon inclusions trapped alongside nanogranitoids in the garnet core are older (>370 Ma) inherited magmatic zircons (see also Walczak et al. 2017), as already observed in other felsic granulites of Southern Bohemia (Kröner et al., 2000).

The only other available systematic database of this type is from the enclaves of the NVP (HO33 and HO50, see caption Fig. 2.7, Acosta-Vigil et al. 2010) and for this reason it was used as a term of comparison to interpret our data, despite the difference in protolith and melt productivity, i.e. metapelitic and 30 vol% melt for the NVP enclaves *versus* metagranitoid and <10 vol% melt for the OSD granulites. Both datasets show consistent patterns and similar (in average) contents of LREE (La, Ce, Pr, Nd) which are partitioned preferentially in the melt produced synchronously with respect to the host garnet (Fig. 2.7b, c). At a closer look the two datasets show some differences in terms of LILE, high field strength elements (HFSE) and first row transition elements (FRTE; Fig. 2.7b). Among the LILE Rb is slightly higher, Cs and Sr slightly lower and Pb significantly lower (>1 order of magnitude) in the OSD inclusions with respect to the NVP inclusions. As HFSE, OSD inclusions show higher Zr and Hf, whereas Th, U, Nb and Ta are significantly lower, whereas FRTE such as V, Zn and Sc are more abundant. LREE show similar

abundance in both datasets, whereas some of the medium rare earths (MREE) like Sm, Eu and Gd are significantly higher in the OSD inclusions – REE heavier than Gd were not measured in the OSD nanogranitoids. In the case of NVP enclaves, the melt trapped in the garnet is interpreted as the result of a dehydration melting reaction involving white mica based on the high concentration of Li and Cs, elements preferentially partitioned in muscovite in a metapelitic system (Acosta-Vigil et al. 2010). Elements preferentially partitioned in biotite, e.g. Rb, Ba and FRTE show instead moderate to low concentration thus suggesting that this mineral was stable during melting production (Acosta-Vigil et al. 2010). Contrastingly, the nanogranitoids hosted in the OSD granulites show lower Cs (7 ppm vs. 31 and 31 ppm in average, see Table 2.2 and Fig. 2.9a), higher Rb (499 vs. 211 and 237 ppm) and Ba (762 vs. 308 and 235 ppm) with respect to NVP inclusions. FRTE, e.g. V and Zn are on average two orders of magnitude and Sc one order of magnitude higher (Table 2.2 and Fig. 2.9b), thus pointing toward biotite/phlogopite consumption during garnet formation near or at the metamorphic peak of the OSD granulites at 2.7 GPa and 875°C (Ferrero et al. 2015). Another element often released by biotite/phlogopite consumption is Ti, but its content is likely to be buffered during melting by the formation of new rutile.

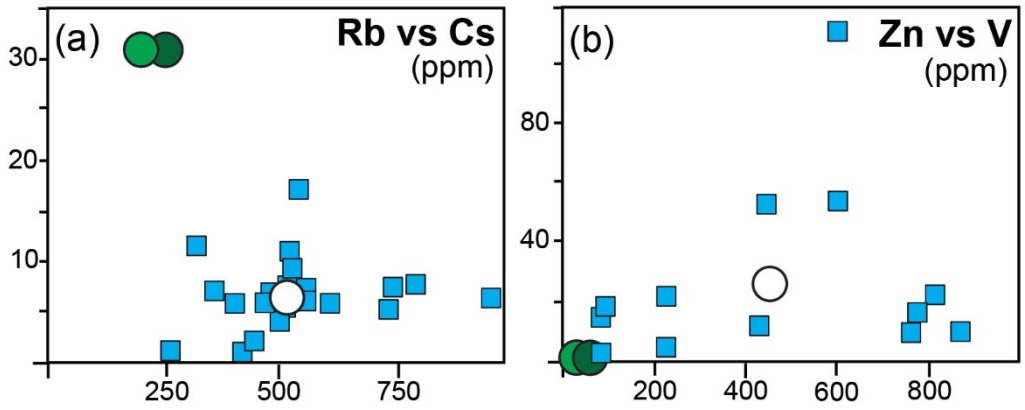

Figure 2.9. Variation diagrams of Rb versus Cs (**a**) and Zn versus V (**b**) for the investigated inclusions (blue circles) and the average of MI in garnet (light and dark green) from Acosta-Vigil *et al.* (2010), see also caption Fig. 7. White circle: average of the nanogranitoid compositions from this study.

As previously discussed, deeply subducted HP/UHP metamorphic terranes of crustal affinity are expected to have melted during decompression for destabilization of phengite, even in the absence in some cases of clear mineralogical relicts, which are often inferred to have been completely erased during post-peak re-equilibration. Now the possibility to discern which OH-bearing phase, biotite/phlogopite versus phengite, was involved in melting via TE investigation of the melt itself provides a powerful tool also to better constrain the geodynamic evolution of deeply

subducted terranes based on the topology of the OH-bearing phase stability curves. The two curves biotite/phlogopite-out and phengite-out show opposite slopes, negative and positive, respectively, with both biotite/phlogopite and phengite stable on the lower T side (Fig. 2.10). The direct consequence of such a different topology is that any dehydration melting reactions involving biotite/phlogopite in the kyanite field will be more likely to occur during the prograde path of the rock as a result of an increase in both P and T. In the case of OSD granulites thus the novel data on TE contents of the nanogranitoids constrain melting to have taken place as the last event of the prograde path of the rock (Fig. 2.10). Dehydration melting involving instead phengite consumption would instead more likely occur as result of decompression, after the rock reached its maximum depth – which may or may not corresponds to the metamorphic thermal peak. From a geodynamic point of view the presence of melt influences the rheological response of subducted bodies to deformation (e.g. Bartoli et al., 2013b) and it is expected to either trigger (when it occurs at the metamorphic peak) or provide further driving force for (when it occurs during decompression) the exhumation of deeply subducted crustal rocks (Hermann and Green, 2001; Labrousse et al., 2011, see also discussion in Ferrero et al. 2015).

2.5 THE MESSAGE OF EXPERIMENTAL PETROLOGY: HOW EXPERIMENTS ON NANOGRANITOIDS HELP TO CONSTRAIN DEEP-MELTING CONDITIONS

The small size and polycrystalline nature of nanogranitoids requires re-homogenization and quenching before in situ analyses of the resulting glass can occur. In the very first case study of melt inclusions in migmatites, in the khondalites of the Kerala Khondalite Belt, Southern India (Cesare et al., 2009; Ferrero, 2010), re-homogenization attempts were initially conducted using a heating stage operating at atmospheric pressure (Ferrero 2010; Cesare et al. 2015). Such attempts invariably resulted in re-melting of the inclusions with extensive melt + garnet interaction, production of new peritectic phases (Cesare et al. 2015) often coupled with the formation of an array of decrepitation cracks (Fig. 2.11a). This outcome is the result of the fact that on re-heating and re-melting the MI experience a significant P increase, up to the entrapment P when re-homogenization is complete. Internal P,T conditions are constrained on a steep isochore (a line in the PT space where the inclusion have constant volume – see e.g. Roedder, 1984), because silicate melts are relatively incompressible (Lowenstern, 1995).

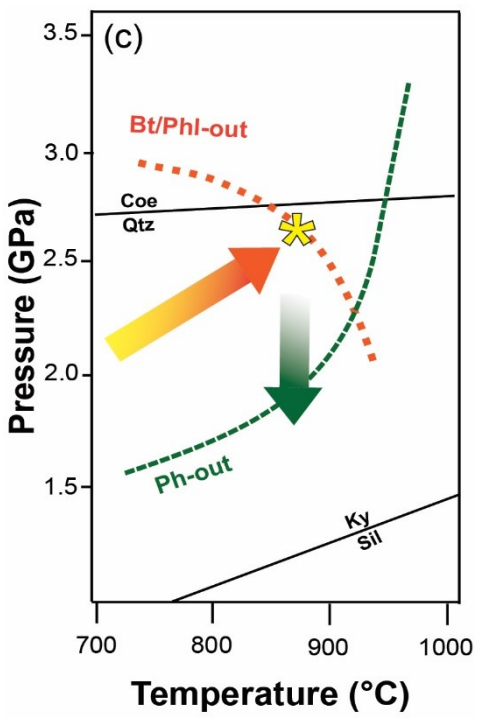

Fig. 2.10 PT diagram showing the biotite/phlogopite-out (Bt/Phl-out) and phengite-out (Ph-out) curves in relationship to the metamorphic peak/melting conditions (yellow star) experienced by the OSD granulites according to re-homogenization experiments (2.7 GPa and 875°C; see also Ferrero *et al.* 2015). Orange arrow: expected prograde subduction-related path of the OSD granulites. Green arrow: generic decompressional path. Bt/Phl-out and Ph-out curves are from (Auzanneau et al., 2006). Quartz-coesite (Qtz, Coe) transition is from (Bose and Ganguly, 1995).

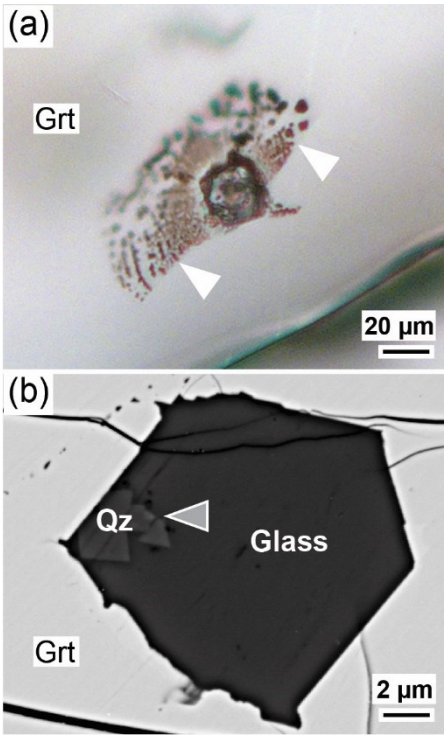

Fig. 2.11 Nanogranitoids after re-homogenization experiments. (**a**) nanogranite from the Kerala Khondalite Belt, Southern India (Ferrero 2010), formed at 0.5 GPa and 950°C (Cesare et al. 2009). This inclusion was re-heated without confining pressure using a LINKAM TS1500 high temperature stage. The inclusion started melting and suffered immediately a catastrophic failure due to extensive decrepitation and formation of a classic decrepitation halo of secondary inclusions (white arrows). (**b**) OSD nanogranitoid re-homogenized in a piston cylinder apparatus with confining P of 2.7 GPa (see point 5 in Fig. 11). The melt inclusion re-homogenized without decrepitation, some quartz is visible on the left side of the inclusion (gray arrow) and it is interpreted as a trapped phase trapped, thus already present during its formation. This is also supported by the fact that the trapped melt is representative of the melt generated during the melting of the OSD granulites as it shows the same composition of inclusions without quartz (Ferrero et al. 2015). The crack visible in the upper part of the figure crosses both glass and host and formed during sample preparation, as visible for the lack of melt in the crack.

The P behavior of the inclusion is independent from that of the host, and each mineral is able to withstand only a certain amount of inclusion overpressurization, for inclusions of a given size, before decrepitation, i.e. opening of cracks, causing stress release and equalization of inclusion internal P and external P. Smaller inclusions must generate higher pressures before decrepitation (Bodnar, 2003). MI in metamorphic rocks form generally several km deep in the crust, and thus the internal P of the inclusions when the inclusion starts to re-melt often largely exceeds the resistance of their host, causing decrepitation, material loss and host-melt interaction (Bartoli et al. 2013a). For this reason the use of a piston cylinder apparatus has become a routine for the re-homogenization of nanogranitoids in metamorphic rocks (Ferrero et al., 2012, 2015, 2016b, 2018a; Bartoli et al., 2013a, 2013b, 2016a; Barich et al., 2014; Carosi et al., 2015; Acosta-Vigil et al., 2016). The confining P applied on the experimental charge in a piston cylinder apparatus "helps" the garnet to perform as an efficient pressure vessel counteracting the inclusion overpressurization, which must be either equal to (Ferrero et al. 2015) or higher (Acosta-Vigil et al. 2016) than the original entrapment P to avoid decrepitation. The experimental T must be as close as possible to the garnet formation temperature, as insufficient temperature will lead to incomplete or no melting, whereas overheating will lead to effects rather similar to insufficient confining pressure, e.g. decrepitation and melt-host interaction, due to increase of the internal P beyond the entrapment conditions (Bartoli et al. 2013a). The most precise knowledge of the conditions at which garnet and melt formed, and thus the melt was trapped, is necessary to perform successful experiments. This information can only be obtained via independent methods such as geothermobarometry and/or thermodynamic modeling.

Experiment	Figures	T(°C)	P (GPa)	t (h)	Melting	Decrepitation	Melt-host interaction	Re-homogenization
1	Fig. 11a	950	2.0	24	X	X (extensive)	-	-
2	Fig. 11b	900	2.0	48	X	X	X (new Grt)	-
3		850	2.0	48	-	-	-	-
4	Fig. 11c	875	2.2	48	X	X	X (new Grt)	-
5	Fig. 11d	875	2.5	48	X	X	-	-
7	Fig. 11e	875	2.7	48	X	-	-	X

Table 2.5. Experimental conditions during the experiments performed for the case study of the OSD nanogranitoids (Ferrero et al. 2015) and related microstructural observations on the experimental products.

Successful experiments allow the direct verification that the polycrystalline aggregate we observe in a nanogranitoid was 1) truly a melt in equilibrium with the host garnet (this condition is required if both melt and garnet are a result of dehydration melting), and 2) that they were in equilibrium at the PT imposed as experimental parameters. Failed experiments, i.e. with textural

evidence of melt-garnet disequilibrium at the inclusion scale, would confirm in turn that the chosen conditions are not representative of the partial melting/inclusion entrapment event. A clear example of this is visible in the experiments performed during the investigation of the OSD nanogranitoids. The metamorphic peak/melting conditions for this case study were poorly defined, thus requiring multiple experiments under variable PT conditions (Table 2.5). The pressure estimates available in the literature include 2.0 GPa (Stipska et al. 2012), 2.7-2.8 GPa (Klemd and Bröcker, 1999), 3.0 GPa (Kryza et al. 1996) or even >30 GPa, in the stability field of coesite, i.e. (Bakun-Czubarow 1991; Bröcker and Klemd 1996), whereas there was general agreement on peak temperature, estimated in the range 900 and 1000 °C. Peak conditions were also calculated by Ferrero et al. (2015) using different geothermobarometers (Fig. 2.12). GASP barometer was used to determine the pressure at which garnet crystallized, which also corresponds to the onset of partial melting, using both the equations of Holdaway, 2001) and Koziol and Newton (1988). Anorthite activity for the GASP barometer was obtained from the bulk composition of the mesoperthite in garnet (similar to the method used in Carswell and O'Brien 1993), whereas grossular activity in garnet was calculated using the activity models from Berman and Aranovich (1996). Our calculations yielded respectively 2.43 GPa and 2.67 GPa, thus narrowing significantly the range of P values proposed in the literature. The minimum temperature for partial melting was calculated as 875°C using the ternary feldspar thermometer (Fuhrman and Lindsley, 1988) on mesoperthite in garnet with activity models from Berman and Aranovich (1996). Mineral compositions are reported in table 2. The starting material for the experiments consisted of garnet chips containing inclusions of different size, from 5 to 50 μm (see Ferrero et al. 2016b for a detailed description of the inclusion appearance). No OH-bearing phase was present in the experimental charges besides the two micas identified in the nanogranitoids and the OH-bearing residual glass identified via Raman mapping (Ferrero et al. 2016b), and no water was added to the experimental capsules. In this way all the melt produced during the experimental run is exclusively the result of inclusion melting. The experiments were performed starting with the lowermost pressure (Fig. 2.12) at 950° (point "1" in Fig. 2.12), then moving to 900° (2) and 850°C. Of this first series of experiments, those at 950 and 900°C showed melting with extensive textural evidence of melt-host interaction (Fig. 2.12b) and, at 950°C, also formation of new peritectic phases, likely aluminosilicates (Fig. 2.12a). The experiment at 850°C showed instead no presence of melt. The subsequent experiments were then performed at 875°C and increasingly higher pressure: at this temperature melting was always achieved inside our inclusions during all the experiments performed under confining P ≤2.5 GPa (Fig. 2.12a,c; see also table 5). New garnet formed in the experiment at 2.0 and 2.2 GPa (Fig. 12a and c) growing on the host garnet.

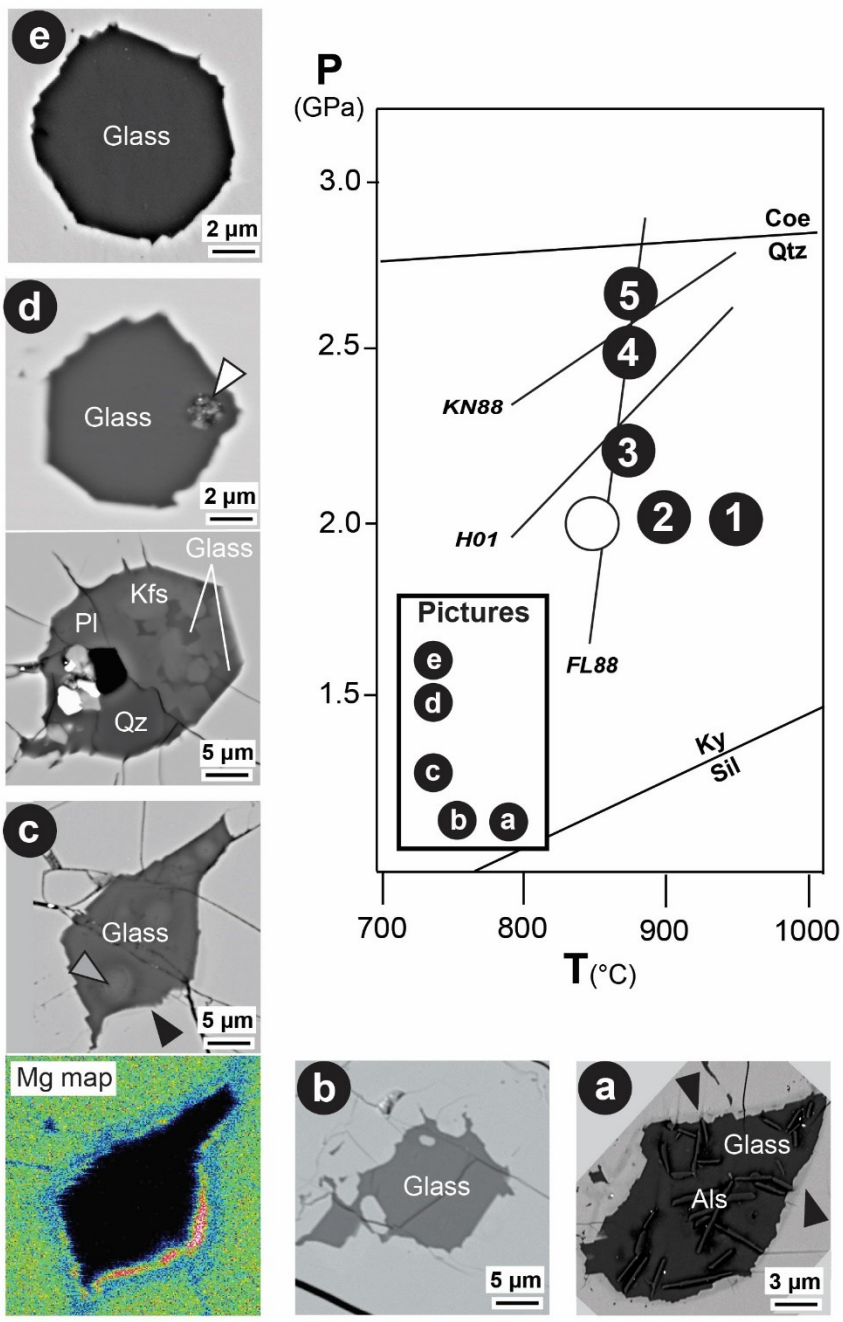

Figure 2.12. Textural evolution of experimental products versus curves calculated with classic geothermobarometry. Multiple experiments performed to achieve complete re-homogenization of OSD nanogranitoids. The experiments showing melt formation are reported in numerals in black circles. White circle: experiment without melt formation. Quartz-coesite (Qtz, Coe) transition is after Bose & Ganguly (1995). KN88: GASP barometer equation from Koziol and Newton (1988); H01: GASP barometer equation from Holdaway (2001) with activity models from Berman and Aranovich (1996) and Fuhrman and Lindsley (1988); FL88: ternary feldspar thermometer from Fuhrman and Lindsley (1988) on mesoperthite as mineral inclusion in MI-bearing garnet. Details on experiment conditions and results are reported in Table 2.5.

The newly formed garnet shows higher Mg (map in Fig. 12c) and lower Ca (composition in Table 2.2). New garnet formation is generally associated with the development of irregular garnet-melt boundaries, suggesting possible garnet consumption and re-precipitation. In the experiment “4” (Fig. 2.12) at 2.5 GPa several cracks of limited extension (they do not reach the boundary garnet-matrix) developed around the larger inclusions where melt formation appears to be only incipient (Fig. 12d below), whereas the smallest inclusions appear to be completely re-melted (Fig. 2.12d above); full re-homogenization is still however not achieved because a shrinkage bubble is still visible. Only at 2.7 GPa confining P the inclusions appear to be fully re-homogenized (Fig. 2.12e, see also Fig. 2.11b) with no evidence of decrepitation and or interaction with the surrounding garnet, e.g. X-ray elemental mapping does not show any zoning or inhomogeneity in the host. Summarizing, the investigation of textural and microchemical features of the experimental products clearly show an evolution in the melt-related microstructures generated during the experimental runs. Experiments at T≥900°C and confining P below 2.7 GPa show clear textural evidence of disequilibrium between melt and garnet, e.g. garnet embayments, melt-host interaction with formation of new phases or decrepitation cracks. Melt-garnet equilibrium appears instead to be achieved at 875°C and 2.7 GPa, where these disequilibrium textures are absent, and EDS elemental maps show absence of zoning in the garnet surrounding the inclusions (See e.g. BSE images Fig. 2.11b and 2.12e). The textural constraints provided by the investigation of the experimental products fit with our geothermobarometric calculations. In the experiments, melt is present at 900°C whereas no melt is observed at 850°C: our calculation based on ternary feldspar thermometer give 875°C, the temperature at which successful re-homogenization was eventually achieved. The confining P of successful experiments, 2.7±0.05 GPa, corresponds within error to the P values obtained using the GASP geobarometer of Holdaway (2001) for T= 875°C using the peak assemblage garnet + mesoperthite + kyanite + quartz. Such a pressure is remarkably higher than the latest calculations performed with the recent thermodynamic databases, 1.8-2.0 GPa of Štípská et al. (2012), but below that of the studies where pseudomorphs after coesite were reported. Our results thus provide clear evidence that all piston cylinder experiments, even the failed ones, can provide robust and completely independent constraints for the mutual stability of melt and garnet, when equilibrium/disequilibrium textures are identified and investigated. Despite being just a by-product of nanogranitoids, such approach may become important to bracket especially the pressure at which partial melting took place in MI-bearing HP/UHP rocks, when clear mineralogical constraints are absent, or for bulk compositions unsuitable for thermodynamic modelling in presence of melting.

Finally it is interesting to note that large melt pockets with more or less euhedral new garnet growing on the inclusion walls have been already reported in experiments under eclogitic conditions (3.0 GPa and 800°C, Perchuk et al., 2008) and also bear some resemblance to the garnet-bearing polycrystalline inclusions in garnet from Faro eclogites, in the Yukon-Tanana terrane (Perchuk et al., 1999). In both cases these microstructures have been interpreted as the result of limited in-situ dehydration melting of a polycrystalline aggregate containing phengite (Lang and Gilotti, 2007), which may destabilize during decompression and generate melt at a local level, i.e. only inside the garnet (see discussion in Cesare et al. 2015). Another possibility, in the light of the failed experiments here discussed, is that these garnet-bearing polycrystalline inclusions in natural HP/UHP garnets may instead represent former nanogranitoids in polymetamorphic garnets, subducted during a second orogenic cycle at high temperature but pressures insufficient to achieve complete re-homogenization of the inclusions – a naturally failed re-homogenization experiment.

2.6 CONCLUSIONS AND FUTURE PERSPECTIVES

The present work provides a comprehensive and timely overview of the results of five years of intense investigation of anatectic melt inclusions in the Bohemian Massif. The finding of numerous case studies of nanogranitoids in an extensively investigated area such as the Bohemian Massif is the best proof that reinvestigation of even very well-known areas, thought to be very well-understood, may help to open up new research avenues, because metamorphic geology itself is under a rapid, continuous and sometimes tumultuous evolution in terms of theories, models and approaches (the “metamorphosis of Metamorphic Petrology” discussed by Spear et al., 2016).

Nanogranitoids still have a large untapped potential, still difficult to completely fathom even after almost a decade of intense investigation. The simple occurrence of nanogranitoids is already a crucial piece in Nature’s puzzle, frequently underappreciated. The identification *per se* of the physical leftovers of melt in form of inclusions constrains beyond doubt the presence of melt at well-defined moments of the rock’s history, in some cases with the possibility to precisely dating the melting event. Often the history of the partial melt is intimately connected to the COHN fluids present in the deep crust, and both need to be thoroughly investigated in order to understand how our planet evolves. The possibility to extracting high quality data directly from natural melt (thus avoiding possible problems of limited representativity of experiments or thermodynamic calculations) opens up the possibility to describing and quantifying melting processes in unprecedented detail. Moreover, whereas most of the results are from silica-rich rocks, melt

inclusions were recently identified and investigated in garnet clinopyroxenites from orogenic peridotites (Borghini et al., in press) and are now under investigation in the Saxo-Thuringian eclogites providing new insights also on how mafic and ultramafic rocks interact with melt when involved in orogenesis.

In conclusion, the idea that anatectic melts can also be hosted in metamorphic minerals (first proposed by Cesare, 2008, see also Cesare et al., 2011) was daring, and shifted the perception of the petrological community from crustal melting as a phenomenon that can only be constrained by re-melting rocks in the laboratory or through sophisticated thermodynamic calculations (Sawyer et al. 2011), to something we can see and “touch” (i.e. analyze) directly in the natural rock. Five years of nanogranitoid investigation in the Bohemian Massif has already produced a large dataset on melting processes and revealed new and unexpected phenomena, such as metastable polymorphs, crustal carbonatites and near-UHP melting of subducted crust. The next few years will see the application of increasingly more sensitive analytical techniques, coupled with a continuously increasing spatial resolution. This will open up even more possibilities to improve understanding of the investigation of processes with planetary-scale implications, such as crustal melting, by peering into few cubic microns of melt sitting in an outcrop in the forests of Central Europe.

3 GRANITOID MELT INCLUSIONS IN OROGENIC PERIDOTITE AND THE ORIGIN OF GARNET CLINOPYROXENITE

ALESSIA BORGHINI[1], SILVIO FERRERO[1,2], BERND WUNDER[3], OSCAR LAURENT[4], PATRICK J. O'BRIEN[1] AND MARTIN A. ZIEMANN[1]

[1]Institute für Geowissenschaften, Universität Potsdam, [2]Musem für Naturkunde (MfN), Berlin, [3]Helmholtz-Zentrum, GFZ, Potsdam, [4]Eidgenössiche Technische Hoschule, ETH, Zurich

Geology (2018), 46 (11): 1007-1010. https://doi.org/10.1130/G45316.1

ABSTRACT

Granitic melt inclusions were found in layers of garnet clinopyroxenites from orogenic peridotites hosted in high pressure felsic granulites of the Granulitgebirge, Central Europe. The inclusions are both glassy and crystallized, and occur as clusters in the garnet. Microstructural features suggest that the inclusions formed while garnet was growing as a peritectic phase likely alongside clinopyroxene. The chemistry of the melt, in particular its trace element signature, shows a crustal contribution, probably due to the involvement of phengite in the melt-producing reaction, most likely in the presence of a fluid. The presence of a granitoid melt in mantle rocks may be the result of localized melting of a phengite-bearing protolith either already present in the peridotites or, more likely, within the local deeply subducted crustal units. In the latter case the melt infiltrated the peridotites and generated pyroxenite via metasomatism. In either case the presence of granitoid inclusions in orogenic peridotite provides a direct evidence for a genetic connection between a high-pressure crustal melt and garnet pyroxenites. The in situ characterization of these remnants of natural melt provides direct quantitative constraints on (one of) the agents responsible for the interaction between crust and mantle.

3.1 INTRODUCTION

Garnet peridotites in (ultra) high pressure ((U)HP) terranes often contains lenses, irregular bodies and dykes of pyroxenite and eclogite (Medaris et al., 1995; Garrido and Bodinier, 1999; Brueckner and Medaris, 2000; Bodinier and Godard, 2014). Whether the origin of the pyroxenite is magmatic, metamorphic, metasomatic or a combination of processes is still debated but certainly interaction with subducted crust, oceanic or continental, plays an important role. Suggested origins include: HP crystal accumulation in magma conduits due to transient melts of variable source, either mantle or subducted oceanic crust (Medaris et al., 1995; Becker, 1996; Bodinier et al., 2008; Bodinier and Godard, 2014; Svojtka et al., 2016 ref. therein); incorporation in the convective mantle of stretched and metamorphosed subducted oceanic and/or lower continental crust (Allègre and Turcotte, 1986; Isabel Varas-Reus et al., 2018); metasomatism by melts with a mantle or crustal origin (Malaspina et al., 2006, 2009; Vrijmoed et al., 2013). The Bohemian Massif represents an excellent setting to study pyroxenite origin because of the presence of numerous peridotite bodies, with layers of pyroxenite, surrounded by HP felsic granulite.

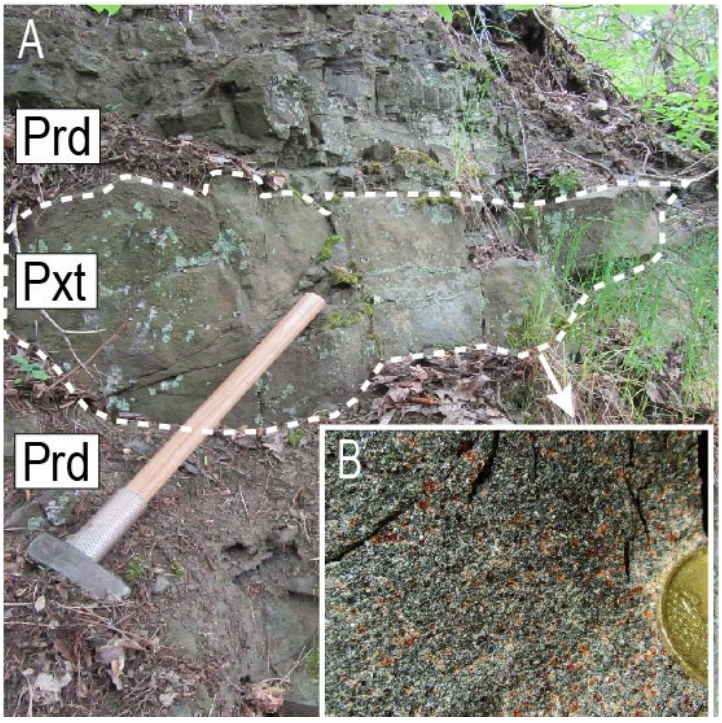

Figure 3.1 Field occurrence of garnet clinopyroxenites. A: foliated body of serpentinized garnet peridotite at Klatschmühle with enclosed a single layer of garnet pyroxenite (Prd = peridotite and Pxt = pyroxenite). B: Close-up of garnet clinopyroxenite (see Appendix 3).

In this study we report the first finding of primary melt inclusions (MI), both glassy and crystallized as “nanogranitoids” (Cesare et al., 2015), in garnet from clinopyroxenites enclosed in

serpentinized garnet peridotites from the Granulitgebirge, northern part of the Bohemian Massif (Fig. 3.1 and S3.1 A-B in the Supplementary material B). In this study we aim to exploit these relicts of natural melt in mantle rocks to investigate the genesis of pyroxenites and, more generally, crust-mantle interactions during continental collision. A large part of the scientific community agrees that melt plays a role in the genesis of mantle pyroxenites (Bodinier and Godard, 2014): our finding now allows us to directly investigate this melt and to provide novel chemical constraints on the melt-related processes in mantle rocks.

3.2 HOST ROCKS AND CHEMISTRY OF THE MELT

The few existing petrological studies available on garnet clinopyroxenites of the Granulitgebirge are limited to the location Reinsdorf (Massone and Bautsch, 2002; Schmädicke et al., 2010). Our samples are from two adjacent localities located 10 km east of Reinsdorf: Rubinberg (locality 1) and Klatschmühle (locality 2). The investigated rocks occur as single layers (Fig. 3.1) with granoblastic texture dominated by crystals of clinopyroxene and garnet (Fig. S3.1 C-D and Table S3.1). Such layers are not in direct contact with the surrounding felsic granulites (Fig. 3.1).

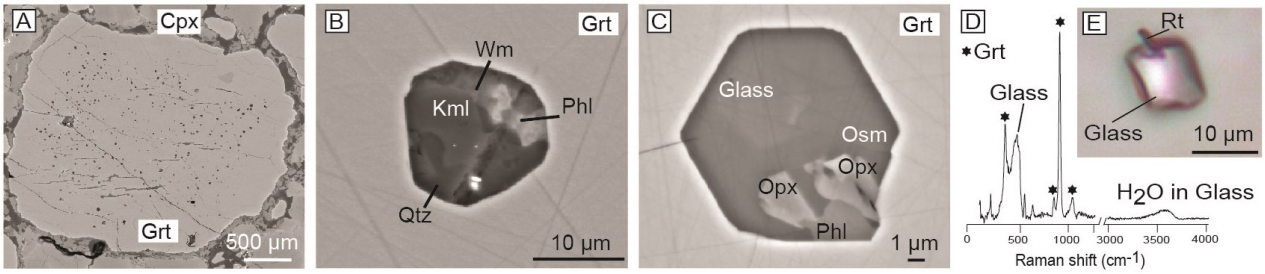

Figure 3.2 Backscattered electron images of nanogranitoids with well-developed negative crystal shape in garnet clinopyroxenites (A-C). A: garnet crystal (Grt) with cluster of nanogranitoids and clinopyroxene (Cpx). B: nanogranitoid microstructures from locality 1 (Loc 1) with kumdykolite (Kml), phlogopite (Phl), quartz (Qtz) and white mica (Wm). C: nanogranitoid microstructures from locality 2 (Loc 2) with osumilite (Osm), phlogopite (Phl), orthopyroxene (Opx) and residual glass. D: Raman spectrum of a preserved glassy inclusion (E) with a trapped rutile (Rt) in Loc1.

Primary glassy inclusions, 2–5 µm in diameter, and nanogranitoids, 5–20 µm, occur together in clusters in the inner part of the garnet (Fig. 3.2A-D) and do not show cracks connecting with the matrix, i.e., they are chemically preserved (Ferrero et al., 2012). Glassy inclusions occur only in locality 1 and they were identified by both optical microscopy and Raman spectroscopy (Fig. 3.2D and E). They have granitic composition with high alkali content (Na_2O+K_2O = 10.5 wt%;

Na_2O/K_2O = 1.10) and low CaO, FeO and MgO (0.45 wt%, 0.56 wt% and 0.22 wt%, respectively; Fig. 3.3). The melt is peraluminous (ASI: $Al_2O_3/(Na_2O+K_2O+CaO)$ = 1.12) and H_2O-bearing (see Table S3.2), as confirmed by Raman spectroscopy (Fig. 3.2E). Nanogranitoids contain kumdykolite or albite, phlogopite, osumilite, kokchetavite, variable amounts of quartz, pyroxene, white mica, and rare carbonate. Kumdykolite and kokchetavite are, respectively, $NaAlSi_3O_8$ and $KAlSi_3O_8$ polymorphs.

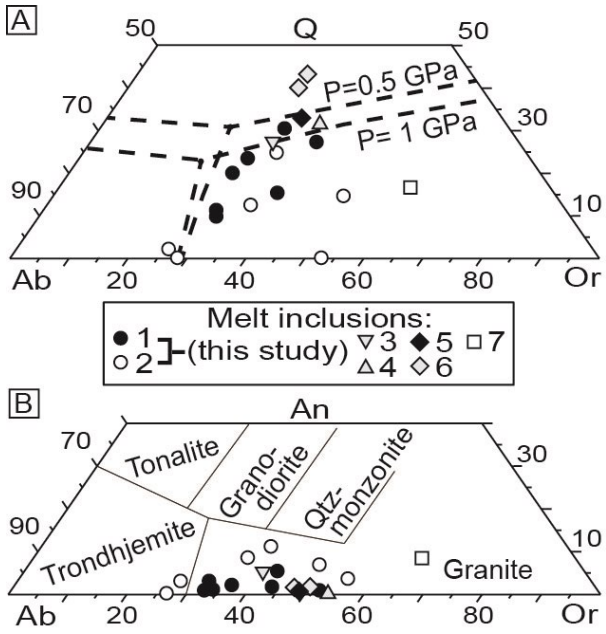

Figure 3.3 CIPW quartz-albite-orthoclase (Q-Ab-Or; A) and anorthite-albite-orthoclase (An-Ab-Or; B) diagrams showing the normative composition of MI from this study (Loc 1 and 2) and the average compositions of MI in peritectic garnets of metagranitoids from (3) Orlica-Śnieżnik Dome, Bohemian Massif (Ferrero et al., 2018b) and (4) La Galite, Tunisia (Ferrero et al., 2014); of metapelites from (5) El Hoyazo (Acosta-Vigil et al., 2007) and (6) Ronda (Ferrero et al., 2012) in southern Spain, and ultramafic granulites from (7) Dronning Maud Land, Antarctica (Ferrero et al., 2018a) (compositions are reported in Table S3.2). Cotectic curves (dashed curves) and minimum melting points (small black dots) for haplogranite composition at a_{H2O} = 0.5. Cotectic curves and the fields in diagram B are from Bartoli et al. (2016).

At locality 2 only nanogranitoids were identified and in order to analyze them they were first re-homogenized to a glass via piston cylinder experiments at 1000 - 1050 °C and 1.5 - 2.2 GPa (see Table S3.2). The chosen conditions are those estimated for the garnet formation (Rötzler et al., 2008) and thus of the melt entrapment. The glass is trondhjemitic to granitic in composition with a high content of alkalis (Na_2O+K_2O = 7.07 wt%; Na_2O/K_2O = 1.14, Fig. 3.3), and slightly higher CaO, FeO and MgO than at locality 1 (1.55 wt%, 1.60 wt% and 0.99 wt%, respectively). The glass is also less peraluminous (ASI = 1.04%) and slightly richer in H_2O (Fig. DR2 and Table DR2). MI from both locations show the same trace element compositions. They are enriched in Li, B, Th and U as well as mantle-incompatible elements (Cs, Rb, Pb and Ba), and show notable negative anomalies in Nb, Ta and Sr (Fig. 3.4A). The LREE are preferentially partitioned into the MI whereas the MREE and the HREE concentrate in the garnet (Fig. 3.4B).

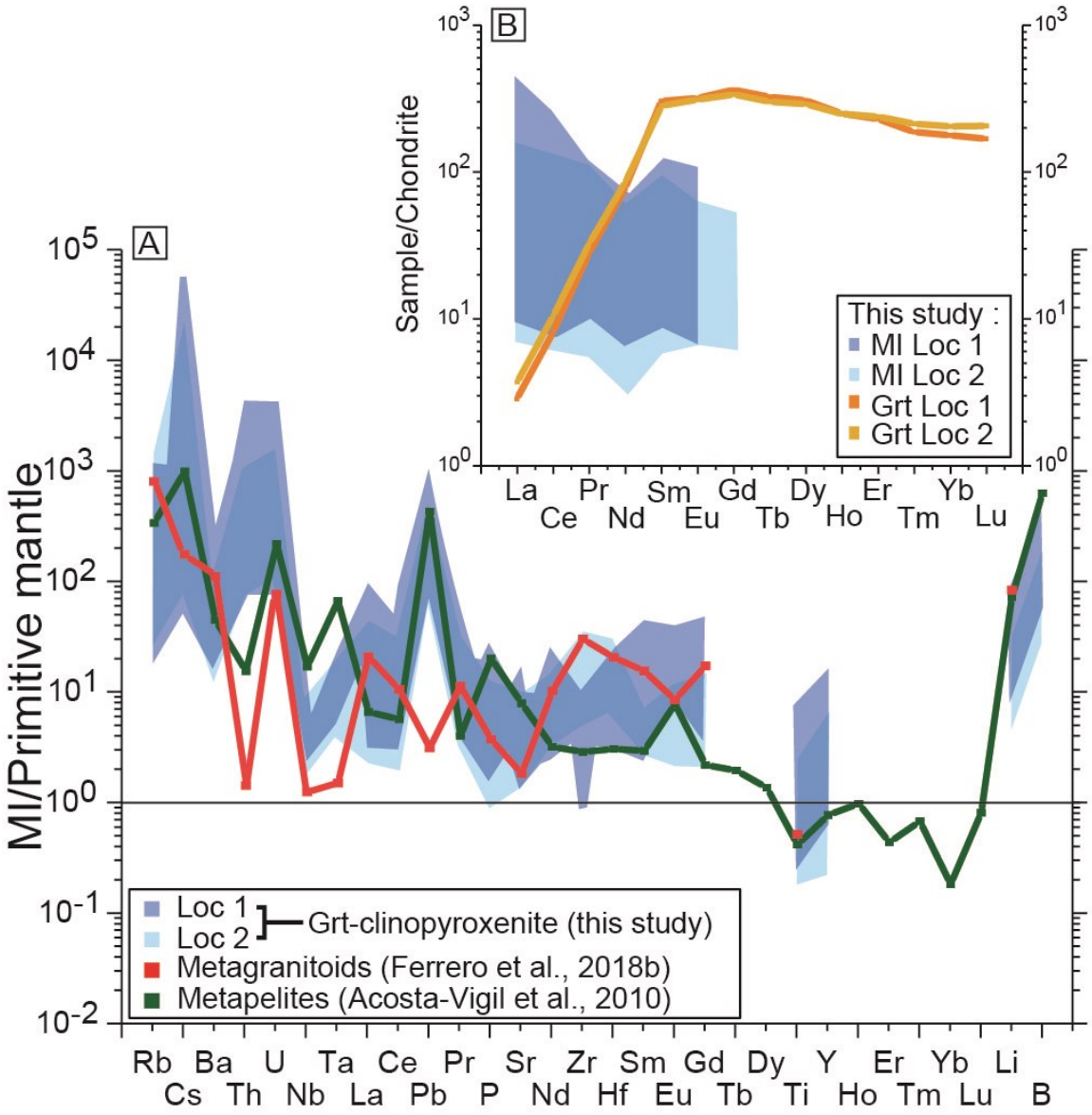

Figure 3.4 A: primitive mantle normalized trace element patterns of MI in garnet from: this study, metagranitoids of Orlica-Śnieżnik Dome and metapelites of El Hoyazo (Acosta-Vigil et al., 2010). El Hoyazo pattern is used for comparison because white mica is involved in the melting producing reaction. B: chondrite normalized REE partition between MI and garnet (see Table S3.4).

3.4 NATURE AND ORIGIN OF THE MELT

Both mineral assemblage and the presence of glassy inclusions in the same cluster support an origin of these inclusions as former droplets of melt (Ferrero et al., 2012), trapped during garnet growth. Most melt compositions in the two localities are granitic with a high alkali content. The reliability of compositions by chemical preservation of the nanogranitoids is

confirmed by the presence of $NaAlSi_3O_8$ and $KAlSi_3O_8$ polymorphs (Ferrero et al., 2016b, 2018a) in crack-free inclusions and by our homogenization experiments, which do not show reactions between melt inclusions and the host garnet (Bartoli et al., 2013a; Ferrero et al., 2018b). Moreover, the melting temperature is consistent with the one determined independently for the formation of the garnet (Rötzler et al., 2008), pointing to no H_2O loss that would then result in re-homogenization at higher temperature (Ferrero et al., 2018b).

As the clinopyroxene is in textural equilibrium with the garnet we can infer a genetic connection between the melt and the pyroxenite as a whole. The granitic nature of the MI is consistent with the involvement of a crustal component in the melt-producing reaction, and the trace element signature of the melt is clearly related to subduction. The MI enrichment in Li, B, Cs, Rb, Pb and Ba strongly suggests that white mica/phengite was the main melt-producing phase (e.g., Liu et al., 2013), similarly to what has been observed in anatectic melts from metapelites (Fig. 3.4A). The enrichment in Th and U, two elements not generally present in micas, might also suggest the involvement of a fluid (Bali et al., 2011). Which are the possible processes that may explain the presence of a granitic melt in orogenic peridotite and how does the melt relate to garnet clinopyroxenite genesis?

3.4.1 LOCALIZED PARTIAL MELTING IN A MARBLE-CAKE MANTLE SCENARIO

So far, the microstructural features of nanogranitoids in silica-poor rocks –both from this study and from the ultramafic granulites of Dronning Maud Land, Antarctica (Ferrero et al., 2018a) – are inclusions in clusters, a negative crystal shape of the inclusions and preserved glass. They appear identical to those reported in silica-rich partially melted rocks both from low-P (Cesare et al., 2015; Bartoli et al., 2016b) and high-P (Ferrero et al., 2016). All the reported cases are interpreted as evidence of partial melting and this process could also explain the genesis of the investigated pyroxenite. Low degrees of partial melting involving white mica, supported by the trace element signature of the melt, could produce simultaneously melt, garnet (and clinopyroxene) also from a mafic protolith (Skjerlie and Patiño-Douce, 2002). Possible protoliths containing white mica are pieces of old oceanic and continental crust incorporated in the mantle during deep subduction and deformed in elongated lenses and bodies, e.g., the marble-cake model of Allègre and Turcotte (1986), recently revisited by Isabel Varas-Reus et al. (2018). However, the lack of clear mineralogical relicts prevents the identification of the protolith, and thus makes this scenario difficult to be constrained in all its parts.

3.4.2 METASOMATISM

Clusters of melt inclusions with a crustal signature in peridotite bodies can be explained also with a melt-rock metasomatic interaction. The trapped melt would then represent the metasomatic agent involved in the reaction with the peridotite responsible for the production of peritectic garnet and clinopyroxene (Rapp et al., 2010) at 1000–1050º C and 1.5–2.2 GPa. In a metasomatism scenario the introduction of the granitoid melt in the peridotites and its entrapment as MI most likely occurred during continental subduction in collisional setting, where magmas with crustal component are common (e.g., Couzinié et al., 2016). The Granulitgebirge is a portion of continental crust subducted to mantle depths which was rapidly exhumed, trapping mantle slices en route (O'Brien, 2000). In this scenario melt-rock interaction would take place during the first stages of exhumation (see metamorphic stages of Schmädicke et al., 2010). Metasomatism has already been proposed for the formation of pyroxenites in other orogenic peridotites, e.g., in the Dabie Shan (UHP Maowu Ultramafic Complex) (Malaspina et al., 2006, 2009), Sulu terranes (UHP unit at Zhimafang, Eastern China) (Malaspina et al., 2009) and in the Svartberget garnet peridotites of the UHP domain of the Western Gneiss Region in Norway (Vrijmoed et al., 2013), but our case study shows some crucial differences. In the Dabie Shan case (Malaspina et al. 2006; 2009) layers of harzburgite, orthopyroxenite and coesite-bearing eclogite occur in garnet-coesite-bearing gneisses. Malaspina et al. (2006) interpreted metasomatism to have occurred via interaction between a hydrous granitic melt and the harzburgites, generating orthopyroxene, garnet and a residual solute-rich aqueous fluid now trapped in garnet as polycrystalline inclusions. Such inclusions contain 10–20 vol% of opaque minerals and 80–90 vol% of hydrous phases and they re-homogenize to a porous quenched material. Conversely, in the Granulitgebirge, the nanogranitoids contain only 20–25 vol% of hydrous minerals and the trapped fluid is a melt with <2 wt.% H_2O, as confirmed by the re-homogenization to a glass.

The Svartberget peridotites show evidence of fluid/melt-rock interaction such as blocks separated by different generation of veins and layers of pyroxenite and eclogite with different composition. Vrijmoed et al. (2013) propose that a "hydrous melt-like transitional fluid" metasomatized the peridotites through a network of thin fissures. The adjacent gneisses are most likely the source of the fluid because they contain, in high concentrations, all the elements added to the metasomatized rocks. Conversely, in the Granulitgebirge, the network of veins is absent and the pyroxenites are lenses in foliated peridotites (Fig. 3.1). Those peridotites are enclosed in partially melted HP granulites which resemble in composition those of the Orlica-Śnieżnik Dome (OSD) which also contain inclusions of crystallized melt (Ferrero et al., 2016). The latter MI and those in garnet-clinopyroxenites are different in both major (see Table S3.2) and trace elements

(Fig. 3.4A), making it unlikely that the granulites are the source of the trapped melt. Considering its geochemical signature, a possible source of the melt could be other crustal rocks subducted during the Variscan orogeny, e.g., UHP phengite-bearing metapelites/eclogites such those in the adjacent Erzgebirge. In this scenario the absence of a network of veins similar to those observed in the Svartberget peridotites could be due to the intense deformation that produces the foliation in the peridotite and transposes the pyroxenite layers within the foliated peridotites.

3.5 CONCLUSIONS AND IMPLICATIONS

This study targets for the first time melt inclusions in metamorphosed mantle rocks in collisional settings and provides novel pieces to the mosaic of knowledge about crust-mantle interaction. Glassy inclusions and nanogranitoids are reported and investigated in garnet-clinopyroxenite hosted in orogenic peridotites from a (U)HP metamorphic terranes. Microstructural and chemical features show that they are primary and thus garnet grew in the presence of melt. Despite the uncertainties regarding the source of the melt, its major and trace element signatures represent direct evidence that a melt with a crustal component directly contributed to the genesis of the pyroxenites of the Granulitgebirge. The chemistry of the crustal melt generated during subduction to mantle depth is a crucial information necessary to quantify processes of deep melting and metasomatization, both via modeling and experimental petrology, as well as to evaluate upper mantle heterogeneity and thus better constrain the different components responsible for the chemical signature of mantle-derived magmas.

4 CRYPTIC METASOMATIC AGENT MEASURED IN SITU IN VARISCAN MANTLE ROCKS: MELT INCLUSIONS IN GARNET OF ECLOGITE/PYROXENITE, GRANULITGEBIRGE, GERMANY

ALESSIA BORGHINI[1], SILVIO FERRERO[1,2], PATRICK J. O'BRIEN[1], OSCAR LAURENT[4], CHRISTINA GÜNTER[1] AND MARTIN A. ZIEMANN[1]

[1]Institute für Geowissenschaften, Universität Potsdam, [2]Musem für Naturkunde (MfN), Berlin, [3]Eidgenössiche Technische Hoschule, ETH, Zurich

Journal of Metamorphic Geology (2020), 38 (3): 207-234, https://doi.org/10.1111/jmg.12519

ABSTRACT

Garnet of eclogite (formerly termed garnet clinopyroxenite) hosted in lenses of orogenic garnet peridotite from the Granulitgebirge, NW Bohemian Massif, contains unique inclusions of granitic melt, now either glassy or crystallized. Analyzed glasses and rehomogenized inclusions are hydrous, peraluminous and enriched in highly incompatible elements characteristic of the continental crust such as Cs, Li, B, Pb, Rb, Th and U. The original melt thus represents a pristine, chemically evolved metasomatic agent which infiltrated the mantle via deep continental subduction during the Variscan orogeny. The bulk chemical composition of the studied eclogites is similar to that of Fe-rich basalt and the enrichment in LILE and U suggest a subduction-related component. All these geochemical features confirm metasomatism. In comparison to other garnet + clinopyroxene-bearing lenses in peridotites of the Bohemian Massif, the studied

samples from Rubinberg and Klatschmühle are more akin to eclogite than pyroxenites, as reflected in high jadeite content in clinopyroxene, relatively low Mg, Cr and Ni but relatively high Ti. However, trace elements of both bulk rock and individual mineral phases show also important differences making these samples rather unique.

Metasomatism involving a melt requiring a trace element pattern very similar to the composition reported here has been suggested for the source region of rocks of the so-called durbachite suite, i.e. ultrapotassic melanosyenites, which are found throughout the high grade Variscan basement. Moreover, the Th, U, Pb, Nb, Ta and Ti patterns of these newly studied melt inclusions strongly resemble those observed for peridotite and its enclosed pyroxenite from the T-7 borehole (Staré, České Středhoři Mountains) in N Bohemia. This suggests that a similar kind of crustal-derived melt was involved also here.

This study of granitic melt inclusions in eclogites from peridotites has provided the first direct characterization of a preserved metasomatic melt, possibly responsible for the metasomatism of several parts of the mantle in the Variscides.

Keywords: clinopyroxenite, eclogite, orogenic peridotite, melt inclusions, metasomatism.

4.1 INTRODUCTION

Orogenic peridotites are ultrabasic bodies tectonically emplaced in suture zones and mountain belts (Bodinier and Godard, 2014). These bodies have attracted the attention of the scientific community because they offer a potential source of information on mantle processes such as the transport, reaction and storage of melts and/or fluids in supra-subduction mantle wedges as well as on subduction/exhumation mechanisms (Allègre and Turcotte, 1986; Bodinier and Godard, 2014 and references therein; Brueckner, 1998). The upper mantle has been shown to be chemically heterogeneous and it is common to find veins, dykes and lenses of websterite, pyroxenite and eclogite in exposed peridotites (Becker, 1996; Bodinier and Godard, 2014; Borghini et al., 2018; Brueckner and Medaris, 2000; Garrido and Bodinier, 1999; Medaris et al., 1995; Svojtka et al., 2016).

Despite decades of research, the origin of pyroxenite and eclogite in orogenic peridotite is still debated although most theories involve a melt component and oceanic (± continental crust). The predominant hypothesis is a high pressure (HP) cumulate origin of garnet and clinopyroxene (Bodinier et al., 1987; Garrido and Bodinier, 1999; Bodinier and Godard, 2014; Svojtka et al.,

2016) from basaltic melts deriving from either the asthenospheric mantle (Becker, 1996; Schmädicke et al., 2010) or mantle metasomatized by melting of subducted oceanic crust (Medaris et al., 1995; Medaris et al., 2005; Schmädicke et al., 2010). Another possibility proposed is a metasomatic interaction between a melt and the mantle peridotite at the margin of a melt conduit (Malaspina et al., 2009; Malaspina et al., 2006; Vrijmoed et al., 2013). Some garnet clinopyroxenites are interpreted as HP recrystallized variants of layers originating as basalts/gabbros (e.g., Obata et al., 2006; Svojtka et al., 2016). These are mostly eclogites but varieties with low-Na clinopyroxene also exist. Moreover, also stress-induced recrystallization of high temperature (1300–1400°C) highly aluminous pyroxene megacrysts can generate, typically at HP and lower temperatures, exsolution-like lamellar garnet and low-Al pyroxene growth (Carswell and Jamtveit, 1990; Faryad et al., 2009; Massonne and Bautsch, 2002; Medaris et al., 2005; Schmädicke et al., 2010). The megacrysts originally formed from interaction between the mantle and mantle-derived melts, which produced mono-mineralic layers of clinopyroxene and/or orthopyroxene and/or garnet (Massonne and Bautsch, 2002; Schmädicke et al., 2010). A full understanding of the formation of pyroxenite and eclogite would thus provide new insights on melt-related processes in mafic and ultramafic rocks and on the nature of crust-mantle interactions in a variety of subduction settings. Typically, investigation of the evolution of these rocks is via trace element and isotope studies. However, the most direct approach to study any deep process involving fluids is clearly to investigate the fluid/melt itself, such as when it is preserved as primary inclusions, thus revealing crucial information about the genesis of both fluid/melt and its host phase (Ferrero and Angel, 2018).

Two localities in the Granulitgebirge (northern part of the Bohemian Massif), Rubinberg and Klatschmühle, show the occurrence of eclogite (formerly termed garnet clinopyroxenite) lenses in orogenic peridotite that is itself enclosed in HP felsic granulite. Primary melt inclusions (MI) were already reported in these eclogites and the melt interpreted has having been directly involved in their formation (Borghini et al., 2018). Whereas these eclogites were already reported in studies on orogenic peridotites and granulites of the Granulitgebirge (Rötzler et al., 2008; Schmädicke et al., 2010), no detailed geochemical and microstructural investigation was ever undertaken, and the presence of preserved melt inclusions went unnoticed until the work of Borghini et al. (2018). The present paper contains the first detailed geochemical dataset on these so far unique melt-bearing garnet + clinopyroxene-rich rocks, and includes analyses of the bulk rock, the main mineral phases and the trapped melt. The aim is to compare this newly acquired geochemical dataset with existing data available in the literature for similar rocks from other localities in the

Bohemian Massif in order to define the role of deep melts in the metasomatic interaction between the crust and the mantle during continental subduction.

4.2 GEOLOGICAL SETTING

The European Variscides are part of a 8000 km long orogenic belt generated after the collision of Laurasia and Gondwana during late Paleozoic (O'Brien and Carswell, 1993; O'Brien, 2000) and exposed in a series of uplifted basement blocks such as the Iberian, Armorican, and Bohemian Massifs and the French Massif Central. At the easternmost part of the chain, the Bohemian Massif, high grade crystalline rocks extend into parts of Germany, the Czech Republic, Poland and Austria (O'Brien and Carswell, 1993; Fig. 4.1).

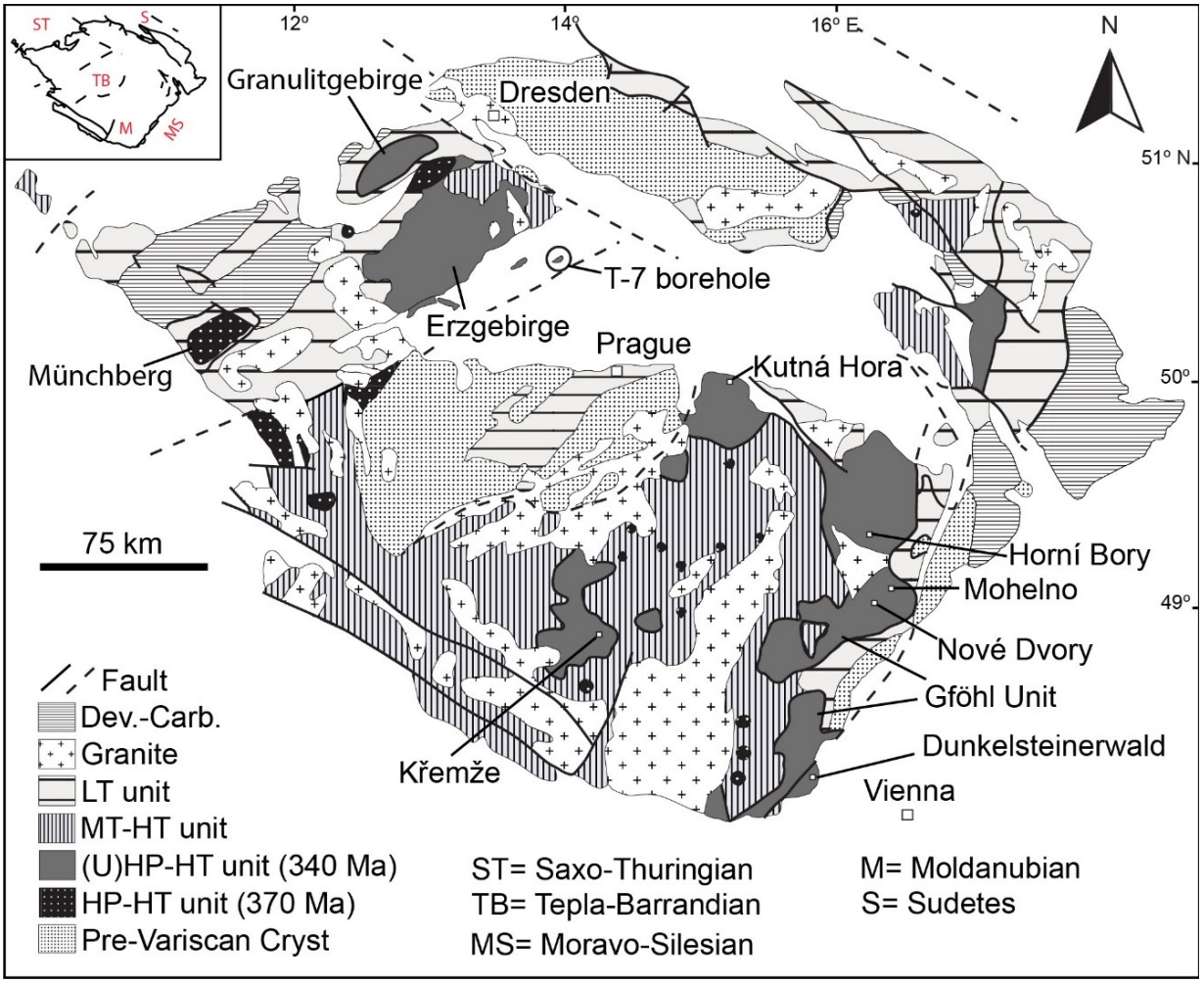

Figure 4.1. Simplified geological map of the Bohemian Massif (modified after Franke and Żelaźniewicz, 2000). The inset reports the different tectonic domains in which the Bohemian Massif is divided.

The Variscan evolution of this basement can be divided into a Devonian oceanic subduction followed by Devonian-Carboniferous deep continental subduction and continental collision, which resulted in high grade metamorphism at different pressures and widespread late intrusion of granitoids (Franke, 2000; O'Brien, 2000; Timmerman, 2008; Scott et al., 2013; Schulmann et al., 2014). Traditionally, the high grade part of the Variscan core is called the Moldanubian Zone whereas a mostly lower grade region to the north is called the Saxothuringian Zone. However, high grade eclogite, granulite and peridotite — including diamond- (Nasdala and Massonne, 2000; Kotková et al., 2011;) and coesite-bearing rocks (Massonne, 2001; Kotková et al., 2011;) — are located in both of these zones, questioning this traditional subdivision (Franke, 1989; Matte et al., 1990; O'Brien and Carswell, 1993; Medaris et al., 1995).

For the most part, older (380-400 Ma) eclogites are associated with spinel peridotites whereas younger, 340 Ma eclogites and so-called HP-granulites (eclogite facies metagranitic rocks) occur with serpentinized garnet peridotites. Such garnet peridotite bodies are reported mainly from six different granulite terrains in the Bohemian Massif: the Saxonian Granulite Complex (Granulitgebirge, Saxothuringian Zone), the Ohře Crystalline complex and České Středohoři Mountains (Saxothuringian Zone, NW of Prague), Sowie Góry (Sudetes, Poland), the Gföhl Unit in South Bohemia, Lower Austria and West Moravia (Medaris & Carswell, 1990). The host rocks in all cases are felsic HP granulites (eclogite facies metagranites with granulite facies overprint; O'Brien and Rötzler, 2003) or their migmatized version, termed Gföhl gneiss (Cooke and O'Brien, 2001).

This study focuses on the Saxonian Granulite complex in the Granulitgebirge.

The Granulitgebirge, well known for the granulite type locality (Weiss, 1803), is located on the north-western portion of the Saxothuringian Zone (eastern Germany) (Fig. 4.1-4.2). It comprises a NE-SW trending dome-like body over 50 km long and 20 km wide mostly made of HP quartzo-feldspathic granulites with minor layers of pyroxene-bearing granulites of intermediate to basic composition which represent the deepest structural unit (Carswell and O'Brien, 1993; O'Brien, 2000, 2006, 2008; O'Brien and Rötzler, 2003; Rötzler et al., 2008). A detachment fault divides the granulite from the lowest structural unit of the Schist Cover. These schists experienced a low pressure (LP) high temperature (HT) metamorphism related to the emplacement of the hot granulites via "hot core complex" extensional mechanism (O'Brien and Carswell, 1993; Reinhardt and Kleemann, 1994). Between these two structural units slivers of cordierite- and garnet-rich gneisses, metaophiolites and orthogneisses may occur. All this complex is then intruded by stocks and sills of monzogranite (O'Brien, 2000; Rötzler et al., 2008; Schmädicke et al., 2010 and references therein; Fig. 4.2).

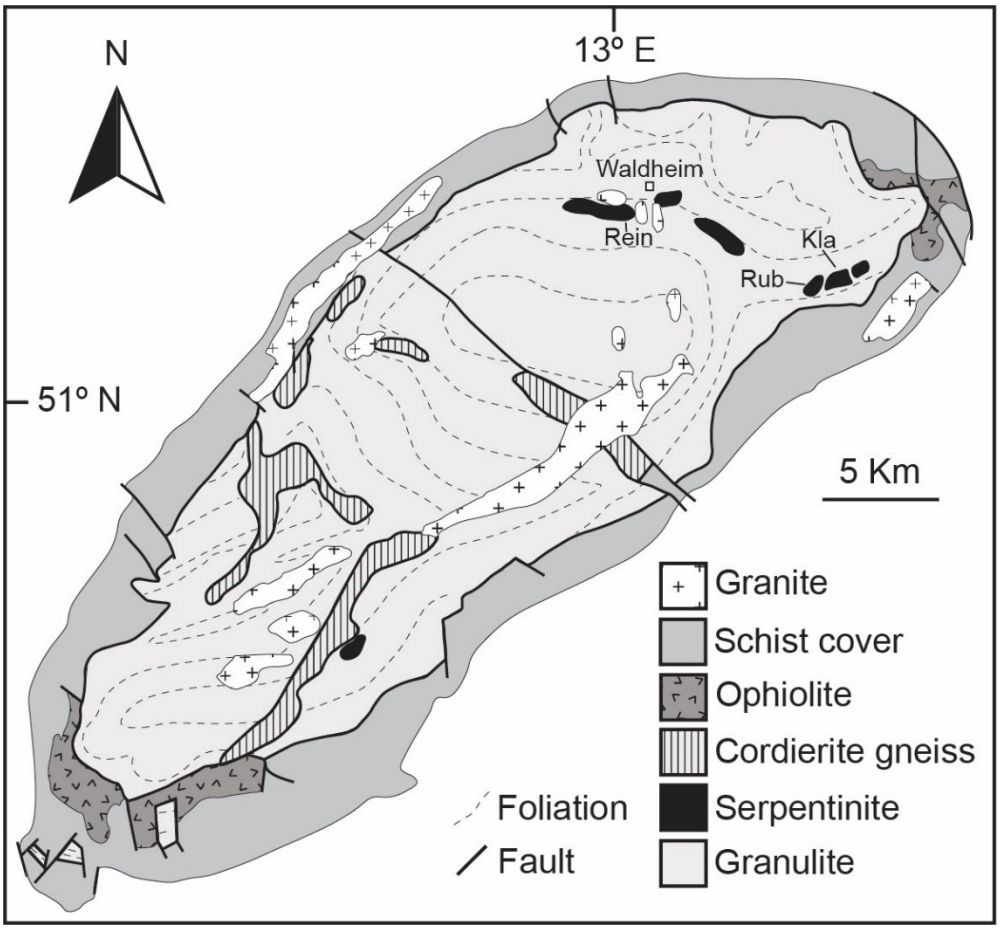

Figure 4.2. Schematic geological map of the Granulitgebirge (modified after Rötzler et al., 2008) with locations of the two selected areas Rub= Rubinberg and Kla= Klatschmühle and the localities with the former clinopyroxene megacrysts (see text for details). Rein = Reinsdorf.

The dominant lithology in the Granulitgebirge consists of granulite with hypersolvus ternary feldspar (now mesoperthite) and quartz with a variable amount of garnet and kyanite along with rutile, apatite and zircon as accessories (Rötzler and Romer, 2001; O'Brien, 2006, 2008;). Granulites have a mylonitic structure with platy quartz and sometimes a banding defined by secondary biotite (O'Brien, 2006, 2008; Rötzler et al., 2008). Geochemical and isotope data suggest that most of the granulites have an igneous origin (Werner, 1987; Rötzler et al., 2008) with a protolith age around *c.* 470-485 Ma (von Quadt, 1993; Kröner et al., 1998; Rötzler et al., 2001, 2004). Enclosed in the felsic rocks are bodies of serpentinized garnet peridotite which in turn contain layers and lenses of garnet + clinopyroxene-rich rocks (O'Brien and Carswell, 1993; Massonne and Bautsch, 2002; O'Brien, 2008; Rötzler et al., 2008; Schmädicke et al., 2010; Borghini et al., 2018).

The P-temperature (T) peak conditions estimated for the granulite and garnet clinopyroxenite are 1000-1015 ºC and 2.0-2.2 GPa (Rötzler et al., 2008), ultra-high temperature (UHP) eclogitic facies, and the metamorphic peak at *c.* 340 Ma (Rötzler and Romer, 2001) was followed by rapid exhumation and cooling to middle crustal levels (O'Brien and Rötzler, 2003). Similar metamorphic ages are observed in comparable felsic granulite-peridotite-pyroxenite complexes rocks elsewhere in the high grade Variscan core, e.g. in the Erzgebirge, North Bohemia, and Gföhl unit of the Moldanubian Zone, thus suggesting a common early evolution. However, the age determined for the pyroxenite of Klatschmühle is instead 380 Ma (von Quadt, 1993) and this aspect will be discussed below (§ 4.6.1).

4.3 METHODS AND SAMPLE SELECTION

The study has been realized on ~30 µm thin- and double-polished thick-sections (150 µm thick). Sample preparation, petrographic study with a polarized-light optical microscope, micro-Raman and electron microprobe (EMP) analysis were performed at the Institut für Geowissenschaften of the University of Potsdam. The micro-Raman analyses were carried out using a HORIBA Jobin Yvon Confocal LabRAM HR 800 equipped with a Peltier cooled multichannel CCD detector and anOlympus BX41 petrographic microscope. The excitation was obtained using an air-cooled Nd:YAG laser (λ=532 nm, laser power on the sample was 2–3 mW) with the 100X objective. The slit width was set to 100 µm and the confocal hole to 200 µm. All the spectra were acquired with a grating of 300 lines/mm using the multiwindows option in the wavenumber range between 100 and 4000 cm^{-1} integrating 3 repetitions of 100s with spectral resolution of about 10 cm^{-1} (see procedure in Ferrero et al., 2015). A microprobe JEOL JXA-8200 was used to analyze glass and rock mineral phases. The analyses of re-homogenized glassy inclusions reported in this paper are the same used for Borghini et al. (2018) and they have been acquired with a beam diameter of 1 µm, 15kV and 3.5 nA. The microprobe has been calibrated with H_2O-bearing leucogranitic glass standards and the same analytical conditions have been applied in each session. The glass standard with H_2O content similar to the glassy inclusions has been used to estimate the correction factor for Na, K, Al and Si because of the common alkali-loss in analyses on alkali-rich melt (Morgan & London, 2005). The field emission gun electron microprobe (FEG-EMP) JEOL Hyperprobe JXA-8500F of the Museum für Naturkunde in Berlin was used to acquire backscattered electron (BSE) images and energy dispersive spectrometer (EDS) elemental maps for high resolution microstructural and microchemical investigation.

The trace element contents were quantified using laser ablation – inductively coupled plasma – mass spectrometry (LA-ICP-MS) at the Department of Earth Sciences, ETH Zürich. The

analyses were performed on one thick section for each locality to study the trace elements of mineral phases and on 21 garnet chips separated from two double-polished thick sections (11 chips for Rubinberg and 10 chips for Klatschmühle) to investigate trace elements in selected, unexposed glassy and crystallized inclusions. For the analyses of trace elements in minerals, a RESOlution (Australian Scientific Instruments/Applied Spectra) laser ablation system equipped with a S-155 dual-volume ablation cell (Laurin Technic, Australia) with an effective volume of ca. 1 cm^3 has been used. For these analyses, a laser repetition rate of 5 Hz, on-sample energy density of ca. 3.5 $J.cm^{-2}$ and spot size of 29 µm has been used. For the MI analyses, the ETH-prototype GeoLas laser ablation system equipped with an Excimer ArF (193 nm) COMPex 102F laser source (Coherent, Germany) has been used. A laser repetition rate of 10 Hz, on-sample energy densities in the range of 5–10 $J.cm^{-2}$ and spot sizes between 10 and 30 µm, based on the different inclusion sizes, has been used. In general, the inclusion diameter was slightly smaller than the selected spot size in order to ablate completely the inclusion and avoid the unrepresentative sampling related to heterogeneity therein. This paper reports a limited version of the MI dataset of Borghini et al. (2018) with a selection of the inclusions with the strongest signal (i.e. highest signal-to-background ratio).

Both laser systems were coupled to an Element XR (Thermo Fischer, Germany) sector-field ICP-MS. The carrier gas consisted of high-purity He (5.0 grade, 0.5 to 1.0 $L.min^{-1}$) to which was admixed make-up Ar gas (6.0 grade, 0.9 to 1.0 $L.min^{-1}$). For all analyses, the instrument was optimized based on ablation of the NIST SRM612 glass (43 µm raster at 5 $\mu m.s^{-1}$, 10 Hz, and 3.5 $J.cm^{-2}$) for highest sensitivity on the high mass range, low production of oxides ($^{248}ThO^+/^{232}Th^+$ <0.4%) and U/Th of ca. 1. The intensities were acquired in low-resolution, peak jumping and triple detector mode, with a dwell time of 10 ms for all elements (total sweep times were 750 ms for minerals and 782 ms for MI). The list of isotopes used for each element are reported in the data repository of Borghini et al., 2018 for the different types of analyses.

The glass reference material NIST SRM610 (Jochum et al., 2011) has been used for drift correction and the quantification of the inclusion analyses, ablated at the same conditions as the unknowns, except for an energy density of *ca.* 5 $J.cm^{-2}$ and spot size of 40 µm for MI analyses (for more details see data repository of Borghini et al., 2018). The USGS glass reference materials GSD-1G and GSE-1G were used as validation reference materials (respectively for minerals and MI analyses) to check the accuracy and reproducibility of the analyses. All data processing was performed offline. The acquired time-resolved signals were processed using the software SILLS (Guillong et al., 2008). EMP concentrations were used as internal standards for deconvolution of host and inclusion signals and relative sensitivity correction for both mineral phases and

inclusions. The EMP concentration of Al_2O_3 has been used as internal standard for garnet whereas CaO has been used for clinopyroxene. For the melt inclusion analyses the EMP concentration of Na_2O in the melt has been used as internal standard whereas FeO (for Rubinberg) and MgO (for Klatschmühle) have been used as matrix-only tracer. The elements more enriched in the host (e.g. Y, HREE) with respect to the inclusions are not quantifiable using this method because of the dominance of the host signal, which prevents the deconvolution software from successfully discriminating and quantifying their concentration in the inclusions.

4.4 FIELD OCCURENCES AND SAMPLE PETROGRAPHY

The investigated garnet + clinopyroxene-rich rocks occur as boudinaged layers surrounded by foliated peridotite at two localities: Rubinberg (RUB; 51º1’57” N, 13º7’37” E) and Klatschmühle (KLA; 51º2’38” N, 13º8’43” E) (Fig. 4.2). At RUB the samples are from an abandoned quarry where one single layer of garnet + clinopyroxene-rich rock, approximately 25 cm thick and 25 m long, is present whereas at KLA the outcrop is on a slope and the single layer is 40 cm thick and 5 m long (Fig. 4.3a–b). The host in both cases is a serpentinized garnet peridotite with foliation defined by lozenge-shaped pyroxene in which coarse grained crystals of garnet (>5 mm in diameter) and fragmented olivine occur as relicts in a matrix dominated by serpentine. The garnet + clinopyroxene-rich layers are oriented parallel to the main foliation in the peridotite and they have sharp contacts with the host.

The garnet + clinopyroxene-rich rocks of the two localities show similar petrographic features (Fig. 4.3c–d). They have a granoblastic texture dominated by slightly variable amounts of garnet (40-45 % in volume) and clinopyroxene (45 %) constituting the assemblage at the HP-UHT metamorphic peak with rutile and ilmenite as accessories. The matrix is medium- to fine-grained and it contains interstitial plagioclase, late brown amphibole — in places associated with ilmenite and apatite (Fig. 4.3f) and rare late biotite. The matrix assemblage represents a post-peak stage in the rock history. Leucocratic pockets (Fig. 4.3e) of fine-grained plagioclase occur in some of the samples and show gradational contact with the host rock. The more retrogressed samples show a larger amount of matrix phases and fresh garnet and clinopyroxene occurring only as relicts.

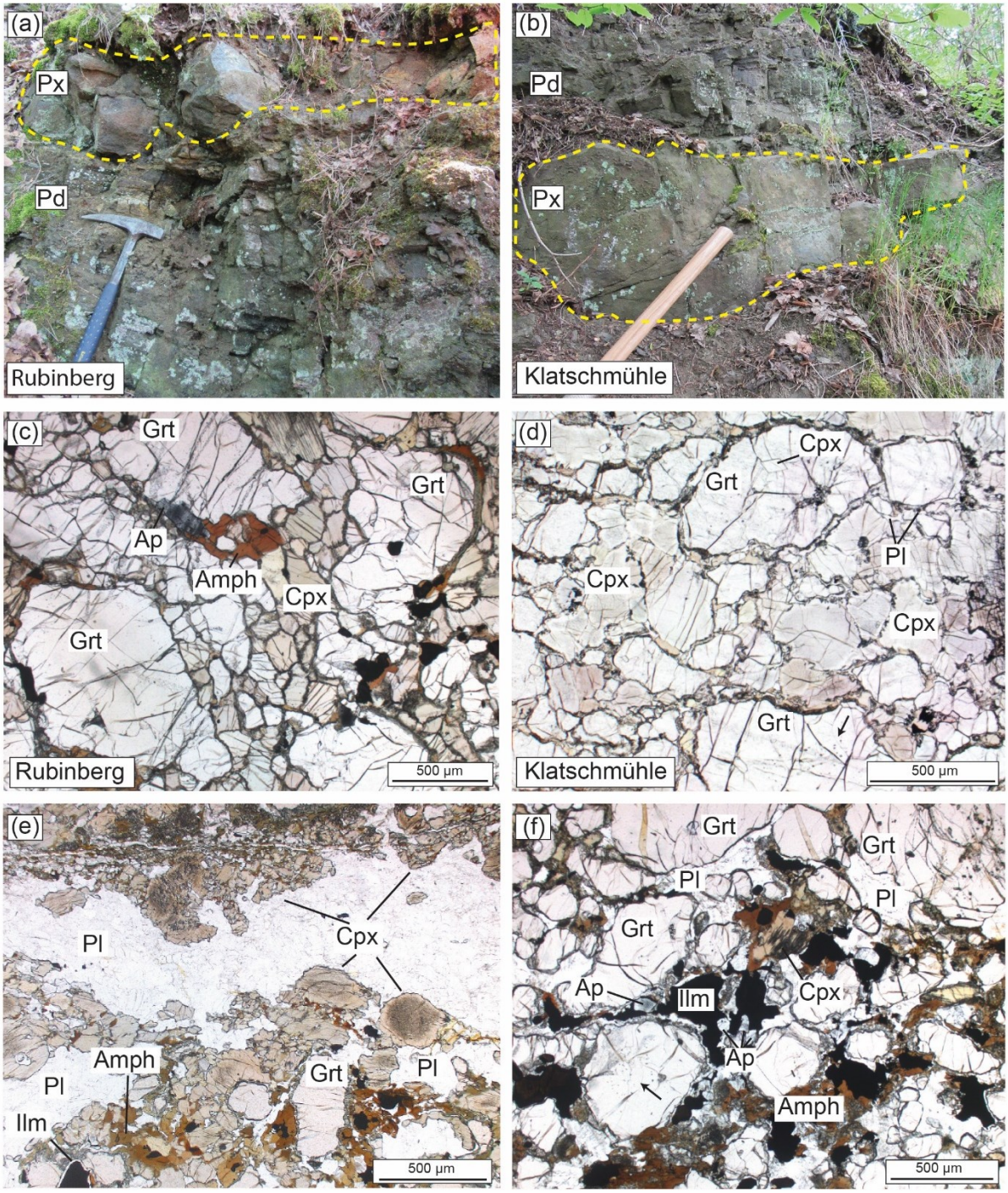

Figure 4.3. Field occurrence of the eclogite, formerly called garnet clinopyroxenite (Px), marked by a yellow dashed line, in Rubinberg (a) and Klatschmühle (b) enclosed in the foliated peridotite (Pd). Plane-polarized photomicrographs of the garnet clinopyroxenites with a granoblastic texture (c - d) dominated by garnet (Grt) and clinopyroxene (Cpx). The matrix contains plagioclase (Pl), both interstitial and in (e) leucocratic pockets, (f) brown amphibole (Amph) in some cases associated with ilmenite (Ilm) and apatite (Ap).

In the investigated samples garnet is euhedral, 1–2 mm in diameter and colorless. It contains clinopyroxene - sometimes rimmed by plagioclase films - rutile, ilmenite and MI mainly organized in clusters or in some cases in secondary/pseudosecondary trails (Fig. 4.4). Dark trails of fluid inclusions crossing the whole crystal are often visible. Garnet often contains cracks filled with plagioclase and green amphibole. Along rims it may be replaced by (i) a symplectite of plagioclase and green amphibole; (ii) plagioclase coronas/films or (iii) brown amphibole in fine-grained films or associated with ilmenite and apatite (Fig. 4.3f). Clinopyroxene is generally 1–3 mm long, subhedral, pale beige and it has a short prismatic shape with often a cloudy core and a clear rim. In the core, it can contain plagioclase in lamellae and blebs and rutile inclusions. Along the rim clinopyroxene is partially replaced by brown amphibole sometimes in an aggregate of ilmenite with or without apatite.

Plagioclase, more abundant in the retrogressed samples, is mainly interstitial. It can also occur in leucocratic pockets. In the fresh samples it forms more or less continuous thin films around garnet (Fig. 4.3d) and clinopyroxene and it shows polysynthetic twinning. In the leucocratic pockets the plagioclase is fine-grained with a patchy extinction and often with subgrain microstructures (Fig. 4.3e). The brown amphibole in the matrix often forms aggregates with ilmenite ± apatite and it is sometimes replaced along the rim by green amphibole. The apatite occurs in almost all the samples and it displays a cloudy core full of CO_2-rich fluid inclusions (verified via micro Raman spectroscopy). Rutile and ilmenite in the matrix are often coarse-grained, with rutile rimmed by ilmenite.

4.5. RESULTS

4.5.1 PETROGRAPHY OF NANOGRANITOIDS AND GLASSY INCLUSIONS

Two types of MI have been identified in garnets based on their microstructural distribution (Fig. 4.4). The first type is dominant and consists of a cluster in the inner part of the garnet (Fig. 4.4a-b–c–d). The random distribution suggests that these MI are primary, thus they were trapped while the garnet was growing (Borghini et al., 2018). The second type of polycrystalline MI was recognized only in three RUB samples and it occurs in trails that cross-cut the crystal and the cluster of primary MI (Fig. 4.4a–e).

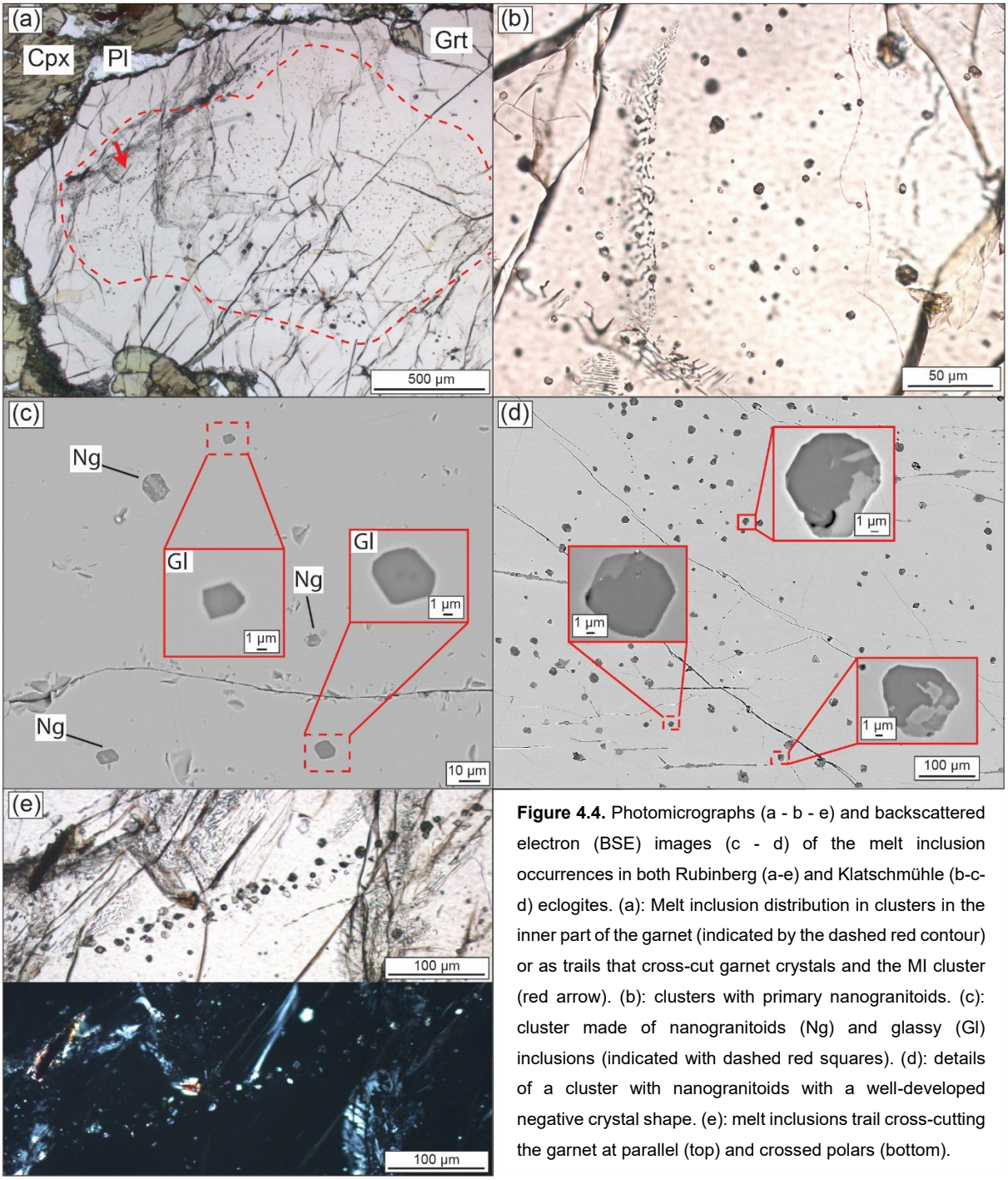

Figure 4.4. Photomicrographs (a - b - e) and backscattered electron (BSE) images (c - d) of the melt inclusion occurrences in both Rubinberg (a-e) and Klatschmühle (b-c-d) eclogites. (a): Melt inclusion distribution in clusters in the inner part of the garnet (indicated by the dashed red contour) or as trails that cross-cut garnet crystals and the MI cluster (red arrow). (b): clusters with primary nanogranitoids. (c): cluster made of nanogranitoids (Ng) and glassy (Gl) inclusions (indicated with dashed red squares). (d): details of a cluster with nanogranitoids with a well-developed negative crystal shape. (e): melt inclusions trail cross-cutting the garnet at parallel (top) and crossed polars (bottom).

They post-date the garnet formation thus they can be interpreted as secondary (Cesare et al., 2015; Ferrero et al., 2018a). For the purpose of this paper we will focus exclusively on the primary inclusions.

Primary MI are either fully glassy or crystallized as nanogranitoids (Cesare et al., 2015). Glassy inclusions, 2–5 µm in diameter, were identified only in RUB samples and are isotropic

under crossed polarizers. They occur in the same cluster with the nanogranitoids but represent just a modest fraction (< 10 %) of the inclusions occurring in the cluster, and they are generally smaller (Fig. 4.4 c and 4.5d). Their shape varies from isometric to prismatic and often they contain rutile. Nanogranitoids, 5–20 μm in diameter, were identified in both localities. They are mostly brown under plane-polarized light, and have a well-developed negative crystal shape, in some cases with minor cracks that do not reach the garnet borders (Fig. 4.5a–c). The mineral assemblage is kumdykolite or albite, phlogopite/biotite, osumilite and kokchetavite, with a variable amount of quartz, pyroxene, carbonate and rare white mica (Fig. 4.5 and 4.6; see also Borghini et al. 2018).

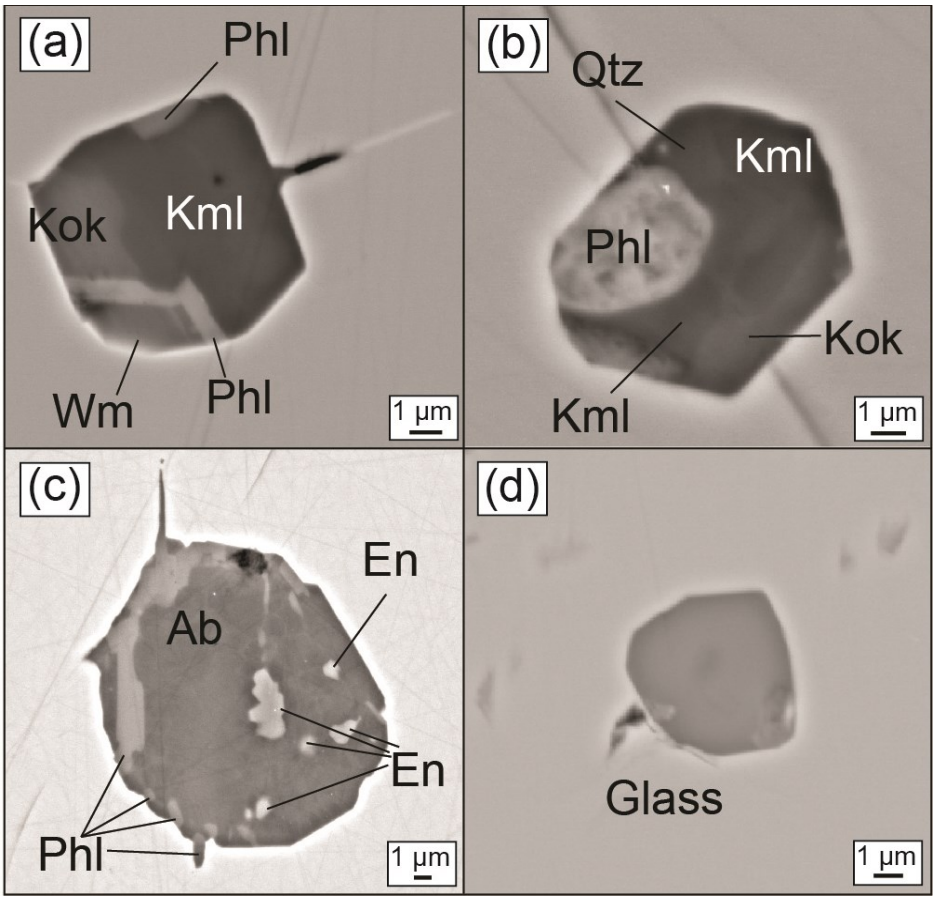

Figure 4.5. BSE images of nanogranitoids and a glass inclusion with a well-developed negative crystal shape. (a): nanogranitoid containing kumdykolite (Kml), kokchetavite (Kok), phlogopite (Phl) and white mica (Wm) with crack of limited extension that does not reach the rim of the host crystal. (b): nanogranitoid that contains also quartz (Qtz), the line crossing the inclusion is not a crack but due to polishing (c): nanogranitoids with phlogopite, enstatite (En) and albite (Ab) and a crack of limited extension that, as for (a), does not reach the rim of the crystal. (d): glassy inclusions with a dark spot in the center due to the microprobe beam damage.

Kokchetavite and carbonate are generally more abundant in RUB samples whereas osumilite, pyroxene and white mica occur more often in KLA.

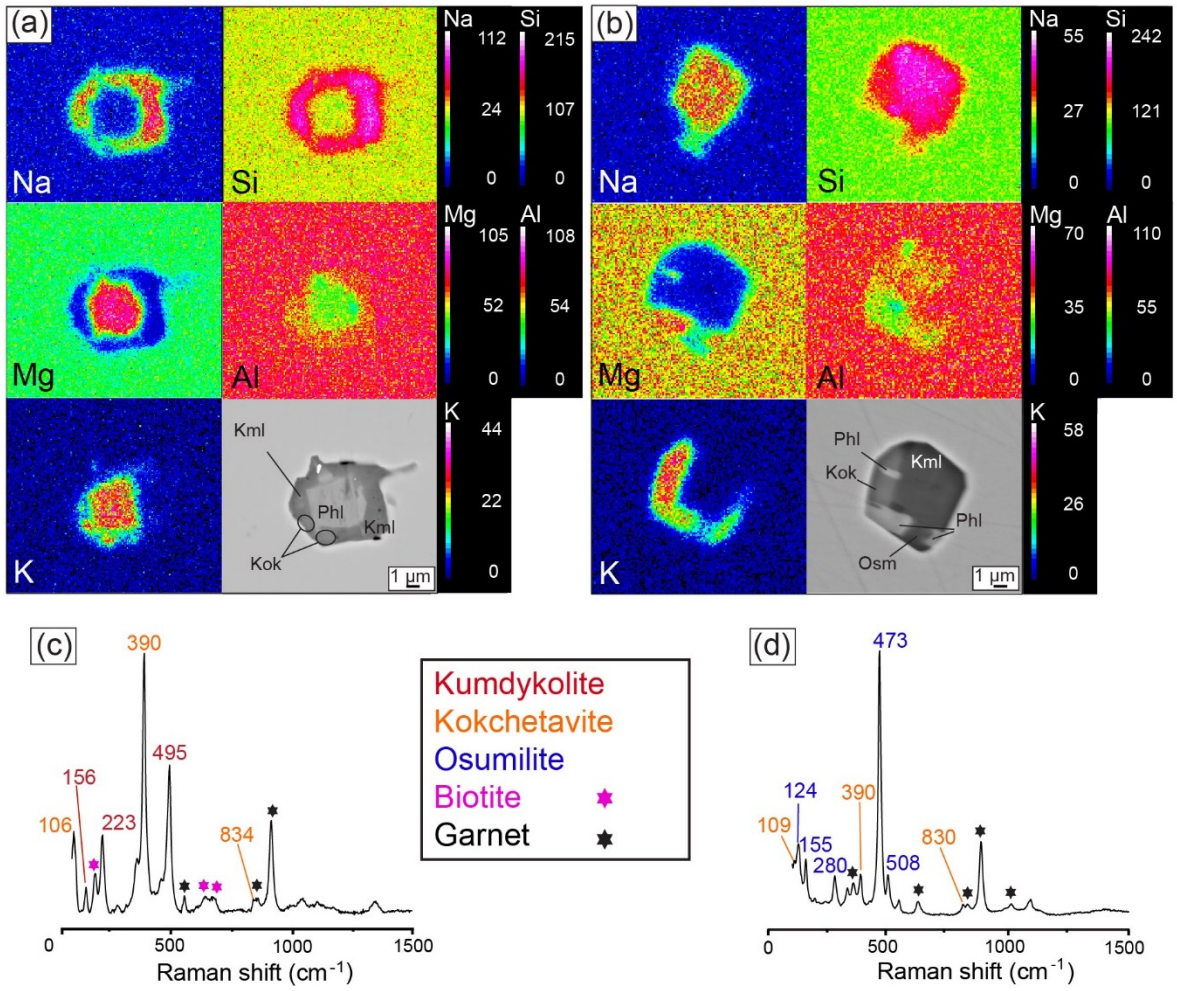

Figure 4.6. (a - b): EDS elemental maps of nanogranitoids with (a) kumdykolite, phlogopite and kokchetavite and (b) kumdykolite, phlogopite, kokchetavite and osumilite (Osm). (c - d) Raman spectra of (c) kumdykolite and kokchetavite and (d) osumilite and kokchetavite.

Kumdykolite, the orthorhombic polymorph of $NaAlSi_3O_8$ and kokchetavite, the hexagonal polymorph of $KAlSi_3O_8$, were reported for the first time together in nanogranitoids by Ferrero et al. (2016b). $NaAlSi_3O_8$ is present mainly in the orthorhombic form i.e. kumdykolite rather than in its triclinic one i.e. albite that is rare and mostly in inclusions showing noticeable cracks. Phlogopite forms euhedral to subhedral lamellae and often nucleates on the inclusion walls (Fig. 4.5 a-b-c and 4.6 b). Osumilite crystals often extend from wall to wall and do not develop an euhedral shape. Kokchetavite has commonly a prismatic elongated shape but in some MI it is

anhedral and crystals often grow associated with kumdykolite. Plagioclase may occur instead of kumdykolite in subhedral tabular crystals. Quartz is always anhedral and interstitial whereas pyroxene (mostly enstatite) is generally subhedral with a prismatic, locally stubby shape. White mica, commonly associated with phlogopite, is mainly subhedral. Overall, nanogranitoids show the following crystallization sequence based on the microstructural features of the phases in the inclusions: biotite, pyroxene, white mica, kumdykolite/albite and kokchetavite, osumilite and quartz.

4.5.2 BULK ROCK GEOCHEMISTRY

The bulk rock composition has been analyzed in three samples from each locality (see average Table 4.1 and complete dataset in the Supplementary material C Table S4.1). Most, though not all, elements show similar abundances in both localities, e.g. Al_2O_3 (RUB 15.6 wt% vs KLA 16 wt%), CaO (12 wt% vs 11.7 wt%), MgO (11.23 wt% vs 11.58 wt%) and MnO (0.24 wt% vs 0.20 wt%). SiO_2 is higher in KLA samples (45.5 wt % vs 43.9 wt %) whereas FeO and TiO_2 contents are higher in those from RUB (FeO: 14.16 wt % vs 12.26 wt %; TiO_2: 1.57 wt % vs 1.01 wt %) and Na_2O is generally high in both with respect to a typical pyroxenite (RUB 1.59 wt % vs KLA 1.94 wt %). The magnesium number (Mg# = [molar Mg/(Mg+Fe^{2+}_{tot}) x 100]) is slightly lower in RUB (58) than in KLA (62) samples. The geochemistry of RUB and KLA samples can be compared with the extensively studied pyroxenites and eclogites in the peridotite bodies of the Gföhl Unit in the Moldanubian Zone as well as with other standard compositions such as N-MORB (data from Workman and Hart, 2005) (Table 4.1 and Fig. 4.7). Whereas pyroxenites and eclogite are present across the whole Bohemian Massif, those from Mohelno, Horní Bory and Nové Dvory were selected for the comparison because these three localities gave their names to the three different type of peridotite of the Moldanubian Zone, as classified by Medaris et al., (2005) based on their chemical features. The SiO_2 contents of the RUB and KLA samples are in the range defined by the whole dataset (43–52 wt%). The Al_2O_3 and MgO contents are similar to those of kyanite eclogite and N-MORB whereas they are higher and remarkably lower, respectively, than for the whole dataset of Moldanubian pyroxenites. The CaO contents of the investigated pyroxenites are instead lower than the kyanite eclogite, and closer to that of the Horní Bory pyroxenite, which has the highest CaO among the Moldanubian pyroxenites and average N-MORB. The RUB and KLA samples show the lowest Mg# of the whole investigated dataset whereas other oxides are higher e.g., FeO in both localities, TiO_2 in RUB and Na_2O in KLA.

Locality	Rubinberg Granulitgebirge (BM)	Klatschmühle Granulitgebirge (BM)	Mohelno Gföhl Unit (BM)	Horní Bory Gföhl Unit (BM)	Nové Dvory Gföhl Unit (BM)							Rubinberg Granulitgebirge (BM)	Klatschmühle Granulitgebirge (BM)	Batan island, Luzon Arc (Philippines)
Sample type	Grt-clinopyroxenite	Grt-clinopyroxenite	Spl-websterite	Ol Grt-clinopyroxenite	ND1: Grt-clinopyroxenite	ND2: Grt-websterite	ND3: Kyanite eclogite	N-MORB	E-MORB	Low-SiO_2 adakite	High-SiO_2 adakite	Granitic melt	Granitic melt	melt in mantle xenoliths in arc lavas
	Bulk	Bulk	Bulk	Bulk	Bulk	Bulk	Bulk	Bulk	Bulk	Bulk	Bulk	MI	MI	MI
No. analyses	3	3	2	1	2	1	3			77	267	7	6	12
wt %														
SiO_2	43.93	46.07	44.45	47.65	43.61	52.15	48.60	49.51	-	56.25	64.8	70.95	64.85	59.22
TiO_2	1.57	0.77	0.11	0.45	0.14	0.22	0.29	0.90	-	1.49	0.56	0.03	0.14	0.19
Al_2O_3	15.57	16.40	5.36	4.89	11.36	5.96	17.58	16.75	-	15.69	16.64	16.84	18.28	17.72
Fe_2O_3	0.00	0.00	3.53	1.73	2.26	1.37	0.00	-	-	-	-	0.00	0.00	-
FeO	14.16	11.62	3.65	5.53	3.96	4.04	5.09	8.05	-	6.47	4.75	0.56	1.60	2.62
MnO	0.24	0.18	0.12	0.14	0.15	0.13	0.10	0.14	-	0.09	0.08	0.03	0.07	0.09
MgO	11.23	10.11	30.89	23.13	23.38	22.73	10.81	9.74	-	5.15	2.18	0.22	0.99	0.79
CaO	12.05	11.89	3.89	12.99	7.07	10.34	14.94	12.50	-	7.69	4.63	0.43	1.55	4.05
Na_2O	1.59	2.22	0.25	0.44	0.37	0.51	1.80	2.18	-	4.11	4.19	5.43	5.52	4.16
K_2O	0.07	0.42	0.02	0.01	0.02	0.04	0.04	0.07	-	2.37	1.97	5.06	5.40	2.94
P_2O_5	0.12	0.16	0.02	0.02	0.04	0.03	0.04	0.10	-	0.66	0.2	0.03	0.27	0.40
LOI	0.12	0.29	7.33	2.64	7.32	2.07	-	-	-	-	-	-	-	-
TOTAL	100.64	100.13	99.59	99.62	99.65	99.59	99.28	99.93	-	99.97	100.00	99.57	98.67	92.18
ASI										0.67	0.95	1.12	1.04	1.02
CaO/Al_2O_3	0.77	0.73	0.73	2.66	0.62	1.73	0.85	0.75	-	0.49	0.28	0.03	0.08	0.23
Mg#	58	61	89	85	88	89	79	71	-	58	45	32	50	34
ppm														
Cr	367	500	-	-			780			157	41	-	-	37
Ni	91	74	1361	878	660	755	113			157	20	-	-	-
Rb	8.13	22	1.87	0.88	0.79	1.62	3.98	0.56	5.04	19	52	176*	265*	-
Cs	22	21	0.37	0.09	0.05	0.34	0.28	0.01	0.06	-	-	45	63	-
Ba	139	142	9.14	2.22	14	162	28	6.30	57	1087	721	678	403	-
Th	1.50	0.60	0.07	0.14	0.12	0.68	b.d.l.	0.12	0.60	-	-	105	39	-
U	1.03	0.20	0.03	0.08	0.07	0.10	b.d.l.	0.05	0.18	-	-	23	13	-
Nb	11	6.53	0.22	0.34	0.17	1.24	0.59	2.33	8.30	11	6.00	2.75	4.08	7.92
Ta	0.83	0.70	-	-	-	-	-	0.13	0.47	-	-	1.01	0.85	-
La	9.20	9.67	0.35	0.80	0.74	5.08	0.34	2.50	6.30	41	19	23	11	51
Ce	21	22	0.80	2.36	2.33	14	1.17	7.50	15	90	38	39	24	81
Pb	4.07	1.60	1.53	2.13	1.08	3.73	-	0.30	0.60	-	-	59	36	-
Pr	2.86	3.00	0.11	0.43	0.39	1.95	0.25	1.32	2.05	-	-	3.48	3.23	-
P	1167	1633	150	200	350	300	367	510	620	-	-	670	460	-
Sr	98	153	10	65	48	138	109	90	155	2051	565	126	128	552
Nd	13	14	0.61	2.55	2.28	8.38	1.29	7.30	9.00	47	18	10	11	19
Zr	69	65	2.84	11	12	18	9.30	74	73	188	108	68	169	186
Hf	2.10	2.13	0.14	0.50	0.40	0.62	0.28	2.05	2.03	-	-	3.71	5.20	-
Sm	3.79	3.70	0.23	0.96	0.95	1.66	0.61	2.63	2.60	7.80	3.40	6.51	4.07	2.51
Eu	1.11	1.09	0.09	0.36	0.27	0.40	0.36	1.02	0.91	2.00	0.90	3.15	2.10	-
Gd	4.88	4.23	0.41	1.42	1.64	1.52	0.74	3.68	2.97	4.80	2.80	-	-	-
Tb	0.90	0.66	0.08	0.25	0.38	0.22	0.17	0.67	0.53	-	-	-	-	-
Dy	5.91	3.71	0.60	1.58	3.00	1.25	1.13	4.55	3.55	2.80	1.90	-	-	1.06
Ti	15700	7667	1050	4500	1400	2200	287	7600	6000	-	-	3105	1454	1140
Y	34	19	5.46	8.87	21	8.52	6.59	28	22	13	10	-	-	5.92
Ho	1.33	0.72	0.14	0.31	0.75	0.22	0.27	1.01	0.79	-	-	-	-	-
Er	4.07	1.91	0.43	0.87	2.57	0.67	0.67	2.97	2.31	1.12	0.96	-	-	-
Tm	0.58	0.25	0.06	0.12	0.42	0.09	0.10	0.46	0.36	-	-	-	-	-
Yb	3.78	1.52	0.45	0.73	2.91	0.58	0.70	3.05	2.37	0.93	0.88	-	-	0.69
Lu	0.57	0.22	0.07	0.10	0.45	0.09	0.10	0.46	0.35	0.08	0.17	-	-	-
Li	n.d.	n.d.	5.67	3.24	11.22	4.67	-	4.30	3.50	-	-	50	52	-
B	n.d.	n.d.	-	-	-	-	-	-	-	-	-	70	58	-

LOI= loss on ignition
b.d.l.= below detection limit
n.d.= not determined
*the trace element averages of the melt are the maximum averages.

Table 4.1. Whole rock major and trace element composition of Rubinberg and Klatschmühle eclogites compared with the Moldanubian pyroxenite (Mohelno, Horní Bory and Nové Dvory) and kyanite eclogite and N- and E-MORB (LOI= loss on ignition).

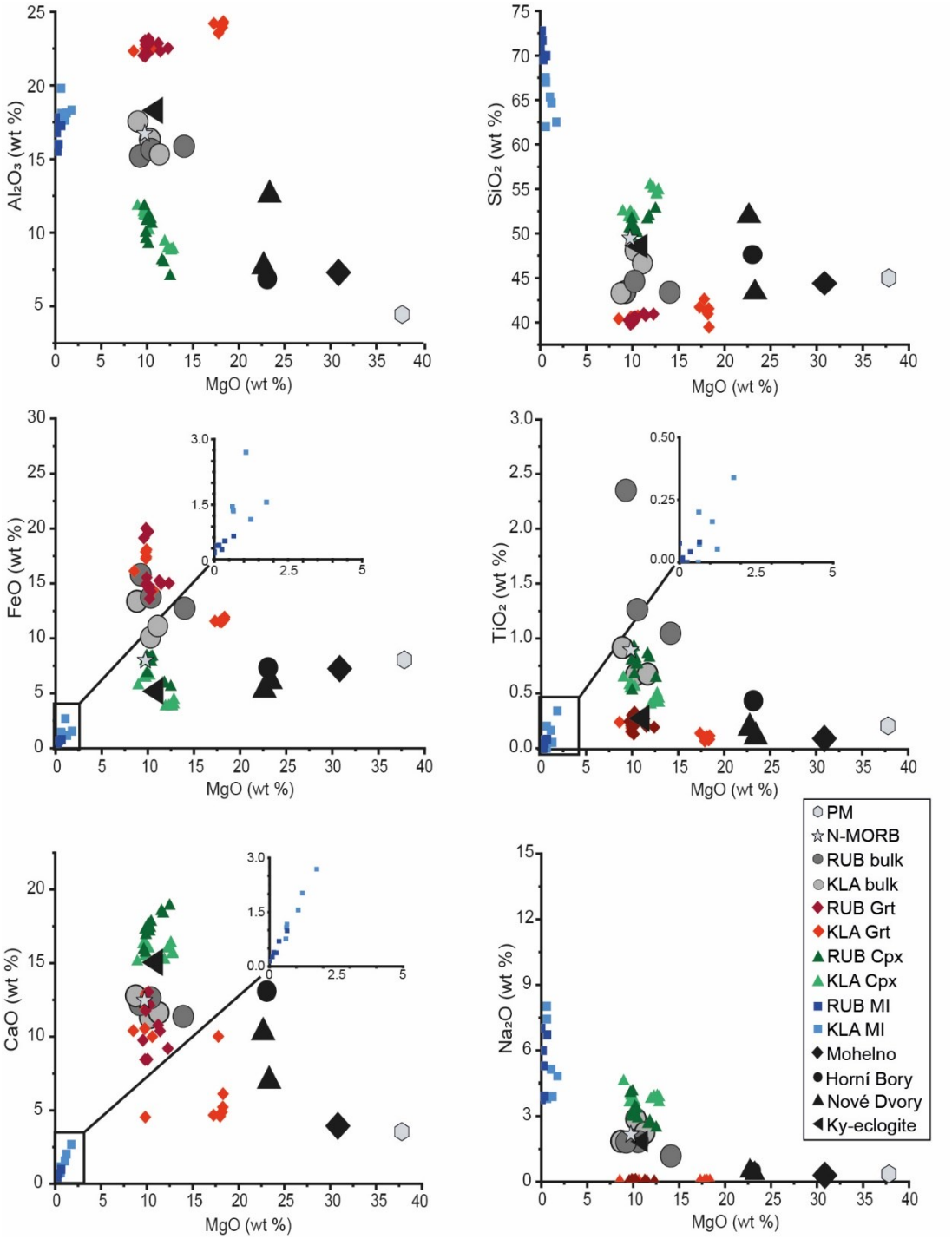

Figure 4.7. Variation of the major oxides relative to the wt. % MgO of whole-rock (see Table 4.1, S4.1 and Suppl. Mat. Borghini et al., 2018), constituent minerals (Grt and Cpx) and melt inclusions of Rubinberg (RUB) and Klatschmühle (KLA) eclogite. They are compared with the pyroxenites (Mohelno, Horní Bory and Nové Dvory; from Svojtka et al., 2016) and kyanite eclogite (Obata et al., 2006) of the Gföhl Unit in the Moldanubian Zone (original

data reported in Table 1), N-MORB (Workman and Hart, 2005; Table 4.1) and primitive mantle (PM; McDonough and Sun, 1995).

The trace element patterns of RUB and KLA samples are similar (Table 4.1 and Fig. 4.8). They both contain high amounts of Large Ion Lithophile Elements (LILE; Rb, Cs and Ba in addition to K) with a very strong Cs positive anomaly, a positive anomaly for U, Ti and to a lesser extent Ta, and a (mostly) slightly negative anomaly for Pb. RUB samples are richer in Cs, U, Nb, Ta and Ti than the KLA ones and show a negative Sr anomaly.

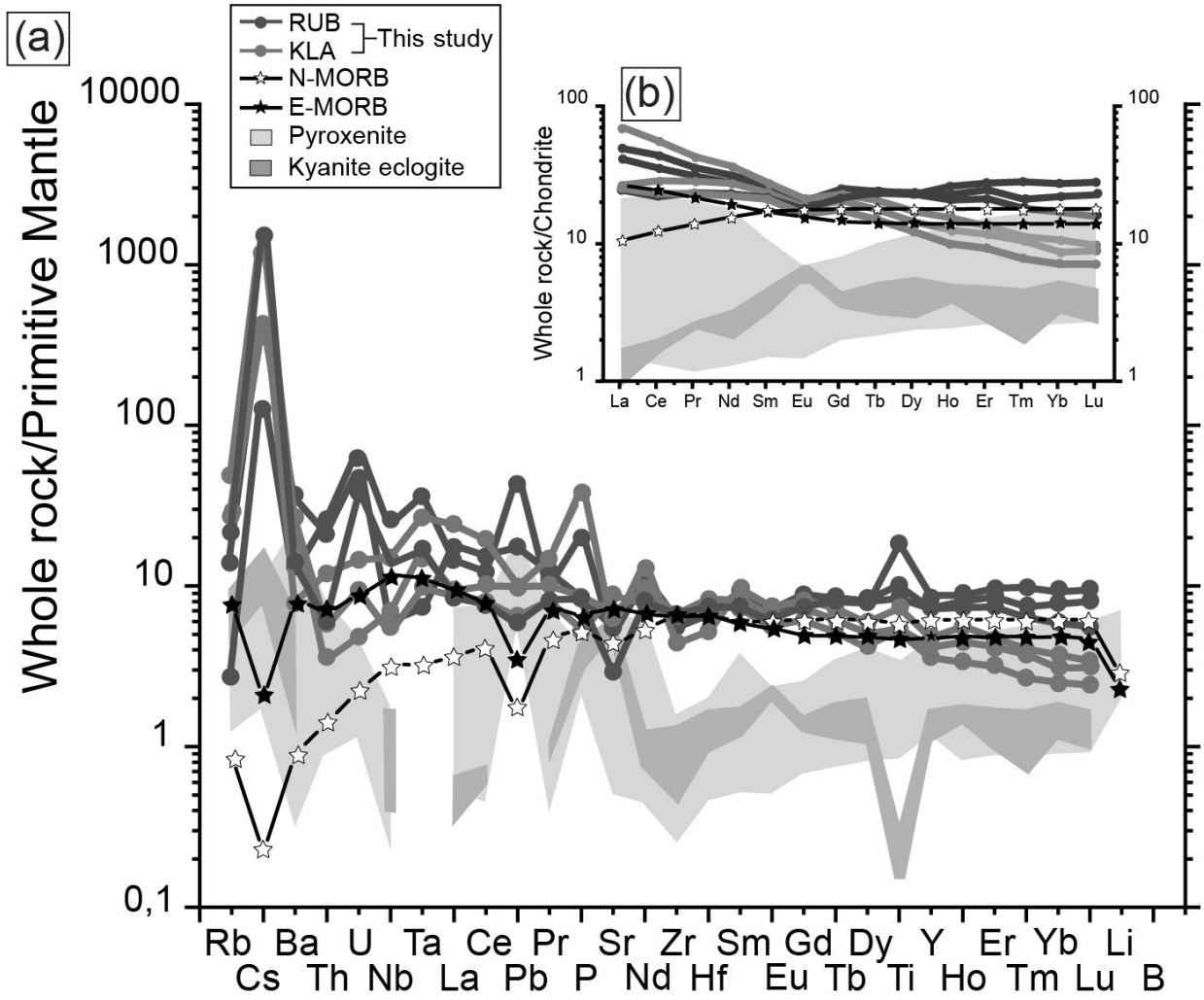

Figure 4.8. Whole-rock trace element patterns (a) and rare earth element (REE) patterns (b) of RUB and KLA (Table 4.1, S4.1 and Suppl. Mat. Borghini et al., 2018) compared with the whole dataset of the Moldanubian pyroxenite and eclogite (references for the data used in the plot are reported in caption to Figure 4.7) and the N- and E-MORB (both from Sun and McDonough, 1989). All the trace element data have been normalized to primitive mantle (Sun and McDonough, 1989 except for B, which is taken from McDonough & Sun, 1995) whereas the REE have been normalized to chondrite (Sun and McDonough, 1989).

The Rare Earth Element (REE) patterns for samples from both localities show no to weak fractionation with KLA samples slightly more fractionated with respect to RUB. For RUB samples, the pattern is almost flat with a slightly higher amount of light rare earth elements (LREE) with respect to the heavy rare earth elements (HREE) with average La_N/Yb_N = 1.87 whereas KLA samples have the same LREE content as RUB ones but show a slight depletion in HREE, resulting in average La_N/Yb_N = 4.4. Samples from both localities have a slightly negative Eu anomaly, and Eu_N/Eu^* ratios [$Eu_N/Eu^*=Eu_N/\sqrt{(Sm_N*Gd_N)}$] are 0.79 for RUB and 0.84 for KLA. The trace element patterns have been compared with the same dataset used for the major elements plus E-MORB (Fig. 8; data from Sun & Mc Donough, 1989). The LILE enrichment and the positive U and Ti anomaly are peculiar features of RUB and KLA samples whereas the negative Pb anomaly is similar to both MORB compositions but completely absent in the dataset of selected Moldanubian rocks, which rather shows instead a clear positive anomaly (Fig. 4.8a). Among the REE, the LREE patterns in RUB and KLA samples are similar to E-MORB but their concentrations are higher than all the other rocks, whereas the HREE are more abundant in RUB rocks and slightly more depleted in KLA samples when compared with the rest of the Moldanubian pyroxenites and both MORB compositions (Fig. 4.8b).

4.5.3 MINERAL CHEMISTRY

The main minerals in the rock representing the high PT stage of the evolution are garnet and clinopyroxene. The major and trace elements for these phases are plotted in Figs. 4.7 & 4.9, where they are compared to whole rock and mineral analyses from comparable rocks from other parts of the Bohemian Massif (the whole dataset is reported in Table 4.2, 4.3 and Table S4.2, S4.3, S4.4, S4.5, S4.6 and S4.7).

Garnet

In sample RUB garnet is in average pyrope (Prp) 39, almandine (Alm) 35, spessartine (Sps) 1 and grossular (Grs) 25 with Mg# =55. In contrast, in Klatschmühle the samples can be divided in two groups based on the different garnet compositions: $Prp_{66}Alm_{24}Sps_0Grs_{10}$ (KLA 1) with a Mg# =74 and $Prp_{37}Alm_{35}Sps_1Grs_{27}$ (KLA 2) with a Mg#=52. In all cases, a thin rim with lower Grs and higher Prp and Alm is discernible (see Fig. S4.1). Garnets from RUB and KLA 2 samples contain less Prp and a lower Mg# with respect to garnets in the Moldanubian garnet pyroxenites ($Prp_{57-71}Alm_{15-21}Sps_{0-1}Grs_{12-22}$; Mg#= 73-82; Svojtka et al., 2016) whereas garnet from specimen KLA 1 is very similar but with a lower Grs and higher Alm content. MI occur in the core of garnets in both RUB, KLA1 and KLA2 samples. Despite showing some compositional differences, both high-Prp and low-Prp garnets contain melt inclusions of essentially the same composition.

Locality	Rubinberg		Klatschmühle			Rubinberg		Klatschmühle	
Phase	Garnet					Clinopyroxene			
Sample name	RUB		KLA 1	KLA 2		RUB		KLA 1	KLA 2
wt %									
SiO_2	40.26	40.99	41.31	40.24		50.41	52.00	54.45	51.89
TiO_2	0.30	0.27	0.11	0.18		0.76	0.82	0.42	0.55
Al_2O_3	22.74	22.86	24.10	22.48		10.97	8.01	8.82	11.64
Fe_2O_3	-	-	-	-		-	-	-	-
FeO	15.55	15.26	11.49	17.28		7.80	5.89	3.80	6.41
MnO	0.27	0.33	0.19	0.34		0.07	0.06	0.02	0.05
MgO	9.88	11.23	18.00	9.80		10.38	11.80	12.62	9.75
CaO	11.77	10.79	4.88	10.41		17.41	18.37	16.32	16.44
Na_2O	0.08	0.04	0.05	0.03		3.36	2.77	3.91	4.03
K_2O	0.00	0.00	0.00	0.00		0.01	0.00	0.06	0.01
P_2O_5	0.10	0.06	0.05	0.06		0.01	0.01	0.01	0.00
TOTAL	100.95	101.84	100.18	100.83		101.17	99.74	100.43	100.77
Mg#	53	57	74	50		70	78	86	73
Si	2.99	3.00	2.96	3.00	Si	1.82	1.90	1.94	1.86
					Al IV	0.18	0.10	0.06	0.14
Ti	0.02	0.01	0.01	0.01	Fe^{+3}	0.00	0.00	0.00	0.00
Al	1.99	1.97	2.04	1.98	*cations T*	2.00	2.00	2.00	2.00
	2.01	1.98	2.04	1.99	Al VI	0.28	0.24	0.31	0.36
					Fe^{+3}	0.10	0.01	0.00	0.03
Fe	0.97	0.93	0.69	1.08	Ti	0.02	0.02	0.01	0.01
Mn	0.02	0.02	0.01	0.02	Cr	0.00	0.00	0.00	0.00
Mg	1.09	1.22	1.93	1.09	Mg	0.56	0.64	0.67	0.52
Ca	0.94	0.85	0.38	0.83	Fe^{+2}	0.14	0.17	0.11	0.16
	3.01	3.02	3.00	3.02	Mn	0.00	0.00	0.00	0.00
					cations M1	1.09	1.09	1.10	1.09
					Ca	0.67	0.72	0.62	0.63
					Na	0.23	0.20	0.27	0.28
					cations M2	0.91	0.91	0.89	0.91
mol %					mol %				
Alm	32	31	23	36					
Prp	36	40	64	36	Jd	19	19	28	27
Sps	1	1	0	1	Quad	74	80	72	70
Grs	31	28	13	28	Ae	7	1	0	2

Table 4.2. Representative garnet and clinopyroxene electron microprobe analyses of Rubinberg and Klatschmühle eclogites. For the garnet: Alm= almandine, Prp= pyrope, Sps= spessartine and Grs= grossular. For the clinopyroxene: Jd= jadeite, Quad= quadrilateral (Ca – Mg – Fe^{2+} pyroxenes) and Ae= aegirine.

Locality	Rubinberg	Klatschmühle			Rubinberg	Klatschmühle		
	Garnet				Clinopyroxene			
Name	1	2	3	4	1	2	3	4
ppm								
Rb	b.d.l.	b.d.l.	b.d.l.	b.d.l.	3.90	3.29	b.d.l.	b.d.l.
Cs	b.d.l.	b.d.l.	b.d.l.	b.d.l.	1.42	1.81	b.d.l.	1.66
Ba	b.d.l.	b.d.l.	b.d.l.	b.d.l.	6.19	30	b.d.l.	16
Th	0.62	0.54	0.77	0.51	14	16	4.50	6.75
U	1.22	1.37	1.28	1.26	2.45	2.69	1.51	2.68
Nb	b.d.l.	b.d.l.	0.11	b.d.l.	0.95	0.73	1.35	1.19
Ta	b.d.l.	b.d.l.	b.d.l.	b.d.l.	0.42	0.37	b.d.l.	0.19
La	0.81	0.82	b.d.l.	b.d.l.	91	116	54	60
Ce	10.2	9.54	2.58	3.40	303	351	201	228
Pb	b.d.l.	b.d.l.	b.d.l.	b.d.l.	7.50	8.39	4.11	7.26
Pr	4.53	4.42	1.45	1.22	47	53	36	39
P	3326	3184	2219	2169	419	487	441	575
Sr	1.57	1.25	b.d.l.	b.d.l.	111	183	292	366
Nd	55	49	22	24	232	258	179	216
Zr	227	231	502	493	850	901	776	1114
Hf	3.88	3.75	5.78	5.62	34	37	33	44
Sm	55	51	39	34	63	66	47	60
Eu	18	19	15	16	14	15	11	14
Gd	42	43	78	74	44	41	33	49
Tb	5.35	5.68	15	15	4.88	4.28	3.00	4.81
Dy	35	31	111	111	27	18	13	23
Ti	12934	12846	6466	8376	49549	58851	35106	51013
Y	179	182	621	596	110	65	4.43	6.19
Ho	6.84	7.54	23	22	4.16	2.57	1.73	3.20
Er	21	21	73	60	10.01	5.20	3.44	6.28
Tm	3.02	2.74	9.59	7.92	1.31	0.54	0.57	0.91
Yb	21	22	63	50	9.34	2.81	1.12	3.68
Lu	2.93	2.83	8.99	6.60	1.00	0.30	0.12	0.49
Li	b.d.l.	b.d.l.	b.d.l.	b.d.l.	87	149	511	534
B	65	53	42	b.d.l.	43	54	27	33

b.d.l= below detection limit

Table 4.3. Representative garnet and clinopyroxene LA-ICP-MS analyses of Rubinberg and Klatschmühle eclogites.

Normalized REE patterns of garnets (Fig. 4.9a) are similar for the LREE: both are depleted with a Ce_N/Yb_N ratio between 0.01 and 0.18. In RUB samples the relative content of medium rare

earth element (MREE, from Gd to Dy) with respect to the LREE is correlated to the Eu anomaly (expressed as the ratio Eu_N/Eu^*).

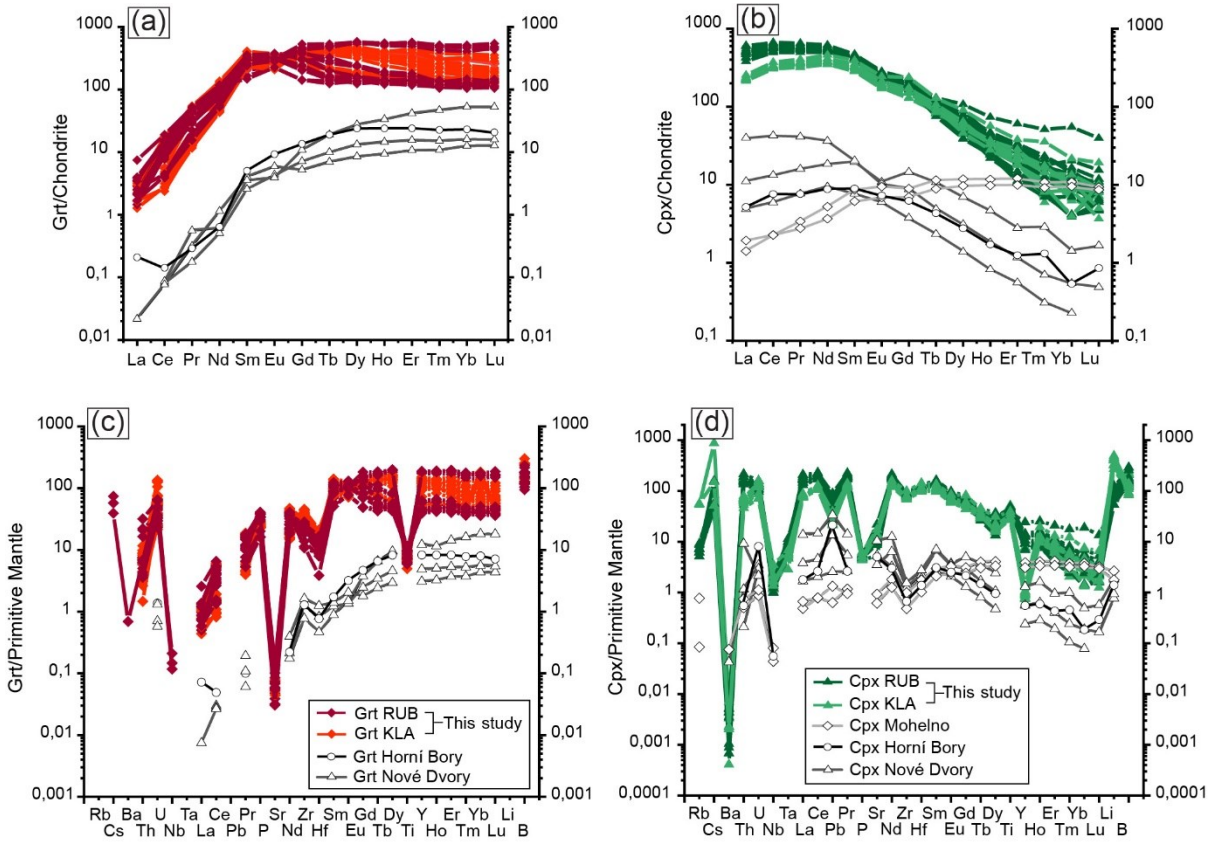

Figure 4.9. REE patterns of RUB and KLA garnet (a) and clinopyroxene (b) (see Table S4.2 and S4.3 respectively) compared with the pyroxenite of the Gföhl Unit in the Moldanubian Zone (same data Figure 4.7) and trace element patterns of RUB and KLA garnet (c) and clinopyroxene (d) compared with the same pyroxenite. For normalized values see caption Figure 4.8.

When the anomaly is positive (Eu_N/Eu^*= 1.26), MREE are more abundant than HREE whereas when the anomaly is negative (Eu_N/Eu^*= 0.87) the amount of MREE is similar to HREE and the pattern is flatter. In specimen KLA 1 the Eu anomaly is slightly negative (Eu_N/Eu^*= 0.93) or absent and the content of MREE is higher than HREE. Furthermore, despite the compositional difference in major elements and in the HREE, the garnets in the two localities have similar trace element patterns (Fig. 4.9c). They are generally depleted in LILE, in some of the High Field Strength Elements (HFSE) such as Nb and Hf, have a negative Sr and Ti anomaly and a positive Th, U and Zr anomaly. Comparison with the trace elements of the Moldanubian dataset shows that RUB and KLA garnets have higher general enrichment in trace elements, a content of LREE almost

two orders of magnitude higher, and in addition the HREE show a much flatter normalized pattern. Mohelno type pyroxenites are not reported because they are garnet-free (Fig. 4.9 a–c).

Clinopyroxene

As for the garnet, clinopyroxene shows variations in composition between the two localities but also within a single sample (Fig. 4.7). In RUB samples the clinopyroxene is generally a sodic diopside with Mg# = 70–74 and an average jadeite (Jd) content of 19 mol % whereas in KLA samples it is an omphacite, Mg- and Na-richer, with Mg# = 73–85 and Jd = 28 mol %. Within a single sample, Al_2O_3 and FeO in clinopyroxene show a negative correlation with MgO whereas SiO_2 and CaO a positive one. TiO_2 and Na_2O contents are rather high for a pyroxenite *s.s.* (Svojtka et al., 2016; see also discussions) and they show a negative correlation with MgO. RUB and KLA clinopyroxenes have lower Mg# and higher Jd content compared to the Moldanubian dataset (Mg# = 89–94; Jd = 3–18 mol %; Svojtka et al., 2016).

The normalized clinopyroxene REE patterns are convex-upward with HREE depletion in both samples (Fig. 4.9b) but with LREE enrichment slightly greater in RUB than in KLA specimens. In both cases the Eu anomaly is slightly negative with a Eu_N/Eu^* of 0.89 and 0.86 for RUB and KLA samples, respectively. Trace element patterns are similar in the two localities (Fig. 9 d), and show enrichment in Cs, Rb, U, Th and Li. In contrast, Nb, Ta, Pb, P and Y show a weak negative anomaly whereas the Ba anomaly is strong. RUB and KLA clinopyroxenes have higher LILE, Th, Li and B with respect to those of the listed Moldanubian pyroxenites whereas Pb and Y anomalies have the opposite trend. Their REE patterns are convex-upward as for the Nové Dvory samples but with higher enrichment (almost two order of magnitude) whereas the pattern is the opposite of the Mohelno type in which the clinopyroxene is richer in HREE because of the absence of garnet (Fig. 4.9d).

Other phases

Plagioclase surrounding garnet and clinopyroxene is typically $Ab_{76}An_{22}Or_2$ and has a similar composition in all the different microstructural positions – interstitial, in leucocratic pockets or as lamellae or blebs along the clinopyroxene cleavage – as well as in the samples from both localities. The dominant brown amphibole, a hornblende with a composition between Mg-hastingsite and pargasite, contains 1.6 wt % TiO_2 and has Mg# of 70 whereas biotite is mainly a phlogopite with 3–3.5 wt % TiO_2 and Mg# of 70 (RUB) or 85 (KLA) (see Table S 4.7).

4.5.4 MELT INCLUSION CHEMISTRY

The major element composition of the melt inclusions in RUB and KLA 1 eclogite samples was already discussed in detail by Borghini et al., 2018 (see data repository for analyses; Figure 4.7 and Table 4.1; see Table S4.8 and S4.9 for the trace element). As the samples RUB and KLA 2 are similar this geochemical study concentrated on the contrasting samples RUB and KLA1. The melt is mainly granitic, hydrous and alkali-rich in both localities. Contents of Al_2O_3, CaO, FeO and TiO_2 correlate positively with MgO, whereas SiO_2 correlates slightly negatively (Fig. 4.7). In terms of trace elements, the melt displays marked enrichment in LILE (Cs, Rb, to a lesser extent Ba), Th, U, Li, B and strong negative anomaly in Ti (partially below the primitive mantle values). The patterns reveal a strong positive anomaly in Pb and to a lesser extent Zr–Hf, and negative anomalies for Nb, Ta and Sr (Fig. 4.10).

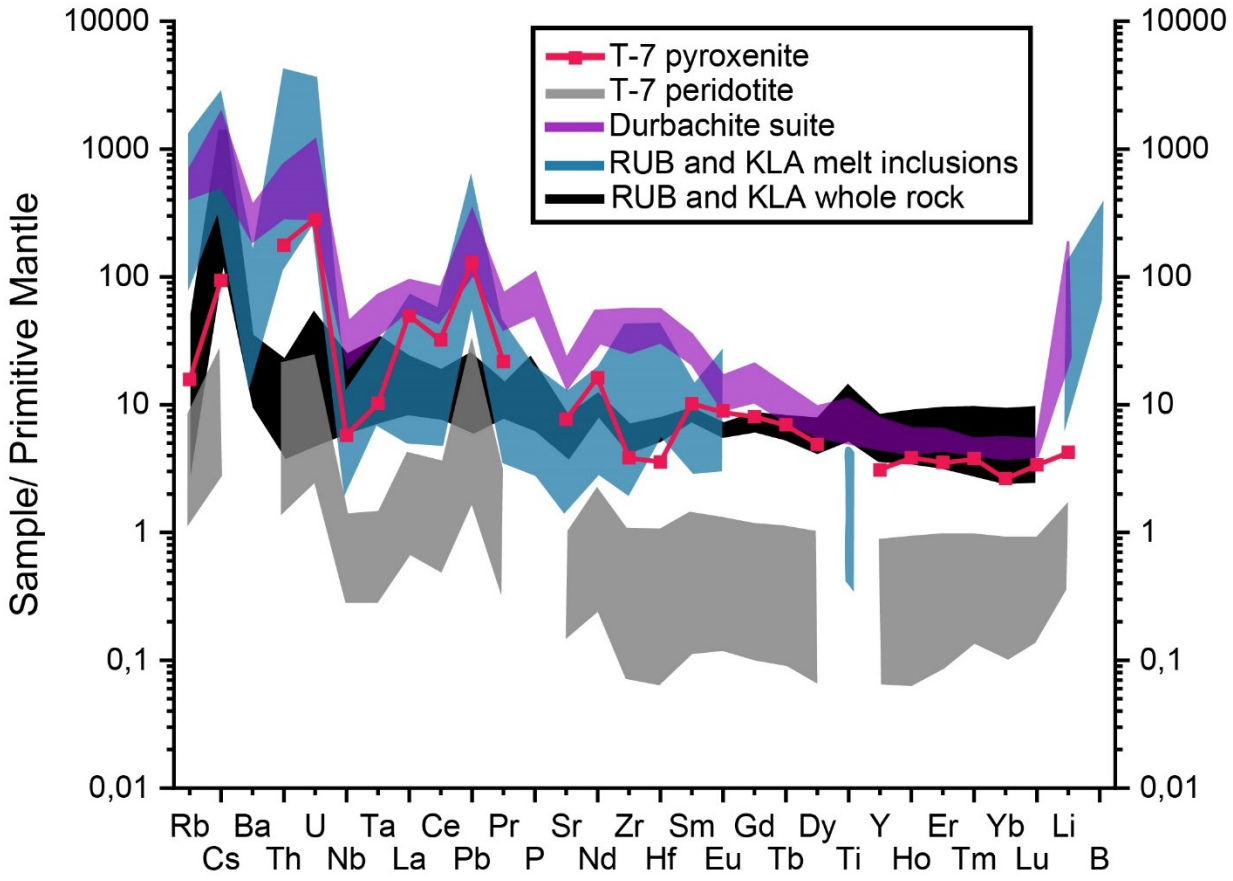

Figure 4.10. Trace element patterns of RUB and KLA melt inclusions compared with the whole-rock trace element patterns of RUB and KLA, the durbachite suite (Janoušek and Holub, 2007) and the peridotite and pyroxenite of the T-7 borehole (Medaris et al., 2015). For normalized values see caption Figure 4.8.

Despite the fact that the Th content is higher in RUB than in KLA 1 inclusions, the trends are very similar in both localities. The melt is also enriched in LREE (Fig. 4.11) with a La_N/Nd_N ratio higher in RUB (average 6.82) than in KLA 1 (average 2.47) samples.

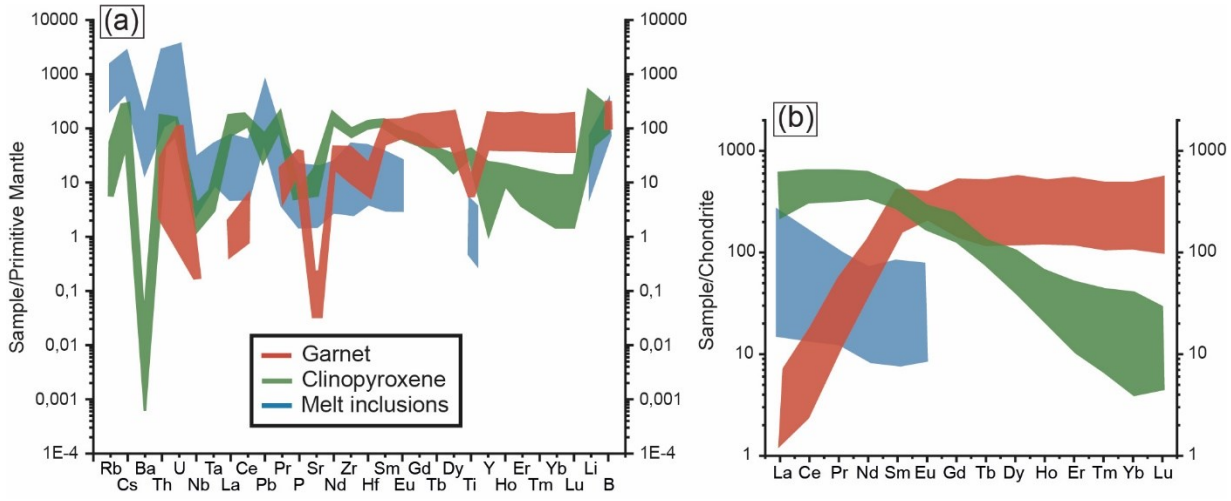

Figure 4.11. Trace element (a) and REE (b) composition patterns of garnet, clinopyroxene and melt inclusions of RUB and KLA eclogites represented together. All the trace element data have been normalized to primitive mantle (Sun and McDonough, 1989 except for B from McDonough and Sun, 1995) whereas the REE have been normalized to chondrite (Sun and McDonough, 1989).

4.6 DISCUSSION

4.6.1 THE TRAPPED MELT AND ITS ORIGIN

The melt trapped in the eclogitic bodies of Klatschmühle and Rubinberg in Granulitgebirge (Bohemian Massif) is granitic in composition, peraluminous and slightly hydrous (< 2 wt% H_2O, Table 4.1). The possibility that this is a supersilicic fluid can be ruled out because the water content in the latter is usually much higher (e.g.25-50 wt %; Frezzotti et al., 2007). The presence of kumdykolite and kokchetavite in the crack-free inclusions supports their chemical preservation (Ferrero et al., 2016b, 2018a) making it highly unlikely that the low H_2O content of the inclusions is the result of H_2O loss.

According to microstructural and geochemical evidences – i.e. granoblastic texture (Fig. 4.3c-d) and REE partitioning with high LREE abundance in clinopyroxene with the same enrichment factor of the HREE in garnet (Fig. 4.11b)- garnets and clinopyroxene formed at peak condition. The melt occurs as primary inclusions in garnet cores thus the melt was trapped at the

metamorphic peak while garnet and clinopyroxene were growing at mantle depth, as already discussed in Borghini et al. (2018).

The melt trace element pattern suggests the involvement of white mica in the melting reaction (see also Acosta-Vigil et al., 2010), which likely occurred in the presence of an aqueous fluid responsible for the high amount of Th and U in the melt (Borghini et al., 2018). A Th, U- rich phase consumed during melting of metasediments is often monazite (Hermann and Rubatto, 2009), but this should be visible in the melt in terms of extensive enrichment in LREE with respect to Th and U, a feature absent in the investigated MI. Also the strong positive Pb anomaly, the depletion in Ti and the negative Nb anomaly (Fig. 4.10) are all typical of a continental crust signature (Hartmann and Wedepohl, 1993). The source of the melt is thus most likely a phengite/muscovite-bearing rock belonging to the continental crust (either a meta-sediment or a meta-granitoid), subducted to mantle depth and melted in the presence of a Th-, U-rich fluid.

Crust-mantle interaction commonly generates adakites, i.e. intermediate to felsic magmatic rocks considered the modern equivalent of the pristine continental crust (i.e. Trondhjemite, Tonalite and Granodiorite suite or TTG; Hastie et al., 2010; Martin et al., 2005). The melt hosted in the inclusions (Table 4.1) is very different from common adakitic melts: 1) it is significantly lower in FeO, MgO, CaO and TiO_2 and richer in K_2O and Na_2O; 2) as for trace elements, the strong positive Sr anomaly and the Ba positive anomaly relatively to Rb, typical of adakites, is completely absent in RUB and KLA melt. Moreover, the generation of adakitic melts generally involves amphibole melting and proceeds via either (i) partial melting of the subducted oceanic slab with later melt enrichment in MgO, Cr and Ni and high Mg# because of interaction with the mantle wedge during ascent or (ii) partial melting of peridotite previously metasomatized by a felsic slab-derived melt (Martin et al., 2005). Both scenarios require amphibole melting, whereas the trapped melt is clearly enriched in elements characteristic of a melting reaction involving white mica (see discussion above).

A possible source for the melt trapped in the studied eclogites could be the Granulitgebirge granulites surrounding the peridotite, as they were already juxtaposed before the granulite metamorphic peak (Schmädicke et al., 2010). This possibility was already ruled out by Borghini et al. (2018) because the melt generated by felsic granulite melting shows a different geochemical signature (Ferrero et al., 2018b). Moreover, the melt-bearing KLA eclogites formed at 380 Ma (von Quadt, 1993) whereas melting in the granulites was likely coeval to the HP metamorphism at 340 Ma (Rötzler and Romer, 2001). Another source already proposed could be an eclogite. From existing studies, the melt derived from such a rock would show very strong enrichment in Sr (Rapp et al., 1991) and would be richer in Rb and Ba than Cs, which is the opposite to the

trends observed in the KLA and RUB MI (Fig. 4.10). It is unlikely that the melt originated from a gabbro or basalt because otherwise it would have a positive Eu, Sr and Ba anomaly due to the consumption of feldspars during the melting reaction (Becker, 1996). The most likely candidates for the source of the melt are deeply subducted metasediments, possibly resembling the younger (336 Ma; Massonne et al., 2007) diamond-bearing phengite gneisses and phengite-bearing high pressure granulites of the Erzgebirge (Schmädicke et al., 1992; Kröner and Willner, 1998; Stöckhert et al., 2009; Massonne and Fockenberg, 2012) where melt was recently identified in inclusions in garnet (Acosta-Vigil et al., 2017).

4.6.1.1 A FORMATION MODEL FOR THE MELT-BEARING ECLOGITES

The source of RUB and KLA granitic melt is crustal and must be located in the subduction zone. During subduction the slab and the mantle wedge are in contact and fluid or melt released from the slab can be transferred to the mantle wedge causing metasomatism (Condamine et al., 2016; Fumagalli et al., 2009; Scambelluri et al., 2006). A similar genetic process may be envisioned for the ultramafic bodies here investigated, where a melt produced via melting of subducted crust migrates to the mantle wedge and causes a metasomatic interaction with an already inhomogeneous peridotite (Fig. 4.12a, see also paragraph § 4.6.5 for the KLA and RUB peridotite chemical features). Then portions of the metasomatized mantle wedge are incorporated in the underlying slab via ductile flow (Fig. 4.12b), as proposed by Brueckner (1998) to explain the juxtaposition of garnet peridotites and continental crust. This scenario is based on the consideration that slab and mantle wedge are gravitationally unstable because of their strong difference in density, considerably higher in the overlying mantle wedge. If the slab at depth becomes hotter and/or wet (the latter possibly because of fluid/melt influx), the peridotite can sink as blobs in the crust, thus sharing afterwards their further evolution with the surrounding subducted crust (Fig. 4.12c).

How the metasomatic melt migrates from the subducting slab into the mantle and how it interacts therein is a complex problem. The two processes proposed for magma migration are porous flow through the grain boundaries and flow through a fracture network (Schiano et al., 2006). The first process would be more likely to promote extensive interaction between melt and peridotite than the second, thus causing the melt to change its original composition. In RUB and KLA case study the melt chemistry suggests that there was no interaction with the peridotite during the migration and before its entrapment as inclusions in the garnet. The melt is indeed poor in MgO, Ni and Cr (Table 1), whereas high-SiO_2 adakite magmas that interact with the mantle wedge peridotite during ascent show high concentrations of such elements (Martin et al., 2005).

In addition, no evidences of peridotite-melt interaction are visible in the field, such as a network of veins in the peridotites around the pyroxenite lenses/layers described here which may be considered indicative of pervasive flow. Therefore, the melt migration process occurred probably via channelized, maybe even fast-travelling flow (as proposed by Vrijmoed et al., 2013) which prevented the melt from interacting with the peridotite and thus preserved its pristine nature. Evidences of these channel were then erased by subsequent deformation and retrogression of the host peridotite after incorporation in the crust.

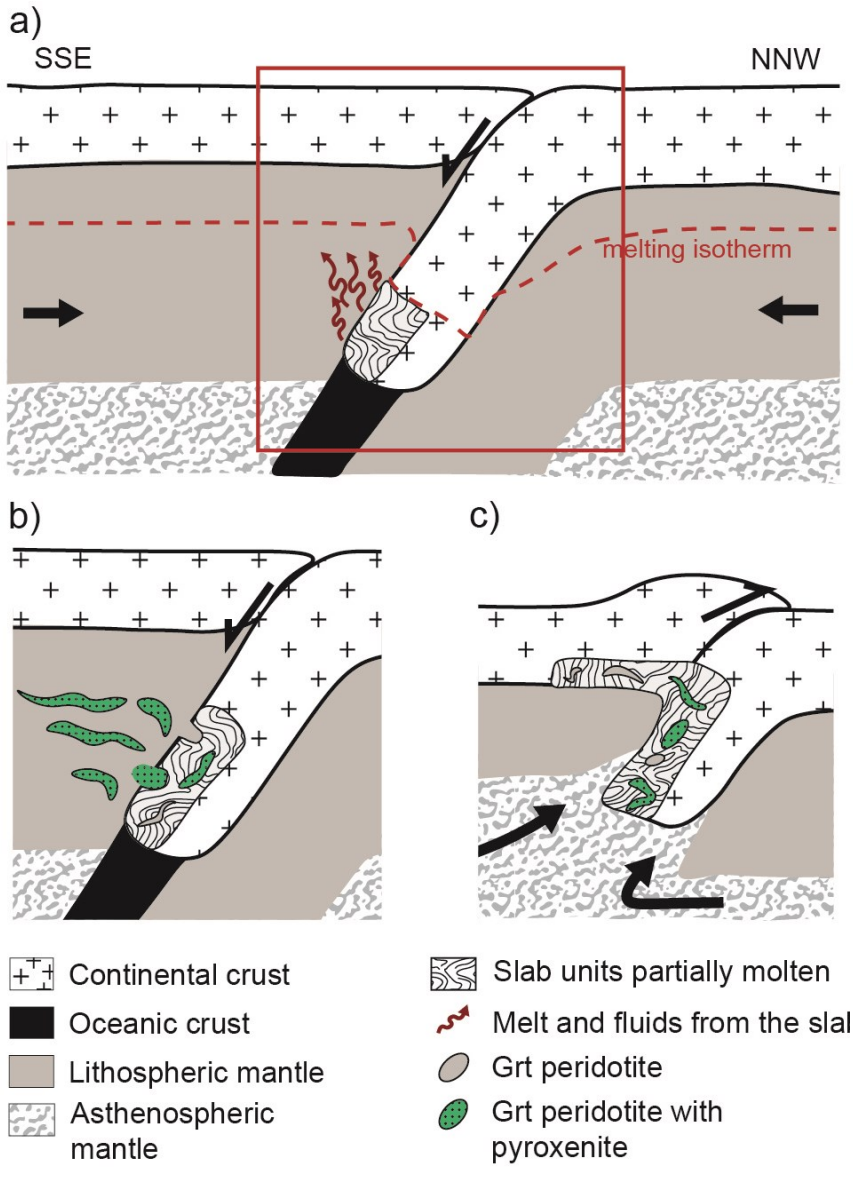

Figure 4.12. Possible scenario for origin and evolution of the peridotite with pyroxenite in the geotectonic setting of the Granulitgebirge: a) HP metamorphism, release of melt and fluids and metasomatism; b) peridotite emplacement in the crust and c) subsequent exhumation of granulites and peridotite with and without pyroxenite. Based on Brueckner, 1998; O'Brien, 2000; Medaris et al., 2005; Janoušek and Holub, 2007.

4.6.2 THE HOST ROCK: A MANTLE ECLOGITE WITH CRUST, SUBDUCTION-RELATED SIGNATURE

Whereas previous works described the investigated rocks as garnet clinopyroxenites, in the present study the term “eclogite” has been chosen to describe them because the newly acquired dataset shows that both major element and mineral compositions of RUB and KLA samples are closer to eclogites, especially the Nové Dvory kyanite eclogites, rather than to pyroxenites of the Moldanubian zone (cf. Medaris et al., 2006 and Fig. 4.7). More in detail, eclogite and pyroxenite of the Moldanubian Zone have been discriminated according to several parameters reported in Table 4.4 such as Na_2O, TiO_2 versus Cr and Ni, Mg# and the Jd content in clinopyroxene (Carswell, 1990; Medaris et al., 1995, 2006; Obata et al., 2006; Gonzaga et al., 2010; Svojtka et al., 2016).

		Garnet pyroxenite	Eclogite	References
Whole rock	**Na_2O**	≤ 0.7 wt%*	> 0.8 wt%	Medaris et al., 1995 Medaris et al., 2006 Svojtka et al., 2016
	TiO_2	lower	higher	Medaris et al., 1995 Obata et al., 2006
	Cr	> 0.15 wt%	< 0.15 wt%	Medaris et al., 1995a Medaris et al., 2006 Obata et al., 2006
	Ni	>400 ppm	<400 ppm	Medaris et al., 1995 Medaris et al., 2006 Svojtka et al., 2016
	Mg#	>80	<80	Medaris et al., 1995a
	Cpx	Augite-diopside or chrome diopside; no omphacite	Omphacite (Jd >20-25 mol%)	Carswell, 1990 Medaris et al., 1995 Gonzaga et al., 2010 Obata et al., 2006

*The Na content is the one reported by Svojtka et al., 2016 for most of the pyroxenites of the Moldanubian zone

Table 4.4. Schematic differences between garnet pyroxenite and eclogite.

All these parameters in RUB and KLA samples are consistent with an eclogite rather than a pyroxenite. The investigated rocks contain $Na_2O \geq 2$ wt% whereas pyroxenites contain generally $Na_2O \leq 1$ wt % (0.7 wt% is the average in the Moldanubian Zone pyroxenites; Svojtka et al., 2016). Significantly, the TiO_2 content in samples RUB and KLA is higher than in the Moldanubian pyroxenites whereas Cr and Ni content are lower, again a feature of eclogites. A typical Moldanubian pyroxenite contains TiO_2 <0.3 wt%, Cr_2O_3 and Ni > 400 ppm in average. Pyroxenite Mg# is generally > 80 whereas for eclogite, and for RUB and KLA, it is lower. Clinopyroxene in RUB and KLA samples has Jd content 19-28 mol %, i.e. it is an omphacite (Jd ≥ 20–25 mol %), as commonly observed in eclogite. In contrast, pyroxenite clinopyroxene is commonly augite-diopside or Cr-diopside.

The investigated eclogites have features more compatible with the oceanic crust than with the mantle peridotites and pyroxenites, notably the low Cr, Ni contents and Mg#, despite being enclosed in mantle rocks. The major element contents are indeed generally very similar to N-MORB, i.e. oceanic crust. For example, Na_2O generally fits in the range of common lower oceanic crust (2.23–3.27 wt %; Coogan, 2014). However, since MgO is lower than in N- and E-MORB, KLA and RUB samples display a typical Fe-rich basaltic composition. Such MgO values are in the range of low-MgO mantle garnet pyroxenite when compared to the database of Isabel Varas-Reus et al. (2018), and their Mg# is the lowest with respect to the other pyroxenites and kyanite eclogite of the Moldanubian Zone. In contrast, Al_2O_3 content is rather high, in the range of high-Al_2O_3 mantle garnet pyroxenite (Isabel Varas-Reus et al., 2018). Consistent with the Fe-rich nature of the rocks, clinopyroxene and garnet are generally more Fe-rich than in the equivalent phases in the other pyroxenites. This feature suggests a protolith derived from, or related to, the oceanic crust.

RUB and KLA samples also show a clear subduction-related trace element signature indicated by enrichment in LILE, positive U anomaly and negative anomalies in Sr and Nb (Fig. 4.8; (Becker, 1996; Zanetti et al., 1999; Becker et al., 2001; Prouteau et al., 2001; Medaris et al., 2015). In particular, the enrichment in Cs, Rb, Li and LREE observed in clinopyroxene is regarded as a monitor of metasomatism in mantle rock: Li in particular is a sensitive tracer of the slab-to-mantle transfer of fluids (Scambelluri et al., 2006 and references therein). Such a subduction-related signature is clearly due to the presence of melt during the crystallization of all the eclogite samples here investigated (RUB, KLA1 and KLA2) despite the slight difference in composition of the host garnet (see Fig. 4.7).

4.6.3 MELT INCLUSIONS PRESERVE THE ORIGINAL METASOMATIC AGENT

In the present study, it is proposed that the melt trapped in the inclusions is of crustal origin (i.e. deeply subducted continental crust), externally derived with respect to the peridotite-pyroxenite-eclogite association, and has acted as a metasomatic agent during the crystallization of the eclogites. This is the first case in which the metasomatic agent – a silicate melt – present at depth within an orogenic peridotite has been studied directly in detail.

Mantle metasomatism by subduction-related melts/fluids has already been extensively studied in several localities worldwide. The main features of metasomatized mantle rocks are whole rock enrichment in K, Rb, Ba, Sr and LREE with respect to HREE and, in case of a modal metasomatism, the crystallization of phlogopite, amphibole and/or orthopyroxene (Schiano et al., 1995; Becker, 1996; Zanetti et al., 1999; Becker et al., 2001; Prouteau et al., 2001; Rampone et al., 2001; Scambelluri et al., 2006; Zhang et al., 2007, 2011). In most of these case studies the composition of the metasomatic agent was inferred from the geochemical signature of bulk rock and/or minerals (Becker, 1996; Zanetti et al., 1999; Becker et al., 2001; Zhang et al., 2007) and only in a few cases was it possible to study directly the metasomatic agent (Schiano et al., 1995) or the remnants of it (Malaspina et al., 2006;2009). The differences between RUB and KLA melt inclusions and the multiphase fluid inclusions described by Malaspina et al. (2006, 2009) are reflected in the mineral assemblages and the result of re-homogenization experiments (see discussion in Borghini et al., 2018).

Melt interpreted as a preserved metasomatic agent in glassy inclusions from spinel-bearing harzburgite xenoliths was reported by Schiano et al. (1995) in arc lavas from the Philippines. There the inclusions occur as trails in the porphyroclasts and isolated in metasomatic minerals, olivine and orthopyroxene. They are either completely glassy (±H_2O ±sulphide) or glassy with daughter minerals such as phlogopite, amphibole, orthopyroxene and clinopyroxene. The reported melt composition is different from the one investigated in this study: SiO_2 content and the alkalis (Na_2O and K_2O) are higher in RUB and KLA MI whereas TiO_2, FeO, P_2O_5 and CaO are higher in the Philippine examples (see composition in Table 4.1). Moreover, sulphides are absent in both Granulitgebirge samples. Schiano et al. (1995) suggested that the melt originated via a small degree of partial melting of the oceanic crust at the garnet-amphibolite/eclogite transition, with garnet, hornblende and clinopyroxene as residual phases. The newly studied eclogites are however different for several reasons: the melt has a different composition; the glass inclusions do not show water shrinkage bubbles and/or sulphides; and the daughter phases are mostly

anhydrous and fill the whole inclusion (Fig. 4.4 and 4.5). Also, there are no clear residual phases: both garnet and clinopyroxene are instead interpreted as the products of reaction at the metamorphic peak. The participation of melt in this process is usually via a peritectic reaction in which a liquid reacts with a solid (in this case a still undefined mafic layer in the mantle; see §6.4 for details) and gives, as a result, other solids without changing its composition. That the melt did not change in composition during the growth of the host garnet is testified by the fact that the primary inclusions show the same composition across the whole garnet, which is moreover not zoned. Alternatively, the melt could just as easily have acted as a kinetic agent, enhancing rapid crystallization of the peak phases, enriching them in specific trace elements but without contributing to their major element chemistry, and locally becoming trapped in the growing garnet.

4.6.3.1 SAME METASOMATIC SIGNATURE, DIFFERENT ROCKS

Remarkably, other rocks in the Bohemian Massif show geochemical signatures requiring a component very close to that of the melt hosted in the investigated eclogites. For instance, unusual melanosyenites in the Bohemian Massif – the so-called durbachite suite – show chemical features similar to the melt trace element pattern, i.e. high LILE (higher Cs then Rb and Ba) and LREE, U, Th and strong Pb positive anomaly and Nb and Ti negative anomaly (Fig. 4.10; Janoušek and Holub, 2007). The durbachite suite has been interpreted as being derived from an anomalous mantle source contaminated by mature crustal material (Janoušek and Holub, 2007), like other potassic mafic magmas that were emplaced throughout the Variscan belt at the same time (von Raumer et al., 2014; Couzinié et al., 2016). In this scenario, a melt similar to the one trapped in the eclogites reported here may represent the crustal component added to the source of such magmas, an occurrence which requires both melts to have been produced by similar source rocks under similar fluid-present conditions.

A melt very similar to the one hosted in KLA and RUB eclogites was most likely also the agent of the reported cryptic metasomatism in garnet peridotite with lenses of phlogopite-garnet pyroxenite in the T-7 borehole in the Saxothuringian Zone (Medaris et al., 2015; Fig. 4.10). These peridotites experienced two types of metasomatism: modal, materialized by the occurrence of phlogopite and small amounts of amphibole, and cryptic, visible as trace element enrichment. The metasomatic agent was interpreted by Medaris et al. (2015) to be subduction-zone related. The trace element patterns of the T-7 peridotites strongly resemble the melt in RUB and KLA MI, in particular in terms of positive anomalies for Th, U and Pb, negative anomalies for Nb, Ta, Sr and Ti strongly supporting the same kind of metasomatic history in all of these widely spaced Saxothuringian peridotite-hosted garnet-clinopyroxene rock.

4.6.4 A CONUNDRUM: ECLOGITES WITH PRESERVED METASOMATIC AGENT AND NO METASOMATIC SIGNATURE

The detailed geochemical investigation of these eclogite and the trapped melt reveals a very puzzling feature: while some key elements enriched in the bulk rock can be attributed to the presence of melt and both garnet and clinopyroxene are to different degrees enriched in incompatible elements, the overall bulk rock trace element pattern of the eclogite does not register the presence of the metasomatic melt, despite the melt being present inside the rock as inclusions.

In terms of modal metasomatism, “classic” metasomatic phases, e.g. phlogopite, amphibole ± apatite, are notably absent from the metamorphic peak assemblage, consistently with the dry character of both main phases (garnet and clinopyroxene). As already made clear in the petrographic descriptions, these “classic” metasomatic phases are present in the matrix together with leucocratic pockets filled with plagioclase (Fig. 4.3e–f) but these represent a later modal metasomatism, that postdates the metamorphic peak and is unrelated to the preserved melt inclusions. Leucocratic pockets have been already reported in the Nové Dvory eclogite where they contain plagioclase, a moderate amount of garnet, clinopyroxene and minor biotite and amphibole (Miyazaki et al., 2016). Clinopyroxene in the latter has been interpreted as having crystallized from a melt with composition close to a HP TTG. The melt pockets in RUB and KLA eclogites however only contain plagioclase, whereas the clinopyroxene belongs to the peak assemblage. Furthermore, the metasomatism of a peridotite by a granitic/granitoid melt is expected to cause abundant crystallization of orthopyroxene with the consequent formation of an Ol-free garnet pyroxenite (Rampone and Morten, 2001). Even aqueous fluids of eclogitic origin can crystalize orthopyroxene in mantle rocks as demonstrated by natural examples (Malaspina et al., 2017), thermodynamic/mass balance studies (Campione et al., 2017) and experimental works (Tiraboschi et al., 2018). RUB and KLA garnet clinopyroxene-rich rocks are orthopyroxene-free, and the production of garnet and clinopyroxene requires a high amount of CaO, an element which is instead not abundant: neither in the melt (CaO in the melt <1 wt%; see Table 4.1) nor in Rubinberg and Klatschmühle peridotite (Schmädicke et al., 2010). This suggests that either a Ca-rich rock layer, such as a gabbro, was already present in the peridotite, or there was another component involved in peak metamorphism, now totally consumed i.e. a CaO- and FeO-rich melt or fluid. The first scenario is more plausible and, either way, the presence of abundant CaO in the system explains the crystallization of clinopyroxene rather than orthopyroxene.

In terms of cryptic metasomatism, the major elements in the eclogite bulk rock analyses, and some of the trace elements, especially Cs and U, are consistent with a crustal and subduction-related signature. A first reasonable inference is that the trapped melt, originating in the crust, should be responsible for such a signature. However, when melt and bulk rock trace elements are compared they appear notably different insofar as that only Cs shows the same degree of enrichment in both, and that most of the normalized patterns are instead rather flat, as expected for an unmetasomatized mantle (Fig. 4.8). As previously discussed, metasomatized peridotites and pyroxenites from the T-7 borehole (Medaris et al., 2015) show instead a signature very similar to the melt trapped in the Granulitgebirge eclogites, despite the apparent absence of MI (Fig. 4.10).

The conundrum of the absence of a metasomatic footprint in rocks containing a metasomatic melt could be solved by taking into account the size of the melt remnants. Despite the fact that MI are abundant in the RUB and KLA eclogites, the overall amount of melt still present in the rock is extremely small, due to the micrometric size of the inclusions, and thus not sufficient to dominate the whole rock signature. Such a minor amount of trace elements enrichment may thus be a direct expression of the limited amount of melt present during peak metamorphism of the eclogites: something also consistent with the absence of classic hydrous metasomatic phases in the peak assemblage. On the other hand, rocks in the T-7 borehole would have experienced a larger influx of melt thus recrystallizing extensively with formation of classic metasomatic phases. According to our hypothesis the two rocks (the investigated eclogites and the mantle rocks from the T-7 borehole) experienced different degrees of metasomatism caused by the infiltration of a similar metasomatic agent, now preserved in the less metasomatized of the two. Clinopyroxene in the Granulitgebirge eclogites seems to be the only peak phase recording the interaction with the melt as it shows enrichment in Rb, Cs, U and Li and possibly LREE even though it is devoid of melt inclusions. Clinopyroxene can trap inclusions (e.g. Veksler et al., 1998; Salvioli-Mariani et al., 2002; Schiano et al., 2004) and their absence can be explained by recrystallization of the clinopyroxene to smaller sized grains which caused the obliteration of the inclusions. This is also supported by the size difference between garnet, generally larger, and clinopyroxene. The simultaneous growth should instead produce crystals with similar size (see Fig. 4.3c-d).

4.6.5 PECULIAR MELT-BEARING ECLOGITES VERSUS OTHERS PYROXENITE/ECLOGITES OF THE BOHEMIAN MASSIF

Mantle-derived garnet clinopyroxenites and associated rocks (eclogites, websterites, garnetites etc.,) have been studied mainly from xenoliths worldwide but the Bohemian Massif, where numerous orogenic garnet- and spinel-bearing peridotite bodies with enclosed pyroxenites

and eclogite are exposed, has presented a fantastic opportunity to study a wide variety of such rocks *in situ*. The formation of the lenses and layers of pyroxenite has been explained by a variety of processes: HP crystal segregation from basaltic melts of different origins; peridotite metasomatism; HP recrystallization of basalts/gabbros, and stress-induced recrystallization of megacrysts. How can the textures, major and trace element data of whole rock, minerals and melt inclusions in the newly studied RUB and KLA samples be explained in terms of these different garnet clinopyroxenite and eclogite types?

The most known and best characterized pyroxenites of the Granulitgebirge are those from Reinsdorf (also called Gilsberg), 10 km west of where samples RUB and KLA were collected (Massonne and Bautsch, 2002; Schmädicke et al., 2010). Reinsdorf pyroxenites are very different from the garnet + clinopyroxene-rich rocks studied here from both microstructural and geochemical viewpoints. The main microstructural difference is the presence in Reinsdorf samples of alternating parallel lamellae of garnet (the minor component) in clinopyroxene (the major phase) surrounded by a recrystallized equigranular garnet + clinopyroxene domain. Clearly, these rocks were originally layers of aluminous, pyroxene megacrysts, which experienced deformation-induced exsolution of garnet and recrystallization at higher pressure (Massonne and Bautsch, 2002). Geochemically, garnet, clinopyroxene and bulk rock all show similar REE trends. Clinopyroxene is richer in LREE and garnet enriched in HREE, but Ce, Pr and Nd are depleted in both minerals as well as in the bulk rock. In comparison, RUB and KLA eclogites have very different textures and show no evidence of exsolution. Also, as garnet preserves clusters of primary melt inclusions its growth took place in presence of melt rather as result of exsolution- or deformation-induced solid-state recrystallization as reported from Reinsdorf. Elsewhere in the Bohemian Massif there are several locations where rocks similar to those of Reinsdorf have been reported e.g., Horní Bory, Biskupice, Nové Dvory, Kutná Hora, Křemže (Czech Republic), Karlstetten and Meidling im Tal (Lower Austria), all belonging to the Moldanubian Zone. Here also other variety of pyroxenites occur and they can be grouped in the three types Mohelno, Horní Bory and Nové Dvory (Medaris et al., 2005; see locations in Fig. 4.1). Precisely those pyroxenites and kyanite eclogite types from the three name-localities have been chosen for the comparison with RUB and KLA samples (Fig. 4.7; see section § 4.6.1 and 4.6.2). In terms of the whole rock major elements data, RUB and KLA samples are very similar, except for a slightly higher TiO_2 and FeO and lower CaO content, to the kyanite eclogite from Nové Dvory: a rock quite different from all the other Moldanubian pyroxenites (Obata et al., 2006; Fig. 4.7; Table 4.1). The comparison of the whole rock trace element patterns shows some peculiar features of RUB and KLA samples: LILE enrichment and positive U and Ti anomalies. The slightly negative Pb anomaly

of RUB and KLA specimens contrasts with a positive Pb anomaly in the Moldanubian samples (Fig. 4.8a). The LREE enrichment in both RUB and KLA analyses is higher than in the whole Moldanubian dataset whereas the comparison of HREE shows higher abundances in RUB but slightly lower values in KLA (Fig. 4.8b). Garnet and clinopyroxene trace element patterns show also that RUB and KLA samples are generally enriched with respect to the Moldanubian ones (Fig. 4.9). Moreover, the clinopyroxene patterns with high LILE, Th, Li and B content, negative Pb anomaly and REE convex-upward pattern, is in strong contrast with those of the Mohelno type that are richer in HREE due to the absence of garnet (Fig. 4.9 b and d). In fact, Mohelno type pyroxenite are spinel- and orthopyroxene-bearing, i.e. websterite (Fig. 4.9d). The three Moldanubian pyroxenite types occur in peridotites attributed to three different mantle environments (Medaris et al., 2005, 2006): suboceanic asthenospheric mantle for the Mohelno type, disrupted mafic-ultramafic cumulate complex for Horní Bory and subcontinental lithospheric mantle for Nové Dvory type. The proposed genesis for those pyroxenites is either as HP cumulates (Svojtka et al., 2016) or due to HP recrystallization of gabbroic cumulates (Obata et al., 2006; Svojtka et al., 2016). The important geochemical differences discussed here suggest then a different genetic process for RUB and KLA samples.

4.6.5.1 ECLOGITE AND PERIDOTITE WITH MULTIPHASE SOLID INCLUSIONS OF THE BOHEMIAN MASSIF

Some of the Bohemian Massif eclogites and peridotites contain multiphase solid inclusions (MSI) that can be compared with the ones investigated in the present paper. MSI were reported in eclogite from Nové Dvory (Faryad et al., 2013) but, with respect to the RUB and KLA nanogranitoids, they contain different modal amounts of phases, different assemblages and thus variable composition. The inclusions in the Nové Dvory eclogites have been interpreted as the result of post-entrapment decomposition of former hydrous minerals included in garnet while it was growing, rather than melt trapped in the garnet. The presence of primary MI and the peculiar trace elements patterns in bulk rock, garnet and clinopyroxene suggest a different genesis for RUB and KLA eclogite with respect to the Nové Dvory equivalents, even though they both form layers in Variscan mantle peridotites. Interestingly some eclogites from Dunkelsteinerwald (Austrian part of the Bohemian Massif) show MSI with aspect and phase assemblage very close to a nanogranitoid (Ferrero et al., 2018b; see Fig. 2 d in Faryad et al., 2013) but interpreted by Faryad et al., 2013 in the same way as for the Nové Dvory examples.

Another location where MSI have been reported in orogenic garnet peridotite is Plešovice in the Blanský Les Massif, South Bohemia (Naemura et al., 2018). Here the inclusions occur in Zn-

poor chromite, have a negative crystal shape and contain mainly hydrous aluminosilicate minerals (phlogopite), phosphates (mainly apatite) and carbonates (calcite and dolomite). The melt composition has been calculated using the mineral proportions and mineral compositions and corresponds to a carbonated potassic silicate melt. This composition is very different from the melt observed in the Rubinberg and Klatschmühle eclogites, although the trace element enrichment patterns, for example positive Th and negative Sr and Ti anomalies in the garnet, are comparable.

Finally, some garnet peridotite from the T-7 borehole, Saxothuringian Zone, contains negative crystal shaped MSI in garnet annuli (Čopjaková and Kotková, 2018). The mineral assemblage of these MSI is however very different from the one reported for RUB and KLA samples, insofar as they contain in variable proportions: barian mica, amphibole, magnesite and dolomite ± other accessory phases. Such MSI have been interpreted, based on the chemical composition on the barian mica alone, as the result of the metasomatism of the mantle wedge via a crustal-derived subduction-related fluid.

4.7 CONCLUSIONS

The eclogites (formerly called pyroxenites) of Rubinberg and Klatschmühle enclosed in the peridotites of the Granulitgebirge contain inclusions of granitic melt occurring as nanogranitoids, a peculiar feature that makes them unique among the pyroxenite/eclogite bodies in orogenic peridotites worldwide. In the present study we report the first detailed geochemical and microstructural study of the eclogite lenses and a metasomatic agent present during subduction in the Variscan orogeny. The melt is granitic, peraluminous, hydrous and enriched in Cs, Li, B, Pb, Rb and Ba, all elements typical of the continental crust. Since such a melt cannot be a product of mantle melting, it is interpreted as the preserved metasomatic agent now stored in inclusions in garnet. This preserved melt is the one that originally infiltrated the rock, and acted as a kinetic agent inducing garnet and clinopyroxene crystallization without contributing to the major element chemistry but just to the enrichment of some specific trace elements.

The host eclogite compositions are close to that of a Fe-rich basalt and the high amounts of Cs and U are also consistent with a subduction-related signature. These different signatures imply that the eclogites formed due to metasomatic interaction between mafic/ultramafic layers in mantle peridotite and a melt produced via partial melting of the deeply subducted continental crust. In fact, the low Mg and high Ca and Fe contents in eclogite can be most likely explained

with the presence in the peridotite of a Ca-rich rock layer now totally consumed, as the preserved melt is not enriched in any of these components.

The trapped melt shows a close resemblance in trace elements with the components of the pattern of the durbachite suite attributed to a mature crustal component, thus suggesting that a melt very similar to the one enclosed in the eclogite was involved in durbachite formation. Some of the elements — Th, U, Pb, Nb, Ta and Ti — in RUB and KLA melt patterns show analogue trends also to the ones in the bulk rock of the peridotite and pyroxenite in the T-7 borehole, suggesting that an akin melt was their metasomatic agent.

Despite the presence of melt inclusions entrapped in the garnet the evidence of metasomatism in the eclogites, both modal and cryptic, is limited. In contrast, the metasomatized peridotite and pyroxenite of the T-7 borehole register the melt signature. This discrepancy can be explained with a different degree of metasomatism, with Granulitgebirge rocks experiencing a more limited influx of the melt, not sufficient to impose its signature. The comparison with other pyroxenites and eclogites of the Bohemian Massif shows some similarities only in terms of major elements with the Nové Dvory kyanite eclogite, whereas the trace elements are very different.

5 MELT INCLUSIONS IN UHP ECLOGITE FROM SAIDENBACH RESERVOIR

5.1 INTRODUCTION

The Erzgebirge, in particular its Gneiss-Eclogite Unit, is renowned in the scientific community for the finding of UHP phases in both felsic and mafic rocks. In fact, at Saidenbach reservoir, coesite is reported either as preserved crystals or polycrystalline quartz pseudomorphs after coesite in garnet and omphacite of eclogites (Massonne, 2001; O'Brien and Ziemann, 2008) and in garnet from granulites exclusively as polycrystalline quartz (Schmädicke et al., 1992). Diamond is so far reported exclusively in quartz-muscovite-kyanite gneisses (Massonne, 1999; Nasdala and Massonne, 2000) but not in the eclogites. The discovery of coesite, microdiamonds and other ultra-high pressure minerals in continental rocks indicates that in collisional settings crustal complexes can be transported very deep into the mantle (Coleman and Wang, 2005), presumably within subduction systems (Brueckner, 1998). Obviously the subduction of continental crust to mantle depth is not just important for the formation of UHP minerals, but also because the break-down of different hydrous phases at different depths releases fluids and silicate melts (Cannao` and Malaspina, 2018), which interact with and metasomatize the mantle wedge (Scambelluri et al., 2006). In some cases, these fluids can be trapped as inclusions whose investigation gives valuable information about the nature of the fluid (e.g. Malaspina et al., 2006, 2009). In the Bohemian Massif, and in particular in the Erzgebirge, evidence of trapped fluids in deeply subducted crustal rocks was reported already in 2001 by Stöckhert, who identified diamonds in polyphase inclusions organized in clusters within garnet of the Saidenbach diamond-bearing gneiss. The authors interpreted the inclusions as a COH + silicate fluid generated in the continental crust (see also Stöckhert et al., 2009). The same inclusions have been interpreted later as nanogranitoids, i.e. former melt droplets, and they represent evidence of anatexis at UHP conditions in the diamond-bearing gneisses (Acosta-Vigil et al., 2017b).

In this study we report the occurrence of melt inclusions, both glassy and as nanogranitoids, organized in clusters in the inner part of the garnet of the UHP eclogite at Saidenbach reservoir. The study of these inclusions was performed using Raman spectroscopy, EDS mapping, microprobe analysis of glass inclusions and LA-ICP-MS analysis (similarly to the

approach described in Chapter 4). The results were then combined with the geochemical investigation of major and trace elements of the whole rock and the peak metamorphic minerals. This investigation allows better understanding of how the melt relates to the host rock and, in particular, clarification as to which of the possible genetic processes is responsible for the formation of these eclogites, in presence of melt, at UHP conditions.

5.2 GEOLOGICAL SETTING

The Erzgebirge belongs to the Bohemian Massif (see Chapter 4 for the Bohemian Massif general description) and more in particular to the Saxothuringian Zone (eastern Germany; see Fig. 4.1 for location; Fig. 5.1). It is an oval-shaped NE-SW trending anticline extending for ~80 km (O'Brien and Carswell, 1993; Willner et al., 1997, 2000; Massonne et al., 2007). According to Willner et al. (2000), the Erzgebirge can be divided in four tectonometamorphic units defined by their dominant rock associations and metamorphic evolution: Phyllite Unit, Red-and-Grey Gneiss Unit, Micaschist-Eclogite Unit and Gneiss-Eclogite Unit (Fig. 5.1). The Phyllite unit is the uppermost one, surrounds the Erzgebirge gneiss dome and contains mainly phyllite, graphitic phyllite, quartzite and amphibolite-chlorite schists with local intercalations of slate and shale (Willner et al., 2000). The Red-and-Grey Gneiss Unit is the lowermost unit exposed and it contains mainly orthogneiss ± migmatitic gneiss with rare intercalations of metapelites, quartzite and garnet amphibolite. The HP rocks occur exclusively in the Micaschist-Eclogite and Gneiss-Eclogite units and the UHP ones are limited to the latter unit. Those two units are interpreted to be exhumed, in the Early Carboniferous, along with rocks that have never experienced HP conditions, within a gneiss dome (Willner et al., 2000). The Micaschist-Eclogite Unit crops out in the western Erzgebirge and contains mica schist and local intercalations of quartzites, orthogneisses, marbles, calc-silicate rocks, LT eclogites, metaconglomerates and amphibolites. The Gneiss-Eclogite Unit is underlying the Micaschist-Eclogite one and crops out mainly in the central Erzgebirge - it corresponds to Unit 1 according to the classification of Schmädicke et al., (1992). This unit represents one of the few metamorphic terranes worldwide with both diamonds and coesite: it contains in fact both diamond-bearing, white mica-rich gneisses (Massonne, 1999; Massonne and Nasdala, 2000; Stöckert et al., 2001) also known as *saidenbachites* (from Saidenbach Reservoir, see map in Massonne, 2001) and coesite-bearing eclogites (Schmädicke et al., 1992, 1995; Massonne, 2001; O'Brien and Ziemann, 2008). The diamond-bearing gneisses occur as lenses in migmatitic quartzo-feldspatic and metapelitic gneisses (Willner et al., 1997; Massonne et al., 2007). Microdiamonds were recognized in polyphase inclusions in garnet (Stöckert et al., 2001, 2009) or in single inclusions in garnet, zircon and kyanite (Nasdala and

Massonne, 2000). In addition, the unit hosts also serpentinized garnet peridotites with layers and lenses of garnet pyroxenites (Schmädicke and Evans, 1997; Massonne and Neuser, 2005). The presence of the UHP rocks suggests that the Erzgebirge contain units belonging to the root of the collisional belt (Willner et al., 2000).

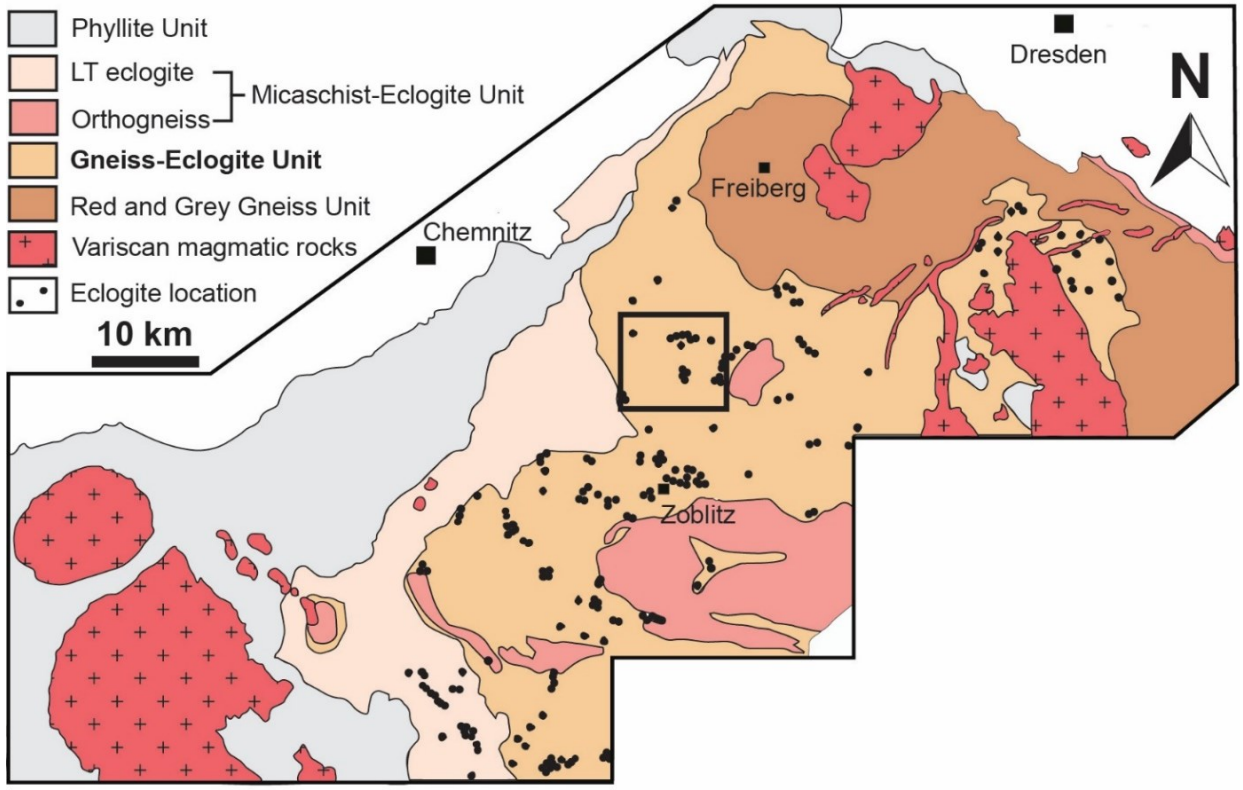

Figure 5.1. Simplified geological map of the Erzgebirge (modified after Willner et al., 2000), the black square indicates the location of Saidenbach Reservoir.

Each unit experienced different P-T conditions but the most extreme were recognized in the *saidenbachites*, ~ 1000°C and >4.5 GPa (Massonne, 1999), as also supported by the finding of α-PbO_2-type structure in the TiO_2 phase (Hwang, 2000). Garnet peridotites belonging to the same unit equilibrated at 900° C and 3.5 GPa (Schmädicke and Evans, 1997) or 1000° C and 4.0 GPa (Massonne and Grosch, 1995). The age of the HP metamorphism is ~340 Ma obtained by U-Pb dating of zircon from the felsic granulites with SIMS and evaporation techniques (Kröner and Willner, 1998; Tichomirowa et al., 2005) but the zircons of the UHP eclogites have been recently dated at 360.5 ± 5.4 Ma and 359.7 ± 5.3 Ma (Schmädicke et al., 2018).

5.3 METHODS

The study of the eclogites has been conducted on 5 thin sections, 5 double-polished thick section (150 μm thick) and on 27 garnets chips from three double-polished thick sections (7 chips for SB_Süd1, 10 for SB-1e and 10 for SB_4) used for the LA-ICP-MS analyses on the melt inclusions. The samples were investigated via an optical microscope with polarized light, Raman spectroscopy and electron microprobe (EMP) at the Institüt für Geowissenschaften of the University of Potsdam in order to determine the mineral assemblage of the nanogranitoids and composition of the mineral phases and glassy inclusions. For the acquisition of the backscattered images (BSE) and the energy dispersive spectrometer (EDS) elemental maps a field emission gun electron microprobe (FEG-EMP) was used at the Museum für Naturkunde in Berlin. The trace element data on mineral phases and melt inclusions were acquired at the Department of Earth Science, ETH Zurich using laser ablation inductively coupled plasma mass spectrometry (LA-ICP-MS). All these methods were used also in Borghini et al. (submitted: Chapter 4) and the reader is referred to this paper/chapter for details of each method.

The rehomogenization experiment was performed with the Multi-anvil module at the Earth Science department “Ardito Desio” of the Universitá degli Studi di Milano. The multi-anvil module is a 6/8 Walker type on a 1000-ton uniaxial press. This multi-anvil can reach maximum pressures of 20 GPa and temperatures up to 2000°C. For the experiment, 3 chips of garnets have been separated from a thick section and put in a Au capsule welded after the filling. The chips are separated from each other and from the capsule walls by SiO_2 powder and the experiment has been run for 24h at 1000°C, 4.5 GPa and dry conditions. The Au capsule has been surrounded by an MgO tube and MgO powder for isolation. This complete assembly is surrounded by a graphite oven and externally by ZrO_2 insulator and inserted into a hole in an octahedron with an edge dimension of 2 cm.

In this chapter we report whole rock data of the three eclogite types, melt major element compositions for types 1 and 2 whereas for the melt trace elements we report only the data of type 1. Major and trace elements of the mineral phases reported here are only from type 1 as well as the major element composition of the rehomogenized nanogranitoids. The general discussion of how melt relates with the host rock is focused on type 1 eclogites.

5.4 SAMPLE DESCRIPTION

The UHP eclogites investigated here are from Saidenbach Reservoir, they occur as lenses and blocks in UHT diamond-bearing gneisses (Massonne, 2001).

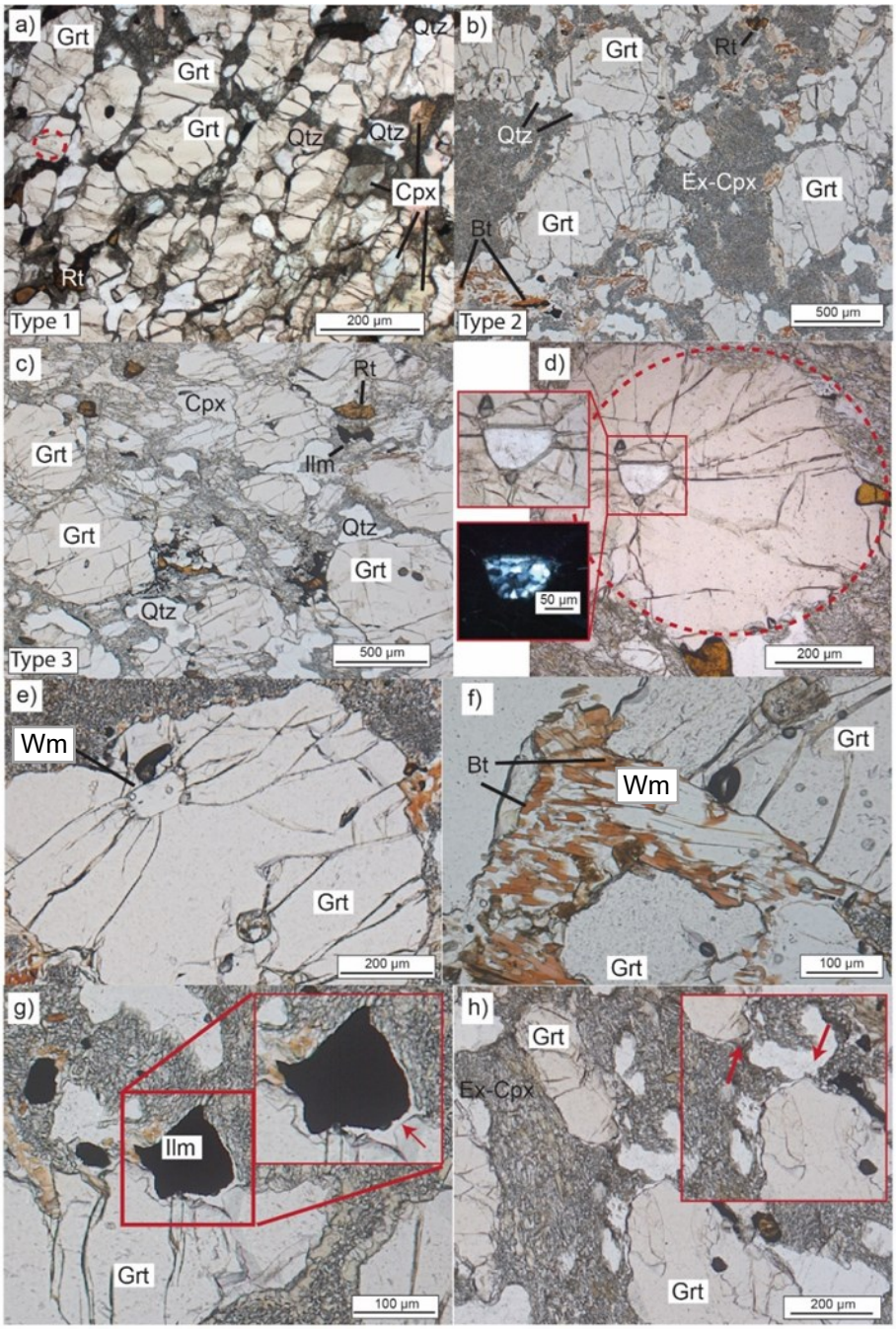

Figure 5.2. Photomicrographs of the three types of Saidenbach UHP eclogite with banded (a) and granoblastic (b-c) texture (the red dash circle indicates a cluster of melt inclusions). The garnet includes: (d) polycrystalline quartz interpreted as a pseudomorph after coesite in the same microstructural position as melt inclusions (indicated with a dashed red circle) and (e) white mica. The latter is also present in the matrix replaced by biotite (f). Thin films of plagioclase can occur along (g) ilmenite and (h) garnet all indicated with the red arrows in the red boxes.

Although layers of eclogite in gneisses occur near the dam, this particular eclogite type is limited to loose boulders in the forest or on the shore of the reservoir, and they are only visible at low water levels (O'Brien and Ziemann, 2008). The eclogite samples come from the southern part of the reservoir, a different location from where the coesite findings have been previously reported (Massonne, 2001; O'Brien and Ziemann). The eclogites targeted in this thesis are classified in three different types based on texture and phases occurrence. Type 1 is banded (sample SB_Süd1-1; Fig. 5.2 a) whereas Type 2 and 3 are granoblastic (samples SB-1e, EAm2, SB 3, SB 4; Fig. 5.2 b-c) and exclusively Type 2 contains white mica (SB-1e and EAm2). In Type 1 the layering is defined by all the main phases, which are generally elongated. Apart from the textural differences and the local presence of white mica, they all show the same main mineral assemblage comprising garnet (~50-45 % in volume), clinopyroxene (or symplectite pseudomorphing it) (~ 40 %), quartz (~ 5-8 %), minor secondary plagioclase (~ 2%) often in aggregates with white mica and biotite, ± apatite, ± white mica, ± biotite and coarse-grained rutile and ilmenite as accessory phases (Fig.5.2).

Garnet is subhedral, colorless in thin section and has an average size of 1-2 mm in diameter. It includes clinopyroxene, rutile, in most of the sample quartz -either as palisade or polycrystalline aggregates surrounded by radial cracks- and melt inclusions (Fig.5.2d). Garnet often shows cracks filled with fine-grained green amphibole or rarely clinozoisite/carbonate (EAm2). Along the rim garnet is generally replaced by green amphibole ± plagioclase and sometimes is rimmed by a discontinuous film of plagioclase. Clinopyroxene is generally smaller than the garnet, colorless, with sub-prismatic shape and showing oblique extinction (~ 45°). Often it is present just as a relict within its replacement product of fine- to very-fine-grained symplectite mainly made of green amphibole, clinopyroxene and plagioclase. Quartz is present in two different microstructural position: (i) in the matrix, medium-grained in type 2 -3 and arranged in medium to fine-grained ribbons in type 1; (ii) included in the garnet and either polycrystalline or as a palisade microstructure, interpreted as a quartz pseudomorph after coesite and in the same microstructural position of the melt inclusions (Fig.5.2d). Plagioclase is mainly interstitial, forming a discontinuous rim around the garnet, ilmenite and rutile, sometimes extremely thin which may be interpreted as a possible melt pseudomorph (Fig. 5.2g-h), or in aggregates with biotite especially as a reaction rim around white mica. In both cases, excluding the thin rims, it exhibits polysynthetic twinning. White mica occurs in type 2 eclogites with subhedral to euhedral shape. In the matrix it is medium to coarse -grained often close to the garnet rim, sometimes associated with plagioclase and replaced along the rim by biotite (Fig. 5.2 e). In one of the samples it can also be found as a subhedral medium- to fine-grained inclusion in the garnet surrounded by radial cracks (Fig. 5.2f).

Apatite is subhedral, fine-grained and with a cloudy core. Biotite is often fine-grained and in an aggregate with plagioclase and in some rare cases is also present in the matrix in subhedral medium-grained flakes/needles (type 1). Rutile is coarse-grained, often rimmed by ilmenite and in type 1 is also elongated marking the banding.

5.5 MELT INCLUSIONS PETROGRAPHY

Melt inclusions, both nanogranitoids and glassy, occur in large clusters in the inner part of the garnet. Their random distribution in the garnet suggest that they are primary and thus trapped during the garnet growth (Roedder, 1984) (Fig.5.3a). The glassy inclusions, 2-4 μm in diameter, were initially identified because they are isotropic under crossed polars and are the first ever reported in eclogites (Fig. 5.3e-f-g-h). They range from isometric to prismatic, can contain rutile or dolomite as accessory phases and often have a shrinkage bubble (Fig. 5.3e-h). They represent less than 10% of the total of inclusions in the cluster. Nanogranitoids are coarser (Fig.5.3b-c-d-e), from 5-20 μm in diameter, they show a well-developed negative crystal shape and some of the bigger ones show also some healed cracks where the garnet shows a clearly different composition, poorer in Mg and richer in Ca (Fig. 5.3 d and 5.4 a). The main mineral assemblage in the nanogranitoids, constant in all the different types of eclogite, includes biotite, calcite, kumdykolite, quartz/very rare cristobalite, a phase with a main Raman peak at 430 cm^{-1}, white mica, kokchetavite, another with the main peak at 412 cm^{-1}, ± graphite (Fig. 5.5). Sometimes nanogranitoids are not fully crystallized and they can also contain some glass identified via Raman spectroscopy. Biotite and white mica are the only euhedral phases and they are both nucleating from the inclusion wall, whereas calcite is generally very small and subhedral. Kumdykolite and kokchetavite are generally subhedral with a prismatic elongated shape and quartz is interstitial (Fig. 5.4).

The two unnamed phases with main peaks respectively at 430 cm^{-1} and 412 cm^{-1} were identified via detailed investigation of the nanogranitoids via Raman spectroscopy (Fig. 5.5e-f). The Raman spectrum of phase 430 shows main peak at 430 cm^{-1}, a secondary at 292 cm^{-1}, minor peaks at 128 and 182 cm^{-1} and further weaker peaks at 240, ±260, ±380, 480 and 820 cm^{-1}. In most of the nanogranitoids multi-window analysis capable of detecting the presence of H_2O also show an OH band typical of the glass associated with this phase (Fig. 5.5e). The phase 412 is much less abundant than the 430 and it is characterized, besides the main peak at 412 cm^{-1} as, secondary peaks at 105 and 831 cm^{-1} and a weaker peak at 470 cm^{-1} (Fig. 5.5f).

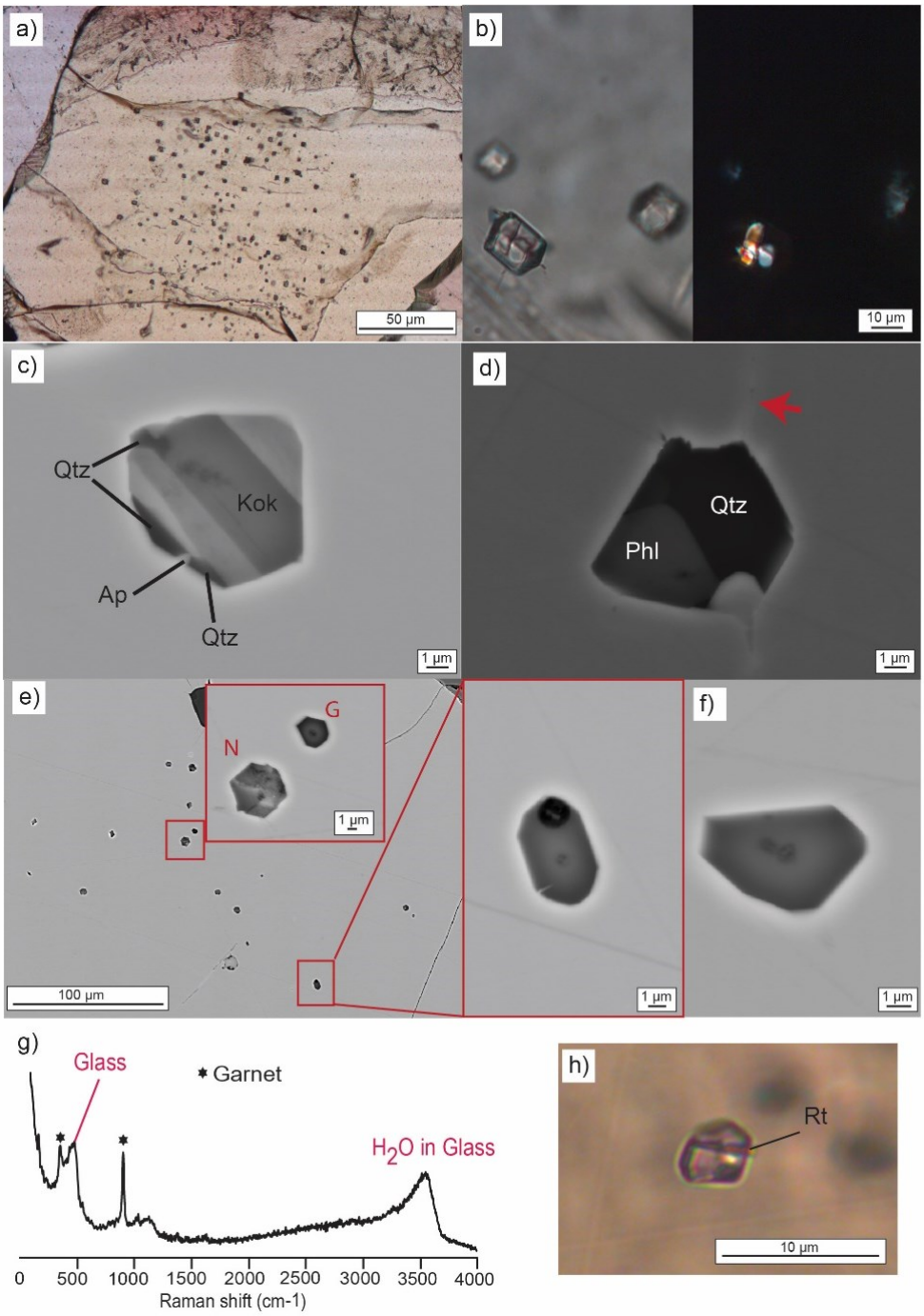

Figure 5.3. Photomicrograph (a-b-h) and backscattered electron (BSE) images (c-d-e-f) of melt inclusion occurrences in UHP eclogite. (a) Melt inclusions are distributed in a cluster in the inner part of the garnet. (b) Part of a nanogranitoids cluster with parallel (left) and cross polars (right). (c): Nanogranitoid containing quartz (Qtz), kokchetavite (Kok) and apatite (Ap). (d): Nanogranitoids containing quartz and phlogopite (Phl) with indicated, with a red arrow, a healed crack with formation of new garnet. (e) Melt inclusion cluster with nanogranitoids (N) and glassy (G) types together, the glass inclusion in the red rectangle has a shrinkage bubble and the dot visible at the center is beam damage of the EPMA. (f) Glassy inclusion. (g) Raman spectrum of a glassy inclusion with indicated the position of the H_2O band. (h) Photomicrograph of a glass inclusion that trapped a rutile.

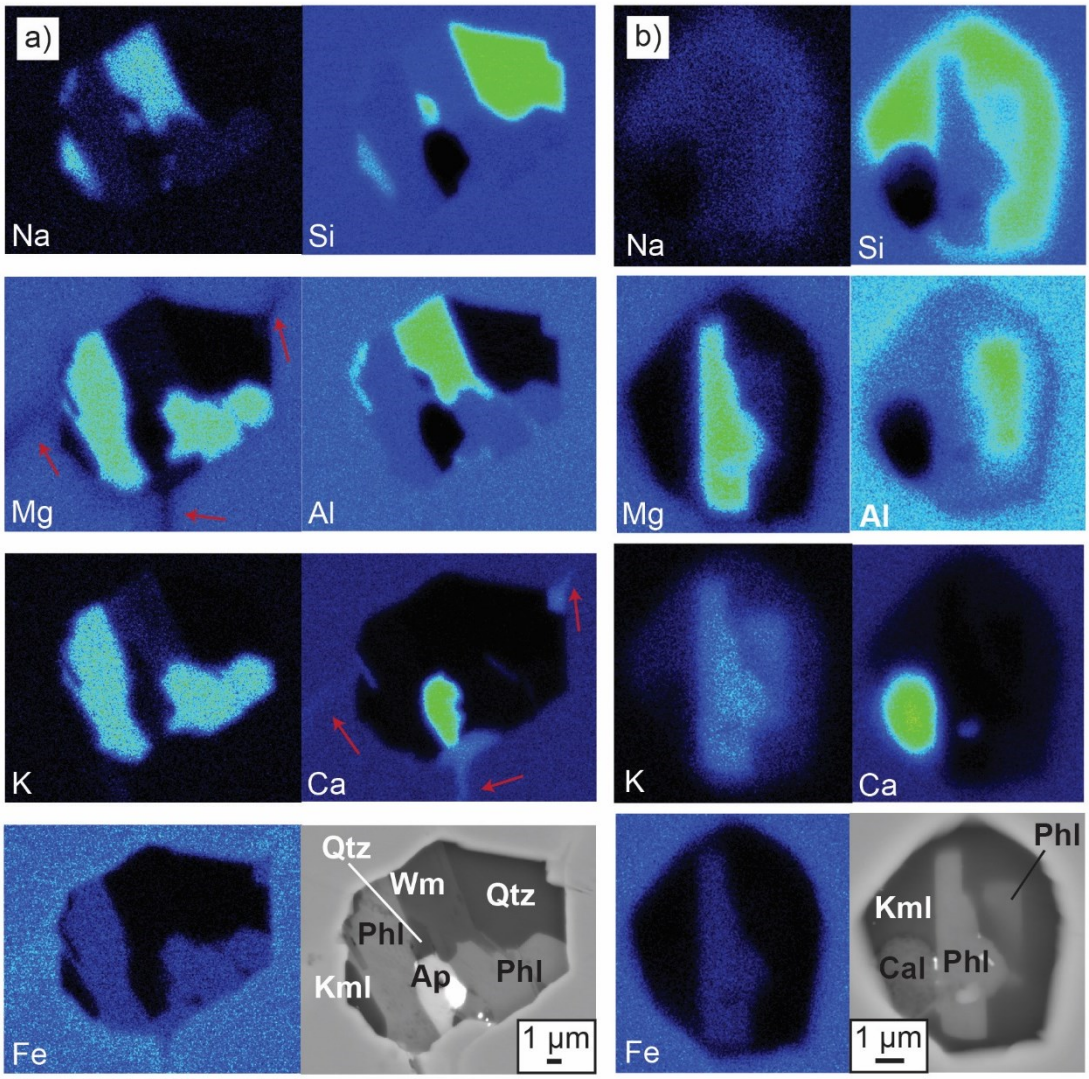

Figure 5.4. EDS (Energy Dispersive Spectrometer) elemental maps of nanogranitoids with (a) phlogopite, kumdykolite, quartz, while mica, apatite and healed cracks with formation of new garnet indicated with the red arrows. (b) nanogranitoid with kumdykolite, phlogopite and calcite.

In back scattered images both phases appear dark grey, similar to quartz, feldspars or glass, suggesting they are both mainly composed by light elements, e.g. with no or very low FeO and MgO. Phase 430 was analyzed via EMPA and shows indeed a composition rich in SiO_2 (75.66 wt% average), Al_2O_3 (15.46 wt %), CaO (3.35 wt%), K_2O (2.43 wt%), Na_2O (2.25 wt%), and poor in FeO (0.94 wt%), MgO (0.15 wt%), TiO_2 (0.04 wt%) and MnO (0.01 wt%) (see Table 5.1).

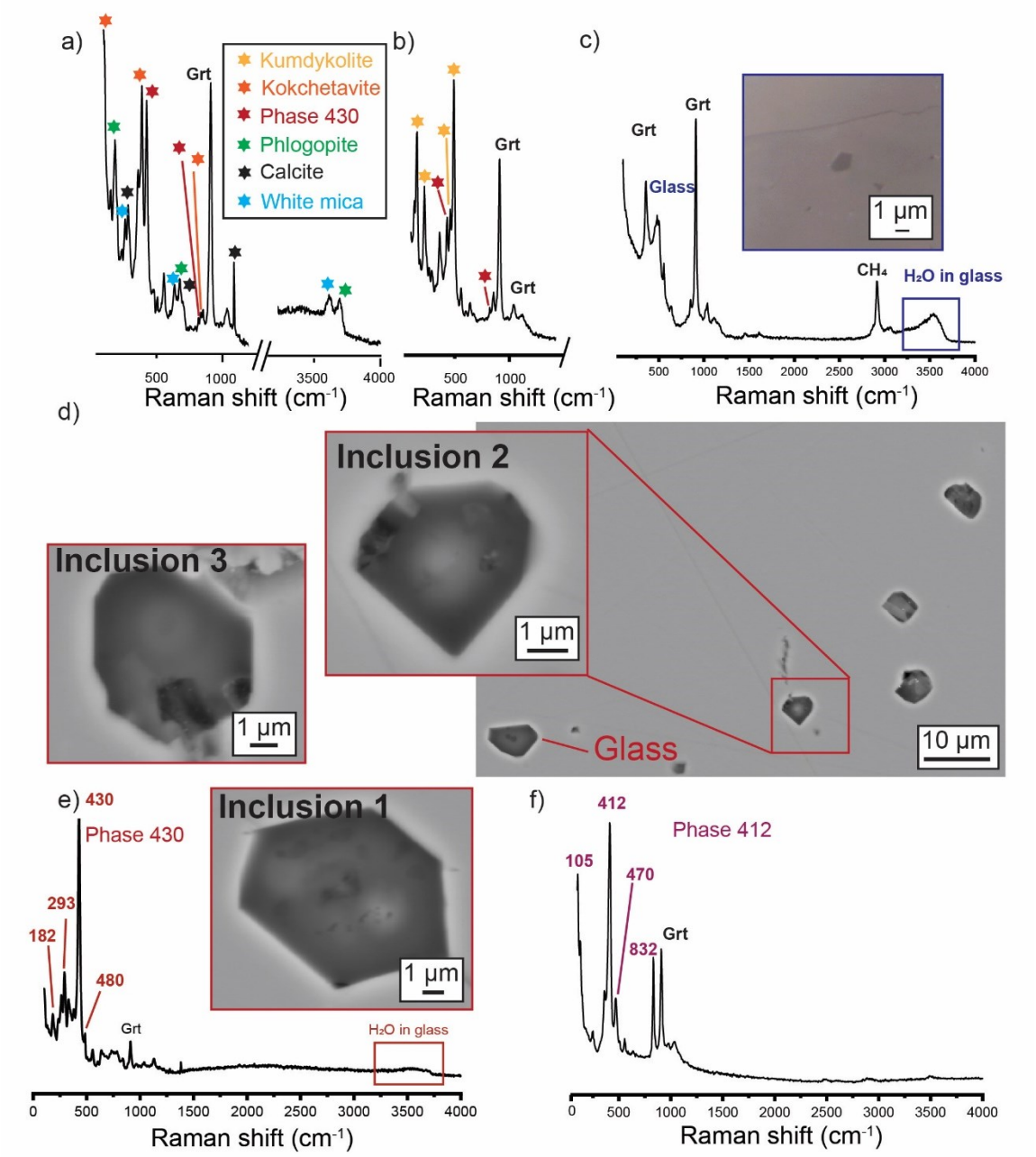

Figure 5.5. Raman spectra of the main phases constituting the nanogranitoids (a-b) and of a rehomogenized glassy inclusion (c): a) kokchetavite (here peaks at 110-391-835 cm^{-1}), phase 430 (peaks 430-820 cm^{-1}), phlogopite (peaks 190-677-3694 cm^{-1}), calcite (peaks 286-710-1089 cm^{-1}) and white mica (peaks 200-260-637-3614 cm^{-1}); b) phase 430 (peaks 430-824 cm^{-1}) and kumdykolite (156-223-462-494 cm^{-1}) and c) re-homogenized inclusions with methane, above the spectrum picture of the inclusion in reflected light. d) BSE images of the inclusions measured with phase 430 (see table 5.1). Raman spectra of phase 430 (e) and 412 (f).

Sample name	Inclusion 1	Inclusion 2	Inclusion 3	Average	Mesoperthite
Name analyses	163	164	165		
References					Data repository Ferrero et al., 2015
wt %					
SiO_2	77.27	74.48	75.22	75.66	65.18
TiO_2	0.02	0.07	0.02	0.04	0.01
Al_2O_3	14.57	14.98	16.84	15.46	19.94
Fe_2O_3	-	-	-	-	-
FeO	1.07	0.94	0.81	0.94	0.25
MnO	0.00	0.02	0.00	0.01	0.01
MgO	0.18	0.21	0.06	0.15	0
CaO	3.06	3.39	3.60	3.35	0.67
Na_2O	2.08	2.11	2.58	2.25	4.48
K_2O	2.36	3.20	1.73	2.43	9.27
P_2O_5	n.a.	n.a.	n.a.	n.a	n.a
LOI	-	-	-	-	-
TOTAL	100.62	99.38	100.85	100.28	99.81

n.a.=not analyzed

Table 5.1. EPMA analyses of the composition of phase 430 and mesoperthite composition (supplementary material of Ferrero et al., 2015) for comparison.

5.6 WHOLE ROCKS, MINERALS AND MELT GEOCHEMISTRY

5.6.1 WHOLE ROCK

The whole rock composition is very similar in all the three different types of eclogite with some slight differences (see Table 5.2). SiO_2 ranges between 51.37 wt % (Type 3) and 53.02 wt% (Type 1), FeO between 11.30 wt% (Type 2) and 13.27 wt% (Type 3), MgO between 7.07 wt % (Type 2) and 5.93 wt% (Type 1) and TiO_2 from 0.92 wt% (Type 2) and 2.00 wt% (Type 3). Al_2O_3 (15.79 wt%), CaO (8.76 wt%), Na_2O (2.59 wt%) and MnO (0.19 wt%) are quite homogeneous in all the samples whereas all the samples are almost devoid of K_2O, i.e. from 0.61 wt% (Type 1) to 0.06 wt % (Type 3): Mg# ranges between 45 (Type 1) and 52 (Type 2).

The trace element patterns of the eclogites are also overall very similar, with a very strong Pb and Ti positive anomaly and a positive anomaly for most of high field strength elements (=HFSE, i.e. Zr, Hf, Nb and Ta) for Type 1 and 3. They all show slight enrichment in Rb and Cs, higher for Type 1 and 2 (Fig. 5.6 a). All the samples show a negative Ba, Eu and Sr anomaly and Type 2 show also a slight negative Nb anomaly but positive Ta, Zr and Hf anomalies less strong then in the other two types.

Sample type (sample name)	Eclogite type 1 (SB_Süd 1)	Eclogite type 2 (SB-1e)	Eclogite type 3 (SB_4)	Eclogite type 3 (SB_3)	Average	Zoesite and phengite-bearing eclogite
Name	1	2	3	4		1
Reference	This study					Skjerlie & Patiño Douce, 2002
wt %						
SiO_2	53.02	51.26	51.74	51.00	51.76	49.96
TiO_2	1.98	0.92	1.86	2.13	1.72	0.76
Al_2O_3	15.49	16.14	15.72	15.8	15.79	19.97
Fe_2O_3	-	-	-	-	-	2.00
FeO	12.79	11.30	12.64	13.9	12.66	4.03
MnO	0.19	0.17	0.18	0.21	0.19	0.11
MgO	5.93	7.07	6.54	6.21	6.44	8.15
CaO	8.19	9.58	8.82	8.45	8.76	12.72
Na_2O	2.69	2.16	3.06	2.44	2.59	2.57
K_2O	0.61	0.44	0.05	0.06	0.29	0.14
P_2O_5	0.09	0.07	0.16	0.22	0.14	-
TOTAL	100.98	99.11	100.77	100.42	100.32	100.41
Mg#	45	52	48	44	47	78
ppm						
Cr	27	84	18	25	39	
Ni	41	38	34	36	37	
Rb	14	10	1.20	1.40	6.53	
Cs	0.70	0.70	0.20	0.10	0.43	
Ba	78	29	13	13	33	
Th	1.30	0.50	0.90	0.90	0.90	
U	0.40	0.30	0.30	0.40	0.35	
Nb	15	5.50	12	16	12	
Ta	1.00	0.50	0.70	0.80	0.75	
La	8.00	2.30	10	16	9.20	
Ce	19	6.40	24	39	22	
Pb	9.20	26	5.00	14	13	
Pr	2.62	1.06	3.41	5.50	3.15	
P	900	700	1600	2200	1350	
Sr	73	54	156	150	108	
Nd	13	6.20	17	25	15	
Zr	220	110	185	272	197	
Hf	5.60	2.70	4.90	6.60	4.95	
Sm	4.02	2.90	4.63	6.61	4.54	
Eu	0.92	0.83	1.29	1.88	1.23	
Gd	5.55	5.06	5.67	7.68	5.99	
Tb	1.03	0.92	0.96	1.18	1.02	
Dy	7.18	5.92	6.06	7.27	6.61	
Ti	19800	9200	18600	21300	17225	
Y	41	30	33	39	36	
Ho	1.59	1.22	1.35	1.55	1.43	
Er	4.96	3.55	3.88	4.65	4.26	
Tm	0.68	0.45	0.52	0.63	0.57	
Yb	4.38	3.11	3.35	4.07	3.73	
Lu	0.66	0.48	0.57	0.67	0.60	
Li	n.d.	n.d.	n.d.	n.d.	n.d.	
B	n.d.	n.d.	n.d.	n.d.	n.d.	

n.d.= not determined

Table 5.2. Whole rock major and trace elements composition of UHP Saidenbach eclogite and major element composition of zoisite and phengite-bearing eclogite (Skjerlie and Patiño Douce, 2002).

The chondrite-normalized rare earth element patterns show enrichment in LREE and a lower content of HREE (La_N/Yb_N 1.31 and 2.53 respectively) for Type 1 and 3, whereas the pattern for Type 2 is depleted in LREE, shows a positive Sm anomaly and the HREE have the same trend as for the other types with La_N/Yb_N=0.53 (Fig. 5.6 b). The Eu_N/Eu^* ratio [$Eu_N/Eu^*=Eu_N/\sqrt{(Sm_N*Gd_N)}$] is 0.60 for Type 1, 0.66 for Type 2 and 0.79 for Type 3. The comparison with N- and E-MORB (both from Sun & McDonough, 1989) show that whereas the enrichment of trace elements is generally similar to E-MORB, Cs and Pb show opposite anomalies.

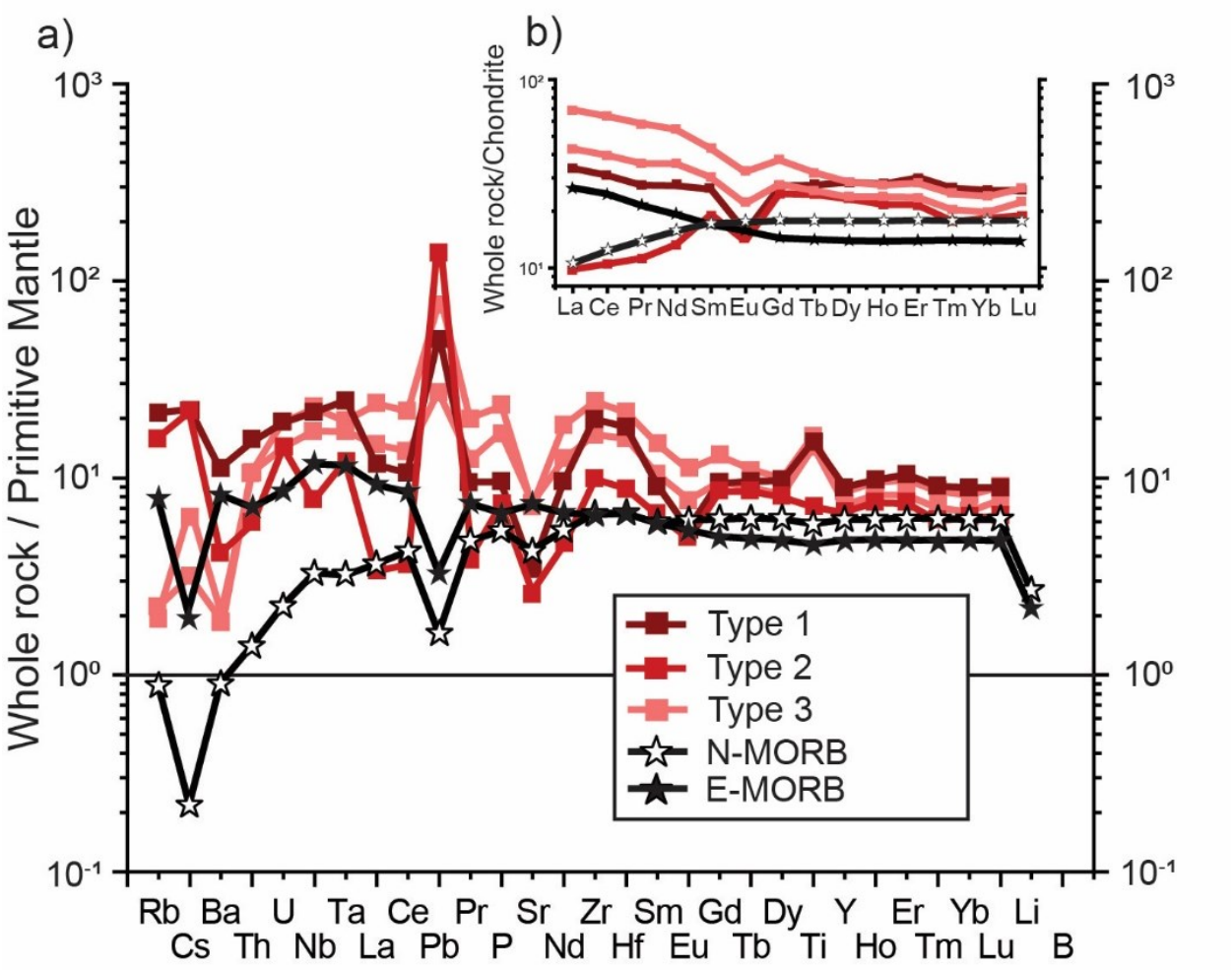

Figure 5.6. Whole rock trace element patterns (a) and rare earth element (REE) patterns (b) of UHP Saidenbach eclogite (see Table 5.2) compared with E- and N-MORB (both from Sun and McDonough, 1989). All the trace element data have been normalized to primitive mantle (Sun and McDonough, 1989 except for B which is taken from McDonough and Sun, 1995) whereas the REE have been normalized to chondrite (Sun and McDonough, 1989).

In terms of REE, the patterns of eclogite Type 1 and 3 have a trend similar to the E-MORB but higher enrichment whereas Type 2 have a trend more similar to N-MORB but with Eu anomalies.

5.6.2 MINERAL PHASES

Representative compositions of garnet and clinopyroxene are reported in Table 5.3 and 5.4 respectively (for the complete dataset see the Supplementary material D Tables S5.1, S5.2, S5.3 and S5.4).

Phase	**Garnet**									
Name	47	48	49	50	63	86	89	112	117	118
wt %										
SiO_2	38.79	38.45	38.54	38.63	39.06	38.39	38.33	38.57	38.75	38.33
TiO_2	0.28	0.26	0.26	0.34	0.08	0.23	0.12	0.28	0.30	0.17
Al_2O_3	21.80	22.10	21.89	21.93	22.05	22.01	21.81	21.86	22.04	22.03
Fe_2O_3										
FeO	19.60	19.57	19.38	19.24	21.06	20.61	21.74	20.34	20.77	21.69
MnO	0.39	0.36	0.30	0.36	0.41	0.39	0.42	0.35	0.39	0.38
MgO	7.95	7.88	8.08	8.12	8.08	7.77	6.99	7.16	7.27	7.29
CaO	9.67	9.91	10.14	10.21	8.37	9.13	9.24	10.07	9.63	8.98
Na_2O	0.10	0.16	0.13	0.13	0.06	0.10	0.09	0.16	0.12	0.06
K_2O	0.00	0.00	0.01	0.00	0.01	0.00	0.00	0.00	0.01	0.01
Cr_2O_3	0.01	0.03	0.02	0.03	0.03	0.05	0.03	0.02	0.02	0.02
P_2O_5										
TOTAL	98.57	98.70	98.74	98.98	99.18	98.61	98.73	98.79	99.27	98.95
Mg#	**41**	**41**	**43**	**43**	**40**	**40**	**36**	**38**	**38**	**37**
Si	**2.99**	**2.97**	**2.97**	**2.97**	**3.00**	**2.97**	**2.98**	**2.99**	**2.99**	**2.97**
Ti	0.02	0.01	0.02	0.02	0.00	0.01	0.01	0.02	0.02	0.01
Al	1.98	2.01	1.99	1.99	2.00	2.01	2.00	2.00	2.00	2.01
	2.00	**2.03**	**2.01**	**2.01**	**2.00**	**2.02**	**2.01**	**2.01**	**2.02**	**2.02**
Fe	1.27	1.26	1.25	1.24	1.35	1.33	1.41	1.32	1.34	1.41
Mn	0.03	0.02	0.02	0.02	0.03	0.03	0.03	0.02	0.03	0.03
Mg	0.91	0.91	0.93	0.93	0.93	0.90	0.81	0.83	0.83	0.84
Ca	0.80	0.82	0.84	0.84	0.69	0.76	0.77	0.84	0.79	0.75
	3.00	**3.01**	**3.04**	**3.03**	**2.99**	**3.01**	**3.02**	**3.00**	**2.99**	**3.02**
mol %										
Alm	**42**	**42**	**41**	**41**	**45**	**44**	**47**	**44**	**45**	**47**
Prp	**30**	**30**	**31**	**31**	**31**	**30**	**27**	**28**	**28**	**28**
Sps	**1**	**1**	**1**	**1**	**1**	**1**	**1**	**1**	**1**	**1**
Grs	**27**	**27**	**28**	**28**	**23**	**25**	**25**	**28**	**27**	**25**

Table 5.3. Representative EMPA major elements analyses of garnet.

Garnets of Type 1 eclogite are homogeneous from core to rim and they are on average $Prp_{29}Alm_{44}Grs_{27}Sps_1$ with an average Mg# of 40. Normalized trace elements (Fig. 5.7 a) show enrichment in U, Th and Sm and a negative anomaly in Ba, Nb, Sr, Ti and Li.

Phase	Clinopyroxene									
								Profile 4		
Name	37	56	119	120	121	122	130	131	132	133
wt %										
SiO_2	55.22	54.86	54.58	55.14	54.65	55.48	50.78	54.97	54.96	54.91
TiO_2	0.33	0.39	0.35	0.34	0.36	0.34	0.43	0.36	0.37	0.33
Al_2O_3	14.13	14.00	13.91	13.88	13.95	13.82	13.58	13.57	13.47	13.41
Fe_2O_3										
FeO	3.48	4.30	3.64	3.73	3.89	3.88	4.32	4.41	4.14	4.04
MnO	0.04	0.06	0.00	0.05	0.02	0.03	0.04	0.07	0.03	0.02
MgO	7.61	7.35	7.64	7.57	7.54	7.41	8.05	7.41	7.44	7.50
CaO	12.75	12.39	12.89	12.78	12.75	12.68	12.10	12.72	12.63	12.70
Na_2O	6.45	6.84	6.54	6.73	6.68	6.38	6.51	6.51	6.53	6.57
K_2O	0.00	0.00	0.00	0.00	0.00	0.00	0.00	0.01	0.01	0.00
Cr_2O_3	0.103	0.03	0.01	0.08	0.05	0.04	0.06	0.06	0.08	0.037
P_2O_5										
TOTAL	100.00	100.18	99.55	100.30	99.89	100.03	95.87	100.10	99.66	99.48
Mg#	**80**	**75**	**79**	**78**	**77**	**77**	**77**	**75**	**76**	**77**
Si	1.96	1.95	1.95	1.95	1.94	1.98	1.87	1.96	1.96	1.96
Ti	0.01	0.01	0.01	0.01	0.01	0.01	0.01	0.01	0.01	0.01
Al	0.59	0.59	0.58	0.58	0.58	0.58	0.59	0.57	0.57	0.57
Fe	0.10	0.13	0.11	0.11	0.12	0.12	0.13	0.13	0.12	0.12
Mn	0.00	0.00	0.00	0.00	0.00	0.00	0.00	0.00	0.00	0.00
Mg	0.40	0.39	0.41	0.40	0.40	0.39	0.44	0.39	0.40	0.40
Ca	0.49	0.47	0.49	0.48	0.49	0.48	0.48	0.49	0.48	0.49
Na	0.44	0.47	0.45	0.46	0.46	0.44	0.47	0.45	0.45	0.46
K	0.00	0.00	0.00	0.00	0.00	0.00	0.00	0.00	0.00	0.00
Cr	0.00	0.00	0.00	0.00	0.00	0.00	0.00	0.00	0.00	0.00
Jd	44	47	45	46	46	44	47	45	45	46

Table 5.4. Representative EMPA major elements analyses of clinopyroxene.

The REE pattern in garnet shows a typical depletion in LREE and enrichment in HREE, coupled with a negative Eu anomaly (Eu_N/Eu^*=0.62) (Fig. 5.7 b). In type 1 eclogite clinopyroxene is often replaced by symplectite. Where preserved, this phase is an omphacite with an average Jd content of 44 mol % and Mg# of 77. Clinopyroxenes are enriched in Li, Th, U and Pb (Fig. 5.7 c). The

REE show a convex-upward shape with an enrichment in LREE and depletion in HREE, La/Yb=21, a negative Eu anomaly (Eu_N/Eu^*=0.66) and a positive anomaly for Gd (Fig. 5.7 d).

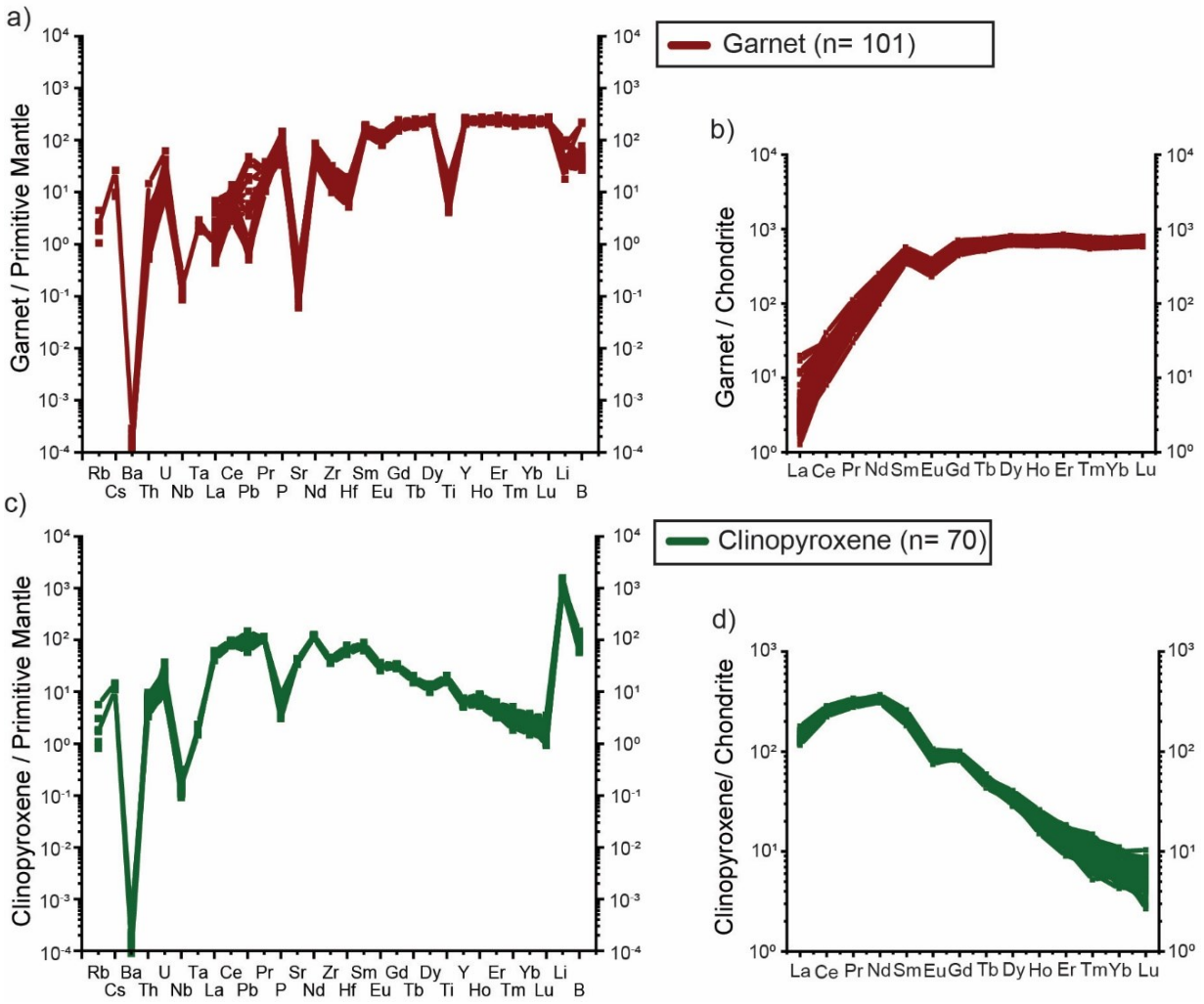

Figure 5.7. Trace elements (a) and REE (b) patterns of garnets and trace elements (c) and REE (d) patterns of clinopyroxene (see Table 5.3 and 5.4). For the normalization values see caption Figure 5.6.

5.6.3 MELT COMPOSITION AND RE-HOMOGENIZATION EXPERIMENTS

The composition of the melt has been determined via microprobe analysis of the glassy inclusions and re-homogenization experiments of the nanogranitoids with a multi-anvil press. The experiment has been performed at 4.5 GPa and 1000°C, with the re-homogenization condition corresponding to the average conditions determined for the Gneiss-Eclogite Unit (see Fig. 5.5c for spectrum rehomogenized glass). Based on the petrographic evidence described above, these

eclogites reached UHP conditions at least in the coesite stability field. The conditions chosen for the experiments correspond to those reported for the diamond-bearing gneisses (Massonne, 1999) and the garnet peridotite (Massonne and Grosch, 1994) that should be the same as for the UHP eclogite and thus for the garnet growth. The glass is granitic, hydrous, high in alkalis with $Na_2O + K_2O$= 9.31 wt% (Na_2O/K_2O = 0.75) and mildly peraluminous (ASI= 1.10) (Fig. 5.8). The melt generally contains small amounts of FeO, MgO, CaO and TiO_2 (0.97 wt%, 0.24 wt%, 0.61 wt% and 0.04 respectively) and on average the H_2O content, determined by difference from the total in the EMPA analyses, is 4.5 wt% (Table 5.5).

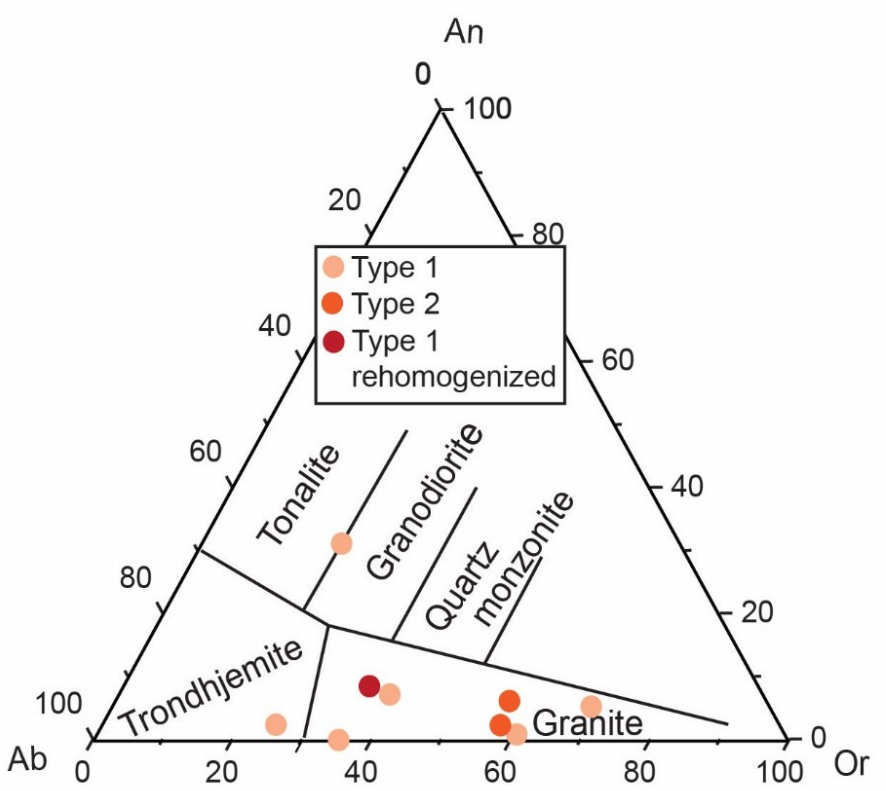

Figure 5.8. CIPW anorthite-albite-orthoclase (An-Ab-Or) diagrams showing normative composition of Type 1 preserved and re-homogenized and type 2 preserved glassy inclusions. The field in the diagram are from (Bartoli et al., 2016a).

The trace element patterns of the melt have been acquired for both inclusions with and without cracks and no substantial differences have been observed, suggesting that decrepitation did not affect melt composition and thus they are both representative of the same melt. The measured inclusions are enriched in LILE -Cs in particular-, Th, U, Pb, Li and B whereas Nb, Nd and Ti show a negative anomaly (Fig. 5.9). The melt is also moderately enriched in LREE (Average in Table 5.6; for the complete dataset see Table S5.5).

Sample type	Melt type 1 eclogite					Melt type 2 eclogite		Melt type 1 rehomogenized inclusion	Average
Name	1	2	3	4	5	6	7	8	
wt %									
SiO_2	70.72	68.69	69.30	70.12	72.86	70.07	66.75	69.16	**69.71**
TiO_2	0.06	0.06	0.04	0.00	0.00	0.05	0.02	0.13	**0.04**
Al_2O_3	14.91	14.35	12.89	15.52	15.01	14.06	14.51	14.90	**14.52**
Fe_2O_3	-	-	-	-	-	-	-	-	**-**
FeO	0.66	1.14	0.81	1.09	0.63	0.80	0.97	1.63	**0.97**
MnO	0.00	0.00	0.00	0.00	0.00	0.00	0.00	0.01	**0.00**
MgO	0.05	0.43	0.11	0.22	0.06	0.17	0.44	0.42	**0.24**
CaO	0.32	0.93	0.41	0.60	0.30	0.43	0.83	1.07	**0.61**
Na_2O	6.16	3.83	3.15	1.70	6.30	3.41	3.29	3.97	**3.98**
K_2O	4.68	4.02	7.09	6.34	3.09	6.94	6.84	3.63	**5.33**
P_2O_5	0.05	0.05	0.00	0.03	0.00	0.07	0.00	0.02	**0.03**
TOTAL	97.61	93.50	93.79	95.64	98.25	96.00	93.64	94.94	**95.42**
H_2O content	2.32	6.47	6.17	4.33	1.72	3.95	6.29	5.06	**4.54**
ASI	0.94	1.16	0.95	1.44	1.05	1.01	1.01	1.20	**1.10**
CaO/Al_2O_3	0.02	0.22	0.23	0.40	0.03	0.03	0.06	0.06	**0.13**
$Na_2O + K_2O$	10.84	7.85	10.24	8.05	9.39	10.35	10.13	7.60	**9.31**
Na_2O / K_2O	1.32	0.95	0.44	0.27	2.04	0.49	0.48	1.09	**0.75**
Mg#	11	40	19	26	15	28	45	31	**27**

Table 5.5. Composition of preserved glassy inclusions of Type 1 and Type 2 Saidenbach eclogite and re-homogenized inclusions of Type 1 eclogite, H_2O determined as difference from the total.

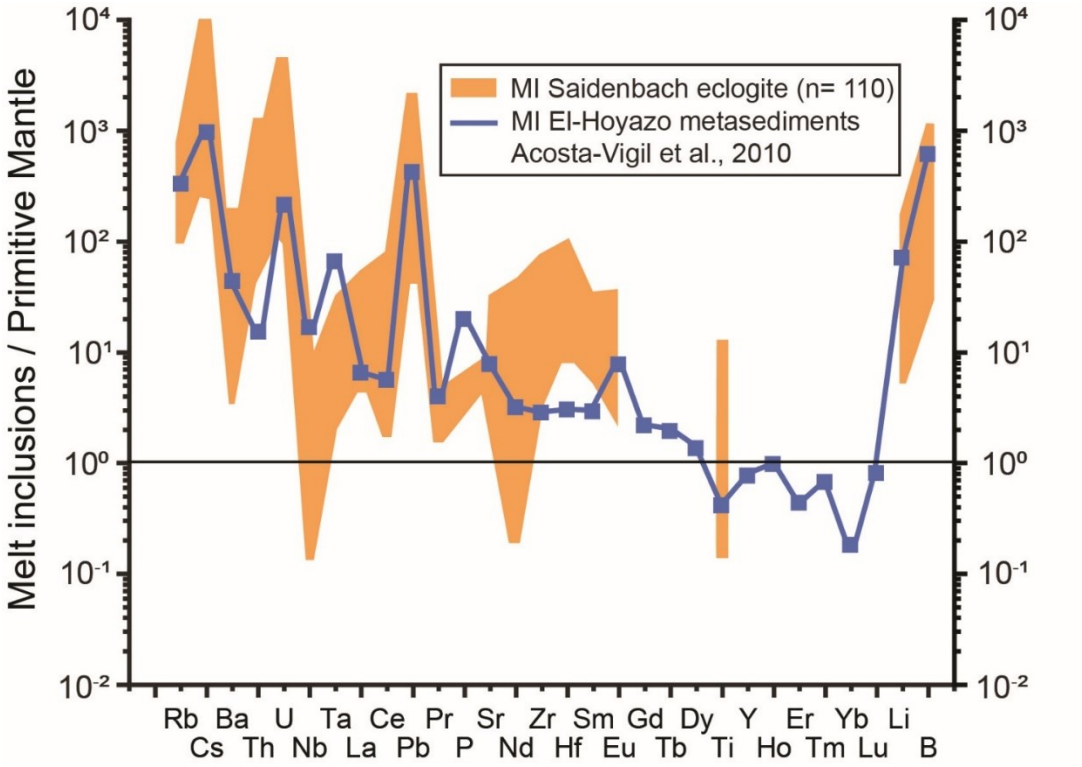

Figure 5.9. Trace elements patterns of the melt inclusions of Saidenbach eclogite compared with the average composition of melt inclusions of the metapelites of El Hoyazo. For the normalization values see caption Figure 5.6.

Sample type	Average melt type 1 eclogite
No. Analyses	110
ppm	
Cr	120
Ni	118
Rb	180
Cs	39
Ba	246
Th	23
U	14
Nb	1.14
Ta	0.44
La	14
Ce	29
Pb	104
Pr	3.01
P	508
Sr	386
Nd	8.52
Zr	261
Hf	8.49
Sm	3.63
Eu	1.69
Gd	-
Tb	-
Dy	-
Ti	1058
Y	-
Ho	-
Er	-
Tm	-
Yb	-
Lu	-
Li	53
B	86

Table 5.6. Maximum average trace elements analyses for the melt inclusions of type 1 Saidenbach eclogite.

5.7 DISCUSSION

The UHP eclogite of Saidenbach Reservoir contains the first preserved glass found in eclogites worldwide (see Cesare et al., 2015 Table 1 for a compilation of melt inclusions finding in metamorphic rocks). As the glassy and crystallized inclusions (nanogranitoids) are in the same cluster, and considering the mineral assemblage in the latter, all the inclusions can be interpreted as former droplets of the same melt, trapped in the garnet while it was growing (Ferrero et al., 2012). Therefore, glassy inclusion composition is representative of the whole melt, as supported by the fact that the compositions of both glassy inclusions and re-homogenized nanogranitoids are similar (Table 5.5). The presence of quartz pseudomorph after coesite in the same microstructural position of the melt inclusions suggests that garnet formation, in presence of melt, took place at UHP conditions.

5.7.1 COMPARISON WITH PREVIOUS INCLUSION STUDIES IN UHP ROCKS

Multiphase solid inclusions (MSI) have been previously reported in UHP eclogite from the Dabie Shan, east-central China (Gao et al., 2012; Liu et al., 2018). However, these MSIs are different from the melt inclusions found in the Erzgebirge in terms of microstructure, mineral assemblages, geochemistry and absence of glass in the Chinese samples. In particular, Gao et al. (2012) reported inclusions with K-feldspar + quartz ± plagioclase and interpreted them as crystallized melt, thus as evidence of partial melting in the UHP eclogite (Gao et al., 2012). However, such inclusions are not preserved as they show radial cracks that suggest decrepitation. Decrepitation and subsequent OH loss may explain furthermore the absence of OH-bearing phases in such inclusions, whereas they are always visible in preserved nanogranitoids. The inclusions described by Liu et al. (2018) contain either quartz and feldspars or quartz and calcite ± other accessory phases. They have regular or irregular shape, protrusion textures, healed cracks around the inclusion and the whole garnet is crossed by a network of thin healed cracks. In terms of trace elements, the inclusions present a dominant Ba positive anomaly, positive anomaly of Pb, U, Li and Sr and a negative anomaly of Th, Zr and Hf. Liu et al. (2018) interpreted the MSI as the result of a reaction between an enclosed mineral, e.g. coesite and rutile, and an external fluid infiltrating the garnet during first stage of exhumation at HP based on their geochemical signature. The Erzgebirge melt inclusions instead range from glassy to polycrystalline in the same cluster, the mineral assemblage is constantly granitic, they have a negative crystal shape and healed cracks with a limited extension and restricted to the larger

inclusions. From the geochemical point of view Cs, Th, U and Pb show a dominant positive anomaly in the same order of magnitude whereas Ba is present in lower concentrations and Zr and Hf here are enriched (Fig. 5.9). These important microstructural and geochemical differences between the Dabie MSI and the Erzgebirge melt inclusions thus suggest a different genetic process for the latter.

5.7.2 EXTERNAL ORIGIN OF THE MELT PRESERVED IN SAIDENBACH UHP ECLOGITE

The investigated melt is granitic, hydrous and enriched in Cs, Th, U, Pb, Li, B, Rb, Zr and Hf whereas it has a negative anomaly in Nb, Nd and Ti. Most of these enrichments are compatible with the involvement of phengite in the melt-producing reaction, based on the comparison with the trace element trends measured in nanogranitoids in the metapelites of El Hoyazo by Acosta-Vigil et al. (2010) (Fig. 5.9). The two melts present some differences, e.g. in the Erzgebirge samples Zr and Hf show a positive anomaly rather than a flat pattern as in El Hoyazo sample, Th is one of the dominant elements in eclogite inclusions whereas in the metapelites it shows a negative anomaly and the Cs concentration is one order of magnitude higher. The very high enrichment in Cs in the Erzgebirge samples cannot in fact be explained exclusively with the involvement of phengite alone, but it may be related to the presence of some fluid during melt production, together with the enrichment in Th and U (Bali et al., 2011; Cannao` and Malaspina, 2018). Some of the features are also typical of the continental crust such as the positive Pb anomaly and the negative one for Nd and Ti (Hartmann and Wedepohl, 1993). All these features make this melt very similar to the one found in eclogites of the Granulitgebirge (see also Borghini et al., submitted), an aspect which will be discussed in detail in the chapter 6 of the present thesis.

There are two possible origins of the melt preserved in these eclogites: internal, via partial melting of phengite-bearing eclogite (where rare phengite is present as a mineral inclusion in garnet, Fig. 5.2), or external, via melting of the surrounding phengite-bearing metasedimentary and metagranitic rocks. Most experiments show that eclogite partial melting generally produces melt with a tonalitic, trondhjemitic or dacitic (in certain case referred to as adakite) rather than granitic composition (Rapp et al., 1991; Peacock et al., 1994; Rapp and Watson, 1995; Yogodzinski et al., 2001; Klemme et al., 2002; Martin et al., 2005; Yaxley et al., 2007; Bouilhol et al., 2015). However, none of the experiments listed above have shown the simultaneous production of peritectic garnet, clinopyroxene and granitic melt as would be required to be the case for the internal production scenario if applied to Saidenbach eclogites. Interestingly, Skjerlie and Patiño Douce (2002) demonstrate that at 3.2 GPa and 1000°C a zoisite- and phengite-

bearing eclogite can produce a true granitic melt via fluid-absent melting. The eclogite used in the latter experiments has a similar amount of Na_2O, higher Al_2O_3, MgO and CaO and lower SiO_2, TiO_2 and FeO (total Fe here reported as FeO; bulk rock reported in Table 5.2) when compared to the three eclogite types investigated in this study. Skjerlie & Patiño Douce (2002) suggest at these P-T conditions zoisite is stable whereas phengite breaks down producing kyanite, garnet and melt but not clinopyroxene. However, in the Saidenbach case study clinopyroxene is abundant and the peak mineral assemblage is devoid of zoisite and kyanite. For all these reasons, an external production of the melt via partial melting of the surrounding phengite-bearing gneisses appears to be the most tenable scenario.

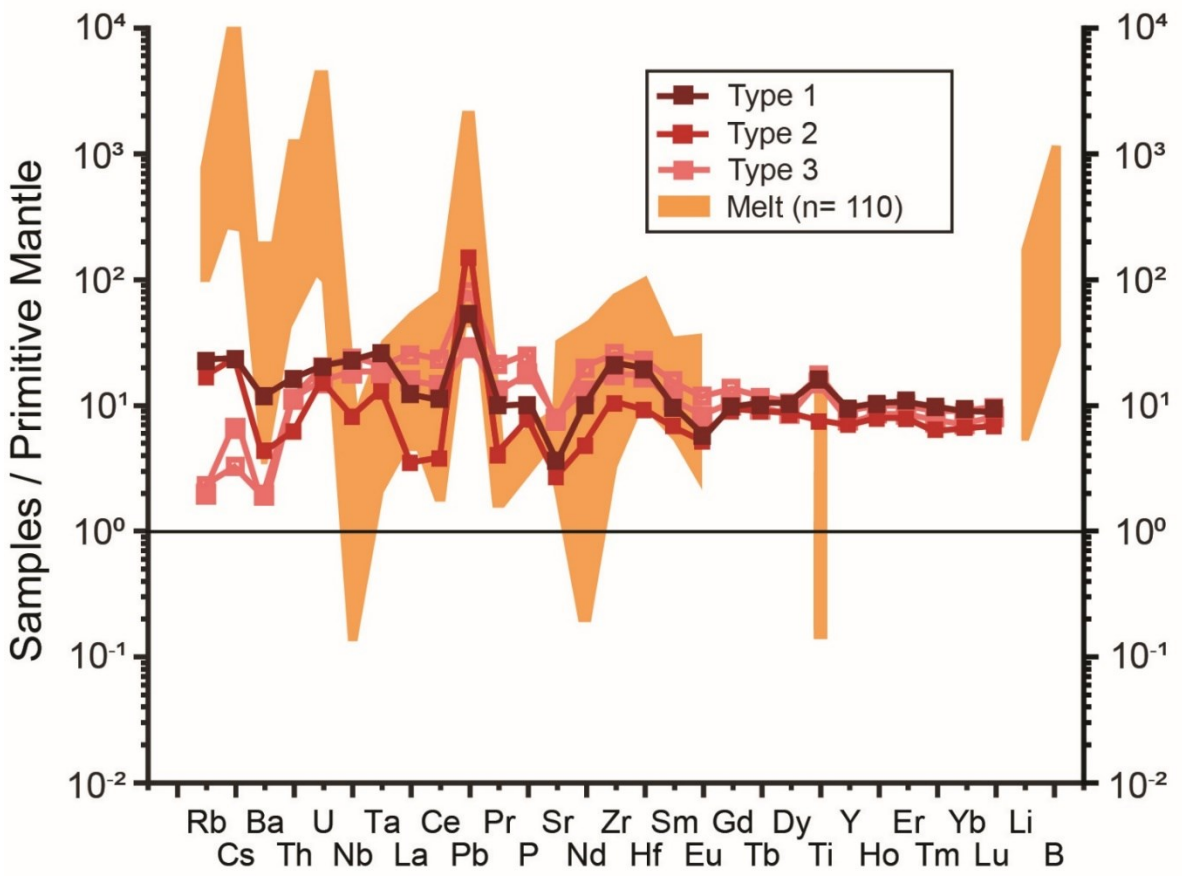

Figure 5.10. Whole rock and melt inclusions trace elements patterns compared. For the normalization values see caption Figure 5.6.

This is also supported by the fact that experiments on phengite bearing metasediments/metagranites have shown that phengite can be stable up to 1000°C with high Ti

content (~2 wt%) before melting to produce granitic melt (Hermann and Spandler, 2008). The melt would have then migrated from the surrounding rocks and metasomatically interacted at UHP conditions with mafic layers to catalyze the Saidenbach eclogite growth studied here. Moreover, the comparison of the whole rock trace element patterns with the melt highlights some common features such as Cs, Pb, Rb, Zr, Hf positive anomalies (Fig. 5.10). Obviously, the whole rock patterns show lower enrichment with respect to the melt because the latter is present in small amounts (see also discussion Chapter 4). It is then likely that the investigated rocks formed as result of a metasomatic reaction between a protolith and a granitic melt that impose the main elements of signature to the whole rock.

5.7.3 CRUSTAL ORIGIN FOR THE HOST ECLOGITE

The most commonly used classifications of eclogites have been proposed by Coleman et al. (1965) and later on by Carswell (1990). In the first case eclogites have been divided in three main groups based on occurrence, bulk rock geochemistry and rock-forming minerals. Group A are eclogites included as xenoliths in kimberlites and basalts or as layers in ultramafic rocks. They are characterized by garnets with high Prp content (> 55 mol%) and clinopyroxene mostly with low Jd content. Group B are eclogites as lenses and bands in migmatite and gneiss terranes. Here the Prp content in the garnet range between 30-55 mol % and the Jd content in the clinopyroxene is moderate. Group C eclogites, in contrast, occur as bands and lenses in ophiolitic sequences. In this group Prp is lower than 30 mol % and the Jd content is the highest but aegirine contents can also be high. Group B and C eclogites have been interpreted by O'Hara and Yoder (1963) as high pressure recrystallization products of basaltic material in subduction zones rather than having formed in the upper mantle. The classification proposed by Carswell, (1990) divides instead the eclogites according to the equilibration temperature and thus different origins. Eclogites equilibrated at high T (>900°C) would originate in the upper mantle and correspond to Group A of Coleman et al. (1965). Medium temperature eclogites (550°<T<900°C) would be related with tectonically thickened continental crust and correspond to the group B (Coleman et al., 1965) whereas low temperature eclogites (T<550°C) would correspond to the Group C (Coleman et al., 1965) and represent recrystallized subducted oceanic crust.

More recent studies of ultra-high pressure subducted continental crust demonstrate that B-type eclogites, i.e., eclogites in gneisses, can form at conditions similar to those formerly expected only for A-type (Carswell et al., 2003). This is the case for the Erzgebirge eclogites. The peak temperatures estimated for the Gneiss-Eclogite Unit to which these eclogites belong range from 900° to 1000°C (Massonne and Grosch, 1995; Schmädicke and Evans, 1997; Massonne,

1999) and this would suggest, according to the Carswell (1990) classification, that the eclogite would be more similar to group A and thus originate in the upper mantle. However, they contain garnet with average Prp content of 29 mol % and the Jd content in clinopyroxene is high (50 mol%), characteristic features of the Group C eclogites of Coleman et al. (1965). The latter interpretation is also supported by the major elements composition of the whole rock, rather close to eclogites of crustal origin and group C. In fact, the investigated eclogites have SiO_2, Al_2O_3, TiO_2 higher than group A whereas FeO and MgO are lower and Na_2O is consistent with the content in common lower oceanic crust (2.23-3.27 wt%; Coogan, 2014; Table 5.2). Thus typically B and C-type eclogites have basaltic protoliths derived from shallow mantle melting processes whereas most (but not all) A-type eclogites resulted from significantly deeper mantle melting processes (Carswell, 1990).

Also the bulk rock trace elements (Fig. 5.6; Table 5.2) show positive anomalies of Pb, Ti, Zr, Hf and Ta, a slight positive anomaly in Rb and Cs and negative anomaly in Eu and Sr. Excluding Cs, Ba, Pb (which are related to the presence of melt +fluid), the samples show a similar trend to E-MORB (Fig. 5.6). The high enrichment in HFSE (Ti, Zr and Hf) is probably related to the presence of rutile in the rock, whereas Eu and Sr negative anomalies could be attributed to the absence of plagioclase in the eclogite protolith. Ba negative anomaly reflects the strong anomaly in both garnet and clinopyroxene. The low content of LREE in type 2 can be explained by the absence of clinopyroxene now totally replaced by a symplectite made of plagioclase, clinopyroxene and green amphibole.

5.7.4 STRANGE PHASES IN NANOGRANITOIDS

The study of nanogranitoid mineral assemblages has revealed the presence of rare polymorphs rather than the conventional phase usually found in granites. Kumdykolite occurs instead of albite, kokchetavite instead of K-feldspar and, less often, cristobalite instead of quartz. Kumdykolite and kokchetavite, as discussed in Chapter 2-3 and 4, have been reported together for the first time in nanogranitoids by Ferrero et al. (2016) and they are indicators of chemically preserved inclusions as they occur just in the crack-free nanogranitoids. In this work we report some additional peculiar phases, identified with their most characteristic peaks as “430” and “412” respectively, which are recurrent in the mineral assemblage observed in the nanogranitoids of the UHP eclogites. Their Raman spectra do not belong to any common phases usually found in nanogranitoids and fluid inclusions (see database of Frezzotti et al., 2012), and in general they do not correspond to any of the phases in existing online databases. In both cases the presence of peaks suggests that they have a crystalline structure, i.e. they are mineral phases rather than

amorphous ones, such as glass, whose spectrum would be characterized by large bands instead of peaks. Backscattered electron images (Fig. 5.5 d) show that both the 430 and 412 phases have features similar to a tectosilicate preferentially constituted by relatively light elements. The position of the main peak can be used as an indication of the silicate and non-silicates classes (i.e. tectosilicates, orthosilicates, phyllosilicates, inosilicates, borates, carbonates, phosphates, sulfates and oxide/hydroxides). In fact, minerals belonging to the same group have the main peak in a rather well-defined range of Raman shift (see Fig. 12 in Frezzotti et al., 2012). This observation confirms that phases 430 and 412 could represent polymorphs of a phase of the tectosilicate group, in which the main peaks range between 420 (cristobalite) to 521 (coesite) cm^{-1} (Frezzotti et al., 2012). For the 412 phase, its main peaks (105-412-470-831) cm^{-1} (Fig. 5.5f) show a similarity with kokchetavite peaks (i.e. 110-395-835 cm^{-1}; Fig. 5.5a and Fig. 3b in Ferrero et al., 2016) whereas for the 430 phase some of the peaks – 430, 488, 820, 131 - are similar to those of a so-called “new phase” reported in experimental products resulting from fast cooling of a glass of anorthitic composition (Daniel et al., 1995). These authors interpret the phase as a possible metastable polymorph of anorthite, but this finding was not investigated further. However, the phase 430 in the nanogranitoids here investigated does not have the chemical composition of an anorthite. In fact, CaO occurs in similar amounts to Na_2O and K_2O (Table 1), a feature possibly consistent with an (unmixed) ternary feldspar. However the comparison with mesoperthite from HP felsic granulites (Ferrero et al., 2015; see also Table 1) excludes this possibility, as phase 430 contains more SiO_2 and CaO and less K_2O, Na_2O and Al_2O_3. Moreover, the frequent presence of glass in Raman spectra acquired on this phase (identified because of its characteristic OH band, see fig. 5.5.e) suggests a close association between phase 430 and glass.

5.8 CONCLUDING REMARKS

Saidenbach eclogite contain a peculiar feature: primary melt inclusions with a granitic composition. The preserved melt is hydrous, rich in alkalis and peraluminous and the trace element signature suggests the involvement of phengite and a subduction zone-related fluid in the melt producing reaction. The melt composition, coupled with the absence of relicts of the prograde and peak mineral assemblage suggest that the melt has been produced externally from a phengite-bearing felsic protolith. The melt then infiltrates previously existent mafic layers and produces eclogites via metasomatic interaction. Moreover, the trace element signature of the whole rock appears to be influenced by the melt and this supports the metasomatism scenario. The presence of melt inclusions and former coesite in the same microstructural position suggest

that the process took place at UHP conditions. Multiphase solid inclusions were reported in UHP eclogite from east-central China but those found in the Erzgebirge samples are unique because 1) of the presence of glass, 2) they contain a mineral assemblage clearly consistent with an originally hydrous granitic melt, and 3) they have an overall excellent preservation state, with only few inclusions showing partially healed cracks. This is the first case study in which it is possible to measure the composition of the melt in natural eclogites directly from preserved glassy inclusions formed under UHP conditions.

6 DISCUSSION AND CONCLUSIONS

This thesis discusses the melt-related processes recorded by mafic rocks involved in continental subduction and collision during the Variscan orogenesis in the Bohemian Massif. Subduction is one of the geological processes through which the crust enters in direct contact with the upper mantle and interacts with it. Crust-mantle interaction via subduction is at the base of most of the processes responsible for mantle heterogeneity such as the formation of HP cumulates, recycling of oceanic crust in the mantle and metasomatism. Several studies, already summarized in the introduction of the present thesis, have shown that crustal fluids and melts can re-fertilize the upper mantle. Pieces of the latter are then incorporated in the subducted crust and exhumed toward the surface, where they can be then studied. How this interaction takes place is, however, still a matter of debate (Brueckner, 1998; Bodinier and Godard, 2014). In this sense, the Bohemian Massif represents the perfect geological setting to tackle this problem. It contains indeed mafic rocks of mantle and crustal affinity that have been involved in continental subduction and occur now in outcrops, embedded in high pressure and ultra-high pressure felsic rocks.

In this thesis I carried out a direct investigation of the fluids/melts responsible for part of the mantle heterogeneity in the Variscan as well as, more in particular, for the crust-mantle interaction and mantle re-fertilization. The approach I used in my thesis, the study of melt inclusions preserved in garnet, is a rather new tool in the investigation of crust-mantle interaction, which I combined with more classic whole rock and mineral phase petrology and geochemistry. Among the several locations of the Bohemian Massif in which melt inclusions occur (Ferrero et al., 2018b) we selected two areas from the Saxothuringian Zone in which inclusions are contained in mafic rocks, i.e., the high pressure (HP) eclogites (formerly pyroxenites) of the Granulitgebirge and the ultrahigh pressure (UHP) eclogites of the Erzgebirge.

In this Chapter I compare the nature of the two melts in order to highlight differences and similarities and then discuss the geodynamic implications to be derived by my results. I then present the research questions still open for investigation and indicate the possible future direction of the study of crust-mantle interaction processes using melt inclusions.

6.1 SIMILAR MELTS IN DIFFERENT ROCKS FROM DIFFERENT SEGMENTS OF THE VARISCAN OROGEN

Eclogites from both the Granulitgebirge and the Erzgebirge contain primary glassy and crystallized melt inclusions in some of the garnet cores. The polycrystalline inclusions have rather similar main mineral assemblages, which include quartz, feldspars (or polymorph of feldspars i.e., kumdykolite and kokchetavite) and OH-bearing phases, thus they are nanogranitoids (Ferrero et al., 2018 and references therein). Moreover, Erzgebirge nanogranitoids contain in abundance two other unknown polymorphs, possibly silica-rich tectosilicates. The same phases have been also observed in the Granulitgebirge nanogranitoids. However, they were far rarer than in the eclogites and for this reason not previously reported in Borghini et al. (2018) and Borghini et al., (submitted). The two mineral assemblages show also some differences in the relative phase abundances: in the Erzgebirge sample mineral assemblage phase 430 and carbonate are more abundant and kokchetavite is scarce with respect to the Granulitgebirge. Conversely, in the latter the inclusions contain also osumilite and pyroxene, absent in the Erzgebirge samples. Another difference is the presence of shrinkage bubbles in the Erzgebirge glassy inclusions.

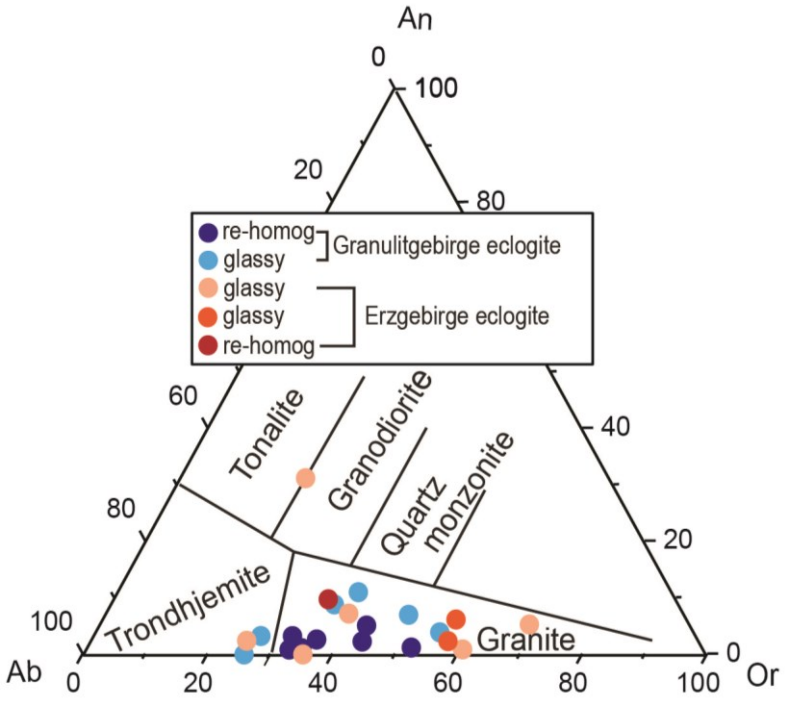

Figure 6.1. CIPW anorthite-albite-orthoclase (An-Ab-Or) diagrams showing normative composition of the glassy and re-homogenized inclusions of the Granulitgebirge eclogite and the glassy (Type 1 and 2) and re-homogenized inclusions (Type 1) of the Erzgebirge eclogite.

In both areas the melt composition is similar in major elements: granitic (Fig. 6.1), hydrous and slightly peraluminous. In both cases the enrichment in MgO, Cr and Ni is not significant and suggests the absence of interaction with the mantle (see Chapter 4) and no change in composition during the migration from the source. Thus the melt preserved in the inclusions can still be considered as the pristine metasomatic agent. The H_2O content of the melts is significantly higher in the Erzgebirge UHP melt with respect to the Granulitgebirge HP one (Table 6.1) and could be related with small differences in the protolith. At higher pressure, melts can also dissolve higher amounts of CO_2 (Ni and Keppler, 2013). This could explain the abundance of carbonates in the nanogranitoid assemblage in the Erzgebirge UHP eclogite.

Locality	Granulitgebirge		Erzgerbirge	
Sample type	**Preserved glassy**	**Re-homogenized**	**Preserved glassy**	**Re-homogenized**
Reference	Data repository Borghini et al., 2018		Chapter 5	
No. analises	6	7	8	1
wt %				
SiO_2	70.95	64.85	69.79	69.16
TiO_2	0.03	0.14	0.03	0.13
Al_2O_3	16.84	18.28	14.46	14.90
FeO	0.56	1.60	0.87	1.63
MnO	0.03	0.07	0.00	0.01
MgO	0.22	0.99	0.21	0.42
CaO	0.43	1.55	0.55	1.07
Na_2O	5.43	5.52	3.98	3.97
K_2O	5.06	5.40	5.57	3.63
P_2O_5	0.03	0.27	0.03	0.02
TOTAL	99.57	98.67	95.27	94.94
H_2O content	0.43	1.33	4.46	5.06
ASI	1.12	1.04	1.08	1.20
CaO/Al_2O_3	0.03	0.08	0.14	0.06
Mg#	0.32	0.50	0.26	0.31

Table 6.1. Average of the melt inclusions major elements composition analyses of the primary and re-homogenized inclusions of the eclogite from Granulitgebirge and Erzgebirge.

In terms of trace elements, the two melts have very similar patterns as they are both enriched in Cs, Pb, Rb, U, Th, Li and B. In the Erzgebirge eclogite Zr and Hf are more abundant, Th and U are less enriched and Nb, Ta, Nd and Eu have a stronger negative anomaly with respect to the melt in the Granulitgebirge (Figure 6.2). The observed differences are overall negligible, and most likely related to slightly different compositions of the two melt sources. Importantly, in both cases the trace element pattern suggests the involvement of phengite and a Cs-, Th- and U-

rich fluid in the melt producing reaction. For both Granulitgebirge and Erzgebirge samples we exclude the possibility of an internally produced melt because that melt has a clearly granitic nature inconsistent with partial melting of either a peridotite (in the first case) or a UHP eclogite (in the second). Such rock types produce generally basaltic or trondhjemitic-tonalitic-dacitic melts respectively. We conclude that the melt was most probably produced externally as a result of melting of two different phengite-bearing source rocks, somewhat similar to those visible in the Erzgebirge (described in detail by Willner et al., 1997, 2000). The two source rocks must have had very similar composition, because they produced similar melts. However, they must have melted at different depth i.e., under HP conditions for the Granulitgebirge melt, and UHP for the Erzgebirge melt as constrained by the metamorphic peak estimates for the two rock types. It is also likely that they melted at different moments during the Variscan orogeny, as supported by the significantly different ages retrieved for the peak assemblages of the two eclogites. In the Granulitgebirge samples the melt was trapped in the garnet at 380 Ma (garnet, clinopyroxene, zircon and whole rock dated with Sm/Nd method; von Quadt, 1993) whereas in the Erzgebirge at 360 Ma (zircons dated with U/Pb SIMS method; Schmädicke et al., 2018).

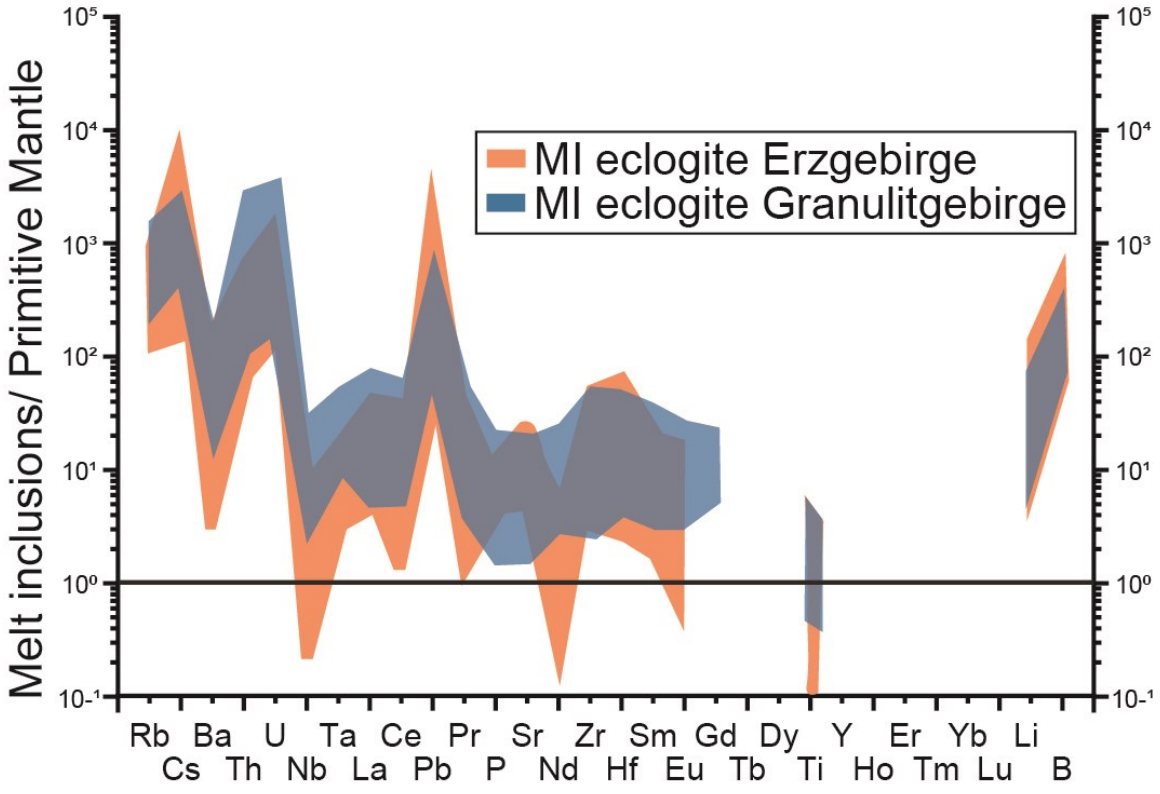

Figure 6.2. Comparison of the trace element patterns of the melt inclusions in garnets of the Granulitgebirge and the Erzgebirge. All the data were normalized to primitive mantle (Sun and McDonough, 1989 except for B which is taken from McDonough & Sun, 1995).

Differences are observed also in the major element compositions of the two eclogites and provide additional constraints for the dynamics of the crust-mantle interaction through space and time (Table 6.2). Whereas both eclogites have similar Al_2O_3, FeO and K_2O contents, in the Granulitgebirge they contain more MgO and CaO and less Na_2O and SiO_2 than in the Erzgebirge.

Sample type (sample name)	Rubinberg Granulitgebirge (RUB, RUB 6 and RUB 11 respectively)			Klatschmühle Granulitgebirge (KLA, KLA 1.2-1 and KLA 2-2)			Eclogite type 1 (SB_Süd 1)	Eclogite type 2 (SB-1e)	Eclogite type 3 (SB_4)	Eclogite type 3 (SB_3)
Reference	Supporting information Borghini et al., submitted						Chapter 5	Chapter 5	Chapter 5	Chapter 5
No. analises	1	1	1	1	1	1	1	1	1	1
wt %										
SiO_2	43.4	43.59	44.81	48.1	46.74	43.38	53.02	51.26	51.74	51.00
TiO_2	2.35	1.07	1.29	0.67	0.69	0.94	1.98	0.92	1.86	2.13
Al_2O_3	15.2	15.85	15.65	16.3	15.41	17.5	15.49	16.14	15.72	15.8
FeO	15.8	12.82	13.87	10.1	11.22	13.53	12.79	11.3	12.64	13.9
MnO	0.26	0.23	0.22	0.15	0.17	0.22	0.19	0.17	0.18	0.21
MgO	9.23	14.04	10.41	10.3	11.14	8.89	5.93	7.07	6.54	6.21
CaO	12.2	11.34	12.61	11.3	11.61	12.76	8.19	9.58	8.82	8.45
Na_2O	1.82	1.14	1.82	2.86	2.03	1.76	2.69	2.16	3.06	2.44
K_2O	0.04	0.02	0.15	0.52	0.53	0.21	0.61	0.44	0.05	0.06
P_2O_5	0.08	0.19	0.08	0.05	0.08	0.36	0.09	0.07	0.16	0.22
TOTAL	100.38	100.29	100.91	100.35	99.62	99.55	100.98	99.11	100.77	100.42
CaO/Al_2O_3	0.80	0.72	0.81	0.69	0.75	0.73	0.53	0.59	0.56	0.53
Mg#	51	66	57	64	64	54	45	52	48	44
ppm										
Cr	200	400	500	500	700	300	27	84	18	25
Ni	80	106	89	90	107	27	41	38	34	36
Rb	14	1.70	8.90	18	31	17	14	10	1.20	1.40
Cs	49	4.00	12	11	37	14	0.70	0.70	0.20	0.10
Ba	99	92	225	186	184	55	78	29	13	13
Th	0.50	2.20	1.80	0.50	0.30	1.00	1.30	0.50	0.90	0.90
U	0.80	1.30	1.00	0.20	0.10	0.30	0.40	0.30	0.30	0.40
Nb	9.90	19	4.30	4.00	4.90	11	15	5.50	12	16
Ta	0.70	1.50	0.30	0.40	0.60	1.10	1.00	0.50	0.70	0.80
La	5.80	9.90	12	6.00	6.40	17	8.00	2.30	10	16
Ce	14	22	27	14	18	34	19	6.40	24	39
Pb	1.10	7.90	3.20	1.20	1.80	1.80	9.20	26	5.00	14
Pr	2.21	2.98	3.39	2.19	2.72	4.08	2.62	1.06	3.41	5.50
P	800	1900	800	500	800	3600	900	700	1600	2200
Sr	62	117	115	185	142	131	73	54	156	150
Nd	11	13	15	10	13	17	13	6.20	17	25
Zr	74	62	71	73	73	49	220	110	185	272
Hf	2.30	2.00	2.00	2.30	2.50	1.60	5.60	2.70	4.90	6.60
Sm	3.31	4.03	4.04	3.22	3.62	4.25	4.02	2.90	4.63	6.61
Eu	1.04	1.10	1.19	0.95	1.07	1.24	0.92	0.83	1.29	1.88
Gd	4.39	5.05	5.21	3.64	4.27	4.78	5.55	5.06	5.67	7.68
Tb	0.87	0.91	0.91	0.56	0.66	0.77	1.03	0.92	0.96	1.18
Dy	5.82	5.87	6.05	3.10	3.67	4.36	7.18	5.92	6.06	7.27
Ti	23500	10700	12900	6700	6900	9400	19800	9200	18600	21300
Y	37	33	33	16	19	21	41	30	33	39
Ho	1.48	1.19	1.31	0.56	0.72	0.89	1.59	1.22	1.35	1.55
Er	4.59	3.51	4.10	1.54	1.96	2.24	4.96	3.55	3.88	4.65
Tm	0.72	0.47	0.55	0.20	0.27	0.29	0.68	0.45	0.52	0.63
Yb	4.66	2.89	3.80	1.22	1.50	1.83	4.38	3.11	3.35	4.07
Lu	0.71	0.41	0.59	0.18	0.23	0.25	0.66	0.48	0.57	0.67
Li	n.d.	n.d.	n.d.	n.d.	n.d.	n.d.	n.d.	n.d.	n.d.	n.d.
B	n.d.	n.d.	n.d.	n.d.	n.d.	n.d.	n.d.	n.d.	n.d.	n.d.

Table 6.2. Whole rock major and trace elements composition of the eclogite of Granulitgebirge and Erzgebirge.

The latter eclogites also contains less Cr and Ni and the Mg# is lower. Such differences reflect the environment in which the two rocks formed as well as the nature of the protolith. Higher Mg#, Cr, Ni content and lower SiO_2 and Na_2O for the Granulitgebirge eclogites suggest the contribution of a mantle component, clearly consistent with their occurrence as layers in orogenic peridotite.

Instead the Erzgebirge eclogites show opposite features, more compatible with shallow mantle melting as in the oceanic crust or rifted continents (see also Chapter 5).

Trace elements (Figure 6.3) show very similar trends for Rb, Ba, Ta, P, Nd and Ti in both eclogites. Pb shows a stronger positive anomaly in the Erzgebirge whereas Cs and U are more abundant in the Granulitgebirge, with Cs two order of magnitude higher. Zr and Hf have opposite trends, with a positive anomaly in the Erzgebirge eclogite and a negative one in the Granulitgebirge eclogite (Figure 6.3a). The REE patterns (Figure 6.3b) are similar for the LREE except for type 2 of the Erzgebirge eclogite, possibly due to the absence of preserved clinopyroxene whereas the HREE of sample KLA (Granulitgebirge) are lower than all the others possibly due to a relatively lower amount of garnet.

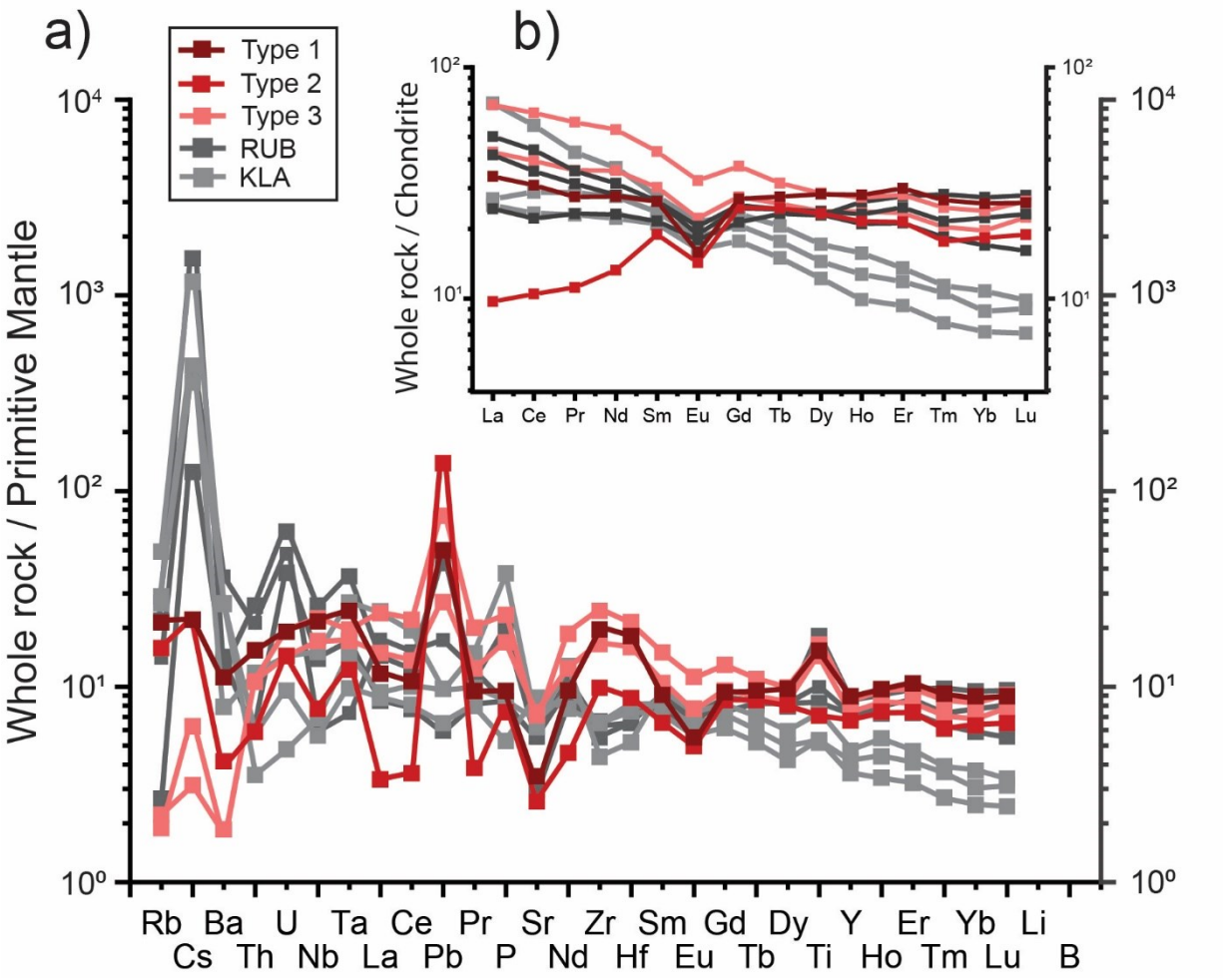

Figure 6.3. Comparison of the trace element patterns of the whole rock of the eclogite of the Granulitgebirge and the Erzgebirge. For the normalization values see caption Fig. 6.2.

The difference in Cs content is most likely related to the higher content of this element in the clinopyroxenes of the Granulitgebirge when compared to those from the Erzgebirge, possibly a

feature inherited by the original protolith infiltrated by the melt in the first location. The significant difference in Pb content between the two eclogites seems decoupled from the melt chemistry, since both melts show indeed the same degree of Pb enrichment. Maybe already the protolith was more enriched in Pb, as expected from crustal rocks.

6.2 FROM MICRO TO MACRO: GEODYNAMIC INSIGHTS AND CONCLUDING REMARKS

So far nanogranitoids were recognized to contain partial melts locally generated, i.e. the host rock in which they occur is likely to be the source of the melt (Cesare et al., 2015). This thesis represents instead the first example of nanogranitoids (and glassy inclusions) preserving a partial melt unrelated to the host rock, and thus interpreted to be metasomatic. In this case the melt inclusions allow the characterization of the metasomatic agent that triggered the transformation of host rock in which they can be found. In the Bohemian Massif this new discovery gives important information about the nature of the agents responsible for the metasomatization of different portions of the orogen. In fact, as discussed in Chapter 4 (Borghini et al., submitted) melts with similar trace element signature are responsible for the metasomatism of the peridotites and pyroxenites of the T-7 borehole in the Saxothuringian zone (see Fig. 4.1 for the location). Moreover, a melt with the similar trace element signature is likely to represent also the mature crustal component that contaminates the mantle sources of the durbachite suite (Moldanubian zone) as shown and discussed in Fig. 4.10.

The Granulitgebirge and Erzgebirge are two separated segments of continental crust, both associated with orogenic peridotite and mafic rocks, yet they belong to the same tectonic unit, i.e. the Saxothuringian Zone. Felsic rocks from both localities show peak metamorphism at 340 Ma, although the Erzgebirge was subducted deeper as suggested by the presence of diamond and coesite. The geodynamic evolution of the Bohemian Massif can be summarized in two stages: an initial oceanic subduction (> 380 Ma) and a subsequent continental subduction with P-T metamorphic peak at 340 Ma followed by rapid exhumation (O'Brien, 2000; Janoušek and Holub, 2007). The Granulitgebirge eclogites are 380 Ma and most likely were formed via a metasomatic interaction between a slab-related melt and the heterogeneous mantle wedge (O'Brien, 2000). A possible source of the melt is the metasedimentary material associated with the oceanic crust. The metasomatized peridotites belonging to the mantle wedge – including now newly-formed eclogite layers- are then emplaced in the subducting continental crust via ductile flow, because of the gravitational instability created by a denser body (peridotite) above a lighter one (continental crust of the subducted slab; Brueckner, 1998 see also discussion in chapter 4). The juxtaposition

between the peridotite and the continental crust would have taken place shortly before the granulite metamorphism at 340 Ma (Schmädicke et al., 2010). As the process continues, the deep subduction of the oceanic crust pulls down also the continental crust, which at depth starts to melt as well. This continental crust, with its own local basaltic dykes, produced melts at depth which then interacted with the enclosed mafic layers: this melt most probably would also have interacted with the mantle wedge. In our opinion one of the examples where this scenario is visible is the Erzgebirge, in which the metasomatism due to infiltrating melt occur at UHP condition according to our results. The upper portion of the subducted continental crust was then exhumed at the same time trapping pieces of the mantle.

In conclusion, the Variscan orogeny in the Bohemian Massif involved the partial melting of several different portions of continental crust during subduction, continental collision and exhumation as confirmed by the large number of locations in which melt inclusions have been reported, scattered across the whole Massif (see Chapter 2, Table 2.1 and Figure 2.1). The silicate melt released from these crustal units represents a potentially very efficient agent capable of metasomatizing not only the mantle wedge but also other portions of the slab on their path upward, eventually influencing also the composition of the late mantle-derived magmatic rocks in the area. Such an interpretation is clearly supported by the strong similarities in the signature of the supposed metasomatic agent in the several occurrences reported and discussed in this thesis, i.e., Granulitgebirge eclogite, Erzgebirge eclogite, T-7 borehole and the crustal component in the durbachite suite.

6.3 OPEN QUESTIONS AND FUTURE INVESTIGATIONS

This thesis still presents some open petrological problems:

Nature of the protolith of the eclogite of both studied areas. In order to solve the problem would be necessary to collect samples with precise structural positions, e.g. along layers in the eclogite of the Erzgebirge and along a transect from the peridotite into the eclogite layer in the Granulitgebirge in order to determine possible differences in mineralogy and composition that would suggest the presence of relict, i.e. pre-metasomatic, phases.

Nature of the Granulitgebirge garnet peridotite. Further trace element analysis of the host garnet peridotites may show to which extent metasomatism also affected the peridotite. The isotopes analyses, Sr in particular, on the peridotite would also allow to define if they belong to the asthenospheric or lithospheric mantle and thus clarify better the geodynamic evolution.

Source of the melt. A systematic study of the melt inclusions in the surrounding felsic rocks in the Erzgebirge (already initiated by other research groups; see Acosta-Vigil et al., 2017 AGU), coupled with a petrological characterization of the relicts of the oceanic suture zone in the Saxothuringian zone, would furthermore help to identify the source of the melting for both case studies.

Nature of the two unknown phases 412 and 430. This could be answered by comparing the Raman spectra collected on the natural samples with more specialized, not easily accessible databases, e.g. of minerals characteristic of ceramic products, and combine this with detailed crystallographic study, such as transmission electron microscope (TEM) and single-crystal X-ray diffraction (Malaspina et al., 2015) on the isolated inclusions containing these phases.

Extending the database. This thesis is one of the first studies of melt inclusions in mafic rocks. Possible further directions of investigation would target the orogenic peridotite with layers of garnet pyroxenite visible at Zöblitz in the Erzgebirge. Moreover, analogue cases of associations of HP felsic rocks with lenses of orogenic peridotites and mafic rocks are also present elsewhere in the Bohemian Massif, in particular in the Gföhl Unit (Moldanubian Zone), thus suggesting a similar geological evolution for this Unit with respect to the Granulitgebirge and Erzgebirge. It would be very interesting to expand the database of investigated melt inclusions in mafic rocks also in this Unit and then compare the results with those from the Saxothuringian Zone to clarify how similar (or different) the geodynamic history is at depth in the different fragments of the Bohemian Massif. Ferrero et al. (2018) already found a good candidate in the UHP eclogite of Dunkelsteinerwald studied by Faryad et al. (2013).

Experimental approach. A further interesting development would be to use the data collected in this thesis to design and perform reaction experiments aimed at recreating the studied eclogite via interaction between suitable mafic/ultramafic protoliths and a silicate melt with composition identical to the one measured in this study. This would offer the possibility to better understand the processes of melt-rock interaction by reproducing nature in the laboratory with unprecedented precision.

REFERENCES

Acosta-Vigil, A., Barich, A., Bartoli, O., Garrido, C.J., Cesare, B., Remusat, L., Poli, S., and Raepsaet, C., 2016, The composition of nanogranitoids in migmatites overlying the Ronda peridotites (Betic Cordillera, S Spain): the anatectic history of a polymetamorphic basement: Contributions to Mineralogy and Petrology, v. 171, p. 1–31, doi:10.1007/s00410-016-1230-3.

Acosta-Vigil, A., Buick, I., Cesare, B., London, D., and Morgan, G.B., 2012, The extent of equilibration between melt and residuum during regional anatexis and its implications for differentiation of the continental crust: A study of partially melted metapelitic enclaves: Journal of Petrology, v. 53, p. 1319–1356, doi:10.1093/petrology/egs018.

Acosta-Vigil, A., Buick, I., Hermann, J., Cesare, B., Rubatto, D., London, D., and Morgan VI, G.B., 2010, Mechanisms of crustal anatexis: A geochemical study of partially melted metapelitic enclaves and host dacite, SE Spain: Journal of Petrology, v. 51, p. 785–821, doi:10.1093/petrology/egp095.

Acosta-Vigil, A., Cesare, B., London, D., and Morgan, G.B., 2007, Microstructures and composition of melt inclusions in a crustal anatectic environment, represented by metapelitic enclaves within El Hoyazo dacites, SE Spain: Chemical Geology, v. 237, p. 450–465, doi:10.1016/j.chemgeo.2006.07.014.

Acosta-Vigil, A., London, D., Morgan, G.B., Cesare, B., Buick, I., Hermann, J., and Bartoli, O., 2017a, Primary crustal melt compositions: Insights into the controls, mechanisms and timing of generation from kinetics experiments and melt inclusions: Lithos, v. 286–287, p. 454–479, doi:10.1016/j.lithos.2017.05.020.

Acosta-Vigil, A., Stöckhert, B., Hermann, J., Yaxley, G., Cesare, B., and Bartoli, O., 2017b, Remelting of nanogranitoids in UHP felsic granulites from Erzgebirge (Bohemian Massif, Germany): American Geophysical Union, Fall Meeting 2017, Abstract #V24B-06.

Agricola, G., 1556, De re metallica: 1st edn. Hieronymous Froben and Nocolaus Episcopius, Basil.

Allegre, C.J., Brévart, O., Dupré, B., and Minster, J.-H., 1980, Isotopic and chemical effects produced in a continuously differentiating convecting earth mantle: Philosophical Transactions of the Royal Society A: Mathematical, Physical and Engineering Sciences, v. 297, p. 447–477.

Allègre, C.J., and Turcotte, D.L., 1986, Implications of a two-component marble-cake mantle: Nature, v. 323, p. 123–127, doi:10.1038/323123a0.

Andersen, T., Austrheim, H., and Burke, E.A.J., 1990, Fluid inclusions in granulites and eclogites from the Bergen Arcs, Caledonides of W. Norway: Mineralogical Magazine, v. 54, p. 145–158.

Anderson, D.L., 1989, Theory of the Earth: Boston, MA, Blackwell scientific publications.

Audetát, A., and Lowenstern, J.B., 2014, Melt inclusions, *in* Holland, H.D. and Turekian, K.K. eds., Treatise on Geochemistry, second edition: Elsevier, Oxford, p. 143- 173.

Auzanneau, E., Vielzeuf, D., and Schmidt, M.W., 2006, Experimental evidence of decompression melting during exhumation of subducted continental crust: Contributions to Mineralogy and Petrology, v. 152, p. 125–148, doi:10.1007/s00410-006-0104-5.

Baker, D.R., 2008, The fidelity of melt inclusions as records of melt composition: Contributions to Mineralogy and Petrology, v. 156, p. 377–395, doi:10.1007/s00410-008-0291-3.

Bakun-Czubarow, N., 1991, Geodynamic significance of the Variscan HP eclogite-granulite series of the Złote Mountains in the Sudetes: Publications of the Institute of Geophysics. A, p. 215–244.

Bali, E., Audétat, A., and Keppler, H., 2011, The mobility of U and Th in subduction zone fluids: An indicator of oxygen fugacity and fluid salinity: Contributions to Mineralogy and Petrology, v. 161, p. 597–613, doi:10.1007/s00410-010-0552-9.

Barich, A., Acosta-Vigil, A., Garrido, C.J., Cesare, B., Tajčmanová, L., and Bartoli, O., 2014, Microstructures and petrology of melt inclusions in the anatectic sequence of Jubrique (Betic Cordillera, S Spain): implications for crustal anatexis: Lithos, v. 206–207, p. 303–320.

Bartoli, O., 2017, Phase equilibria modelling of residual migmatites and granulites: An evaluation of the melt-reintegration approach: Journal of Metamorphic Geology, v. 35, p. 919–942, doi:10.1111/jmg.12261.

Bartoli, O., 2019, Reintegrating nanogranitoid inclusion composition to reconstruct the prograde history of melt-depleted rocks: Geoscience Frontiers, v. 10, p. 517–525, doi:10.1016/j.gsf.2018.02.002.

Bartoli, O., Acosta-Vigil, A., and Cesare, B., 2015, High-temperature metamorphism and crustal melting: Working with melt inclusions: Periodico di Mineralogia, v. 84, p. 0–24, doi:10.2451/2015PM00xx.

Bartoli, O., Acosta-Vigil, A., Ferrero, S., and Cesare, B., 2016a, Granitoid magmas preserved as melt inclusions in high-grade metamorphic rocks: American Mineralogist, v. 101, p. 1543–1559, doi:10.2138/am-2016-5541CCBYNCND.

Bartoli, O., Acosta-Vigil, A., Tajčmanová, L., Cesare, B., and Bodnar, R.J., 2016b, Using nanogranitoids and phase equilibria modeling to unravel anatexis in the crustal footwall of the Ronda peridotites (Betic Cordillera, S Spain): Lithos, v. 256–257, p. 282–299, doi:10.1016/j.lithos.2016.03.016.

Bartoli, O., Cesare, B., Poli, S., Acosta-Vigil, A., Esposito, R., Turina, A., Bodnar, R.J., Angel, R.J., and Hunter, J., 2013a, Nanogranite inclusions in migmatitic garnet: Behavior during piston-cylinder remelting experiments: Geofluids, v. 13, p. 405–420, doi:10.1111/gfl.12038.

Bartoli, O., Cesare, B., Poli, S., Bodnar, R.J., Acosta-Vigil, A., Frezzotti, M.L., and Meli, S., 2013b, Recovering the composition of melt and the fluid regime at the onset of crustal anatexis and S-type granite formation: Geology, v. 41, p. 115–118, doi:10.1130/G33455.1.

Bartoli, O., Cesare, B., Remusat, L., Acosta-Vigil, A., and Poli, S., 2014, The H2O content of granite embryos: Earth and Planetary Science Letters, v. 395, p. 281–290.

Bea, F., 1996, Controls on the trace element composition of crustal melts: Earth and Environmental Science Transactions of the Royal Society of Edinburgh, v. 87, p. 33–41.

Becker, H., 1996, Crustal trace element and isotopic signatures in garnet pyroxenites from garnet peridotite massifs from Lower Austria: Journal of Petrology, v. 37, p. 272–286, doi:10.1093/petrology/37.4.785.

Becker, H., 1997, Petrological constraints on the cooling history of high-temperature garnet peridotite massifs in lower Austria: Contributions to Mineralogy and Petrology, v. 128, p. 272–286, doi:10.1007/s004100050308.

Becker, H., and Altherr, R., 1992, Evidence from ultra-high-pressure marbles for recycling of sediments into the mantle: Nature, v. 358, p. 745–748.

Becker, H., Jochum, K.P., and Carlson, R.W., 2000, Trace element fractionation during dehydration of eclogites from high-pressure terranes and the implications for element fluxes in subduction zones: Chemical Geology, v. 163, p. 65–99, doi:10.1016/S0009-2541(99)00071-6.

Becker, H., Shirey, S.B., and Carlson, R.W., 2001, Effects of melt percolation on the Re-Os systematics of periodites from a Paleozoic convergent plate margin: Earth and Planetary Science Letters, v. 188, p. 107–121, doi:10.1016/S0012-821X(01)00308-9.

Berman, R.G., and Aranovich, L.Y., 1996, Optimized standard state and solution properties of minerals: Contributions to Mineralogy and Petrology, v. 126, p. 1–24.

Blichert-Toft, J., Albarède, F., and Kornprobst, J., 1999, Lu-Hf Isotope Systematics of Garnet Pyroxenites from Beni Bousera, Morocco: Implications for Basalt Origin: Science, v. 283, p. 1303–1306, doi:10.1126/science.283.5406.1303.

Bodinier, J.-L., Garrido, C.J., Chanefo, I., Bruguier, O., and Gervilla, F., 2008, Origin of pyroxenite-peridotite veined mantle by refertilization reactions: Evidence from the Ronda peridotite (Southern Spain): Journal of Petrology, v. 49, p. 999–1025, doi:10.1093/petrology/egn014.

Bodinier, J.-L., and Godard, M., 2014, Orogenic, Ophiolitic, and Abyssal Peridotites: Elsevier Ltd., v. 3, 103–167 p., doi:10.1016/B978-0-08-095975-7.00204-7.

Bodinier, J.-L., Guiraud, M., Fabriès, J., Dostal, J., and Dupuy, C., 1987, Petrogenesis of layered pyroxenites from the Lherz, Freychinède and Prades ultramafic bodies (Ariège, French Pyrénées): Geochimica et Cosmochimica Acta, v. 51, p. 279–290.

Bodinier, J.-L., Menzies, M.A., Shimizu, N., Frey, F.A., and McPherson, E., 2004, Silicate, Hydrous and Carbonate Metasomatism at Lherz, France: Contemporaneous Derivatives of Silicate Melt-Harzburgite Reaction: Journal of Petrology, v. 45, p. 299–320, doi:10.1093/petrology/egg107.

Bodinier, J.L., Vasseur, G., Vernieres, J., Dupuy, C., and Fabries, J., 1990, Mechanisms of Mantle Metasomatism: Geochemical Evidence from the Lherz Peridotite: Journal of Petrology, v. 31, p. 597–628.

Bodnar, R.J., 2003, Introduction to aqueous fluid systems, *in* Samson, I., Anderson, A., and Marshall, D., eds., Fluid Inclusions: Analysis and interpretation, Mineralogical Association of Canada, Quebec City, Short Course, v. 32, p. 81–99.

Boehnke, P., Watson, E.B., Trail, D., Harrison, T.M., and Schmitt, A.K., 2013, Zircon saturation re-revisited: Chemical Geology, v. 351, p. 324–334.

Borghini, A., Ferrero, S., Wunder, B., Laurent, O., O'Brien, P.J., and Ziemann, M.A., 2018, Granitoid melt inclusions in orogenic peridotite and the origin of garnet clinopyroxenite: Geology, v. 46, p. 1007–1010, doi:10.1130/G45316.1.

Bose, K., and Ganguly, J., 1995, Quartz-coesite transition revisited: Reversed experimental determination at 500-1200 °C and retrieved thermochemical properties: American Mineralogist, v. 80, p. 231–238.

Bouilhol, P., Magni, V., van Hunen, J., and Kaislaniemi, L., 2015, A numerical approach to melting in warm subduction zones: Earth and Planetary Science Letters, v. 411, p. 37–44, doi:10.1016/j.epsl.2014.11.043.

Bouzek, J., Koutecký, D., and Simon, K., 1989, Tin and Prehistoric Mining in the Erzgebirge (Ore Mountains): Some New Evidence: Oxford Journal of Archaeology, v. 8, p. 203–212, doi:10.1111/j.1468-0092.1989.tb00200.x.

Boyd, F.R., and Meyer, H.O.A., 1979, The mantle sample: inclusions in kimberlites and other volcanics: American Geophysical Union, Washington D.C., v. 2.

Bröcker, M., and Klemd, R., 1996, Ultrahigh-pressure metamorphism in the Śnieżnik Mountains (Sudetes, Poland): PT constraints and geological implications: The Journal of Geology, v. 104, p. 417–433.

Bröcker, M., Klemd, R., Cosca, M., Brock, W., Larionov, A.N., and Rodionov, N., 2009, The timing of eclogite facies metamorphism and migmatization in the Orlica–Śnieżnik complex, Bohemian Massif: constraints from a multimethod geochronological study: Journal of Metamorphic Geology, v. 27, p. 385–403.

Brueckner, H.K., 1998, Sinking intrusion model for the emplacement of garnet-bearing peridotites into continent collision orogens: Geology, v. 26, p. 631–634.

Brueckner, H.K., and Medaris, L.G., 2000, A general model for the intrusion and evolution of “mantle” garnet peridotites in high-pressure and ultra-high-pressure metamorphic terranes: Journal of Metamorphic Geology, v. 18, p. 123–133.

Budzyń, B., Jastrzębski, M., Kozub-Budzyń, G.A., and Konečný, P., 2015, Monazite Th-U-total Pb geochronology and PT thermodynamic modelling in a revision of the HP-HT metamorphic record in granulites from Stary Gierałtów (NE Orlica-Śnieżnik Dome, SW Poland): Geological Quarterly, v. 59, p. 700–717.

Campione, M., Tumiati, S., and Malaspina, N., 2017, Primary spinel + chlorite inclusions in mantle garnet formed at ultrahigh-pressure: Geochemical Prespective Letters, p. 19–23, doi:10.7185/geochemlet.1730.

Cannao`, E., and Malaspina, N., 2018, From oceanic to continental subduction: Implications for the geochemical and redox evolutuion of the supra-subduction mantle: Geosphere, v. 14, p. 2311–2336.

Carosi, R., Montomoli, C., Langone, A., Turina, A., Cesare, B., Iaccarino, S., Fascioli, L., Visonà, D., and Ronchi, A., 2015, Eocene partial melting recorded in peritectic garnets from kyanite-gneiss, Greater Himalayan Sequence, central Nepal: Geological Society, London, Special Publications, v. 412, p. 111–129.

Carroll, M.R., and Wyllie, P.J., 1990, The system tonalite-H2O at 15 kbar and the genesis of calc- alkaline magmas: American Mineralogist, v. 75, p. 345–357.

Carswell, D.A., 1990, Eclogite and eclogite facies: definitions and classification, *in* Carswell, D.A., ed., Eclogite facies rocks: Blackie, Glasgow, p. 1–13.

Carswell, D.A., and Jamtveit, B., 1990, Variscan Sm-Nd ages for the high-pressure metamorphism in the Moldanubian Zone of the Bohemian Massif, Lower Austria: Neues Jahrbuch für Mineralogie-Abhandlungen, v. 162, p. 69–78.

Carswell, D.A., and O’Brien, P.J., 1993, Thermobarometry and Geotectonic Significance of High-Pressure Granulites: Examples from the Moldanubian Zone of the Bohemian Massif in lower Austria: Journal of Petrology, v. 34, p. 427–459, doi:10.1093/petrology/34.3.427.

Carswell, D.A., Compagnoni, R., and Rolfo, F., 2003, Ultrahigh pressure metamorphism: The Mineralogical Society of Great Britain and Ireland, v. 5.

Carvalho, B.B., Bartoli, O., Ferri, F., Cesare, B., Ferrero, S., Remusat, L., Capizzi, L.S., and Poli, S., 2018, Anatexis and fluid regime of the deep continental crust: New clues from melt and fluid inclusions in metapelitic migmatites from Ivrea Zone (NW Italy): Journal of Metamorphic Geology, p. 1–25, doi:10.1111/jmg.12463.

Cesare, B., 1995, Graphite precipitation in C-O-H fluid inclusions: closed system compositional and density changes, and thermobarometric implications: Contributions to Mineralogy and Petrology, v. 122, p. 25–33, doi:10.1007/s004100050110.

Cesare, B., 2008, Crustal melting: working with enclaves, *in* Sawyer E.W. and Brown, M., eds., Working with migmatites: Quebec Mineralogical Association of Canada, Short Course Series, v. 38, p. 37 - 55.

Cesare, B., and Gomez-Pugnaire, M.T., 2001, Crustal melting in the Alboran Domain: Constraints from xenoliths of the Neogene Volcanic province: Physics and Chemistry of the Earth, v. 4–5, p. 255–260.

Cesare, B., Acosta-Vigil, A., Bartoli, O., and Ferrero, S., 2015, What can we learn from melt inclusions in migmatites and granulites? Lithos, v. 239, p. 186–216, doi:10.1016/j.lithos.2015.09.028.

Cesare, B., Acosta-vigil, A., Ferrero, S., Bartoli, O., Eds, I., Forster, M.A., Gerald, J.D.F., and Acosta-vigil, A., 2011, Melt inclusions in migmatites and granulites, *in* Forster, M.A., and Gerald, J.D., eds., The Science of Microstructure - Part II: Journal of the Virtual Explorer, Electronic Edition, v. 38, doi:10.3809/jvirtex.2011.00268.

Cesare, B., Ferrero, S., Salvioli-Mariani, E., Pedron, D., and Cavallo, A., 2009, "Nanogranite" and glassy inclusions: The anatectic melt in migmatites and granulites: Geology, v. 37, p. 627–630, doi:10.1130/G25759A.1.

Cesare, B., Maineri, C., Baron Toaldo, A., Pedron, D., and Acosta Vigil, A., 2007, Immiscibility between carbonic fluids and granitic melts during crustal anatexis: A fluid and melt inclusion study in the enclaves of the Neogene Volcanic Province of SE Spain: Chemical Geology, v. 237, p. 433–449, doi:10.1016/j.chemgeo.2006.07.013.

Cesare, B., Meli, S., Nodari, L., and Russo, U., 2005, Fe^{3+} reduction during biotite melting in graphitic metapelites: Another origin of CO_2 in granulites: Contributions to Mineralogy and Petrology, v. 149, p. 129–140, doi:10.1007/s00410-004-0646-3.

Cesare, B., Salvioli Mariani, E., and Venturelli, G., 1997, Crustal anatexis and melt extraction during deformation in the restitic xenoliths at El Joyazo (SE Spain): Mineralogical Magazine, v. 61, p. 15–27, doi:10.1180/minmag.1997.061.404.03.

Clarke, G.L., Daczko, N.R., and Miescher, D., 2013, Identifying relic igneous garnet and clinopyroxene in eclogite and granulite, Breaksea orthogneiss, New Zealand: Journal of Petrology, v. 54, p. 1921–1938, doi:10.1093/petrology/egt036.

Clemens, J.D., 2009, The message in the bottle: "Melt" inclusions in migmatitic garnets: Geology, v. 37, p. 671–672, doi:10.1130/focus072009.1.

Coleman, R.G., and Wang, X., 2005, Ultrahigh pressure metamorphism: Cambridge University Press.

Coleman, R.G., Lee, D.E., Beatty, L.B., and Brannock, W.W., 1965, Eclogites and Eclogites: Their differences and similarities: GSA Bulletin, v. 76, p. 300, doi:https://doi.org/10.1130/0016-7606(1965)76[483:EAETDA]2.0.CO;2.

Condamine, P., Médard, E., and Devidal, J.L., 2016, Experimental melting of phlogopite-peridotite in the garnet stability field: Contributions to Mineralogy and Petrology, v. 171, doi:10.1007/s00410-016-1306-0.

Coogan, L.A., 2014, The lower oceanic crust, *in* Rudnick, R.L., ed., The Crust: Elsivier, Treatise on Geochemistry (Second Edition), v. 4, p. 497–541.

Cooke, R.A., and O'Brien, P.J., 2001, Resolving the relationship between high P-T rocks and gneisses in collisional terranes: An example from the Gföhl gneiss-granulite association in the Moldanubian Zone, Austria: Lithos, v. 58, p. 33–54, doi:10.1016/S0024-4937(01)00049-4.

Čopjaková, R., and Kotková, J., 2018, Composition of barian mica in multiphase solid inclusions from orogenic garnet peridotites as evidence of mantle metasomatism in a subduction zone setting: Contributions to Mineralogy and Petrology, v. 173, doi.org/10.1007/s00410-018-1534-6.

Couzinié, S., Laurent, O., Moyen, J.F., Zeh, A., Bouilhol, P., and Villaros, A., 2016, Post-collisional magmatism: Crustal growth not identified by zircon Hf–O isotopes: Earth and Planetary Science Letters, v. 456, p. 182–195, doi:10.1016/j.epsl.2016.09.033.

Don, J., Dumicz, M., Wojciechowska, I., and Zelazniewicz, A., 1990, Lithology and tectonics of the Orlica-Snieznik Dome, Sudetes-Recent state of knowledge: Neues Jahrbuch für Geologie und Paläontologie. Abhandlungen, v. 179, p. 159–188.

Downes, H., 2007, Origin and significance of spinel and garnet pyroxenites in the shallow lithospheric mantle: Ultramafic massifs in orogenic belts in Western Europe and NW Africa: Lithos, v. 99, p. 1–24, doi:10.1016/j.lithos.2007.05.006.

Elliott, T., Plank, T., Zindler, A., White, W., and Bourdon, B., 1997, Element trasport from slab to volcanic front at the Mariana arc: Journal of Geophysical Research, v. 102, p. 14,991-15,018.

Falloon, T.J., Green, D.H., Hatton, C.J., and Harris, K.L., 1988, Anhydrous partial melting of a fertile and depleted peridotite from 2 to 30 kb and application to basalt petrogenesis: Journal of Petrology, v. 29, p. 1257–1282, doi:10.1093/petrology/29.6.1257.

Falloon, T., Green, D., O'Neill, H.S., and Hibberson, W., 1997, Experimental tests of low degree peridotite partial melt compositions: implications for the nature of anhydrous near-solidus peridotite melts at 1 GPa: Earth and Planetary Science Letters, v. 152, p. 149–162, doi:10.1016/S0012-821X(97)00155-6.

Faryad, S.W., Dolejš, D., and Machek, M., 2009, Garnet exsolution in pyroxene from clinopyroxenites in the Moldanubian zone: Constraining the early pre-convergence history of ultramafic rocks in the Variscan orogen: Journal of Metamorphic Geology, v. 27, p. 655–671, doi:10.1111/j.1525-1314.2009.00834.x.

Faryad, S.W., Jedlicka, R., and Ettinger, K., 2013, Subduction of lithospheric upper mantle recorded by solid phase inclusions and compositional zoning in garnet: Example from the Bohemian Massif: Gondwana Research, v. 23, p. 944–955, doi:10.1016/j.gr.2012.05.014.

Ferrero, S., 2010, Anatectic melting in a metapelitic system: a fluid and melt inclusion study [Ph.D. thesis]: Padova, Dipartimento di Geoscienze, Universitá degli studi di Padova, 140 p.

Ferrero, S., and Angel, R.J., 2018, Micropetrology: Are Inclusions Grains of Truth? Journal of Petrology, v. 59, p. 1671–1700, doi:10.1093/petrology/egy075.

Ferrero, S., Bartoli, O., Cesare, B., Salvioli-Mariani, E., Acosta-Vigil, A., Cavallo, A., Groppo, C., and Battiston, S., 2012, Microstructures of melt inclusions in anatectic metasedimentary rocks: Journal of Metamorphic Geology, v. 30, p. 303–322, doi:10.1111/j.1525-1314.2011.00968.x.

Ferrero, S., Bodnar, R.J., Cesare, B., and Viti, C., 2011, Re-equilibration of primary fluid inclusions in peritectic garnet from metapelitic enclaves, El Hoyazo, Spain: Lithos, v. 124, p. 117–131, doi:10.1016/j.lithos.2010.09.004.

Ferrero, S., Braga, R., Berkesi, M., Cesare, B., and Laridhi Ouazaa, N., 2014, Production of metaluminous melt during fluid-present anatexis: An example from the Maghrebian basement, La Galite Archipelago, central Mediterranean: Journal of Metamorphic Geology, v. 32, p. 209–225, doi:10.1111/jmg.12068.

Ferrero, S., Godard, G., Palmieri, R., Wunder, B., and Cesare, B., 2018a, Partial melting of ultramafic granulites from Dronning Maud Land, Antarctica: Constraints from melt inclusions and thermodynamic modeling: American Mineralogist, v. 103, p. 610–622, doi:10.2138/am-2018-6214.

Ferrero, S., O'Brien, P.J., Borghini, A., Wunder, B., Wälle, M., Günter, C., and Ziemann, M.A., 2018b, A treasure chest full of nanogranitoids : an archive to investigate crustal melting in the Bohemian Massif, *in* Ferrero, S., Lanari, P., Goncalves, P. & Grosch, E.G., eds., Metamorphic Geology: Microscale to Mountain Belts: Geological Society, London, Special Publication, v. 478.

Ferrero, S., Wunder, B., Walczak, K., O'Brien, P.J., and Ziemann, M.A., 2015, Preserved near ultrahigh-pressure melt from continental crust subducted to mantle depths: Geology, v. 43, p. 447–450, doi:10.1130/G36534.1.

Ferrero, S., Wunder, B., Ziemann, M.A., Wälle, M., and O'Brien, P.J., 2016a, Carbonatitic and granitic melts produced under conditions of primary immiscibility during anatexis in the lower crust: Earth and Planetary Science Letters, v. 454, p. 121–131, doi:10.1016/j.epsl.2016.08.043.

Ferrero, S., Ziemann, M.A., Angel, R.J., O'Brien, P.J., and Wunder, B., 2016b, Kumdykolite, kokchetavite, and cristobalite crystallized in nanogranites from felsic granulites, Orlica-Snieznik Dome (Bohemian Massif): not an evidence for ultrahigh-pressure conditions: Contributions to Mineralogy and Petrology, v. 171, p. 1–12, doi:10.1007/s00410-015-1220-x.

Förster, M.W., Prelević, D., Schmück, H.R., Buhre, S., Veter, M., Mertz-Kraus, R., Foley, S.F., and Jacob, D.E., 2017, Melting and dynamic metasomatism of mixed harzburgite + glimmerite mantle source: Implications for the genesis of orogenic potassic magmas: Chemical Geology, v. 455, p. 182–191, doi:10.1016/j.chemgeo.2016.08.037.

Franke, W., 1989, Tectonostratigraphic units in the Variscan belt of central Europe: Geological Society of America Special Paper, v. 230, p. 67–90.

Franke, W., 2000, The mid-European segment of the Variscides: tectonostratigraphic units, terrane boundaries and plate tectonic evolution: Geological Society, London, Special Publications, v. 179, p. 35–61, doi:10.1144/gsl.sp.2000.179.01.05.

Franke, W., and Żelaźniewicz, A., 2000, The eastern termination of the Variscides: terrane correlation and kinematic evolution: Geological Society, London, Special Publications, v. 179, p. 63–86.

Frets, E.C., Tommasi, A., Garrido, C., Vauchez, A., Mainprice, D., Kamaltarguisti, and Amri, I., 2014, The Beni Bousera peridotite (Rif Belt, Morocco): An oblique-slip low-angle shear zone thinning the subcontinental mantle lithosphere: Journal of Petrology, v. 55, p. 283–313, doi:10.1093/petrology/egt067.

Frey, F.A., 1980, The origin of pyroxenite and garnet pyroxenite from Salt Lake Crater, Oahu, Hawaii: trace element evidence: American Journal of Science, v. 280-A, p. 427–449.

Frey, F.A., and Prinz, M., 1978, Ultramafic inclusions from San Carlos, Arizona: Petrologic and geochemical data bearing on their petrogenesis: Earth and Planetary Science Letters, v. 38, p. 129–176.

Frezzotti, M.L., Ferrando, S., Dallai, L., and Compagnoni, R., 2007, Intermediate alkali - Alumino-silicate aqueous solutions released by deeply subducted continental crust: Fluid evolution in UHP OH-rich topaz - kyanite quartzites from Donghai (Sulu, China): Journal of Petrology, v. 48, p. 1219–1241, doi:10.1093/petrology/egm015.

Frezzotti, M.L., Tecce, F., and Casagli, A., 2012, Raman spectroscopy for fluid inclusion analysis: Journal of Geochemical Exploration, v. 112, p. 1–20, doi:10.1016/j.gexplo.2011.09.009.

Fuhrman, M.L., and Lindsley, D.H., 1988, Ternary-feldspar modeling and thermometry: American mineralogist, v. 73, p. 201–215.

Fumagalli, P., Zanchetta, S., and Poli, S., 2009, Alkali in phlogopite and amphibole and their effects on phase relations in metasomatized peridotites: A high-pressure study: Contributions to Mineralogy and Petrology, v. 158, p. 723–737, doi:10.1007/s00410-009-0407-4.

Gao, X.Y., Chen, Y.X., and Zhang, Q.Q., 2017, Multiphase solid inclusions in ultrahigh-pressure metamorphic rocks: A snapshot of anatectic melts during continental collision: Journal of Asian Earth Sciences, v. 145, p. 192–204, doi:10.1016/j.jseaes.2017.03.036.

Gao, X.Y., Zheng, Y.F., and Chen, Y.X., 2012, Dehydration melting of ultrahigh-pressure eclogite in the Dabie orogen: Evidence from multiphase solid inclusions in garnet: Journal of Metamorphic Geology, v. 30, p. 193–212, doi:10.1111/j.1525-1314.2011.00962.x.

Garrido, C.J., and Bodinier, J.-L., 1999, Diversity of Mafic Rocks in the Ronda Peridotite: Evidence for Pervasive Melt-Rock Reaction during Heating of Subcontinental Lithosphere by Upwelling Asthenosphere: Journal of Petrology, v. 40, p. 729–754, doi:10.1093/petroj/40.5.729.

Gast, P.W., Tilton, G.R., and Hedge, C., 1964, Isotopic composition of lead and strontium from Ascension and Gough Islands: Science, v. 145, p. 1181–1185, doi:10.1126/science.145.3637.1181.

Gonzaga, R.G., Lowry, D., Jacob, D.E., LeRoex, A., Schulze, D., and Menzies, M.A., 2010, Eclogites and garnet pyroxenites: Similarities and differences: Journal of Volcanology and Geothermal Research, v. 190, p. 235–247, doi:10.1016/j.jvolgeores.2009.08.022.

Gordon, S.M., Schneider, D.A., Manecki, M., and Holm, D.K., 2005, Exhumation and metamorphism of an ultrahigh-grade terrane: geochronometric investigations of the Sudete Mountains (Bohemia), Poland and Czech Republic: Journal of the Geological Society, v. 162, p. 841–855.

Green, D.H., 1973, Experimental melting studies on a model upper mantle composition at high pressure under water-saturated and water-undersaturated conditions: Earth and Planetary Science Letters, v. 19, p. 37–53.

Guillong, M., Meier, D.L., Allan, M.M., Heinrich, C.A., and Yardley, B.W.D., 2008, SILLS: A Matlab-Based Program for the Reduction of Laser Ablation ICP–MS Data of Homogeneous Materials and Inclusions: Mineralogical Association of Canada Short Course, v. 40, p. 328–333.

Halter, W.E., Pettke, T., Heinrich, C.A., and Rothen-Rutishauser, B., 2002, Major to trace element analysis of melt inclusions by laser-ablation ICP-MS: methods of quantification: Chemical Geology, v. 183, p. 63–86, doi:10.1016/S0009-2541(01)00372-2.

Hartmann, G., and Wedepohl, K.H., 1993, The composition of peridotite tectonites from the Ivrea Complex, northern Italy: Residues from melt extraction: Geochimica et Cosmochimica Acta, v. 57, p. 1761–1782.

Hermann, J., and Green, D.H., 2001, Experimental constraints on high pressure melting in subducted crust: Earth and Planetary Science Letters, v. 188, p. 149–168, doi:10.1016/S0012-821X(01)00321-1.

Hermann, J., and Rubatto, D., 2009, Accessory phase control on the trace element signature of sediment melts in subduction zones: Chemical Geology, v. 265, p. 512–526, doi:10.1016/j.chemgeo.2009.05.018.

Hermann, J., and Spandler, C.J., 2008, Sediment melts at sub-arc depths: An experimental study: Journal of Petrology, v. 49, p. 717–740, doi:10.1093/petrology/egm073.

Herzberg, C., and Zhang, J., 1996, Melting experiments on anhydrous peridotite KLB-1: Compositions of magmas in the upper mantle and transition zone: Journal of Geophysical Research: Solid Earth, v. 101, p. 8271–8295, doi:10.1029/96jb00170.

Hirose, K., and Kushiro, I., 1993, Partial melting of dry peridotite at high pressure: Determination of compositions of melts segregated from peridotite using aggregates of diamond: Earth and Planetary Science Letters, v. 114, p. 477–489.

Hirschmann, M.M., 2000, Mantle solidus: Experimental constraints and the effects of peridotite composition: Geochemistry, Geophysics, Geosystems, v. 1, doi:10.1029/2000GC000070.

Hirschmann, M.M., and Stolper, E.M., 1996, A possible role for garnet pyroxenite in the origin of the “garnet signature” in MORB: Contributions to Mineralogy and Petrology, v. 124, p. 185–208, doi:10.1007/s004100050184.

Hirschmann, M.M., Ghiorso, M.S., Wasylenki, L.E., Asimow, P.D., and Stolper, E.M., 1998, Calculation of peridotite partial melting from thermodynamic models of minerals and melts. I. Review of methods and comparison with experiments: Journal of

Petrology, v. 39, p. 1091–1115, doi:10.1093/petroj/39.6.1091.

Holdaway, M.J., 2001, Recalibration of the GASP geobarometer in light of recent garnet and plagioclase activity models and versions of the garnet-biotite geothermometer: American Mineralogist, v. 86, p. 1117–1129.

Holloway, J.R., 1976, Fluids in the evolution of granitic magmas: Consequences of finite CO2 solubility: Bulletin of the Geological Society of America, v. 87, p. 1513–1518, doi:10.1130/0016-7606(1976)87<1513:FITEOG>2.0.CO;2.

Holness, M.B., and Sawyer, E.W., 2008, On the pseudomorphing of melt-filled pores during the crystallization of migmatites: Journal of Petrology, v. 49, p. 1343–1363, doi:10.1093/petrology/egn028.

Holness, M.B., Cesare, B., and Sawyer, E.W., 2011, Melted rocks under the microscope: Microstructures and their interpretation: Elements, v. 7, p. 247–252, doi:10.2113/gselements.7.4.247.

Huizenga, J.M., Van Reenen, D., and Touret, J.L.R., 2014, Fluid-rock interaction in retrograde granulites of the Southern Marginal Zone, Limpopo high grade terrain, South Africa: Geoscience Frontiers, v. 5, p. 673–682.

Hwang, S., 2000, Nanometer-Size α-PbO2–Type TiO2 in Garnet: A Thermobarometer for Ultrahigh-Pressure Metamorphism: Science, v. 288, p. 321–324, doi:10.1126/science.288.5464.321.

Hyndman, R.D., and Peacock, S.M., 2003, Serpentinization of the forearc mantle: Earth and Planetary Science Letters, v. 212, p. 417–432, doi:10.1016/S0012-821X(03)00263-2.

Irving, A.J., 1980, Petrology and geochemistry of composite ultramafic xenoliths in alkalic basalts and implications for magmatic processes within the mantle: American Journal of Science, v. 280, p. 389–426.

Isabel Varas-Reus, M., Garrido, C.J., Marchesi, C., Bosch, D., and Hidas, K., 2018, Genesis of Ultra-High Pressure Garnet Pyroxenites in Orogenic Peridotites and its Bearing on the Compositional Heterogeneity of the Earth's Mantle: Geochimica and Cosmochimica Acta, v. 232, p. 303-328, doi:10.1016/j.gca.2018.04.033.

Janoušek, V., and Holub, F. V., 2007, The causal link between HP-HT metamorphism and ultrapotassic magmatism in collisional orogens: Case study from the Moldanubian Zone of the Bohemian Massif: Proceedings of the Geologists' Association, v. 118, p. 75–86, doi:10.1016/S0016-7878(07)80049-6.

Janoušek, V., Finger, F., Roberts, M., Fryda, J., Pin, C., and Dolejš, 2004, Deciphering the petrogenesis of deeply buried granites: whole-rock geochemical constraints on the origin of largely undepleted felsic granulites from the Moldanubian Zone of the Bohemian Massif: Transactions of the Royal Society of Edinburgh: Earth Science, v. 95, p. 141–159, doi:10.1017/S0263593300000985.

Janousek, V., Krenn, E., Finger, F., Mikova, J., and Fryda, J., 2007, Hyperpotassic granulites from the Blanský les Massif (Moldanubian Zone, Bohemian Massif) revisited: Journal of Geosciences, v. 52, p. 73-112, doi:10.3190/jgeosci.010.

Jochum, K.P., et al., 2011, Determination of Reference Values for NIST SRM 610--617 Glasses Following ISO Guidelines: Geostandards and Geoanalytical Research, v. 35, p. 397–429, doi:10.1111/j.1751-908X.2011.00120.x.

Johannes, W., and Holtz, F., 1996, Petrogenesis and Experimental Petrology of Granitic Rocks: Springer, Berlin.

Johnson, T.E., Brown, M., Gardiner, N.J., Kirkland, C.L., and Smithies, H.R., 2017, Earth's first stable continents did not form by subduction: Nature, v. 543, p. 239–242, doi:10.1038/nature21383.

Kalt, A., Berger, A., and Blümel, P., 1999, Metamorphic evolution of cordierite-bearing migmatites from the Bayerische Wald (Variscan Belt, Germany): Journal of Petrology, v. 40, p. 601–627, doi:10.1093/petroj/40.4.601.

Kawamoto, T., and Holloway, J.R., 1997, Melting temperature and partial melt chemistry to H2O-saturated mantle peridotite to 11 gigapascals: Science, v. 276, p. 240–243, doi:10.1126/science.276.5310.240.

Kelemen, P.B., Hirth, G., Shimizu, N., Spiegelman, M., and Dick, H.J.B., 1997, A review of melt migration processes in the adiabatically upwelling mantle beneath oceanic spreading ridges: Philosophical Transactions of the Royal Society A: Mathematical, Physical and Engineering Sciences, v. 355, p. 283–318, doi:10.1098/rsta.1997.0010.

Kessel, R., Pettke, T., and Fumagalli, P., 2015, Melting of metasomatized peridotite at 4–6 GPa and up to 1200 °C: an experimental approach: Contributions to Mineralogy and Petrology, v. 169, p. 1–19, doi:10.1007/s00410-015-1132-9.

Klemd, R., and Bröcker, M., 1999, Fluid influence on mineral reactions in ultrahigh-pressure granulites: a case study in the Śnieżnik Mts.(West Sudetes, Poland): Contributions to Mineralogy and Petrology, v. 136, p. 358–373.

Klemme, S., Blundy, J.D., and Wood, B.J., 2002, Experimental constraints on major and trace element partitioning during partial melting of eclogite: Geochimica et Cosmochimica Acta, v. 66, p. 3109–3123, doi:10.1016/S0016-7037(02)00859-1.

Kobayashi, T., Hirajima, T., Kawakami, T., and Svojtka, M., 2011, Metamorphic history of garnet-rich gneiss at Ktiš in the Lhenice shear zone, Moldanubian Zone of the southern Bohemian Massif, inferred from inclusions and compositional zoning of garnet: Lithos, v. 124, p. 46–65, doi:10.1016/j.lithos.2010.11.003.

Kogiso, T., Hirschmann, M.M., and Reiners, P.W., 2004, Length scales of mantle heterogeneities and their relationship to ocean island basalt geochemistry: Geochimica et Cosmochimica Acta, v. 68, p. 345–360, doi:10.1016/S0016-7037(03)00419-8.

Kornprobst, J., Piboule, M., Roden, M., and Tabit, A., 1990, Corundum-bearing garnet clinopyroxenites at Beni Bousera (Morocco): Original plagioclase-rich gabbros recrystallized at depth within the mantle? Journal of Petrology, v. 31, p. 717–745, doi:10.1093/petrology/31.3.717.

Kotková, J., O'Brien, P.J., and Ziemann, M.A., 2011, Diamond and coesite discovered in Saxony-type granulite: Solution to the Variscan garnet peridotite enigma: Geology, v. 39, p. 667–670, doi:10.1130/G31971.1.

Kotkova, J., Skoda, R., and Machovic, V., 2014, Kumdykolite from the ultrahigh-pressure granulite of the Bohemian Massif: American Mineralogist, v. 99, p. 1798–1801, doi:10.2138/am.2014.4889.

Koziol, A.M., and Newton, R.C., 1988, Redetermination of the anorthite breakdown reaction and improvement of the plagioclase-garnet-Al2SiO5-quartz geobarometer: American Mineralogist, v. 73, p. 216–223.

Kröner, A., Jaeckel, P., Hegner, E., and Opletal, M., 2001, Single zircon ages and whole-rock Nd isotopic systematics of early Palaeozoic granitoid gneisses from the Czech and Polish Sudetes (Jizerské hory, Krkonoše Mountains and Orlice-Sněžník Complex): International Journal of Earth Sciences, v. 90, p. 304–324.

Kröner, A., Jaeckel, P., Reischmann, T., and Kroner, U., 1998, Further evidence for an early Carboniferous (~340 Ma) age of high-grade metamorphism in the Saxonian granulite complex: Geologische Rundschau, v. 86, p. 751–766, doi:10.1007/PL00009939.

Kröner, A., and Willner, 1998, Time of formation and peak of Variscan HP-HT metamorphism of quartz-feldspar rocks in the central Erzgebirge, Saxony, Germany: Contributions to Mineralogy and Petrology, v. 132, p. 1–20, doi:10.1007/s004100050401.

Kröner, A., O'Brien, P.J., Nemchin, A.A., and Pidgeon, R.T., 2000, Zircon ages for high pressure granulites from South Bohemia, Czech Republic, and their connection to Carboniferous high temperature processes: Contributions to Mineralogy and Petrology, v. 138, p. 127–142.

Kryza, R., Pin, C., and Vielzeuf, D., 1996, High-pressure granulites from the Sudetes (south-west Poland): Evidence of crustal subduction and collisional thickening in the Variscan Belt: Journal of Metamorphic Geology, v. 14, p. 531–546, doi:10.1046/j.1525-1314.1996.03710.x.

Kushiro, I., 1972, Effect of water on the composition of magmas formed at high pressures: Journal of Petrology, v. 13, p. 311–334, doi:10.1093/petrology/13.2.311.

Labrousse, L., Prouteau, G., and Ganzhorn, A.C., 2011, Continental exhumation triggered by partial melting at ultrahigh pressure: Geology, v. 39, p. 1171–1174, doi:10.1130/G32316.1.

Lamadrid, H.M., Lamb, W.M., Santosh, M., and Bodnar, R.J., 2014, Raman spectroscopic characterization of H2O in CO2-rich fluid inclusions in granulite facies metamorphic rocks: Gondwana Research, v. 26, p. 301–310.

Lambart, S., Baker, M.B., and Stolper, E.M., 2016, The role of pyroxenite in basalt genesis: Melt-Px, a melting parameterization for mantle pyroxenites between 0.9 and 5 GPa: Journal of Geophysical Research: Solid Earth, v. 121, p. 5708–5735, doi:10.1002/2015JB012762.Received.

Lambart, S., Laporte, D., Provost, A., and Schiano, P., 2012, Fate of pyroxenite-derived melts in the peridotitic mantle: Thermodynamic and experimental constraints: Journal of Petrology, v. 53, p. 451–476, doi:10.1093/petrology/egr068.

Lambart, S., Laporte, D., and Schiano, P., 2013, Markers of the pyroxenite contribution in the major-element compositions of oceanic basalts: Review of the experimental constraints: Lithos, v. 160–161, p. 14–36, doi:10.1016/j.lithos.2012.11.018.

Lang, H.M., and Gilotti, J.A., 2007, Partial melting of metapelites at ultrahigh-pressure conditions, Greenland Caledonides: Journal of Metamorphic Geology, v. 25, p. 129–147, doi:10.1111/j.1525-1314.2006.00687.x.

Lange, U., Bröcker, M., Armstrong, R., Trapp, E., and Mezger, K., 2005, Sm–Nd and U–Pb dating of high-pressure granulites from the Złote and Rychleby Mts (Bohemian Massif, Poland and Czech Republic): Journal of Metamorphic Geology, v. 23, p. 133–145.

Le Breton, N., and Thompson, A.B., 1988, Fluid-absent (dehydration) melting of biotite in metapelites in the early stages of crustal anatexis: Contributions to Mineralogy and Petrology, v. 99, p. 226–237.

Liu, Q., Hermann, J., and Zhang, J., 2013, Polyphase inclusions in the Shuanghe UHP eclogites formed by subsolidus transformation and incipient melting during exhumation of deeply subducted crust: Lithos, v. 177, p. 91–109, doi:10.1016/j.lithos.2013.06.010.

Liu, P., Zhang, J., Massonne, H.-J.J., and Jin, Z., 2018, Polyphase solid-inclusions formed by interactions between infiltrating fluids and precursor minerals enclosed in garnet of UHP rocks from the Dabie Shan, China: American Mineralogist, v. 103, p. 1663–1673, doi:10.2138/am-2018-6395.

Lowenstern, J.B., 1995, Applications of silicate-melt inclusions to the study of magmatic volatiles, *in* Thompson, J.F.H., ed., Magma, Fluids and Ore Deposits: Mineralogical Association of Canada Short Course, v. 23, p. 71–99.

Lundstrom, C.C., and Glazner, A.F., 2016, Silicic magmatism and the volcanic–plutonic connection: Elements, v. 12, p. 91–96.

Luvizotto, G.L., Zack, T., Meyer, H.P., Ludwig, T., Triebold, S., Kronz, A., Münker, C., Stockli, D.F., Prowatke, S., and Klemme, S., 2009, Rutile crystals as potential trace element and isotope mineral standards for microanalysis: Chemical Geology, v. 261, p. 346–369.

Malaspina, N., Alvaro, M., Campione, M., Wilhelm, H., and Nestola, F., 2015, Dynamics of mineral crystallization from precipitated slab-derived fluid phase: first in situ synchrotron X-ray measurements: Contributions to Mineralogy and Petrology, v. 169, doi:10.1007/s00410-015-1121-z.

Malaspina, N., Hermann, J., and Scambelluri, M., 2009, Fluid/mineral interaction in UHP garnet peridotite: Lithos, v. 107, p. 38–52, doi:10.1016/j.lithos.2008.07.006.

Malaspina, N., Hermann, J., Scambelluri, M., and Compagnoni, R., 2006, Polyphase inclusions in garnet-orthopyroxenite (Dabie Shan, China) as monitors for metasomatism and fluid-related trace element transfer in subduction zone peridotite: Earth and Planetary Science Letters, v. 249, p. 173–187, doi:10.1016/j.epsl.2006.07.017.

Malaspina, N., Langenhorst, F., Tumiati, S., Campione, M., Frezzotti, M.L., and Poli, S., 2017, The redox budget of crust-derived fluid phases at the slab-mantle interface: Geochemica et Cosmochimica Acta, v. 209, p. 70–84, doi:http://dx.doi.org/10.1016/j.gca.2017.04.004.

Mallik, A., and Dasgupta, R., 2012, Reaction between MORB-eclogite derived melts and fertile peridotite and generation of ocean island basalts: Earth and Planetary Science Letters, v. 329–330, p. 97–108, doi:10.1016/j.epsl.2012.02.007.

Marchesi, C., Garrido, C.J., Bosch, D., Bodinier, J.L., Gervilla, F., and Hidas, K., 2013, Mantle refertilization by melts of crustal-derived garnet pyroxenite: Evidence from the Ronda peridotite massif, southern Spain: Earth and Planetary Science Letters, v. 362, p. 66–75, doi:10.1016/j.epsl.2012.11.047.

Martin, H., Smithies, R.H., Rapp, R., Moyen, J.F., and Champion, D., 2005, An overview of adakite, tonalite-trondhjemiten-granodiorite (TTG), and sanukitoid: Relationships and some implications for crustal evolution: Lithos, v. 79, p. 1–24, doi:10.1016/j.lithos.2004.04.048.

Massonne, H.-J., 1999, A new occurrence of microdiamonds in quartzofeldspathic rocks of the Saxonian Erzgebirge, Germany, and their metamorphic evolution, *in* Proceedings of the 7th International Kimberlite Conference, Cape Town, p. 552–554.

Massonne, H.-J.J., 2001, First find of coesite in the ultrahigh-pressure metamorphic area of the central Erzgebirge, Germany: European Journal of Mineralogy, v. 13, p. 565–570, doi:10.1127/0935-1221/2001/0013-0565.

Massonne, H., 2011, Occurrences and PT Conditions of High and Ultrahigh Pressure Rocks in the Bohemian Massif: Geolines, v. 23, p. 18–26, http://geolines.gli.cas.cz/index.php?id=volume23.

Massone, H.J., and Bautsch, H.-J., 2002, An unusual garnet pyroxenite from the granulitgebirge, Germany: Origin in the transition zone (>400 km depths) or in a shallower upper mantle region? International Geology Review, v. 44, p. 779–796, doi:10.2747/0020-6814.44.9.779.

Massonne, H.-J., and Fockenberg, T., 2012, Melting of metasedimentary rocks at ultrahigh pressure — Insights from experiments and thermodynamic calculations: Lithosphere, v. 4, p. 269–285, doi:10.1130/L185.1.

Massonne, H.-J., and Grosch, U., 1995, PT evolution of palaeozoic garnet peridotites from the Saxonian Erzgebirge and the Aheim region, W. Norway, *in* International Kimberlite Conference: Extended Abstracts, v. 6, p. 353–355.

Massonne, H.-J., and Neuser, R.D., 2005, Ilmenite exolution in olivine from the serpentinite body at Zöblitz, Saxonian Erzgebirge - microstructural evidence using EBSD: Mineralogical Magazine, v. 69, p. 119–124.

Massonne, H.-J., and O'Brien, P.J., 2003, The Bohemian massif and the NW Himalaya, *in* Carswell, D.A., and Compagnoni, R., eds., Ultrahigh pressure metamorphism: EMU Notes in Mineralogy, v. 5, p. 145–187.

Massonne, H.-J., Kennedy, A., Nasdala, L., and Theye, T., 2007, Dating of zircon and monazite from diamondiferous

quartzofeldspathic rocks of the Saxonian Erzgebirge – hints at burial and exhumation velocities: Mineralogical Magazine, v. 71, p. 407–425, doi:10.1180/minmag.2007.071.4.407.

Matte, P., 1998, Continental subduction and exhumation of HP rocks in Paleozoic orogenic belts: Uralides and Variscides: Geologiska Foreningen i Stockholm Forhandlingar, v. 120, p. 209–222, doi:10.1080/11035899801202209.

Matte, P., Maluski, H., Rajlich, P., and Franke, W., 1990, Terrane boundaries in the Bohemian Massif: result of large-scale Variscan shearing: Tectonophysics, v. 177, p. 151–170.

McDonough, W.F., and Sun, S. -S., 1995, The composition of the Earth: Chemical Geology, v. 120, p. 223–253.

Medaris, L.G., 1999, Garnet Peridotites in Eurasian High-Pressure and Ultrahigh-Pressure Terranes : A Diversity of Origins and Thermal Histories: International Geology Review, v. 41, p. 799–815, doi:10.1080/00206819909465170.

Medaris, L.G., and Carswell, D.A., 1990, Petrogenesis of Mg-Cr garnet peridotites in European metamorphic belts, *in* Carswell D. A., ed., Eclogite facies rocks: Blackie, Glasgow, p. 260–290.

Medaris, L.G., Ackerman, L., Jelínek, E., Michels, Z.D., Erban, V., and Kotková, J., 2015, Depletion, cryptic metasomatism, and modal metasomatism (refertilization) of Variscan lithospheric mantle: Evidence from major elements, trace elements, and Sr-Nd-Os isotopes in a Saxothuringian garnet peridotite: Lithos, v. 226, p. 81–97, doi:10.1016/j.lithos.2014.10.007.

Medaris, L.G., Beard, and Jelínek, E., 2006, Mantle-Derived, UHP Garnet Pyroxenite and Eclogite in the Moldanubian Gföhl Nappe, Bohemian Massif: A Geochemical Review, New P-T Determinations, and Tectonic Interpretation: International Geology Review, v. 48, p. 765–777, doi:10.2747/0020-6814.48.9.765.

Medaris, L.G., Beard, B.L., Johnson, C.M., Valley, J.W., Spicuzza, M.J., Jelínek, E., and Mísâr, Z., 1995, Garnet pyroxenite and eclogite in the Bohemian Massif: geochemical evidence for Variscan recycling of subducted lithosphere: Geologische Rundschau, v. 84, p. 489–505, doi:10.1007/BF00284516.

Medaris, L.G., Jelínek, E., Beard, B.L., Valley, J.W., Spicuzza, M.J., and Strnad, L., 2013, Garnet pyroxenite in the biskupice peridotite, Bohemian Massif: Anatomy of a variscan high-pressure cumulate: Journal of Geosciences (Czech Republic), v. 58, p. 3–19, doi:10.3190/jgeosci.131.

Medaris, L.G., Wang, H., Jelínek, E., Mihaljevič, M., and Jakeš, P., 2005, Characteristics and origins of diverse Variscan peridotites in the Gföhl Nappe, Bohemian Massif, Czech Republic: Lithos, v. 82, p. 1–23, doi:10.1016/j.lithos.2004.12.004.

Miyazaki, T., Nakamura, D., Tamura, A., Svojtka, M., Arai, S., and Hirajima, T., 2016, Evidence for partial melting of eclogite from the Moldanubian Zone of the Bohemian Massif, Czech Republic: Journal of Mineralogical and Petrological Sciences, v. 111, p. 405–419, doi:10.2465/jmps.151029c.

Montanini, A., and Tribuzio, R., 2015, Evolution of recycled crust within the mantle: Constraints from the garnet pyroxenites of the External Ligurian ophiolites (northern Apennines, Italy): Geology, v. 43, p. 1–4, doi:10.1130/G36877.1.

Montanini, A., Tribuzio, R., and Thirlwall, M., 2012, Garnet clinopyroxenite layers from the mantle sequences of the Northern Apennine ophiolites (Italy): Evidence for recycling of crustal material: Earth and Planetary Science Letters, v. 351–352, p. 171–181, doi:10.1016/j.epsl.2012.07.033.

Montel, J.-M., and Vielzeuf, D., 1997, Partial melting of metagreywackes, Part II. Compositions of minerals and melts: Contributions to Mineralogy and Petrology, v. 128, p. 176–196.

Morgan, G.B., and London, D., 1996, Optimizing the electron microprobe analysis of hydrous alkali aluminosilicate glasses: American Mineralogist, v. 81, p. 1176–1185.

Morgan, G.B., and London, D., 2005, Effect of current density on the electron microprobe analysis of alkali aluminosilicate glasses: American Mineralogist, v. 90, p. 1131–1138.

Morishita, T., Arai, S., Gervilla, F., and Green, D.H., 2003, Closed-system geochemical recycling of crustal materials in alpine-type peridotite: Geochimica et Cosmochimica Acta, v. 67, p. 303–310.

Moyen, J., and Martin, H., 2012, Forty years of TTG research: Lithos, v. 148, p. 312–336, doi:10.1016/j.lithos.2012.06.010.

Naemura, K., Hirajima, T., Svojtka, M., Shimizu, I., and Iizuka, T., 2018, Fossilized melts in mantle wedge peridotites: Scientific Reports, v. 8, p. 1–12, doi:10.1038/s41598-018-28264-6.

Nasdala, L., and Massonne, H.-J., 2000, Microdiamonds from the Saxonian Erzgebirge, Germany: in situ micro-Raman characterisation: European Journal of Mineralogy, v. 12, p. 495–498, doi:10.1127/0935-1221/2000/0012-0495.

Neubauer, F., 2009, Geology of Europe: GEOLOGY-Volume IV, p. 198.

Ni, H., and Keppler, H., 2013, Carbon in silicate melts: Reviews in Mineralogy and Geochemistry, v. 75, p. 251–287, doi:10.2138/rmg.2013.75.9.

Nixon, P.H., Rogers, N.W., Gibson, I.L., and Grey, A., 1981, Depleted and fertile mantle xenoliths from southern African kimberlites: Annual Reviews on Earth and Planetary Science, v. 9, p. 285–309.

O'Brien, P.J., 2000, The fundamental Variscan problem: high-temperature metamorphism at different depths and high-pressure metamorphism at different temperatures: Geological Society, London, Special Publications, v. 179, p. 369–386, doi:10.1144/GSL.SP.2000.179.01.22.

O'Brien, P.J., 2006, Type-locality granulites: High-pressure rocks formed at eclogite-facies conditions: Mineralogy and Petrology, v. 86, p. 161–175, doi:10.1007/s00710-005-0108-2.

O'Brien, P.J., 2008, Challenges in high-pressure granulite metamorphism in the era of pseudosections: Reaction textures, compositional zoning and tectonic interpretation with examples from the Bohemian Massif: Journal of Metamorphic Geology, v. 26, p. 235–251, doi:10.1111/j.1525-1314.2007.00758.x.

O'Brien, P.J., and Carswell, D.A., 1993, Tectonometamorphic Evolution of the Bohemian Massif - Evidence from High-Pressure Metamorphic Rocks: Geologische Rundschau, v. 82, p. 531–555.

O'Brien, P.J., and Rötzler, J., 2003, High-pressure granulites: Formation, recovery of peak conditions and implications for tectonics: Journal of Metamorphic Geology, v. 21, p. 3–20, doi:10.1046/j.1525-1314.2003.00420.x.

O'Brien, P.J., and Ziemann, M.A., 2008, Preservation of coesite in exhumed eclogite: insights from Raman mapping: European Journal of Mineralogy, v. 20, p. 827–834, doi:10.1127/0935-1221/2008/0020-1883.

O'Hara, M.J., and Yoder, H.S., 1963, Partial melting of the mantle: Carnegie Institution of Washington Yearbook, v. 62, p. 66–71.

Obata, M., and Morten, L., 1987, Transformation of spinel lherzolite to garnet lherzolite in ultramafic lenses of the austridic crystalline complex, Northern Italy: Journal of Petrology, v. 28, p. 599–623, doi:10.1093/petrology/28.3.599.

Obata, M., Hirajima, T., and Svojtka, M., 2006, Origin of eclogite and garnet pyroxenite from the Moldanubian Zone of the Bohemian Massif, Czech Republic and its implication to other mafic layers embedded in orogenic peridotites: Mineralogy and Petrology, v. 88, p. 321–340, doi:10.1007/s00710-006-0158-0.

Oliver, G.J.H., Corfu, F., and Krogh, T.E., 1993, U-Pb ages from SW Poland: evidence for a Caledonian suture zone between Baltica and Gondwana: Journal of the Geological Society, v. 150, p. 355–369.

Peacock, S.M., Rushmer, T., and Thompson, A.B., 1994, Partial Melting of Subducting Oceanic-Crust: Earth and Planetary Science Letters, v. 121, p. 227–244, doi:10.1016/0012-821x(94)90042-6.

Pearson, D.G., Davies, G.R., and Nixon, P.H., 1993, Geochemical constraints on the petrogenesis of diamond facies pyroxenites from the Beni Bousera peridotite massif, North Morocco: Journal of Petrology, v. 34, p. 125–172.

Pearson, D.G., Davies, G.R., Nixon, P.H., Greenwood, P.B., and Mattey, D.P., 1991, Oxygen isotope evidence for the origin of pyroxenites in the Beni Bousera peridotite massif, North Morocco: derivation from subducted oceanic lithosphere: Earth and Planetary Science Letters, v. 102, p. 289–301, doi:10.1016/0012-821X(91)90024-C.

Pearson, D.G., and Nowell, G.M., 2004, Re-Os and Lu-Hf Isotope Constraints on the Origin and Age of Pyroxenites from the Beni Bousera Peridotite Massif: Implications for Mixed Peridotite-Pyroxenite Mantle Sources: Journal of Petrology, v. 45, p. 439–455, doi:10.1093/petrology/egg102.

Perchuk, A., Philippot, P., Erdmer, P., and Fialin, M., 1999, Rates of thermal equilibration at the onset of subduction deduced from diffusion modeling of eclogitic garnets, Yukon-Tanana terrane, Canada: Geology, v. 27, p. 531–534.

Perchuk, A.L., Yapaskurt, V.O., and Davydova, V. V, 2008, Melt inclusions in eclogite garnet : experimental study of natural processes: Russian Geology and Geophysics, v. 49, p. 310–312, doi:10.1016/j.rgg.2007.10.009.

Perraki, M., and Faryad, S.W., 2014, First finding of microdiamond, coesite and other UHP phases in felsic granulites in the Moldanubian Zone: Implications for deep subduction and a revised geodynamic model for Variscan Orogeny in the Bohemian Massif: Lithos, v. 202–203, p. 157–166, doi:10.1016/j.lithos.2014.05.025.

Pertermann, M., and Hirschmann, M.M., 2003, Anhydrous Partial Melting Experiments on MORB-like Eclogite: Phase Relations, Phase Compositions and Mineral-Melt Partitioning of Major Elements at 2 - 3 GPa: Journal of Petrology, v. 44, p. 2173–2201, doi:10.1093/petrology/egg074.

Prouteau, G., Scaillet, B., and Pichavant, M., 2001, Hydrous Silicic Melts Derived From Subducted Oceanic Crust: Nature, v. 410, p. 197–200.

von Quadt, A., 1993, The Saxonian Granulite Massif: new aspects from geochronological studies: Geologische Rundschau, v. 82, p. 516–530, doi:10.1007/BF00212414.

Raffone, N., Le Fèvre, B., Ottolini, L., Vannucci, R., and Zanetti, A., 2006, Light-lithophile element metasomatism of finero peridotite (W ALPS): A secondary-ion mass spectrometry study: Microchimica Acta, v. 155, p. 251–255, doi:10.1007/s00604-006-0551-8.

Rampone, E., and Morten, L., 2001, Records of Crustal Metasomatism in the Garnet Peridotites of the Ulten Zone (Upper Austroalpine, Eastern Alps): Journal of Petrology, v. 42, p. 207–219, doi:10.1093/petrology/42.1.207.

Rapp, R.P., and Watson, E.B., 1995, Dehydration melting of metabasalt at 8 - 32 kbar: Implications for continental growth and crust-mantle recycling: Journal of Petrology, v. 36, p. 891–931, doi:10.1093/petrology/36.4.891.

Rapp, R.P., Norman, M.D., Laporte, D., Yaxley, G.M., Martin, H., and Foley, S.F., 2010, Continet formation in the Archean and chemical evolution of the cratonic lithosphere: melt-rock reaction experiments at 3-4 GPa and petrogenesis of Archean Mg-Diorites (Sanukitoids): Journal of Petrology, v. 51, p. 1237–1266, doi:10.1093/petrology/egq017.

Rapp, R.P., Watson, E.B., and Miller, C.F., 1991, Partial melting of amphibolite/eclogite and the origin of Archean trondhjemites and tonalites: Precambrian Research, v. 51, p. 1–25, doi:10.1016/0301-9268(91)90092-O.

von Raumer, J.F., Finger, F., Veselá, P., and Stampfli, G.M., 2014, Durbachites-Vaugnerites - a geodynamic marker in the central European Variscan orogen: Terra Nova, v. 26, p. 85–95, doi:10.1111/ter.12071.

Reinhardt, J., and Kleemann, U., 1994, Extensional unroofing of granulitic lower crust and related low-pressure, high-temperature metamorphism in the Saxonian Granulite Massif, Germany: Tectonophysics, v. 238, p. 71–94, doi:10.1016/0040-1951(94)90050-7.

Roedder, E., 1984, Volume 12: Fluid inclusions: Reviews in mineralogy, v. 12.

Van Roermund, H.L.M., Carswell, D.A., Drury, M.R., and Heijboer, T.C., 2002, Microdiamonds in a megacrystic garnet websterite pod from Bardane on the island of Fjørtoft, western Norway: Evidence for diamond formation in mantle rocks durind deep continetal subduction: Geology, v. 30, p. 959–962.

Romer, R.L., and Rötzler, J., 2001, P-T-t Evolution of Ultrahigh-Temperature Granulites from the Saxon Granulite Massif , Germany . Part II : Geochronology: Journal of Petrology, v. 42, p. 2015–2032.

Rötzler, J., and Romer, R.L., 2001, P-T-t Evolution of Ultrahigh-Temperature Granulites from the Saxon Granulite Massif , Germany . Part I: Petrology: Journal of Petrology, v. 42, p. 1995–2013.

Rötzler, J., and Romer, R.L., 2001, P–T–t evolution of ultrahigh-temperature granulites from the Saxon Granulite Massif, Germany. Part II: Geochronology: Journal of Petrology, v. 42, p. 1995–2013.

Rötzler, J., Hagen, B., and Hoernes, S., 2008, Geothermometry of the ultrahigh-temperature Saxon granulites revisited. Part I: New evidence from key mineral assemblages and reaction textures: European Journal of Mineralogy, v. 20, p. 1097–1115, doi:10.1127/0935-1221/2008/0020-1857.

Rötzler, J., Kurze, M., Linnemann, U., and Tröger, K.-A., 1992, Zur Petrogenese im Sächsischen Granulitgebirge: die pyroxenfreien Granulite und die Metapelite: Geotektonische Forschungen, v.77, p. 1 - 100.

Rötzler, J., Romer, R.L., Budzinski, H., and Oberhänsli, R., 2004, Ultrahigh-temperature high-pressure granulites from Tirschheim, Saxon Granulite Massif, Germany: P-T-t path and geotectonic implications: European Journal of Mineralogy, v. 16, p. 917–937, doi:10.1127/0935-1221/2004/0016-0917.

Salvioli-Mariani, E., Mattioli, M., Renzulli, A., and Serri, G., 2002, Silicate melt inclusions in the cumulate minerals of gabbroic nodules from Stromboli Volcano (Aeolian Islands, Italy): main components of the fluid phase and crystallization temperatures: v. 66, p. 969–984, doi:10.1180/0026461026660071.

Sawyer, E.W., Cesare, B., and Brown, M., 2011, When the continental crust melts: Elements, v. 7, p. 229–234.

Scaillet, B., and Prouteau, G., 2001, Oceanic Slab Melting and Mantle Metasomatism: Science Progress, v. 84, p. 335–354, doi:10.3184/003685001783238943.

Scambelluri, M., Cannao`, E., and Gilio, M., 2019, The water and fluid-mobile element cycles during serpentinite subduction. A review: European Journal of Mineralogy, v. 31, p. 405–428, doi:https://doi.org/10.1127/ejm/2019/0031-2842.

Scambelluri, M., Hermann, J., Morten, L., and Rampone, E., 2006, Melt- versus fluid-induced metasomatism in spinel to garnet wedge peridotites (Ulten Zone, Eastern Italian Alps): Clues from trace element and Li abundances: Contributions to Mineralogy and Petrology, v. 151, p. 372–394, doi:10.1007/s00410-006-0064-9.

Schantl, P., Hauzenberger, C., Finger, F., and Linner, M., 2018, Garnet growth history in granulites from the southeastern Moldanubain Zone (Bohemian Massif) revealed by Zr in rutile thermometry, mineral inclusions and trace element zoning, *in* EGU General Assembly Conference Abstracts, v. 20, p. 10054.

Schiano, P., Clocchiatti, R., Boivin, P., and Medard, E., 2004, The nature of melt inclusions inside minerals in an ultramafic cumulate from Adak volcanic center, aleutian arc: implications for the origin of high-Al basalts: Chemical Geology, v. 203, p. 169–179, doi:10.1016/j.chemgeo.2003.10.001.

Schiano, P., Clocchiatti, R., Shimizu, N., Maury, R.C., Jochum, K.P., and Hofmann, A.W., 1995, Hydrous, silica-rich melts in the sub-arc mantle and their relationship with erupted arc lavas: Nature, v. 377, p. 595–600, doi:10.1038/377595a0.

Schiano, P., Provost, A., Clocchiatti, R., and Faure, F., 2006, Transcrystalline melt migration and earth's mantle: Science, v. 314, p. 970–974, doi:10.1126/science.1132485.

Schmädicke, E., and Evans, B.W., 1997, Garnet-bearing ultramafic rocks from the Erzgebirge, and their relation to other settings in the Bohemian Massif: Contributions to Mineralogy and Petrology, v. 127, p. 57–74, doi:10.1007/s004100050265.

Schmädicke, E., Gose, J., and Will, T.M., 2010, The P-T evolution of ultra high temperature garnet-bearing ultramafic rocks from the Saxonian Granulitgebirge Core Complex, Bohemian Massif: Journal of Metamorphic Geology, v. 28, p. 489–508, doi:10.1111/j.1525-1314.2010.00876.x.

Schmädicke, E., Mezger, K., Cosca, M.A., and Okrusch, M., 1995, Variscan Sm-Nd and Ar-Ar ages of eclogite facies rocks from the Erzgebirge, Bohemian Massif: Journal of Metamorphic Geology, v. 13, p. 537–552, doi:10.1111/j.1525-1314.1995.tb00241.x.

Schmädicke, E., Okrusch, M., and Schmidt, W., 1992, Eclogite-facies rocks in the Saxonoian Erzgebirge, Germany: high pressure metamorphism under contrasting P-T conditions: Contributions to Mineralogy and Petrology, v. 110, p. 226–241.

Schmädicke, E., Will, T.M., Ling, X., Li, X.H., and Li, Q.L., 2018, Rare peak and ubiquitous post-peak zircon in eclogite: Constraints for the timing of UHP and HP metamorphism in Erzgebirge, Germany: Lithos, v. 322, p. 250–267, doi:10.1016/j.lithos.2018.10.017.

Schmidt, G., Witt-Eickschen, G., Palme, H., Seck, H., Spettel, B., and Kratz, K.L., 2003, Highly siderophile elements (PGE, Re and Au) in mantle xenoliths from the West Eifel volcanic field (Germany): Chemical Geology, v. 196, p. 77–105, doi:10.1016/S0009-2541(02)00408-4.

Schulmann, K., Lexa, O., Janoušek, V., Lardeaux, J.M., and Edel, J.B., 2014, Anatomy of a diffuse cryptic suture zone: An example from the Bohemian Massif, European variscides: Geology, v. 42, p. 275–278, doi:10.1130/G35290.1.

Scott, J.M., Konrad-Schmolke, M., O'Brien, P.J., and Günter, C., 2013, High-T, low-P formation of rare olivine-bearing symplectites in Variscan eclogite: Journal of Petrology, v. 54, p. 1375–1398, doi:10.1093/petrology/egt015.

Skjerlie, K.P., and Patiño Douce, A.E., 2002, The fluid-absent partial melting of a zoisite-bearing quartz eclogite from 1.0 to 3.2 GPa; implications for melting in thickened continetal crust and for subduction-zone processes: Journal of Petrology, v. 43, p. 291–314, doi:10.1093/petrology/43.2.291.

Sláma, J., Košler, J., Condon, D.J., Crowley, J.L., Gerdes, A., Hanchar, J.M., Horstwood, M.S.A., Morris, G.A., Nasdala, L., and Norberg, N., 2008, Plešovice zircon—a new natural reference material for U–Pb and Hf isotopic microanalysis: Chemical Geology, v. 249, p. 1–35.

Slupski, P., Ferrero, S., and Walczak, K., 2018, Former melt inclusions in garnets from granulites of the Góry Sowie Block, NE Bohemian Massif, *in* EGU General Assembly Conference Abstracts, v. 20, p. 15214.

Sobolev, A.V., Asafov, E.V., Gurenko, A.A., Arndt, N.T., Batanova, V.G., Portnyagin, M.V., Garbe-Schönberg, D., Wilson, A.H., and Byerly, G.R., 2019, Deep hydrous mantle reservoir provides evidence for crustal recycling before 3.3 billion years ago: Nature, v. 571, p. 555 - 559, doi:10.13140/RG.2.2.15896.44801.

Sobolev, A. V. et al., 2007, The amount of recycled crust in sources of mantle-derived melts: Science, v. 316, p. 412–418, doi:10.1126/science.1138113.

Sorger, D., Hauzenberger, C.A., Linner, M., Iglseder, C., and Finger, F., 2018, Carboniferous polymetamorphism recorded in paragneiss-migmatites from the Bavarian Unit (Moldanubian Superunit, Upper Austria): Implications for the tectonothermal evolution at the end of the Variscan orogeny: Journal of Petrology, v. 59, p. 1359–1382, doi:10.1093/petrology/egy063.

Spear, F.S., Pattison, D.R.M., and Cheney, J.T., 2016, The metamorphosis of metamorphic petrology: Geological Society of America Special Paper, v. 523, p. 31–74, doi:10.1130/2016.2523(02).

Stepanov, A.S., Hermann, J., Rubatto, D., Korsakov, A.V., and Danyushevsky, L.V., 2016, Melting history of an ultrahigh-pressure paragneiss revealed by multiphase solid inclusions in garnet, Kokchetav massif, Kazakhstan: Journal of Petrology, v. 57, p.

1531–1554, doi:10.1093/petrology/egw049.

Štípská, P., Chopin, F., Skrzypek, E., Schulmann, K., Pitra, P., Lexa, O., Martelat, J.E., Bollinger, C., and Žáčková, E., 2012, The juxtaposition of eclogite and mid-crustal rocks in the Orlica–Śnieżnik Dome, Bohemian Massif: Journal of Metamorphic Geology, v. 30, p. 213–234.

Štípská, P., Schulmann, K., and Kröner, A., 2004, Vertical extrusion and middle crustal spreading of omphacite granulite: a model of syn-convergent exhumation (Bohemian Massif, Czech Republic): Journal of Metamorphic Geology, v. 22, p. 179–198.

Stöckhert, B., Duyster, J., Trepmann, C., and Massonne, H.-J., 2001, Microdiamond daughter crystals precipitated from supercritical COH + silicate fluids included in garnet, Erzgebirge, Germany: Geology, v. 29, p. 391–394, doi:10.1130/0091-7613(2001)029<0391:MDCPFS>2.0.CO;2.

Stöckhert, B., Trepmann, C.A., and Massone, H.-J., 2009, Decrepitated UHP fluid inclusions : about diverse phase assemblages and extreme decompression rates (Erzgebirge, Germany): Journal of Geosciences (Czech Republic), v. 27, p. 673–684, doi:10.1111/j.1525-1314.2009.00835.x.

Stracke, A., 2012, Earth's heterogeneous mantle: A product of convection-driven interaction between crust and mantle: Chemical Geology, v. 330–331, p. 274–299, doi:10.1016/j.chemgeo.2012.08.007.

Suen, C.J., and Frey, F.A., 1987, Origins of the mafic and ultramafic rocks in the Ronda peridotite: Earth and Planetary Science Letters, v. 85, p. 183–202, doi:10.1016/0012-821X(87)90031-8.

Sun, S.-S., and McDonough, W.F., 1989, Chemical and isotopic systematics of oceanic basalts: implications for mantle composition and processes: Geological Society, London, Special Publications, v. 42, p. 313–345, doi:10.1144/GSL.SP.1989.042.01.19.

Svojtka, M., Ackerman, L., Medaris, L.G., Hegner, E., Valley, J.W., Hirajima, T., Jelínek, E., and Hrstka, T., 2016, Petrological, geochemical and Sr-Nd-O Isotopic Constraints on the Origin of Garnet and Spinel Pyroxenites from the Moldanubian Zone of the Bohemian Massif: Journal of Petrology, v. 57, p. 897–920, doi:10.1093/petrology/egw025.

Tacchetto, T., Bartoli, O., Cesare, B., Berkesi, Ḿarta, Aradi, L.E., Dumond, G., and Szabó, C., 2018, Multiphase inclusions in peritectic garnet from granulites of the Athabasca granulite terrane (Canada): Evidence of carbon recycling during Neoarchean crustal melting: Chemical Geology, v. 508, p. 197–209.

Takahashi, E., and Kushiro, I., 1983, Melting of a dry peridotite at high pressures and basalt magma genesis: American Mineralogist, v. 68, p. 859–879, doi:10.1144/gsjgs.139.6.0771.

Tamic, N., Behrens, H., and Holtz, F., 2001, The solubility of H2O and CO2 in rhyolitic melts in equilibrium with a mixed CO2–H2O fluid phase: Chemical Geology, v. 174, p. 333–347.

Taylor, J.W., 1983, Erzgebirge Tin: a Closer Look: Oxford Journal of Archaeology, v. 2, p. 295–298, doi:10.1111/j.1468-0092.1983.tb00344.x.

Thompson, A.B., 1988, Dehydration melting of crustal rocks: Rendiconti della societa italiana di mineralogia e petrologia, v. 43, p. 41–60.

Tichomirowa, M., Whitehouse, M.J., and Nasdala, L., 2005, Resorption, growth, solid state recrystallisation, and annealing of granulite facies zircon - A case study from the Central Erzgebirge, Bohemian Massif: Lithos, v. 82, p. 25–50, doi:10.1016/j.lithos.2004.12.005.

Timmerman, M.J., 2008, Palaeozoic magmatism, *in* Mccann, T., ed., The Geology of Central Europe. Volume 1: Precambrian and Paleozoic: London, Geological Society, p. 665–748.

Tiraboschi, C., Tumiati, S., Sverjensky, D., Pettke, T., Ulmer, P., and Poli, S., 2018, Experimental determination of magnesia and silica solubilities in graphite-saturated and redox-buffered high-pressure COH fluids in equilibrium with forsterite + enstatite and magnesite + enstatite: Contributions to Mineralogy and Petrology, v. 173, doi:10.1007/s00410-017-1427-0.

Touret, J.L.R., 2001, Fluids in metamorphic rocks: Lithos, v. 55, p. 1–25, doi:10.1016/S0024-4937(00)00036-0.

Tsunogae, T., Santosh, M., and Dubessy, J., 2008, Fluid characteristics of high-to ultrahigh-temperature metamorphism in southern India: a quantitative Raman spectroscopic study: Precambrian Research, v. 162, p. 198–211.

Tumiati, S., Thöni, M., Nimis, P., Martin, S., and Mair, V., 2003, Matle-crust interactions during Variscan subduction in the Eastern Alps (Nonsberg-Ulten Zone): geochronology and new petrological constraints: Earth and Planetary Science Letters, p. 1–18.

Turniak, K., Mazur, S., and Wysoczański, R., 2000, SHRIMP zircon geochronology and geochemistry of the Orlica-Śnieżnik gneisses (Variscan belt of Central Europe) and their tectonic implications: Geodinamica Acta, v. 13, p. 293–312.

Veksler, I.V., Nielsen, T.F.D., and Sokolov, S.V., 1998, Mineralogy of Crystallized Melt Inclusions from Gardiner and Kovdor Ultramafic Alkaline Complexes: Implications for Carbonatite Genesis: Journal of Petrology, v. 39, p. 2015–2031, doi.org/10.1093/petroj/39.11-12.2015.

Vernon, R.H., 2011, Microstructures of melt-bearing regional metamorphic rocks: Geological Society of America Memoirs, v. 207, p. 1–11.

Vielzeuf, D., and Montel, J.M., 1994, Partial melting of metagreywackes. Part I. Fluid-absent experiments and phase relationships: Contributions to Mineralogy and Petrology, v. 117, p. 375–393.

Vrána, S., 1989, Perpotassic granulites from southern Bohemia: Contributions to Mineralogy and Petrology, v. 103, p. 510–522, doi:10.1007/BF01041756.

Vrána, S., Janoušek, V., and Franěk, J., 2013, Contrasting mafic to felsic HP-HT granulites of the Blanský les Massif (Moldanubian Zone of southern Bohemia): Complexity of mineral assemblages and metamorphic reactions: Journal of Geosciences, v. 58, p. 347–378, doi:10.3190/jgeosci.157.

Vrijmoed, J.C., Austrheim, H., John, T., Hin, R.C., Corfu, F., and Davies, G.R., 2013, Metasomatism in the ultrahigh-pressure svartberget garnet-peridotite (Western gneiss region, Norway): Implications for thetransport of crust-derived fluids within the mantle: Journal of Petrology, v. 54, p. 1815–1848, doi:10.1093/petrology/egt032.

Walczak, K., 2011, Interpretation of Sm-Nd and Lu-Hf dating of garnets from high pressure and high temperature rocks in the light of the trace elements distribution [Ph. D. thesis]: Krakow, Polish Academy of Sciences Institute of Geological Sciences, 146 p.

Walczak, K., Anczkiewicz, R., Szczepański, J., Rubatto, D., and Košler, J., 2017, Combined garnet and zircon geochronology of the ultra-high temperature metamorphism: constraints on the rise of the Orlica-Śnieżnik Dome, NE Bohemian Massif, SW Poland: Lithos, v. 292, p. 388–400.

Wannhoff, I., Ferrero, S., O'Brien, P.J., Ziemann, M.A., and Hecht, L., 2018, Evidence for fluid-melt immiscibility during partial melting in the Oberpfalz migmatites, Moldanubian Zone (Bohemian Massif), *in* EGU General Assembly Conference Abstracts, v. 20, p. 1673.

Weinberg, R.F., and Hasalová, P., 2015, Water-fluxed melting of the continental crust: A review: Lithos, v. 212–215, doi:10.1016/j.lithos.2014.08.021.

Weiss, C.S., 1803, Ueber die Gebirgsart des Sächsischen Erzgebirges welche unter dem Namen Weiss-Stein neuerlich bekannt gemacht worden ist.: Neue Schriften gesellschaft naturforschender Freunde, v. 4, p. 342–366.

Werner, C.D., 1987, Saxonian granulites: a contribution to the geochemical diagnosis of the original rocks in high-metamorphic complexes: Gerlands Beiträge zur Geophysik, v. 96, p. 271–290.

Whitney, D.L., and Evans, B.W., 2010, Abbreviations for names of rock-forming minerals: American Mineralogist, v. 95, p. 185–187.

Willner, A.P., Krohe, A., and Maresch, W. V., 2000, Interrelated P-T-t-d Paths in the Variscan Erzgebirge Dome (Saxony, Germany): Constraints on the rapid exhumation of HP rocks from the root zone of a collisional orogen: International Geology Review, v. 42, p. 64–85.

Willner, A.P., Rötzler, K., and Maresch, W. V., 1997, Pressure - Temperature and fluid evolution of quartzo-feldspathic metamorphic rocks with a relic high-pressure, granulite-facies history from the Central Erzgebirge (Saxony, Germany): Journal of Petrology, v. 38, p. 307–336, doi:10.1093/petroj/38.3.307.

Woodland, a. B., Kornprobst, J., McPherson, E., Bodinier, J.-L., and Menzies, M. a., 1996, Metasomatic interactions in the lithospheric mantle: petrologic evidence from the Lherz massif, French Pyrenees: Chemical Geology, v. 134, p. 83–112, doi:10.1016/S0009-2541(96)00082-4.

Workman, R.K., and Hart, S.R., 2005, Major and Trace Element Composition of the Depleted MORB Mantle (DMM): Earth and Planetary Science Letters, v. 231, p. 53–72, doi:10.1016/j.epsl.2004.12.005.

Xia, Q.-X., and Zhou, L.-G., 2017, Different origins of garnet in high pressure to ultrahigh pressure metamorphic rocks: Journal of Asian Earth Sciences, v. 145, p. 130–148.

Yakymchuk, C., 2017, Behaviour of apatite during partial melting of metapelites and consequences for prograde suprasolidus monazite growth: Lithos, v. 274-275, p. 412–426, doi.org/10.1016/j.lithos.2017.01.009.

Yaxley, G.M., and Green, D.H., 1998, Reactions between eclogite and peridotite: mantle refertilisation by subduction of oceanic crust: Schweizerische Mineralogische Und Petrographische Mitteilungen, v. 78, p. 243–255.

Yaxley, G.M., Sobolev, A. V., and Sobolev, G.M.Y.Æ.A. V, 2007, High-pressure partial melting of gabbro and its role in the Hawaiian

magma source: Contributions to Mineralogy and Petrology, v. 154, p. 371–383, doi:10.1007/s00410-007-0198-4.

Yogodzinski, G.M., Lees, J.M., Churikova, T.G., Dorendorf, F., Wöerner, G., and Volynets, O.N., 2001, Geochemical evidence for the melting of subducting oceanic lithosphere at plate edges: Nature, v. 409, p. 500–504, doi:10.1038/35054039.

Zanetti, A., Mazzucchelli, M., Rivalenti, G., and Vannucci, R., 1999, The Finero phlogopite-peridotite massif: an example of subduction-related metasomatism: Contributions to Mineralogy and Petrology, v. 134, p. 107–122, doi:10.1007/s004100050472.

Zhang, Z.M., Dong, X., Liou, J.G., Liu, F., Wang, W., and Yui, F., 2011, Metasomatism of garnet peridotite from Jiangzhuang, southern Sulu UHP belt: Constraints on the interactions between crust and mantle rocks during subduction of continental lithosphere: Journal of Metamorphic Geology, v. 29, p. 917–937, doi:10.1111/j.1525-1314.2011.00947.x.

Zhang, R.Y., Li, T., Rumble, D., Yui, T.-F., Li, L., Yang, J.S., Pan, Y., and Liou, J.G., 2007, Multiple metasomatism in Sulu ultrahigh-P garnet peridotite constrained by petrological and geochemical investigations: Journal of Metamorphic Geology, v. 25, p. 149–164, doi:10.1111/j.1525-1314.2006.00683.x.

SUPPLEMENTARY MATERIAL

A. SUPPLEMENTARY MATERIAL CHAPTER 2

	Nanogranitoids in OSD granulites																										
(ppm)	***1***	***2***	***3***	***4***	***5***	***6***	***7***	***8***	***9***	***10***	***11***	***12***	***13***	***14***	***15***	***16***	***17***	***18***	***19***	***20***	***21***	***22***	***23***	***24***	***25***	***26***	***27***	**Av.**
Li	57	-	42	91	20	-	43		146	149	51	196	-	37	245	85	-	-	176	-	-	32	-	115	196	-		**105**
B	<57	<56	<27	<26	<10	<20	<35	<216	<21	<18	<10	<129	<91	<40	<247	<13	<429	<197	<24	<65	<126	<16	<67	<38	<27	<198	<122	**-**
P	<189	<192	<127	<125	<49	<103	<117	<702	90	<63	57	<437	<313	<153	1077	<58.9	<1731	<804	<98	<279	<523	184	<286	<114	<79	<544	<337	**352**
Sc	<3	40	29	7	17	<1.7	10	<14	22	<1.2	5	14	<5.7	57	<17	<0.9	<29	<12	<1.6	<4.2	<8	<1	<4	30	<1.4	<10.9	12	**22**
Ti	827	<28	762	2271	521	502	<15	465	791	869	98	<56	<44	523	<142	40	<211	<106	93	317	192	230	196	1153	2689	<75	213	**671**
V	4	51	20	49	9	11	15	10	-	-	4	29	-	52	10	14	22	-	23	11	16	2	-	-	53	-	-	**21**
Co	8	<1.1	<0.8	26	<0.3	9	2	<5	14	17	2	11	<2	<1	<7	12	<13	<6	14	<2	9	3	<1	<1	31	<3.6	10	**12**
Zn	154		69	1246	145	215	82	767	406	1007	225		362	448	874	80	816	390	222	431	772	67	33	695	597	-	805	**455**
Rb	524	502	554	555	102	603	508	528	444	489	740	724	516	406	529	268	535	356	417	465	783	511	318	957	469	520	378	**507**
Sr	30	32	32	28	219	28	28	30	90	17	45	23	37	13	28	39	39	22	42	19	40	24	13	15	81	27	11	**39**
Zr	165	50	143	168	<0.2	66	147	206	150	116	205	64	41	295	66	23	150	276	88	127	108	38	130	163	14	91	155	**125**
Nb	1.0	0.9	0.9	0.8	0.2	1.1	0.6	<1.5	1.5	0.9	0.4	<1	<0.7	0.7	<2.5	0.2	<3.7	<1.4	0.3	0.8	<1.2	0.2	<0.4	2.3	2.6	<1.4	<0.7	**0.9**
Cs	6.4	4.8	6.5	7.3	<0.2	6.1	5.7	7.0	2.1	4.1	7.5	5.5	7.1	6.0	6.6	0.9	17.3	6.9	0.9	5.9	7.8	10.9	11.4	6.6	6.3	9.2	-	**6.7**
Ba	791	608	543	678	1958	714	733	712	1265	784	950	624	597	445	251	2064	427	586	1155	441	643	980	592	614	383	795	450	**770**
La	23.2	17.7	16.7	23.8	2.5	6.5	2.1	5.6	27.4	4.0	2.8	13.9	8.0	9.4	2.3	6.6	1.6	3.5	11.6	45.3	47.4	13.5	3.9	3.4	21.1	6.6	10.6	**12.6**
Ce	40.0	17.1	29.6	54.0	5.8	7.6	2.7	10.3	37.5	7.2	5.7	5.5	10.0	16.6	2.8	1.9	5.9	4.0	3.0	62.7	62.4	29.3	8.9	7.1	<0.1	10.7	26.2	**18.3**
Pr	4.1	0.6	3.2	7.0	0.4	0.8	<0.1	0.9	6.3	0.7	0.6	3.4	<0.38	2.1	1.1	1.1	<1.4	<0.7	2.2	5.5	5.8	4.8	0.3	1.1	2.0	1.1	3.9	**2.6**
Nd	2.6	<0.2	14.9	24.0	3.7	<0.3	<0.4	4.9	24.4	2.0	1.6	19.6	<1.7	11.3	<4.2	3.1	<6.8	<2.9	3.7	9.2	9.7	24.2	3.7	13.9	<0.4	<2.3	26.0	**11.3**
Sm	1.7	<0.4	11.5	<0.4	3.4	<0.4	<0.5	5.3	10.5	<0.16	1.1	14.4	<1.9	8.3	<4.7	<0.2	<8.3	<3.8	<0.4	<1.5	<3	3.2	2.0	12.8	<0.4	<1.4	9.2	**7.0**
Eu	<0.2	<0.2	0.7	<0.2	1.2	<0.2	<0.2	1.7	1.8	<0.1	<0.06	<0.82	<0.6	1.3	<2	<0.07	<3.7	<1.6	<0.2	<0.6	<1.2	0.2	<0.4	2.7	<0.2	<1.2	1.7	**1.4**
Gd	<0.6	3.6	16.9	<0.5	0.5	<0.5	<0.7	<5	14.4	<0.4	<0.2	18.1	<2	13.3	<5.8	<0.3	<13	<6.1	<0.7	<2.2	<3.6	<0.4	6.2	16.3	<0.7	<4.7	8.9	**10.9**
Hf	5.3	2.4	5.3	6.6	<0.1	3.3	4.6	9.6	5.2	4.4	7.1	2.9	3.4	8.3	<2.7	1.9	6.2	7.0	3.1	4.8	3.9	1.0	3.4	5.4	1.9	2.5	5.9	**4.6**
Ta	<0.10	<0.09	<0.05	<0.05	<0.03	<0.06	<0.02	<0.74	<0.05	<0.03	0.0	<0.37	<0.27	<0.1	<0.7	<0.03	<1.2	<0.54	<0.08	<0.2	<0.3	<0.02	<0.2	<0.1	0.1	<0.16	<0.3	**0.1**
Pb	0.5	0.3	0.9	0.3	0.3	0.5	0.3	<0.6	0.4	0.4	0.2	<0.5	0.4	0.8	<0.8	0.2	<2.5	<2	0.2	1.5	<0.9	<0.1	0.6	0.4	<0.1	<1.1	0.6	**0.5**
Th	0.2	0.2	0.1	<0.06	<0.01	<0.05	<0.04	<0.4	0.1	0.0	0.1	<0.1	<0.2	0.1	<0.6	0.03	<0.9	<0.6	0.1	0.4	0.6	0.3	0.2	0.1	<0.03	<0.2	<0.2	**0.2**
U	0.5	0.5	1.1	0.3	0.1	0.1	0.7	0.4	1.0	0.4	1.0	0.4	0.4	1.2	0.5	0.2	0.5	1.4	0.2	0.9	0.3	0.9	0.5	0.7	0.2	0.2	0.5	**0.6**
Tb	-	-	-	-	-	-	-	-	-	-	-	-	-	-	-	-	-	-	-	-	-	-	-	-	-	-	-	-
Dy	-	-	-	-	-	-	-	-	-	-	-	-	-	-	-	-	-	-	-	-	-	-	-	-	-	-	-	-
Ho	-	-	-	-	-	-	-	-	-	-	-	-	-	-	-	-	-	-	-	-	-	-	-	-	-	-	-	-
Er	-				-	-	-	-	-	-	-	-	-	-	-	-	-	-	-	-	-	-	-	-	-	-	-	-
Tm					-	-	-	-	-	-	-	-	-	-	-	-	-	-	-	-	-	-	-	-	-	-	-	-
Yb					-	-	-	-	-	-	-	-	-	-	-	-	-	-	-	-	-	-	-	-	-	-	-	-
Lu					-	-	-	-	-	-	-	-	-	-	-	-	-	-	-	-	-	-	-	-	-	-	-	-

Table S2.1 Dataset of trace element analyses on melt inclusions from high pressure felsic granulites

B. SUPPLEMENTARY MATERIAL CHAPTER 3

GEOLOGICAL SETTING

The Granulitgebirge is located on the north-western portion of the Bohemian Massif, in the Saxonthuringian Zone (eastern Germany) (Fig. S3.1A-B). It is a dome-like body over 45 km long mainly composed of high pressure quarzo-feldspatic granulites with minor layers of pyroxene-bearing granulites of intermediate to basic composition (O'Brien and Rötzler, 2003). The main mineral assemblage in the granulites consists of hypersolvus ternary feldspar (now mesoperthite) and quartz with a variable amount of garnet, kyanite and rutile (Rötzler et al., 1992; Rötzler and Romer, 2001). In addition, bodies of serpentinized peridotites occur in the granulites and contain layers and lenses of garnet clinopyroxenites investigated in this study. The P-T peak conditions determined for the granulites are 1000-1015ºC and 2.0-2.2 GPa (Rötzler et al., 2008) and the age of the metamorphism is c. 340 Ma (von Quadt, 1993; Kröner and Willner, 1998; Romer and Rötzler, 2001). The metamorphic peak was followed by rapid exhumation and cooling to middle crustal level (O'Brien and Rötzler, 2003). The samples investigated have been collected in two localities 1 km apart: Rubinberg (locality 1, 51º1'57"N, 13º7'37"E) and Klatschmühle (locality 2, 51º2'38"N, 13º8'43"E).

PETROGRAPHY

The samples from the two localities have different bulk composition, ultrabasic (locality 1=Loc 1) to basic (locality 2=Loc 2) (see Table S3.1). In both localities they show a granoblastic texture dominated for the 80-85 % in volume by garnet (slightly more abundant in Loc 1) and clinopyroxene (slightly more abundant in Loc 2) porphyroblasts (see Figure S3.1 C-D). Interstitial plagioclase is more abundant in Loc 1 whereas post-peak biotite (more abundant in Loc 2) and two generations of later amphibole occur in the matrix with rutile and ilmenite as accessories. Garnet (1-2 mm in size) includes, besides nanogranitoids, clinopyroxene, plagioclase (sometimes forms aggregates with clinopyroxene), rutile and ilmenite. The garnet composition is different in the two localities, pyrope-rich (66%) in Loc 1 whereas in Loc 2 the amount of pyrope, almandine and grossular is similar (see Table S3.1). Moreover, in Loc 2 the garnet rim shows a slight zoning with increase of iron at the expense of calcium, not related with the distribution of the inclusions. No compositional differences were observed between MI-bearing and MI-free garnets. Clinopyroxene (1mm in size) often shows a cloudy core and a clear rim. It can contain, in the core, lamellae and blebs of plagioclase. Clinopyroxene is richer in the Jd component in Loc 2 (see Table S3.1).

METHODS

Raman spectroscopy: The instrument used for the Raman analyses is the HORIBA Jobin Yvon LabRAM HR 800 of the Institut für Erd- und Umweltwissenschaften of the University of Potsdam. It consists of a Peltier cooled multichannel CCD detector and an Olympus BX41 petrographic microscope. The laser used for the excitation is an air-cooled Nd:YAG (λ=532 nm, the laser power on the sample was 2-3 mW)

with a grating 300 lines/mm, slit width set to 100 μm and confocal hole to 200 μm. We acquired all the spectra using a 100x objective and the multiwindows option in the range between 100 cm^{-1} and 4000 cm^{-1} integrating 3 repetitions of 100s with spectral resolution of 10 cm^{-1} (see procedure in Ferrero et al., 2015).

FESEM and microprobe: High resolution microstructural and microchemical investigation were performed using the field-emission microprobe JEOL Hyperprobe JXA-8500F of the Museum für Naturkunde in Berlin.

We used the microprobe JEOL JXA-8200 of the Institut für Erd- und Umweltwissenschaften of the University of Potsdam to analyze glass and mineral phases. The parameters used for the glasses analyses are: 15 kV, 3.5 nA and a beam diameter of 1μm. The calibration was done using H_2O-bearing leucogranitic glass standards. During analyses of alkali-rich melt is common to have alkali-loss (Morgan and London, 2005) and the correction factor for Na, K, Al and Si is estimated by analyzing the leucogranitic standards with similar water content (3.1 wt% for the glasses of both localities) and applying, during each analytical session, the same analytical conditions (see also Ferrero et al., 2012, 2015).

Piston cylinder apparatus for re-homogenization experiments: The starting material consists of 8 different garnet crystals extracted from a double-polished thick section (150 μm). We separated 20 garnet chips with crack-free, unexposed nanogranitoids. The nanogranitoids in the selected chips are representative of the inclusion population because in the studied samples they always show the same mineral assemblage. We used for both experiments platinum capsules of 4 mm length and 3 mm diameter, cold sealed after the filling. We inserted in the capsule garnet chips and quartz powder for the first experiment (KLA_1, 3 chips) and chips and magnesium monoxide powder for the second one (KLA_4, 17 chips) and we ran the first one for 24 hours while the second ran at least for 7 hours (see Table S3.3). The capsule is embedded in an assemblage that in the inner part is made of crushable alumina (Al_2O_3) and then all the assemblage is placed in a talc-pyrex-graphite-pressure cell. The pressure of the experiments is calibrated using the quartz-coesite transition and the accuracy estimated is +/- 0.05 GPa. We used type S thermocouple (Pt/PtRh10) to control the temperature and the uncertainty is assumed to be +/- 10 ºC (Frei et al., 2009). In both cases we performed the experiment in dry conditions since previous works showed no compositional difference between microcrack-free nanogranitoids re-homogenized under presence or absence of water (Bartoli et al., 2013a). At the end of each experiment we quenched the experimental charges at high pressure waiting to reach ambient temperature before unloading the machine. After the quenching we mounted the experimental charges in epoxy and we polished it in order to expose the re-homogenized inclusions (see Bartoli et al., 2013 for more details about the approach and its benefits and limits).

LA ICP-MS (Laser Ablation Inductively Coupled Plasma Mass Spectrometry): we performed trace elements analyses of the inclusions and minerals using a GeoLas ArF (193 nm) Excimer laser ablation system (Coherent, Germany) coupled to an Element XR (Thermo Fischer, Germany) sector-field ICP-MS, at the Department of Earth Sciences, ETH Zürich. We selected 21 garnet chips with crack-free unexposed glassy inclusions and nanogranitoids from a double polished thick section (150 μm) (11 chips for Loc 1 and 10 chips for Loc 2).

We used a repetition rate of 10 Hz, energy densities on sample in the range 5-10 J.cm^{-2} and spot sizes from 10 to 30 μm depending on the size of the inclusions. The spot size was selected to be slightly larger than the inclusion diameter, to as completely ablate the inclusion in order to avoid the unrepresentative sampling related to the heterogeneities therein. The sample aerosol was transported to the ICP-MS using He (5.0 grade) carrier gas at ca. 1.1 L.min^{-1} flow, to which was admixed make up gas (6.0 grade Ar) at ca. 1.0 L.min^{-1} prior to introduction into the plasma. The instrument was optimized for highest sensitivity on the high mass range (^{238}U, ^{232}Th) while keeping low the production of oxides (^{248}ThO^{+}/^{232}Th^{+} <0.15%) and doubly charged ions (^{138}Ba++/^{138}Ba+ <1%).

Every analyses consisted of 30 s gas blank followed by ablation of the mineral and inclusion. The following isotopes were recorded in mass jump mode (dwell time in ms between brackets): ^{7}Li (10), ^{11}B (10), ^{23}Na (10), ^{24}Mg (5), ^{27}Al (5), ^{29}Si (5), ^{31}P (10), ^{39}K (10), ^{43}Ca (5), ^{45}Sc (5), ^{49}Ti (10), ^{51}V (5), ^{53}Cr (5), ^{55}Mn (5), ^{57}Fe (5), ^{59}Co (5), ^{62}Ni (10), ^{63}Cu (10), ^{66}Zn (5), ^{85}Rb (10), ^{88}Sr (10), ^{89}Y (10), ^{90}Zr (25), ^{93}Nb (25), ^{133}Cs (10), ^{137}Ba (10), ^{139}La (50), ^{140}Ce (50), ^{141}Pr (50), ^{146}Nd (50), ^{147}Sm (25), ^{151}Eu (25), ^{157}Gd (25), ^{178}Hf (25), ^{181}Ta (25), ^{208}Pb (10), ^{232}Th (25), ^{238}U (25). The corresponding sweep time was 0.932 s and the total measurement time ca. 245 s (260 replicates).

All data processing was performed offline. The NIST SRM610 reference material (Jochum et al., 2011), ablated using 10 Hz, ca. 5 J.cm^{-2} and 40 μm spot size, was used to perform drift correction and quantification of the inclusion analyses. Both, the inclusion and the host are contributing to the signal, to which is then applied a deconvolution as described by Halter et al., (2002). The acquired time-resolved signals were processed using the software SILLS (Guillong et al., 2008). Internal standards used for deconvolution and relative sensitivity correction were the concentrations determined by EMP of Na_2O as inclusion-dominated tracer in both localities and FeO (Loc 1) and MgO (Loc 2) as host-dominated tracers. The elements that are strongly enriched in the host (e.g. Fe, Mg, HREE, transition elements) compared to the inclusions are not quantifiable in the latter using this method because of the dominance of the host signal (see average of values in Table S3.4).

TABLES

	Loc 1 (Rubinberg)		Loc 2 (Klatschmühle)	
	Grt	Cpx	Grt	Cpx
wt%	357G_KLA	138	5G_4.4-1	176
SiO_2	41,92	48,74	38,53	54,45
TiO_2	0,15	0,97	0,13	0,42
Al_2O_3	23,94	12,71	22,86	8,82
Fe_2O_3	0,00	0,00	0,00	0,00
FeO	11,91	6,28	18,70	3,80
MnO	0,21	0,08	0,38	0,02
MgO	18,54	10,03	9,73	12,62
CaO	3,91	18,77	9,22	16,32
Na_2O	0,00	3,09	0,00	3,91
K_2O	0,00	0,00	0,00	0,06
Cr_2O_3	0,00	0,00	0,00	0,00
TOTAL	100,58	100,67	99,55	100,42
	12 (O)	6 (O)	12 (O)	6 (O)
Si	2,988	1,760	2,926	1,939
Ti	0,008	0,026	0,007	0,011
Al	1,006	0,541	1,023	0,371
Fe^{+3}	0,000	0,103	0,000	0,001
Fe^{+2}	0,710	0,087	1,188	0,112
Mn	0,012	0,000	0,025	0,000
Mg	1,969	0,540	1,102	0,670
Ca	0,299	0,726	0,750	0,623
Na	0,000	0,216	0,000	0,270
K	0,000	-	0,000	-
Cr	0,000	0,000	0,000	0,000
Alm/Ac	24	6	39	0
Pyp/Jd	66	18	36	28
Sps/Di	0	76	1	72
Grs	10		24	

Table S3.1. Representative analyses of garnet and clinopyroxene in the two localities

	Preserved glassy inclusions Loc 1 (Rubinberg)								Re-homogenized nanogranitoids Loc 2 (Klatschmühle)							OSZ (3)	La Galite (4)	El Hoyazo (5)	Ronda (6)		Dronning Maud Land (7)	Loc 1	Loc 2
Name	21C	23C	24C	26C	29C	30C	33C	Loc 1_AV	11C	9C2	13C	11C2	9-18-19C	16C2	Loc 2_AV	average	average	average	re-homog_av	glassy_av	average	Bulk	Bulk
SiO_2	70,01	70,86	71,83	69,99	69,51	72,75	71,68	70,95	67,53	67,02	64,70	65,34	62,52	61,99	64,85	68,71	74,05	71,26	68,78	69,69	65,67	43,4	48,10
TiO_2	0,02	0,00	0,08	0,08	0,04	0,00	0,00	0,03	0,00	0,07	0,05	0,16	0,34	0,20	0,14	0,10	0,04	0,1	0,08	0,08	0,08	2,35	0,67
Al_2O_3	16,99	17,80	17,53	17,26	16,01	16,79	15,52	16,84	17,66	18,11	18,13	17,65	18,33	19,80	18,28	13,58	12,07	14,44	11,42	11,8	17,00	15,2	16,30
Fe_2O_3	0,00	0,00	0,00	0,00	0,00	0,00	0,00	0,00	0,00	0,00	0,00	0,00	0,00	0,00	0,00	0,00	0,00	0	0,00	0,00	0,00	0	0,00
FeO	0,56	0,45	0,39	0,79	0,67	0,57	0,48	0,56	1,46	1,35	1,17	2,70	1,56	1,38	1,60	2,02	1,30	1,72	1,59	1,2	1,47	15,8	10,10
MnO	0,00	0,04	0,04	0,00	0,11	0,00	0,00	0,03	0,19	0,00	0,17	0,00	0,03	0,00	0,07	0,00	0,08	0,08	0,14	0,09	0,03	0,26	0,15
MgO	0,10	0,04	0,00	0,65	0,35	0,16	0,25	0,22	0,61	0,65	1,23	1,07	1,77	0,63	0,99	0,08	0,11	0,05	0,12	0,07	0,98	9,23	10,30
CaO	0,27	0,14	0,14	0,98	0,70	0,39	0,38	0,43	0,76	1,16	2,03	1,56	2,69	1,08	1,55	0,76	0,27	0,6	0,44	0,39	1,14	12,2	11,30
Na_2O	5,30	3,75	7,02	6,72	3,91	6,00	5,30	5,43	8,02	3,80	3,90	5,14	4,84	7,44	5,52	4,24	3,47	3,61	2,74	3,09	2,38	1,82	2,86
K_2O	6,07	5,98	4,92	4,79	4,60	4,51	4,53	5,06	4,11	7,44	4,32	4,81	7,47	4,23	5,40	4,50	5,88	4,97	4,00	4,19	8,45	0,04	0,52
P_2O_5	0,00	0,00	0,00	0,00	0,00	0,16	0,02	0,03	0,07	0,44	0,41	0,15	0,21	0,37	0,27	0,02	0,06	0,37	0,35	0,18	0,01	0,08	0,05
TOTAL	99,33	99,06	101,96	101,27	95,91	101,34	98,15	99,57	100,42	100,04	96,11	98,58	99,76	97,13	98,67	94,02	97,30	97,20	89,66	90,78	97,22	100,38	100,35
Q	14,76	25,40	11,55	9,34	26,51	19,47	22,04	18,44	2,10	13,12	19,37	10,35	,00	,00	7,49	23,53	29,90	29,49	35,97	34,23	14,39	,00	,00
C	1,22	4,90	,39	,00	3,33	1,70	1,27	1,83	,00	2,73	4,33	1,49	,00	1,92	1,74	0,41	0,00	2,92	2,58	1,90	1,88	,00	,00
Or	35,89	35,32	29,10	28,31	27,20	26,68	26,75	29,89	24,31	43,95	25,56	28,44	44,15	24,98	31,90	26,61	34,72	29,37	23,64	24,76	49,95	,24	3,07
Ab	44,85	31,73	59,38	56,87	33,09	50,77	44,81	45,93	67,89	32,19	32,97	43,51	39,59	62,93	46,51	35,87	29,35	30,55	23,19	26,15	20,17	8,69	16,47
An	1,31	,70	,71	2,78	3,45	,91	1,73	1,66	,02	2,92	7,41	6,79	6,24	2,92	4,38	3,62	0,00	0,56	,00	,76	5,60	33,19	30,10
Hy	1,25	1,01	,68	2,08	2,25	1,45	1,50	1,46	3,14	3,98	5,44	7,35	,00	1,26	3,53	3,74	2,32	3,27	3,35	2,41	5,06	,00	,00
ASI	1,08	1,38	1,02	0,96	1,26	1,09	1,09	1,12	0,93	1,10	1,23	1,07	0,88	1,05	1,04	1,03	0,96	1,16	1,18	1,14	1,12	0,60	0,63
H_2O by diff	0,67	0,94	-1,96	-1,27	4,09	-1,34	1,85	0,43	-0,42	-0,04	3,89	1,42	0,24	2,87	1,33	5,98	2,70	2,80	10,34	9,22	2,78	-0,38	-0,35
Mg#	0,24	0,13	0,00	0,60	0,45	0,33	0,49	0,32	0,40	0,46	0,62	0,41	0,66	0,45	0,50	0,06	0,12	0,05	0,11	0,09	0,54	0,51	0,64
K_2O/Na_2O	1,15	1,59	0,70	0,71	1,18	0,75	0,85	0,99	0,51	1,96	1,11	0,94	1,54	0,57	1,10	1,06	1,69	1,38	1,46	1,36	3,55	0,02	0,18
K_2O/H_2O	9,00	6,36	-2,52	-3,78	1,12	-3,37	2,45	1,32	-9,82	-195,02	1,11	3,40	31,16	1,47	-27,95	0,75	2,18	1,77	0,39	0,45	3,05	-0,11	-1,48

Table S3.2. EMP (electron microprobe) analyses of preserved glassy inclusions (Rubinberg, from 6 different garnets) and re-homogenized (Klatschmühle, from 4 different garnets) and the compositions of MI (glassy and re-homogenized nanogranitoids) plotted in Fig. 3.2 (the numbers correspond to the ones in the figure) and the bulk rock compositions of the investigated samples (Loc 1 and Loc 2). OSZ: Orlica-Śnieżnik Dome. ASI: Alumina Saturation Index (molar $Al_2O_3/CaO+Na_2O+K_2O$). Mg#= molar MgO/(MgO+FeO)

EXPERIMENTAL PARAMETERS					RESULTS		
Experiment Name	Temperature (°C)	Pressure (GPa)	Duration (h)	Matarials in the capsule	Complete re-homogenization	Decrepitation	Melt-host interaction
KLA_1	1000	2.2	24	Chips + quartz powder	X	-	X (very limited to not investigated inclusions)
KLA_4	1050	1.5	at least 7	Chips + MgO powder	X	-	X (limited to not investigated inclusions, new Grt)

Table S3.3. Re-homogenization experiment performed for the nanogranitoids of Klatschmühle (Loc 2) with experimental parameters and microstructural observations.

	Loc 1			Loc 2			OSZ	El Hoyazo
samples type:	Av_MI	AV_Grt	Bulk	Av_MI	Av_Grt	Bulk	Av_MI	Av_MI
No. analyses:	168	94	1	64	65	1	30	20
ppm								
Rb	176	29	14	265	26	18	499	211
Cs	64	149	49	64	64	11	6,67	31
Ba	678	32	99	416	31	186	762	308
Th	108	0,73	0,5	41	0,45	0,5	0,21	1,3
U	23	0,85	0,8	14	1,41	0,2	1,59	4,5
Nb	2,76	0,13	9,9	3,97	0,13	4	0,89	12
Ta	b.d.l.	0,11	0,7	0,55	0,28	0,4	0,06	2,7
La	25	0,91	5,8	12	0,67	6	14	4,5
Ce	41	6,65	14	25	4,92	14	19	10
Pb	62	0,56	1,1	37	0,73	1,2	0,58	78
Pr	3,98	3,21	2,21	3,17	2,65	2,19	3,09	1,1
P	1412	2865	n.d.	568	2593	n.d.	352	1890
Sr	127	2,06	62	138	2,37	185	39	165
Nd	11	41	11	11	36	10	14	4,3
Zr	71	264	74	171	394	73	334	32
Hf	2,96	3,51	2,3	5,03	5,00	2,3	6,29	0,94
Sm	8,35	44	3,31	3,18	46	3,22	6,82	1,3
Eu	3,94	18	1,04	1,25	18	0,95	1,42	1,3
Gd	2,32	69	4,39	12	74	3,64	10	1,3
Tb	n.d.	11	0,87	n.d.	12	0,56	n.d.	0,21
Dy	n.d.	74	5,82	n.d.	78	3,1	n.d.	1
Ti	3846	10496	n.d.	1601	9909	n.d.	671	541
Y	19	385	37	9,35	385	15,5	n.d.	3,5
Ho	n.d.	14	1,48	n.d.	14	0,56	n.d.	0,16
Er	n.d.	40	4,59	n.d.	38	1,54	n.d.	0,21
Tm	n.d.	5,53	0,72	n.d.	4,76	0,2	n.d.	0,05
Yb	n.d.	36	4,66	n.d.	30	1,22	n.d.	0,09
Lu	n.d.	5,38	0,71	n.d.	4,26	0,18	n.d.	0,06
Li	49	63	n.d.	31	218	n.d.	132	114
B	63	45	n.d.	32	55	n.d.	b.d.l.	185

Table S3.4. Averages of LA-ICP-MS analyses of MI in the two localities of this sudy, Orlica-Śnieżnik Dome(OSZ) and El Hoyazo (see also Fig. 3.3A); Grt average values (Fig. 3.3B) and bulk rock trace element compositions in the two localities. n.d= not determined. b.d.l= below detection limit.

FIGURES

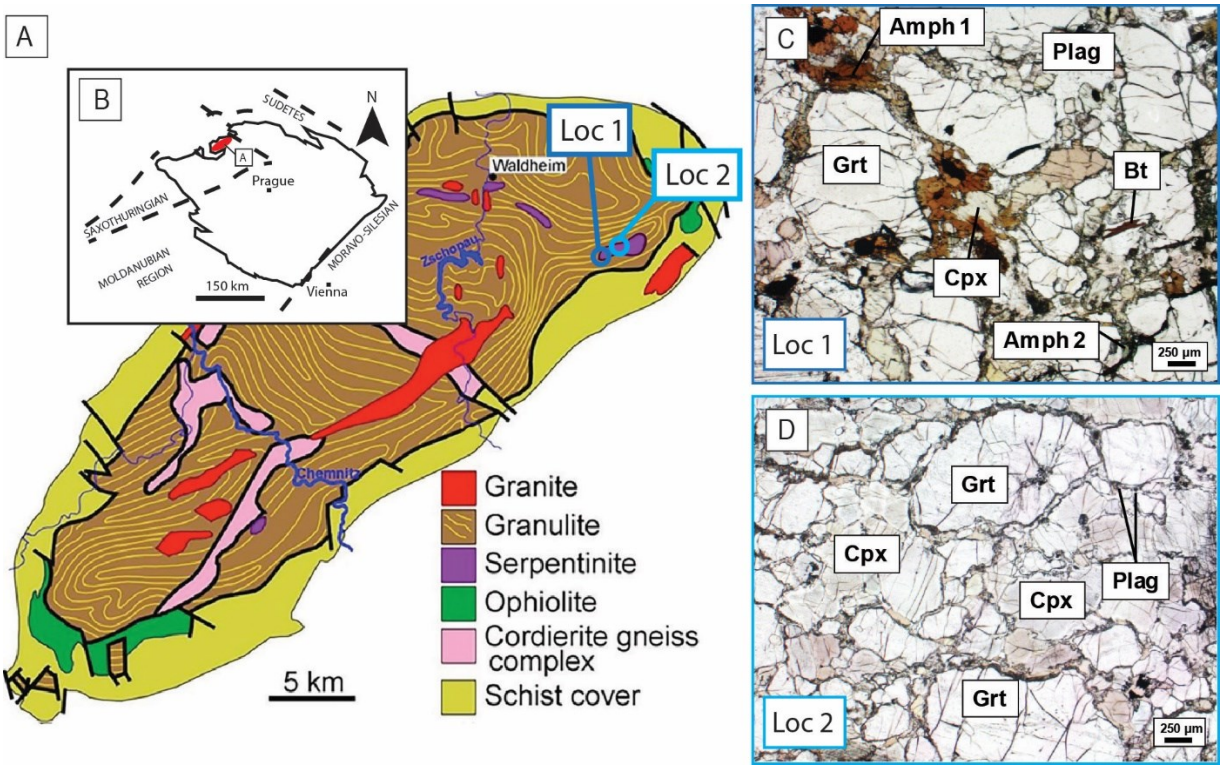

Figure S3.1. A) Schematic geology of the Granulitgebirge in the Bohemian Massif (B) with the two sampling localities (adapted from Rötzler, 1992). Photomicrograph of the Loc 1 (C) and Loc 2 (D) garnet clinopyroxenites.

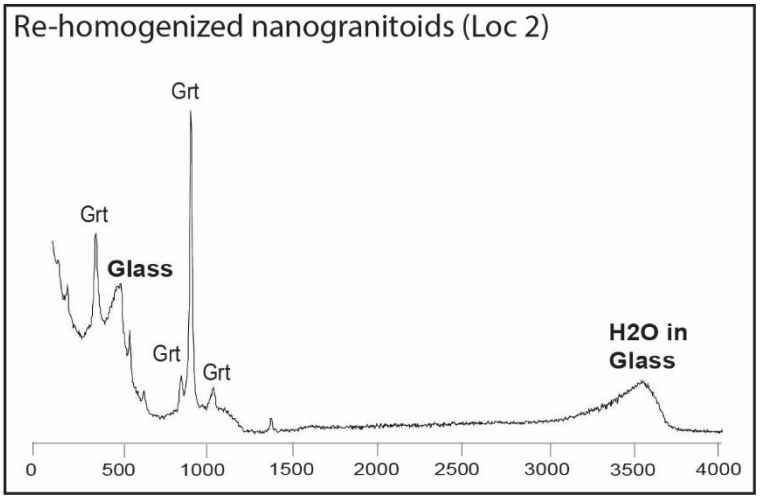

Figure S3.2. Raman spectrum of a water-bearing glass of Loc 2 after the re-homogenization experiment (see Table S3.2).

C. SUPPLEMENTARY MATERIAL CHAPTER 4

TABLES

Sample type	Grt-clinopyroxenite			Grt-clinopyroxenite				
Name	RUB	RUB 6	RUB 11	KLA	KLA 1.2-1	KLA 2-2	**AV_RUB**	**AV_KLA**
No. analyses	1	1	1	1	1	1	**3**	**3**
wt %								
SiO_2	43.4	43.59	44.81	48.1	46.74	43.38	**43.93**	**45.50**
TiO_2	2.35	1.07	1.29	0.67	0.69	0.94	**1.57**	**1.01**
Al_2O_3	15.2	15.85	15.65	16.3	15.41	17.5	**15.57**	**15.93**
Fe_2O_3	0	0	0	0.00	0	0	**0.00**	**0.00**
FeO	15.8	12.82	13.87	10.1	11.22	13.53	**14.16**	**12.26**
MnO	0.26	0.23	0.22	0.15	0.17	0.22	**0.24**	**0.20**
MgO	9.23	14.04	10.41	10.3	11.14	8.89	**11.23**	**11.58**
CaO	12.2	11.34	12.61	11.3	11.61	12.76	**12.05**	**11.75**
Na_2O	1.82	1.14	1.82	2.86	2.03	1.76	**1.59**	**1.94**
K_2O	0.04	0.02	0.15	0.52	0.53	0.21	**0.07**	**0.23**
P_2O_5	0.08	0.19	0.08	0.05	0.08	0.36	**0.12**	**0.11**
LOI	0.04	0.34	-0.03	0.24	0.78	-0.16	**0.12**	**0.18**
TOTAL	100.42	100.63	100.88	100.59	100.4	99.39	**100.64**	**100.70**
CaO/Al_2O_3	0.80	0.72	0.81	0.69	0.75	0.73	**0.77**	**0.74**
Mg#	51	66	57	64	64	54	**57.87**	**62.39**
ppm								
Cr	200	400	500	500	700	300	**367**	**467**
Ni	80	106	89	90	107	27	**91**	**95**
Rb	14	1.70	8.90	18	31	17	**8.13**	**9.63**
Cs	49	4.00	12	11	37	14	**22**	**9.17**
Ba	99	92	225	186	184	55	**139**	**168**
Th	0.50	2.20	1.80	0.50	0.30	1.00	**1.50**	**1.50**
U	0.80	1.30	1.00	0.20	0.10	0.30	**1.03**	**0.83**
Nb	9.90	19	4.30	4.00	4.90	11	**11**	**8.93**
Ta	0.70	1.50	0.30	0.40	0.60	1.10	**0.83**	**0.73**
La	5.80	9.90	12	6.00	6.40	17	**9.20**	**9.27**
Ce	14	22	27	14	18	34	**21**	**21**
Pb	1.10	7.90	3.20	1.20	1.80	1.80	**4.07**	**4.10**
Pr	2.21	2.98	3.39	2.19	2.72	4.08	**2.86**	**2.85**
P	800	1900	800	500	800	3600	**1167**	**1067**
Sr	62	117	115	185	142	131	**98**	**139**
Nd	11	13	15	10	13	17	**13**	**13**
Zr	74	62	71	73	73	49	**69**	**68**
Hf	2.30	2.00	2.00	2.30	2.50	1.60	**2.10**	**2.10**
Sm	3.31	4.03	4.04	3.22	3.62	4.25	**3.79**	**3.76**
Eu	1.04	1.10	1.19	0.95	1.07	1.24	**1.11**	**1.08**
Gd	4.39	5.05	5.21	3.64	4.27	4.78	**4.88**	**4.63**
Tb	0.87	0.91	0.91	0.56	0.66	0.77	**0.90**	**0.79**
Dy	5.82	5.87	6.05	3.10	3.67	4.36	**5.91**	**5.01**
Ti	23500	10700	12900	6700	6900	9400	**15700**	**10100**
Y	37	33	33	16	19	21	**34**	**27**
Ho	1.48	1.19	1.31	0.56	0.72	0.89	**1.33**	**1.02**
Er	4.59	3.51	4.10	1.54	1.96	2.24	**4.07**	**3.05**
Tm	0.72	0.47	0.55	0.20	0.27	0.29	**0.58**	**0.41**
Yb	4.66	2.89	3.80	1.22	1.50	1.83	**3.78**	**2.64**
Lu	0.71	0.41	0.59	0.18	0.23	0.25	**0.57**	**0.39**
Li	n.d.	n.d.	n.d.	n.d.	n.d.	n.d.	**n.d.**	**n.d.**
B	n.d.	n.d.	n.d.	n.d.	n.d.	n.d.	**n.d.**	**n.d.**

n.d= not determined

Table S4.1 Major and trace element composition of the eclogite whole rock from Rubinberg and Klatschmühle.

Major elements

	Rubinberg												Klatschmühle											
Name	3	4	8	127	134	135	4	27	53	113	131	164	311	316	319	324	330	332	1	9	25	211	243	312
wt. %																								
SiO_2	40.58	40.63	40.26	40.20	40.19	40.28	40.99	40.78	40.94	39.99	40.22	39.79	39.47	41.72	40.95	41.31	41.55	42.63	40.58	40.40	40.24	40.74	40.32	40.57
TiO_2	0.33	0.29	0.30	0.21	0.21	0.24	0.27	0.20	0.19	0.13	0.24	0.15	0.11	0.14	0.08	0.11	0.08	0.07	0.16	0.24	0.18	0.27	0.15	0.20
Al_2O_3	22.80	22.91	22.74	23.01	23.06	23.17	22.86	22.33	22.54	22.19	22.04	21.98	24.33	24.21	23.94	24.10	24.21	23.56	22.28	22.33	22.48	22.50	22.52	22.77
Fe_2O_3																								
FeO	14.44	14.28	15.55	14.71	14.91	13.62	15.26	14.98	15.03	19.73	19.14	20.02	11.95	11.57	11.65	11.49	11.75	11.53	18.07	16.13	17.28	14.40	17.88	17.43
MnO	0.27	0.27	0.27	0.26	0.24	0.22	0.33	0.35	0.36	0.46	0.42	0.50	0.25	0.17	0.17	0.19	0.21	0.22	0.34	0.34	0.34	0.29	0.34	0.32
MgO	10.15	10.31	9.88	10.21	9.78	10.18	11.23	11.44	12.30	10.08	9.58	9.80	18.32	17.29	18.20	18.00	18.29	17.80	9.86	8.52	9.80	10.60	9.78	9.83
CaO	12.21	12.14	11.77	12.26	12.52	13.05	10.79	10.40	9.20	8.46	9.76	8.45	4.54	6.12	4.67	4.88	4.60	5.22	10.02	12.90	10.41	11.95	10.00	10.55
Na_2O	0.08	0.08	0.08	0.01	0.00	0.07	0.04	0.04	0.01	0.01	0.02	0.01	0.08	0.06	0.03	0.05	0.02	0.01	0.04	0.03	0.03	0.03	0.02	0.05
K_2O	0.01	0.01	0.00	0.01	0.00	0.00	0.00	0.00	0.00	0.01	0.01	0.00	0.00	0.00	0.01	0.00	0.00	0.01	0.00	0.00	0.00	0.00	0.00	0.01
P_2O_5	0.09	0.08	0.10	0.04	0.08	0.07	0.06	0.07	0.03	0.06	0.09	0.04	0.06	0.06	0.06	0.05	0.08	0.07	0.05	0.07	0.06	0.08	0.08	0.07
TOTAL	100.95	100.99	100.95	100.91	100.98	#####	101.84	100.58	100.60	101.11	101.52	100.74	99.11	101.34	99.76	100.18	100.79	101.10	101.41	100.97	100.83	100.84	101.10	101.79
Mg#	56	56	53	55	54	57	57	58	59	48	47	47	73	73	74	74	74	73	49	48	50	57	49	50
Si	**3.00**	**3.00**	**2.99**	**2.97**	**2.97**	**2.97**	**3.00**	**3.01**	**3.01**	**2.99**	**3.00**	**2.99**	**2.88**	**2.97**	**2.95**	**2.96**	**2.96**	**3.03**	**3.01**	**3.01**	**3.00**	**3.01**	**3.00**	**3.00**
Ti	0.02	0.02	0.02	0.01	0.01	0.01	0.01	0.01	0.01	0.01	0.01	0.01	0.01	0.01	0.00	0.01	0.00	0.00	0.01	0.01	0.01	0.01	0.01	0.01
Al	1.98	1.99	1.99	2.01	2.01	2.02	1.97	1.95	1.96	1.96	1.94	1.95	2.09	2.03	2.04	2.04	2.04	1.97	1.95	1.96	1.98	1.96	1.98	1.98
	2.00	**2.01**	**2.01**	**2.02**	**2.02**	**2.03**	**1.98**	**1.96**	**1.97**	**1.96**	**1.95**	**1.96**	**2.10**	**2.04**	**2.04**	**2.04**	**2.04**	**1.98**	**1.96**	**1.98**	**1.99**	**1.97**	**1.98**	**1.99**
Fe	0.89	0.88	0.97	0.91	0.92	0.84	0.93	0.93	0.92	1.23	1.19	1.26	0.73	0.69	0.70	0.69	0.70	0.68	1.12	1.01	1.08	0.89	1.11	1.08
Mn	0.02	0.02	0.02	0.02	0.02	0.01	0.02	0.02	0.02	0.03	0.03	0.03	0.02	0.01	0.01	0.01	0.01	0.01	0.02	0.02	0.02	0.02	0.02	0.02
Mg	1.12	1.13	1.09	1.13	1.08	1.12	1.22	1.26	1.35	1.12	1.06	1.10	1.99	1.83	1.96	1.93	1.95	1.88	1.09	0.95	1.09	1.17	1.09	1.08
Ca	0.97	0.96	0.94	0.97	0.99	1.03	0.85	0.82	0.73	0.68	0.78	0.68	0.36	0.47	0.36	0.38	0.35	0.40	0.80	1.03	0.83	0.95	0.80	0.83
	2.99	**2.99**	**3.01**	**3.02**	**3.01**	**3.01**	**3.02**	**3.03**	**3.02**	**3.07**	**3.07**	**3.07**	**3.09**	**3.00**	**3.03**	**3.00**	**3.01**	**2.98**	**3.03**	**3.01**	**3.02**	**3.02**	**3.02**	**3.01**
mol %																								
Alm	**30**	**29**	**32**	**30**	**31**	**28**	**31**	**31**	**31**	**40**	**39**	**41**	**24**	**23**	**23**	**23**	**23**	**23**	**37**	**33**	**36**	**29**	**37**	**36**
Prp	**37**	**38**	**36**	**37**	**36**	**37**	**40**	**42**	**45**	**37**	**35**	**36**	**64**	**61**	**65**	**64**	**65**	**63**	**36**	**32**	**36**	**39**	**36**	**36**
Sps	**0.56**	**0.56**	**0.56**	**0.54**	**0.50**	**0.46**	**0.68**	**0.71**	**0.73**	**0.95**	**0.86**	**1.04**	**0.50**	**0.35**	**0.35**	**0.39**	**0.41**	**0.43**	**0.71**	**0.71**	**0.72**	**0.59**	**0.72**	**0.66**
Grs	**32**	**32**	**31**	**32**	**33**	**34**	**28**	**27**	**24**	**22**	**25**	**22**	**11**	**16**	**12**	**13**	**12**	**13**	**26**	**34**	**28**	**31**	**26**	**28**

Table S4.2. Major element composition of garnets from Rubinberg and Klatschmühle

Trace element

ppm	Rubinberg																			
Rb	b.d.l.	b.d.l.	b.d.l.	b.d.l.	b.d.l.	b.d.l.	b.d.l.	b.d.l.	b.d.l.	b.d.l.	b.d.l.	b.d.l.	b.d.l.	b.d.l.	b.d.l.	b.d.l.	b.d.l.	b.d.l.	b.d.l.	b.d.l.
Cs	b.d.l.	1.26	b.d.l.	b.d.l.	2.367	b.d.l.	b.d.l.	b.d.l.	b.d.l.	b.d.l.	b.d.l.	b.d.l.	b.d.l.	b.d.l.	b.d.l.	b.d.l.	b.d.l.	b.d.l.	1.84	b.d.l.	b.d.l.
Ba	b.d.l.	4.83	b.d.l.	b.d.l.	b.d.l.	b.d.l.	b.d.l.	b.d.l.	b.d.l.	b.d.l.	b.d.l.	b.d.l.	b.d.l.	b.d.l.	b.d.l.	b.d.l.	b.d.l.	b.d.l.	b.d.l.	b.d.l.	b.d.l.
Th	0.65	0.58	0.62	0.54	0.49	1.89	1.79	1.40	0.63	2.70	0.59	0.59	0.52	0.53	0.32	0.37	0.43	0.33	0.54	0.30
U	1.09	1.35	1.22	1.37	1.15	0.61	0.82	0.70	0.67	1.32	0.53	1.04	0.93	0.78	0.56	0.49	0.98	0.77	0.63	0.72
Nb	b.d.l.	0.10	b.d.l.	b.d.l.	b.d.l.	b.d.l.	0.08	b.d.l.	b.d.l.	b.d.l.	b.d.l.	b.d.l.	b.d.l.	0.15	b.d.l.	b.d.l.	b.d.l.	b.d.l.	b.d.l.	b.d.l.
Ta	b.d.l.	b.d.l.	b.d.l.	b.d.l.	b.d.l.	b.d.l.	b.d.l.	b.d.l.	b.d.l.	b.d.l.	b.d.l.	b.d.l.	b.d.l.	b.d.l.	b.d.l.	b.d.l.	b.d.l.	b.d.l.	b.d.l.	b.d.l.
La	0.84	1.77	0.81	0.82	0.53	0.40	b.d.l.	b.d.l.	0.35	0.60	0.39	0.91	0.91	0.95	0.67	b.d.l.	0.50	b.d.l.	0.40	0.50
Ce	8.27	12	10	9.54	7.28	2.53	2.68	2.39	5.36	2.74	6.26	8.75	9.52	9.30	9.98	4.72	6.99	7.55	5.78	5.13
Pb	b.d.l.	b.d.l.	b.d.l.	b.d.l.	b.d.l.	b.d.l.	b.d.l.	b.d.l.	b.d.l.	b.d.l.	b.d.l.	b.d.l.	b.d.l.	b.d.l.	b.d.l.	b.d.l.	b.d.l.	b.d.l.	b.d.l.	b.d.l.
Pr	4.12	4.88	4.53	4.42	4.34	1.47	1.49	1.81	2.91	2.11	2.97	4.14	4.56	4.96	4.40	3.31	4.07	3.16	2.76	2.76
P	3268	3298	3326	3184	3223	1523	1526	1549	2192	1912	3684	3794	3892	2772	2163	2953	3176	3593	3592	3558
Sr	1.20	2.13	1.57	1.25	0.67	0.64	b.d.l.	b.d.l.	0.82	1.15	1.01	1.50	1.79	2.80	2.93	b.d.l.	0.67	1.45	1.21	b.d.l.
Nd	52	54	55	49	47	25	31	29	39	26	43	50	49	55	53	34	48	51	35	36
Zr	262	243	227	231	287	296	309	318	251	276	292	207	154	121	127	283	282	292	292	297
Hf	2.81	4.23	3.88	3.75	2.78	5.14	4.57	3.87	4.58	4.46	3.79	2.85	2.45	2.68	1.19	3.19	3.69	4.45	3.62	4.32
Sm	51	50	55	51	43	38	41	37	44	39	43	49	32	23	25	47	45	55	51	45
Eu	21	19	18	19	20	17	17	18	18	16	19	18	13	13	13	18	22	22	20	18
Gd	48	50	42	43	62	90	89	92	109	96	75	41	29	29	29	76	71	64	74	81
Tb	5.98	5.83	5.35	5.68	7.52	18	18	19	20	18	11	6.15	4.63	5.12	4.72	12	7.77	7.43	9.88	11
Dy	35	33	35	31	42	144	135	148	144	144	60	38	35	40	41	61	42	41	59	62
Ti	12646	12974	12934	12846	11393	7681	8338	8307	10254	8116	10259	12163	12579	15035	14025	9693	10558	10898	9831	9306
Y	189	188	179	182	209	838	841	855	791	837	269	195	190	199	206	267	224	208	247	288
Ho	7.20	7.46	6.84	7.54	7.80	31	31	30	28	31	9.61	7.09	7.98	7.05	7.77	9.86	8.71	8.17	9.87	11
Er	23	20	21	21	23	93	91	94	81	88	24	19	21	24	23	27	24	23	23	30
Tm	2.97	3.37	3.02	2.74	2.68	13	12	13	11	12	3.78	2.80	2.81	3.52	3.11	3.42	3.46	3.60	3.46	3.34
Yb	20	18	21	22	19	78	84	87	69	80	22	18	20	19	20	22	22	20	22	25
Lu	3.28	2.72	2.93	2.83	3.25	11	12	14	12	12	2.67	3.29	3.19	3.25	2.82	3.69	3.85	3.50	3.38	3.41
Li	b.d.l.	b.d.l.	b.d.l.	b.d.l.	b.d.l.	b.d.l.	b.d.l.	b.d.l.	b.d.l.	b.d.l.	b.d.l.	b.d.l.	b.d.l.	b.d.l.	b.d.l.	b.d.l.	b.d.l.	b.d.l.	b.d.l.	b.d.l.
B	47	70	65	53	28	44	37	51	36	55	b.d.l.	36	b.d.l.	46	31	b.d.l.	b.d.l.	38	39	35

Detection limits

ppm	Rubinberg																			
Rb	4.12	3.85	3.89	3.85	4.67	4.64	4.09	4.76	4.22	4.14	4.97	4.26	4.13	4.18	4.01	4.04	4.18	4.01	4.59	4.47
Cs	1.26	1.15	1.19	1.14	1.26	1.40	1.17	1.32	1.30	1.25	1.55	1.24	1.22	1.26	1.25	1.23	1.21	1.18	1.36	1.28
Ba	3.34	3.10	3.66	3.46	4.22	3.94	3.30	4.24	3.51	3.53	4.13	3.23	3.37	3.53	3.20	3.44	3.69	3.54	3.90	4.35
Th	0.10	0.02	0.08	0.07	0.12	0.11	0.03	0.13	0.12	0.07	0.04	0.03	0.09	0.03	0.03	0.11	0.08	0.03	0.13	0.03
U	0.09	0.07	0.02	0.06	0.11	0.13	0.08	0.08	0.02	0.09	0.20	0.16	0.07	0.03	0.14	0.22	0.14	0.11	0.08	0.13
Nb	0.17	0.06	0.28	0.24	0.07	0.31	0.07	0.10	0.07	0.22	0.30	0.23	0.18	0.07	0.19	0.07	0.23	0.07	0.27	0.07
Ta	0.13	0.14	0.16	0.17	0.16	0.21	0.19	0.29	0.15	0.14	0.21	0.22	0.18	0.20	0.15	0.18	0.22	0.21	0.17	0.26
La	0.11	0.23	0.22	0.25	0.12	0.31	0.30	0.31	0.25	0.20	0.29	0.22	0.20	0.29	0.30	0.36	0.23	0.33	0.29	0.29
Ce	0.22	0.13	0.16	0.22	0.27	0.19	0.21	0.28	0.27	0.29	0.37	0.26	0.26	0.22	0.29	0.17	0.26	0.34	0.24	0.33
Pb	0.55	0.57	0.40	0.55	0.55	0.61	0.50	0.52	0.40	0.53	0.59	0.48	0.52	0.44	0.57	0.47	0.47	0.49	0.44	0.51
Pr	0.12	0.13	0.11	0.09	0.04	0.12	0.12	0.23	0.04	0.15	0.20	0.14	0.04	0.15	0.13	0.10	0.13	0.10	0.14	0.21
P	83	79	79	79	87	94	84	94	89	84	107	89	87	91	91	89	88	89	96	93
Sr	0.62	0.47	0.57	0.50	0.65	0.60	0.61	0.67	0.62	0.51	0.78	0.65	0.66	0.66	0.59	0.68	0.64	0.66	0.68	0.69
Nd	1.30	0.74	0.63	1.50	1.11	1.27	0.82	1.69	0.96	1.19	1.06	1.29	1.07	1.05	0.58	0.61	0.75	0.22	1.39	1.18
Zr	0.80	0.66	0.69	0.83	0.76	0.84	0.73	0.68	0.79	1.11	1.50	1.32	0.91	1.09	1.10	0.91	0.73	1.09	1.03	0.97
Hf	0.10	0.09	0.25	0.26	0.46	0.14	0.12	0.16	0.38	0.10	0.17	0.11	0.11	0.11	0.11	0.11	0.11	0.30	0.43	0.33
Sm	0.83	0.21	0.60	1.10	0.27	0.33	0.98	0.37	0.25	0.23	0.89	0.24	0.24	1.13	0.87	0.26	0.26	0.25	1.00	0.28
Eu	0.20	0.31	0.33	0.31	0.23	0.36	0.26	0.32	0.32	0.42	0.48	0.27	0.21	0.32	0.32	0.37	0.39	0.52	0.37	0.24
Gd	1.55	1.44	0.22	0.89	1.08	1.16	1.77	1.62	1.14	1.34	1.91	1.21	0.97	1.41	1.13	1.49	0.90	1.84	1.77	1.80
Tb	0.03	0.03	0.03	0.09	0.11	0.15	0.12	0.15	0.17	0.09	0.13	0.04	0.12	0.20	0.15	0.15	0.15	0.18	0.04	0.11
Dy	0.14	0.13	0.13	0.37	0.16	0.49	0.17	0.22	0.43	0.14	0.55	0.15	0.15	0.16	0.54	0.16	0.71	0.16	0.72	0.17
Ti	38	36	35	33	37	25	24	20	23	31	30	27	30	33	27	35	31	30	31	28
Y	0.26	0.37	0.38	0.32	0.29	0.43	0.33	0.42	0.42	0.23	0.40	0.47	0.33	0.35	0.33	0.39	0.32	0.36	0.45	0.52
Ho	0.03	0.11	0.11	0.03	0.04	0.05	0.04	0.05	0.10	0.03	0.06	0.10	0.04	0.04	0.04	0.04	0.15	0.04	0.15	0.04
Er	0.11	0.09	0.10	0.49	0.33	0.15	0.13	0.17	0.11	0.11	0.57	0.11	0.11	0.11	0.11	0.12	0.12	0.32	0.14	0.45
Tm	0.03	0.03	0.03	0.09	0.11	0.05	0.10	0.05	0.15	0.03	0.06	0.10	0.12	0.15	0.04	0.17	0.15	0.04	0.04	0.04
Yb	0.16	0.14	0.41	0.15	0.51	0.22	0.19	0.58	0.17	0.16	0.27	0.17	0.47	0.18	0.17	0.18	0.49	0.78	0.55	0.19
Lu	0.08	0.07	0.03	0.03	0.09	0.04	0.03	0.10	0.08	0.10	0.13	0.12	0.03	0.08	0.08	0.11	0.08	0.08	0.12	0.03
Li	24.55	24.24	23.51	23.64	27	29	26	29	28	28	35	29	29	29	30	31	31	31	33	34
B	24.94	22.65	22.72	21.58	26	30	27	32	28	24	34	29	29	30	28	33	33	31	32	31

Table S4.3. Trace elements composition of garnets from Rubinberg

Trace element

ppm	Klatschmühle																			
Rb	b.d.l.	b.d.l.	b.d.l.	b.d.l.	b.d.l.	b.d.l.	b.d.l.	b.d.l.	b.d.l.	b.d.l.	b.d.l.	b.d.l.	b.d.l.	b.d.l.	b.d.l.	b.d.l.	b.d.l.	b.d.l.	b.d.l.	b.d.l.
Cs	b.d.l.	b.d.l.	b.d.l.	b.d.l.	b.d.l.	b.d.l.	b.d.l.	b.d.l.	b.d.l.	b.d.l.	b.d.l.	b.d.l.	b.d.l.	b.d.l.	b.d.l.	b.d.l.	b.d.l.	b.d.l.	b.d.l.	b.d.l.
Ba	b.d.l.	b.d.l.	b.d.l.	b.d.l.	b.d.l.	b.d.l.	b.d.l.	b.d.l.	b.d.l.	b.d.l.	b.d.l.	b.d.l.	b.d.l.	b.d.l.	b.d.l.	b.d.l.	b.d.l.	b.d.l.	b.d.l.	b.d.l.
Th	0.77	0.51	0.38	0.38	0.35	0.51	0.99	0.70	0.26	0.32	0.63	0.59	0.58	0.54	0.74	0.22	0.12	0.60	b.d.l.	0.83
U	1.28	1.26	1.10	0.82	1.34	1.43	0.82	1.61	1.55	1.20	2.63	2.22	2.84	2.77	2.66	0.52	0.84	0.50	0.45	1.17
Nb	0.11	b.d.l.	b.d.l.	b.d.l.	b.d.l.	b.d.l.	b.d.l.	b.d.l.	b.d.l.	b.d.l.	b.d.l.	b.d.l.	b.d.l.	b.d.l.	b.d.l.	b.d.l.	b.d.l.	b.d.l.	b.d.l.	b.d.l.
Ta	b.d.l.	b.d.l.	b.d.l.	b.d.l.	b.d.l.	b.d.l.	b.d.l.	b.d.l.	b.d.l.	b.d.l.	b.d.l.	b.d.l.	b.d.l.	b.d.l.	b.d.l.	b.d.l.	b.d.l.	b.d.l.	b.d.l.	b.d.l.
La	b.d.l.	b.d.l.	b.d.l.	b.d.l.	b.d.l.	b.d.l.	b.d.l.	b.d.l.	b.d.l.	b.d.l.	0.51	0.71	0.51	0.76	0.58	0.39	0.30	b.d.l.	b.d.l.	b.d.l.
Ce	2.58	3.40	2.53	2.45	2.79	2.77	2.44	2.48	2.95	3.41	9.45	11	9.82	11	11	1.63	1.72	1.69	1.93	1.45
Pb	b.d.l.	b.d.l.	b.d.l.	b.d.l.	b.d.l.	b.d.l.	b.d.l.	b.d.l.	b.d.l.	b.d.l.	b.d.l.	b.d.l.	b.d.l.	b.d.l.	b.d.l.	b.d.l.	b.d.l.	b.d.l.	b.d.l.	b.d.l.
Pr	1.45	1.22	1.63	1.77	2.10	1.29	1.63	1.80	2.11	3.35	4.81	4.77	5.18	4.63	4.68	1.10	1.11	1.48	1.45	1.22
P	2219	2169	2528	2481	2618	2275	2320	2265	2694	2380	2162	2171	2615	2841	2588	2423	2411	2263	2218	2399
Sr	b.d.l.	b.d.l.	b.d.l.	b.d.l.	b.d.l.	b.d.l.	b.d.l.	0.94	b.d.l.	1.65	1.49	1.09	1.24	1.09	1.43	b.d.l.	b.d.l.	b.d.l.	b.d.l.	b.d.l.
Nd	22	24	25	27	26	25	30	29	25	28	57	64	61	57	59	22	20	24	20	21
Zr	502	493	457	453	440	508	488	444	423	437	366	352	323	302	333	392	422	411	411	447
Hf	5.78	5.62	5.74	6.01	5.35	5.34	6.58	5.89	4.95	6.13	4.64	4.40	3.69	4.63	5.23	5.35	5.39	4.28	5.98	5.34
Sm	39	34	37	37	41	36	39	43	48	46	62	59	62	55	54	35	41	34	33	38
Eu	15	16	14	16	17	14	18	16	17	22	21	20	19	19	20	12	15	15	15	15
Gd	78	74	73	78	83	72	85	84	74	67	60	50	49	43	60	86	81	93	84	86
Tb	15	15	14	15	14	16	13	16	16	14	7.71	8.18	6.27	8.45	7.46	16	15	17	17	16
Dy	111	111	104	100	90	115	118	96	101	80	46	45	47	49	48	123	120	117	103	110
Ti	6466	8376	8724	9437	10184	7875	9187	9024	9348	10490	12301	12569	11812	11835	11916	9135	9055	9212	9015	9274
Y	621	596	537	479	431	618	545	462	425	331	234	238	235	241	236	691	653	573	497	567
Ho	23	22	20	19	16	23	23	16	18	14	11	9.33	9.37	9.11	9.02	23	22	19	16	20
Er	73	60	55	51	40	65	53	46	38	34	28	27	25	27	30	71	63	48	42	54
Tm	9.59	7.92	6.59	5.54	4.89	7.62	7.75	5.45	4.15	3.79	3.37	3.48	3.34	3.32	3.59	7.86	8.31	5.87	4.80	6.56
Yb	63	50	41	33	31	54	36	33	24	26	29	24	24	20	23	55	41	36	28	40
Lu	8.99	6.60	5.27	4.80	4.24	7.27	4.68	4.12	3.48	3.66	2.85	3.13	3.34	3.46	3.52	8.10	5.65	4.65	3.75	4.92
Li	b.d.l.	b.d.l.	b.d.l.	b.d.l.	b.d.l.	b.d.l.	b.d.l.	b.d.l.	b.d.l.	b.d.l.	b.d.l.	b.d.l.	b.d.l.	b.d.l.	b.d.l.	b.d.l.	b.d.l.	b.d.l.	b.d.l.	b.d.l.
B	42	b.d.l.	b.d.l.	b.d.l.	38	77	b.d.l.	90	b.d.l.	73	b.d.l.	44.22	53.07	54.86	b.d.l.	b.d.l.	b.d.l.	42.74	b.d.l.	b.d.l.

Detection limits

ppm	Klatschmühle																			
Rb	4.52	4.45	4.48	4.51	4.15	5.76	6.36	5.32	7.44	6.49	5.61	4.80	5.41	5.17	4.86	4.89	4.89	4.93	4.78	4.63
Cs	1.36	1.29	1.33	1.30	1.31	1.68	1.90	1.53	2.22	1.93	1.68	1.35	1.59	1.49	1.41	1.38	1.38	1.47	1.37	1.30
Ba	4.51	5.04	4.99	4.08	4.61	6.27	8.64	6.03	8.45	7.77	5.45	5.24	6.68	5.57	5.87	5.02	4.17	5.10	5.88	6.21
Th	0.08	0.03	0.03	0.03	0.03	0.15	0.22	0.06	0.19	0.21	0.19	0.04	0.20	0.15	0.04	0.12	0.04	0.12	0.15	0.11
U	0.14	0.16	0.14	0.20	0.03	0.17	0.25	0.06	0.09	0.23	0.22	0.15	0.19	0.14	0.14	0.16	0.13	0.22	0.21	0.26
Nb	0.07	0.20	0.20	0.30	0.18	0.37	0.20	0.45	0.60	0.24	0.39	0.09	0.41	0.31	0.34	0.25	0.24	0.50	0.44	0.23
Ta	0.25	0.18	0.23	0.22	0.23	0.44	0.32	0.19	0.41	0.25	0.31	0.21	0.21	0.39	0.30	0.27	0.33	0.43	0.34	0.23
La	0.30	0.40	0.28	0.26	0.25	0.30	0.45	0.22	0.56	0.53	0.26	0.30	0.25	0.16	0.28	0.38	0.26	0.34	0.37	0.37
Ce	0.36	0.33	0.31	0.29	0.28	0.30	0.47	0.35	0.53	0.34	0.40	0.24	0.35	0.26	0.28	0.44	0.49	0.43	0.33	0.45
Pb	0.24	0.55	0.50	0.59	0.43	0.56	0.78	0.76	1.17	1.04	0.75	0.60	0.75	0.67	0.84	0.51	0.58	0.44	0.54	0.54
Pr	0.04	0.17	0.13	0.14	0.14	0.05	0.12	0.24	0.28	0.14	0.07	0.13	0.32	0.06	0.20	0.27	0.05	0.19	0.14	0.19
P	107	107	105	104	100	140	152	118	165	149	117	97	110	109	104	118	112	121	120	110
Sr	0.75	0.69	0.75	0.74	0.72	0.99	0.95	0.72	1.19	1.01	0.70	0.81	0.84	0.84	0.78	1.01	0.92	1.08	0.90	0.81
Nd	0.90	0.92	1.21	0.80	1.49	1.67	2.08	1.43	1.89	2.98	1.53	0.98	1.12	1.97	1.46	1.09	1.34	1.33	0.84	1.01
Zr	0.92	1.18	1.08	0.78	1.04	1.13	1.44	1.22	1.28	1.75	1.14	0.63	1.14	1.17	0.93	1.15	0.68	1.34	1.18	0.92
Hf	0.41	0.12	0.41	0.11	0.11	0.46	0.83	0.25	0.36	0.43	0.21	0.16	0.17	0.18	0.17	0.58	0.44	0.71	0.16	0.15
Sm	0.27	0.26	0.75	0.25	0.25	1.02	0.82	0.54	0.79	0.95	1.77	0.35	1.03	1.25	0.97	0.36	0.35	0.35	0.34	0.33
Eu	0.34	0.30	0.23	0.08	0.39	0.47	0.66	0.43	0.62	0.81	0.51	0.51	0.49	0.46	0.45	0.53	0.63	0.50	0.32	0.65
Gd	1.98	2.14	1.55	1.50	1.86	1.71	3.06	1.98	3.04	2.41	1.46	1.68	2.07	1.50	1.62	2.35	2.34	1.95	1.95	2.38
Tb	0.14	0.20	0.23	0.11	0.15	0.20	0.23	0.20	0.30	0.27	0.07	0.18	0.16	0.19	0.15	0.15	0.33	0.23	0.15	0.14
Dy	0.17	0.69	0.17	0.60	0.16	0.26	0.55	0.36	0.53	0.64	0.31	0.23	0.25	0.26	0.63	0.83	0.23	0.87	0.23	0.22
Ti	37	36	32	35	32	30	22	27	37	41	27	23	24	27	25	28	32	35	28	30
Y	0.51	0.40	0.34	0.32	0.42	0.51	0.54	0.48	0.62	0.65	0.54	0.51	0.34	0.36	0.48	0.55	0.35	0.56	0.52	0.40
Ho	0.11	0.11	0.11	0.04	0.11	0.06	0.13	0.09	0.13	0.16	0.08	0.26	0.06	0.07	0.23	0.06	0.16	0.06	0.06	0.05
Er	0.50	0.12	0.35	0.45	0.12	0.19	0.42	0.28	0.81	0.48	0.23	0.18	0.19	0.20	0.19	0.18	0.70	0.18	0.62	0.68
Tm	0.04	0.04	0.11	0.04	0.10	0.17	0.13	0.09	0.13	0.15	0.08	0.06	0.21	0.06	0.20	0.06	0.16	0.06	0.06	0.05
Yb	0.19	0.52	0.67	0.89	0.18	1.08	1.34	0.81	1.42	1.27	0.35	0.26	0.96	1.28	0.28	0.94	0.26	0.77	0.26	0.24
Lu	0.09	0.09	0.15	0.09	0.03	0.19	0.10	0.07	0.24	0.12	0.18	0.12	0.05	0.18	0.12	0.16	0.20	0.20	0.16	0.17
Li	33	34	33	34	32	36	40	32	45	41	36	31	33	32	31	38	37	40	36	37
B	31	33	35	33	31	39	51	39	53	50	46	38	41	39	39	42	35	41	36	41

Table S4.4. Trace elements composition of garnets from Klatschmühle.

Major elements

	Rubinberg												Klatschmühle											
Name	253	255	256	257	258	259	75	84	92	118	155	188	173	174	175	176	177	178	52	71	77	228	258	305
wt. %																								
SiO_2	51.70	50.09	50.63	50.10	50.41	50.09	52.86	51.64	52.00	50.48	50.89	49.69	54.85	55.42	54.84	54.45	55.04	54.35	51.89	51.84	51.79	51.91	52.44	52.41
TiO_2	0.52	0.81	0.87	0.67	0.76	0.76	0.64	0.85	0.82	0.91	0.92	0.79	0.41	0.40	0.45	0.42	0.42	0.50	0.55	0.57	0.54	0.56	0.64	0.58
Al_2O_3	10.82	10.87	11.84	11.18	10.97	10.63	7.09	8.16	8.01	10.03	9.26	9.60	8.89	9.38	8.85	8.82	8.92	8.77	11.64	11.38	11.20	10.15	11.81	11.12
Fe_2O_3																								
FeO	6.81	8.21	7.87	7.96	7.80	8.29	5.55	5.84	5.89	8.02	8.10	8.33	4.39	3.80	3.97	3.80	3.83	3.84	6.41	6.46	6.43	6.58	5.72	6.68
MnO	0.04	0.08	0.06	0.06	0.07	0.08	0.05	0.05	0.06	0.12	0.09	0.07	0.06	0.07	0.07	0.02	0.03	0.04	0.05	0.07	0.05	0.09	0.06	0.11
MgO	9.93	10.31	9.68	10.17	10.38	10.48	12.49	11.60	11.80	9.84	10.12	9.87	12.82	11.93	12.82	12.62	12.27	12.63	9.75	9.61	9.69	10.21	8.96	9.79
CaO	16.92	17.15	15.93	17.62	17.41	17.81	18.89	18.52	18.37	17.29	17.55	15.73	15.59	15.22	15.68	16.32	15.98	16.36	16.44	16.26	16.27	15.99	15.10	15.43
Na_2O	4.14	3.35	4.07	3.43	3.36	2.90	2.48	2.64	2.77	3.14	3.28	2.98	3.62	3.77	3.86	3.91	3.89	3.81	4.03	3.61	3.68	3.63	4.59	3.92
K_2O	0.00	0.04	0.06	0.01	0.01	0.03	0.00	0.00	0.00	0.01	0.00	0.01	0.01	0.02	0.02	0.06	0.01	0.01	0.01	0.01	0.01	0.00	0.01	0.01
P_2O_5	0.023	0.004	0.02	0.00	0.013	0.014	0.04	0.02	0.01	0.02	0.01	0.03	0.03	0.01	0.01	0.01	0.02	0.02	0.00	0.04	0.02	0.01	0.01	0.00
TOTAL	100.91	100.91	101.03	101.21	101.17	101.10	100.08	99.33	99.74	99.85	100.22	97.11	100.66	100.02	100.55	100.43	100.40	100.32	100.77	99.85	99.69	99.12	99.33	100.04
Mg#	**72**	**69**	**69**	**69**	**70**	**69**	**80**	**78**	**78**	**69**	**69**	**68**	**84**	**85**	**85**	**86**	**85**	**85**	**73**	**73**	**73**	**73**	**74**	**72**
Si	1.85	1.81	1.82	1.80	1.81	1.81	1.92	1.89	1.90	1.85	1.86	1.88	1.96	1.99	1.95	1.94	1.96	1.94	1.86	1.89	1.89	1.90	1.91	1.90
Ti	0.01	0.02	0.02	0.02	0.02	0.02	0.02	0.02	0.02	0.02	0.03	0.02	0.01	0.01	0.01	0.01	0.01	0.01	0.01	0.02	0.01	0.02	0.02	0.02
Al	0.46	0.46	0.50	0.47	0.47	0.45	0.30	0.35	0.34	0.43	0.40	0.43	0.37	0.40	0.37	0.37	0.38	0.37	0.49	0.49	0.48	0.44	0.51	0.48
Fe	0.20	0.25	0.24	0.24	0.23	0.25	0.17	0.18	0.18	0.25	0.25	0.26	0.13	0.11	0.12	0.11	0.11	0.11	0.19	0.20	0.20	0.20	0.17	0.20
Mn	0.20	0.25	0.24	0.24	0.23	0.25	0.00	0.00	0.00	0.00	0.00	0.00	0.13	0.11	0.12	0.11	0.11	0.11	0.00	0.00	0.00	0.00	0.00	0.00
Mg	0.53	0.56	0.52	0.55	0.56	0.57	0.68	0.63	0.64	0.54	0.55	0.56	0.68	0.64	0.68	0.67	0.65	0.67	0.52	0.52	0.53	0.56	0.49	0.53
Ca	0.65	0.66	0.61	0.68	0.67	0.69	0.74	0.73	0.72	0.68	0.69	0.64	0.60	0.59	0.60	0.62	0.61	0.63	0.63	0.63	0.63	0.63	0.59	0.60
Na	0.29	0.23	0.28	0.24	0.23	0.20	0.17	0.19	0.20	0.22	0.23	0.22	0.25	0.26	0.27	0.27	0.27	0.26	0.28	0.25	0.26	0.26	0.32	0.28
K	0.00	0.00	0.00	0.00	0.00	0.00	0.00	0.00	0.00	0.00	0.00	0.00	0.00	0.00	0.00	0.00	0.00	0.00	0.00	0.00	0.00	0.00	0.00	0.00
Jd	**29**	**23**	**28**	**24**	**23**	**20**	**17**	**19**	**20**	**22**	**23**	**22**	**25**	**26**	**27**	**27**	**27**	**26**	**28**	**25**	**26**	**26**	**32**	**28**

Table S4.5. Major composition of clinopyroxenes from Rubinberg and Klatschmühle

Trace element

	Rubinberg																		Klatschmühle											
ppm																														
Rb	b.d.l.	b.d.l.	b.d.l.	b.d.l.	b.d.l.	b.d.l.	b.d.l.	b.d.l.	b.d.l.	b.d.l.	3.90	3.29	4.74	4.56	5.81	5.52	b.d.l.	4.00	b.d.l.	35.76	b.d.l.	b.d.l.	b.d.l.	b.d.l.	34	b.d.l.	b.d.l.	b.d.l.	b.d.l.	b.d.l.
Cs	b.d.l.	b.d.l.	b.d.l.	b.d.l.	b.d.l.	b.d.l.	b.d.l.	b.d.l.	b.d.l.	b.d.l.	1.42	1.81	b.d.l.	b.d.l.	2.70	b.d.l.	b.d.l.	5.07	b.d.l.	4.78	b.d.l.	1.66	b.d.l.	b.d.l.	28	b.d.l.	b.d.l.	b.d.l.	b.d.l.	b.d.l.
Ba	b.d.l.	b.d.l.	7.31	2.88	b.d.l.	4.79	b.d.l.	b.d.l.	b.d.l.	b.d.l.	6.19	30	25	35	31	37	23	16	b.d.l.	14	b.d.l.	16	b.d.l.	b.d.l.	49	b.d.l.	b.d.l.	b.d.l.	b.d.l.	4.73	b.d.l.
Th	18.43	16.12	13.94	15.78	16	16	15	12	14	13	14	16	13	13	14	16	15	12	5.75	3.94	4.50	6.75	5.26	4.89	5.42	5.44	5.87	6.08	6.10	6.30
U	3.34	3.34	3.34	2.90	2.50	2.93	2.92	2.07	2.31	2.61	2.45	2.69	2.33	2.50	2.27	2.61	2.96	2.20	2.04	1.48	1.51	2.68	1.98	1.82	2.64	2.48	2.76	3.09	2.82	2.87
Nb	1.75	1.81	0.87	1.71	1.60	1.08	1.69	1.20	1.28	1.11	0.95	0.73	0.82	0.71	0.84	0.89	1.06	1.04	1.30	1.21	1.35	1.19	1.61	1.52	1.80	2.52	1.42	0.98	0.83	1.17
Ta	0.28	0.25	0.28	0.38	0.23	0.32	0.34	0.40	0.47	0.32	0.42	0.37	0.23	b.d.l.	0.19	0.28	0.36	0.20	0.23	b.d.l.	b.d.l.	0.19	0.26	0.12	0.24	0.28	0.29	0.23	0.21	b.d.l.
La	121	117	102	124	122	116	111	99	111	111	91	116	125	131	141	141	144	116	54	55	54	60	53	52	53	55	52	57	51	55
Ce	366	356	322	370	352	343	347	314	337	341	303	351	365	384	408	404	395	352	207	205	201	228	192	197	195	207	200	202	188	196
Pb	10	8.14	10	13	12	10	9.69	7.35	8.30	7.19	7.50	8.39	12	13	14	17	14	13	6.21	5.18	4.11	7.26	3.96	5.36	4.50	4.63	4.11	5.55	5.48	3.94
Pr	55	55	50	55	53	54	52	50	52	53	47	53	56	58	61	62	58	51	34	36	36	39	34	32	34	36	35	34	30	35
P	554	520	445	507	544	495	551	467	510	521	419	487	438	465	538	594	521	514	503	495	441	575	425	416	511	487	521	483	456	482
Sr	301	251	195	310	331	319	237	209	224	203	111	183	244	246	256	293	337	463	267	295	292	366	282	294	306	286	262	279	269	286
Nd	272	263	248	260	269	258	254	235	246	241	232	258	257	263	289	286	261	256	193	192	179	216	166	164	173	180	175	175	162	163
Zr	932	852	859	932	929	890	910	910	896	918	850	901	863	894	957	1013	995	948	826	836	776	1114	821	806	820	898	827	778	763	798
Hf	33	32	36	39	36	37	35	38	36	37	34	37	36	32	38	40	44	40	35	36	33	44	32	31	32	36	32	32	30	31
Sm	72	61	63	65	63	60	62	62	63	63	63	66	63	64	70	72	67	65	50	54	47	60	43	44	48	51	50	50	45	45
Eu	14	16	12	14	14	13	15	14	15	15	14	15	14	15	16	16	15	14	11	12	11	14	12	9.89	11	11	11	12	10	11
Gd	37	34	31	38	33	36	34	36	40	39	44	41	40	39	44	47	41	37	37	35	33	49	33	31	31	36	33	32	26	27
Tb	3.01	3.32	3.31	3.49	3.12	2.82	3.24	4.58	4.48	4.49	4.88	4.28	3.99	3.91	4.66	4.71	3.32	3.70	4.12	4.00	3.00	4.81	3.58	3.16	3.85	3.63	3.57	3.30	3.22	3.52
Dy	13	12	13	9.82	11	9.95	13	18	19	18	27	18	17	18	22	20	15	14	18	16	13	23	14	13	14	15	13	15	11	12
Ti	65756	58976	53519	67083	63868	61928	62857	55690	####	57220	49549	58851	50437	52989	59549	63833	65603	55344	39108	38270	35106	51013	35906	35082	36699	45494	43931	37516	36567	38251
Y	34	35	41	31	31	32	35	61	62	61	110	65	60	57	64	65	49	43	4.82	4.70	4.43	6.19	4.31	3.95	4.03	4.19	3.58	3.36	3.38	3.55
Ho	1.36	1.43	1.53	1.39	1.45	1.37	1.24	2.43	2.27	2.27	4.16	2.57	2.11	2.34	2.47	2.66	1.74	1.66	1.89	1.87	1.73	3.20	1.67	1.92	1.66	2.09	2.04	1.87	1.53	1.59
Er	2.09	2.47	3.22	1.83	2.29	1.87	2.08	4.68	4.51	5.57	10	5.20	3.96	5.17	4.99	5.52	3.18	3.32	3.72	4.18	3.44	6.28	3.30	3.42	3.80	4.69	3.32	2.95	3.36	3.05
Tm	0.21	0.20	0.28	0.29	0.18	0.18	0.20	0.48	0.44	0.59	1.31	0.54	0.38	0.41	0.46	0.59	0.47	0.32	0.32	0.45	0.57	0.91	0.28	0.42	0.37	0.37	0.38	0.25	0.15	0.21
Yb	0.71	0.66	1.51	1.86	0.70	1.18	0.69	1.74	2.31	2.61	9.34	2.81	2.21	2.04	3.45	2.41	1.56	1.67	1.91	1.58	1.12	3.68	1.67	1.86	1.06	2.28	1.56	0.67	1.31	1.46
Lu	0.12	0.15	0.16	0.12	0.21	0.13	0.12	0.23	0.24	0.21	1.00	0.30	0.25	0.28	0.39	0.25	0.27	0.17	0.26	0.20	0.12	0.49	0.30	0.13	0.18	0.23	0.18	0.26	b.d.l.	0.09
Li	162	170	85	174	187	184	128	153	185	177	87	149	116	119	112	165	141	203	438	523	511	534	656	719	703	790	654	665	642	736
B	87	69	63	64	87	77	62	39	42	48	43	54	44	38	36	50	44	36	28	42	27	33	b.d.l.	38	26	37	b.d.l.	b.d.l.	b.d.l.	25

Detection limits

	Rubinberg																		Klatschmühle											
ppm																														
Rb	2.79	2.73	2.38	2.95	3.08	2.95	2.76	3.26	3.26	3.11	3.03	3.26	2.92	2.94	3.05	3.00	3.02	3.20	2.58	2.70	2.51	3.27	2.55	2.60	2.57	2.72	2.46	2.43	2.43	2.44
Cs	0.80	0.83	0.69	0.89	0.89	0.84	0.83	0.97	0.98	0.97	0.87	0.99	0.88	0.88	0.91	0.93	0.87	0.95	0.78	0.84	0.77	0.93	0.75	0.77	0.77	0.84	0.69	0.70	0.78	0.73
Ba	2.44	2.69	2.13	2.65	2.20	2.05	2.65	2.90	2.88	2.81	2.10	2.17	2.72	2.26	2.44	2.94	2.90	2.76	3.05	3.16	3.01	3.72	3.40	3.78	3.57	3.09	2.94	2.96	2.82	2.93
Th	0.01	0.02	0.01	0.06	0.02	0.02	0.05	0.02	0.02	0.02	0.05	0.02	0.02	0.05	0.08	0.02	0.05	0.02	0.02	0.08	0.06	0.03	0.02	0.06	0.08	0.06	0.08	0.02	0.13	0.10
U	0.07	0.07	0.01	0.09	0.06	0.08	0.02	0.06	0.07	0.06	0.08	0.10	0.07	0.07	0.05	0.05	0.09	0.05	0.11	0.10	0.11	0.09	0.15	0.09	0.06	0.10	0.14	0.11	0.10	0.12
Nb	0.13	0.17	0.12	0.12	0.15	0.18	0.14	0.17	0.14	0.17	0.15	0.14	0.04	0.13	0.19	0.12	0.24	0.05	0.12	0.25	0.17	0.16	0.04	0.04	0.13	0.04	0.20	0.17	0.24	0.16
Ta	0.09	0.10	0.10	0.10	0.13	0.13	0.15	0.10	0.10	0.12	0.11	0.14	0.09	0.21	0.12	0.09	0.09	0.15	0.09	0.12	0.19	0.16	0.18	0.10	0.19	0.15	0.20	0.18	0.11	0.21
La	0.12	0.14	0.11	0.11	0.14	0.10	0.21	0.23	0.19	0.24	0.18	0.16	0.11	0.20	0.13	0.16	0.17	0.28	0.19	0.15	0.14	0.10	0.21	0.18	0.23	0.22	0.20	0.25	0.24	0.24
Ce	0.17	0.18	0.13	0.15	0.17	0.16	0.15	0.18	0.09	0.21	0.20	0.18	0.22	0.23	0.10	0.16	0.15	0.24	0.11	0.21	0.20	0.29	0.20	0.25	0.26	0.12	0.17	0.15	0.28	0.21
Pb	0.34	0.36	0.29	0.33	0.40	0.41	0.39	0.32	0.31	0.41	0.36	0.49	0.35	0.31	0.30	0.33	0.42	0.45	0.23	0.24	0.28	0.30	0.24	0.28	0.37	0.18	0.15	0.31	0.30	0.32
Pr	0.10	0.11	0.07	0.14	0.11	0.08	0.06	0.07	0.10	0.07	0.09	0.09	0.08	0.09	0.07	0.11	0.13	0.14	0.07	0.11	0.11	0.21	0.15	0.07	0.07	0.12	0.12	0.16	0.13	0.13
P	57	57	49	61	60	61	56	68	69	67	62	67	64	65	64	64	67	70	58	62	59	77	62	64	62	64	65	65	71	67
Sr	0.39	0.42	0.32	0.39	0.39	0.38	0.35	0.45	0.52	0.42	0.42	0.41	0.42	0.48	0.44	0.47	0.48	0.49	0.44	0.46	0.43	0.50	0.49	0.51	0.47	0.57	0.49	0.44	0.50	0.49
Nd	0.81	0.82	0.73	0.67	1.19	1.11	0.73	1.06	0.72	0.15	0.61	0.53	0.63	0.58	0.98	0.86	0.58	0.92	0.95	0.56	0.60	0.55	0.64	0.43	0.74	0.64	0.55	0.86	0.68	0.64
Zr	0.53	0.47	0.46	0.52	0.49	0.57	0.52	0.55	0.77	0.63	0.63	0.63	0.42	0.56	0.53	0.70	0.85	0.90	0.45	0.57	0.64	0.85	0.82	0.55	0.61	0.48	0.63	0.65	0.66	0.66
Hf	0.06	0.21	0.05	0.07	0.07	0.07	0.07	0.07	0.08	0.08	0.07	0.07	0.07	0.07	0.07	0.07	0.30	0.23	0.08	0.09	0.08	0.10	0.23	0.08	0.35	0.08	0.08	0.08	0.24	0.09
Sm	0.14	0.14	0.13	0.17	0.66	0.73	0.16	0.17	0.19	0.17	0.56	0.63	0.57	0.17	0.69	0.17	0.18	0.52	0.17	0.52	0.48	0.22	0.18	0.17	0.52	0.64	0.18	0.18	0.19	0.20
Eu	0.18	0.20	0.11	0.20	0.18	0.18	0.28	0.05	0.29	0.35	0.23	0.05	0.23	0.27	0.19	0.27	0.06	0.17	0.27	0.27	0.31	0.34	0.16	0.21	0.30	0.27	0.06	0.33	0.42	0.41
Gd	0.74	0.85	0.67	1.00	0.92	0.86	0.62	1.21	0.94	0.81	0.79	0.74	1.13	0.77	1.07	1.07	0.84	0.78	1.28	0.95	1.00	2.23	1.18	1.01	1.38	1.19	0.94	1.09	1.08	1.18
Tb	0.02	0.08	0.06	0.06	0.02	0.10	0.02	0.07	0.10	0.09	0.06	0.07	0.07	0.10	0.07	0.08	0.07	0.15	0.09	0.08	0.09	0.18	0.13	0.11	0.12	0.18	0.11	0.15	0.12	0.14
Dy	0.08	0.09	0.08	0.27	0.10	0.27	0.10	0.11	0.12	0.11	0.10	0.11	0.09	0.29	0.11	0.28	0.11	0.11	0.31	0.12	0.31	0.15	0.12	0.11	0.43	0.12	0.12	0.12	0.13	0.34
Ti	20	20	18	21	21	15	17	19	18	16	18	17	15	23	18	19	18	19	16	15	16	19	16	13	17	18	14	14	15	21
Y	0.18	0.22	0.20	0.19	0.16	0.26	0.21	0.25	0.26	0.29	0.32	0.34	0.25	0.27	0.24	0.25	0.25	0.25	0.29	0.23	0.27	0.36	0.17	0.22	0.28	0.39	0.29	0.18	0.23	0.24
Ho	0.06	0.02	0.02	0.08	0.07	0.02	0.02	0.03	0.03	0.03	0.02	0.03	0.02	0.03	0.03	0.03	0.07	0.03	0.03	0.03	0.08	0.04	0.03	0.08	0.03	0.03	0.03	0.08	0.03	0.03
Er	0.06	0.06	0.20	0.29	0.08	0.20	0.07	0.08	0.09	0.08	0.20	0.29	0.30	0.08	0.27	0.08	0.38	0.24	0.08	0.09	0.23	0.11	0.09	0.08	0.26	0.32	0.38	0.09	0.10	0.26
Tm	0.02	0.02	0.06	0.08	0.02	0.02	0.06	0.03	0.03	0.03	0.07	0.07	0.02	0.07	0.03	0.02	0.03	0.03	0.10	0.03	0.03	0.04	0.03	0.03	0.03	0.08	0.03	0.08	0.09	0.03
Yb	0.33	0.10	0.39	0.12	0.12	0.11	0.29	0.12	0.13	0.34	0.31	0.12	0.46	0.33	0.33	0.12	0.12	0.13	0.13	0.14	0.13	0.77	0.54	0.47	0.56	0.13	0.37	0.45	0.40	0.38
Lu	0.05	0.05	0.02	0.02	0.02	0.07	0.06	0.06	0.02	0.02	0.05	0.02	0.07	0.06	0.08	0.02	0.02	0.02	0.06	0.02	0.06	0.13	0.08	0.02	0.02	0.10	0.08	0.06	0.13	0.06
Li	16	16	14	18	18	17	17	22	22	21	19	21	20	21	21	21	22	24	18	18	18	24	20	20	21	21	21	21	22	21
B	17	16	14	19	16	17	17	21	20	21	20	21	19	21	21	21	22	23	24	23	22	24	21	17	23	22	26	22	26	23

Table S4.6. Trace elements composition of clinopyroxene from Klatschmühle.

Plagioclase

Location	Rubinberg					Klatschmühle			
Sample	RUB 11	RUB 11	RUB 11	3.1	4.4-1	KLA 1-2.1	KLA	KLA 2-2	KLA 1-2.1
Microstructural position	Interstitial	Inclusion in Grt	Leucocratic pocket	Symplectite	Lamellae in Cpx	Interstitial	Inclusion in Grt	Leucocratic pocket	Symplectite
wt%									
SiO_2	63.18	64.34	62.65	62.58	62.49	62.80	65.60	65.70	62.06
TiO_2	0.04	0.02	0.02	0.01	0.03	0.00	0.01	0.03	0.04
Al_2O_3	23.21	22.85	23.41	24.47	24.14	23.57	23.03	21.80	23.62
FeO	0.09	0.33	0.07	0.40	0.32	0.14	0.14	0.07	0.19
MnO	0.00	0.01	0.00	0.00	0.03	0.01	0.00	0.00	0.02
MgO	0.00	0.00	0.00	0.01	0.02	0.00	0.01	0.00	0.01
CaO	3.98	3.45	4.21	5.31	5.25	4.59	3.78	2.20	4.60
Na_2O	8.47	9.12	8.44	8.82	8.95	8.50	9.67	9.19	8.49
K_2O	0.50	0.23	0.46	0.22	0.24	0.06	0.12	0.93	0.05
P_2O_5	0.02	0.01	0.02	0.01	0.00	0.02	0.04	0.00	0.00
Total	99.48	100.36	99.28	101.82	101.47	99.70	102.42	99.92	99.09
Or%	3	1	3	1	1	0	1	6	0
An%	20	17	21	25	24	23	18	11	23
Ab%	77	82	76	74	75	77	82	83	77

Amphibole

Location	Rubinberg				Klatschmühle			
Sample	RUB 6	RUB 6	RUB 11	RUB 11	KLA2-2	KLA 2-2	KLA	KLA
wt%								
SiO_2	40.65	40.73	40.85	40.99	41.29	41.72	43.98	43.98
TiO_2	0.58	0.59	3.07	3.09	1.93	1.64	2.09	2.09
Al_2O_3	18.36	18.52	14.01	14.05	16.11	15.60	16.03	16.03
FeO	9.60	9.77	12.69	12.27	10.89	10.00	5.72	5.72
MnO	0.11	0.11	0.11	0.08	0.11	0.08	0.04	0.04
MgO	13.85	13.91	12.05	12.06	13.02	13.74	15.92	15.92
CaO	11.26	11.19	10.78	11.17	10.28	10.99	11.24	11.24
Na_2O	3.40	3.45	2.79	2.79	3.32	3.19	3.05	3.05
K_2O	0.01	0.01	1.31	1.07	0.36	0.33	1.15	1.15
P_2O_5								
Total	97.82	98.28	97.66	97.56	97.33	97.29	99.21	99.21
Mg#	0.72	0.72	0.63	0.64	0.68	0.71	0.67	0.83
Calculation scheme	∑13	∑13	∑13	∑13	∑13	∑13	∑13	∑13
Amphibole group	Ca	Ca	Ca	Ca	Ca	Ca	Ca	Ca
(Ca+Na) (B)	2.00	2.00	2.00	2.00	2.00	2.00	2.00	2.00
Na (B)	0.29	0.31	0.30	0.24	0.42	0.31	0.32	0.32
(Na+K) (A)	0.65	0.64	0.74	0.76	0.57	0.64	0.71	0.71
Mg/(Mg+Fe2)	0.92	0.93	0.70	0.68	0.85	0.84	0.88	0.88
Fe3/(Fe3+Alvi)	0.51	0.53	0.49	0.35	0.55	0.50	0.22	0.22
Sum of S2	13.00	13.00	13.00	13.00	13.00	13.00	13.00	13.00
	Mg-hastingsite	Mg-hastigsite	Ti-pargasite	Ti-ferroan pargasite	Mg-hastingsite	Mg-hastigsite	Pargasite	Pargasite

Phlogopite

Location	Rubinberg			Klatschmühle		
Sample	4-4.1	3.1 b	3.1 b	KLA	KLA	KLA
wt%						
SiO_2	36.36	35.66	35.70	39.31	39.40	38.31
TiO_2	3.20	3.37	1.51	4.04	4.07	3.47
Al_2O_3	16.05	16.08	17.12	15.34	15.51	16.66
FeO	13.75	11.64	11.51	5.89	6.20	6.14
MnO	0.02	0.05	0.04	0.00	0.02	0.00
MgO	14.97	15.23	17.59	20.42	20.10	20.11
CaO	0.00	0.16	0.07	0.00	0.00	0.01
Na_2O	0.46	0.29	0.29	0.84	0.62	0.57
K_2O	8.99	8.94	8.52	8.78	9.31	9.25
Total	93.79	91.43	92.36	94.61	95.24	94.51
XMg	0.66	0.70	0.73	0.86	0.85	0.85
XFe	0.34	0.30	0.27	0.14	0.15	0.15

Table S 4.7. Major element analyses of selected plagioclase, amphibole and biotite.

Trace element

Rubinberg

ppm																								
Rb	396	259	452	57	548	285	215	221	194	190	224	296	494	422	319	441	453	669	780	613	612	552	356	314
Cs	36	21	35	21	33	23	16	18	11	12	12	21	45	62	21	43	38	62	40	26	33	33	12	16
Ba	440	258	902	657	850	551	519	247	383	424	375	451	581	484	599	685	481	480	1042	1353	821	232	1082	300
Th	46	34	95	113	60	17	91	34	28	293	151	358	151	160	175	358	105	5.26	47	45	166	305	245	3.52
U	15	16	32	19	10	26	25	24	27	41	32	46	64	13	45	33	29	5.19	13	17	31	29	25	3.04
Nb	1.92	b.d.l.	1.75	2.89	b.d.l.	b.d.l.	2.04	b.d.l.	b.d.l.	2.38	1.86	2.40	1.76	2.64	2.43	2.88	1.64	b.d.l.	3.99	6.30	1.32	b.d.l.	4.40	1.44
Ta	b.d.l.	b.d.l.	0.41	0.22	b.d.l.	b.d.l.	b.d.l.	b.d.l.	b.d.l.	b.d.l.	b.d.l.	b.d.l.	0.36	b.d.l.	0.40	0.54	b.d.l.	b.d.l.	b.d.l.	b.d.l.	b.d.l.	b.d.l.	b.d.l.	b.d.l.
La	11	2.53	65	35	11	4.87	12	6.28	4.35	42	16	29	54	25	46	43	18	16	16	16	49	50	58	11
Ce	19	7.60	92	51	17	7.42	22	7.54	9.74	65	24	55	75	51	71	76	33	19	26	21	80	85	102	22
Pb	28	18	44	62	36	67	34	63	98	111	73	41	58	7.83	70	100	75	b.d.l.	42	44	57	59	152	46
Pr	2.05	2.12	7.67	3.07	5.56	b.d.l.	1.86	b.d.l.	1.42	2.80	0.85	5.86	4.55	3.59	5.66	5.75	4.08	4.12	b.d.l.	b.d.l.	4.92	6.99	5.98	b.d.l.
P	b.d.l.	b.d.l.	2438	463	b.d.l.	b.d.l.	562	368	704	787	663	b.d.l.	330	b.d.l.	744	1262	b.d.l.	360	b.d.l.	b.d.l.	813	2208	1179	b.d.l.
Sr	48	41	83	261	44	70	80	48	40	63	60	82	65	63	87	86	65	39	115	99	107	24	90	72
Nd	5.41	18	10	4.27	19	b.d.l.	7.46	b.d.l.	4.19	11	4.41	12	4.30	5.39	12	12	8.05	9.58	23	b.d.l.	15	12	14	5.01
Zr	20	57	42	66	26	50	62	42	64	68	76	59	87	48	65	76	36	65	85	43	77	b.d.l.	23	6.83
Hf	b.d.l.	b.d.l.	0.98	3.14	11	3.91	2.83	b.d.l.	b.d.l.	1.92	3.63	1.56	2.38	b.d.l.	2.53	2.38	1.65	b.d.l.	3.55	4.64	4.08	b.d.l.	3.07	b.d.l.
Sm	b.d.l.	b.d.l.	b.d.l.	b.d.l.	b.d.l.	b.d.l.	b.d.l.	b.d.l.	4.48	b.d.l.	b.d.l.	b.d.l.	2.27	b.d.l.	0.47	b.d.l.	4.81	8.02	b.d.l.	b.d.l.	b.d.l.	b.d.l.	b.d.l.	b.d.l.
Eu	b.d.l.	b.d.l.	b.d.l.	0.38	b.d.l.	b.d.l.	b.d.l.	b.d.l.	b.d.l.	b.d.l.	b.d.l.	b.d.l.	b.d.l.	b.d.l.	0.60	b.d.l.	4.89	1.98	13	b.d.l.	b.d.l.	b.d.l.	b.d.l.	b.d.l.
Gd	b.d.l.	b.d.l.	b.d.l.	b.d.l.	b.d.l.	b.d.l.	b.d.l.	b.d.l.	b.d.l.	b.d.l.	n.d.	n.d.	n.d.	n.d.	n.d.	n.d.	n.d.	n.d.	n.d.	n.d.	n.d.	n.d.	n.d.	n.d.
Tb	n.d.	n.d.	n.d.	n.d.	n.d.	n.d.	n.d.	n.d.	n.d.	n.d.	n.d.	n.d.	n.d.	n.d.	n.d.	n.d.	n.d.	n.d.	n.d.	n.d.	n.d.	n.d.	n.d.	n.d.
Dy	n.d.	n.d.	n.d.	n.d.	n.d.	n.d.	n.d.	n.d.	n.d.	n.d.	n.d.	n.d.	n.d.	n.d.	n.d.	n.d.	n.d.	n.d.	n.d.	n.d.	n.d.	n.d.	n.d.	n.d.
Ti	b.d.l.	2347	220	2509	b.d.l.	b.d.l.	1448	543	896	2712	2313	3469	1339	b.d.l.	2315	2704	4853	871	4841	b.d.l.	3304	b.d.l.	141	b.d.l.
Y	n.d.	n.d.	n.d.	n.d.	n.d.	n.d.	n.d.	n.d.	n.d.	n.d.	n.d.	n.d.	n.d.	n.d.	n.d.	n.d.	n.d.	n.d.	n.d.	n.d.	n.d.	n.d.	n.d.	n.d.
Ho	n.d.	n.d.	n.d.	n.d.	n.d.	n.d.	n.d.	n.d.	n.d.	n.d.	n.d.	n.d.	n.d.	n.d.	n.d.	n.d.	n.d.	n.d.	n.d.	n.d.	n.d.	n.d.	n.d.	n.d.
Er	n.d.	n.d.	n.d.	n.d.	n.d.	n.d.	n.d.	n.d.	n.d.	n.d.	n.d.	n.d.	n.d.	n.d.	n.d.	n.d.	n.d.	n.d.	n.d.	n.d.	n.d.	n.d.	n.d.	n.d.
Tm	n.d.	n.d.	n.d.	n.d.	n.d.	n.d.	n.d.	n.d.	n.d.	n.d.	n.d.	n.d.	n.d.	n.d.	n.d.	n.d.	n.d.	n.d.	n.d.	n.d.	n.d.	n.d.	n.d.	n.d.
Yb	n.d.	n.d.	n.d.	n.d.	n.d.	n.d.	n.d.	n.d.	n.d.	n.d.	n.d.	n.d.	n.d.	n.d.	n.d.	n.d.	n.d.	n.d.	n.d.	n.d.	n.d.	n.d.	n.d.	n.d.
Lu	n.d.	n.d.	n.d.	n.d.	n.d.	n.d.	n.d.	n.d.	n.d.	n.d.	n.d.	n.d.	n.d.	n.d.	n.d.	n.d.	n.d.	n.d.	n.d.	n.d.	n.d.	n.d.	n.d.	n.d.
Li	b.d.l.	b.d.l.	b.d.l.	19	b.d.l.	32	43	32	28	b.d.l.	b.d.l.	19	b.d.l.	340	20	32	29	b.d.l.	72	82	20	b.d.l.	38	80
B	66	b.d.l.	69	19	b.d.l.	74	49	64	62	45	44	66	85	b.d.l.	76	78	59	64	b.d.l.	85	112	78	113	b.d.l.

Detection limits

Rubinberg

ppm																								
Rb	3.37	5.70	1.28	4.26	22	3.44	3.08	6.19	3.35	4.23	4.39	3.01	1.95	3.87	0.68	1.24	4.43	4.74	11	6.91	3.08	4.84	5.36	6.62
Cs	2.05	3.53	0.89	2.27	12	2.16	1.80	3.03	1.84	2.07	2.50	1.52	1.09	2.45	0.37	0.65	2.24	2.60	6.56	3.81	1.49	2.61	3.06	3.61
Ba	21	44	9.93	20	62	16	13	23	14	17	20	14	10	20	2.62	6.34	23	21	53	34	12	19	14	30
Th	0.54	0.80	0.20	0.35	2.49	0.23	0.24	0.60	0.39	0.38	0.54	0.25	0.29	0.34	0.07	0.13	0.82	0.79	1.33	0.66	0.39	0.60	0.61	0.64
U	0.51	1.06	0.21	0.59	2.07	0.37	0.42	0.82	0.37	0.56	0.52	0.33	0.24	0.43	0.09	0.15	0.75	0.70	1.49	1.00	0.36	0.38	0.71	0.77
Nb	1.27	2.08	0.49	0.85	5.53	1.12	0.81	1.23	0.85	1.02	1.19	0.73	0.90	1.52	0.20	0.27	1.37	1.48	1.95	1.50	0.95	1.17	0.87	0.93
Ta	0.59	1.08	0.26	0.64	2.62	0.44	0.43	0.66	0.42	0.60	0.81	0.56	0.28	0.49	0.10	0.19	0.79	0.90	1.60	1.41	0.52	0.90	0.87	0.86
La	1.42	2.48	0.60	1.38	5.77	0.89	0.95	1.52	0.70	1.03	1.28	0.85	0.61	1.06	0.16	0.39	1.26	1.20	3.72	2.25	0.81	1.48	1.42	1.90
Ce	1.69	3.22	0.76	1.53	5.17	0.96	0.93	1.67	0.86	1.16	1.44	0.85	0.70	1.41	0.19	0.38	1.61	1.57	3.92	2.32	0.92	1.40	1.32	2.05
Pb	1.49	3.94	0.71	1.83	12	2.31	2.00	3.09	1.77	2.46	2.75	1.78	1.56	2.52	0.55	0.61	3.28	4.35	8.22	5.24	1.68	2.38	3.12	4.15
Pr	0.74	1.53	0.35	0.59	2.34	0.67	0.61	0.87	0.44	0.55	0.84	0.49	0.43	0.86	0.10	0.19	0.79	0.99	2.58	1.63	0.52	0.92	0.69	1.12
P	159	325	83	114	766	168	142	248	146	179	204	137	120	230	34	68	257	322	444	278	111	225	255	304
Sr	5.79	11	2.43	5.89	20	4.03	3.77	6.52	3.35	4.72	5.07	3.29	2.79	4.46	0.78	1.49	5.38	6.98	13	10	3.26	5.88	6.41	7.42
Nd	3.60	5.44	1.38	4.34	16	3.31	2.68	4.98	2.70	2.69	3.64	2.50	1.89	4.51	0.48	0.92	4.02	4.39	10	6.70	2.63	3.10	5.44	4.19
Zr	5.06	10	1.86	3.53	20	3.32	3.00	5.45	2.72	3.82	4.37	2.98	1.85	4.28	0.69	1.28	4.56	4.69	12	8.68	2.84	4.22	5.50	6.59
Hf	2.03	1.85	0.87	0.93	7.77	0.85	1.24	1.52	0.75	1.44	2.49	1.35	0.58	1.90	0.17	0.31	1.64	3.10	3.41	3.42	0.94	1.19	1.60	1.70
Sm	3.47	5.64	1.21	3.13	12	1.85	1.98	4.84	1.62	4.04	4.37	2.02	1.25	2.72	0.37	0.67	3.47	3.27	7.77	9.14	2.04	4.02	5.09	5.35
Eu	1.87	2.87	0.77	1.43	7.50	1.26	1.47	2.23	1.22	1.55	1.86	0.98	0.61	1.39	0.23	0.52	1.92	1.77	3.96	3.56	1.27	2.13	2.01	2.33
Gd	6.22	10	2.38	6.18	29	5.01	4.48	9.23	3.14	4.62	n.d.	n.d.	n.d.	n.d.	n.d.	n.d.	n.d.	n.d.	n.d.	n.d.	n.d.	n.d.	n.d.	n.d.
Tb	n.d.	n.d.	n.d.	n.d.	n.d.	n.d.	n.d.	n.d.	n.d.	n.d.	n.d.	n.d.	n.d.	n.d.	n.d.	n.d.	n.d.	n.d.	n.d.	n.d.	n.d.	n.d.	n.d.	n.d.
Dy	n.d.	n.d.	n.d.	n.d.	n.d.	n.d.	n.d.	n.d.	n.d.	n.d.	n.d.	n.d.	n.d.	n.d.	n.d.	n.d.	n.d.	n.d.	n.d.	n.d.	n.d.	n.d.	n.d.	n.d.
Ti	59	122	25	54	229	52	49	61	38	60	80	45	33	76	11	16	69	86	196	130	47	75	76	89
Y	n.d.	n.d.	n.d.	n.d.	n.d.	n.d.	n.d.	n.d.	n.d.	n.d.	n.d.	n.d.	n.d.	n.d.	n.d.	n.d.	n.d.	n.d.	n.d.	n.d.	n.d.	n.d.	n.d.	n.d.
Ho	n.d.	n.d.	n.d.	n.d.	n.d.	n.d.	n.d.	n.d.	n.d.	n.d.	n.d.	n.d.	n.d.	n.d.	n.d.	n.d.	n.d.	n.d.	n.d.	n.d.	n.d.	n.d.	n.d.	n.d.
Er	n.d.	n.d.	n.d.	n.d.	n.d.	n.d.	n.d.	n.d.	n.d.	n.d.	n.d.	n.d.	n.d.	n.d.	n.d.	n.d.	n.d.	n.d.	n.d.	n.d.	n.d.	n.d.	n.d.	n.d.
Tm	n.d.	n.d.	n.d.	n.d.	n.d.	n.d.	n.d.	n.d.	n.d.	n.d.	n.d.	n.d.	n.d.	n.d.	n.d.	n.d.	n.d.	n.d.	n.d.	n.d.	n.d.	n.d.	n.d.	n.d.
Yb	n.d.	n.d.	n.d.	n.d.	n.d.	n.d.	n.d.	n.d.	n.d.	n.d.	n.d.	n.d.	n.d.	n.d.	n.d.	n.d.	n.d.	n.d.	n.d.	n.d.	n.d.	n.d.	n.d.	n.d.
Lu	n.d.	n.d.	n.d.	n.d.	n.d.	n.d.	n.d.	n.d.	n.d.	n.d.	n.d.	n.d.	n.d.	n.d.	n.d.	n.d.	n.d.	n.d.	n.d.	n.d.	n.d.	n.d.	n.d.	n.d.
Li	34	62	14	43	104	18	17	30	17	20	24	16	12	24	3.72	7.36	25	29	70	44	17	31	34	36
B	34	72	16	44	152	32	28	47	28	32	38	25	20	35	5.38	10	38	45	117	76	23	42	45	55

Table S 4.8. Trace element compositions with the detection limits of the Rubinberg melt inclusions.

Trace element

Klatschmühle

ppm																								
Rb	303	191	562	309	286	142	851	588	600	418	339	380	318	390	201	196	734	477	372	257	409	508	222	494
Cs	24	59	44	25	17	19	93	51	55	20	23	46	25	23	21	20	61	31	20	16	44	73	32	45
Ba	569	412	752	582	130	369	370	94	236	96	1358	284	224	367	374	162	132	212	220	176	200	116	338	395
Th	91	62	175	46	11	27	58	2.86	30	63	18	39	60	78	30	24	35	19	46	22	28	26	49	34
U	29	21	74	19	b.d.l.	17	23	3.66	11	20	10	11	20	32	13	7.50	15	6.54	16	6.32	13	7.67	15	15
Nb	6.94	4.73	19	2.95	2.58	5.29	4.64	1.82	3.08	5.90	4.25	4.77	5.57	9.18	4.77	2.15	2.44	3.51	3.61	2.09	3.14	2.24	3.59	3.26
Ta	b.d.l.	0.71	1.95	0.55	b.d.l.	0.47	0.79	b.d.l.	0.95	1.13	0.58	0.64	0.77	0.87	0.47	0.39	b.d.l.	0.81	0.78	0.89	0.53	0.50	0.46	0.57
La	25	15	43	11	7.01	8.68	14	3.37	11	19	5.14	9.19	17	32	9.88	5.77	15	6.26	14	10	7.91	7.53	16	8.48
Ce	58	32	99	21	14	20	30	7.77	33	42	12	16	32	57	23	17	46	15	35	29	21	16	34	18
Pb	51	44	95	74	26	64	45	18	20	76	13	30	21	65	33	16	26	16	15	22	29	20	35	42
Pr	8.85	4.31	12	2.28	b.d.l.	2.61	4.28	b.d.l.	4.37	5.44	1.19	2.74	3.64	5.01	2.54	1.81	6.13	1.62	4.65	3.77	2.17	1.33	3.90	2.74
P	376	409	b.d.l.	775	316	1463	b.d.l.	653	374	1229	132	b.d.l.	277.65	b.d.l.	162	504	399	b.d.l.	801	b.d.l.	534	478	629	398
Sr	169	87	201	129	42	96	87	35	60	42	1784	86	96	125	109	47	b.d.l.	408	34	53	b.d.l.	31	154	104
Nd	17	17	34	9.51	6.07	12	13	b.d.l.	14	20	3.67	5.86	14	12	4.18	4.84	20	b.d.l.	18	7.23	6.47	5.37	12	9.72
Zr	368	251	592	186	35	126	286	151	274	378	141	260	288	401	164	126	224	119	282	224	154	125	178	199
Hf	9.68	5.96	14	6.09	2.66	1.94	6.77	4.02	6.03	7.21	3.08	5.55	7.14	9.85	3.52	3.14	7.74	3.12	9.07	6.22	5.44	2.76	6.16	5.82
Sm	b.d.l.	b.d.l.	16	2.95	b.d.l.	7.53	2.39	b.d.l.	b.d.l.	4.43	b.d.l.	b.d.l.	b.d.l.	b.d.l.	1.86	b.d.l.	b.d.l.	2.18	2.39	b.d.l.	b.d.l.	b.d.l.	1.27	b.d.l.
Eu	b.d.l.	1.03	2.86	b.d.l.	b.d.l.	b.d.l.	b.d.l.	b.d.l.	b.d.l.	4.21	b.d.l.	b.d.l.	b.d.l.	b.d.l.	b.d.l.	b.d.l.	b.d.l.	b.d.l.	b.d.l.	b.d.l.	b.d.l.	b.d.l.	0.50	b.d.l.
Gd	n.d.	n.d.	n.d.	n.d.	n.d.	n.d.	n.d.	n.d.	n.d.	n.d.	n.d.	n.d.	n.d.	n.d.	n.d.	n.d.	n.d.	n.d.	n.d.	n.d.	n.d.	n.d.	n.d.	n.d.
Tb	n.d.	n.d.	n.d.	n.d.	n.d.	n.d.	n.d.	n.d.	n.d.	n.d.	n.d.	n.d.	n.d.	n.d.	n.d.	n.d.	n.d.	n.d.	n.d.	n.d.	n.d.	n.d.	n.d.	n.d.
Dy	n.d.	n.d.	n.d.	n.d.	n.d.	n.d.	n.d.	n.d.	n.d.	n.d.	n.d.	n.d.	n.d.	n.d.	n.d.	n.d.	n.d.	n.d.	n.d.	n.d.	n.d.	n.d.	n.d.	n.d.
Ti	4370	1933	6122	1211	599	2556	2067	1262	1838	1141	2255	1164	2190	3374	2220	1236	761	1236	1735	749	1501	1173	1627	2524
Y	n.d.	n.d.	n.d.	n.d.	n.d.	n.d.	n.d.	n.d.	n.d.	n.d.	n.d.	n.d.	n.d.	n.d.	n.d.	n.d.	n.d.	n.d.	n.d.	n.d.	n.d.	n.d.	n.d.	n.d.
Ho	n.d.	n.d.	n.d.	n.d.	n.d.	n.d.	n.d.	n.d.	n.d.	n.d.	n.d.	n.d.	n.d.	n.d.	n.d.	n.d.	n.d.	n.d.	n.d.	n.d.	n.d.	n.d.	n.d.	n.d.
Er	n.d.	n.d.	n.d.	n.d.	n.d.	n.d.	n.d.	n.d.	n.d.	n.d.	n.d.	n.d.	n.d.	n.d.	n.d.	n.d.	n.d.	n.d.	n.d.	n.d.	n.d.	n.d.	n.d.	n.d.
Tm	n.d.	n.d.	n.d.	n.d.	n.d.	n.d.	n.d.	n.d.	n.d.	n.d.	n.d.	n.d.	n.d.	n.d.	n.d.	n.d.	n.d.	n.d.	n.d.	n.d.	n.d.	n.d.	n.d.	n.d.
Yb	n.d.	n.d.	n.d.	n.d.	n.d.	n.d.	n.d.	n.d.	n.d.	n.d.	n.d.	n.d.	n.d.	n.d.	n.d.	n.d.	n.d.	n.d.	n.d.	n.d.	n.d.	n.d.	n.d.	n.d.
Lu	n.d.	n.d.	n.d.	n.d.	n.d.	n.d.	n.d.	n.d.	n.d.	n.d.	n.d.	n.d.	n.d.	n.d.	n.d.	n.d.	n.d.	n.d.	n.d.	n.d.	n.d.	n.d.	n.d.	n.d.
Li	b.d.l.	b.d.l.	34	30	b.d.l.	b.d.l.	12	b.d.l.	25	b.d.l.	46	b.d.l.	9.98	b.d.l.	25	b.d.l.	b.d.l.	225	b.d.l.	b.d.l.	b.d.l.	45	28	b.d.l.
B	b.d.l.	b.d.l.	51	55	45	42	42	53	54	b.d.l.	b.d.l.	b.d.l.	24	39	23	b.d.l.	b.d.l.	87	b.d.l.	b.d.l.	27	b.d.l.	25	b.d.l.

Detection limits

Klatschmühle

ppm																								
Rb	5.85	1.39	2.75	1.30	2.29	1.42	1.40	2.98	2.57	4.07	0.85	2.64	1.00	2.48	1.06	0.85	5.88	8.47	3.88	2.95	1.81	1.46	0.84	2.39
Cs	3.63	0.77	1.52	0.83	1.98	1.26	0.83	2.21	1.55	2.41	0.38	1.19	0.51	1.63	0.45	0.56	3.12	5.09	2.10	2.23	0.87	1.01	0.44	1.30
Ba	44	13	17	12	29	18	15	35	26	43	8.39	22.85	9.39	30.15	9.59	13	22	33	14	14	8.60	11	5.06	17
Th	0.65	0.15	0.15	0.12	0.23	0.20	0.30	0.49	0.25	0.65	0.05	0.16	0.09	0.23	0.11	0.09	0.32	0.19	0.28	0.17	0.08	0.16	0.10	0.28
U	1.09	0.27	0.47	0.26	0.84	0.44	0.35	0.84	0.67	1.00	0.22	0.53	0.20	0.68	0.21	0.32	0.42	0.54	0.28	0.36	0.16	0.23	0.12	0.39
Nb	1.78	0.42	0.93	0.32	0.58	0.62	0.25	1.24	0.93	1.26	0.27	0.41	0.22	0.59	0.33	0.48	1.07	0.93	0.88	0.83	0.39	0.44	0.24	0.71
Ta	1.09	0.26	0.34	0.14	0.54	0.34	0.34	0.74	0.52	1.02	0.12	0.48	0.17	0.67	0.18	0.29	0.56	0.73	0.43	0.34	0.19	0.24	0.12	0.37
La	2.46	0.76	1.05	0.69	1.66	0.97	0.77	2.02	1.46	2.47	0.43	1.43	0.47	1.79	0.49	0.74	1.00	1.74	0.83	0.81	0.53	0.50	0.25	0.83
Ce	2.97	0.87	1.14	0.96	2.31	1.29	1.02	2.19	1.79	2.90	0.59	1.35	0.58	2.00	0.60	0.87	1.12	1.78	0.98	0.95	0.51	0.57	0.28	1.05
Pb	4.24	0.92	1.49	1.23	2.36	1.94	1.06	2.44	2.22	3.35	0.73	2.41	0.65	2.34	0.71	0.95	2.26	2.83	1.33	1.11	0.72	0.74	0.50	1.50
Pr	1.47	0.38	0.57	0.35	1.05	0.68	0.46	1.19	0.76	1.15	0.20	0.76	0.24	0.75	0.31	0.41	0.67	0.92	0.50	0.47	0.24	0.33	0.13	0.56
P	180	60	78	53	122	83	61	138	108	180	35	100	36	125	37	56	100	164	77	71	44	48	25	79
Sr	9.85	2.81	4.39	3.02	7.26	3.95	3.40	7.84	5.72	9.49	1.81	5.23	2.02	6.48	1.97	3.03	4.26	7.34	3.47	3.31	2.04	2.47	1.22	3.68
Nd	6.44	1.86	3.00	1.50	4.43	2.34	1.73	5.99	4.38	5.56	0.92	3.19	1.08	4.34	1.25	1.96	3.37	5.01	2.02	2.62	1.37	1.37	0.71	2.68
Zr	6.63	1.76	3.09	1.69	4.67	2.82	1.74	4.89	3.36	6.53	1.24	2.47	1.14	4.35	1.30	1.74	3.47	5.20	2.87	2.85	1.40	1.75	0.98	2.83
Hf	2.01	0.87	1.42	0.63	2.14	1.04	0.73	2.09	1.08	2.12	0.56	1.17	0.19	0.99	0.30	0.41	0.94	1.53	0.68	0.74	0.67	0.76	0.16	1.07
Sm	4.60	1.76	1.52	1.23	2.26	1.10	0.99	4.87	2.51	2.83	0.49	2.73	0.44	2.30	0.96	1.72	2.85	1.83	2.12	2.20	0.76	1.61	0.74	2.60
Eu	2.08	0.85	1.19	0.58	1.64	1.10	0.89	2.10	1.96	2.88	0.35	1.14	0.43	1.76	0.47	0.76	1.61	1.84	0.85	1.00	0.37	0.77	0.33	1.15
Gd	n.d.	n.d.	n.d.	n.d.	n.d.	n.d.	n.d.	n.d.	n.d.	n.d.	n.d.	n.d.	n.d.	n.d.	n.d.	n.d.	n.d.	n.d.	n.d.	n.d.	n.d.	n.d.	n.d.	n.d.
Tb	n.d.	n.d.	n.d.	n.d.	n.d.	n.d.	n.d.	n.d.	n.d.	n.d.	n.d.	n.d.	n.d.	n.d.	n.d.	n.d.	n.d.	n.d.	n.d.	n.d.	n.d.	n.d.	n.d.	n.d.
Dy	n.d.	n.d.	n.d.	n.d.	n.d.	n.d.	n.d.	n.d.	n.d.	n.d.	n.d.	n.d.	n.d.	n.d.	n.d.	n.d.	n.d.	n.d.	n.d.	n.d.	n.d.	n.d.	n.d.	n.d.
Ti	86	23	39	26	75	41	28	54	54	86	18	47	18	65	17	24	46	62	28	38	15	20	14	42
Y	n.d.	n.d.	n.d.	n.d.	n.d.	n.d.	n.d.	n.d.	n.d.	n.d.	n.d.	n.d.	n.d.	n.d.	n.d.	n.d.	n.d.	n.d.	n.d.	n.d.	n.d.	n.d.	n.d.	n.d.
Ho	n.d.	n.d.	n.d.	n.d.	n.d.	n.d.	n.d.	n.d.	n.d.	n.d.	n.d.	n.d.	n.d.	n.d.	n.d.	n.d.	n.d.	n.d.	n.d.	n.d.	n.d.	n.d.	n.d.	n.d.
Er	n.d.	n.d.	n.d.	n.d.	n.d.	n.d.	n.d.	n.d.	n.d.	n.d.	n.d.	n.d.	n.d.	n.d.	n.d.	n.d.	n.d.	n.d.	n.d.	n.d.	n.d.	n.d.	n.d.	n.d.
Tm	n.d.	n.d.	n.d.	n.d.	n.d.	n.d.	n.d.	n.d.	n.d.	n.d.	n.d.	n.d.	n.d.	n.d.	n.d.	n.d.	n.d.	n.d.	n.d.	n.d.	n.d.	n.d.	n.d.	n.d.
Yb	n.d.	n.d.	n.d.	n.d.	n.d.	n.d.	n.d.	n.d.	n.d.	n.d.	n.d.	n.d.	n.d.	n.d.	n.d.	n.d.	n.d.	n.d.	n.d.	n.d.	n.d.	n.d.	n.d.	n.d.
Lu	n.d.	n.d.	n.d.	n.d.	n.d.	n.d.	n.d.	n.d.	n.d.	n.d.	n.d.	n.d.	n.d.	n.d.	n.d.	n.d.	n.d.	n.d.	n.d.	n.d.	n.d.	n.d.	n.d.	n.d.
Li	38	11	19	14	28	17	10	30	22	38	7	18	7	24	7	11	46	71	32	28	14	17	9	26
B	56	14	25	16	41	24	17	47	35	53	10	29	10	32	10	18	46	72	33	29	17	20	11	27

Table S 4.9. Trace element compositions with the detection limits of the Rubinberg melt inclusions.

FIGURE

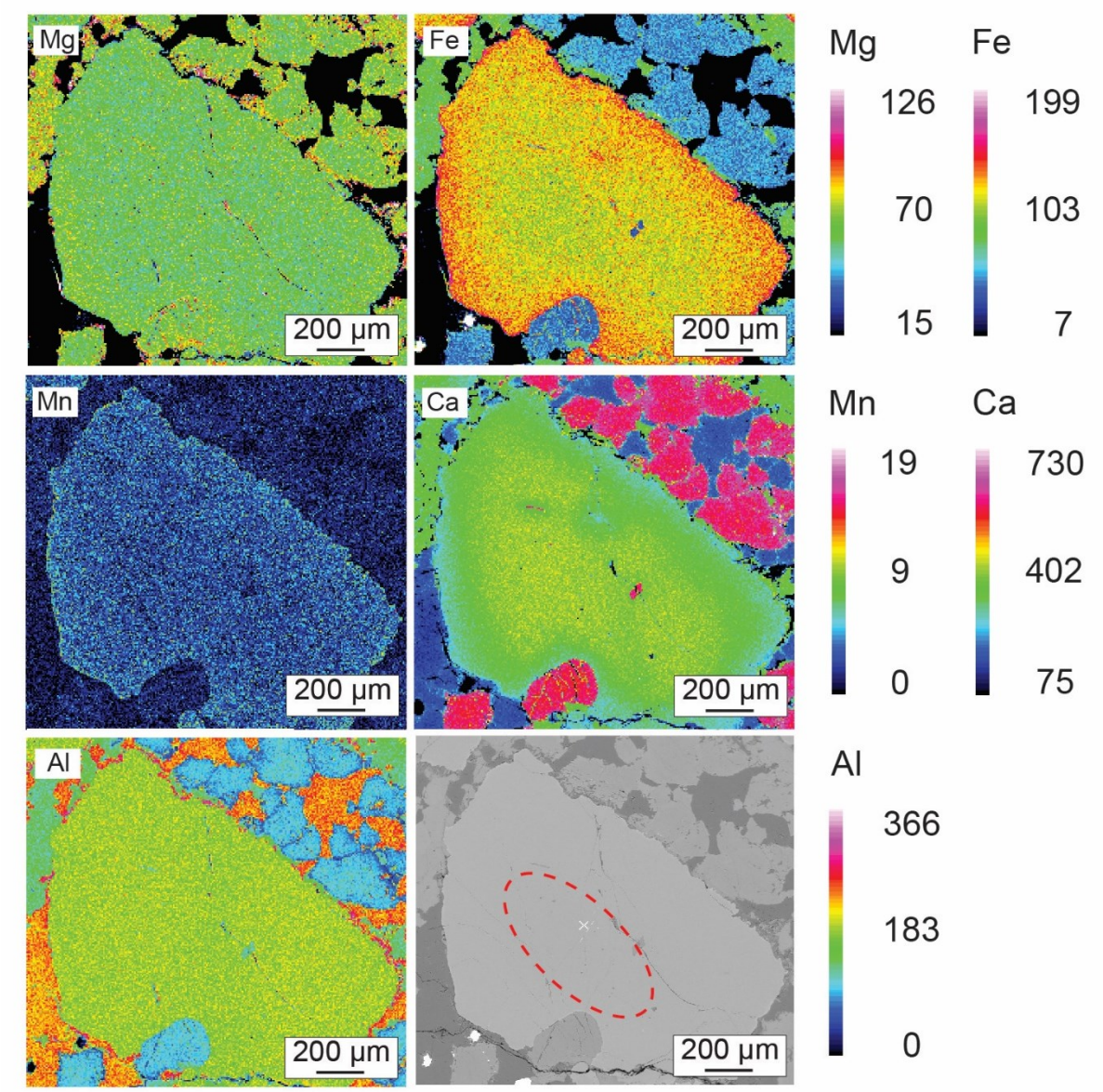

Figure S4.1. Compositional map of a garnet containing melt inclusions (red ellipse on the bottom right of the figure) of a sample from Rubinberg.

D. SUPPLEMENTARY MATERIAL CHAPTER 5

Garnet

					Profile 2												
Name	51	52	53	54	64	65	66	67	68	69	70	71	72	73	74	75	77
wt %																	
SiO_2	38.78	38.96	38.95	38.95	38.69	38.85	38.65	39.12	38.99	38.81	39.30	38.96	39.03	38.92	38.66	38.99	38.74
TiO_2	0.34	0.33	0.29	0.22	0.23	0.25	0.30	0.36	0.35	0.34	0.35	0.38	0.37	0.31	0.32	0.31	0.19
Al_2O_3	21.85	22.10	22.15	22.21	21.88	21.66	21.67	21.79	21.83	21.92	21.71	21.97	21.75	21.89	22.04	21.98	22.08
Fe_2O_3																	
FeO	19.48	19.40	19.80	20.09	20.13	20.04	19.66	19.26	19.37	19.44	19.50	19.56	19.07	19.22	19.29	19.51	20.21
MnO	0.35	0.30	0.36	0.40	0.36	0.36	0.35	0.33	0.36	0.31	0.34	0.34	0.34	0.37	0.33	0.38	0.39
MgO	8.00	7.88	7.93	8.00	7.99	7.91	7.96	7.82	7.94	8.00	7.95	7.93	7.99	8.15	7.89	8.09	8.02
CaO	10.09	10.02	9.93	9.46	9.42	9.49	9.72	10.06	10.08	10.03	10.10	10.02	10.02	10.09	10.03	9.87	9.01
Na_2O	0.09	0.13	0.13	0.10	0.06	0.06	0.07	0.06	0.12	0.12	0.09	0.10	0.12	0.08	0.11	0.10	0.07
K_2O	0.00	0.00	0.00	0.00	0.00	0.00	0.00	0.00	0.00	0.00	0.01	0.01	0.00	0.01	0.00	0.00	0.00
Cr_2O_3	0.02	0.03	0.01	0.00	0.03	0.04	0.00	0.00	0.01	0.02	0.00	0.05	0.00	0.00	0.01	0.01	0.03
P_2O_5																	
TOTAL	99.00	99.14	99.55	99.42	98.77	98.66	98.40	98.83	99.04	98.99	99.33	99.31	98.69	99.03	98.69	99.23	98.73
Mg#	**42**	**42**	**42**	**41**	**41**	**41**	**42**	**42**	**42**	**42**	**42**	**42**	**43**	**43**	**42**	**42**	**41**
Si	**2.98**	**2.99**	**2.98**	**2.98**	**2.98**	**3.00**	**2.99**	**3.01**	**2.99**	**2.98**	**3.01**	**2.99**	**3.00**	**2.99**	**2.98**	**2.99**	**2.99**
Ti	0.02	0.02	0.02	0.01	0.01	0.01	0.02	0.02	0.02	0.02	0.02	0.02	0.02	0.02	0.02	0.02	0.01
Al	1.98	2.00	2.00	2.01	1.99	1.97	1.98	1.97	1.98	1.99	1.96	1.99	1.97	1.98	2.00	1.99	2.01
	2.00	**2.02**	**2.01**	**2.02**	**2.00**	**1.99**	**1.99**	**1.99**	**2.00**	**2.01**	**1.98**	**2.01**	**1.99**	**2.00**	**2.02**	**2.00**	**2.02**
Fe	1.25	1.24	1.27	1.29	1.30	1.29	1.27	1.24	1.24	1.25	1.25	1.25	1.23	1.23	1.24	1.25	1.30
Mn	0.02	0.02	0.02	0.03	0.02	0.02	0.02	0.02	0.02	0.02	0.02	0.02	0.02	0.02	0.02	0.02	0.03
Mg	0.92	0.90	0.90	0.91	0.92	0.91	0.92	0.90	0.91	0.92	0.91	0.91	0.92	0.93	0.91	0.92	0.92
Ca	0.83	0.82	0.81	0.78	0.78	0.79	0.81	0.83	0.83	0.83	0.83	0.82	0.83	0.83	0.83	0.81	0.74
	3.03	**2.99**	**3.01**	**3.00**	**3.02**	**3.01**	**3.02**	**2.98**	**3.01**	**3.01**	**3.01**	**3.01**	**2.99**	**3.02**	**3.00**	**3.01**	**2.99**
mol %																	
Alm	**41**	**42**	**42**	**43**	**43**	**43**	**42**	**41**	**41**	**41**	**42**	**42**	**41**	**41**	**41**	**42**	**44**
Prp	**30**	**30**	**30**	**30**	**30**	**30**	**30**	**30**	**30**	**30**	**30**	**30**	**31**	**31**	**30**	**31**	**31**
Sps	**1**	**1**	**1**	**1**	**1**	**1**	**1**	**1**	**1**	**1**	**1**	**1**	**1**	**1**	**1**	**1**	**1**
Grs	**27**	**28**	**27**	**26**	**26**	**26**	**27**	**28**	**28**	**27**	**28**	**27**	**28**	**27**	**28**	**27**	**25**

Table S5.1. Major elements composition of garnets.

Garnet

						Profile 3									Profile 4								
Name	78	79	80	81	82	83	84	85	87	88	90	91	92	93	94	95	96	97	98
wt %																			
SiO_2	38.95	38.55	38.44	38.44	38.42	38.81	38.70	39.11	38.97	39.48	38.21	38.27	38.22	39.09	38.73	37.94	38.30	38.52	38.73
TiO_2	0.12	0.26	0.27	0.28	0.29	0.20	0.25	0.30	0.12	0.17	0.26	0.31	0.33	0.27	0.31	0.31	0.25	0.31	0.19
Al_2O_3	21.83	21.78	21.85	22.01	22.02	21.84	21.85	21.73	22.18	19.90	21.86	21.79	21.79	21.74	21.70	21.82	21.78	21.89	22.11
Fe_2O_3																			
FeO	20.82	20.40	20.05	19.78	20.11	20.15	20.25	20.01	21.18	22.80	20.77	20.69	20.52	20.49	20.26	20.68	20.78	20.83	21.12
MnO	0.38	0.40	0.40	0.42	0.41	0.39	0.36	0.34	0.40	0.42	0.40	0.37	0.36	0.40	0.34	0.38	0.42	0.38	0.39
MgO	7.70	7.65	7.79	7.75	7.74	7.70	7.67	7.58	7.58	6.71	7.11	7.09	7.01	7.02	6.97	6.96	7.00	7.12	7.19
CaO	8.90	9.57	9.65	9.80	9.75	9.68	9.79	9.92	8.89	8.60	9.71	10.00	10.16	10.16	10.24	10.14	9.88	9.64	9.41
Na_2O	0.08	0.06	0.08	0.09	0.07	0.12	0.08	0.10	0.09	0.11	0.10	0.10	0.13	0.09	0.15	0.08	0.07	0.10	0.07
K_2O	0.01	0.01	0.00	0.01	0.00	0.01	0.00	0.01	0.00	0.00	0.02	0.00	0.00	0.00	0.00	0.01	0.00	0.00	0.01
Cr_2O_3	0.00	0.02	0.00	0.03	0.04	0.05	0.01	0.00	0.07	0.00	0.00	0.01	0.00	0.00	0.02	0.00	0.00	0.05	0.02
P_2O_5																			
TOTAL	98.77	98.68	98.53	98.62	98.84	98.93	98.96	99.11	99.47	98.19	98.44	98.62	98.52	99.24	98.71	98.32	98.47	98.85	99.22
Mg#	**40**	**40**	**41**	**41**	**41**	**40**	**40**	**40**	**39**	**34**	**38**	**38**	**38**	**38**	**38**	**37**	**37**	**38**	**38**
Si	**3.01**	**2.98**	**2.98**	**2.97**	**2.97**	**2.99**	**2.99**	**3.01**	**2.99**	**3.10**	**2.97**	**2.97**	**2.97**	**3.01**	**3.00**	**2.96**	**2.98**	**2.98**	**2.99**
Ti	0.01	0.02	0.02	0.02	0.02	0.01	0.01	0.02	0.01	0.01	0.02	0.02	0.02	0.02	0.02	0.02	0.01	0.02	0.01
Al	1.99	1.99	1.99	2.01	2.00	1.99	1.99	1.97	2.01	1.84	2.01	2.00	2.00	1.97	1.98	2.01	2.00	2.00	2.01
	1.99	**2.00**	**2.01**	**2.02**	**2.02**	**2.00**	**2.00**	**1.99**	**2.02**	**1.85**	**2.02**	**2.01**	**2.02**	**1.99**	**2.00**	**2.03**	**2.01**	**2.02**	**2.02**
Fe	1.34	1.32	1.30	1.28	1.30	1.30	1.31	1.29	1.36	1.49	1.35	1.34	1.33	1.32	1.31	1.35	1.35	1.35	1.36
Mn	0.02	0.03	0.03	0.03	0.03	0.03	0.02	0.02	0.03	0.03	0.03	0.02	0.02	0.03	0.02	0.02	0.03	0.03	0.03
Mg	0.89	0.88	0.90	0.89	0.89	0.89	0.88	0.87	0.87	0.78	0.82	0.82	0.81	0.81	0.81	0.81	0.81	0.82	0.83
Ca	0.74	0.79	0.80	0.81	0.81	0.80	0.81	0.82	0.73	0.72	0.81	0.83	0.85	0.84	0.85	0.85	0.82	0.80	0.78
	2.99	**3.02**	**3.02**	**3.01**	**3.02**	**3.01**	**3.02**	**3.00**	**2.99**	**3.03**	**3.01**	**3.02**	**3.02**	**2.99**	**2.99**	**3.03**	**3.02**	**3.00**	**2.99**
mol %																			
Alm	**45**	**44**	**43**	**42**	**43**	**43**	**43**	**43**	**46**	**49**	**45**	**44**	**44**	**44**	**44**	**45**	**45**	**45**	**46**
Prp	**30**	**29**	**30**	**30**	**29**	**29**	**29**	**29**	**29**	**26**	**27**	**27**	**27**	**27**	**27**	**27**	**27**	**27**	**28**
Sps	**1**	**1**	**1**	**1**	**1**	**1**	**1**	**1**	**1**	**1**	**1**	**1**	**1**	**1**	**1**	**1**	**1**	**1**	**1**
Grs	**25**	**26**	**26**	**27**	**27**	**27**	**27**	**27**	**24**	**24**	**27**	**28**	**28**	**28**	**28**	**28**	**27**	**27**	**26**

Table S5.1. Continued.

Garnet

	Profile 5									Profile 6						
Name	99	100	101	102	103	105	106	107	108	109	110	111	113	114	115	116
wt %																
SiO_2	38.78	38.34	38.84	39.27	38.81	38.69	38.84	38.44	38.53	38.63	38.62	38.04	38.88	38.32	38.71	39.09
TiO_2	0.22	0.22	0.24	0.27	0.28	0.28	0.19	0.13	0.23	0.20	0.25	0.24	0.36	0.32	0.31	0.30
Al_2O_3	21.92	21.91	21.72	21.82	21.81	21.85	21.87	22.14	22.11	21.99	21.94	20.71	22.15	22.03	22.03	21.93
Fe_2O_3																
FeO	21.17	20.61	20.30	20.42	20.28	20.41	20.82	21.35	21.36	21.57	20.80	22.69	20.27	20.12	20.46	20.46
MnO	0.40	0.35	0.37	0.37	0.38	0.34	0.38	0.39	0.38	0.40	0.37	0.35	0.40	0.38	0.42	0.42
MgO	7.44	7.34	7.12	7.16	7.08	7.10	7.26	7.43	7.38	7.22	7.32	7.38	7.08	7.15	7.10	7.10
CaO	9.26	9.64	10.07	10.22	10.20	10.18	9.69	9.12	9.14	8.97	9.52	9.01	10.22	10.22	10.21	10.03
Na_2O	0.11	0.15	0.13	0.09	0.10	0.15	0.11	0.10	0.08	0.09	0.10	0.15	0.09	0.09	0.07	0.15
K_2O	0.00	0.00	0.01	0.00	0.00	0.00	0.00	0.00	0.01	0.00	0.00	0.04	0.00	0.00	0.01	0.00
Cr_2O_3	0.05	0.03	0.01	0.00	0.02	0.01	0.01	0.00	0.00	0.04	0.02	0.03	0.01	0.02	0.00	0.00
P_2O_5																
TOTAL	99.34	98.60	98.80	99.63	98.94	99.01	99.16	99.10	99.21	99.09	98.93	98.61	99.47	98.65	99.31	99.46
Mg#	**38**	**39**	**38**	**38**	**38**	**38**	**38**	**38**	**38**	**37**	**38**	**37**	**38**	**39**	**38**	**38**
Si	**2.99**	**2.98**	**3.00**	**3.01**	**3.00**	**2.99**	**3.00**	**2.97**	**2.97**	**2.99**	**2.99**	**2.98**	**2.99**	**2.97**	**2.98**	**3.00**
Ti	0.01	0.01	0.01	0.02	0.02	0.02	0.01	0.01	0.01	0.01	0.01	0.01	0.02	0.02	0.02	0.02
Al	1.99	2.00	1.98	1.97	1.99	1.99	1.99	2.02	2.01	2.00	2.00	1.91	2.01	2.01	2.00	1.99
	2.00	**2.02**	**1.99**	**1.99**	**2.00**	**2.01**	**2.00**	**2.02**	**2.02**	**2.02**	**2.01**	**1.93**	**2.03**	**2.03**	**2.02**	**2.00**
Fe	1.36	1.34	1.31	1.31	1.31	1.32	1.34	1.38	1.38	1.39	1.35	1.49	1.30	1.30	1.32	1.31
Mn	0.03	0.02	0.02	0.02	0.03	0.02	0.02	0.03	0.02	0.03	0.02	0.02	0.03	0.02	0.03	0.03
Mg	0.85	0.85	0.82	0.82	0.81	0.82	0.83	0.86	0.85	0.83	0.84	0.86	0.81	0.83	0.82	0.81
Ca	0.76	0.80	0.83	0.84	0.84	0.84	0.80	0.76	0.76	0.74	0.79	0.76	0.84	0.85	0.84	0.83
	3.01	**3.01**	**2.99**	**2.99**	**2.99**	**3.00**	**3.00**	**3.02**	**3.01**	**3.00**	**3.00**	**3.13**	**2.98**	**3.00**	**3.00**	**2.98**
mol %																
Alm	**45**	**44**	**44**	**44**	**44**	**44**	**45**	**46**	**46**	**47**	**45**	**48**	**44**	**43**	**44**	**44**
Prp	**28**	**28**	**27**	**27**	**27**	**27**	**28**	**28**	**28**	**28**	**28**	**28**	**27**	**27**	**27**	**27**
Sps	**1**	**1**	**1**	**1**	**1**	**1**	**1**	**1**	**1**	**1**	**1**	**1**	**1**	**1**	**1**	**1**
Grs	**25**	**27**	**28**	**28**	**28**	**28**	**27**	**25**	**25**	**25**	**26**	**24**	**28**	**28**	**28**	**28**

Table S5.1. Continued.

Clinopyroxene

	Profile 1							Profile 2												Cpx in symplectites	
Name	38	39	40	41	44	45	46	55	57	58	59	60	61	62	123	124	126	127	128	134	136
wt %																					
SiO_2	55.07	54.95	55.02	55.21	55.09	54.85	55.25	55.12	55.07	55.22	54.94	55.38	55.20	55.66	55.49	55.47	54.72	55.05	55.47	53.66	52.24
TiO_2	0.38	0.39	0.38	0.31	0.38	0.31	0.32	0.35	0.42	0.38	0.39	0.37	0.30	0.35	0.35	0.35	0.36	0.35	0.38	0.35	0.55
Al_2O_3	13.84	14.02	14.00	13.97	14.04	13.91	13.99	13.83	13.94	13.95	13.88	13.87	13.96	13.86	13.92	13.93	14.00	13.82	13.85	6.95	11.56
Fe_2O_3																					
FeO	3.91	4.25	4.28	4.04	4.13	3.82	3.70	3.73	4.44	4.37	4.27	4.21	3.97	3.81	3.97	3.89	3.96	3.92	3.78	4.50	4.34
MnO	0.04	0.04	0.03	0.03	0.05	0.06	0.04	0.02	0.03	0.05	0.04	0.03	0.05	0.03	0.03	0.01	0.05	0.02	0.03	0.04	0.02
MgO	7.58	7.42	7.34	7.40	7.41	7.56	7.68	7.56	7.26	7.30	7.33	7.31	7.49	7.48	7.61	7.45	7.45	7.48	7.59	12.21	9.78
CaO	12.52	12.50	12.46	12.55	12.39	12.76	12.95	12.73	12.39	12.47	12.56	12.61	12.56	12.63	12.79	12.70	12.54	12.70	12.81	19.60	17.35
Na_2O	6.52	6.64	6.49	6.48	6.80	6.79	6.81	6.62	6.57	6.48	6.74	6.55	6.68	6.65	6.56	6.67	6.75	6.82	6.65	2.93	4.15
K_2O	0.00	0.01	0.00	0.01	0.00	0.01	0.00	0.00	0.00	0.00	0.00	0.00	0.00	0.00	0.01	0.01	0.00	0.01	0.01	0.00	0.01
Cr_2O_3	0.09	0.08	0.06	0.05	0.02	0.04	0.05	0.03	0.05	0.01	0.03	0.07	0.06	0.07	0.06	0.06	0.09	0.06	0.04	0.06	0.04
P_2O_5																					
TOTAL	99.94	100.31	100.07	100.04	100.31	100.10	100.79	99.98	100.16	100.23	100.18	100.39	100.27	100.53	100.78	100.55	99.90	100.22	100.60	100.29	100.04
Mg#	**78**	**76**	**75**	**77**	**76**	**78**	**79**	**78**	**74**	**75**	**75**	**76**	**77**	**78**	**77**	**77**	**77**	**77**	**78**	**83**	**80**
Si	1.96	1.95	1.96	1.97	1.95	1.94	1.94	1.96	1.96	1.96	1.95	1.97	1.96	1.97	1.96	1.96	1.95	1.95	1.96	1.94	1.88
Ti	0.01	0.01	0.01	0.01	0.01	0.01	0.01	0.01	0.01	0.01	0.01	0.01	0.01	0.01	0.01	0.01	0.01	0.01	0.01	0.01	0.01
Al	0.58	0.59	0.59	0.59	0.59	0.58	0.58	0.58	0.58	0.59	0.58	0.58	0.58	0.58	0.58	0.58	0.59	0.58	0.58	0.30	0.49
Fe	0.12	0.13	0.13	0.12	0.12	0.11	0.11	0.11	0.13	0.13	0.13	0.13	0.12	0.11	0.12	0.12	0.12	0.12	0.11	0.14	0.13
Mn	0.00	0.00	0.00	0.00	0.00	0.00	0.00	0.00	0.00	0.00	0.00	0.00	0.00	0.00	0.00	0.00	0.00	0.00	0.00	0.00	0.00
Mg	0.40	0.39	0.39	0.39	0.39	0.40	0.40	0.40	0.39	0.39	0.39	0.39	0.40	0.39	0.40	0.39	0.39	0.40	0.40	0.66	0.52
Ca	0.48	0.48	0.48	0.48	0.47	0.48	0.49	0.48	0.47	0.48	0.48	0.48	0.48	0.48	0.48	0.48	0.48	0.48	0.48	0.76	0.67
Na	0.45	0.46	0.45	0.45	0.47	0.47	0.46	0.46	0.45	0.45	0.46	0.45	0.46	0.46	0.45	0.46	0.47	0.47	0.46	0.20	0.29
K	0.00	0.00	0.00	0.00	0.00	0.00	0.00	0.00	0.00	0.00	0.00	0.00	0.00	0.00	0.00	0.00	0.00	0.00	0.00	0.00	0.00
Cr	0.00	0.00	0.00	0.00	0.00	0.00	0.00	0.00	0.00	0.00	0.00	0.00	0.00	0.00	0.00	0.00	0.00	0.00	0.00	0.00	0.00
Jd	45	46	45	45	47	47	46	46	45	45	46	45	46	46	45	46	47	47	46	20	29

Table S5.2 Major element composition of clinopyroxenes

Garnet

Name ppm	1	2	3	4	5	6	7	8	9	10	11	12	13	14	15	16	17	18	19	20	21	22
Cr	2830	3571	3709	3727	3549	3492	3705	3542	3409	1569	1199	1250	1906	1969	1524	1353	1534	1675	1595	1503	1179	1167
Ni	89	142	150	148	106	116	119	122	143	35	226	78	47	62	38	b.d.l.	219	49	43	45	48	b.d.l.
Rb	b.d.l.	b.d.l.	b.d.l.	b.d.l.	0.67	b.d.l.	b.d.l.	b.d.l.	b.d.l.	b.d.l.	b.d.l.	b.d.l.	b.d.l.	b.d.l.	b.d.l.	b.d.l.	b.d.l.	b.d.l.	b.d.l.	b.d.l.	b.d.l.	1.53
Cs	b.d.l.	b.d.l.	b.d.l.	b.d.l.	b.d.l.	b.d.l.	b.d.l.	0.26	b.d.l.	b.d.l.	b.d.l.	b.d.l.	b.d.l.	b.d.l.	b.d.l.	b.d.l.	b.d.l.	b.d.l.	b.d.l.	b.d.l.	b.d.l.	0.85
Ba	b.d.l.	b.d.l.	b.d.l.	b.d.l.	b.d.l.	b.d.l.	b.d.l.	b.d.l.	0.85	b.d.l.	b.d.l.	b.d.l.	b.d.l.	b.d.l.	b.d.l.	b.d.l.	1.15	b.d.l.	b.d.l.	0.80	b.d.l.	1.98
Th	0.06	0.24	0.29	0.24	0.13	0.29	0.20	0.11	0.18	0.27	0.22	0.33	0.25	0.25	0.24	0.16	0.16	0.19	0.21	0.27	0.36	1.25
U	0.57	0.79	0.69	0.90	0.64	0.73	0.88	0.64	0.64	0.55	0.68	0.69	0.62	0.39	0.51	0.40	0.47	0.44	0.45	0.50	0.58	1.30
Nb	0.08	0.12	0.10	0.11	0.08	b.d.l.	b.d.l.	0.10	0.06	b.d.l.	0.07	0.11	b.d.l.	0.11	0.08	0.07	b.d.l.	b.d.l.	b.d.l.	b.d.l.	b.d.l.	b.d.l.
Ta	b.d.l.	b.d.l.	b.d.l.	b.d.l.	b.d.l.	b.d.l.	b.d.l.	b.d.l.	b.d.l.	b.d.l.	b.d.l.	b.d.l.	b.d.l.	b.d.l.	b.d.l.	b.d.l.	b.d.l.	b.d.l.	0.07	b.d.l.	b.d.l.	b.d.l.
La	0.42	0.83	1.02	1.22	0.34	0.63	0.83	0.60	0.55	0.76	2.96	0.68	0.82	0.90	1.10	0.55	2.66	0.81	0.91	0.94	1.01	1.53
Ce	6.57	12	15	13	8.08	7.34	12	8.62	10	13	18	14	14	13	17	11	16	10	15	14	17	17
Pb	b.d.l.	b.d.l.	b.d.l.	b.d.l.	b.d.l.	b.d.l.	b.d.l.	0.86	b.d.l.	b.d.l.	3.10	b.d.l.	b.d.l.	b.d.l.	b.d.l.	b.d.l.	8.88	7.05	b.d.l.	b.d.l.	b.d.l.	6.27
Pr	4.39	6.47	7.69	7.02	4.60	4.68	6.25	5.27	6.19	7.06	8.01	7.64	7.90	6.97	7.98	6.72	7.62	5.78	7.54	7.83	8.17	8.10
P	5275	7917	6033	5139	5892	6818	6190	7536	6892	7832	7529	8376	11268	11952	7808	7868	8009	12257	12509	8718	7885	7155
Sr	3.82	6.22	8.08	7.01	4.07	4.30	5.84	4.40	5.59	6.33	8.43	6.99	6.72	6.81	8.77	5.27	7.01	4.35	7.13	6.28	7.41	8.22
Nd	63	85	92	92	69	70	86	76	82	90	93	92	88	87	94	83	87	78	86	92	93	93
Zr	232	272	292	284	214	210	261	236	263	278	264	275	287	300	360	276	312	255	272	279	288	300
Hf	3.56	5.12	4.87	5.48	3.69	4.10	4.39	4.24	4.43	4.60	4.02	4.45	5.20	4.75	5.70	4.55	5.04	4.29	4.94	4.19	4.84	6.13
Sm	64	66	73	74	68	71	74	72	71	69	69	71	69	72	74	72	74	66	60	60	58	61
Eu	18	18	17	19	19	19	22	20	20	19	18	18	18	18	20	19	19	18	16	15	14	16
Gd	120	110	106	124	123	128	128	125	128	114	109	106	111	122	132	126	124	112	103	94	90	91
Tb	23	22	22	22	24	24	24	24	24	23	22	22	23	24	25	25	24	22	20	21	20	20
Dy	180	166	163	168	182	179	183	181	186	171	164	169	170	176	187	187	185	173	164	162	164	165
Ti	12635	18862	18639	17879	13544	13170	15389	14358	14005	19734	20573	22223	19373	17387	14771	12877	14618	17939	19619	23147	24936	22858
Y	1036	943	929	960	991	983	1011	983	1031	1007	996	1010	996	1024	1093	1090	1093	992	963	990	1036	1039
Ho	40	36	35	37	39	38	39	39	40	38	38	37	37	38	41	41	41	37	35	36	38	39
Er	114	105	103	108	114	111	114	112	120	113	116	116	112	114	122	122	124	112	110	113	124	126
Tm	16	15	14	15	15	15	16	16	17	16	16	17	15	16	17	17	17	16	15	17	18	19
Yb	105	97	96	97	101	101	106	103	111	106	111	110	106	111	113	115	118	106	105	112	125	127
Lu	16	15	15	15	15	15	16	16	16	17	18	18	17	17	18	18	18	16	17	18	20	20
Li	52	69	67	62	49	61	76	72	61	73	161	74	76	74	65	60	122	65	62	68	76	59
B	12	b.d.l.	b.d.l.	14	12	b.d.l.	b.d.l.	10	12	b.d.l.	15	b.d.l.	11	b.d.l.	b.d.l.	b.d.l.	13	18	b.d.l.	b.d.l.	b.d.l.	23

b.d.l= below detection limit

Table S5.3 Trace element composition of garnets.

Garnet

Name ppm	23	24	25	26	27	28	29	30	31	32	33	34	35	36	37	38	39	40	41	42	43	44
Cr	1175	1409	1549	1246	1263	1268	1282	1277	1256	1283	1223	1294	1165	1137	1256	1230	1730	1866	2115	2224	2309	2153
Ni	41	207	b.d.l.	b.d.l.	38	b.d.l.	43	33	57	38	b.d.l.	49	b.d.l.	b.d.l.	57	57	56	238	84	61	98	76
Rb	b.d.l.	b.d.l.	b.d.l.	b.d.l.	b.d.l.	b.d.l.	b.d.l.	b.d.l.	b.d.l.	b.d.l.	b.d.l.	b.d.l.	2.82	b.d.l.	b.d.l.	b.d.l.	b.d.l.	b.d.l.	b.d.l.	b.d.l.	b.d.l.	b.d.l.
Cs	b.d.l.	b.d.l.	b.d.l.	b.d.l.	b.d.l.	b.d.l.	b.d.l.	b.d.l.	b.d.l.	b.d.l.	b.d.l.	b.d.l.	b.d.l.	b.d.l.	b.d.l.	b.d.l.	b.d.l.	0.32	b.d.l.	b.d.l.	b.d.l.	b.d.l.
Ba	b.d.l.	b.d.l.	b.d.l.	b.d.l.	b.d.l.	b.d.l.	0.89	b.d.l.	b.d.l.	1.58	b.d.l.	b.d.l.	b.d.l.	b.d.l.	b.d.l.	b.d.l.	b.d.l.	b.d.l.	b.d.l.	b.d.l.	b.d.l.	b.d.l.
Th	0.32	0.27	0.06	0.24	0.36	0.23	0.28	0.15	0.30	0.33	0.33	0.23	0.15	0.14	0.15	0.18	0.14	0.14	0.13	0.20	0.43	0.32
U	0.54	0.62	0.30	0.71	0.47	0.50	0.54	0.84	0.56	0.48	0.48	0.67	0.51	0.54	0.64	0.68	0.39	0.42	0.50	0.50	0.47	0.49
Nb	0.08	0.09	0.08	b.d.l.	b.d.l.	b.d.l.	b.d.l.	b.d.l.	0.10	b.d.l.	b.d.l.	b.d.l.	b.d.l.	0.10	0.12	b.d.l.	b.d.l.	0.10	b.d.l.	0.09	b.d.l.	0.13
Ta	b.d.l.	b.d.l.	b.d.l.	b.d.l.	b.d.l.	b.d.l.	0.07	b.d.l.	b.d.l.	b.d.l.	b.d.l.	b.d.l.	b.d.l.	b.d.l.	b.d.l.	b.d.l.	b.d.l.	b.d.l.	b.d.l.	b.d.l.	b.d.l.	b.d.l.
La	1.13	1.92	0.52	0.63	1.21	0.70	1.08	0.49	0.76	1.14	1.32	0.72	0.47	0.89	0.70	0.76	0.58	2.68	0.77	0.74	1.37	0.96
Ce	16	15	6.96	12	18	13	15	11	15	16	18	13	10.64	10.98	14.21	14.12	8.41	14.64	11.51	12.83	16.98	14.75
Pb	0.15	9.79	b.d.l.	b.d.l.	0.12	b.d.l.	b.d.l.	b.d.l.	0.17	0.13	b.d.l.	b.d.l.	b.d.l.	b.d.l.	b.d.l.	b.d.l.	b.d.l.	1.12	b.d.l.	b.d.l.	0.22	b.d.l.
Pr	8.56	6.98	4.14	6.97	9.09	7.59	7.69	7.03	7.50	7.99	7.87	7.17	6.31	6.95	7.30	7.28	5.24	6.21	6.14	7.04	8.19	7.15
P	8208	8019	11107	12440	13139	12803	13211	12978	10979	11382	14046	14019	8765	8120	4706	4438	7308	7169	11590	10138	11370	11043
Sr	7.35	5.79	3.11	6.17	9.03	6.10	7.48	4.53	7.22	8.13	7.93	6.08	5.03	6.14	4.70	4.58	4.57	7.15	4.89	5.73	7.98	6.98
Nd	92	90	57	84	89	85	90	82	94	90	85	89	87	87	90	86	75	80	79	83	88	83
Zr	297	273	156	282	299	288	303	286	305	297	292	284	291	324	200	196	223	270	259	255	265	264
Hf	5.21	4.37	2.88	5.45	5.28	5.31	4.84	4.46	4.53	5.11	5.59	4.39	5.25	5.34	2.96	3.04	4.32	4.98	4.21	4.52	4.57	4.19
Sm	64	71	63	67	62	64	63	65	65	61	68	65	71	73	79	77	66	69	62	54	55	58
Eu	15	19	18	19	18	18	18	16	16	17	17	18	20	19	20	21	18	19	16	14	13	16
Gd	98	112	112	116	108	104	106	109	105	108	106	109	126	124	131	132	123	123	105	91	95	94
Tb	21	23	22	23	22	22	21	21	22	22	20	22	24	24	26	26	24	24	21	20	19	20
Dy	166	174	176	174	169	168	164	162	167	163	160	166	186	185	205	202	182	182	160	154	157	153
Ti	24313	21166	8629	17286	18858	18995	19346	19027	19951	20205	20211	19246	14731	13781	7864	7753	11058	12989	18156	19227	19496	19031
Y	1040	1036	1028	1032	1014	1009	998	993	1002	991	977	996	1099	1111	1216	1202	1057	1061	947	940	948	938
Ho	39	39	38	39	37	37	37	37	36	35	36	37	41	41	45	44	39	39	35	35	34	33
Er	122	117	116	117	114	114	113	111	113	110	106	109	117	122	141	142	119	119	104	103	99	100
Tm	18	17	17	17	16	16	16	16	16	15	15	16	17	17	20	20	16	17	15	15	14	15
Yb	126	118	115	113	112	110	110	110	107	109	102	102	118	113	130	130	108	112	101	99	100	101
Lu	19	18	17	17	17	17	17	17	16	17	16	16	18	18	20	20	16	17	16	15	15	15
Li	70	131	58	54	59	62	61	54	58	55	68	60	49	51	44	43	54	129	69	73	67	66
B	10	12	b.d.l.	b.d.l.	b.d.l.	b.d.l.	b.d.l.	b.d.l.	b.d.l.	b.d.l.	b.d.l.	b.d.l.	b.d.l.	b.d.l.	b.d.l.	b.d.l.	b.d.l.	63	b.d.l.	8.72	b.d.l.	b.d.l.

Table S5.3. Continued.

Garnet

Name ppm	45	46	47	48	49	50	51	52	53	54	55	56	57	58	59	60	61	62	63	64	65	66
Cr	2169	1956	2358	2300	2375	2510	2310	2364	2350	1728	1554	814	834	812	825	842	852	788	731	783	634	714
Ni	76	132	96	49	50	56	87	47	49	38	50	36	b.d.l.	41	32	40	44	b.d.l.	b.d.l.	b.d.l.	b.d.l.	67
Rb	b.d.l.	b.d.l.	b.d.l.	b.d.l.	b.d.l.	b.d.l.	b.d.l.	b.d.l.	b.d.l.	b.d.l.	b.d.l.	b.d.l.	b.d.l.	b.d.l.	b.d.l.	b.d.l.	b.d.l.	b.d.l.	b.d.l.	b.d.l.	b.d.l.	b.d.l.
Cs	b.d.l.	b.d.l.	b.d.l.	b.d.l.	b.d.l.	b.d.l.	b.d.l.	b.d.l.	b.d.l.	b.d.l.	b.d.l.	b.d.l.	b.d.l.	b.d.l.	b.d.l.	b.d.l.	b.d.l.	b.d.l.	b.d.l.	b.d.l.	b.d.l.	b.d.l.
Ba	b.d.l.	2.02	b.d.l.	b.d.l.	b.d.l.	b.d.l.	b.d.l.	b.d.l.	b.d.l.	b.d.l.	b.d.l.	b.d.l.	b.d.l.	b.d.l.	b.d.l.	b.d.l.	1	b.d.l.	b.d.l.	b.d.l.	b.d.l.	b.d.l.
Th	0.26	0.21	0.32	0.10	0.11	0.06	0.09	0.08	0.06	0.13	0.11	0.13	0.09	0.21	0.26	0.16	0.23	0.15	0.16	0.13	0.24	0.09
U	0.40	0.49	0.33	0.30	0.34	0.38	0.24	0.44	0.29	0.24	0.46	0.33	0.34	0.37	0.34	0.38	0.29	0.31	0.48	0.33	0.37	0.33
Nb	0.15	b.d.l.	0.10	b.d.l.	0.11	b.d.l.	b.d.l.	b.d.l.	0.08	0.09	b.d.l.	b.d.l.	b.d.l.	b.d.l.	b.d.l.	b.d.l.	b.d.l.	0.08	b.d.l.	0.12	b.d.l.	b.d.l.
Ta	b.d.l.	b.d.l.	b.d.l.	b.d.l.	0.09	b.d.l.	b.d.l.	b.d.l.	b.d.l.	b.d.l.	b.d.l.	0.09	b.d.l.	b.d.l.	b.d.l.	b.d.l.	b.d.l.	b.d.l.	0.12	b.d.l.	b.d.l.	b.d.l.
La	0.77	3.99	2.95	0.57	0.80	0.46	0.45	0.42	0.47	0.45	0.84	0.66	0.45	0.63	1.16	0.89	0.76	0.75	0.66	0.53	1.19	0.60
Ce	13.51	19.43	10.69	4.87	6.43	7.25	6.45	6.38	6.61	6.21	12.25	9.73	9.79	11.27	16.08	15.42	13.18	12.43	13.54	10	17	9.18
Pb	0.09	0.64	1.91	0.13	0.17	b.d.l.	b.d.l.	b.d.l.	b.d.l.	0.12	b.d.l.	b.d.l.	0.13	b.d.l.	b.d.l.	b.d.l.	b.d.l.	b.d.l.	b.d.l.	b.d.l.	b.d.l.	b.d.l.
Pr	6.95	7.69	3.79	2.82	3.92	4.51	4.00	3.77	4.01	3.88	6.55	6.03	5.91	6.76	8.26	7.92	6.58	6.94	6.95	5.63	8.59	5.68
P	10896	5903	7060	7521	7509	6492	7403	8913	8869	4909	4343	6103	7877	8536	9786	9775	8935	8281	7492	5976	5363	7821
Sr	6.84	7.66	3.14	1.81	3.93	3.18	2.84	2.47	2.61	2.29	6.00	4.32	3.89	5.24	7.34	7.34	5.18	5.25	5.88	4.41	7.84	3.97
Nd	86	86	48	46	52	66	61	55	57	54	78	78	79	85	96	97	92	89	89	81	98	80
Zr	270	282	110	112	150	179	155	141	158	152	272	234	235	282	295	302	288	292	296	258	346	274
Hf	5.21	4.10	1.97	1.59	2.16	3.04	2.37	2.16	3.03	2.41	3.78	4.31	3.85	5.14	5.42	5.44	4.87	3.92	4.63	4.33	5.16	4.74
Sm	66	73	52	55	61	67	64	58	64	60	67	73	73	74	72	74	80	81	78	72	83	77
Eu	16	19	16	17	16	19	18	17	18	18	21	20	19	20	19	19	21	21	20	20	23	20
Gd	108	121	112	109	117	118	117	109	109	117	123	125	123	122	115	118	120	120	126	130	142	128
Tb	21	23	23	22	22	22	22	21	22	23	23	24	24	23	22	23	23	23	23	25	27	24
Dy	162	181	174	172	171	170	164	163	163	179	181	185	182	177	171	175	176	175	175	191	202	187
Ti	18399	13047	5281	5618	9855	14049	11972	10511	11866	8744	9861	11662	13064	15997	18298	18352	17850	17349	16424	12607	14141	15135
Y	972	1083	1053	1033	1014	990	989	967	990	1084	1070	1124	1088	1058	1025	1045	1032	1022	1048	1116	1184	1117
Ho	35	40	38	38	36	35	35	35	37	40	38	41	40	39	37	38	38	38	37	42	43	41
Er	107	117	116	112	107	108	106	103	104	117	115	125	120	120	111	115	112	110	116	125	133	122
Tm	15	16	16	16	15	15	15	15	15	17	16	18	17	17	16	16	15	15	17	18	19	19
Yb	101	110	106	106	102	100	99	102	102	111	108	117	114	110	109	106	108	109	110	120	124	120
Lu	15	17	16	16	15	15	15	15	15	17	16	18	18	17	17	17	18	17	17	19	19	18
Li	70	58	46	42	58	55	52	54	59	43	28	57	56	61	65	54	64	59	60	55	49	63
B	b.d.l.	66	16	10	b.d.l.	b.d.l.	b.d.l.	b.d.l.	b.d.l.	b.d.l.	b.d.l.	b.d.l.	b.d.l.	b.d.l.	8.32	b.d.l.	b.d.l.	8.39	b.d.l.	8.14	b.d.l.	b.d.l.

Table S5.3. Continued.

Garnet

Name ppm	67	68	69	70	71	72	73	74	75	76	77	78	79	80	81	82	83	84	85	86	87	88
Cr	689	700	721	707	695	697	695	728	728	612	610	702	808	766	1453	1624	1581	1054	979	1150	1255	1195
Ni	b.d.l.	51	84	b.d.l.	b.d.l.	b.d.l.	b.d.l.	40.5764	42.7366	b.d.l.	b.d.l.	38	b.d.l.	b.d.l.	b.d.l.	45	b.d.l.	66	b.d.l.	54	55	58
Rb	b.d.l.	b.d.l.	b.d.l.	b.d.l.	b.d.l.	b.d.l.	b.d.l.	b.d.l.	b.d.l.	b.d.l.	1.69	b.d.l.	1.28	b.d.l.	b.d.l.	b.d.l.	b.d.l.	b.d.l.	b.d.l.	b.d.l.	b.d.l.	b.d.l.
Cs	b.d.l.	b.d.l.	b.d.l.	b.d.l.	b.d.l.	b.d.l.	b.d.l.	b.d.l.	b.d.l.	b.d.l.	b.d.l.	b.d.l.	b.d.l.	b.d.l.	b.d.l.	b.d.l.	b.d.l.	b.d.l.	b.d.l.	b.d.l.	b.d.l.	b.d.l.
Ba	b.d.l.	b.d.l.	b.d.l.	1.57	b.d.l.	b.d.l.	b.d.l.	b.d.l.	b.d.l.	b.d.l.	b.d.l.	b.d.l.	b.d.l.	b.d.l.	b.d.l.	b.d.l.	b.d.l.	b.d.l.	b.d.l.	b.d.l.	b.d.l.	b.d.l.
Th	0.16	0.09	0.10	b.d.l.	b.d.l.	0.06	0.09	0.15	0.23	0.10	0.18	0.16	0.14	0.16	0.06	0.10	0.06	0.14	0.07	0.08	0.04	0.11
U	0.27	0.40	0.30	0.23	0.34	0.17	0.38	0.36	0.41	0.31	0.40	0.41	0.35	0.46	0.32	0.31	0.21	0.37	0.43	0.30	0.46	0.36
Nb	0.08	b.d.l.	b.d.l.	b.d.l.	b.d.l.	0.09	b.d.l.	b.d.l.	0.10	b.d.l.	b.d.l.	b.d.l.	0.09	0.07	0.13	b.d.l.	b.d.l.	b.d.l.	b.d.l.	0.12	0.13	b.d.l.
Ta	b.d.l.	b.d.l.	b.d.l.	b.d.l.	b.d.l.	b.d.l.	b.d.l.	b.d.l.	b.d.l.	b.d.l.	b.d.l.	b.d.l.	b.d.l.	b.d.l.	b.d.l.	b.d.l.	b.d.l.	b.d.l.	b.d.l.	b.d.l.	b.d.l.	b.d.l.
La	0.63	0.44	1.48	0.96	4.73	0.71	1.11	0.51	0.81	0.38	0.67	0.75	0.42	0.83	0.66	1.15	0.30	0.66	0.52	0.46	0.57	0.59
Ce	8.67	7.56	10	7.00	19	6.45	15	11	13	8.11	13	11	10	13	6.49	9.42	6.95	6.82	8.31	10	10	8.46
Pb	b.d.l.	b.d.l.	b.d.l.	b.d.l.	b.d.l.	0.71	b.d.l.	b.d.l.	0.14	b.d.l.	b.d.l.	b.d.l.	b.d.l.	b.d.l.	b.d.l.	3.62	0.12	b.d.l.	b.d.l.	0.16	b.d.l.	b.d.l.
Pr	5.50	4.67	4.71	4.17	5.40	4.14	8.50	6.50	7.67	5.37	7.40	5.92	5.80	7.35	4.19	4.73	4.58	4.07	4.83	5.47	5.61	4.56
P	9274	8584	7075	7993	8150	7796	4975	6882	9271	7006	7715	9558	8254	3137	4959	5334	5765	5115	5578	6070	5987	5495
Sr	3.46	1.89	2.44	1.26	2.55	1.40	6.96	4.89	6.55	2.28	4.83	4.33	3.58	5.01	2.73	3.69	2.95	2.14	2.96	4.20	4.93	3.49
Nd	69	68	73	58	65	55	102	87	91	78	88	76	78	91	58	62	63	56	64	75	74	67
Zr	258	206	178	161	153	143	306	312	303	258	292	259	222	246	182	176	162	141	180	222	230	184
Hf	4.43	3.27	3.89	2.26	2.54	2.34	3.79	4.61	4.71	3.93	4.23	4.54	3.55	2.96	3.86	2.85	2.32	1.93	3.70	4.31	3.69	2.78
Sm	73	75	65	63	69	63	78	80	76	74	72	77	75	75	62	63	65	61	68	69	69	68
Eu	19	18	18	19	19	16	20	20	20	19	20	19	19	21	18	19	19	19	18	19	18	17
Gd	123	118	118	120	119	118	130	123	118	118	116	114	120	131	117	109	112	117	117	113	111	108
Tb	24	23	24	23	23	23	26	24	23	23	23	23	23	25	22	22	22	22	23	22	22	22
Dy	181	176	165	170	174	178	193	181	177	180	178	173	174	190	176	173	168	171	169	162	166	172
Ti	17125	15789	14056	12978	11220	8471	12598	15382	18321	15340	18730	17129	12978	8941	8636	8911	9982	9950	13935	16504	15117	11617
Y	1064	1046	1036	1031	1043	1047	1175	1124	1074	1082	1066	1063	1065	1165	1058	1032	1016	1019	977	976	968	1004
Ho	39	38	37	36	38	37	44	41	38	40	38	39	38	40	38	37	37	36	34	35	36	37
Er	116	115	115	112	113	118	130	124	117	120	116	118	117	127	116	115	110	112	110	109	110	112
Tm	17	16	16	16	16	16	19	17	17	17	17	17	16	19	16	17	16	15	16	15	16	15
Yb	111	113	113	110	109	110	128	117	111	115	115	117	114	123	106	109	105	105	105	106	104	107
Lu	18	17	18	16	17	17	19	19	18	18	18	18	18	19	16	17	16	17	16	17	17	17
Li	65	73	136	53	65	56	49	54	63	49	55	71	60	44	47	53	49	43	54	62	56	50
B	b.d.l.	b.d.l.	13	b.d.l.	b.d.l.	12	b.d.l.	b.d.l.	b.d.l.	b.d.l.	b.d.l.	b.d.l.	b.d.l.	b.d.l.	b.d.l.	14	b.d.l.	b.d.l.	b.d.l.	b.d.l.	b.d.l.	b.d.l.

Table S5.3. Continued.

Garnet

Name ppm	89	90	91	92	93	94	95	96	97	98	99	100	101
Cr	1035	1327	1677	1433	493	541	671	650	688	656	680	613	684
Ni	41	51	b.d.l.	42	44	b.d.l.	b.d.l.	b.d.l.	39	50	49	b.d.l.	b.d.l.
Rb	b.d.l.	1.14	b.d.l.	b.d.l.	b.d.l.	1.16	b.d.l.	b.d.l.	b.d.l.	b.d.l.	b.d.l.	b.d.l.	1.50
Cs	b.d.l.	b.d.l.	b.d.l.	b.d.l.	b.d.l.	b.d.l.	b.d.l.	b.d.l.	b.d.l.	b.d.l.	b.d.l.	b.d.l.	b.d.l.
Ba	b.d.l.	b.d.l.	b.d.l.	1	b.d.l.	b.d.l.	b.d.l.	b.d.l.	b.d.l.	b.d.l.	b.d.l.	b.d.l.	b.d.l.
Th	0.10	0.18	0.06	0.07	0.31	0.20	0.12	0.08	0.16	0.12	0.08	0.07	0.05
U	0.46	0.48	0.25	0.36	0.41	0.38	0.34	0.35	0.39	0.36	0.44	0.20	0.21
Nb	b.d.l.	b.d.l.	b.d.l.	b.d.l.	0.11	b.d.l.	b.d.l.	0.07	b.d.l.	0.20	b.d.l.	b.d.l.	b.d.l.
Ta	b.d.l.	b.d.l.	b.d.l.	b.d.l.	b.d.l.	b.d.l.	b.d.l.	b.d.l.	b.d.l.	b.d.l.	b.d.l.	b.d.l.	b.d.l.
La	0.55	0.45	0.45	0.54	1.88	1.11	0.60	0.67	0.81	0.43	0.68	0.75	0.45
Ce	10	10	6.51	7.19	25	16	10	11	13	11	11	12	10
Pb	b.d.l.	b.d.l.	b.d.l.	b.d.l.	b.d.l.	b.d.l.	b.d.l.	b.d.l.	b.d.l.	b.d.l.	b.d.l.	b.d.l.	b.d.l.
Pr	5.43	5.68	3.68	4.08	11	8.24	5.82	6.35	7.06	6.32	6.06	6.14	5.40
P	5578	5290	7228	4373	4488	5120	8220	9253	9056	7201	7258	7697	8013
Sr	4.17	4.25	2.67	2.86	7.48	6.91	3.99	4.67	5.39	4.80	3.96	3.58	3.86
Nd	78	74	55	60	118	105	88	91	90	87	86	86	73
Zr	225	218	151	153	355	350	262	270	286	269	258	262	253
Hf	3.62	4.21	2.78	2.17	4.87	5.19	4.74	4.07	4.68	4.55	4.34	5.10	4.33
Sm	70	68	61	64	86	88	80	82	83	84	86	78	76
Eu	19	20	16	19	23	23	21	21	20	21	22	20	19
Gd	117	111	110	123	146	145	133	129	127	130	126	128	123
Tb	22	22	22	25	27	28	25	24	23	24	25	23	24
Dy	165	170	169	188	208	206	188	180	181	182	188	179	177
Ti	17427	18100	8773	6674	12136	13456	15094	16829	17979	17103	15119	15520	13823
Y	982	988	976	1021	1213	1239	1134	1094	1081	1103	1128	1061	1114
Ho	36	36	37	41	45	45	42	40	39	38	40	38	38
Er	112	109	107	124	136	136	128	120	117	119	121	115	120
Tm	16	16	16	17	19	19	18	17	16	16	17	15	17
Yb	106	101	98	114	120	123	109	111	108	109	113	107	110
Lu	17	17	16	18	19	19	18	17	17	16	18	17	18
Li	53	52	49	44	42	49	57	60	67	60	67	58	59
B	b.d.l.	b.d.l.	7.93	10	b.d.l.	b.d.l.	b.d.l.	b.d.l.	b.d.l.	b.d.l.	b.d.l.	b.d.l.	b.d.l.

Table S5.3. Continued.

Clinopyroxene

Name ppm	1	2	3	4	5	6	7	8	9	10	11	12	13	14	15	16	17	18
Cr	2213	2134	1821	1880	1909	1907	1909	1890	1898	1970	1869	1794	1868	1914	1878	2700	3387	4250
Ni	486	486	493	497	538	466	495	501	509	491	495	477	473	476	512	1124	1124	1087
Rb	b.d.l.	0.69	0.52	b.d.l.	b.d.l.	b.d.l.	b.d.l.	b.d.l.	b.d.l.	b.d.l.	1.09	b.d.l.	b.d.l.	b.d.l.	b.d.l.	b.d.l.	b.d.l.	b.d.l.
Cs	b.d.l.	b.d.l.	b.d.l.	0.36	b.d.l.	b.d.l.	b.d.l.	b.d.l.	b.d.l.	b.d.l.	0.35	b.d.l.	b.d.l.	b.d.l.	b.d.l.	b.d.l.	b.d.l.	b.d.l.
Ba	1.25	1.29	1.14	0.93	1.37	b.d.l.	0.62	b.d.l.	b.d.l.	b.d.l.	2.63	b.d.l.	b.d.l.	b.d.l.	0.86	b.d.l.	b.d.l.	b.d.l.
Th	0.83	0.60	0.68	0.60	0.66	0.53	0.45	0.49	0.43	0.52	0.46	0.33	0.28	0.39	0.46	0.49	0.37	0.38
U	0.26	0.26	0.27	0.17	0.31	0.19	0.23	0.26	0.24	0.17	0.29	0.18	0.22	0.21	0.19	0.30	0.17	0.21
Nb	0.11	0.11	0.13	0.17	0.15	0.17	0.07	0.11	0.13	0.12	0.21	0.15	0.13	0.12	0.10	0.10	b.d.l.	0.16
Ta	0.06	b.d.l.	0.06	b.d.l.	b.d.l.	b.d.l.	b.d.l.	b.d.l.	b.d.l.	b.d.l.	b.d.l.	b.d.l.	0.07	b.d.l.	b.d.l.	b.d.l.	b.d.l.	b.d.l.
La	42	38	39	39	39	37	36	36	34	36	35	33	33	32	32	30	31	30
Ce	176	168	170	169	165	167	166	169	166	164	164	158	159	154	155	148	142	142
Pb	23	21	21	22	21	20	19	22	20	20	20	17	19	19	19	14	15	18
Pr	32	31	31	30	29	30	29	30	31	30	31	29	30	30	29	28	29	27
P	615	584	572	654	532	692	602	709	583	610	811	789	749	663	618	486	416	476
Sr	921	904	899	879	883	884	882	908	899	897	895	873	874	856	830	803	814	843
Nd	153	146	149	147	143	147	149	149	151	151	144	147	146	150	146	156	152	149
Zr	501	486	479	465	457	461	475	484	493	475	493	494	490	464	451	398	412	428
Hf	24	22	22	21	21	22	22	22	24	21	22	24	22	21	18	18	18	19
Sm	32	31	31	30	28	28	29	30	30	29	29	29	29	30	31	33	33	31
Eu	5.11	5.20	4.83	4.31	4.92	4.39	4.66	4.65	5.40	4.79	4.79	4.61	5.44	4.80	5.02	5.56	5.26	4.77
Gd	19	19	18	19	19	18	19	18	20	18	17	17	18	18	17	18	18	17
Tb	2.03	2.06	2.04	1.97	2.08	2.04	2.12	2.01	1.96	1.78	1.88	1.92	2.00	1.76	1.80	1.98	1.68	1.82
Dy	10	10	10	8.50	10	9.38	10	9.03	10	10	8.52	9.37	9.14	8.72	8.97	7.70	7.55	7.96
Ti	27079	26577	26039	25774	25536	26163	25762	26429	26647	26333	27112	26338	26326	25705	25124	20266	21167	22517
Y	33	33	32	31	33	32	32	33	34	33	33	31	31	31	29	27	26	26
Ho	1.48	1.42	1.43	1.30	1.34	1.37	1.33	1.29	1.40	1.26	1.39	1.25	1.32	1.25	1.32	1.01	1.04	1.08
Er	2.89	2.81	2.82	2.87	2.82	2.88	2.63	2.95	2.90	2.80	2.98	2.66	3.06	2.43	2.48	2.15	1.90	1.78
Tm	0.27	0.34	0.29	0.38	0.34	0.27	0.27	0.34	0.29	0.30	0.29	0.29	0.27	0.26	0.28	0.18	0.21	0.29
Yb	1.71	1.66	1.64	1.27	1.89	1.68	1.41	1.62	1.28	1.64	1.78	1.37	1.56	1.06	1.62	0.84	1.16	1.08
Lu	0.26	0.17	0.20	0.15	0.17	0.17	0.13	0.21	0.19	0.22	0.20	0.14	0.17	0.18	0.18	0.17	0.16	0.12
Li	2355	2262	2268	2331	2228	2203	2194	2212	2295	2370	2537	2393	2391	2375	2448	1697	1739	1683
B	24	24	25	23	19	19	21	22	19	26	24	19	24	20	25	29	20	20

b.d.l= below detection limit

Table S5.4. Clinopyroxenes trace elements composition.

Clinopyroxene

Name ppm	19	20	21	22	23	24	25	26	27	28	29	30	31	32	33	34	35	36
Cr	4003	3824	3787	3736	3940	4003	3973	5006	4782	3844	3632	3593	3310	4477	4586	4131	3442	4460
Ni	1072	1158	1053	1118	1058	1216	1214	1131	1098	1268	1317	1223	1192	1213	1261	1196	1123	1170
Rb	b.d.l.	b.d.l.	b.d.l.	b.d.l.	b.d.l.	b.d.l.	b.d.l.	3.58	b.d.l.	b.d.l.	b.d.l.	b.d.l.	b.d.l.	b.d.l.	b.d.l.	b.d.l.	b.d.l.	b.d.l.
Cs	0.43	b.d.l.	b.d.l.	b.d.l.	b.d.l.	b.d.l.	b.d.l.	0.47	b.d.l.	b.d.l.	b.d.l.	b.d.l.	b.d.l.	b.d.l.	b.d.l.	b.d.l.	b.d.l.	b.d.l.
Ba	b.d.l.	b.d.l.	b.d.l.	b.d.l.	b.d.l.	b.d.l.	1.59	b.d.l.	b.d.l.	1.19	1.32	b.d.l.	b.d.l.	b.d.l.	b.d.l.	b.d.l.	b.d.l.	b.d.l.
Th	0.42	0.38	0.49	0.53	0.34	0.47	0.73	0.66	0.51	0.44	0.40	0.41	0.51	0.43	0.34	0.34	0.29	0.39
U	0.29	0.19	0.27	0.25	0.27	0.35	0.53	0.43	0.28	0.33	0.21	0.21	0.26	0.48	0.28	0.38	0.23	0.23
Nb	0.10	b.d.l.	b.d.l.	0.16	0.13	b.d.l.	b.d.l.	b.d.l.	0.13	0.13	0.08	0.13	0.08	b.d.l.	b.d.l.	b.d.l.	b.d.l.	b.d.l.
Ta	b.d.l.	b.d.l.	b.d.l.	b.d.l.	b.d.l.	b.d.l.	b.d.l.	b.d.l.	b.d.l.	b.d.l.	b.d.l.	b.d.l.	b.d.l.	b.d.l.	b.d.l.	b.d.l.	b.d.l.	b.d.l.
La	30	31	32	30	29	30	32	31	33	31	31	31	33	33	28	27	29	30
Ce	144	145	149	144	145	149	150	148	149	148	145	153	155	164	140	136	138	147
Pb	19	20	17	14	17	19	13	12	27	20	20	20	17	15	12	11	13	16
Pr	28	28	29	29	29	31	30	30	29	29	29	30	29	32	29	28	26	29
P	432	596	463	383	351	453	297	361	372	375	439	455	366	423	362	461	399	477
Sr	855	862	845	796	822	839	755	757	891	864	868	869	884	867	779	757	819	835
Nd	144	150	156	153	150	154	168	158	143	151	152	151	161	165	155	147	145	151
Zr	443	444	414	408	394	419	408	414	399	483	486	485	482	488	477	478	486	493
Hf	19	19	19	17	18	20	19	20	16	21	21	21	22	20	19	19	19	20
Sm	31	31	34	34	32	30	34	36	32	31	31	30	32	34	34	32	30	31
Eu	5.23	4.77	5.63	5.29	4.90	5.69	5.57	5.12	4.65	5.61	5.29	5.21	5.09	5.60	5.46	4.86	4.68	5.04
Gd	19	17	18	17	17	19	19	18	17	18	19	18	17	18	19	18	19	18
Tb	1.68	1.83	1.77	1.79	1.80	1.84	1.74	1.72	1.81	1.93	1.88	1.96	1.82	1.93	1.82	1.78	1.82	1.84
Dy	7.75	8.44	7.38	7.53	8.04	7.88	7.64	8.08	8.50	9.20	8.85	9.48	8.28	8.39	8.86	8.44	9.40	8.32
Ti	23734	24637	22534	21065	20088	20381	19729	19311	20571	21538	23693	24510	24154	23878	23288	23914	24467	24511
Y	27	27	25	26	24	25	26	23	25	28	30	28	26	28	27	26	27	27
Ho	1.00	0.96	1.05	1.03	1.06	1.14	0.97	0.93	0.95	1.20	1.31	1.18	1.28	1.07	1.06	1.07	0.87	1.07
Er	2.37	2.11	1.84	1.92	1.85	1.81	1.82	1.78	1.96	2.45	2.37	2.13	2.09	2.31	1.97	2.22	1.57	2.30
Tm	0.18	0.29	0.22	0.22	0.15	0.18	0.19	0.21	0.19	0.28	0.24	0.19	0.23	0.20	0.25	0.24	0.17	0.22
Yb	1.29	1.12	0.87	1.16	0.90	1.22	0.81	0.99	1.06	0.82	1.10	1.15	1.09	1.08	1.05	0.80	0.94	0.79
Lu	0.16	0.12	0.10	0.10	0.13	0.11	0.11	0.10	0.12	0.23	0.16	0.18	0.11	0.12	0.12	0.11	0.08	0.17
Li	1688	1760	1850	1850	1830	2078	1785	1830	2247	1978	1905	1779	1627	1694	1747	1702	1540	1701
B	20	22	20	44	25	18	29	29	22	30	28	21	17	20	24	25	26	20

b.d.l= below detection limit

Table S5.4. Continued.

Clinopyroxene

Name	37	38	39	40	41	42	43	44	45	46	47	48	49	50	51	52	53	54
ppm																		
Cr	4712	3655	3941	4072	4178	4088	4140	4167	4523	4475	3698	4262	4497	4437	4165	4033	4217	4645
Ni	1185	1189	1203	1210	1223	1313	1259	1312	1228	1204	1049	914	900	874	927	857	992	788
Rb	b.d.l.	b.d.l.	b.d.l.	b.d.l.	b.d.l.	b.d.l.	b.d.l.	b.d.l.	b.d.l.	b.d.l.	b.d.l.	b.d.l.	b.d.l.	b.d.l.	b.d.l.	b.d.l.	b.d.l.	b.d.l.
Cs	b.d.l.	b.d.l.	b.d.l.	b.d.l.	b.d.l.	b.d.l.	b.d.l.	b.d.l.	b.d.l.	b.d.l.	b.d.l.	b.d.l.	b.d.l.	b.d.l.	b.d.l.	b.d.l.	b.d.l.	b.d.l.
Ba	b.d.l.	b.d.l.	b.d.l.	b.d.l.	b.d.l.	b.d.l.	b.d.l.	b.d.l.	b.d.l.	b.d.l.	b.d.l.	1.19	b.d.l.	b.d.l.	b.d.l.	b.d.l.	b.d.l.	b.d.l.
Th	0.31	0.30	0.35	0.40	0.37	0.51	0.41	0.35	0.46	0.37	0.69	0.51	0.51	0.58	0.55	0.55	0.50	0.58
U	0.25	0.39	0.40	0.30	0.37	0.42	0.40	0.43	0.30	0.23	0.45	0.45	0.37	0.41	0.33	0.32	0.37	0.32
Nb	0.08	0.12	0.09	0.10	0.10	0.09	b.d.l.	0.12	b.d.l.	0.09	0.17	0.08	b.d.l.	b.d.l.	b.d.l.	0.11	b.d.l.	0.09
Ta	b.d.l.	b.d.l.	b.d.l.	b.d.l.	b.d.l.	b.d.l.	b.d.l.	b.d.l.	b.d.l.	b.d.l.	b.d.l.	b.d.l.	b.d.l.	b.d.l.	b.d.l.	b.d.l.	b.d.l.	b.d.l.
La	28	29	32	32	31	34	33	32	32	32	30	29	28	31	29	29	30	29
Ce	144	153	155	156	154	157	156	152	149	149	144	143	144	147	147	143	144	138
Pb	15	11	16	17	16	19	17	22	19	18	14	18	19	19	20	17	15	18
Pr	29	30	32	30	30	31	30	29	30	29	28	28	29	29	29	29	29	27
P	480	398	373	424	386	394	374	565	471	374	445	467	383	485	484	445	288	487
Sr	817	716	821	879	854	907	871	841	840	831	746	833	763	852	858	823	779	812
Nd	148	172	162	163	159	161	170	157	158	155	162	147	157	158	153	155	156	147
Zr	493	477	475	490	486	499	486	460	468	450	508	515	507	514	504	494	486	470
Hf	22	21	21	22	20	22	21	20	21	20	24	23	23	22	22	23	23	21
Sm	32	40	33	36	33	33	35	34	33	34	32	33	34	33	34	32	32	33
Eu	5.21	6.07	5.38	5.43	5.77	5.21	4.53	5.33	5.66	5.29	5.82	5.27	6.05	5.61	5.06	5.32	5.63	5.39
Gd	18	21	19	18	20	20	19	18	19	19	18	18	18	19	18	20	19	18
Tb	1.85	2.22	1.88	1.84	1.92	2.03	2.07	2.01	1.93	1.88	1.84	1.93	1.78	1.94	1.87	2.04	1.99	1.82
Dy	7.49	8.08	8.36	8.40	7.37	9.58	8.80	7.20	7.37	8.14	8.24	7.85	8.43	8.28	8.23	9.28	8.69	8.31
Ti	22310	20762	21671	23336	22819	23824	21977	22514	22515	20902	22479	25311	24127	24721	23844	23016	21724	22480
Y	26	24	25	26	26	28	27	26	26	26	26	27	26	26	26	26	26	26
Ho	0.98	0.86	1.14	1.22	1.13	0.99	0.91	1.10	1.00	0.90	1.09	1.08	1.15	1.09	1.08	1.06	1.11	1.01
Er	1.97	1.49	1.91	2.05	2.10	2.17	2.10	1.89	1.80	1.96	1.77	2.27	1.85	1.98	1.98	1.86	2.37	2.18
Tm	0.18	0.19	0.23	0.26	0.18	0.21	0.21	0.29	0.15	0.25	0.13	0.24	0.17	0.32	0.25	0.19	0.21	0.28
Yb	1.01	1.11	0.77	0.99	1.02	1.56	1.32	0.82	0.92	0.80	0.97	1.30	1.05	0.93	1.08	1.12	0.81	0.80
Lu	0.10	0.10	0.11	0.11	0.16	0.17	0.11	0.20	0.11	0.09	0.20	0.12	0.08	0.16	0.13	0.10	0.13	0.12
Li	1911	1408	1448	1607	1813	1705	1823	2001	1866	1773	1941	1901	2100	1734	1882	1921	1953	1871
B	23	24	18	24	22	30	25	19	24	19	34	24	36	25	30	28	36	26

b.d.l= below detection limit

Table S5.4. Continued.

Clinopyroxene

Name	55	56	57	58	59	60	61	62	63	64	65	66	67	68	69	70
ppm																
Cr	3808	3742	3449	3036	3542	3673	4393	4367	4741	5533	4830	4747	4464	4255	4630	4302
Ni	820	782	784	804	809	834	863	963	1021	944	1006	1224	1053	1018	954	899
Rb	b.d.l.	b.d.l.	b.d.l.	b.d.l.	b.d.l.	b.d.l.	b.d.l.	b.d.l.	b.d.l.	1.92	b.d.l.	b.d.l.	1.17	b.d.l.	b.d.l.	b.d.l.
Cs	b.d.l.	b.d.l.	b.d.l.	b.d.l.	b.d.l.	b.d.l.	b.d.l.	b.d.l.	b.d.l.	b.d.l.	b.d.l.	b.d.l.	b.d.l.	0.44	b.d.l.	b.d.l.
Ba	b.d.l.	b.d.l.	1.34	b.d.l.	b.d.l.	b.d.l.	b.d.l.	b.d.l.	b.d.l.	b.d.l.	b.d.l.	b.d.l.	2.87	b.d.l.	b.d.l.	b.d.l.
Th	0.55	0.60	0.70	0.55	0.46	0.65	0.35	0.47	0.56	0.57	0.63	0.56	0.28	0.35	0.48	0.49
U	0.36	0.31	0.39	0.30	0.28	0.45	0.33	0.37	0.57	0.46	0.51	0.47	0.78	0.41	0.39	0.46
Nb	0.06	0.11	0.09	0.10	0.08	b.d.l.	b.d.l.	b.d.l.	b.d.l.	0.12	b.d.l.	0.23	b.d.l.	0.14	0.14	b.d.l.
Ta	b.d.l.	b.d.l.	b.d.l.	b.d.l.	b.d.l.	0.09	b.d.l.	0.08	b.d.l.	0.08	b.d.l.	b.d.l.	b.d.l.	b.d.l.	b.d.l.	0.10
La	29	29	30	30	29	30	28	28	30	30	29	29	32	30	30	30
Ce	142	141	149	147	147	143	137	144	147	144	141	148	147	144	147	141
Pb	16	17	21	15	16	21	11	11	14	14	14	15	21	20	21	19
Pr	27	28	29	30	31	29	28	28	29	28	29	29	30	28	30	28
P	506	561	517	440	537	385	506	540	419	477	506	516	416	473	444	343
Sr	805	821	869	800	790	855	709	721	788	812	804	802	765	834	867	832
Nd	152	150	155	157	155	154	155	159	159	155	149	159	153	152	154	153
Zr	477	482	493	496	492	482	447	465	479	483	472	484	484	466	485	475
Hf	21	22	24	22	22	22	19	19	19	20	19	17	23	22	24	24
Sm	33	29	30	34	36	32	35	35	32	35	33	35	35	32	31	33
Eu	5.90	4.83	5.61	5.35	5.38	5.00	5.22	5.29	6.15	5.36	5.14	5.20	5.49	5.39	5.62	5.91
Gd	18	17	18	20	20	19	19	18	17	20	19	18	21	18	20	19
Tb	1.87	2.06	1.94	1.94	1.98	1.96	1.91	1.74	1.61	1.73	1.98	1.87	2.02	1.87	1.89	1.95
Dy	7.72	8.61	9.23	7.80	8.48	8.79	7.66	7.39	8.11	8.31	8.39	8.68	8.83	8.18	9.05	8.60
Ti	23838	24757	26343	25699	25269	23079	21876	22983	24103	24680	25184	24622	23675	24285	25359	24066
Y	28	28	28	28	28	27	24	24	26	27	26	27	29	25	28	28
Ho	1.09	1.09	1.02	1.24	1.04	1.08	0.91	0.96	0.93	1.02	1.19	0.90	1.26	1.08	1.12	1.15
Er	2.18	2.11	2.56	2.32	1.90	2.08	1.91	1.70	2.32	2.11	1.78	2.54	2.65	2.25	2.12	2.16
Tm	0.20	0.21	0.24	0.21	0.19	0.24	0.19	0.17	0.22	0.21	0.23	0.15	0.32	0.16	0.25	0.22
Yb	0.87	0.84	1.11	1.25	1.09	0.89	1.10	0.89	0.81	1.16	1.03	0.72	1.57	0.93	0.92	1.42
Lu	0.12	0.13	0.14	0.07	0.13	0.10	0.12	0.11	0.11	0.07	0.19	0.12	0.21	0.13	0.18	0.14
Li	1790	1754	1790	1728	1734	2076	1720	1745	1693	1708	1727	1924	1826	1626	1747	1986
B	31	24	25	28	26	27	26	25	22	25	25	36	43	29	29	26

b.d.l= below detection limit

Table S5.4. Continued.

Melt inclusions

Name ppm	1	2	3	4	5	6	7	8	9	10	11	12	13	14	15	16	17	18	19	20
Cr	b.d.l.	b.d.l.	b.d.l.	b.d.l.	b.d.l.	b.d.l.	b.d.l.	95.17124	b.d.l.	b.d.l.	b.d.l.	b.d.l.	b.d.l.	b.d.l.	b.d.l.	b.d.l.	b.d.l.	b.d.l.	b.d.l.	b.d.l.
Ni	b.d.l.	b.d.l.	b.d.l.	b.d.l.	b.d.l.	b.d.l.	b.d.l.	b.d.l.	b.d.l.	b.d.l.	b.d.l.	52	b.d.l.	b.d.l.	b.d.l.	b.d.l.	b.d.l.	b.d.l.	b.d.l.	b.d.l.
Rb	143	250	251	216	155	225	172	180	166	141	217	169	222	209	265	159	248	427	269	347
Cs	15	30	35	57	27	79	19	18	16	14	70	34	84	47	135	15	96	319	61	39
Ba	229	81	229	147	242	540	438	372	275	304	163	171	140	117	101	211	89	41	90	14
Th	20	56	7	32	14	23	25	5.61	35	29	25	25	28	14	11	18	9.31	4.18	4.73	7.56
U	12	36	14	64	11	11	14	2.38	17	15	18	13	27	11	9.41	7.92	10	11	6.36	5.07
Nb	0.61	3.25	0.68	1.26	0.46	0.61	0.65	0.34	0.59	0.40	0.71	0.68	b.d.l.	0.41	0.61	0.68	0.57	1.16	0.52	b.d.l.
Ta	0.17	0.71	0.13	1.37	0.15	b.d.l.	0.18	b.d.l.	0.16	0.21	0.16	0.22	b.d.l.	0.17	b.d.l.	0.17	b.d.l.	b.d.l.	0.18	b.d.l.
La	12	11	8.54	6.73	10	14	10	12	105	16	14	13	17	8.69	11	10	10	10	8.10	12.78
Ce	24	20	19	9.41	19	26	14	19	236	30	28	29	34	15	20	19	26	23	21	2.22
Pb	64	102	47	111	18	93	89	26	115	87	70	93	48	76	58	67	27	94	32	3.38
Pr	1.84	1.60	0.67	b.d.l.	1.16	2.64	0.99	b.d.l.	29	3.00	2.10	1.38	2.87	0.40	2.66	1.87	2.43	b.d.l.	1.09	b.d.l.
P	b.d.l.	b.d.l.	b.d.l.	179	b.d.l.	1739	b.d.l.	508	3064	b.d.l.	b.d.l.	b.d.l.	b.d.l.	254	b.d.l.	b.d.l.	b.d.l.	b.d.l.	b.d.l.	b.d.l.
Sr	254	205	288	251	83	388	381	351	592	329	385	294	364	210	477	323	425	562	363	104
Nd	4.84	b.d.l.	b.d.l.	24	0.95	11	b.d.l.	b.d.l.	98	b.d.l.	2.65	4.71	b.d.l.	5.54	5.55	2.76	3.42	b.d.l.	b.d.l.	b.d.l.
Zr	219	811	273	200	129	273	183	64	263	212	246	186	226	126	217	249	195	49	70	b.d.l.
Hf	6.64	29	7.59	2.81	4.83	5.18	6.90	3.32	8.50	6.70	7.71	7.05	6.44	4.47	4.88	8.08	5.59	b.d.l.	1.81	b.d.l.
Sm	b.d.l.	b.d.l.	b.d.l.	5.49	3.25	11.42	b.d.l.	1.42	10.61	b.d.l.	3.09	b.d.l.	b.d.l.	3.35	5.37	b.d.l.	b.d.l.	b.d.l.	b.d.l.	b.d.l.
Eu	b.d.l.	0.84	b.d.l.	0.22	b.d.l.	3.69	3.46	b.d.l.	b.d.l.	b.d.l.	b.d.l.	0.07	b.d.l.	0.21	b.d.l.	0.67	b.d.l.	b.d.l.	b.d.l.	b.d.l.
Gd	b.d.l.	b.d.l.	b.d.l.	27	2.81	11	6.72	b.d.l.	b.d.l.	b.d.l.	b.d.l.	b.d.l.	b.d.l.	b.d.l.	b.d.l.	b.d.l.	b.d.l.	b.d.l.	b.d.l.	b.d.l.
Tb	b.d.l.	b.d.l.	b.d.l.	3.03	b.d.l.	1.78	b.d.l.	b.d.l.	b.d.l.	b.d.l.	b.d.l.	b.d.l.	b.d.l.	0.84	b.d.l.	0.02	b.d.l.	b.d.l.	b.d.l.	b.d.l.
Dy	b.d.l.	b.d.l.	b.d.l.	27	2.47	37	b.d.l.	b.d.l.	b.d.l.	b.d.l.	b.d.l.	b.d.l.	b.d.l.	b.d.l.	b.d.l.	b.d.l.	b.d.l.	b.d.l.	b.d.l.	b.d.l.
Ti	b.d.l.	b.d.l.	b.d.l.	219	b.d.l.	b.d.l.	b.d.l.	b.d.l.	b.d.l.	b.d.l.	b.d.l.	b.d.l.	b.d.l.	599	6599	b.d.l.	1702	b.d.l.	b.d.l.	b.d.l.
Y	b.d.l.	b.d.l.	b.d.l.	130	b.d.l.	130	b.d.l.	0.88	b.d.l.	b.d.l.	b.d.l.	b.d.l.	b.d.l.	10	20	0.33	b.d.l.	b.d.l.	b.d.l.	b.d.l.
Ho	b.d.l.	b.d.l.	b.d.l.	7.24	b.d.l.	5.42	b.d.l.	1.94	b.d.l.	b.d.l.	b.d.l.	b.d.l.	b.d.l.	b.d.l.	0.32	b.d.l.	0.09	b.d.l.	b.d.l.	b.d.l.
Er	b.d.l.	0.60	b.d.l.	20	b.d.l.	28	b.d.l.	6.61	b.d.l.	b.d.l.	b.d.l.	b.d.l.	b.d.l.	0.14	2.93	b.d.l.	b.d.l.	b.d.l.	b.d.l.	b.d.l.
Tm	b.d.l.	1.17	b.d.l.	4.88	0.33	3.77	b.d.l.	0.10	b.d.l.	b.d.l.	b.d.l.	b.d.l.	b.d.l.	b.d.l.	0.42	0.47	b.d.l.	b.d.l.	b.d.l.	b.d.l.
Yb	b.d.l.	6.18	b.d.l.	30	b.d.l.	23	b.d.l.	4.75	b.d.l.	b.d.l.	b.d.l.	b.d.l.	b.d.l.	b.d.l.	2.05	0.76	b.d.l.	b.d.l.	b.d.l.	b.d.l.
Lu	b.d.l.	b.d.l.	b.d.l.	4.64	b.d.l.	4.32	b.d.l.	1.02	b.d.l.	b.d.l.	b.d.l.	b.d.l.	b.d.l.	1.11	0.47	0.43	b.d.l.	b.d.l.	b.d.l.	b.d.l.
Li	20	b.d.l.	44	b.d.l.	b.d.l.	b.d.l.	b.d.l.	b.d.l.	b.d.l.	28	b.d.l.	b.d.l.	23	b.d.l.	44	20	47	b.d.l.	31	b.d.l.
B	63	52	44	138	42	68	111	54	72	60	92	70	108	34	79	43	67	101	114	b.d.l.

b.d.l.= below detection limit

Table S5.5. Trace elements composition of the melt inclusions.

Melt inclusions

Name ppm	21	22	23	24	25	26	27	28	29	30	31	32	33	34	35	36	37	38	39	40
Cr	b.d.l.	b.d.l.	b.d.l.	b.d.l.	b.d.l.	b.d.l.	b.d.l.	b.d.l.	b.d.l.	b.d.l.	b.d.l.	b.d.l.	b.d.l.	b.d.l.	b.d.l.	b.d.l.	b.d.l.	b.d.l.	b.d.l.	b.d.l.
Ni	b.d.l.	b.d.l.	b.d.l.	b.d.l.	b.d.l.	b.d.l.	b.d.l.	b.d.l.	b.d.l.	b.d.l.	b.d.l.	b.d.l.	b.d.l.	b.d.l.	b.d.l.	b.d.l.	b.d.l.	b.d.l.	b.d.l.	b.d.l.
Rb	551	284	224	214	169	165	276	212	194	279	287	148	296	85	141	216	166	252	78	170
Cs	155	78	52	41	12	19	85	32	132	114	80	10	31	9.16	8.85	25	23	61	9.47	27
Ba	115	79	123	106	76	69	77	109	105	168	62	215	435	178	323	77	201	186	1005	236
Th	8.54	6.06	11	10	5.36	8.63	5.88	8.75	11	26	5.70	16	37	15	20	27	16	36	91	25
U	14	6.91	9.10	7.30	3.14	5.87	7.21	6.38	8.16	19	4.96	7.49	14	2.74	7.94	13	7.00	19	14	8.97
Nb	b.d.l.	0.67	0.47	0.44	b.d.l.	0.59	b.d.l.	0.46	0.33	b.d.l.	0.82	0.74	2.79	b.d.l.	0.93	b.d.l.	1.17	0.62	b.d.l.	0.73
Ta	b.d.l.	b.d.l.	b.d.l.	b.d.l.	b.d.l.	b.d.l.	b.d.l.	b.d.l.	b.d.l.	b.d.l.	b.d.l.	0.48	b.d.l.	b.d.l.	0.12	b.d.l.	b.d.l.	0.81	b.d.l.	0.27
La	4.87	8.09	17	9.18	3.12	6.94	4.20	8.86	9.59	27	4.37	11	14	39	10	16	8.66	5.77	29	13
Ce	19	18	34	22	9.07	17	10	17	16	62	2.55	26	34	73	17	19	13	b.d.l.	88	23
Pb	158	33	33	33	33	33	33	33	33	33	33	26	140	110	102	214	76	356	129	80
Pr	b.d.l.	b.d.l.	3.73	2.71	0.58	1.93	1.87	0.30	2.05	11	b.d.l.	3.72	11	5.92	1.41	6.90	b.d.l.	b.d.l.	b.d.l.	1.47
P	b.d.l.	b.d.l.	b.d.l.	b.d.l.	b.d.l.	b.d.l.	3125	b.d.l.	b.d.l.	8008	b.d.l.	b.d.l.	3151	b.d.l.	b.d.l.	7580	b.d.l.	b.d.l.	b.d.l.	b.d.l.
Sr	120	341	578	379	47	374	370	375	467	1041	111	379	724	303	415	568	349	751	273	421
Nd	b.d.l.	b.d.l.	2.86	14	b.d.l.	b.d.l.	2.36	0.64	4.23	47	b.d.l.	13	22	b.d.l.	b.d.l.	b.d.l.	b.d.l.	b.d.l.	b.d.l.	2.55
Zr	155	82	153	202	b.d.l.	211	107	138	111	686	42	250	480	b.d.l.	259	772	195	248	82	291
Hf	4.48	3.08	1.76	4.64	b.d.l.	7.44	6.07	4.55	4.57	22	4.97	8.37	18	b.d.l.	8.01	20	4.80	16	b.d.l.	8.95
Sm	b.d.l.	b.d.l.	4.98	12	b.d.l.	b.d.l.	b.d.l.	b.d.l.	b.d.l.	14	b.d.l.	6.14	25	b.d.l.	b.d.l.	b.d.l.	b.d.l.	b.d.l.	b.d.l.	b.d.l.
Eu	b.d.l.	b.d.l.	1.63	1.61	b.d.l.	b.d.l.	b.d.l.	b.d.l.	1.38	2.96	b.d.l.	3.36	b.d.l.	b.d.l.	b.d.l.	7.05	2.83	b.d.l.	21	b.d.l.
Gd	b.d.l.	b.d.l.	b.d.l.	11	b.d.l.	2.11	b.d.l.	b.d.l.	b.d.l.	41	b.d.l.	7.42	b.d.l.	b.d.l.	b.d.l.	b.d.l.	18	b.d.l.	b.d.l.	b.d.l.
Tb	b.d.l.	b.d.l.	0.97	3.66	b.d.l.	b.d.l.	2.02	0.11	b.d.l.	25	b.d.l.	2.05	5.41	b.d.l.	b.d.l.	b.d.l.	b.d.l.	b.d.l.	11	b.d.l.
Dy	b.d.l.	b.d.l.	6.40	35	b.d.l.	b.d.l.	22	b.d.l.	b.d.l.	b.d.l.	b.d.l.	15	b.d.l.	b.d.l.	b.d.l.	b.d.l.	b.d.l.	b.d.l.	b.d.l.	b.d.l.
Ti	b.d.l.	b.d.l.	b.d.l.	1558	b.d.l.	b.d.l.	596	b.d.l.	b.d.l.	5546	b.d.l.	1806	b.d.l.	b.d.l.	b.d.l.	7967	124	b.d.l.	b.d.l.	b.d.l.
Y	b.d.l.	b.d.l.	30	130	b.d.l.	b.d.l.	96	b.d.l.	b.d.l.	271	b.d.l.	b.d.l.	b.d.l.	b.d.l.	b.d.l.	b.d.l.	b.d.l.	b.d.l.	b.d.l.	b.d.l.
Ho	b.d.l.	b.d.l.	2.80	5.83	b.d.l.	b.d.l.	11	b.d.l.	b.d.l.	15	b.d.l.	b.d.l.	b.d.l.	b.d.l.	b.d.l.	b.d.l.	b.d.l.	b.d.l.	b.d.l.	b.d.l.
Er	b.d.l.	b.d.l.	19	20	b.d.l.	b.d.l.	15	b.d.l.	b.d.l.	b.d.l.	b.d.l.	7.10	b.d.l.	b.d.l.	b.d.l.	b.d.l.	b.d.l.	b.d.l.	b.d.l.	b.d.l.
Tm	b.d.l.	b.d.l.	0.15	4.89	b.d.l.	b.d.l.	3	b.d.l.	b.d.l.	35	b.d.l.	4.08	b.d.l.	b.d.l.	b.d.l.	b.d.l.	b.d.l.	b.d.l.	b.d.l.	b.d.l.
Yb	b.d.l.	b.d.l.	0.35	33	b.d.l.	b.d.l.	14	b.d.l.	b.d.l.	28	b.d.l.	8.11	b.d.l.	b.d.l.	b.d.l.	12	b.d.l.	b.d.l.	b.d.l.	b.d.l.
Lu	b.d.l.	b.d.l.	2.16	2.52	b.d.l.	b.d.l.	1	b.d.l.	b.d.l.	7.84	b.d.l.	0.94	b.d.l.	b.d.l.	b.d.l.	b.d.l.	b.d.l.	b.d.l.	6.78	b.d.l.
Li	b.d.l.	b.d.l.	37	b.d.l.	73	38	b.d.l.	30	76	b.d.l.	b.d.l.	b.d.l.	b.d.l.	b.d.l.	b.d.l.	b.d.l.	b.d.l.	117	b.d.l.	b.d.l.
B	229	77	108	42	65	65	112	49	100	306	b.d.l.	16	b.d.l.	b.d.l.	25	b.d.l.	78	177	b.d.l.	37

Table S5.5. Continued

Melt inclusions

Name ppm	41	42	43	44	45	46	47	48	49	50	51	52	53	54	55	56	57	58	59	60
Cr	b.d.l.	b.d.l.	b.d.l.	b.d.l.	b.d.l.	b.d.l.	b.d.l.	b.d.l.	b.d.l.	b.d.l.	b.d.l.	b.d.l.	b.d.l.	b.d.l.	b.d.l.	b.d.l.	b.d.l.	b.d.l.	b.d.l.	b.d.l.
Ni	b.d.l.	b.d.l.	b.d.l.	b.d.l.	b.d.l.	b.d.l.	b.d.l.	b.d.l.	b.d.l.	b.d.l.	b.d.l.	b.d.l.	b.d.l.	b.d.l.	b.d.l.	b.d.l.	b.d.l.	b.d.l.	b.d.l.	b.d.l.
Rb	169	242	144	182	168	202	128	118	186	195	212	259	206	242	247	182	181	226	192	168
Cs	15	79	17	31	19	29	10	11	24	34	59	148	104	90	59	27	21	55	27	16
Ba	204	135	316	144	234	350	169	153	247	222	141	130	61	121	120	156	145	151	158	164
Th	20	11	29	24	15	38	21	13	23	18	13	13	10	17	15	11	6.62	19	11	3.35
U	9.02	10	16	11	7.17	14	7.99	6.37	11	9.48	2.94	12	9.25	9.43	12	5.66	3.56	7.74	10	9.25
Nb	1.01	0.55	1.38	0.98	0.66	1.33	1.50	0.72	1.49	0.65	0.97	0.77	0.79	0.31	1.30	0.74	0.65	0.71	0.37	0.34
Ta	0.15	0.11	0.23	0.24	0.21	0.32	0.20	0.16	0.30	0.16	0.17	0.23	b.d.l.	b.d.l.	0.23	b.d.l.	0.16	0.28	0.10	b.d.l.
La	8.96	8.62	18	5.95	8.19	19	12	5.83	18	11	11	13	8.97	13	12	11	5.09	10	1.90	1.13
Ce	18	19	40	14	17	35	22	10	37	23	23	32	25	29	30	26	10	19	16	4.80
Pb	42	115	93	238	22	149	82	20	100	80	95	169	14	94	42	151	55	110	76	100
Pr	0.91	1.99	4.25	2.32	1.14	2.74	1.37	0.89	4.14	3.78	2.63	5.25	3.20	3.06	4.02	2.38	0.65	1.10	1.51	0.56
P	b.d.l.	b.d.l.	b.d.l.	b.d.l.	b.d.l.	59	1573	b.d.l.	b.d.l.	b.d.l.	b.d.l.	b.d.l.	b.d.l.	b.d.l.	b.d.l.	b.d.l.	b.d.l.	b.d.l.	b.d.l.	b.d.l.
Sr	248	455	423	69	457	549	253	135	477	334	314	266	651	429	269	365	184	431	375	356
Nd	b.d.l.	3.03	23	17	2.40	3.63	5.11	b.d.l.	3.96	3.92	8.28	6.37	8.17	b.d.l.	8.60	10	b.d.l.	5.30	b.d.l.	10
Zr	258	223	614	307	216	465	341	184	374	287	20	237	153	50	290	156	104	159	70	332
Hf	5.00	5.98	17	10	7.56	13	10	5.89	13	10	2.57	6.60	4.50	0.64	7.17	4.71	3.86	4.39	7.64	8.89
Sm	b.d.l.	b.d.l.	10	2.76	2.41	b.d.l.	3.26	b.d.l.	4.16	b.d.l.	b.d.l.	b.d.l.	1.41	b.d.l.	7.55	10	b.d.l.	b.d.l.	11	b.d.l.
Eu	b.d.l.	1.24	0.71	2.42	b.d.l.	b.d.l.	0.65	b.d.l.	0.27	b.d.l.	2.08	b.d.l.	23	b.d.l.	b.d.l.	0.51	b.d.l.	b.d.l.	2.45	b.d.l.
Gd	b.d.l.	b.d.l.	7.83	2.92	b.d.l.	b.d.l.	b.d.l.	b.d.l.	b.d.l.	b.d.l.	b.d.l.	b.d.l.	b.d.l.	b.d.l.	7.64	b.d.l.	b.d.l.	b.d.l.	17	b.d.l.
Tb	b.d.l.	0.39	1.69	b.d.l.	b.d.l.	b.d.l.	b.d.l.	b.d.l.	b.d.l.	b.d.l.	b.d.l.	b.d.l.	b.d.l.	b.d.l.	0.35	1.83	0.38	1.93	3.09	0.23
Dy	b.d.l.	b.d.l.	8.96	10	b.d.l.	b.d.l.	0.64	b.d.l.	5.11	5.86	b.d.l.	b.d.l.	b.d.l.	b.d.l.	b.d.l.	4.92	b.d.l.	18	22	11
Ti	b.d.l.	b.d.l.	568	592	b.d.l.	b.d.l.	190	b.d.l.	b.d.l.	b.d.l.	1095	b.d.l.	548	b.d.l.	2980	b.d.l.	b.d.l.	b.d.l.	1250	691
Y	b.d.l.	b.d.l.	52	57	b.d.l.	b.d.l.	12	b.d.l.	b.d.l.	b.d.l.	7.95	b.d.l.	b.d.l.	b.d.l.	b.d.l.	30	b.d.l.	49	105	71
Ho	b.d.l.	b.d.l.	3.72	1.97	b.d.l.	b.d.l.	b.d.l.	b.d.l.	b.d.l.	1.83	1.96	b.d.l.	b.d.l.	b.d.l.	b.d.l.	1.78	0.34	5.14	5.78	4.03
Er	b.d.l.	b.d.l.	15	15	b.d.l.	b.d.l.	b.d.l.	b.d.l.	b.d.l.	3.53	b.d.l.	b.d.l.	b.d.l.	b.d.l.	3.70	7.83	1.70	2.65	12	13
Tm	b.d.l.	b.d.l.	2.52	1.23	b.d.l.	b.d.l.	b.d.l.	b.d.l.	0.43	1.38	b.d.l.	0.21	b.d.l.	b.d.l.	b.d.l.	1.11	0.07	3.12	3.02	0.55
Yb	b.d.l.	3.17	16	17	b.d.l.	b.d.l.	b.d.l.	b.d.l.	b.d.l.	5.36	b.d.l.	b.d.l.	b.d.l.	b.d.l.	b.d.l.	11	3.93	5.15	15	5.95
Lu	b.d.l.	0.72	2.09	1.04	b.d.l.	b.d.l.	b.d.l.	b.d.l.	b.d.l.	0.58	0.61	b.d.l.	b.d.l.	b.d.l.	b.d.l.	0.93	0.85	2.22	1.63	3.02
Li	34	29	b.d.l.	b.d.l.	b.d.l.	b.d.l.	b.d.l.	16	b.d.l.	b.d.l.	39	b.d.l.	25	b.d.l.	b.d.l.	20	b.d.l.	b.d.l.	38	b.d.l.
B	26	84	51	65	24	51	45	31	41	62	62	107	70	139	43	61	14	67	70	75

Table S5.5. Continued

Melt inclusions

Name ppm	61	62	63	64	65	66	67	68	69	70	71	72	73	74	75	76	77	78	79	80
Cr	b.d.l.	b.d.l.	b.d.l.	b.d.l.	b.d.l.	b.d.l.	b.d.l.	b.d.l.	b.d.l.	b.d.l.	b.d.l.	b.d.l.	b.d.l.	b.d.l.	b.d.l.	b.d.l.	b.d.l.	b.d.l.	b.d.l.	b.d.l.
Ni	b.d.l.	b.d.l.	b.d.l.	b.d.l.	b.d.l.	b.d.l.	b.d.l.	b.d.l.	b.d.l.	b.d.l.	b.d.l.	b.d.l.	b.d.l.	b.d.l.	b.d.l.	b.d.l.	b.d.l.	b.d.l.	b.d.l.	b.d.l.
Rb	172	175	173	129	170	153	176	217	110	125	119	152	123	163	159	113	131	63	112	108
Cs	30	12	21	17	26	15	30	39	10	11	51	40	51	47	77	12	4.05	b.d.l.	8.94	10
Ba	173	161	159	223	115	187	102	102	224	201	499	101	294	177	b.d.l.	838	254	53	212	252
Th	16	12	14	14	26	22	14	18	12	21	99	15	6.27	3.55	b.d.l.	3.82	38	26	35	36
U	11	5.07	3.07	0.70	14	8.89	8.27	7.44	6.97	5.57	53	8.91	1.05	1.38	b.d.l.	41	31	2.94	17	19
Nb	0.89	0.75	b.d.l.	b.d.l.	1.67	0.99	0.42	0.46	9.27	0.68	2.12	0.50	1.45	0.29	2.03	3.00	2.47	b.d.l.	1.32	0.48
Ta	0.27	b.d.l.	b.d.l.	b.d.l.	0.23	0.22	0.12	0.12	0.49	0.14	0.71	0.25	b.d.l.	b.d.l.	b.d.l.	0.71	b.d.l.	b.d.l.	0.31	0.12
La	5.56	21	9.28	11	8.60	10	10	7.29	20	3.69	53	3.70	4.25	2.92	b.d.l.	13	16	18	10	24
Ce	15	30	2.65	23	20	19	21	14	53	6.27	126	8.48	10	8.33	b.d.l.	44	37	41	20	39
Pb	68	12	85	66	37	10	32	68	74	10	338	22	21	103	b.d.l.	613	274	68	74	95
Pr	0.54	1.69	b.d.l.	b.d.l.	4.06	1.60	1.99	b.d.l.	7.19	b.d.l.	14	b.d.l.	b.d.l.	0.56	b.d.l.	11	12	1.26	2.15	3.58
P	b.d.l.	b.d.l.	b.d.l.	b.d.l.	b.d.l.	b.d.l.	b.d.l.	b.d.l.	b.d.l.	b.d.l.	b.d.l.	b.d.l.	2510	b.d.l.	b.d.l.	b.d.l.	b.d.l.	b.d.l.	b.d.l.	b.d.l.
Sr	667	33	260	337	189	301	451	405	438	185	1065	45	551	454	b.d.l.	3044	232	52	214	279
Nd	2.07	b.d.l.	20	16	19	0.40	6.02	b.d.l.	17	b.d.l.	49	b.d.l.	13	6.51	b.d.l.	b.d.l.	b.d.l.	b.d.l.	b.d.l.	4.71
Zr	352	158	194	58	492	233	244	72	282	194	837	152	b.d.l.	35	b.d.l.	1014	383	b.d.l.	263	280
Hf	7.51	6.62	10	0.94	14	6.17	6.47	3.86	8.68	6.41	25	6.09	1.96	4.36	b.d.l.	32	14	5.75	7.57	8.30
Sm	8.40	12	b.d.l.	b.d.l.	9.29	b.d.l.	0.73	b.d.l.	0.94	b.d.l.	17	b.d.l.	b.d.l.	10	b.d.l.	46	10	b.d.l.	b.d.l.	3.81
Eu	3.31	1.27	b.d.l.	b.d.l.	4.42	b.d.l.	b.d.l.	b.d.l.	0.41	b.d.l.	2.43	b.d.l.	b.d.l.	5.01	b.d.l.	26	7.67	3.73	b.d.l.	b.d.l.
Gd	10	b.d.l.	75	11	25	b.d.l.	b.d.l.	b.d.l.	b.d.l.	b.d.l.	18	b.d.l.	b.d.l.	26	b.d.l.	b.d.l.	b.d.l.	b.d.l.	b.d.l.	b.d.l.
Tb	1.53	4.93	0.71	4.39	3.07	b.d.l.	b.d.l.	b.d.l.	b.d.l.	b.d.l.	0.25	b.d.l.	b.d.l.	3.97	b.d.l.	b.d.l.	7.03	7.06	b.d.l.	0.59
Dy	2.20	35	51	b.d.l.	12	b.d.l.	b.d.l.	b.d.l.	b.d.l.	b.d.l.	2.68	b.d.l.	b.d.l.	28	b.d.l.	20	b.d.l.	b.d.l.	b.d.l.	b.d.l.
Ti	831	b.d.l.	b.d.l.	3142	3238	b.d.l.	b.d.l.	b.d.l.	16933	b.d.l.	b.d.l.	b.d.l.	b.d.l.	432	b.d.l.	b.d.l.	884	b.d.l.	b.d.l.	b.d.l.
Y	18	146	244	b.d.l.	102	b.d.l.	b.d.l.	b.d.l.	b.d.l.	b.d.l.	107	b.d.l.	b.d.l.	32	b.d.l.	18	37	b.d.l.	b.d.l.	b.d.l.
Ho	1.50	b.d.l.	5.44	b.d.l.	5.20	b.d.l.	b.d.l.	b.d.l.	b.d.l.	b.d.l.	b.d.l.	b.d.l.	b.d.l.	7.54	b.d.l.	b.d.l.	b.d.l.	0.86	b.d.l.	1.00
Er	3.23	14	34	b.d.l.	11	b.d.l.	b.d.l.	b.d.l.	b.d.l.	b.d.l.	15	b.d.l.	3.73	30	b.d.l.	62	42	73	b.d.l.	b.d.l.
Tm	b.d.l.	0.53	b.d.l.	3.06	2.32	b.d.l.	b.d.l.	b.d.l.	b.d.l.	b.d.l.	0.17	b.d.l.	b.d.l.	5.10	b.d.l.	4.75	10	b.d.l.	b.d.l.	b.d.l.
Yb	9.46	57	34	23	19	b.d.l.	b.d.l.	b.d.l.	b.d.l.	b.d.l.	8.56	b.d.l.	2.29	32	b.d.l.	57	18	b.d.l.	b.d.l.	4.01
Lu	0.45	5.36	b.d.l.	b.d.l.	3.59	b.d.l.	b.d.l.	b.d.l.	b.d.l.	b.d.l.	1.45	b.d.l.	1.72	2.83	b.d.l.	b.d.l.	2.32	b.d.l.	b.d.l.	0.10
Li	b.d.l.	b.d.l.	b.d.l.	b.d.l.	40	5.71	24	28	30	23	b.d.l.	b.d.l.	124	35	b.d.l.	b.d.l.	b.d.l.	b.d.l.	11	16
B	74	102	162	149	b.d.l.	38	99	57	28	20	295	74	b.d.l.	88	b.d.l.	211	b.d.l.	b.d.l.	46	42

Table S5.5. Continued

Melt inclusions

Name ppm	81	82	83	84	85	86	87	88	89	90	91	92	93	94	95	96	97	98	99	100
Cr	b.d.l.	b.d.l.	b.d.l.	b.d.l.	b.d.l.	b.d.l.	b.d.l.	b.d.l.	b.d.l.	b.d.l.	b.d.l.	b.d.l.	b.d.l.	b.d.l.	b.d.l.	b.d.l.	b.d.l.	b.d.l.	b.d.l.	b.d.l.
Ni	b.d.l.	b.d.l.	b.d.l.	b.d.l.	b.d.l.	b.d.l.	b.d.l.	b.d.l.	b.d.l.	b.d.l.	b.d.l.	b.d.l.	47	65	b.d.l.	b.d.l.	b.d.l.	b.d.l.	b.d.l.	b.d.l.
Rb	128	73	120	125	95	108	180	95	132	110	119	127	114	176	85	117	198	204	163	166
Cs	13	3.76	20	12	64	11	46	24	7.20	13	21	18	11	11	39	11	36	18	24	58
Ba	452	492	363	452	244	324	920	80	326	325	219	154	498	438	1416	522	260	282	275	239
Th	20	41	51	43	20	39	116	48	22	52	16	36	21	20	27	14	23	29	25	70
U	20	19	24	20	85	13	54	14	12	14	7.84	19	11	13	21	7.48	17	10	18	35
Nb	1.70	8.28	1.23	1.59	0.91	2.35	b.d.l.	b.d.l.	0.64	0.85	2.66	1.81	0.71	0.61	5.21	0.28	0.47	0.44	0.47	0.89
Ta	0.31	b.d.l.	b.d.l.	0.20	0.38	0.82	b.d.l.	b.d.l.	b.d.l.	b.d.l.	b.d.l.	b.d.l.	0.25	0.18	0.85	0.09	0.11	b.d.l.	0.15	0.23
La	16	b.d.l.	12	16	6.57	12	22	89	4.49	11	19	8.84	11	13	28	3.20	10	12	20	40
Ce	34	b.d.l.	23	35	15	29	19	166	11	96	46	22	22	31	69	7.49	22	21	47	83
Pb	186	214	167	152	18	58	221	44	48	115	206	183	92	122	42	19	22	56	74	333
Pr	3.56	b.d.l.	3.19	3.43	2.64	2.81	0.83	19	1.36	7.05	5.35	2.04	2.14	3.84	6.14	0.54	1.78	1.11	5.50	8.22
P	b.d.l.	1462	b.d.l.	b.d.l.	b.d.l.	b.d.l.	b.d.l.	1959	b.d.l.	b.d.l.	1770	b.d.l.	b.d.l.	b.d.l.	b.d.l.	b.d.l.	b.d.l.	b.d.l.	b.d.l.	b.d.l.
Sr	607	338	526	350	98	289	1283	512	307	243	184	151	331	318	776	140	266	103	303	1026
Nd	11	20	b.d.l.	5.20	9.36	5.62	b.d.l.	77	b.d.l.	71	15	b.d.l.	b.d.l.	13	b.d.l.	2	b.d.l.	b.d.l.	23	33
Zr	461	383	572	352	200	243	791	248	218	289	145	248	244	251	433	165	362	167	300	869
Hf	13	15	10	11	3.80	11	42	15	7.24	15	4.40	5.27	6.29	8.73	24	4.43	9.44	5.75	8.82	25
Sm	4.56	b.d.l.	b.d.l.	b.d.l.	18	b.d.l.	b.d.l.	b.d.l.	b.d.l.	b.d.l.	b.d.l.	b.d.l.	b.d.l.	5.07	b.d.l.	b.d.l.	b.d.l.	b.d.l.	3.58	b.d.l.
Eu	b.d.l.	b.d.l.	0.54	b.d.l.	3.53	b.d.l.	b.d.l.	3.68	b.d.l.	b.d.l.	0.90	b.d.l.	b.d.l.	1.65	b.d.l.	b.d.l.	b.d.l.	3.33	b.d.l.	b.d.l.
Gd	b.d.l.	16	b.d.l.	b.d.l.	b.d.l.	0.72	6.70	12	b.d.l.	b.d.l.	b.d.l.	b.d.l.	b.d.l.	3.23	b.d.l.	b.d.l.	b.d.l.	0.53	2.70	b.d.l.
Tb	b.d.l.	b.d.l.	b.d.l.	b.d.l.	b.d.l.	1.94	5.76	9.19	b.d.l.	b.d.l.	0.43	b.d.l.	b.d.l.	b.d.l.	b.d.l.	b.d.l.	b.d.l.	b.d.l.	b.d.l.	b.d.l.
Dy	2.07	1.03	b.d.l.	b.d.l.	16	9.26	b.d.l.	46	b.d.l.	b.d.l.	9.90	b.d.l.	b.d.l.	0.97	b.d.l.	b.d.l.	b.d.l.	b.d.l.	2.61	b.d.l.
Ti	b.d.l.	13361	b.d.l.	b.d.l.	954	b.d.l.	b.d.l.	b.d.l.	b.d.l.	25861	3318	1248	b.d.l.	672	b.d.l.	204	b.d.l.	b.d.l.	295	b.d.l.
Y	b.d.l.	57	b.d.l.	b.d.l.	b.d.l.	b.d.l.	b.d.l.	b.d.l.	b.d.l.	85	69	b.d.l.	b.d.l.	b.d.l.	b.d.l.	b.d.l.	b.d.l.	b.d.l.	b.d.l.	b.d.l.
Ho	b.d.l.	b.d.l.	b.d.l.	b.d.l.	3.90	b.d.l.	7.47	14	b.d.l.	b.d.l.	5.97	b.d.l.	b.d.l.	b.d.l.	b.d.l.	b.d.l.	b.d.l.	b.d.l.	b.d.l.	b.d.l.
Er	b.d.l.	b.d.l.	b.d.l.	b.d.l.	8.94	b.d.l.	b.d.l.	b.d.l.	b.d.l.	54	8.55	b.d.l.	b.d.l.	b.d.l.	b.d.l.	b.d.l.	b.d.l.	5.06	0.55	b.d.l.
Tm	b.d.l.	b.d.l.	b.d.l.	b.d.l.	1.71	b.d.l.	b.d.l.	b.d.l.	b.d.l.	15	4.28	b.d.l.	b.d.l.	b.d.l.	b.d.l.	b.d.l.	b.d.l.	0.53	b.d.l.	b.d.l.
Yb	1.00	b.d.l.	b.d.l.	b.d.l.	8.18	14	100	38	b.d.l.	122	10	b.d.l.	b.d.l.	0.45	b.d.l.	b.d.l.	b.d.l.	b.d.l.	4.58	14
Lu	b.d.l.	b.d.l.	b.d.l.	b.d.l.	0.77	2.43	1.87	8.30	b.d.l.	6.95	2.10	b.d.l.	b.d.l.	0.41	b.d.l.	b.d.l.	b.d.l.	b.d.l.	b.d.l.	b.d.l.
Li	b.d.l.	b.d.l.	b.d.l.	26	b.d.l.	31	198	b.d.l.	b.d.l.	b.d.l.	b.d.l.	118	16	19	243	21	17	23	22	39
B	65	b.d.l.	123	68	26	48	216	b.d.l.	b.d.l.	132	113	63	50	37	50	10	71	54	36	170

Table S5.5. Continued

Melt inclusions

Name ppm	101	102	103	104	105	106	107	108	109	110
Cr	b.d.l.	b.d.l.	b.d.l.	b.d.l.	b.d.l.	b.d.l.	b.d.l.	b.d.l.	b.d.l.	b.d.l.
Ni	b.d.l.	b.d.l.	b.d.l.	b.d.l.	b.d.l.	b.d.l.	b.d.l.	b.d.l.	b.d.l.	b.d.l.
Rb	166	188	183	111	284	158	167	132	143	109
Cs	21	23	18	38	24	10	28	14	12	9.93
Ba	270	354	312	275	188	352	308	230	413	338
Th	28	26	19	46	63	15	58	13	20	13
U	10	16	9.52	28	33	8.88	36	9.43	12	9.14
Nb	0.77	1.18	0.84	0.10	1.17	0.16	b.d.l.	0.46	0.64	0.44
Ta	0.22	0.23	0.16	0.10	b.d.l.	0.08	b.d.l.	0.10	0.26	0.26
La	9.57	20	13	7.03	24	8.51	22	6.89	8.86	6.65
Ce	21	44	29	14	59	19	47	16	22	19
Pb	71	238	37	103	146	9	835	56	85	49
Pr	1.93	4.67	2.62	0.35	8.55	1.72	b.d.l.	1.46	2.60	2.54
P	b.d.l.	b.d.l.	b.d.l.	b.d.l.	1243	b.d.l.	b.d.l.	b.d.l.	b.d.l.	b.d.l.
Sr	226	340	205	688	475	120	175	247	298	234
Nd	3	15	6	1	31	0	2	1	2	11
Zr	112	362	94	542	649	188	491	184	254	231
Hf	5.05	8.58	3.62	17	18	3.41	9.75	4.88	6.52	6.35
Sm	b.d.l.	24	b.d.l.	b.d.l.	6.01	b.d.l.	b.d.l.	b.d.l.	b.d.l.	2.63
Eu	0.23	7.23	b.d.l.	2.62	0.73	b.d.l.	5.40	0.38	b.d.l.	1.17
Gd	b.d.l.	15	b.d.l.	b.d.l.	4.87	b.d.l.	b.d.l.	b.d.l.	14	b.d.l.
Tb	b.d.l.	1.04	b.d.l.	b.d.l.	1.80	b.d.l.	b.d.l.	b.d.l.	b.d.l.	b.d.l.
Dy	b.d.l.	1.53	b.d.l.	b.d.l.	10	b.d.l.	24	b.d.l.	5.19	b.d.l.
Ti	b.d.l.	2469	b.d.l.	b.d.l.	1347	b.d.l.	b.d.l.	b.d.l.	b.d.l.	543
Y	b.d.l.	b.d.l.	b.d.l.	b.d.l.	58	b.d.l.	b.d.l.	b.d.l.	b.d.l.	b.d.l.
Ho	b.d.l.	3.26	b.d.l.	b.d.l.	6.41	b.d.l.	b.d.l.	b.d.l.	3.66	b.d.l.
Er	b.d.l.	23	b.d.l.	b.d.l.	15	b.d.l.	b.d.l.	b.d.l.	b.d.l.	1.86
Tm	b.d.l.	3.91	b.d.l.	b.d.l.	2.13	b.d.l.	b.d.l.	b.d.l.	1.99	0.51
Yb	b.d.l.	12	b.d.l.	1.47	8.01	b.d.l.	b.d.l.	b.d.l.	b.d.l.	3.52
Lu	b.d.l.	0.14	b.d.l.	b.d.l.	1.03	b.d.l.	b.d.l.	b.d.l.	b.d.l.	0.80
Li	16	27	14	16	b.d.l.	16	b.d.l.	20	b.d.l.	12
B	96	56	44	122	26	23	189	33	54	41

Table S5.5. Continued

APPENDIX

A1. GARNET ANALYSES FROM RUBINBERG

Rubinberg Garnets

Name	1	5	10	9	13	20	21	22	30	40	41	42	44	45	46	54	55	56	59	60
wt. %																				
SiO_2	38.59	38.53	38.48	39.84	40.06	40.05	40.13	39.75	40.16	40.48	40.50	39.91	40.63	40.35	40.48	40.13	39.70	40.15	40.29	40.01
TiO_2	0.13	0.13	0.24	0.14	0.12	0.16	0.11	0.05	0.15	0.22	0.09	0.11	0.33	0.24	0.30	0.20	0.23	0.26	0.30	0.21
Al_2O_3	22.77	22.86	22.77	22.61	22.47	22.77	22.82	22.83	22.94	22.95	22.78	22.97	22.91	22.86	22.82	22.89	23.00	22.79	22.78	22.91
FeO	18.39	18.70	17.53	19.21	19.37	19.10	19.51	20.36	17.97	16.50	20.37	20.08	15.21	15.22	15.27	17.32	18.16	17.11	16.64	17.53
MnO	0.37	0.38	0.35	0.39	0.44	0.45	0.39	0.47	0.34	0.28	0.48	0.45	0.24	0.23	0.29	0.35	0.38	0.36	0.32	0.34
MgO	9.65	9.73	8.91	9.91	9.94	9.42	9.95	10.38	9.75	9.65	10.05	10.12	10.26	10.17	10.11	10.03	9.31	9.68	9.57	9.43
CaO	9.82	9.22	11.35	8.57	8.30	9.01	8.21	6.98	10.12	11.65	7.18	7.72	11.78	11.78	11.72	10.32	10.68	11.10	11.58	10.69
Na_2O	0.04	0.02	0.02	0.04	0.03	0.00	0.02	0.03	0.01	0.02	0.03	0.01	0.02	0.04	0.08	0.06	0.06	0.03	0.04	0.02
K_2O	0.01	0.01	0.00	0.00	0.00	0.01	0.00	0.01	0.00	0.00	0.01	0.01	0.00	0.00	0.00	0.00	0.00	0.00	0.00	0.00
P_2O_5	0.07	0.05	0.07	0.07	0.05	0.05	0.02	0.04	0.06	0.05	0.04	0.03	0.05	0.06	0.04	0.06	0.08	0.08	0.06	0.06
TOTAL	99.83	99.62	99.72	100.77	100.78	101.01	101.16	100.89	101.50	101.79	101.53	101.39	101.44	100.94	101.13	101.34	101.60	101.55	101.56	101.20
Mg#	48	48	48	48	48	47	48	48	49	51	47	47	55	54	54	51	48	50	51	49
Si	**2.93**	**2.93**	**2.92**	**2.98**	**3.00**	**2.99**	**2.99**	**2.98**	**2.98**	**2.98**	**3.01**	**2.97**	**2.99**	**2.99**	**2.99**	**2.98**	**2.95**	**2.98**	**2.98**	**2.98**
Ti	0.01	0.01	0.01	0.01	0.01	0.01	0.01	0.00	0.01	0.01	0.01	0.01	0.02	0.01	0.02	0.01	0.01	0.01	0.02	0.01
Al	2.04	2.05	2.04	2.00	1.98	2.00	2.00	2.01	2.01	1.99	1.99	2.02	1.99	1.99	1.99	2.00	2.02	1.99	1.99	2.01
	2.04	**2.05**	**2.05**	**2.00**	**1.99**	**2.01**	**2.01**	**2.02**	**2.01**	**2.01**	**2.00**	**2.02**	**2.00**	**2.01**	**2.00**	**2.01**	**2.03**	**2.01**	**2.00**	**2.02**
Fe	1.17	1.19	1.11	1.20	1.21	1.19	1.22	1.27	1.11	1.02	1.27	1.25	0.94	0.94	0.94	1.07	1.13	1.06	1.03	1.09
Mn	0.02	0.02	0.02	0.02	0.03	0.03	0.02	0.03	0.02	0.02	0.03	0.03	0.02	0.01	0.02	0.02	0.02	0.02	0.02	0.02
Mg	1.09	1.10	1.01	1.11	1.11	1.05	1.10	1.16	1.08	1.06	1.11	1.12	1.13	1.12	1.11	1.11	1.03	1.07	1.06	1.05
Ca	0.80	0.75	0.92	0.69	0.67	0.72	0.66	0.56	0.80	0.92	0.57	0.62	0.93	0.93	0.93	0.82	0.85	0.88	0.92	0.85
	3.08	**3.06**	**3.07**	**3.02**	**3.01**	**2.99**	**3.00**	**3.02**	**3.02**	**3.02**	**2.98**	**3.02**	**3.01**	**3.01**	**3.00**	**3.02**	**3.04**	**3.03**	**3.02**	**3.01**
mol %																				
Alm	**38**	**39**	**36**	**40**	**40**	**40**	**41**	**42**	**37**	**34**	**42**	**41**	**31**	**31**	**31**	**36**	**37**	**35**	**34**	**36**
Prp	**35**	**36**	**33**	**37**	**37**	**35**	**37**	**38**	**36**	**35**	**37**	**37**	**37**	**37**	**37**	**37**	**34**	**35**	**35**	**35**
Sps	**1**	**1**	**1**	**1**	**1**	**1**	**1**	**1**	**1**	**1**	**1**	**1**	**1**	**0**	**1**	**1**	**1**	**1**	**1**	**1**
Grs	**26**	**24**	**30**	**23**	**22**	**24**	**22**	**19**	**27**	**31**	**19**	**20**	**31**	**31**	**31**	**27**	**28**	**29**	**30**	**28**

Table A1. Major element composition of Rubinberg garnets.

Rubinberg Garnets

Name	61	65	66	67	68	77	78	79	80	88	89	90	91	101	102	103	104	105	106	107	108
wt. %																					
SiO_2	39.88	39.91	40.49	39.99	40.15	39.79	39.99	39.77	39.76	39.84	39.40	39.61	39.35	40.05	39.78	39.73	40.01	40.53	40.52	40.60	40.36
TiO_2	0.14	0.16	0.27	0.17	0.31	0.15	0.23	0.10	0.22	0.13	0.24	0.24	0.19	0.12	0.13	0.08	0.13	0.26	0.26	0.27	0.23
Al_2O_3	23.00	22.79	22.76	22.75	22.82	22.73	22.71	22.99	22.53	22.86	22.78	22.91	22.68	22.69	22.91	22.72	22.78	23.06	22.95	23.00	22.83
FeO	20.09	19.47	14.98	19.77	15.91	19.99	17.69	21.19	19.32	19.82	17.18	16.16	17.22	20.52	20.75	21.29	21.13	14.71	14.53	14.64	15.87
MnO	0.43	0.42	0.25	0.33	0.31	0.44	0.33	0.50	0.40	0.47	0.35	0.28	0.37	0.48	0.49	0.49	0.45	0.32	0.28	0.27	0.30
MgO	9.93	9.27	9.93	9.31	9.62	9.04	9.22	9.75	8.90	9.64	9.21	9.59	9.84	9.63	9.51	9.86	9.59	10.84	11.18	10.72	9.81
CaO	7.85	9.45	12.09	9.10	11.92	9.01	10.98	7.21	10.01	8.31	11.26	11.61	10.36	7.74	7.94	7.35	7.73	11.46	11.04	11.63	11.58
Na_2O	0.03	0.05	0.07	0.00	0.10	0.01	0.02	0.00	0.02	0.00	0.04	0.06	0.02	0.02	0.03	0.01	0.03	0.05	0.05	0.06	0.04
K_2O	0.00	0.00	0.00	0.00	0.01	0.01	0.00	0.00	0.00	0.01	0.01	0.00	0.01	0.00	0.01	0.00	0.01	0.00	0.00	0.00	0.00
P_2O_5	0.06	0.06	0.07	0.09	0.08	0.07	0.09	0.04	0.07	0.06	0.06	0.04	0.04	0.07	0.04	0.05	0.04	0.05	0.03	0.05	0.05
TOTAL	101.39	101.59	100.90	101.51	101.23	101.23	101.24	101.55	101.24	101.13	100.51	100.50	100.09	101.32	101.58	101.58	101.88	101.27	100.84	101.24	101.06
Mg#	47	46	54	46	52	45	48	45	45	46	49	51	50	46	45	45	45	57	58	57	52
Si	**2.97**	**2.98**	**3.00**	**2.98**	**2.98**	**2.98**	**2.98**	**2.97**	**2.98**	**2.98**	**2.96**	**2.96**	**2.96**	**2.99**	**2.97**	**2.97**	**2.98**	**2.98**	**2.99**	**2.99**	**2.99**
Ti	0.01	0.01	0.01	0.01	0.02	0.01	0.01	0.01	0.01	0.01	0.01	0.01	0.01	0.01	0.01	0.00	0.01	0.01	0.01	0.01	0.01
Al	2.02	2.00	1.99	2.00	2.00	2.01	1.99	2.02	1.99	2.01	2.02	2.02	2.01	2.00	2.02	2.00	2.00	2.00	1.99	1.99	1.99
	2.03	**2.01**	**2.00**	**2.01**	**2.01**	**2.02**	**2.01**	**2.03**	**2.00**	**2.02**	**2.03**	**2.03**	**2.02**	**2.00**	**2.02**	**2.01**	**2.01**	**2.01**	**2.01**	**2.01**	**2.01**
Fe	1.25	1.21	0.93	1.23	0.99	1.25	1.10	1.32	1.21	1.24	1.08	1.01	1.08	1.28	1.30	1.33	1.32	0.90	0.90	0.90	0.98
Mn	0.03	0.03	0.02	0.02	0.02	0.03	0.02	0.03	0.03	0.03	0.02	0.02	0.02	0.03	0.03	0.03	0.03	0.02	0.02	0.02	0.02
Mg	1.10	1.03	1.10	1.04	1.06	1.01	1.02	1.09	0.99	1.07	1.03	1.07	1.10	1.07	1.06	1.10	1.06	1.19	1.23	1.17	1.08
Ca	0.63	0.75	0.96	0.73	0.95	0.72	0.88	0.58	0.80	0.67	0.91	0.93	0.83	0.62	0.64	0.59	0.62	0.90	0.87	0.92	0.92
	3.01	**3.03**	**3.00**	**3.02**	**3.02**	**3.01**	**3.02**	**3.02**	**3.03**	**3.01**	**3.04**	**3.03**	**3.05**	**3.01**	**3.02**	**3.05**	**3.03**	**3.02**	**3.01**	**3.01**	**3.00**
mol %																					
Alm	**42**	**40**	**31**	**41**	**33**	**42**	**36**	**44**	**40**	**41**	**36**	**33**	**36**	**43**	**43**	**44**	**43**	**30**	**30**	**30**	**33**
Prp	**37**	**34**	**37**	**34**	**35**	**34**	**34**	**36**	**33**	**36**	**34**	**35**	**36**	**36**	**35**	**36**	**35**	**39**	**41**	**39**	**36**
Sps	**1**	**1**	**1**	**1**	**1**	**1**	**1**	**1**	**1**	**1**	**1**	**1**	**1**	**1**	**1**	**1**	**1**	**1**	**1**	**1**	**1**
Grs	**21**	**25**	**32**	**24**	**31**	**24**	**29**	**19**	**26**	**22**	**30**	**31**	**27**	**21**	**21**	**19**	**20**	**30**	**29**	**30**	**31**

Table A1. Continued.

Rubinberg Garnets

Name	115	116	117	118	119	128	129	148	149	150	151	152	153	154	155	156	157	159	160	161	162
wt. %																					
SiO_2	39.95	39.75	40.40	40.46	40.12	40.57	40.52	40.37	40.19	40.44	40.11	40.30	40.48	40.27	40.38	40.29	40.37	40.04	40.25	40.28	40.50
TiO_2	0.13	0.17	0.32	0.27	0.21	0.23	0.31	0.15	0.22	0.17	0.16	0.20	0.21	0.24	0.22	0.22	0.20	0.17	0.18	0.17	0.26
Al_2O_3	22.80	22.87	23.03	22.97	22.89	23.65	23.05	23.14	23.23	23.18	23.10	23.24	23.11	23.18	23.23	23.21	23.10	23.07	23.08	23.19	23.06
FeO	20.56	19.38	14.18	14.58	18.18	13.66	14.30	15.74	14.23	14.62	15.35	15.27	14.27	13.74	13.83	14.22	14.99	15.39	15.65	15.41	14.36
MnO	0.45	0.38	0.23	0.27	0.42	0.20	0.21	0.30	0.19	0.23	0.29	0.28	0.23	0.20	0.21	0.25	0.28	0.27	0.30	0.26	0.27
MgO	9.69	9.29	10.57	10.69	9.56	10.50	9.86	10.47	10.03	9.99	9.93	10.15	9.78	10.19	10.21	9.93	10.40	10.11	10.62	10.12	9.97
CaO	7.62	9.60	12.13	12.14	10.11	12.95	12.86	11.09	12.72	12.42	11.60	11.82	12.71	12.98	12.98	12.93	11.45	11.66	10.74	11.93	12.99
Na_2O	0.03	0.05	0.08	0.01	0.05	0.05	0.07	0.01	0.01	0.02	0.00	0.03	0.03	0.01	0.07	0.02	0.02	0.04	0.00	0.03	0.02
K_2O	0.00	0.00	0.01	0.01	0.00	0.00	0.00	0.01	0.00	0.00	0.01	0.01	0.02	0.01	0.00	0.01	0.01	0.00	0.01	0.02	0.00
P_2O_5	0.05	0.06	0.06	0.08	0.04	0.08	0.09	0.07	0.09	0.06	0.06	0.06	0.05	0.06	0.09	0.09	0.06	0.07	0.06	0.07	0.06
TOTAL	101.27	101.55	101.02	101.48	101.58	101.89	101.26	101.35	100.90	101.13	100.61	101.35	100.88	100.89	101.20	101.17	100.87	100.82	100.88	101.48	101.49
Mg#	46	46	57	57	48	58	55	54	56	55	54	54	55	57	57	55	55	54	55	54	55
Si	**2.99**	**2.97**	**2.98**	**2.97**	**2.98**	**2.96**	**2.99**	**2.98**	**2.97**	**2.98**	**2.98**	**2.97**	**2.99**	**2.97**	**2.97**	**2.97**	**2.98**	**2.97**	**2.98**	**2.97**	**2.98**
Ti	0.01	0.01	0.02	0.02	0.01	0.01	0.02	0.01	0.01	0.01	0.01	0.01	0.01	0.01	0.01	0.01	0.01	0.01	0.01	0.01	0.01
Al	2.01	2.01	2.00	1.99	2.00	2.03	2.00	2.01	2.02	2.01	2.02	2.02	2.01	2.02	2.02	2.02	2.01	2.02	2.01	2.01	2.00
	2.02	**2.02**	**2.02**	**2.00**	**2.01**	**2.05**	**2.02**	**2.02**	**2.03**	**2.02**	**2.03**	**2.03**	**2.02**	**2.03**	**2.03**	**2.03**	**2.02**	**2.03**	**2.02**	**2.02**	**2.01**
Fe	1.28	1.21	0.87	0.90	1.13	0.83	0.88	0.97	0.88	0.90	0.95	0.94	0.88	0.85	0.85	0.88	0.93	0.95	0.97	0.95	0.88
Mn	0.03	0.02	0.01	0.02	0.03	0.01	0.01	0.02	0.01	0.01	0.02	0.02	0.01	0.01	0.01	0.02	0.02	0.02	0.02	0.02	0.02
Mg	1.08	1.03	1.16	1.17	1.06	1.14	1.08	1.15	1.10	1.10	1.10	1.12	1.08	1.12	1.12	1.09	1.15	1.12	1.17	1.11	1.09
Ca	0.61	0.77	0.96	0.96	0.80	1.01	1.01	0.88	1.01	0.98	0.92	0.93	1.01	1.03	1.02	1.02	0.91	0.93	0.85	0.94	1.02
	3.00	**3.03**	**3.01**	**3.04**	**3.02**	**3.00**	**2.99**	**3.02**	**3.00**	**3.00**	**2.99**	**3.01**	**2.98**	**3.01**	**3.01**	**3.01**	**3.00**	**3.02**	**3.01**	**3.02**	**3.02**
mol %																					
Alm	**43**	**40**	**29**	**29**	**37**	**28**	**29**	**32**	**29**	**30**	**32**	**31**	**30**	**28**	**28**	**29**	**31**	**32**	**32**	**31**	**29**
Prp	**36**	**34**	**39**	**39**	**35**	**38**	**36**	**38**	**37**	**37**	**37**	**37**	**36**	**37**	**37**	**36**	**38**	**37**	**39**	**37**	**36**
Sps	**1**	**1**	**0**	**1**	**1**	**0**	**0**	**1**	**0**	**0**	**1**	**1**	**0**	**0**	**0**	**1**	**1**	**1**	**1**	**1**	**1**
Grs	**20**	**25**	**32**	**31**	**27**	**34**	**34**	**29**	**34**	**33**	**31**	**31**	**34**	**34**	**34**	**34**	**30**	**31**	**28**	**31**	**34**

Table A1. Continued.

Rubinberg Garnets

Name	163	164	165	166	167	168	169	170	191	192	193	194	195	196	201	202	203	237	238	239	240
wt. %																					
SiO_2	40.57	40.35	40.30	40.14	40.20	40.36	40.55	40.24	40.38	40.14	40.33	40.48	40.21	40.11	40.41	40.28	40.57	40.08	40.11	39.70	39.88
TiO_2	0.24	0.20	0.18	0.15	0.23	0.25	0.25	0.14	0.12	0.19	0.15	0.24	0.24	0.19	0.16	0.22	0.15	0.17	0.21	0.22	0.23
Al_2O_3	23.07	23.11	23.10	23.37	22.95	23.15	23.03	23.27	23.35	23.20	23.23	23.34	23.48	23.43	23.21	23.03	23.01	22.79	22.60	22.56	22.77
FeO	14.09	14.13	15.63	15.94	14.75	14.44	13.98	15.56	16.59	14.45	14.11	13.59	13.74	15.47	15.62	15.10	15.38	18.10	17.10	17.11	16.98
MnO	0.20	0.21	0.30	0.26	0.26	0.20	0.22	0.27	0.38	0.27	0.23	0.18	0.21	0.26	0.30	0.23	0.24	0.39	0.35	0.33	0.33
MgO	10.04	10.05	10.29	10.71	9.73	9.96	9.95	10.17	10.75	10.06	10.39	10.08	10.11	10.31	10.09	9.81	10.22	9.52	8.58	8.82	8.91
CaO	13.01	12.75	11.23	10.72	12.75	12.92	13.04	11.62	9.73	12.68	12.46	13.08	13.11	11.46	11.81	12.25	11.48	10.16	12.16	11.80	11.94
Na_2O	0.06	0.00	0.02	0.01	0.05	0.06	0.05	0.03	0.04	0.05	0.03	0.05	0.06	0.02	0.03	0.04	0.01	0.02	0.05	0.03	0.04
K_2O	0.00	0.00	0.00	0.01	0.00	0.01	0.00	0.02	0.00	0.00	0.01	0.00	0.01	0.00	0.00	0.00	0.00	0.00	0.01	0.02	0.00
P_2O_5	0.05	0.07	0.05	0.05	0.08	0.10	0.06	0.05	0.03	0.06	0.07	0.07	0.07	0.07	0.06	0.07	0.04	0.07	0.06	0.07	0.05
TOTAL	101.34	100.86	101.08	101.38	101.00	101.44	101.13	101.37	101.37	101.09	101.00	101.12	101.23	101.31	101.68	101.04	101.12	101.29	101.23	100.66	101.13
Mg#	56	56	54	55	54	55	56	54	54	55	57	57	57	54	54	54	54	48	47	48	48
Si	**2.98**	**2.98**	**2.98**	**2.96**	**2.98**	**2.97**	**2.99**	**2.97**	**2.97**	**2.96**	**2.97**	**2.98**	**2.96**	**2.96**	**2.97**	**2.98**	**2.99**	**2.98**	**2.99**	**2.98**	**2.97**
Ti	0.01	0.01	0.01	0.01	0.01	0.01	0.01	0.01	0.01	0.01	0.01	0.01	0.01	0.01	0.01	0.01	0.01	0.01	0.01	0.01	0.01
Al	2.00	2.01	2.01	2.03	2.00	2.01	2.00	2.02	2.03	2.02	2.02	2.02	2.04	2.04	2.01	2.01	2.00	2.00	1.99	1.99	2.00
	2.01	**2.02**	**2.02**	**2.04**	**2.02**	**2.02**	**2.01**	**2.03**	**2.03**	**2.03**	**2.03**	**2.04**	**2.05**	**2.05**	**2.02**	**2.02**	**2.01**	**2.01**	**2.00**	**2.01**	**2.01**
Fe	0.87	0.87	0.97	0.98	0.91	0.89	0.86	0.96	1.02	0.89	0.87	0.84	0.85	0.95	0.96	0.93	0.95	1.13	1.07	1.07	1.06
Mn	0.01	0.01	0.02	0.02	0.02	0.01	0.01	0.02	0.02	0.02	0.01	0.01	0.01	0.02	0.02	0.01	0.02	0.02	0.02	0.02	0.02
Mg	1.10	1.11	1.13	1.18	1.07	1.09	1.09	1.12	1.18	1.11	1.14	1.11	1.11	1.13	1.11	1.08	1.12	1.06	0.95	0.99	0.99
Ca	1.02	1.01	0.89	0.85	1.01	1.02	1.03	0.92	0.77	1.00	0.98	1.03	1.03	0.91	0.93	0.97	0.91	0.81	0.97	0.95	0.95
	3.01	**3.00**	**3.01**	**3.02**	**3.02**	**3.01**	**3.00**	**3.01**	**3.00**	**3.02**	**3.01**	**2.98**	**3.00**	**3.01**	**3.02**	**3.00**	**3.00**	**3.02**	**3.01**	**3.03**	**3.02**
mol %																					
Alm	**29**	**29**	**32**	**32**	**30**	**30**	**29**	**32**	**34**	**30**	**29**	**28**	**28**	**32**	**32**	**31**	**32**	**37**	**35**	**35**	**35**
Prp	**37**	**37**	**38**	**39**	**36**	**36**	**36**	**37**	**39**	**37**	**38**	**37**	**37**	**38**	**37**	**36**	**38**	**35**	**32**	**33**	**33**
Sps	**0**	**0**	**1**	**1**	**1**	**0**	**0**	**1**	**1**	**1**	**0**	**0**	**0**	**1**	**1**	**0**	**1**	**1**	**1**	**1**	**1**
Grs	**34**	**34**	**30**	**28**	**34**	**34**	**34**	**30**	**26**	**33**	**33**	**35**	**34**	**30**	**31**	**32**	**30**	**27**	**32**	**31**	**32**

Table A1. Continued.

Rubinberg Garnets

Name	241	242	243	244	245	246	247	248	249	250	251	254	315	1	2	3	4	5	6	7	8
wt. %																					
SiO_2	40.09	39.98	40.19	40.19	40.12	40.08	40.19	40.44	40.06	40.00	39.82	40.15	40.21	41.57	41.38	41.06	40.99	40.99	40.73	40.82	40.90
TiO_2	0.25	0.20	0.22	0.23	0.32	0.30	0.31	0.30	0.27	0.22	0.22	0.17	0.11	0.16	0.18	0.21	0.27	0.25	0.22	0.24	0.26
Al_2O_3	22.50	22.78	22.61	22.83	22.58	22.87	22.82	22.70	22.79	22.86	22.85	22.72	23.51	23.38	22.98	22.93	22.86	22.79	22.74	22.75	22.78
FeO	16.94	16.99	16.99	16.40	15.73	15.62	15.41	15.64	15.80	17.09	18.01	17.67	16.33	16.05	15.79	15.14	15.26	15.57	15.63	15.68	15.84
MnO	0.36	0.33	0.35	0.37	0.30	0.30	0.34	0.25	0.28	0.34	0.39	0.39	0.32	0.36	0.34	0.33	0.33	0.32	0.32	0.29	0.29
MgO	9.02	9.04	9.11	9.22	9.15	9.15	9.22	9.12	8.95	9.10	9.71	9.27	11.12	13.83	13.04	11.88	11.23	10.78	10.65	10.52	10.57
CaO	11.71	11.81	11.75	12.17	12.60	12.70	12.75	12.77	12.72	11.70	10.17	10.60	9.89	6.58	8.15	9.90	10.79	11.18	11.23	11.25	11.33
Na_2O	0.08	0.03	0.03	0.10	0.06	0.03	0.06	0.06	0.10	0.07	0.02	0.00	0.00	0.02	0.03	0.03	0.04	0.01	0.07	0.02	0.03
K_2O	0.00	0.01	0.00	0.00	0.01	0.00	0.01	0.00	0.00	0.00	0.00	0.00	0.01	0.01	0.00	0.01	0.00	0.00	0.00	0.00	0.00
P_2O_5	0.06	0.04	0.05	0.05	0.06	0.06	0.03	0.07	0.06	0.07	0.06	0.05	0.06	0.07	0.07	0.06	0.06	0.04	0.07	0.06	0.09
TOTAL	101.01	101.20	101.31	101.55	100.91	101.10	101.13	101.35	101.03	101.44	101.25	101.02	101.53	102.01	101.97	101.55	101.84	101.92	101.67	101.63	102.07
Mg#	**49**	**49**	**49**	**50**	**51**	**51**	**52**	**51**	**50**	**49**	**49**	**48**	**55**	**61**	**60**	**58**	**57**	**55**	**55**	**54**	**54**
Si	**2.99**	**2.98**	**2.99**	**2.98**	**2.99**	**2.98**	**2.98**	**2.99**	**2.98**	**2.97**	**2.97**	**2.99**	**2.96**	**3.00**	**3.00**	**3.00**	**3.00**	**3.00**	**2.99**	**3.00**	**3.00**
Ti	0.01	0.01	0.01	0.01	0.02	0.02	0.02	0.02	0.02	0.01	0.01	0.01	0.01	0.01	0.01	0.01	0.01	0.01	0.01	0.01	0.01
Al	1.98	2.00	1.98	1.99	1.98	2.00	2.00	1.98	2.00	2.00	2.01	2.00	2.04	1.99	1.97	1.97	1.97	1.97	1.97	1.97	1.97
	1.99	**2.01**	**1.99**	**2.01**	**2.00**	**2.02**	**2.01**	**2.00**	**2.01**	**2.02**	**2.02**	**2.01**	**2.04**	**2.00**	**1.98**	**1.99**	**1.98**	**1.98**	**1.98**	**1.98**	**1.98**
Fe	1.06	1.06	1.06	1.02	0.98	0.97	0.96	0.97	0.98	1.06	1.12	1.10	1.00	0.97	0.96	0.93	0.93	0.95	0.96	0.96	0.97
Mn	0.02	0.02	0.02	0.02	0.02	0.02	0.02	0.02	0.02	0.02	0.02	0.02	0.02	0.02	0.02	0.02	0.02	0.02	0.02	0.02	0.02
Mg	1.00	1.00	1.01	1.02	1.02	1.01	1.02	1.01	0.99	1.01	1.08	1.03	1.22	1.49	1.41	1.29	1.22	1.18	1.17	1.15	1.15
Ca	0.94	0.94	0.94	0.97	1.01	1.01	1.01	1.01	1.01	0.93	0.81	0.85	0.78	0.51	0.63	0.78	0.85	0.88	0.88	0.89	0.89
	3.02	**3.02**	**3.03**	**3.03**	**3.02**	**3.01**	**3.01**	**3.00**	**3.01**	**3.02**	**3.04**	**3.00**	**3.02**	**2.99**	**3.02**	**3.02**	**3.02**	**3.02**	**3.03**	**3.02**	**3.03**
mol %																					
Alm	**35**	**35**	**35**	**34**	**32**	**32**	**32**	**32**	**33**	**35**	**37**	**37**	**33**	**32**	**32**	**31**	**31**	**32**	**32**	**32**	**32**
Prp	**33**	**33**	**33**	**34**	**34**	**34**	**34**	**34**	**33**	**33**	**36**	**34**	**40**	**50**	**47**	**43**	**40**	**39**	**38**	**38**	**38**
Sps	**1**	**1**	**1**	**1**	**1**	**1**	**1**	**1**	**1**	**1**	**1**	**1**	**1**	**1**	**1**	**1**	**1**	**1**	**1**	**1**	**1**
Grs	**31**	**31**	**31**	**32**	**33**	**34**	**34**	**34**	**34**	**31**	**27**	**28**	**26**	**17**	**21**	**26**	**28**	**29**	**29**	**29**	**29**

Table A1. Continued.

Rubinberg Garnets

Name	9	10	11	12	13	14	15	16	17	18	19	20	21	22	23	24	25	26	28	29	30
wt. %																					
SiO_2	40.92	40.92	41.41	41.17	41.39	41.41	41.34	41.31	41.16	41.33	41.45	41.38	41.21	41.25	41.46	41.05	41.07	40.77	40.47	40.57	40.56
TiO_2	0.25	0.27	0.20	0.06	0.07	0.11	0.13	0.12	0.14	0.10	0.10	0.14	0.15	0.11	0.13	0.17	0.11	0.20	0.21	0.23	0.25
Al_2O_3	22.68	22.77	22.99	23.33	23.24	23.21	23.01	23.16	22.88	23.27	23.44	23.37	23.07	23.27	23.20	23.14	22.58	22.45	22.18	22.23	22.13
FeO	15.71	15.19	15.90	16.61	16.33	15.76	15.70	15.55	15.65	15.61	15.62	15.50	15.50	15.81	15.74	16.05	17.64	15.42	15.41	15.29	15.70
MnO	0.31	0.33	0.37	0.35	0.37	0.38	0.37	0.36	0.37	0.36	0.29	0.37	0.32	0.37	0.36	0.35	0.42	0.31	0.30	0.33	0.31
MgO	10.79	11.20	12.87	13.96	14.38	13.97	13.96	13.92	13.85	14.12	14.30	13.90	13.74	14.31	13.89	13.65	12.87	12.52	10.58	10.38	10.36
CaO	11.23	10.75	8.04	6.07	5.65	6.53	6.64	6.75	6.70	6.60	6.10	6.76	7.00	6.13	6.66	6.98	6.17	8.59	11.22	11.41	11.37
Na_2O	0.05	0.05	0.04	0.00	0.03	0.03	0.03	0.05	0.04	0.01	0.01	0.01	0.00	0.04	0.04	0.05	0.03	0.03	0.05	0.04	0.03
K_2O	0.02	0.01	0.00	0.00	0.00	0.00	0.01	0.01	0.00	0.01	0.00	0.00	0.00	0.00	0.00	0.00	0.00	0.00	0.00	0.01	0.00
P_2O_5	0.07	0.08	0.10	0.03	0.07	0.08	0.06	0.05	0.03	0.04	0.07	0.07	0.06	0.05	0.06	0.04	0.06	0.08	0.06	0.07	0.05
TOTAL	102.02	101.56	101.91	101.59	101.52	101.47	101.24	101.28	100.82	101.43	101.37	101.50	101.05	101.32	101.55	101.47	100.95	100.36	100.48	100.54	100.75
Mg#	**55**	**57**	**59**	**60**	**61**	**61**	**61**	**61**	**61**	**62**	**62**	**62**	**61**	**62**	**61**	**60**	**57**	**59**	**55**	**55**	**54**
Si	**3.00**	**3.00**	**3.01**	**2.99**	**3.00**	**3.01**	**3.01**	**3.00**	**3.01**	**3.00**	**3.00**	**3.00**	**3.00**	**3.00**	**3.01**	**2.99**	**3.02**	**3.01**	**3.01**	**3.01**	**3.01**
Ti	0.01	0.01	0.01	0.00	0.00	0.01	0.01	0.01	0.01	0.01	0.01	0.01	0.01	0.01	0.01	0.01	0.01	0.01	0.01	0.01	0.01
Al	1.96	1.97	1.97	2.00	1.99	1.99	1.97	1.98	1.97	1.99	2.00	2.00	1.98	1.99	1.98	1.99	1.96	1.95	1.94	1.95	1.94
	1.97	**1.98**	**1.98**	**2.00**	**1.99**	**1.99**	**1.98**	**1.99**	**1.98**	**1.99**	**2.01**	**2.00**	**1.99**	**2.00**	**1.99**	**1.99**	**1.96**	**1.96**	**1.96**	**1.96**	**1.95**
Fe	0.96	0.93	0.97	1.01	0.99	0.96	0.96	0.95	0.96	0.95	0.95	0.94	0.94	0.96	0.95	0.98	1.09	0.95	0.96	0.95	0.97
Mn	0.02	0.02	0.02	0.02	0.02	0.02	0.02	0.02	0.02	0.02	0.02	0.02	0.02	0.02	0.02	0.02	0.03	0.02	0.02	0.02	0.02
Mg	1.18	1.22	1.39	1.51	1.55	1.51	1.51	1.51	1.51	1.53	1.54	1.50	1.49	1.55	1.50	1.48	1.41	1.38	1.17	1.15	1.15
Ca	0.88	0.84	0.63	0.47	0.44	0.51	0.52	0.53	0.52	0.51	0.47	0.52	0.55	0.48	0.52	0.54	0.49	0.68	0.89	0.91	0.90
	3.04	**3.02**	**3.01**	**3.02**	**3.01**	**3.00**	**3.01**	**3.00**	**3.01**	**3.01**	**2.98**	**2.99**	**3.00**	**3.01**	**3.00**	**3.03**	**3.01**	**3.03**	**3.04**	**3.03**	**3.04**
mol %																					
Alm	**32**	**31**	**32**	**33**	**33**	**32**	**32**	**31**	**32**	**31**	**32**	**31**	**31**	**32**	**32**	**32**	**36**	**31**	**31**	**31**	**32**
Prp	**39**	**41**	**46**	**50**	**52**	**50**	**50**	**50**	**50**	**51**	**52**	**50**	**50**	**51**	**50**	**49**	**47**	**45**	**39**	**38**	**38**
Sps	**1**	**1**	**1**	**1**	**1**	**1**	**1**	**1**	**1**	**1**	**1**	**1**	**1**	**1**	**1**	**1**	**1**	**1**	**1**	**1**	**1**
Grs	**29**	**28**	**21**	**16**	**15**	**17**	**17**	**18**	**17**	**17**	**16**	**18**	**18**	**16**	**17**	**18**	**16**	**22**	**29**	**30**	**30**

Table A1. Continued.

Rubinberg Garnets

Name	31	32	33	34	35	36	37	38	39	41	42	43	44	45	46	47	48	49	50	51	52
wt. %																					
SiO_2	40.29	40.34	40.51	40.70	41.11	41.22	41.27	41.29	41.17	41.31	41.32	41.08	41.10	38.90	41.07	41.15	41.16	41.41	41.30	41.37	41.04
TiO_2	0.22	0.27	0.22	0.18	0.15	0.10	0.18	0.14	0.15	0.15	0.17	0.20	0.22	0.18	0.15	0.17	0.11	0.11	0.14	0.13	0.13
Al_2O_3	22.10	22.12	22.20	22.50	22.71	22.75	22.89	22.97	23.16	22.85	22.77	22.76	22.77	24.08	22.80	22.72	23.02	23.12	22.98	22.87	22.71
FeO	15.44	15.14	15.09	15.16	15.60	16.10	15.95	15.85	15.55	15.43	15.29	15.38	15.26	15.13	15.34	15.59	15.71	16.33	15.78	15.60	15.25
MnO	0.29	0.29	0.32	0.31	0.35	0.36	0.38	0.35	0.36	0.32	0.34	0.31	0.34	0.38	0.37	0.34	0.31	0.34	0.44	0.34	0.37
MgO	10.29	10.46	11.05	12.42	13.54	14.02	13.69	13.51	13.79	13.43	13.12	12.80	12.58	13.89	13.50	13.57	13.90	13.89	14.03	13.81	12.70
CaO	11.35	11.35	10.87	8.98	6.97	5.96	6.74	7.18	6.99	7.29	7.94	8.48	8.80	8.06	7.49	6.94	6.54	6.17	6.47	6.87	8.54
Na_2O	0.06	0.05	0.03	0.04	0.00	0.02	0.03	0.01	0.05	0.03	0.02	0.03	0.06	0.00	0.02	0.03	0.00	0.00	0.01	0.02	0.01
K_2O	0.00	0.00	0.00	0.01	0.00	0.00	0.00	0.00	0.00	0.00	0.00	0.00	0.00	0.00	0.00	0.01	0.00	0.00	0.01	0.00	0.01
P_2O_5	0.08	0.09	0.09	0.06	0.06	0.07	0.01	0.06	0.07	0.05	0.06	0.06	0.09	0.07	0.07	0.06	0.04	0.03	0.05	0.07	0.04
TOTAL	100.12	100.12	100.37	100.35	100.49	100.59	101.12	101.36	101.28	100.86	101.02	101.10	101.21	100.69	100.80	100.49	100.74	101.35	101.13	100.98	100.73
Mg#	**54**	**55**	**57**	**59**	**61**	**61**	**60**	**60**	**61**	**61**	**60**	**60**	**59**	**62**	**61**	**61**	**61**	**60**	**61**	**61**	**60**
Si	**3.01**	**3.01**	**3.01**	**3.00**	**3.02**	**3.02**	**3.01**	**3.01**	**3.00**	**3.02**	**3.02**	**3.01**	**3.01**	**2.86**	**3.01**	**3.02**	**3.01**	**3.01**	**3.01**	**3.02**	**3.01**
Ti	0.01	0.01	0.01	0.01	0.01	0.01	0.01	0.01	0.01	0.01	0.01	0.01	0.01	0.01	0.01	0.01	0.01	0.01	0.01	0.01	0.01
Al	1.95	1.95	1.94	1.96	1.96	1.96	1.97	1.97	1.99	1.97	1.96	1.96	1.96	2.09	1.97	1.96	1.98	1.98	1.97	1.96	1.96
	1.96	**1.96**	**1.96**	**1.97**	**1.97**	**1.97**	**1.98**	**1.98**	**2.00**	**1.98**	**1.97**	**1.97**	**1.98**	**2.10**	**1.97**	**1.97**	**1.99**	**1.99**	**1.98**	**1.97**	**1.97**
Fe	0.96	0.94	0.94	0.94	0.96	0.99	0.97	0.97	0.95	0.94	0.93	0.94	0.93	0.93	0.94	0.96	0.96	0.99	0.96	0.95	0.94
Mn	0.02	0.02	0.02	0.02	0.02	0.02	0.02	0.02	0.02	0.02	0.02	0.02	0.02	0.02	0.02	0.02	0.02	0.02	0.03	0.02	0.02
Mg	1.15	1.16	1.22	1.37	1.48	1.53	1.49	1.47	1.50	1.46	1.43	1.40	1.37	1.52	1.47	1.48	1.51	1.50	1.52	1.50	1.39
Ca	0.91	0.91	0.86	0.71	0.55	0.47	0.53	0.56	0.55	0.57	0.62	0.67	0.69	0.64	0.59	0.55	0.51	0.48	0.50	0.54	0.67
	3.04	**3.03**	**3.04**	**3.03**	**3.01**	**3.01**	**3.01**	**3.01**	**3.01**	**3.00**	**3.00**	**3.02**	**3.02**	**3.12**	**3.02**	**3.00**	**3.00**	**3.00**	**3.01**	**3.01**	**3.02**
mol %																					
Alm	**32**	**31**	**31**	**31**	**32**	**33**	**32**	**32**	**31**	**31**	**31**	**31**	**31**	**30**	**31**	**32**	**32**	**33**	**32**	**32**	**31**
Prp	**38**	**38**	**40**	**45**	**49**	**51**	**49**	**49**	**50**	**49**	**48**	**46**	**45**	**49**	**49**	**49**	**50**	**50**	**51**	**50**	**46**
Sps	**1**	**1**	**1**	**1**	**1**	**1**	**1**	**1**	**1**	**1**	**1**	**1**	**1**	**1**	**1**	**1**	**1**	**1**	**1**	**1**	**1**
Grs	**30**	**30**	**28**	**23**	**18**	**16**	**17**	**19**	**18**	**19**	**21**	**22**	**23**	**20**	**19**	**18**	**17**	**16**	**17**	**18**	**22**

Table A1. Continued.

A2. GARNET ANALYSES FROM KLATSCHMÜHLE

Klatschmühle Garnet (KLA 1)

Name	313	314	334	335	338	343	344	356	357	359	360	200	201	202	203	204	205	206	207	208
wt. %																				
SiO_2	35.33	34.03	41.60	42.07	41.50	41.84	41.82	41.65	41.92	42.11	41.79	41.8	41.9	42.1	42.0	42.1	42.01	42.32	42.35	42.41
TiO_2	0.15	0.13	0.19	0.07	0.11	0.10	0.20	0.11	0.15	0.30	0.09	0.1	0.1	0.1	0.0	0.1	0.04	0.06	0.04	0.09
Al_2O_3	24.04	23.90	23.61	24.12	23.75	24.25	23.80	24.18	23.94	23.89	24.26	24.0	24.2	24.3	24.1	24.2	24.10	24.16	24.05	24.21
FeO	11.56	11.46	10.95	11.66	11.12	11.63	11.73	11.53	11.91	12.03	11.66	13.9	12.4	12.0	12.0	12.0	11.84	12.02	11.99	12.09
MnO	0.25	0.19	0.21	0.23	0.23	0.21	0.22	0.20	0.21	0.22	0.21	0.2	0.2	0.2	0.3	0.2	0.21	0.25	0.24	0.20
MgO	18.31	17.98	15.93	18.01	15.39	18.19	17.73	18.91	18.54	18.65	18.62	17.1	18.1	18.4	18.5	18.4	18.61	18.49	18.71	18.47
CaO	4.15	4.95	8.24	4.79	8.73	4.47	5.06	4.08	3.91	3.94	4.13	4.2	4.1	4.1	4.0	4.0	4.04	4.03	4.02	3.98
Na_2O	0.05	0.07	0.05	0.04	0.03	0.00	0.06	0.03	0.03	0.07	0.02	0.0	0.1	0.0	0.0	0.0	0.05	0.04	0.03	0.01
K_2O	0.00	0.01	0.01	0.00	0.01	0.01	0.02	0.01	0.00	0.01	0.00	0.0	0.0	0.0	0.0	0.0	0.01	0.00	0.01	0.00
P_2O_5	0.04	0.09	0.06	0.04	0.06	0.05	0.06	0.03	0.06	0.04	0.05	0.1	0.1	0.1	0.1	0.1	0.05	0.06	0.09	0.09
TOTAL	93.88	92.82	100.84	101.03	100.92	100.73	100.71	100.73	100.66	101.25	100.82	101.2	100.9	101.1	100.9	101.0	100.84	101.33	101.40	101.45
Mg#	**74**	**74**	**72**	**73**	**71**	**74**	**73**	**75**	**73**	**73**	**74**	**68**	**72**	**73**	**73**	**73**	**74**	**73**	**74**	**73**
Si	**2.74**	**2.68**	**2.99**	**2.99**	**2.98**	**2.98**	**2.99**	**2.96**	**2.99**	**2.99**	**2.97**	**2.99**	**2.98**	**2.98**	**2.99**	**2.99**	**2.99**	**2.99**	**2.99**	**3.00**
Ti	0.01	0.01	0.01	0.00	0.01	0.01	0.01	0.01	0.01	0.02	0.00	0.00	0.00	0.00	0.00	0.00	0.00	0.00	0.00	0.00
Al	2.19	2.22	2.00	2.02	2.01	2.04	2.01	2.03	2.01	2.00	2.03	2.02	2.03	2.03	2.02	2.02	2.02	2.01	2.00	2.02
	2.20	2.23	2.01	2.02	2.02	2.04	2.02	2.03	2.02	2.01	2.04	2.03	2.04	2.03	2.02	2.03	2.02	2.02	2.01	2.02
Fe	0.75	0.75	0.66	0.69	0.67	0.69	0.70	0.69	0.71	0.71	0.69	0.83	0.74	0.71	0.71	0.71	0.70	0.71	0.71	0.71
Mn	0.02	0.01	0.01	0.01	0.01	0.01	0.01	0.01	0.01	0.01	0.01	0.02	0.01	0.01	0.02	0.01	0.01	0.01	0.01	0.01
Mg	2.11	2.11	1.70	1.91	1.65	1.93	1.89	2.01	1.97	1.97	1.97	1.82	1.92	1.94	1.96	1.95	1.97	1.95	1.97	1.95
Ca	0.34	0.42	0.63	0.36	0.67	0.34	0.39	0.31	0.30	0.30	0.31	0.32	0.31	0.31	0.31	0.31	0.31	0.31	0.30	0.30
	3.22	3.30	3.01	2.98	3.00	2.98	2.99	3.02	2.99	3.00	2.99	2.98	2.98	2.98	2.99	2.98	3.00	2.98	3.00	2.97
mol %																				
Alm	**23**	**23**	**22**	**23**	**22**	**23**	**23**	**23**	**24**	**24**	**23**	**28**	**25**	**24**	**24**	**24**	**23**	**24**	**24**	**24**
Prp	**66**	**64**	**57**	**64**	**55**	**65**	**63**	**67**	**66**	**66**	**66**	**61**	**64**	**65**	**65**	**65**	**66**	**65**	**66**	**65**
Sps	**1**	**0**	**0**	**0**	**0**	**0**	**0**	**0**	**0**	**0**	**0**	**1**	**0**	**0**	**1**	**0**	**0**	**0**	**0**	**0**
Grs	**11**	**13**	**21**	**12**	**22**	**11**	**13**	**10**	**10**	**10**	**11**	**11**	**11**	**10**	**10**	**10**	**10**	**10**	**10**	**10**

Table A2. Major element composition of Klatschmühle garnets.

Klatschmühle Garnet (KLA 1)

Name	209	210	211	212	213	214	215	216	217	218	219	220	221	222	223	224	225	226	227	228
wt. %																				
SiO_2	42.03	41.81	41.92	41.98	42.21	42.15	42.29	42.20	42.15	41.94	41.84	42.09	41.59	42.03	41.85	41.97	41.88	41.73	41.69	41.93
TiO_2	0.04	0.06	0.10	0.06	0.09	0.08	0.10	0.09	0.08	0.09	0.09	0.06	0.09	0.10	0.08	0.09	0.08	0.08	0.09	0.08
Al_2O_3	24.16	24.15	24.35	24.12	24.12	24.12	24.24	24.16	24.07	24.32	24.06	24.11	24.12	24.22	24.23	24.17	24.18	24.18	23.99	24.12
FeO	11.89	11.84	11.99	12.00	11.89	11.91	11.84	12.02	11.97	11.83	11.89	11.86	11.49	11.92	11.93	12.01	11.98	11.93	11.64	11.86
MnO	0.20	0.20	0.21	0.22	0.21	0.21	0.23	0.20	0.25	0.21	0.23	0.24	0.22	0.24	0.24	0.20	0.21	0.21	0.23	0.22
MgO	18.53	18.67	18.48	18.50	18.63	18.61	18.41	18.56	18.56	18.60	18.48	18.56	18.52	18.57	18.51	18.53	18.61	18.47	18.60	18.52
CaO	4.02	3.95	3.96	4.05	3.97	3.95	3.97	3.99	4.02	3.99	4.06	4.01	4.06	3.98	4.05	4.01	4.00	4.00	3.99	4.10
Na_2O	0.02	0.01	0.04	0.03	0.00	0.00	0.01	0.02	0.04	0.02	0.06	0.01	0.33	0.04	0.01	0.04	0.02	0.04	0.00	0.04
K_2O	0.00	0.01	0.01	0.02	0.01	0.01	0.01	0.01	0.01	0.00	0.01	0.01	0.01	0.00	0.01	0.01	0.00	0.01	0.00	0.01
P_2O_5	0.09	0.07	0.06	0.06	0.07	0.07	0.07	0.07	0.07	0.06	0.07	0.07	0.05	0.07	0.07	0.07	0.06	0.06	0.08	0.06
TOTAL	100.88	100.67	101.00	100.93	101.10	101.03	101.08	101.23	101.08	100.98	100.65	100.92	100.10	101.06	100.89	100.98	100.93	100.60	100.24	100.82
Mg#	**74**	**74**	**73**	**73**	**74**	**74**	**73**	**73**	**73**	**74**	**73**	**74**	**74**	**74**	**73**	**73**	**73**	**73**	**74**	**74**
Si	**2.99**	**2.98**	**2.98**	**2.98**	**2.99**	**2.99**	**3.00**	**2.99**	**2.99**	**2.98**	**2.98**	**2.99**	**2.98**	**2.98**	**2.98**	**2.98**	**2.98**	**2.98**	**2.98**	**2.98**
Ti	0.00	0.00	0.01	0.00	0.00	0.00	0.01	0.00	0.00	0.00	0.00	0.00	0.01	0.01	0.00	0.00	0.00	0.00	0.00	0.00
Al	2.02	2.03	2.04	2.02	2.01	2.02	2.02	2.02	2.01	2.03	2.02	2.02	2.03	2.03	2.03	2.02	2.03	2.03	2.02	2.02
	2.03	2.03	2.04	2.02	2.02	2.02	2.03	2.02	2.02	2.04	2.03	2.02	2.04	2.03	2.03	2.03	2.03	2.04	2.03	2.03
Fe	0.71	0.71	0.71	0.71	0.70	0.71	0.70	0.71	0.71	0.70	0.71	0.70	0.69	0.71	0.71	0.71	0.71	0.71	0.70	0.71
Mn	0.01	0.01	0.01	0.01	0.01	0.01	0.01	0.01	0.01	0.01	0.01	0.01	0.01	0.01	0.01	0.01	0.01	0.01	0.01	0.01
Mg	1.96	1.98	1.96	1.96	1.97	1.97	1.94	1.96	1.96	1.97	1.96	1.96	1.98	1.96	1.96	1.96	1.97	1.96	1.98	1.96
Ca	0.31	0.30	0.30	0.31	0.30	0.30	0.30	0.30	0.31	0.30	0.31	0.30	0.31	0.30	0.31	0.30	0.30	0.31	0.31	0.31
	2.99	3.00	2.98	3.00	2.99	2.99	2.96	2.99	2.99	2.99	3.00	2.99	2.99	2.99	2.99	2.99	3.00	2.99	3.00	2.99
mol %																				
Alm	**24**	**24**	**24**	**24**	**24**	**24**	**24**	**24**	**24**	**24**	**24**	**24**	**23**	**24**	**24**	**24**	**24**	**24**	**23**	**24**
Prp	**66**	**66**	**66**	**65**	**66**	**66**	**66**	**66**	**66**	**66**	**66**	**66**	**66**	**66**	**66**	**66**	**66**	**66**	**66**	**66**
Sps	**0**	**0**	**0**	**0**	**0**	**0**	**0**	**0**	**0**	**0**	**0**	**0**	**0**	**0**	**0**	**0**	**0**	**0**	**0**	**0**
Grs	**10**	**10**	**10**	**10**	**10**	**10**	**10**	**10**	**10**	**10**	**10**	**10**	**10**	**10**	**10**	**10**	**10**	**10**	**10**	**10**

Table A2. Continued

Klatschmühle Garnet (KLA 1)

Name	229	230	231	232	233	234	235	236	237	238	239	240	241	242	243	244	245	246	247	248
wt. %																				
SiO_2	42.06	41.93	42.05	42.17	42.14	42.06	41.74	41.85	41.91	41.78	41.70	41.80	41.65	41.99	42.01	41.89	42.13	42.39	41.98	42.11
TiO_2	0.08	0.04	0.05	0.12	0.10	0.11	0.13	0.11	0.06	0.03	0.10	0.08	0.09	0.06	0.08	0.08	0.08	0.05	0.09	0.09
Al_2O_3	24.13	24.35	24.32	24.34	24.29	24.09	24.11	24.32	24.13	24.21	24.22	24.21	24.10	23.99	24.09	24.05	24.16	24.13	24.18	24.08
FeO	11.67	11.84	11.73	11.89	11.83	11.80	11.89	11.86	11.87	11.95	11.88	11.77	11.91	11.86	11.82	11.74	11.89	11.88	11.87	11.95
MnO	0.22	0.19	0.19	0.20	0.20	0.24	0.20	0.23	0.23	0.20	0.23	0.28	0.23	0.23	0.18	0.23	0.15	0.22	0.22	0.21
MgO	18.53	18.70	18.27	18.55	18.57	18.49	18.53	18.44	18.57	18.48	18.47	18.53	18.58	18.61	18.58	18.46	18.47	18.51	18.56	18.48
CaO	4.08	4.08	4.05	4.07	4.03	4.01	4.03	4.05	3.99	4.03	4.03	4.07	3.99	3.97	3.99	4.00	4.02	4.02	4.08	4.06
Na_2O	0.04	0.05	0.05	0.03	0.00	0.00	0.07	0.01	0.05	0.01	0.05	0.05	0.01	0.03	0.02	0.02	0.03	0.04	0.08	0.02
K_2O	0.01	0.02	0.01	0.02	0.00	0.01	0.01	0.01	0.01	0.01	0.00	0.01	0.00	0.01	0.01	0.01	0.01	0.00	0.02	0.01
P_2O_5	0.07	0.05	0.09	0.08	0.07	0.06	0.04	0.07	0.06	0.07	0.09	0.07	0.08	0.06	0.04	0.08	0.06	0.06	0.09	0.06
TOTAL	100.78	101.14	100.64	101.34	101.16	100.78	100.62	100.86	100.76	100.68	100.63	100.73	100.55	100.73	100.76	100.45	100.90	101.21	100.99	100.99
Mg#	**74**	**74**	**74**	**74**	**74**	**74**	**74**	**73**	**74**	**73**	**73**	**74**	**74**	**74**	**74**	**74**	**73**	**73**	**74**	**73**
Si	**2.99**	**2.97**	**2.99**	**2.98**	**2.98**	**2.99**	**2.98**	**2.98**	**2.98**	**2.98**	**2.97**	**2.98**	**2.97**	**2.99**	**2.99**	**2.99**	**2.99**	**3.00**	**2.98**	**2.99**
Ti	0.00	0.00	0.00	0.01	0.01	0.01	0.01	0.01	0.00	0.00	0.01	0.00	0.00	0.00	0.00	0.00	0.00	0.00	0.00	0.00
Al	2.02	2.03	2.04	2.03	2.03	2.02	2.03	2.04	2.02	2.03	2.04	2.03	2.03	2.01	2.02	2.02	2.02	2.01	2.02	2.02
	2.03	2.04	2.04	2.04	2.03	2.02	2.03	2.04	2.03	2.03	2.04	2.04	2.03	2.02	2.02	2.03	2.03	2.02	2.03	2.02
Fe	0.69	0.70	0.70	0.70	0.70	0.70	0.71	0.71	0.71	0.71	0.71	0.70	0.71	0.71	0.70	0.70	0.71	0.70	0.70	0.71
Mn	0.01	0.01	0.01	0.01	0.01	0.01	0.01	0.01	0.01	0.01	0.01	0.02	0.01	0.01	0.01	0.01	0.01	0.01	0.01	0.01
Mg	1.96	1.98	1.94	1.96	1.96	1.96	1.97	1.95	1.97	1.96	1.96	1.97	1.98	1.97	1.97	1.96	1.95	1.95	1.96	1.96
Ca	0.31	0.31	0.31	0.31	0.31	0.31	0.31	0.31	0.30	0.31	0.31	0.31	0.31	0.30	0.30	0.31	0.31	0.31	0.31	0.31
	2.98	3.00	2.95	2.98	2.98	2.98	3.00	2.98	2.99	2.99	2.99	2.99	3.01	3.00	2.99	2.98	2.98	2.97	2.99	2.99
mol %																				
Alm	**23**	**23**	**24**	**24**	**24**	**24**	**24**	**24**	**24**	**24**	**24**	**23**	**24**	**24**	**24**	**23**	**24**	**24**	**24**	**24**
Prp	**66**	**66**	**66**	**66**	**66**	**66**	**66**	**66**	**66**	**66**	**66**	**66**	**66**	**66**	**66**	**66**	**66**	**66**	**66**	**65**
Sps	**0**	**0**	**0**	**0**	**0**	**0**	**0**	**0**	**0**	**0**	**0**	**1**	**0**	**0**	**0**	**0**	**0**	**0**	**0**	**0**
Grs	**10**	**10**	**10**	**10**	**10**	**10**	**10**	**10**	**10**	**10**	**10**	**10**	**10**	**10**	**10**	**10**	**10**	**10**	**10**	**10**

Table A2. Continued

Klatschmühle Garnet (KLA 2)

Name	269	270	271	272	273	274	275	276	310	311	313	314	315	316	317	2	3	4	5	6	8	10	11	12
wt. %																								
SiO_2	40.6	40.7	40.6	40.5	40.6	40.4	40.5	40.7	40.4	40.4	40.6	40.5	40.6	40.4	40.5	39.95	39.82	40.03	40.16	40.07	40.22	40.46	40.54	40.43
TiO_2	0.2	0.2	0.2	0.2	0.2	0.2	0.1	0.1	0.1	0.2	0.2	0.2	0.2	0.2	0.2	0.21	0.19	0.18	0.17	0.15	0.17	0.25	0.21	0.24
Al_2O_3	22.8	22.8	22.7	22.8	22.8	22.7	22.8	22.8	23.0	22.9	22.9	22.8	22.6	22.7	23.0	22.09	22.22	22.30	22.23	22.36	22.81	22.54	22.39	22.42
FeO	15.4	15.7	16.1	16.9	17.1	17.8	18.4	18.9	19.2	17.4	17.7	17.4	16.9	17.2	17.9	17.35	17.63	17.69	17.99	18.40	18.37	14.48	15.08	14.38
MnO	0.3	0.3	0.3	0.3	0.3	0.4	0.4	0.5	0.5	0.4	0.4	0.3	0.3	0.3	0.5	0.35	0.36	0.33	0.37	0.43	0.41	0.28	0.28	0.26
MgO	9.6	9.7	9.7	9.7	9.6	10.0	10.8	12.0	10.8	10.3	10.0	9.8	9.7	10.0	11.4	8.97	9.30	9.38	9.86	10.34	10.24	8.81	9.03	8.87
CaO	12.3	12.1	11.9	10.9	10.8	9.8	8.2	6.6	7.8	9.8	10.0	10.6	11.0	10.5	8.0	11.34	10.58	10.45	9.67	8.68	8.84	14.04	13.46	13.84
Na_2O	0.0	0.0	0.0	0.0	0.0	0.0	0.0	0.0	0.0	0.0	0.0	0.0	0.1	0.1	0.0	0.03	0.06	0.02	0.02	0.00	0.03	0.04	0.01	0.05
K_2O	0.0	0.0	0.0	0.0	0.0	0.0	0.0	0.0	0.0	0.0	0.0	0.0	0.0	0.0	0.0	0.00	0.01	0.00	0.00	0.01	0.00	0.00	0.00	0.00
P_2O_5	0.1	0.1	0.1	0.1	0.1	0.1	0.1	0.0	0.1	0.1	0.1	0.1	0.1	0.1	0.1	0.04	0.06	0.04	0.02	0.03	0.04	0.05	0.04	0.07
TOTAL	101.2	101.5	101.6	101.4	101.4	101.4	101.2	101.7	101.7	101.4	101.8	101.7	101.3	101.4	101.4	100.32	100.23	100.42	100.49	100.47	101.13	100.94	101.05	100.55
Mg#	52	52	52	51	50	50	51	53	50	51	50	50	51	51	53	48	48	49	49	50	50	52	52	52
Si	3.00	3.00	2.99	3.00	3.00	2.99	3.00	2.99	2.98	2.98	2.99	2.99	3.01	2.99	2.98	3.00	3.00	3.00	3.01	3.00	2.99	3.00	3.01	3.01
Ti	0.01	0.01	0.01	0.01	0.01	0.01	0.01	0.01	0.01	0.01	0.01	0.01	0.01	0.01	0.01	0.01	0.01	0.01	0.01	0.01	0.01	0.01	0.01	0.01
Al	1.98	1.98	1.98	1.99	1.99	1.98	1.99	1.98	2.00	1.99	1.99	1.99	1.97	1.98	2.00	1.96	1.97	1.97	1.96	1.97	2.00	1.97	1.96	1.97
	2.00	1.99	1.99	2.00	2.00	1.99	1.99	1.98	2.01	2.01	2.00	2.00	1.98	1.99	2.01	1.97	1.98	1.98	1.97	1.98	2.01	1.99	1.97	1.98
Fe	0.95	0.97	1.00	1.05	1.06	1.11	1.14	1.16	1.18	1.08	1.09	1.08	1.05	1.07	1.10	1.09	1.11	1.11	1.13	1.15	1.14	0.90	0.94	0.90
Mn	0.02	0.02	0.02	0.02	0.02	0.02	0.03	0.03	0.03	0.02	0.02	0.02	0.02	0.02	0.03	0.02	0.02	0.02	0.02	0.03	0.03	0.02	0.02	0.02
Mg	1.05	1.06	1.07	1.07	1.05	1.11	1.19	1.31	1.19	1.14	1.10	1.08	1.07	1.10	1.25	1.01	1.04	1.05	1.10	1.15	1.13	0.97	1.00	0.98
Ca	0.97	0.96	0.94	0.87	0.86	0.78	0.65	0.52	0.62	0.78	0.79	0.84	0.87	0.83	0.63	0.91	0.85	0.84	0.78	0.70	0.70	1.12	1.07	1.10
	3.00	3.01	3.02	3.00	2.99	3.02	3.01	3.03	3.02	3.02	3.01	3.01	3.01	3.02	3.01	3.03	3.03	3.02	3.03	3.03	3.01	3.01	3.02	3.00
mol %																								
Alm	32	32	33	35	35	37	38	38	39	36	36	36	35	35	37	36	37	37	37	38	38	30	31	30
Prp	35	35	35	36	35	37	40	43	39	38	37	36	36	36	42	33	34	35	36	38	38	32	33	33
Sps	1	1	1	1	1	1	1	1	1	1	1	1	1	1	1	1	1	1	1	1	1	1	1	1
Grs	33	32	31	29	29	26	22	17	20	26	26	28	29	28	21	30	28	28	26	23	23	37	35	37

Table A2. Continued

Klatschmühle Garnet (KLA 2)

Name	13	14	15	16	17	22	23	24	26	27	28	29	30	31	32	33	34	35	36	37
wt. %																				
SiO_2	40.49	40.28	40.26	40.25	40.53	40.40	40.34	40.23	40.10	40.26	40.34	40.07	40.19	40.41	40.59	40.28	40.50	40.15	40.38	40.21
TiO_2	0.22	0.18	0.18	0.15	0.12	0.11	0.12	0.15	0.17	0.18	0.18	0.21	0.16	0.07	0.10	0.08	0.11	0.18	0.16	0.10
Al_2O_3	22.60	22.65	22.49	22.85	22.74	22.79	22.73	22.57	22.23	22.51	22.44	22.27	22.47	22.59	23.04	22.80	22.74	22.58	22.64	22.63
FeO	15.94	16.58	17.84	18.46	18.74	18.88	18.51	18.38	17.21	16.99	16.87	17.16	17.73	18.65	19.05	18.89	18.60	18.05	18.33	18.41
MnO	0.26	0.30	0.37	0.37	0.36	0.34	0.38	0.34	0.30	0.31	0.33	0.33	0.32	0.36	0.38	0.41	0.41	0.36	0.38	0.35
MgO	8.90	8.99	9.53	10.36	11.01	10.97	10.76	10.36	9.64	9.47	9.33	9.48	9.71	11.04	11.20	11.03	10.58	9.93	10.01	10.27
CaO	13.01	11.92	10.44	8.52	7.48	7.51	7.84	8.77	10.78	11.03	11.30	11.05	9.97	7.48	7.24	7.53	8.21	9.48	9.43	9.17
Na_2O	0.02	0.04	0.03	0.06	0.03	0.03	0.02	0.03	0.03	0.05	0.00	0.05	0.00	0.05	0.01	0.04	0.03	0.05	0.00	0.02
K_2O	0.00	0.00	0.00	0.00	0.00	0.00	0.00	0.00	0.00	0.01	0.01	0.00	0.00	0.00	0.00	0.00	0.00	0.00	0.00	0.00
P_2O_5	0.04	0.04	0.07	0.07	0.04	0.05	0.03	0.05	0.06	0.06	0.07	0.05	0.04	0.06	0.05	0.04	0.06	0.06	0.08	0.05
TOTAL	101.48	100.97	101.19	101.09	101.05	101.07	100.73	100.87	100.52	100.87	100.86	100.68	100.59	100.70	101.64	101.10	101.22	100.85	101.40	101.22
Mg#	49.9	49.1	48.8	50.0	51.1	50.9	50.9	50.1	50.0	49.8	49.6	49.6	49.4	51.3	51.2	51.0	50.3	49.5	49.3	49.8
Si	3.00	3.00	3.00	2.99	3.00	3.00	3.00	3.00	3.00	3.00	3.01	3.00	3.00	3.01	2.99	2.99	3.00	3.00	3.00	2.99
Ti	0.01	0.01	0.01	0.01	0.01	0.01	0.01	0.01	0.01	0.01	0.01	0.01	0.01	0.00	0.01	0.00	0.01	0.01	0.01	0.01
Al	1.97	1.99	1.97	2.00	1.99	1.99	1.99	1.98	1.96	1.98	1.97	1.96	1.98	1.98	2.00	2.00	1.99	1.99	1.98	1.98
	1.98	2.00	1.98	2.01	1.99	2.00	2.00	1.99	1.97	1.99	1.98	1.98	1.99	1.99	2.01	2.00	1.99	2.00	1.99	1.99
Fe	0.99	1.03	1.11	1.15	1.16	1.17	1.15	1.14	1.08	1.06	1.05	1.07	1.11	1.16	1.17	1.17	1.15	1.13	1.14	1.14
Mn	0.02	0.02	0.02	0.02	0.02	0.02	0.02	0.02	0.02	0.02	0.02	0.02	0.02	0.02	0.02	0.03	0.03	0.02	0.02	0.02
Mg	0.98	1.00	1.06	1.15	1.22	1.21	1.19	1.15	1.08	1.05	1.04	1.06	1.08	1.22	1.23	1.22	1.17	1.10	1.11	1.14
Ca	1.03	0.95	0.83	0.68	0.59	0.60	0.63	0.70	0.86	0.88	0.90	0.89	0.80	0.60	0.57	0.60	0.65	0.76	0.75	0.73
	3.02	3.00	3.02	3.00	3.00	3.00	2.99	3.02	3.04	3.01	3.01	3.04	3.01	3.00	3.00	3.02	3.00	3.01	3.02	3.04
mol %																				
Alm	33	34	37	38	39	39	38	38	35	35	35	35	37	39	39	39	38	37	38	38
Prp	33	33	35	38	41	40	40	38	35	35	34	35	36	41	41	40	39	37	37	37
Sps	1	1	1	1	1	1	1	1	1	1	1	1	1	1	1	1	1	1	1	1
Grs	34	32	28	23	20	20	21	23	28	29	30	29	27	20	19	20	22	25	25	24

Table A2. Continued

Klatschmühle Garnet (KLA 2)

Name	38	39	40	41	42	43	44	45	46	47	48	49	209	210	213	214	215	216	217	218
wt. %																				
SiO_2	40.35	40.37	40.51	40.69	40.70	40.53	40.34	40.72	40.48	40.44	40.51	40.77	40.63	40.74	40.65	40.73	40.79	41.00	40.98	40.84
TiO_2	0.17	0.15	0.10	0.09	0.08	0.20	0.20	0.22	0.21	0.19	0.13	0.12	0.19	0.20	0.26	0.23	0.23	0.27	0.23	0.23
Al_2O_3	22.54	22.72	22.72	22.95	22.73	22.59	22.30	22.31	22.46	22.48	22.66	22.87	22.73	22.37	22.71	22.51	22.78	22.64	22.45	22.60
FeO	18.00	18.84	18.80	19.35	18.63	17.73	16.04	15.01	15.78	17.26	18.50	18.81	17.11	15.16	13.57	13.38	13.52	13.63	13.45	13.45
MnO	0.33	0.36	0.39	0.42	0.38	0.36	0.26	0.25	0.31	0.35	0.37	0.40	0.35	0.32	0.31	0.28	0.27	0.28	0.25	0.28
MgO	9.83	10.79	11.11	11.41	11.06	9.73	8.77	8.85	8.77	9.57	10.76	11.27	10.19	10.40	10.71	10.95	10.83	10.85	10.93	10.81
CaO	9.67	8.22	7.37	6.63	7.73	10.14	12.75	13.60	13.21	10.97	8.24	7.17	10.59	11.60	12.15	12.19	12.24	12.26	12.29	12.24
Na_2O	0.06	0.02	0.00	0.01	0.02	0.02	0.02	0.05	0.04	0.05	0.03	0.03	0.04	0.02	0.06	0.07	0.05	0.04	0.07	0.07
K_2O	0.00	0.00	0.01	0.00	0.00	0.01	0.01	0.00	0.00	0.00	0.00	0.00	0.00	0.00	0.01	0.00	0.00	0.01	0.01	0.01
P_2O_5	0.06	0.04	0.04	0.06	0.04	0.04	0.03	0.02	0.05	0.05	0.06	0.04	0.06	0.06	0.04	0.07	0.06	0.06	0.05	0.06
TOTAL	100.89	101.46	101.00	101.53	101.31	101.28	100.67	100.96	101.22	101.26	101.17	101.42	101.79	100.79	100.35	100.26	100.66	100.93	100.57	100.44
Mg#	**49**	**51**	**51**	**51**	**51**	**49**	**49**	**51**	**50**	**50**	**51**	**52**	**51**	**55**	**58**	**59**	**59**	**59**	**59**	**59**
Si	**3.00**	**2.99**	**3.00**	**3.00**	**3.01**	**3.01**	**3.01**	**3.02**	**3.00**	**3.00**	**3.00**	**3.01**	**2.99**	**3.01**	**3.00**	**3.01**	**3.00**	**3.01**	**3.02**	**3.01**
Ti	0.01	0.01	0.01	0.00	0.00	0.01	0.01	0.01	0.01	0.01	0.01	0.01	0.01	0.01	0.01	0.01	0.01	0.01	0.01	0.01
Al	1.98	1.98	1.99	1.99	1.98	1.97	1.96	1.95	1.96	1.97	1.98	1.99	1.97	1.95	1.98	1.96	1.98	1.96	1.95	1.96
	1.99	**1.99**	**1.99**	**2.00**	**1.98**	**1.99**	**1.97**	**1.96**	**1.98**	**1.98**	**1.99**	**2.00**	**1.98**	**1.96**	**1.99**	**1.97**	**1.99**	**1.97**	**1.96**	**1.98**
Fe	1.12	1.17	1.17	1.19	1.15	1.10	1.00	0.93	0.98	1.07	1.15	1.16	1.05	0.94	0.84	0.83	0.83	0.84	0.83	0.83
Mn	0.02	0.02	0.02	0.03	0.02	0.02	0.02	0.02	0.02	0.02	0.02	0.03	0.02	0.02	0.02	0.02	0.02	0.02	0.02	0.02
Mg	1.09	1.19	1.23	1.25	1.22	1.08	0.98	0.98	0.97	1.06	1.19	1.24	1.12	1.15	1.18	1.21	1.19	1.19	1.20	1.19
Ca	0.77	0.65	0.59	0.52	0.61	0.81	1.02	1.08	1.05	0.87	0.65	0.57	0.84	0.92	0.96	0.97	0.97	0.96	0.97	0.97
	3.00	3.03	3.00	3.00	3.01	3.00	3.01	3.01	3.02	3.02	3.01	2.99	3.03	3.02	3.00	3.02	3.00	3.01	3.01	3.00
mol %																				
Alm	**37**	**38**	**39**	**40**	**38**	**37**	**33**	**31**	**32**	**35**	**38**	**39**	**35**	**31**	**28**	**27**	**28**	**28**	**27**	**28**
Prp	**36**	**39**	**41**	**42**	**41**	**36**	**32**	**33**	**32**	**35**	**39**	**41**	**37**	**38**	**39**	**40**	**40**	**40**	**40**	**40**
Sps	**1**	**1**	**1**	**1**	**1**	**1**	**1**	**1**	**1**	**1**	**1**	**1**	**1**	**1**	**1**	**1**	**1**	**1**	**1**	**1**
Grs	**26**	**22**	**19**	**17**	**20**	**27**	**34**	**36**	**35**	**29**	**22**	**19**	**28**	**30**	**32**	**32**	**32**	**32**	**32**	**32**

Table A2. Continued

Klatschmühle Garnet (KLA 2)

Name	219	220	221	223	224	241	242	244	245	246	247	248	249	250	251	252	265	266	267	268
wt. %																				
SiO_2	40.90	40.96	40.93	40.78	40.58	40.94	40.47	40.37	40.31	40.49	40.32	40.52	40.32	43.24	40.72	40.81	40.67	40.47	40.41	40.67
TiO_2	0.21	0.25	0.27	0.18	0.19	0.14	0.17	0.19	0.22	0.20	0.17	0.16	0.20	0.18	0.20	0.16	0.16	0.18	0.22	0.21
Al_2O_3	22.74	22.68	22.52	22.61	22.67	22.91	22.77	22.51	22.47	22.49	22.72	22.64	22.61	22.64	22.86	22.97	22.97	22.73	22.65	22.52
FeO	13.74	14.04	14.19	16.06	17.26	18.35	18.29	17.18	16.41	16.77	17.52	17.65	17.32	13.78	17.69	18.19	18.30	17.09	15.81	15.25
MnO	0.25	0.26	0.28	0.33	0.38	0.48	0.40	0.38	0.36	0.33	0.37	0.39	0.31	0.33	0.42	0.39	0.41	0.31	0.30	0.30
MgO	10.79	10.81	10.65	9.91	10.42	11.75	10.67	9.48	9.30	9.43	9.88	9.82	9.55	7.75	10.24	11.51	11.14	9.34	9.25	9.52
CaO	12.16	12.12	12.12	11.46	9.73	7.10	8.69	10.92	11.70	11.59	10.10	10.27	10.88	8.72	9.71	7.87	7.99	11.54	12.31	12.39
Na_2O	0.03	0.05	0.07	0.03	0.01	0.03	0.04	0.02	0.03	0.06	0.03	0.04	0.05	0.76	0.02	0.00	0.02	0.05	0.05	0.02
K_2O	0.01	0.00	0.00	0.00	0.01	0.00	0.00	0.00	0.00	0.01	0.00	0.01	0.00	0.09	0.01	0.00	0.00	0.00	0.00	0.00
P_2O_5	0.05	0.05	0.08	0.07	0.08	0.05	0.06	0.04	0.06	0.06	0.06	0.05	0.05	0.06	0.05	0.06	0.05	0.06	0.05	0.07
TOTAL	100.79	101.12	100.96	101.33	101.21	101.67	101.46	101.03	100.78	101.30	101.08	101.46	101.19	96.64	101.83	101.89	101.64	101.66	100.96	100.85
Mg#	**58**	**58**	**57**	**52**	**52**	**53**	**51**	**50**	**50**	**50**	**50**	**50**	**50**	**50**	**51**	**53**	**52**	**49**	**51**	**53**
Si	**3.01**	**3.01**	**3.01**	**3.01**	**3.00**	**3.01**	**2.99**	**3.00**	**3.00**	**3.00**	**2.99**	**3.00**	**2.99**	**3.25**	**3.00**	**2.99**	**2.99**	**2.99**	**3.00**	**3.01**
Ti	0.01	0.01	0.01	0.01	0.01	0.01	0.01	0.01	0.01	0.01	0.01	0.01	0.01	0.01	0.01	0.01	0.01	0.01	0.01	0.01
Al	1.97	1.96	1.95	1.97	1.98	1.98	1.98	1.97	1.97	1.97	1.99	1.98	1.98	2.01	1.98	1.99	1.99	1.98	1.98	1.97
	1.98	**1.98**	**1.97**	**1.98**	**1.99**	**1.99**	**1.99**	**1.98**	**1.98**	**1.98**	**2.00**	**1.99**	**1.99**	**2.02**	**1.99**	**1.99**	**2.00**	**1.99**	**1.99**	**1.98**
Fe	0.85	0.86	0.87	0.99	1.07	1.13	1.13	1.07	1.02	1.04	1.09	1.09	1.08	0.87	1.09	1.12	1.13	1.06	0.98	0.95
Mn	0.02	0.02	0.02	0.02	0.02	0.03	0.03	0.02	0.02	0.02	0.02	0.02	0.02	0.02	0.03	0.02	0.03	0.02	0.02	0.02
Mg	1.18	1.18	1.17	1.09	1.15	1.29	1.18	1.05	1.03	1.04	1.09	1.08	1.06	0.87	1.12	1.26	1.22	1.03	1.02	1.05
Ca	0.96	0.95	0.96	0.91	0.77	0.56	0.69	0.87	0.93	0.92	0.80	0.82	0.87	0.70	0.77	0.62	0.63	0.91	0.98	0.98
	3.00	3.01	3.02	3.01	3.01	3.00	3.02	3.01	3.01	3.02	3.01	3.02	3.02	2.46	3.01	3.02	3.00	3.02	3.00	3.00
mol %																				
Alm	**28**	**29**	**29**	**33**	**35**	**38**	**37**	**35**	**34**	**34**	**36**	**36**	**36**	**35**	**36**	**37**	**37**	**35**	**33**	**32**
Prp	**39**	**39**	**39**	**36**	**38**	**43**	**39**	**35**	**34**	**34**	**36**	**36**	**35**	**35**	**37**	**42**	**41**	**34**	**34**	**35**
Sps	**1**	**1**	**1**	**1**	**1**	**1**	**1**	**1**	**1**	**1**	**1**	**1**	**1**	**1**	**1**	**1**	**1**	**1**	**1**	**1**
Grs	**32**	**32**	**32**	**30**	**26**	**19**	**23**	**29**	**31**	**30**	**27**	**27**	**29**	**29**	**25**	**20**	**21**	**30**	**33**	**33**

Table A2. Continued

A3. CLINOPYROXENE ANALYSES FROM RUBINBERG

Clinopyroxene Rubinberg

Name	2	6	13	2(3)	10	14	15	16	25	26	28	31	35	37	38	48	49	50	62	63
wt %																				
SiO_2	50.07	49.22	49.07	48.43	48.96	48.89	48.90	48.67	49.00	48.90	49.54	48.91	48.14	48.76	48.32	48.75	48.99	48.94	48.91	48.87
TiO_2	0.80	0.83	0.63	0.72	0.66	0.71	0.58	0.63	0.75	0.79	0.91	0.86	0.77	0.59	0.62	0.78	0.65	0.78	0.81	0.70
Al_2O_3	8.71	10.07	6.97	8.35	7.03	8.51	7.66	8.26	7.89	8.79	8.91	10.50	8.60	8.57	7.30	9.42	7.42	8.54	8.35	7.70
FeO	9.57	8.24	10.37	10.43	9.12	10.57	10.12	10.69	9.47	10.11	10.38	8.72	9.90	9.80	10.21	10.41	10.22	10.18	10.33	10.24
MnO	0.05	0.08	0.14	0.14	0.13	0.18	0.15	0.15	0.12	0.11	0.11	0.12	0.12	0.10	0.13	0.07	0.09	0.10	0.14	0.13
MgO	10.33	10.70	11.98	11.75	13.52	11.39	11.77	11.96	11.69	11.27	10.89	11.27	10.87	10.69	11.80	11.08	12.01	11.27	11.32	11.52
CaO	17.95	18.26	19.53	18.96	18.73	18.78	19.47	18.71	20.02	18.37	17.91	17.73	18.44	18.60	19.50	18.27	20.27	18.99	19.16	19.86
Na_2O	2.60	2.43	1.29	1.53	1.42	1.90	1.60	1.68	1.53	2.02	2.44	2.63	2.05	1.95	1.41	2.13	1.34	1.86	1.76	1.47
K_2O	0.03	0.02	0.11	0.14	0.07	0.05	0.09	0.11	0.06	0.07	0.06	0.03	0.13	0.06	0.11	0.14	0.13	0.09	0.06	0.08
Cr_2O_3	0.00	0.00	0.00	0.00	0.00	0.00	0.00	0.00	0.00	0.00	0.00	0.00	0.00	0.00	0.00	0.00	0.00	0.00	0.00	0.00
TOTAL	100.12	99.85	100.09	100.46	99.64	100.97	100.33	100.85	100.52	100.42	101.16	100.77	99.01	99.11	99.40	101.03	101.12	100.75	100.84	100.57
Mg#	**66**	**70**	**67**	**67**	**73**	**66**	**67**	**67**	**69**	**67**	**65**	**70**	**66**	**66**	**67**	**65**	**68**	**66**	**66**	**67**
Si	1.84	1.81	1.82	1.79	1.81	1.79	1.80	1.78	1.80	1.80	1.81	1.78	1.80	1.82	1.80	1.78	1.80	1.80	1.80	1.80
Ti	0.02	0.02	0.02	0.02	0.02	0.02	0.02	0.02	0.02	0.02	0.03	0.02	0.02	0.02	0.02	0.02	0.02	0.02	0.02	0.02
Al	0.38	0.44	0.30	0.36	0.31	0.37	0.33	0.36	0.34	0.38	0.38	0.45	0.38	0.38	0.32	0.41	0.32	0.37	0.36	0.33
Fe	0.29	0.25	0.32	0.32	0.28	0.32	0.31	0.33	0.29	0.31	0.32	0.26	0.31	0.31	0.32	0.32	0.31	0.31	0.32	0.32
Mn	0.00	0.00	0.00	0.00	0.00	0.00	0.00	0.00	0.00	0.00	0.00	0.00	0.00	0.00	0.00	0.00	0.00	0.00	0.00	0.00
Mg	0.57	0.59	0.66	0.65	0.74	0.62	0.65	0.65	0.64	0.62	0.59	0.61	0.60	0.59	0.66	0.60	0.66	0.62	0.62	0.63
Ca	0.71	0.72	0.78	0.75	0.74	0.74	0.77	0.73	0.79	0.72	0.70	0.69	0.74	0.74	0.78	0.71	0.80	0.75	0.75	0.78
Na	0.19	0.17	0.09	0.11	0.10	0.13	0.11	0.12	0.11	0.14	0.17	0.19	0.15	0.14	0.10	0.15	0.10	0.13	0.13	0.11
K	0.00	0.00	0.01	0.01	0.00	0.00	0.00	0.00	0.00	0.00	0.00	0.00	0.01	0.00	0.01	0.01	0.01	0.00	0.00	0.00
Cr	0.00	0.00	0.00	0.00	0.00	0.00	0.00	0.00	0.00	0.00	0.00	0.00	0.00	0.00	0.00	0.00	0.00	0.00	0.00	0.00
Jd	**19**	**17**	**9**	**11**	**10**	**13**	**11**	**12**	**11**	**14**	**17**	**19**	**15**	**14**	**10**	**15**	**10**	**13**	**13**	**11**

Table A3. Major element composition of Rubinberg clinopyroxene.

Clinopyroxene Rubinberg

Name	64	69	70	71	76	84	85	86	87	92	93	94	95	96	109	110	120	121	122	130
wt %																				
SiO_2	46.93	48.68	48.55	48.68	48.81	48.48	47.35	47.78	47.73	48.91	49.04	48.40	48.23	48.51	49.49	48.31	49.25	49.54	49.04	49.36
TiO_2	0.91	0.68	0.67	0.65	0.66	0.80	0.99	0.77	0.81	0.84	0.75	0.91	0.79	0.77	0.88	0.79	0.64	0.74	0.88	0.80
Al_2O_3	9.06	7.67	8.24	7.52	7.83	8.05	8.36	8.00	8.71	9.60	8.35	7.53	7.90	7.82	5.01	6.94	7.94	9.35	8.98	12.82
FeO	12.42	11.32	11.32	11.75	10.26	10.27	11.52	11.01	11.68	10.25	9.80	10.41	10.46	10.10	10.35	11.60	8.95	9.75	9.98	5.98
MnO	0.16	0.16	0.22	0.20	0.10	0.12	0.14	0.11	0.15	0.09	0.13	0.15	0.17	0.09	0.15	0.20	0.10	0.11	0.12	0.05
MgO	11.72	11.49	11.34	12.04	11.84	11.83	11.93	12.14	11.69	10.88	11.57	12.16	12.30	12.13	12.61	12.16	11.78	10.85	11.14	10.20
CaO	17.33	19.11	17.87	18.90	19.97	19.71	18.29	18.52	17.80	17.89	19.68	19.56	19.28	19.59	21.21	18.98	20.21	18.44	18.57	18.80
Na_2O	1.78	1.65	1.67	1.56	1.49	1.44	1.78	1.69	1.96	2.14	1.56	1.42	1.39	1.51	1.00	1.48	1.45	2.40	2.04	3.00
K_2O	0.14	0.03	0.05	0.03	0.05	0.11	0.22	0.14	0.11	0.04	0.06	0.09	0.07	0.07	0.07	0.16	0.05	0.07	0.08	0.00
Cr_2O_3	0.00	0.00	0.00	0.00	0.00	0.00	0.00	0.00	0.00	0.00	0.00	0.00	0.00	0.00	0.00	0.00	0.00	0.00	0.00	0.00
TOTAL	100.45	100.79	99.92	101.32	101.00	100.80	100.58	100.17	100.64	100.65	100.94	100.62	100.58	100.59	100.76	100.61	100.36	101.24	100.82	101.01
Mg#	**63**	**64**	**64**	**65**	**67**	**67**	**65**	**66**	**64**	**65**	**68**	**68**	**68**	**68**	**68**	**65**	**70**	**66**	**67**	**75**
Si	1.73	1.79	1.81	1.78	1.79	1.78	1.74	1.76	1.75	1.79	1.80	1.78	1.78	1.78	1.83	1.78	1.81	1.80	1.80	1.77
Ti	0.03	0.02	0.02	0.02	0.02	0.02	0.03	0.02	0.02	0.02	0.02	0.03	0.02	0.02	0.02	0.02	0.02	0.02	0.02	0.02
Al	0.39	0.33	0.36	0.33	0.34	0.35	0.36	0.35	0.38	0.42	0.36	0.33	0.34	0.34	0.22	0.30	0.34	0.40	0.39	0.54
Fe	0.38	0.35	0.35	0.36	0.31	0.32	0.35	0.34	0.36	0.31	0.30	0.32	0.32	0.31	0.32	0.36	0.28	0.30	0.31	0.18
Mn	0.00	0.00	0.00	0.00	0.00	0.00	0.00	0.00	0.00	0.00	0.00	0.00	0.00	0.00	0.00	0.00	0.00	0.00	0.00	0.00
Mg	0.64	0.63	0.63	0.66	0.65	0.65	0.65	0.67	0.64	0.60	0.63	0.67	0.68	0.66	0.69	0.67	0.65	0.59	0.61	0.55
Ca	0.69	0.75	0.71	0.74	0.78	0.78	0.72	0.73	0.70	0.70	0.77	0.77	0.76	0.77	0.84	0.75	0.80	0.72	0.73	0.72
Na	0.13	0.12	0.12	0.11	0.11	0.10	0.13	0.12	0.14	0.15	0.11	0.10	0.10	0.11	0.07	0.11	0.10	0.17	0.14	0.21
K	0.01	0.00	0.00	0.00	0.00	0.00	0.01	0.01	0.01	0.00	0.00	0.00	0.00	0.00	0.00	0.01	0.00	0.00	0.00	0.00
Cr	0.00	0.00	0.00	0.00	0.00	0.00	0.00	0.00	0.00	0.00	0.00	0.00	0.00	0.00	0.00	0.00	0.00	0.00	0.00	0.00
Jd	**13**	**12**	**12**	**11**	**11**	**10**	**13**	**12**	**14**	**15**	**11**	**10**	**10**	**11**	**7**	**11**	**10**	**17**	**14**	**21**

Table A3. Continued.

Clinopyroxene Rubinberg

Name	132	137	138	139	140	141	158	177	178	179	180	181	182	183	199	200	209	210	211	212
wt %																				
SiO_2	49.08	48.94	48.74	48.65	48.34	48.53	50.18	48.46	48.52	48.51	48.43	48.80	48.65	48.64	50.59	50.17	48.70	48.45	49.17	49.43
TiO_2	0.95	1.02	0.97	0.98	1.01	0.98	0.77	1.05	0.79	0.85	0.96	1.06	0.98	0.74	0.62	0.71	0.93	0.80	0.90	0.86
Al_2O_3	11.98	12.61	12.71	12.98	13.17	12.57	14.76	12.63	13.95	13.55	13.30	12.55	12.78	13.64	14.17	14.48	12.55	11.84	11.99	13.99
FeO	5.81	6.19	6.28	6.66	6.86	6.84	4.42	6.82	6.16	6.37	6.74	6.61	6.34	6.58	4.38	4.74	6.78	6.88	6.61	5.86
MnO	0.02	0.05	0.08	0.05	0.03	0.05	0.03	0.03	0.09	0.03	0.07	0.09	0.05	0.05	0.04	0.05	0.07	0.08	0.02	0.04
MgO	10.11	10.42	10.03	10.29	10.24	10.35	9.23	10.30	9.56	9.76	9.99	10.10	9.89	9.78	9.47	9.57	10.45	11.08	10.31	9.32
CaO	18.66	18.71	18.77	18.62	18.87	19.12	17.62	18.69	18.37	19.02	18.54	19.04	19.08	19.06	17.52	17.74	19.36	20.38	19.08	18.05
Na_2O	2.60	3.01	3.09	2.80	2.82	2.70	4.09	2.86	3.23	2.88	3.13	2.77	2.90	2.85	4.26	4.09	2.38	1.93	2.73	3.51
K_2O	0.01	0.01	0.00	0.03	0.03	0.00	0.00	0.01	0.00	0.01	0.01	0.01	0.01	0.01	0.00	0.00	0.01	0.01	0.01	0.00
Cr_2O_3		0.00	0.00	0.00	0.00	0.00	0.00	0.00	0.00	0.00	0.00	0.00	0.00	0.00	0.00	0.00	0.00	0.00	0.00	0.00
TOTAL	99.22	100.96	100.67	101.05	101.36	101.14	101.10	100.85	100.67	100.97	101.18	101.03	100.68	101.35	101.04	101.56	101.24	101.46	100.81	101.06
Mg#	**76**	**75**	**74**	**73**	**73**	**73**	**79**	**73**	**73**	**73**	**73**	**73**	**74**	**73**	**79**	**78**	**73**	**74**	**74**	**74**
Si	1.80	1.76	1.76	1.75	1.74	1.75	1.79	1.75	1.75	1.75	1.74	1.76	1.76	1.75	1.80	1.78	1.76	1.75	1.78	1.77
Ti	0.03	0.03	0.03	0.03	0.03	0.03	0.02	0.03	0.02	0.02	0.03	0.03	0.03	0.02	0.02	0.02	0.03	0.02	0.02	0.02
Al	0.52	0.53	0.54	0.55	0.56	0.53	0.62	0.54	0.59	0.58	0.56	0.53	0.54	0.58	0.59	0.60	0.53	0.50	0.51	0.59
Fe	0.18	0.19	0.19	0.20	0.21	0.21	0.13	0.21	0.19	0.19	0.20	0.20	0.19	0.20	0.13	0.14	0.20	0.21	0.20	0.18
Mn	0.00	0.00	0.00	0.00	0.00	0.00	0.00	0.00	0.00	0.00	0.00	0.00	0.00	0.00	0.00	0.00	0.00	0.00	0.00	0.00
Mg	0.55	0.56	0.54	0.55	0.55	0.56	0.49	0.55	0.51	0.52	0.54	0.54	0.53	0.52	0.50	0.51	0.56	0.60	0.56	0.50
Ca	0.73	0.72	0.73	0.72	0.73	0.74	0.67	0.72	0.71	0.73	0.71	0.74	0.74	0.73	0.67	0.67	0.75	0.79	0.74	0.69
Na	0.18	0.21	0.22	0.20	0.20	0.19	0.28	0.20	0.23	0.20	0.22	0.19	0.20	0.20	0.29	0.28	0.17	0.13	0.19	0.24
K	0.00	0.00	0.00	0.00	0.00	0.00	0.00	0.00	0.00	0.00	0.00	0.00	0.00	0.00	0.00	0.00	0.00	0.00	0.00	0.00
Cr	0.00	0.00	0.00	0.00	0.00	0.00	0.00	0.00	0.00	0.00	0.00	0.00	0.00	0.00	0.00	0.00	0.00	0.00	0.00	0.00
Jd	**18**	**21**	**22**	**20**	**20**	**19**	**28**	**20**	**23**	**20**	**22**	**19**	**20**	**20**	**29**	**28**	**17**	**13**	**19**	**24**

Table A3. Continued.

Clinopyroxene Rubinberg

Name	213	214	215	216	217	218	219	220	221	222	223	224	225	226	227	228	229	230	236	252
wt %																				
SiO_2	48.18	48.53	48.76	48.90	48.93	49.10	49.35	49.47	49.31	49.47	48.42	49.06	49.18	49.34	49.20	48.96	49.87	48.15	51.38	50.80
TiO_2	1.01	0.99	1.00	1.08	1.02	0.93	0.88	0.93	0.82	0.84	0.61	0.84	0.85	0.87	0.91	0.90	0.76	0.95	0.49	0.58
Al_2O_3	13.57	13.01	12.66	13.08	13.22	13.56	13.72	13.81	13.84	14.02	13.93	13.75	13.99	13.92	13.83	13.52	13.04	13.38	11.34	11.71
FeO	6.59	6.78	6.34	6.37	6.37	6.20	6.21	6.10	6.13	5.88	5.75	5.80	5.82	6.01	6.19	6.30	5.97	6.42	6.21	6.80
MnO	0.03	0.05	0.08	0.00	0.06	0.05	0.04	0.02	0.04	0.04	0.02	0.03	0.05	0.05	0.05	0.03	0.06	0.08	0.00	0.07
MgO	9.54	10.02	10.35	9.97	9.97	9.78	9.67	9.59	9.56	9.55	10.31	9.46	9.41	9.53	9.52	9.69	9.71	9.58	9.89	9.54
CaO	18.88	18.89	19.16	18.61	18.32	18.20	18.02	17.97	17.72	17.74	18.30	18.09	18.19	18.12	18.12	18.24	18.98	18.49	17.36	16.95
Na_2O	2.99	2.80	2.61	2.99	3.03	3.28	3.48	3.40	3.45	3.63	3.33	3.58	3.44	3.59	3.38	3.25	3.33	2.98	3.90	4.32
K_2O	0.01	0.01	0.00	0.01	0.01	0.01	0.00	0.00	0.01	0.01	0.01	0.01	0.01	0.01	0.01	0.03	0.02	0.02	0.00	0.01
Cr_2O_3	0.00	0.00	0.00	0.00	0.00	0.00	0.00	0.00	0.00	0.00	0.00	0.00	0.00	0.00	0.00	0.00	0.00	0.00	0.00	0.00
TOTAL	100.80	101.07	100.96	101.02	100.93	101.10	101.37	101.28	100.86	101.20	100.66	100.62	100.95	101.44	101.21	100.92	101.74	100.04	100.56	100.77
Mg#	**72**	**73**	**74**	**74**	**74**	**74**	**74**	**74**	**74**	**74**	**76**	**74**	**74**	**74**	**73**	**73**	**74**	**73**	**74**	**71**
Si	1.74	1.75	1.76	1.76	1.76	1.76	1.77	1.77	1.77	1.77	1.74	1.76	1.77	1.76	1.76	1.76	1.78	1.75	1.85	1.82
Ti	0.03	0.03	0.03	0.03	0.03	0.03	0.02	0.02	0.02	0.02	0.02	0.02	0.02	0.02	0.02	0.02	0.02	0.03	0.01	0.02
Al	0.58	0.55	0.54	0.56	0.56	0.57	0.58	0.58	0.59	0.59	0.59	0.58	0.59	0.59	0.58	0.57	0.55	0.57	0.48	0.50
Fe	0.20	0.20	0.19	0.19	0.19	0.19	0.19	0.18	0.18	0.18	0.17	0.17	0.17	0.18	0.19	0.19	0.18	0.20	0.19	0.20
Mn	0.00	0.00	0.00	0.00	0.00	0.00	0.00	0.00	0.00	0.00	0.00	0.00	0.00	0.00	0.00	0.00	0.00	0.00	0.00	0.00
Mg	0.51	0.54	0.56	0.54	0.54	0.52	0.52	0.51	0.51	0.51	0.55	0.51	0.50	0.51	0.51	0.52	0.52	0.52	0.53	0.51
Ca	0.73	0.73	0.74	0.72	0.71	0.70	0.69	0.69	0.68	0.68	0.70	0.70	0.70	0.69	0.70	0.70	0.73	0.72	0.67	0.65
Na	0.21	0.20	0.18	0.21	0.21	0.23	0.24	0.24	0.24	0.25	0.23	0.25	0.24	0.25	0.24	0.23	0.23	0.21	0.27	0.30
K	0.00	0.00	0.00	0.00	0.00	0.00	0.00	0.00	0.00	0.00	0.00	0.00	0.00	0.00	0.00	0.00	0.00	0.00	0.00	0.00
Cr	0.00	0.00	0.00	0.00	0.00	0.00	0.00	0.00	0.00	0.00	0.00	0.00	0.00	0.00	0.00	0.00	0.00	0.00	0.00	0.00
Jd	**21**	**20**	**18**	**21**	**21**	**23**	**24**	**24**	**24**	**25**	**23**	**25**	**24**	**25**	**24**	**23**	**23**	**21**	**27**	**30**

Table A3. Continued.

Clinopyroxene Rubinberg

Name	61	62	63	64	65	66	67	68	69	70	71	72	73	74	76	77	78	79	80	81
wt %																				
SiO_2	51.30	50.25	51.86	51.57	51.68	51.77	52.08	52.19	52.32	51.74	51.90	52.28	52.58	52.87	52.86	52.66	52.07	52.05	51.58	50.57
TiO_2	0.96	0.89	0.80	0.99	0.84	0.92	0.86	0.87	0.70	0.91	0.80	0.75	0.70	0.59	0.71	0.72	0.82	0.84	0.91	1.10
Al_2O_3	8.99	8.02	8.05	8.87	8.24	8.02	8.00	8.14	7.81	8.60	7.79	7.78	7.37	7.01	6.68	7.58	7.87	8.07	8.26	8.78
FeO	5.72	5.75	5.81	5.90	6.05	6.25	5.83	5.86	6.06	5.70	5.50	5.77	5.57	5.55	5.60	5.63	5.82	5.73	5.76	6.44
MnO	0.10	0.04	0.04	0.06	0.06	0.07	0.07	0.07	0.04	0.04	0.08	0.06	0.07	0.06	0.05	0.08	0.06	0.06	0.06	0.09
MgO	11.83	10.99	11.89	11.87	12.54	12.20	11.73	11.94	12.13	11.93	12.04	12.01	12.04	12.23	12.82	12.14	11.95	11.93	11.78	11.59
CaO	18.76	18.36	18.75	18.55	18.30	18.02	18.70	18.44	18.50	18.78	19.30	18.50	18.63	18.82	19.19	18.54	18.35	18.51	18.72	18.32
Na_2O	2.31	2.44	2.49	2.46	2.34	2.58	2.66	2.74	2.59	2.49	2.20	2.64	2.70	2.60	2.28	2.85	2.67	2.66	2.49	2.57
K_2O	0.00	0.01	0.00	0.00	0.00	0.00	0.00	0.00	0.00	0.00	0.00	0.00	0.00	0.01	0.00	0.00	0.00	0.00	0.01	0.00
Cr_2O_3	0.03	0.05	0.09	0.04	0.04	0.05	0.05	0.07	0.07	0.03	0.03	0.06	0.05	0.00	0.06	0.05	0.03	0.02	0.04	0.03
TOTAL	99.99	96.79	99.79	100.30	100.08	99.89	99.98	100.32	100.22	100.22	99.65	99.85	99.70	99.73	100.25	100.25	99.64	99.87	99.62	99.49
Mg#	**79**	**77**	**79**	**78**	**79**	**78**	**78**	**78**	**78**	**79**	**80**	**79**	**79**	**80**	**80**	**79**	**79**	**79**	**78**	**76**
Si	1.87	1.90	1.89	1.87	1.88	1.89	1.90	1.89	1.90	1.88	1.90	1.91	1.92	1.93	1.92	1.91	1.90	1.90	1.89	1.85
Ti	0.03	0.03	0.02	0.03	0.02	0.03	0.02	0.02	0.02	0.02	0.02	0.02	0.02	0.02	0.02	0.02	0.02	0.02	0.03	0.03
Al	0.39	0.36	0.35	0.38	0.35	0.34	0.34	0.35	0.33	0.37	0.34	0.33	0.32	0.30	0.29	0.32	0.34	0.35	0.36	0.38
Fe	0.17	0.18	0.18	0.18	0.18	0.19	0.18	0.18	0.18	0.17	0.17	0.18	0.17	0.17	0.17	0.17	0.18	0.17	0.18	0.20
Mn	0.00	0.00	0.00	0.00	0.00	0.00	0.00	0.00	0.00	0.00	0.00	0.00	0.00	0.00	0.00	0.00	0.00	0.00	0.00	0.00
Mg	0.64	0.62	0.65	0.64	0.68	0.66	0.64	0.65	0.66	0.65	0.66	0.65	0.66	0.67	0.69	0.66	0.65	0.65	0.64	0.63
Ca	0.73	0.74	0.73	0.72	0.71	0.70	0.73	0.72	0.72	0.73	0.76	0.72	0.73	0.74	0.75	0.72	0.72	0.72	0.73	0.72
Na	0.16	0.18	0.18	0.17	0.17	0.18	0.19	0.19	0.18	0.18	0.16	0.19	0.19	0.18	0.16	0.20	0.19	0.19	0.18	0.18
K	0.00	0.00	0.00	0.00	0.00	0.00	0.00	0.00	0.00	0.00	0.00	0.00	0.00	0.00	0.00	0.00	0.00	0.00	0.00	0.00
Cr	0.00	0.00	0.00	0.00	0.00	0.00	0.00	0.00	0.00	0.00	0.00	0.00	0.00	0.00	0.00	0.00	0.00	0.00	0.00	0.00
Jd	**16**	**18**	**18**	**17**	**17**	**18**	**19**	**19**	**18**	**18**	**16**	**19**	**19**	**18**	**16**	**20**	**19**	**19**	**18**	**18**

Table A3. Continued.

Clinopyroxene Rubinberg

Name	82	83	85	86	87	88	89	90	91	93	94	95	96	97	98	99	101	116	117	119
wt %																				
SiO_2	51.51	51.36	50.68	50.89	51.08	50.55	51.68	51.68	51.92	52.36	51.98	51.76	50.94	51.78	52.02	51.80	51.94	50.84	50.48	50.58
TiO_2	0.90	0.86	1.02	0.92	1.05	1.09	0.92	0.84	0.84	0.77	0.85	0.84	1.00	0.64	0.61	0.94	0.65	0.68	0.94	0.92
Al_2O_3	8.11	8.13	8.25	8.11	8.43	8.72	8.28	8.17	7.96	7.92	8.09	8.12	8.42	8.62	8.70	8.91	8.10	8.47	10.14	10.03
FeO	6.05	5.94	6.33	6.14	6.01	5.77	5.90	5.94	6.16	5.68	6.01	6.01	5.83	5.32	5.40	5.25	5.64	8.29	8.21	7.86
MnO	0.05	0.07	0.04	0.06	0.06	0.07	0.02	0.07	0.06	0.06	0.05	0.03	0.06	0.07	0.04	0.06	0.05	0.13	0.09	0.06
MgO	11.82	11.66	11.89	11.79	11.43	11.77	11.50	11.77	11.77	11.72	11.80	11.80	12.10	11.85	11.72	11.99	12.13	10.75	9.71	9.72
CaO	18.16	18.27	18.07	18.36	18.37	18.70	18.58	18.43	18.33	18.42	18.35	18.47	17.64	18.81	18.80	18.69	18.55	18.07	17.28	17.15
Na_2O	2.71	2.55	2.67	2.74	2.59	2.54	2.76	2.74	2.81	2.83	2.79	2.63	2.52	2.75	2.61	2.65	2.61	2.66	3.06	3.22
K_2O	0.01	0.00	0.00	0.01	0.01	0.00	0.00	0.00	0.00	0.00	0.00	0.00	0.01	0.01	0.00	0.00	0.00	0.01	0.01	0.01
Cr_2O_3	0.06	0.02	0.04	0.05	0.03	0.01	0.02	0.03	0.02	0.08	0.03	0.00	0.02	0.05	0.01	0.03	0.02	0.06	0.07	0.06
TOTAL	99.39	98.86	98.99	99.07	99.05	99.20	99.66	99.67	99.86	99.83	99.93	99.66	98.54	99.90	99.90	100.31	99.68	99.96	99.98	99.60
Mg#	**78**	**78**	**77**	**77**	**77**	**78**	**78**	**78**	**77**	**79**	**78**	**78**	**79**	**80**	**79**	**80**	**79**	**70**	**68**	**69**
Si	1.89	1.89	1.86	1.87	1.88	1.86	1.89	1.89	1.89	1.91	1.89	1.89	1.88	1.88	1.89	1.88	1.89	1.87	1.85	1.86
Ti	0.02	0.02	0.03	0.03	0.03	0.03	0.03	0.02	0.02	0.02	0.02	0.02	0.03	0.02	0.02	0.03	0.02	0.02	0.03	0.03
Al	0.35	0.35	0.36	0.35	0.37	0.38	0.36	0.35	0.34	0.34	0.35	0.35	0.37	0.37	0.37	0.38	0.35	0.37	0.44	0.43
Fe	0.19	0.18	0.19	0.19	0.19	0.18	0.18	0.18	0.19	0.17	0.18	0.18	0.18	0.16	0.16	0.16	0.17	0.25	0.25	0.24
Mn	0.00	0.00	0.00	0.00	0.00	0.00	0.00	0.00	0.00	0.00	0.00	0.00	0.00	0.00	0.00	0.00	0.00	0.00	0.00	0.00
Mg	0.65	0.64	0.65	0.65	0.63	0.64	0.63	0.64	0.64	0.64	0.64	0.64	0.67	0.64	0.64	0.65	0.66	0.59	0.53	0.53
Ca	0.71	0.72	0.71	0.72	0.72	0.74	0.73	0.72	0.72	0.72	0.72	0.72	0.70	0.73	0.73	0.73	0.72	0.71	0.68	0.68
Na	0.19	0.18	0.19	0.20	0.18	0.18	0.20	0.19	0.20	0.20	0.20	0.19	0.18	0.19	0.18	0.19	0.18	0.19	0.22	0.23
K	0.00	0.00	0.00	0.00	0.00	0.00	0.00	0.00	0.00	0.00	0.00	0.00	0.00	0.00	0.00	0.00	0.00	0.00	0.00	0.00
Cr	0.00	0.00	0.00	0.00	0.00	0.00	0.00	0.00	0.00	0.00	0.00	0.00	0.00	0.00	0.00	0.00	0.00	0.00	0.00	0.00
Jd	**19**	**18**	**19**	**20**	**18**	**18**	**20**	**19**	**20**	**20**	**20**	**19**	**18**	**19**	**18**	**19**	**18**	**19**	**22**	**23**

Table A3. Continued.

Clinopyroxene Rubinberg

Name	120	121	122	123	124	125	127	149	150	151	152	153	154	156	157	158	159	160	185	186
wt %																				
SiO_2	50.68	50.12	50.52	50.69	50.45	50.68	51.13	50.20	50.30	50.61	50.40	50.66	50.69	51.54	50.37	50.06	50.71	50.18	49.40	50.16
TiO_2	0.97	0.89	0.75	0.87	0.95	0.88	0.80	0.83	0.98	0.89	0.92	0.96	0.87	0.55	0.92	0.85	0.74	0.89	0.91	0.88
Al_2O_3	9.89	9.47	8.09	8.94	9.62	9.61	8.47	9.04	8.25	9.19	9.76	9.24	9.27	8.23	9.45	9.49	8.47	8.15	9.46	9.79
FeO	7.92	8.00	8.47	8.55	8.19	8.00	8.53	8.42	8.57	8.31	8.19	8.15	8.03	7.88	7.82	8.24	8.00	8.31	8.17	7.95
MnO	0.09	0.10	0.10	0.10	0.11	0.07	0.10	0.13	0.10	0.07	0.12	0.10	0.11	0.12	0.07	0.11	0.09	0.11	0.10	0.09
MgO	9.88	10.87	11.37	10.47	10.13	9.88	10.66	10.61	11.34	10.14	9.98	10.14	10.10	10.36	10.15	10.22	10.19	10.75	10.08	9.77
CaO	17.30	17.90	18.33	17.42	17.63	17.35	17.83	17.86	18.79	17.59	17.26	17.52	17.75	17.47	17.37	17.40	17.89	18.58	18.09	17.09
Na_2O	3.21	2.71	2.31	2.95	2.97	3.16	2.64	2.72	1.98	3.05	3.19	3.07	3.15	3.37	3.26	3.15	3.07	2.56	2.79	3.21
K_2O	0.00	0.02	0.06	0.01	0.01	0.00	0.01	0.02	0.05	0.02	0.01	0.01	0.00	0.03	0.00	0.01	0.01	0.01	0.02	0.00
Cr_2O_3	0.06	0.04	0.08	0.03	0.04	0.05	0.01	0.02	0.08	0.06	0.06	0.04	0.05	0.07	0.09	0.10	0.05	0.03	0.03	0.02
TOTAL	100.00	100.13	100.08	100.02	100.11	99.67	100.19	99.85	100.43	99.93	99.86	99.89	100.02	99.61	99.50	99.62	99.22	99.55	99.04	98.95
Mg#	**69**	**71**	**71**	**69**	**69**	**69**	**69**	**69**	**70**	**69**	**68**	**69**	**69**	**70**	**70**	**69**	**69**	**70**	**69**	**69**
Si	1.86	1.83	1.86	1.86	1.85	1.86	1.88	1.85	1.85	1.86	1.85	1.86	1.86	1.89	1.85	1.84	1.87	1.85	1.83	1.86
Ti	0.03	0.02	0.02	0.02	0.03	0.02	0.02	0.02	0.03	0.02	0.03	0.03	0.02	0.02	0.03	0.02	0.02	0.02	0.03	0.02
Al	0.43	0.41	0.35	0.39	0.42	0.42	0.37	0.39	0.36	0.40	0.42	0.40	0.40	0.36	0.41	0.41	0.37	0.35	0.41	0.43
Fe	0.24	0.24	0.26	0.26	0.25	0.25	0.26	0.26	0.26	0.25	0.25	0.25	0.25	0.24	0.24	0.25	0.25	0.26	0.25	0.25
Mn	0.00	0.00	0.00	0.00	0.00	0.00	0.00	0.00	0.00	0.00	0.00	0.00	0.00	0.00	0.00	0.00	0.00	0.00	0.00	0.00
Mg	0.54	0.59	0.62	0.57	0.55	0.54	0.58	0.58	0.62	0.55	0.55	0.55	0.55	0.57	0.56	0.56	0.56	0.59	0.56	0.54
Ca	0.68	0.70	0.72	0.68	0.69	0.68	0.70	0.70	0.74	0.69	0.68	0.69	0.70	0.69	0.68	0.68	0.71	0.74	0.72	0.68
Na	0.23	0.19	0.16	0.21	0.21	0.23	0.19	0.19	0.14	0.22	0.23	0.22	0.22	0.24	0.23	0.22	0.22	0.18	0.20	0.23
K	0.00	0.00	0.00	0.00	0.00	0.00	0.00	0.00	0.00	0.00	0.00	0.00	0.00	0.00	0.00	0.00	0.00	0.00	0.00	0.00
Cr	0.00	0.00	0.00	0.00	0.00	0.00	0.00	0.00	0.00	0.00	0.00	0.00	0.00	0.00	0.00	0.00	0.00	0.00	0.00	0.00
Jd	**23**	**19**	**16**	**21**	**21**	**23**	**19**	**19**	**14**	**22**	**23**	**22**	**22**	**24**	**23**	**22**	**22**	**18**	**20**	**23**

Table A3. Continued.

Clinopyroxene Rubinberg

Name	187	189	190	191	192	
wt %						
SiO_2	50.38	50.22	50.05	49.67	48.53	48.76
TiO_2	0.84	0.87	0.91	0.99	0.87	1.01
Al_2O_3	9.81	9.70	9.72	9.76	8.19	9.08
FeO	7.85	7.83	7.97	8.50	9.64	8.42
MnO	0.11	0.08	0.08	0.10	0.15	0.08
MgO	9.71	9.85	9.81	10.05	11.12	10.61
CaO	16.71	17.18	17.19	17.47	18.97	17.80
Na_2O	3.52	3.30	3.21	2.92	1.72	2.61
K_2O	0.01	0.00	0.01	0.01	0.01	0.00
Cr_2O_3	0.07	0.06	0.06	0.03	0.02	0.03
TOTAL	99.00	99.09	99.00	99.48	99.23	98.41
Mg#	**69**	**69**	**69**	**68**	**67**	**69**
Si	1.86	1.85	1.85	1.83	1.81	1.82
Ti	0.02	0.02	0.03	0.03	0.02	0.03
Al	0.43	0.42	0.42	0.42	0.36	0.40
Fe	0.24	0.24	0.25	0.26	0.30	0.26
Mn	0.00	0.00	0.00	0.00	0.00	0.00
Mg	0.53	0.54	0.54	0.55	0.62	0.59
Ca	0.66	0.68	0.68	0.69	0.76	0.71
Na	0.25	0.24	0.23	0.21	0.12	0.19
K	0.00	0.00	0.00	0.00	0.00	0.00
Cr	0.00	0.00	0.00	0.00	0.00	0.00
Jd	**25**	**24**	**23**	**21**	**12**	**19**

Table A3. Continued.

A4. CLINOPYROXENE ANALYSES FROM KLATSCHMÜHLE

Clinopyroxene Klatschmühle

Name	164	166	167	168	169	170	171	172	179	180	181	182	183	184	185	186	187	188	189	190
wt %																				
SiO_2	54.96	53.87	52.83	53.67	53.48	53.65	53.73	53.60	54.25	54.58	54.22	54.20	54.32	54.49	54.90	54.48	54.46	54.10	54.09	54.23
TiO_2	0.40	0.34	0.31	0.48	0.52	0.47	0.53	0.52	0.44	0.43	0.43	0.43	0.44	0.45	0.41	0.43	0.48	0.49	0.45	0.46
Al_2O_3	8.74	7.57	7.50	8.40	9.03	9.00	9.20	9.14	8.84	8.83	8.78	8.58	8.91	8.57	8.54	8.62	8.87	9.03	8.88	8.79
FeO	3.67	3.28	3.34	4.94	3.88	4.16	3.97	3.91	3.68	3.49	3.77	3.92	3.56	4.14	3.90	3.94	3.79	3.68	3.67	4.02
MnO	0.01	0.02	0.05	0.07	0.05	0.06	0.07	0.03	0.06	0.04	0.06	0.09	0.05	0.04	0.00	0.07	0.01	0.09	0.05	0.08
MgO	12.74	12.79	13.30	14.41	12.74	12.94	12.58	12.26	12.16	12.37	12.51	12.75	12.22	13.06	12.82	12.88	12.67	12.69	12.20	12.71
CaO	16.53	17.63	21.14	16.74	17.60	16.69	16.85	16.76	16.78	16.80	16.36	16.16	16.76	15.94	16.45	16.37	16.59	16.83	16.98	16.47
Na_2O	3.97	3.54	1.97	2.52	3.08	3.17	3.60	3.64	3.98	3.86	3.85	3.99	4.05	3.66	3.64	3.82	3.78	3.83	3.99	3.75
K_2O	0.02	0.04	0.01	0.01	0.01	0.01	0.01	0.01	0.01	0.01	0.01	0.01	0.01	0.01	0.01	0.01	0.01	0.01	0.00	0.02
Cr_2O_3	0.00	0.00	0.00	0.00	0.00	0.00	0.00	0.00	0.00	0.00	0.00	0.00	0.00	0.00	0.00	0.00	0.00	0.00	0.00	0.00
TOTAL	101.04	99.07	100.44	101.22	100.38	100.16	100.54	99.86	100.21	100.40	100.00	100.12	100.31	100.37	100.67	100.61	100.65	100.74	100.30	100.52
Mg#	**86**	**87**	**88**	**84**	**85**	**85**	**85**	**85**	**85**	**86**	**86**	**85**	**86**	**85**	**85**	**85**	**86**	**86**	**86**	**85**
Si	1.94	1.95	1.90	1.91	1.92	1.93	1.92	1.93	1.94	1.95	1.94	1.94	1.94	1.95	1.95	1.94	1.94	1.92	1.93	1.93
Ti	0.01	0.01	0.01	0.01	0.01	0.01	0.01	0.01	0.01	0.01	0.01	0.01	0.01	0.01	0.01	0.01	0.01	0.01	0.01	0.01
Al	0.36	0.32	0.32	0.35	0.38	0.38	0.39	0.39	0.37	0.37	0.37	0.36	0.37	0.36	0.36	0.36	0.37	0.38	0.37	0.37
Fe	0.11	0.10	0.10	0.15	0.12	0.13	0.12	0.12	0.11	0.10	0.11	0.12	0.11	0.12	0.12	0.12	0.11	0.11	0.11	0.12
Mn	0.00	0.00	0.00	0.00	0.00	0.00	0.00	0.00	0.00	0.00	0.00	0.00	0.00	0.00	0.00	0.00	0.00	0.00	0.00	0.00
Mg	0.67	0.69	0.71	0.76	0.68	0.69	0.67	0.66	0.65	0.66	0.67	0.68	0.65	0.70	0.68	0.68	0.67	0.67	0.65	0.68
Ca	0.63	0.68	0.82	0.64	0.68	0.64	0.64	0.65	0.64	0.64	0.63	0.62	0.64	0.61	0.63	0.62	0.63	0.64	0.65	0.63
Na	0.27	0.25	0.14	0.17	0.21	0.22	0.25	0.25	0.28	0.27	0.27	0.28	0.28	0.25	0.25	0.26	0.26	0.26	0.28	0.26
K	0.00	0.00	0.00	0.00	0.00	0.00	0.00	0.00	0.00	0.00	0.00	0.00	0.00	0.00	0.00	0.00	0.00	0.00	0.00	0.00
Cr	0.00	0.00	0.00	0.00	0.00	0.00	0.00	0.00	0.00	0.00	0.00	0.00	0.00	0.00	0.00	0.00	0.00	0.00	0.00	0.00
Jd	**27**	**25**	**14**	**17**	**21**	**22**	**25**	**25**	**28**	**27**	**27**	**28**	**28**	**25**	**25**	**26**	**26**	**26**	**28**	**26**

Table A4. Major element composition of Klatschmühle clinopyroxene.

Clinopyroxene Klatschmühle

Name	191	192	193	194	195	196	197	199	267	269	270	271	272	273	274	275	276	277	278	279
wt %																				
SiO_2	53.72	54.17	53.82	53.98	53.73	53.10	53.05	53.77	55.10	52.50	52.56	53.31	53.13	53.42	53.40	53.73	53.93	51.58	54.01	54.21
TiO_2	0.50	0.48	0.51	0.53	0.56	0.61	0.48	0.38	0.38	0.51	0.45	0.44	0.45	0.49	0.45	0.40	0.44	0.75	0.45	0.45
Al_2O_3	9.04	8.80	8.83	8.62	8.80	8.73	8.14	7.69	8.11	8.67	9.25	9.10	9.15	9.33	9.52	9.22	9.21	10.91	9.36	9.37
FeO	3.93	3.87	4.02	4.33	3.65	3.69	3.98	3.63	3.73	3.90	3.98	4.32	4.02	3.88	3.32	3.61	4.05	4.50	3.59	3.79
MnO	0.08	0.05	0.05	0.08	0.05	0.00	0.04	0.03	0.00	0.04	0.03	0.06	0.00	0.06	0.06	0.02	0.05	0.05	0.06	0.05
MgO	12.27	12.62	12.70	13.33	12.48	12.45	12.73	13.18	12.92	12.92	12.68	13.00	12.39	12.11	11.56	12.12	12.25	12.97	11.90	12.18
CaO	17.01	17.03	16.98	17.00	18.16	18.92	19.82	17.39	17.15	19.23	17.47	16.41	16.53	16.36	16.90	16.26	15.71	14.97	16.21	16.04
Na_2O	3.71	3.50	3.40	3.25	3.33	2.95	2.57	3.54	3.71	2.58	3.22	3.54	3.72	4.17	4.27	4.24	4.05	3.97	4.32	4.18
K_2O	0.01	0.02	0.02	0.01	0.00	0.01	0.01	0.02	0.01	0.01	0.03	0.02	0.01	0.02	0.02	0.01	0.01	0.06	0.02	0.02
Cr_2O_3	0.00	0.00	0.00	0.00	0.00	0.00	0.00	0.00	0.00	0.00	0.00	0.00	0.00	0.00	0.00	0.00	0.00	0.00	0.00	0.00
TOTAL	100.27	100.53	100.34	101.15	100.74	100.47	100.83	99.62	101.12	100.36	99.66	100.19	99.38	99.83	99.50	99.61	99.69	99.73	99.93	100.29
Mg#	**85**	**85**	**85**	**85**	**86**	**86**	**85**	**87**	**86**	**86**	**85**	**84**	**85**	**85**	**86**	**86**	**84**	**84**	**86**	**85**
Si	1.92	1.93	1.93	1.92	1.92	1.90	1.90	1.93	1.95	1.89	1.89	1.91	1.91	1.91	1.92	1.92	1.94	1.84	1.93	1.93
Ti	0.01	0.01	0.01	0.01	0.01	0.02	0.01	0.01	0.01	0.01	0.01	0.01	0.01	0.01	0.01	0.01	0.01	0.02	0.01	0.01
Al	0.38	0.37	0.37	0.36	0.37	0.37	0.34	0.33	0.34	0.37	0.39	0.38	0.39	0.39	0.40	0.39	0.39	0.46	0.39	0.39
Fe	0.12	0.12	0.12	0.13	0.11	0.11	0.12	0.11	0.11	0.12	0.12	0.13	0.12	0.12	0.10	0.11	0.12	0.13	0.11	0.11
Mn	0.00	0.00	0.00	0.00	0.00	0.00	0.00	0.00	0.00	0.00	0.00	0.00	0.00	0.00	0.00	0.00	0.00	0.00	0.00	0.00
Mg	0.65	0.67	0.68	0.71	0.66	0.67	0.68	0.71	0.68	0.69	0.68	0.69	0.67	0.65	0.62	0.65	0.66	0.69	0.63	0.65
Ca	0.65	0.65	0.65	0.65	0.69	0.73	0.76	0.67	0.65	0.74	0.67	0.63	0.64	0.63	0.65	0.62	0.60	0.57	0.62	0.61
Na	0.26	0.24	0.24	0.22	0.23	0.21	0.18	0.25	0.25	0.18	0.22	0.25	0.26	0.29	0.30	0.29	0.28	0.27	0.30	0.29
K	0.00	0.00	0.00	0.00	0.00	0.00	0.00	0.00	0.00	0.00	0.00	0.00	0.00	0.00	0.00	0.00	0.00	0.00	0.00	0.00
Cr	0.00	0.00	0.00	0.00	0.00	0.00	0.00	0.00	0.00	0.00	0.00	0.00	0.00	0.00	0.00	0.00	0.00	0.00	0.00	0.00
Jd	**26**	**24**	**24**	**22**	**23**	**21**	**18**	**25**	**25**	**18**	**22**	**25**	**26**	**29**	**30**	**29**	**28**	**27**	**30**	**29**

Table A4. Continued.

Clinopyroxene Klatschmühle

Name	280	281	282	283	284	285	286	287	288	289	290	291	292	293	294	295	296	297	298	299
wt %																				
SiO_2	54.39	54.18	54.31	53.96	54.27	54.20	54.35	54.38	54.05	53.91	53.80	53.67	53.74	53.94	53.66	53.52	53.50	53.22	53.22	53.32
TiO_2	0.45	0.39	0.43	0.42	0.45	0.44	0.45	0.45	0.41	0.44	0.41	0.42	0.38	0.44	0.40	0.42	0.46	0.46	0.48	0.45
Al_2O_3	9.47	9.37	9.52	9.49	9.31	9.25	9.40	9.29	9.02	9.03	9.11	9.05	9.13	8.87	9.00	8.94	8.82	9.03	9.06	9.15
FeO	3.46	3.65	3.55	3.37	3.71	3.72	3.47	3.64	3.55	3.52	3.70	3.55	3.69	3.91	3.82	3.87	4.30	3.94	3.96	3.92
MnO	0.06	0.04	0.06	0.05	0.02	0.00	0.02	0.05	0.02	0.04	0.06	0.04	0.06	0.06	0.03	0.07	0.02	0.03	0.03	0.03
MgO	11.60	11.99	11.87	11.64	12.15	12.44	11.99	12.03	12.36	12.47	12.40	12.01	12.08	12.42	12.60	12.41	12.97	12.59	12.39	12.54
CaO	16.29	15.82	16.15	16.20	16.00	15.92	16.27	16.21	16.18	16.27	16.24	16.73	16.72	16.43	16.48	16.68	15.96	16.57	16.72	16.66
Na_2O	4.37	4.44	4.48	4.40	4.24	4.27	4.27	4.39	4.15	4.00	4.05	4.19	4.11	4.09	3.93	3.77	3.75	3.76	3.82	3.75
K_2O	0.01	0.01	0.01	0.01	0.00	0.00	0.01	0.01	0.01	0.00	0.01	0.01	0.01	0.01	0.01	0.01	0.02	0.02	0.01	0.01
Cr_2O_3	0.00	0.00	0.00	0.00	0.00	0.00	0.00	0.00	0.00	0.00	0.00	0.00	0.00	0.00	0.00	0.00	0.00	0.00	0.00	0.00
TOTAL	100.09	99.87	100.36	99.55	100.14	100.24	100.22	100.43	99.75	99.67	99.77	99.66	99.91	100.16	99.91	99.68	99.80	99.61	99.68	99.82
Mg#	86	85	86	86	85	86	86	85	86	86	86	86	85	85	85	85	84	85	85	85
Si	1.94	1.93	1.93	1.94	1.94	1.93	1.94	1.93	1.93	1.93	1.93	1.92	1.92	1.93	1.92	1.92	1.92	1.91	1.91	1.91
Ti	0.01	0.01	0.01	0.01	0.01	0.01	0.01	0.01	0.01	0.01	0.01	0.01	0.01	0.01	0.01	0.01	0.01	0.01	0.01	0.01
Al	0.40	0.39	0.40	0.40	0.39	0.39	0.39	0.39	0.38	0.38	0.38	0.38	0.39	0.37	0.38	0.38	0.37	0.38	0.38	0.39
Fe	0.10	0.11	0.11	0.10	0.11	0.11	0.10	0.11	0.11	0.11	0.11	0.11	0.11	0.12	0.11	0.12	0.13	0.12	0.12	0.12
Mn	0.00	0.00	0.00	0.00	0.00	0.00	0.00	0.00	0.00	0.00	0.00	0.00	0.00	0.00	0.00	0.00	0.00	0.00	0.00	0.00
Mg	0.62	0.64	0.63	0.62	0.65	0.66	0.64	0.64	0.66	0.67	0.66	0.64	0.64	0.66	0.67	0.67	0.69	0.67	0.66	0.67
Ca	0.62	0.61	0.62	0.62	0.61	0.61	0.62	0.62	0.62	0.62	0.62	0.64	0.64	0.63	0.63	0.64	0.61	0.64	0.64	0.64
Na	0.30	0.31	0.31	0.31	0.29	0.29	0.29	0.30	0.29	0.28	0.28	0.29	0.29	0.28	0.27	0.26	0.26	0.26	0.27	0.26
K	0.00	0.00	0.00	0.00	0.00	0.00	0.00	0.00	0.00	0.00	0.00	0.00	0.00	0.00	0.00	0.00	0.00	0.00	0.00	0.00
Cr	0.00	0.00	0.00	0.00	0.00	0.00	0.00	0.00	0.00	0.00	0.00	0.00	0.00	0.00	0.00	0.00	0.00	0.00	0.00	0.00
Jd	30	31	31	31	29	29	29	30	29	28	28	29	29	28	27	26	26	26	27	26

Table A4. Continued.

Clinopyroxene Klatschmühle

Name	300	301	302	303	312	315	317	318	320	325	331	333	336	337	339	345	346	347	355	358	362
wt %																					
SiO_2	51.64	53.11	53.02	52.41	50.95	45.98	54.87	55.68	54.35	54.62	54.13	54.28	54.96	54.66	53.43	52.68	54.27	55.50	55.43	53.82	54.84
TiO_2	0.41	0.47	0.48	0.48	0.46	0.43	0.41	0.47	0.51	0.37	0.45	0.59	0.37	0.45	0.63	0.54	0.49	0.40	0.56	0.50	0.45
Al_2O_3	9.35	8.88	8.97	8.73	9.02	9.69	9.07	9.31	9.73	8.57	9.90	10.04	9.66	10.49	10.86	9.06	9.77	7.32	8.56	8.22	9.52
FeO	4.99	4.41	3.74	3.60	4.04	3.57	3.03	3.19	3.54	3.27	3.58	3.54	3.16	3.05	3.47	3.88	3.61	4.07	3.50	4.14	3.71
MnO	0.04	0.08	0.03	0.05	0.06	0.03	0.00	0.04	0.04	0.05	0.04	0.06	0.05	0.00	0.05	0.05	0.05	0.05	0.04	0.06	0.00
MgO	14.51	13.10	12.39	12.57	12.57	11.60	12.09	11.84	12.10	12.51	12.03	12.01	11.72	11.13	11.36	14.16	12.03	13.80	12.39	13.37	12.07
CaO	15.22	16.41	18.02	19.10	16.21	16.09	17.15	16.44	16.36	16.91	16.44	17.32	16.24	16.04	17.50	17.93	16.69	16.37	16.46	17.04	16.14
Na_2O	3.14	3.46	3.40	2.80	3.84	4.16	4.09	4.28	4.08	4.15	4.34	3.81	4.39	4.19	3.97	2.33	4.00	3.59	4.22	3.32	4.11
K_2O	0.04	0.01	0.00	0.01	0.01	0.01	0.00	0.01	0.01	0.02	0.01	0.02	0.03	0.03	0.02	0.02	0.00	0.02	0.01	0.01	0.00
Cr_2O_3	0.00	0.00	0.00	0.00	0.00	0.00	0.00	0.00	0.00	0.00	0.00	0.00	0.00	0.00	0.00	0.00	0.00	0.00	0.00	0.00	0.00
TOTAL	99.33	99.93	100.05	99.76	97.17	91.55	100.71	101.26	100.72	100.46	100.92	101.66	100.57	100.04	101.27	100.65	100.91	101.12	101.18	100.47	100.86
Mg#	84	84	86	86	85	85	88	87	86	87	86	86	87	87	85	87	86	86	86	85	85
Si	1.86	1.91	1.90	1.89	1.87	1.78	1.95	1.97	1.93	1.94	1.91	1.91	1.95	1.95	1.89	1.88	1.93	1.97	1.96	1.92	1.95
Ti	0.01	0.01	0.01	0.01	0.01	0.01	0.01	0.01	0.01	0.01	0.01	0.02	0.01	0.01	0.02	0.01	0.01	0.01	0.01	0.01	0.01
Al	0.40	0.38	0.38	0.37	0.39	0.44	0.38	0.39	0.41	0.36	0.41	0.42	0.40	0.44	0.45	0.38	0.41	0.31	0.36	0.35	0.40
Fe	0.15	0.13	0.11	0.11	0.12	0.12	0.09	0.09	0.11	0.10	0.11	0.10	0.09	0.09	0.10	0.12	0.11	0.12	0.10	0.12	0.11
Mn	0.00	0.00	0.00	0.00	0.00	0.00	0.00	0.00	0.00	0.00	0.00	0.00	0.00	0.00	0.00	0.00	0.00	0.00	0.00	0.00	0.00
Mg	0.78	0.70	0.66	0.68	0.69	0.67	0.64	0.62	0.64	0.66	0.63	0.63	0.62	0.59	0.60	0.75	0.64	0.73	0.65	0.71	0.64
Ca	0.59	0.63	0.69	0.74	0.64	0.67	0.65	0.62	0.62	0.64	0.62	0.65	0.62	0.61	0.66	0.69	0.63	0.62	0.62	0.65	0.61
Na	0.22	0.24	0.24	0.20	0.27	0.31	0.28	0.29	0.28	0.29	0.30	0.26	0.30	0.29	0.27	0.16	0.28	0.25	0.29	0.23	0.28
K	0.00	0.00	0.00	0.00	0.00	0.00	0.00	0.00	0.00	0.00	0.00	0.00	0.00	0.00	0.00	0.00	0.00	0.00	0.00	0.00	0.00
Cr	0.00	0.00	0.00	0.00	0.00	0.00	0.00	0.00	0.00	0.00	0.00	0.00	0.00	0.00	0.00	0.00	0.00	0.00	0.00	0.00	0.00
Jd	22	24	24	20	27	31	28	29	28	29	30	26	30	29	27	16	28	25	29	23	28

Table A4. Continued.

Clinopyroxene Klatschmühle

Name	21	50	51	53	54	55	56	57	58	59	60	61	62	63	64	65	66	67	68	69
wt %																				
SiO_2	49.03	51.43	51.58	51.45	50.98	50.55	51.37	51.62	51.34	51.03	50.19	50.96	51.38	55.17	51.18	51.61	51.64	51.09	50.64	51.15
TiO_2	0.78	0.64	0.58	0.60	0.68	0.67	0.65	0.54	0.60	0.64	0.70	0.68	0.63	0.52	0.63	0.59	0.60	0.65	0.63	0.61
Al_2O_3	10.19	11.44	11.63	11.68	11.29	11.50	11.56	11.41	11.50	11.50	10.25	11.37	11.42	15.35	11.33	11.38	11.42	11.02	10.87	10.82
FeO	7.74	6.71	6.46	6.65	6.73	6.74	6.35	6.71	6.57	6.53	6.89	6.20	6.01	3.69	6.08	5.90	5.88	5.96	6.26	7.25
MnO	0.12	0.06	0.08	0.07	0.06	0.08	0.05	0.08	0.10	0.07	0.08	0.06	0.06	0.04	0.05	0.09	0.04	0.04	0.07	0.04
MgO	11.51	10.02	9.79	9.99	10.18	10.29	9.68	9.98	9.92	10.05	11.14	9.64	9.62	6.61	9.44	9.48	9.50	9.29	9.71	10.43
CaO	17.99	17.03	16.61	16.54	17.57	17.87	16.87	16.79	16.90	17.33	18.46	16.52	16.14	12.55	16.13	15.91	15.82	15.81	15.81	16.65
Na_2O	1.85	3.56	3.82	3.74	3.19	3.02	3.63	3.85	3.70	3.49	2.58	3.94	4.25	5.23	4.24	4.55	4.63	4.13	3.72	3.00
K_2O	0.01	0.00	0.01	0.00	0.00	0.00	0.00	0.01	0.00	0.00	0.00	0.00	0.00	0.02	0.01	0.00	0.00	0.01	0.00	0.00
Cr_2O_3	0.06	0.05	0.00	0.05	0.01	0.04	0.03	0.02	0.03	0.01	0.02	0.05	0.04	0.03	0.03	0.02	0.06	0.04	0.03	0.02
TOTAL	99.26	100.93	100.54	100.77	100.69	100.78	100.18	101.00	100.65	100.65	100.31	99.42	99.54	99.20	99.11	99.52	99.59	98.03	97.73	99.97
Mg#	**73**	**73**	**73**	**73**	**73**	**73**	**73**	**73**	**73**	**73**	**74**	**73**	**74**	**76**	**73**	**74**	**74**	**74**	**73**	**72**
Si	1.81	1.85	1.86	1.85	1.84	1.83	1.86	1.85	1.85	1.84	1.83	1.86	1.86	2.00	1.87	1.87	1.87	1.89	1.88	1.87
Ti	0.02	0.02	0.02	0.02	0.02	0.02	0.02	0.01	0.02	0.02	0.02	0.02	0.02	0.01	0.02	0.02	0.02	0.02	0.02	0.02
Al	0.44	0.49	0.49	0.50	0.48	0.49	0.49	0.48	0.49	0.49	0.44	0.49	0.49	0.66	0.49	0.49	0.49	0.48	0.48	0.47
Fe	0.24	0.20	0.19	0.20	0.20	0.20	0.19	0.20	0.20	0.20	0.21	0.19	0.18	0.11	0.19	0.18	0.18	0.18	0.19	0.22
Mn	0.00	0.00	0.00	0.00	0.00	0.00	0.00	0.00	0.00	0.00	0.00	0.00	0.00	0.00	0.00	0.00	0.00	0.00	0.00	0.00
Mg	0.63	0.54	0.53	0.54	0.55	0.55	0.52	0.53	0.53	0.54	0.60	0.52	0.52	0.36	0.51	0.51	0.51	0.51	0.54	0.57
Ca	0.71	0.66	0.64	0.64	0.68	0.69	0.66	0.65	0.65	0.67	0.72	0.64	0.63	0.49	0.63	0.62	0.61	0.63	0.63	0.65
Na	0.13	0.25	0.27	0.26	0.22	0.21	0.26	0.27	0.26	0.24	0.18	0.28	0.30	0.37	0.30	0.32	0.32	0.30	0.27	0.21
K	0.00	0.00	0.00	0.00	0.00	0.00	0.00	0.00	0.00	0.00	0.00	0.00	0.00	0.00	0.00	0.00	0.00	0.00	0.00	0.00
Cr	0.00	0.00	0.00	0.00	0.00	0.00	0.00	0.00	0.00	0.00	0.00	0.00	0.00	0.00	0.00	0.00	0.00	0.00	0.00	0.00
Jd	**13**	**25**	**27**	**26**	**22**	**21**	**26**	**27**	**26**	**24**	**18**	**28**	**30**	**37**	**30**	**32**	**32**	**30**	**27**	**21**

Table A4. Continued.

Clinopyroxene Klatschmühle

Name	70	72	73	74	75	76	78	79	80	91	105	106	225	226	227	229	230	231	232	233
wt %																				
SiO_2	51.35	52.94	52.25	51.62	51.17	51.27	51.90	51.71	51.56	51.61	49.00	49.26	51.33	51.24	51.69	53.10	52.25	51.19	50.50	50.66
TiO_2	0.64	0.54	0.58	0.56	0.68	0.60	0.54	0.59	0.57	0.62	0.59	0.61	0.77	0.68	0.61	0.49	0.54	0.59	0.73	0.83
Al_2O_3	11.39	11.53	11.65	11.72	10.61	11.37	11.30	11.27	11.44	10.75	13.78	13.51	11.24	10.77	10.04	9.93	10.19	10.41	10.04	10.42
FeO	6.45	6.20	6.06	6.59	6.75	6.82	6.19	6.34	6.33	6.13	5.60	5.51	6.36	5.78	7.33	6.19	6.58	6.76	6.80	6.28
MnO	0.07	0.08	0.09	0.05	0.06	0.06	0.04	0.06	0.05	0.06	0.03	0.04	0.06	0.09	0.09	0.06	0.07	0.10	0.08	0.07
MgO	9.81	9.25	9.47	9.78	10.19	10.02	9.66	9.77	9.75	9.71	9.32	9.25	10.09	10.64	10.83	10.05	10.31	10.38	10.93	10.42
CaO	16.35	15.47	15.79	15.94	17.23	16.62	16.05	15.80	16.01	16.43	18.83	18.61	16.48	14.99	15.91	15.07	16.03	16.77	17.95	17.89
Na_2O	3.59	3.81	4.05	3.73	3.00	3.26	3.87	3.78	3.71	3.80	2.91	3.07	3.52	3.71	3.40	3.77	3.72	3.36	2.56	2.84
K_2O	0.01	0.00	0.00	0.00	0.01	0.00	0.00	0.02	0.00	0.02	0.03	0.01	0.00	0.01	0.00	0.03	0.00	0.00	0.00	0.00
Cr_2O_3	0.01	0.02	0.04	0.03	0.06	0.05	0.04	0.06	0.03	0.05	0.06	0.02	0.12	0.10	0.06	0.10	0.09	0.12	0.11	0.14
TOTAL	99.67	99.85	99.97	100.01	99.75	100.06	99.57	99.39	99.43	99.17	100.14	99.88	99.96	98.00	99.95	98.78	99.77	99.67	99.73	99.53
Mg#	**73**	**73**	**74**	**73**	**73**	**72**	**74**	**73**	**73**	**74**	**75**	**75**	**74**	**77**	**72**	**74**	**74**	**73**	**74**	**75**
Si	1.87	1.93	1.89	1.87	1.87	1.87	1.89	1.89	1.88	1.89	1.78	1.79	1.87	1.89	1.88	1.95	1.90	1.87	1.85	1.86
Ti	0.02	0.01	0.02	0.02	0.02	0.02	0.01	0.02	0.02	0.02	0.02	0.02	0.02	0.02	0.02	0.01	0.01	0.02	0.02	0.02
Al	0.49	0.49	0.50	0.50	0.46	0.49	0.48	0.48	0.49	0.46	0.59	0.58	0.48	0.47	0.43	0.43	0.44	0.45	0.43	0.45
Fe	0.20	0.19	0.18	0.20	0.21	0.21	0.19	0.19	0.19	0.19	0.17	0.17	0.19	0.18	0.22	0.19	0.20	0.21	0.21	0.19
Mn	0.00	0.00	0.00	0.00	0.00	0.00	0.00	0.00	0.00	0.00	0.00	0.00	0.00	0.00	0.00	0.00	0.00	0.00	0.00	0.00
Mg	0.53	0.50	0.51	0.53	0.56	0.54	0.52	0.53	0.53	0.53	0.50	0.50	0.55	0.59	0.59	0.55	0.56	0.56	0.60	0.57
Ca	0.64	0.60	0.61	0.62	0.68	0.65	0.63	0.62	0.63	0.64	0.73	0.73	0.64	0.59	0.62	0.59	0.62	0.66	0.70	0.70
Na	0.25	0.27	0.28	0.26	0.21	0.23	0.27	0.27	0.26	0.27	0.21	0.22	0.25	0.26	0.24	0.27	0.26	0.24	0.18	0.20
K	0.00	0.00	0.00	0.00	0.00	0.00	0.00	0.00	0.00	0.00	0.00	0.00	0.00	0.00	0.00	0.00	0.00	0.00	0.00	0.00
Cr	0.00	0.00	0.00	0.00	0.00	0.00	0.00	0.00	0.00	0.00	0.00	0.00	0.00	0.00	0.00	0.00	0.00	0.00	0.00	0.00
Jd	**25**	**27**	**28**	**26**	**21**	**23**	**27**	**27**	**26**	**27**	**21**	**22**	**25**	**26**	**24**	**27**	**26**	**24**	**18**	**20**

Table A4. Continued.

Clinopyroxene Klatschmühle

Name	234	235	236	237	238	239	240	253	254	255	256	257	259	260	261	262	263	264	290	292
wt %																				
SiO_2	51.54	51.88	51.97	52.39	52.52	52.50	51.49	51.83	51.85	52.00	52.29	52.47	52.51	52.43	52.93	52.80	52.14	51.28	51.92	51.05
TiO_2	0.66	0.65	0.55	0.55	0.59	0.60	0.69	0.73	0.65	0.73	0.69	0.65	0.67	0.56	0.63	0.55	0.59	0.73	0.73	0.90
Al_2O_3	10.46	10.86	10.92	11.09	11.11	11.08	10.88	11.19	11.31	11.69	11.57	11.64	11.77	11.67	11.79	11.81	11.74	10.69	10.32	10.47
FeO	6.86	6.10	6.31	6.04	5.80	5.80	6.50	6.90	6.20	6.40	5.82	5.84	5.77	5.67	5.62	5.77	6.17	6.11	6.08	5.97
MnO	0.10	0.07	0.05	0.08	0.07	0.04	0.08	0.06	0.08	0.07	0.03	0.07	0.06	0.06	0.06	0.06	0.02	0.09	0.03	0.09
MgO	10.62	9.87	10.03	9.58	9.65	9.52	10.03	9.94	9.55	9.60	9.38	9.19	9.03	9.28	9.23	9.31	9.50	10.48	10.18	10.42
CaO	15.89	16.11	15.60	15.75	15.62	15.63	16.35	15.50	15.75	15.17	15.58	15.43	15.17	15.15	15.11	15.27	15.69	17.45	17.13	17.59
Na_2O	3.55	3.92	3.77	4.07	4.39	4.22	3.42	3.73	4.08	4.23	4.28	4.44	4.62	4.46	4.56	4.43	4.14	3.08	3.41	3.05
K_2O	0.01	0.01	0.00	0.00	0.00	0.00	0.01	0.00	0.00	0.00	0.01	0.00	0.01	0.00	0.02	0.00	0.00	0.01	0.00	0.00
Cr_2O_3	0.06	0.10	0.06	0.09	0.08	0.09	0.08	0.08	0.09	0.07	0.06	0.05	0.06	0.07	0.06	0.08	0.04	0.09	0.07	0.06
TOTAL	99.74	99.55	99.26	99.63	99.82	99.46	99.54	99.96	99.57	99.97	99.71	99.79	99.65	99.35	100.02	100.08	100.03	99.99	99.88	99.61
Mg#	**73**	**74**	**74**	**74**	**75**	**75**	**73**	**72**	**73**	**73**	**74**	**74**	**74**	**74**	**75**	**74**	**73**	**75**	**75**	**76**
Si	1.88	1.89	1.90	1.90	1.90	1.91	1.88	1.88	1.89	1.88	1.90	1.90	1.90	1.90	1.91	1.91	1.89	1.87	1.89	1.87
Ti	0.02	0.02	0.02	0.02	0.02	0.02	0.02	0.02	0.02	0.02	0.02	0.02	0.02	0.02	0.02	0.01	0.02	0.02	0.02	0.02
Al	0.45	0.47	0.47	0.48	0.47	0.47	0.47	0.48	0.49	0.50	0.49	0.50	0.50	0.50	0.50	0.50	0.50	0.46	0.44	0.45
Fe	0.21	0.19	0.19	0.18	0.18	0.18	0.20	0.21	0.19	0.19	0.18	0.18	0.17	0.17	0.17	0.17	0.19	0.19	0.19	0.18
Mn	0.00	0.00	0.00	0.00	0.00	0.00	0.00	0.00	0.00	0.00	0.00	0.00	0.00	0.00	0.00	0.00	0.00	0.00	0.00	0.00
Mg	0.58	0.54	0.55	0.52	0.52	0.52	0.55	0.54	0.52	0.52	0.51	0.50	0.49	0.50	0.50	0.50	0.51	0.57	0.55	0.57
Ca	0.62	0.63	0.61	0.61	0.61	0.61	0.64	0.60	0.61	0.59	0.60	0.60	0.59	0.59	0.58	0.59	0.61	0.68	0.67	0.69
Na	0.25	0.28	0.27	0.29	0.31	0.30	0.24	0.26	0.29	0.30	0.30	0.31	0.32	0.31	0.32	0.31	0.29	0.22	0.24	0.22
K	0.00	0.00	0.00	0.00	0.00	0.00	0.00	0.00	0.00	0.00	0.00	0.00	0.00	0.00	0.00	0.00	0.00	0.00	0.00	0.00
Cr	0.00	0.00	0.00	0.00	0.00	0.00	0.00	0.00	0.00	0.00	0.00	0.00	0.00	0.00	0.00	0.00	0.00	0.00	0.00	0.00
Jd	**25**	**28**	**27**	**29**	**31**	**30**	**24**	**26**	**29**	**30**	**30**	**31**	**32**	**31**	**32**	**31**	**29**	**22**	**24**	**22**

Table A4. Continued.

Clinopyroxene Klatschmühle

Name	293	294	295	296	297	298	299	300	301	302	303	304	306	307	308	309	318	319	320	321
wt %																				
SiO_2	52.20	52.38	53.07	52.90	52.85	50.67	52.57	51.74	51.26	51.59	52.12	52.60	52.04	51.34	51.19	50.53	51.21	52.38	52.57	52.83
TiO_2	0.78	0.71	0.69	0.66	0.61	0.65	0.64	0.62	0.93	0.89	0.63	0.58	0.63	0.84	0.90	0.96	0.83	0.70	0.66	0.65
Al_2O_3	11.25	11.28	11.27	11.21	11.44	11.32	11.20	10.86	10.58	8.65	11.38	11.37	11.20	10.67	10.24	9.43	10.67	11.38	11.31	11.21
FeO	6.25	6.17	5.83	5.99	6.01	7.79	6.37	8.60	6.53	6.54	6.56	6.39	6.64	6.77	6.90	6.74	5.98	6.20	6.17	6.16
MnO	0.06	0.08	0.07	0.04	0.06	0.06	0.06	0.09	0.10	0.10	0.06	0.06	0.11	0.08	0.06	0.05	0.08	0.10	0.06	0.09
MgO	9.54	9.34	9.06	9.16	9.06	10.58	9.32	10.76	10.31	11.17	9.57	9.41	9.61	10.28	10.59	11.26	9.97	9.34	9.29	9.07
CaO	15.66	15.43	15.12	15.28	15.32	14.08	15.39	13.81	16.72	18.71	15.62	15.38	15.64	16.65	17.23	18.51	17.52	15.63	15.34	15.14
Na_2O	4.04	4.22	4.46	4.50	4.40	3.51	4.53	3.66	3.31	2.51	3.87	4.38	3.79	3.16	2.98	2.38	3.21	4.17	4.48	4.27
K_2O	0.01	0.01	0.01	0.00	0.02	0.02	0.00	0.01	0.00	0.00	0.00	0.00	0.00	0.00	0.00	0.00	0.00	0.01	0.00	0.00
Cr_2O_3	0.09	0.13	0.09	0.08	0.11	0.07	0.04	0.07	0.11	0.12	0.10	0.12	0.09	0.10	0.12	0.06	0.07	0.07	0.08	0.05
TOTAL	99.87	99.75	99.65	99.82	99.90	98.75	100.12	100.21	99.85	100.29	99.89	100.29	99.75	99.89	100.19	99.92	99.54	99.97	99.95	99.48
Mg#	**73**	**73**	**73**	**73**	**73**	**71**	**72**	**69**	**74**	**75**	**72**	**72**	**72**	**73**	**73**	**75**	**75**	**73**	**73**	**72**
Si	1.89	1.90	1.93	1.92	1.91	1.86	1.90	1.88	1.87	1.88	1.89	1.90	1.90	1.87	1.86	1.85	1.87	1.90	1.90	1.93
Ti	0.02	0.02	0.02	0.02	0.02	0.02	0.02	0.02	0.03	0.02	0.02	0.02	0.02	0.02	0.02	0.03	0.02	0.02	0.02	0.02
Al	0.48	0.48	0.48	0.48	0.49	0.49	0.48	0.46	0.45	0.37	0.49	0.48	0.48	0.46	0.44	0.41	0.46	0.49	0.48	0.48
Fe	0.19	0.19	0.18	0.18	0.18	0.24	0.19	0.26	0.20	0.20	0.20	0.19	0.20	0.21	0.21	0.21	0.18	0.19	0.19	0.19
Mn	0.00	0.00	0.00	0.00	0.00	0.00	0.00	0.00	0.00	0.00	0.00	0.00	0.00	0.00	0.00	0.00	0.00	0.00	0.00	0.00
Mg	0.52	0.51	0.49	0.49	0.49	0.58	0.50	0.58	0.56	0.61	0.52	0.51	0.52	0.56	0.57	0.61	0.54	0.50	0.50	0.49
Ca	0.61	0.60	0.59	0.59	0.59	0.55	0.60	0.54	0.65	0.73	0.61	0.59	0.61	0.65	0.67	0.73	0.69	0.61	0.59	0.59
Na	0.28	0.30	0.31	0.32	0.31	0.25	0.32	0.26	0.23	0.18	0.27	0.31	0.27	0.22	0.21	0.17	0.23	0.29	0.31	0.30
K	0.00	0.00	0.00	0.00	0.00	0.00	0.00	0.00	0.00	0.00	0.00	0.00	0.00	0.00	0.00	0.00	0.00	0.00	0.00	0.00
Cr	0.00	0.00	0.00	0.00	0.00	0.00	0.00	0.00	0.00	0.00	0.00	0.00	0.00	0.00	0.00	0.00	0.00	0.00	0.00	0.00
Jd	**28**	**30**	**31**	**32**	**31**	**25**	**32**	**26**	**23**	**18**	**27**	**31**	**27**	**22**	**21**	**17**	**23**	**29**	**31**	**30**

Table A4. Continued.